

AD-772 774

STOL TACTICAL AIRCRAFT INVESTIGATION--
EXTERNALLY BLOWN FLAP. VOLUME IV.
ANALYSIS OF WIND TUNNEL DATA

Patrick P. Papp, et al

Rockwell International Corporation

Prepared for:

Air Force Flight Dynamics Laboratory

April 1973

DISTRIBUTED BY:

NTIS

National Technical Information Service
U. S. DEPARTMENT OF COMMERCE
5285 Port Royal Road, Springfield Va. 22151

NOTICE

When Government drawings, specifications, or other data are used for any purpose other than in connection with a definitely related Government procurement operation, the United States Government thereby incurs no responsibility nor any obligation whatsoever; and the fact that the government may have formulated, furnished, or in any way supplied the said drawings, specifications, or other data, is not to be regarded by implication or otherwise as in any manner licensing the holder or any other person or corporation, or conveying any rights or permission to manufacture, use, or sell any patented invention that may in any way be related thereto.

ACCESSION for	
NTIS	Write Section <input checked="" type="checkbox"/>
DDC	add Section <input type="checkbox"/>
ORIGINATED	<input type="checkbox"/>
JUSTIFICATION	
BY	
CLASSIFICATION CODES	
SPECIAL	
A	

Copies of this report should not be returned unless return is required by security considerations, contractual obligations, or notice on a specific document.

Security Classification

DOCUMENT CONTROL DATA - R & D

(Security classification of title, body of abstract and indexing annotation must be entered when the overall report is classified)

1. ORIGINATING ACTIVITY (Corporate author) Los Angeles Aircraft Division Rockwell International Corporation Los Angeles International Airport, L.A., Calif., 90009		2a. REPORT SECURITY CLASSIFICATION Unclassified	
3. REPORT TITLE STOL Tactical Aircraft Investigation, Externally Blown Flap, Volume IV Analysis of Wind Tunnel Data		2b. GROUP	
4. DESCRIPTIVE NOTES (Type of report and inclusive dates) Final Report (10 June 1971 to 10 December 1972)			
5. AUTHOR(S) (First name, middle initial, last name) Patrick P. Papp Ralph A. Quam Gerald A. Freeman			
6. REPORT DATE April 1974	7a. TOTAL NO. OF PAGES 426 420	7b. NO. OF REFS 2	
8a. CONTRACT OR GRANT NO. F33615-71-C-1760	8b. ORIGINATOR'S REPORT NUMBER(S)		
8c. PROJECT NO. 643A - Task 0020	8d. OTHER REPORT NO(S) (Any other numbers that may be assigned this report) AFFDL-TR-73-20 Volume IV		
10. DISTRIBUTION STATEMENT Approved for public release; distribution unlimited.			
11. SUPPLEMENTARY NOTES		12. SPONSORING MILITARY ACTIVITY Air Force Flight Dynamics Laboratory (PTA), Wright Patterson AFB, Ohio, 45433	
13. ABSTRACT <p>The basic objective of the work reported herein was to provide a broader technology base to support the development of a medium STOL Transport (MST) airplane. This work was limited to the application of the externally blown flap (EBF) powered lift concept.</p> <p>The technology of EBF STOL aircraft has been investigated through analytical studies, wind tunnel testing, flight simulator testing, and design trade studies. The results obtained include development of methods for the estimation of the aerodynamic characteristics of an EBF configuration, STOL performance estimation methods, safety margins for takeoff and landing, wind tunnel investigation of the effects of varying EBF system geometry parameters, configuration definition to meet MST requirements, trade data on performance and configuration requirement variations, flight control system mechanization trade data, handling qualities characteristics; piloting procedures, and effects of applying an air cushion landing system to the MST.</p> <p>From an overall assessment of study results, it is concluded that the EBF concept provides a practical means of obtaining STOL performance for an MST with relatively low risk.</p>			

DD FORM 1473

Security Classification

**Best
Available
Copy**

Security Classification

14. KEY WORDS	LINK A		LINK B		LINK C	
	ROLE	WT	ROLE	WT	ROLE	WT
STOL Transport Externally Blown Flaps Medium STOL Transport Wind Tunnel Data Engine Simulators						

AFFDL-TR-73-20
Volume IV

**STOL TACTICAL AIRCRAFT INVESTIGATION-
EXTERNALLY BLOWN FLAP**

Volume IV

Analysis of Wind Tunnel Data

P. P. PAPP

R. A. QUAM

G. A. FREEMAN

*LOS ANGELES AIRCRAFT DIVISION
ROCKWELL INTERNATIONAL CORPORATION*

TECHNICAL REPORT AFFDL-TR-73-20, VOLUME IV

APRIL 1973

Approved for public release; distribution unlimited


**AIR FORCE FLIGHT DYNAMICS LABORATORY
AIR FORCE SYSTEMS COMMAND
WRIGHT-PATTERSON AIR FORCE BASE, OHIO**

FOREWORD

This report was prepared for the Prototype Division of the Air Force Flight Dynamics Laboratory by the Los Angeles Aircraft Division, Rockwell International. The work was performed as part of the STOL tactical aircraft investigation program under USAF contract F33615-71-C-1760, project 643A0020. Daniel E. Fraga, AFFDL/PTA, was the Air Force program manager, and Garland S. Oates, Jr., AFFDL/PTA, was the Air Force technical manager. Marshall H. Roe was the program manager for Rockwell.

This investigation was conducted during the period from 10 June 1971 through 9 December 1972. This final report is published in six volumes and was originally published as Rockwell report NA-72-868. This report was submitted for approval on 9 December 1972.

This technical report has been reviewed and is approved.


E. J. Cross, Jr.
Lt Col, USAF
Chief, Prototype Division

ABSTRACT

The basic objective of the work reported herein was to provide a broader technology base to support the development of a medium STOL Transport (MST) airplane. This work was limited to the application of the externally blown flap (EBF) powered lift concept.

The technology of EBF STOL aircraft has been investigated through analytical studies, wind tunnel testing, flight simulator testing, and design trade studies. The results obtained include development of methods for the estimation of the aerodynamic characteristics of an EBF configuration, STOL performance estimation methods, safety margins for takeoff and landing, wind tunnel investigation of the effects of varying EBF system geometry parameters, configuration definition to meet MST requirements, trade data on performance and configuration requirement variations, flight control system mechanization trade data, handling qualities characteristics, piloting procedures, and effects of applying an air cushion landing system to the MST.

From an overall assessment of study results, it is concluded that the EBF concept provides a practical means of obtaining STOL performance for an MST with relatively low risk. Some improvement in EBF performance could be achieved with further development - primarily wind tunnel testing. Further work should be done on optimization of flight controls, definition of flying qualities requirements, and development of piloting procedures. Considerable work must be done in the area of structural design criteria relative to the effects of engine exhaust impingement on the wing and flap structure.

This report is arranged in six volumes:

Volume I - Configuration Definition

Volume II - Design Compendium

Volume III - Performance Methods and Takeoff and Landing Rules

Volume IV - Analysis of Wind Tunnel Data

Volume V - Flight Control Technology

Part I - Control System Mechanization Trade Studies

Part II - Simulation Studies/Flight Control System Validation

Part III - Stability and Control Derivative Accuracy
Requirements and Effects of Augmentation System Design

Volume VI - Air Cushion Landing System Trade Study

This Volume IV represents analysis of wind tunnel data obtained at the Lockheed/Georgia Company's Low Speed Wind Tunnel at Marietta, Georgia between the dates of 3 April 1972 and 19 May 1972. The basic wind tunnel data is presented in Rockwell report NA-72-670, Appendix A, dated 24 August 1972 and titled, "STOL Tactical Aircraft Investigation Wind Tunnel Test Data of an Externally Blown Flap Model;" Contract F33615-71-C-1760, Appendix A, Plotted Figures, Volumes I, II, and III of XIV.

The data presented herein was obtained using the Rockwell 7-percent scale wind tunnel model of a STOL transport employing externally blown flaps.

TABLE OF CONTENTS

Section	Page
I INTRODUCTION	1
II MODEL DIMENSIONS AND NOMENCLATURE AND PHOTOGRAPHS	3
III WIND TUNNEL TEST RUN LOG SUMMARY	59
IV WING SWEEP	75
4.1 Effects on Lift	75
4.2 Effects on Drag	75
4.3 Effects on Pitching Moment	76
V ASPECT RATIO	89
5.1 Effects on Lift	89
5.2 Effects on Drag	90
5.3 Effects on Pitching Moment	90
VI DOWNWASH	101
6.1 Effects of Power	101
6.2 Effects of Engine Nozzle Deflection and Flap Deflection	102
6.3 Effects of Various Leading Edge Devices	102
6.4 Effects of Engine Spanwise Location	102
VII REYNOLDS NUMBER	133
7.1 Effects on Longitudinal Aerodynamic Parameters	133
7.2 Effects on Lateral-Directional Aerodynamic Parameters	133
7.3 Effects on Horizontal Tail Angle of Attack	133
VIII FLAP SPAN	145
8.1 Effects on Longitudinal Aerodynamic Parameters	145
IX HORIZONTAL TAIL AND ELEVATOR EFFECTIVENESS	153
9.1 Horizontal Tail Effectiveness	153
9.2 Effect of Horizontal Tail Leading Edge Flap	153
9.3 Elevator Effectiveness	154

Section		Page
X	LEADING EDGE DEVICES	167
	10.1 Effect of Leading Edge Kruegers	167
	10.2 Comparison of Leading Edge BLC With Leading Edge Kruegers	168
XI	NACELLE LOCATION VARIATION	
	11.1 Effects of Longitudinal and Vertical Engine Location Perturbation on Longitudinal Aerodynamic Parameters	177
	11.2 Effects of Engine Spanwise Perturbation	177
	11.3 Comparison of "Fixed" and "Swivel" Pylons	178
XII	FLAP CHARACTERISTICS	193
	12.1 Power-Off Lift Capability	193
	12.2 Static Turning Angles and Efficiencies	194
	12.3 Flap Gap Optimization for Double and Triple Slotted Flaps	194
	12.4 Powered Lift Capability	195
	12.5 Power Effects on Drag	196
	12.6 Power Effects on Pitching Moment	197
	12.7 Flap Deflection and Power Effects on Aerodynamic Center Location	198
	12.8 Effects of Flap Inlet Fairing on Longitudinal Aerodynamic Parameters	199
XIII	WING SPOILERS	287
	13.1 BLC Effects on Longitudinal Aerodynamic Parameters	287
	13.2 Effects on Longitudinal Aerodynamic Parameters When Used as Aerodynamic Braking Devices	287
XIV	ROLL CONTROL	303
	14.1 Roll Due to Failed Engine	303
	14.2 Effect of Tail on Rolling Moment	304
	14.3 Effect of Slotted Kruegers and Flap Van. Spoiler on Rolling Moment	304
	14.4 Roll Increment Due to Ailerons and Spoiler Deflection	305
	14.5 Rolling Moments Due to Blown Aileron	307
	14.6 Spoiler Effectiveness With Failed Engine	308

Section		Page
XV	DIRECTIONAL CONTROL	359
	15.1 Directional Stability - Flaps Up and Flaps Down	359
	15.2 Dorsal Optimization	359
	15.3 Yaw Characteristics With Engine Failure	360
	15.4 Rudder Effectiveness and Efficiency	361
XVI	CONCLUSIONS	399
	REFERENCES	401

LIST OF MODEL ILLUSTRATIONS

Number		Page
2.1	Three View, 0.07183 Scale STOL Transport Model	5
2.2	General View	7
2.3	Double Slotted Flap Detail	8
2.4	Triple Slotted Flap Detail	9
2.5	Triple Slotted Flap Upper Surface Details	10
2.6	Basic Configuration Up Deflected Nozzle with Type II Pylon	11
2.7	Basic Configuration Up Deflected Nozzle with Type I Pylon	12
2.8	Krueger Flap Detail	13
2.9	Tip Spoiler with Double Slotted Flap	14
2.10	Tip Spoiler with Aileron Using BLC	15
2.11	Tail Assembly with Large Dorsal	16
2.12	Downwash Rake with Smaller Dorsal	17
12.1	Wing Flap - Double Slotted Inboard Section	200
12.2	Wing Flap - Triple Slotted Inboard Section	201
14.1	Aileron-Outboard Wing Flap - Double Slotted - MST W.T. Model	309
14.2	Aileron-Outboard Wing Flap - Triple Slotted - MST W.T. Model	310
14.3	Trailing Edge Roll Control Devices	311
14.4	Leading Edge Roll Control Devices	312

LIST OF FIGURES

Figure	Page
4.1.1 Change in Lift Coefficient due to Change in Wing Sweep Angle ($\alpha = 0^\circ$)	77
4.1.2 Change in Lift Coefficient due to Change in Wing Sweep Angle ($\alpha = 8^\circ$)	78
4.1.3 Wing Sweep Angle Effects on Lift Coefficient at Constant Angle of Attack ($\alpha = 0^\circ$)	79
4.1.4 Wing Sweep Angle Effect on Lift Coefficient at Constant Angle of Attack ($\alpha = 8^\circ$)	80
4.2.1 Change in Total Drag Coefficient Due to Change in Wing Sweep Angle ($\alpha = 0^\circ$)	81
4.2.2 Change in Total Drag Coefficient due to Change in Wing Sweep Angle ($\alpha = 8^\circ$)	82
4.2.3 Wing Sweep Angle Effects on Total Drag Coefficient at Constant Angle of Attack ($\alpha = 0^\circ$)	83
4.2.4 Wing Sweep Angle Effects on Total Drag Coefficient at Constant Angle of Attack ($\alpha = 8^\circ$)	84
4.3.1 Change of Pitching Moment Coefficient due to Change in Wing Sweep Angle ($\alpha = 0^\circ$)	85
4.3.2 Change of Pitching Moment Coefficient due to Change in Wing Sweep Angle ($\alpha = 8^\circ$)	86
4.3.3 Wing Sweep Angle Effects on Pitching Moment Coefficient at Constant Angle of Attack ($\alpha = 0^\circ$)	87
4.3.4 Wing Sweep Angle Effects on Pitching Moment Coefficient at Constant Angle of Attack ($\alpha = 8^\circ$)	88
5.1.1 Effect of Aspect Ratio Change on Lift Coefficient	91
5.1.2 Total Powered Lift Coefficient for AR = 7 Wing	92
5.1.3 Total Powered Lift Coefficient for AR = 10 Wing	93
5.2.1 Effect of Aspect Ratio Change on Drag Coefficient	94
5.2.2 Total Powered Drag Coefficient for AR = 7 Wing	95
5.2.3 Total Powered Drag Coefficient for AR = 10 Wing	96
5.3.1 Effect of Aspect Ratio Change on Pitching Moment Coefficient	97
5.3.2 Total Powered Pitching Moment Coefficient for AR = 7 Wing	98
5.3.3 Total Powered Pitching Moment Coefficient for AR = 10 Wing	99
6.1.1 Effect of Flap and Nozzle Angles on Downwash Variation with Lift Change due to Power	104
6.1.2 Power Effects on Downwash Factor at Constant Angle of Attack	105
6.1.3 Effect of Spanwise Engine Location and Leading Edge Devices on Downwash Variation with Lift Change due to Power	106

Figure		Page
6.1.4	Power Effects on Downwash Factor at Constant Angle of Attack. .	107
6.1.5	Variation of Horiz. Tail Angle with Angle of Attack - Effects of Power (Short Chord Krueger).	108
6.1.6	Variation of Horiz. Tail Angle with Angle of Attack - Effects of Power (Long Chord Krueger) ,	109
6.1.7	Variation of Horiz. Tail Angle with Angle of Attack - Effects of Power (L.E. BLC)	110
6.1.8	Variation of Horiz. Tail Angle with Angle of Attack - Effect of Power (Spread Engines)	111
6.2.1	Effects of Flap and Engine Nozzle Deflection on Powered Horizontal Tail Angle	112
6.2.2	Horiz. Tail Angle vs Angle of Attack - $C_T = 0$	113
6.2.3	Spanwise Variation of Horizontal Tail Angle at $\alpha = +1.2^\circ$, $C_T = 0$	114
6.2.4	Horiz. Tail Angle vs Angle of Attack - $C_T = 1.0$	115
6.2.5	Spanwise Variation of Horizontal Tail Angle at $\alpha = +1.2^\circ$, $C_T = 1.0$	116
6.2.6	Horiz. Tail Angle vs Angle of Attack - $C_T = 2.0$	117
6.2.7	Spanwise Variation of Horizontal Tail Angle at $\alpha = +1.2^\circ$, $C_T = 2.0$	118
6.2.8	Horiz. Tail Angle vs Angle of Attack - $C_T = 3.0$	119
6.2.9	Spanwise Variation of Horizontal Tail Angle at $\alpha = +1.2^\circ$, $C_T = 3.0$	120
6.2.10	Horiz. Tail Angle vs Angle of Attack - $C_T = 3.3$	121
6.2.11	Spanwise Variation of Horizontal Tail Angle at $\alpha = +1.2^\circ$, $C_T = 3.3$	122
6.3.1	Effects of Various Leading Edge Devices on Powered Hori- zontal Tail Angle	123
6.3.2	Horiz. Tail Angle vs Angle of Attack - $C_T = 0$	124
6.3.3	Horiz. Tail Angle vs Angle of Attack - $C_T = 1.0$	125
6.3.4	Horiz. Tail Angle vs Angle of Attack - $C_T = 2.0$	126
6.3.5	Horiz. Tail Angle vs Angle of Attack - $C_T = 3.0$	127
6.3.6	Horiz. Tail Angle vs Angle of Attack - $C_T = 3.3$	128
6.4.1	Variation of Horiz. Tail Angle with Angle of Attack - Effect of Spanwise Engine Location, $C_T = 0$ and 1.0	129
6.4.2	Variation of Horiz. Tail Angle with Angle of Attack - Effect of Spanwise Engine Location, $C_T = 2.0$ and 3.0	130
6.4.3	Spanwise Variation of Horizontal Tail Angle at $\alpha_{FRL} = 0^\circ$	131

Figure		Page
6.4.4	Spanwise Variation of Horizontal Tail Angle at $\alpha_{FRL} = 0^\circ$ - Spread Engines	132
7.1.1	Reynolds Number Effect on Lift Coefficient	134
7.1.2	Effect of Reynolds Number on Drag Coefficient	135
7.1.3	Effects of Reynolds Number on Pitching Moment Coefficient	136
7.2.1	Effect of Reynolds Number on Dihedral Effect, $\alpha = 0^\circ$	137
7.2.2	Effect of Reynolds Number on Dihedral Effect, $\alpha = 12^\circ$	138
7.2.3	Effects of Reynolds Number on Yawing Moment Coefficient at Zero Alpha	139
7.2.4	Effects of Reynolds Number on Yawing Moment Coefficient at Alpha of 12 Degrees	141
7.3.1	Reynolds Number Effects on Horizontal Tail Angle, K_4	143
7.3.2	Reynolds Number Effects on Horizontal Tail Angle, K_{25}	144
8.1.1	Flap Span Effects on Lift Coefficient - $C_T = 0$	146
8.1.2	Flap Span Effects on Lift Coefficient - $C_T = 2.0$	147
8.1.3	Flap Span Effects on Drag Coefficient - $C_T = 0$	148
8.1.4	Flap Span Effects on Drag Coefficient - $C_T = 2.0$	149
8.1.5	Flap Span Effect on Pitching Moment Coefficient - $C_T = 0$	150
8.1.6	Flap Span Effect on Pitching Moment Coefficient - $C_T = 2.0$	151
9.1.1	Change in Horizontal Tail Pitching Moment Coefficient due to Engine Power Effects at $i_t = 0^\circ$	155
9.1.2	Change in Horizontal Tail Angle-of-Attack Static Stability due to Engine Power Effects at $i_t = 0^\circ$	156
9.1.3	Effects of Power on Horizontal Tail Pitching Moment Coefficient, $\delta_f = 25^\circ/50^\circ$	157
9.1.4	Effects of Power on Horizontal Tail Pitching Moment Coefficient, $\delta_f = 35^\circ/60^\circ$	158
9.2.1	Elevator Control Effectiveness	159
9.3.1	Effects of Elevator Deflection on Model Lift Coefficient for Varying Stabilizer Angles	160
9.3.2	Effects of Elevator Deflection on Model Drag Coefficient for Varying Stabilizer Angles	161
9.3.3	Effects of Elevator Deflection on Model Pitching Moment Coefficient for Varying Stabilizer Angles	162
9.3.4	Change in Total Model Lift Coefficient due to Elevator Deflection	163
9.3.5	Change in Total Model Drag Coefficient due to Elevator Deflection	164
9.3.6	Change in Total Model Pitching Moment Coefficient due to Elevator Deflection	165

Figure	Page
10.1.1 Effect of Inboard Krueger - $C_T = 0$	169
10.1.2 Effect of Wing Leading Edge Flaps (Kruegers) - $C_T = 0$. . .	170
10.1.3 Effect of Inboard Krueger - $C_T = 2.0$	171
10.1.4 Effect of Wing Leading Edge Flap (Kruegers) - $C_T = 2.0$. . .	172
10.1.5 Effect of Wing Leading Edge Flap (Kruegers) - $C_T = 2.0$. . .	173
10.2.1 Comparison of Outboard L.E. Devices	174
10.2.2 Effect of Power on Maximum Lift Coefficient for Various Outboard Leading Edge Devices	175
11.1.1 Change in Lift Coefficient due to a Rearward Shift in Engine Nacelle Location from the Basic Configuration . . .	179
11.1.2 Change in Drag Coefficient due to a Rearward Shift in Engine Nacelle Location from the Basic Configuration . . .	180
11.1.3 Change in Pitching Moment Coefficient due to a Rearward Shift in Engine Nacelle Location from the Basic Configuration	181
11.1.4 Change in Lift Coefficient due to a Vertical Shift in Engine Nacelle Location from the Basic Configuration . . .	182
11.1.5 Change in Drag Coefficient due to a Vertical Shift in Engine Nacelle Location from the Basic Configuration . . .	183
11.1.6 Change in Pitching Moment Coefficient due to a Vertical Shift in Engine Nacelle Location from the Basic Configuration	184
11.2.1 Effect of Engine Spanwise Location on Lift Coefficient due to Power	185
11.2.2 Effect of Engine Spanwise Location on Drag Coefficient due to Power	186
11.2.3 Effect of Engine Spanwise Location on Pitching Moment Coefficient due to Power	187
11.2.4 Effect of Engine Spanwise Location on Directional Stability Derivative	188
11.2.5 Effect of Engine Spanwise Location on Dihedral Effect Derivative	189
11.2.6 Effect of Engine Spanwise Location on Side Force Derivative	190
11.3.1 Effect of Pylon (Swivel vs Fixed) - $C_T = 0$	191
11.3.2 Effect of Pylon (Swivel vs Fixed) - $C_T = 2.0$	192
12.1.1 Power Off Longitudinal Characteristics Clean Wing	202
12.1.2 Power Off Lift Capability	203
12.1.3 Power Off Lift Capability - Double Slotted Flap	204

Figure		Page
12.1.4	Power Off Double and Triple Slotted Flap Lift Capability .	205
12.1.5	T.S. Flap Characteristics	206
12.1.6	Power Off Double and Triple Slotted Flap Lift Capability (Trimmed)	207
12.2.1	Summary of Turning Efficiency and Turning Angles	208
12.3.1	Flap Gap Optimization	209
12.3.2	Effects of Flap Gap Variation on Power Off Lift Coefficient	210
12.3.3	Effects of Flap Gap Variation on Powered Lift Coefficient.	211
12.3.4	Lift Coefficient Variation vs Spoiler Deflection Angle at $\alpha = 0^\circ$ and α at C_{Lmax}	212
12.3.5	Effects of Flap Gap Variation on Power Off Drag Coefficient	213
12.3.6	Effects of Flap Gap Variation on Powered Drag Coefficient.	214
12.3.7	Power Off Drag vs Percent Flap Gap Variation for Lines of Constant Lift	215
12.3.8	Powered Drag vs Percent Flap Gap Variation for Lines of Constant Lift	216
12.3.9	Effect of Flap Gap on Optimum Lift of Double Slotted Flaps at $\delta = 0^\circ$	217
12.3.10	Flap Gap Optimization	218
12.3.11	Effects of Flap Gap Variation on Power-Off Lift Coefficient	219
12.3.12	Effects of Flap Gap Variation on Powered Lift Coefficient.	221
12.3.13	Lift Coefficient Variation vs Spoiler Deflection Angle at $\alpha = 0^\circ$ and α at C_{Lmax}	222
12.3.14	Effects of Flap Gap Variation on Power-Off Drag Coefficient	223
12.3.15	Effects of Flap Gap Variation on Powered Drag Coefficient.	224
12.3.16	Power-Off Drag Coefficient vs Percent Flap Gap Variation for Lines of Constant Lift Coefficient	225
12.3.17	Powered Drag Coefficient vs Percent Flap Gap Variation for Lines of Constant Powered Lift Coefficient	226
12.3.18	Effect of Flap Gap on Optimum Lift of Triple Slotted Flaps at $\delta = 0^\circ$	227
12.4.1	Power Effects on Double Slotted Flap Lift Capability . . .	228
12.4.2	Effects of Flap Deflection on Powered Lift Coefficient . .	229
12.4.3	Effects of Flap Deflection on Powered Lift Coefficient . .	230
12.4.4	Effect of Power on Lift Coefficient - Double Slotted Flap.	231
12.4.5	Effect of Power on Lift Coefficient - Double Slotted Flap.	232
12.4.6	Double Slotted Flap Characteristics	233

Figure		Page
12.4.7	Effect of Power on Lift Coefficient - Double Slotted Flap.	235
12.4.8	Double Slotted Flap Characteristics.	237
12.4.9	Power Effects on Triple Slotted Flap Lift Capability . . .	239
12.4.10	Effects of Flap Deflection on Powered Lift Coefficient . .	240
12.4.11	Effects of Flap Direction Lift Control on Powered Lift Coefficient.	241
12.4.12	Effects of Flap Deflection on Powered Lift Coefficient . .	242
12.4.13	T.S. Flap Characteristics.	243
12.4.14	Triple Slotted Flap Characteristics.	245
12.4.15	Triple Slotted Flap Characteristics.	246
12.4.16	Triple Slotted Flap Characteristics.	247
12.5.1	Power Effects on Double Slotted Flap Drag Coefficient. . .	248
12.5.2	Effects of Flap Direct Drag Control on Powered Drag Coefficient.	249
12.5.3	Effects of Flap Direct Drag Control on Powered Drag Coefficient.	250
12.5.4	Effect of Flaps on Power off Drag Coefficient.	251
12.5.5	Double Slotted Flap Characteristics.	252
12.5.6	Effect of Power on Drag Coefficient.	253
12.5.7	Power Effects on Triple Slotted Flap Drag Coefficient. . .	254
12.5.8	Effects of Flap Direct Drag Control on Powered Drag Coefficient.	255
12.5.9	Effects of Flap Direct Drag Control on Powered Drag Coefficient.	256
12.5.10	Effects of Flap Direct Drag Control on Powered Drag Coefficient.	257
12.5.11	T.S. Flap Characteristics	258
12.5.12	Triple Slotted Flap Characteristics.	259
12.5.13	Triple Slotted Flap Characteristics.	261
12.5.14	Triple Slotted Flap Characteristics.	263
12.5.15	Variation of Inlet Momentum Drag Coefficient with Nozzle Thrust Coefficient	265
12.6.1	Power Effects on Double Slotted Flap Pitching Moment Coefficient.	266
12.6.2	Effects of Last Flap Segment Deflection on Powered Pitching Moment Coefficient	267
12.6.3	Effects of Last Flap Segment Deflection on Powered Pitching Moment Coefficient	268
12.6.4	Double Slotted Flap Lift and Pitching Moment Characteristics	269
12.6.5	Double vs Triple Slotted Flap Pitching Moment Comparison .	270

Figure	Page
12.6.6 Double Slotted Flap Lift and Pitching Moment Characteristics . .	271
12.6.7 Effect of Power on Pitching Moment Coefficient - Double Slotted Flap	272
12.6.8 Effect of Power on Pitching Moment Coefficient - Double Slotted Flap	273
12.6.9 Effect of Power on Pitching Moment Coefficient - Double Slotted Flaps	274
12.6.10 Power Effects on Triple Slotted Flap Pitching Moment Coefficient	275
12.6.11 Effects of Last Flap Segment Deflection on Powered Pitching Moment Coefficient	276
12.6.12 Effects of Last Flap Segment Deflection on Powered Pitching Moment Coefficient	277
12.6.13 Effects of Last Flap Segment Deflection on Powered Pitching Moment Coefficient	278
12.6.14 Triple Slotted Flap Characteristics	279
12.7.1 Flap Deflection Effect on Aerodynamic Center Location for Double and Triple Slotted Flap Configuration - $C_T = 0$	280
12.7.2 Flap Deflection Effect on Aerodynamic Center Location for Double and Triple Slotted Flap Configurations - $C_T = 2.0$	281
12.7.3 Flap Deflection Effect on Aerodynamic Center Location for Double and Triple Slotted Flap Configurations - $C_T = 3.28$	282
12.7.4 Engine Blowing Effect on Aerodynamic Center Location for Double and Triple Slotted Flap Configurations	283
12.8.1 Effect of Flap Entry Fairing - C_L	284
12.8.2 Effect of Flap Entry Fairing - C_D	285
12.8.3 Effect of Flap Entry Fairing - C_m	286
13.1.1 Effects of Wing Trailing Edge, Full Span Spoiler Deflection - Power off	289
13.1.2 Effects of Wing Trailing Edge, Full Span Spoiler Deflection - Powered	290
13.1.3 Effect of Partial Span Spoiler Deployment - $C_T = 2.0$	291
13.1.4 Effect of Partial Span Spoiler Deployment - $C_T = 3.28$	292
13.1.5 Effect of Partial Span Spoiler Deployment - $C_T = 2.0$	293
13.1.6 Effect of Partial Span Spoiler Deployment - $C_T = 3.28$	294
13.1.7 Deflected Spoiler Effects on Longitudinal Characteristics	295
13.1.8 Deflected Spoiler Effects on Longitudinal Characteristics	296
13.2.1 Effect of Raising Five Spoiler Panels to 50° , Right Wing Only . .	297

Figure		Page
13.2.2	Effect of Full Span Spoiler Deployment	298
13.2.3	Effect of Raising Five Spoiler Panels to 50°, Right Wing Only	299
13.2.4	Effect of Full Span Spoiler Deployment	300
13.2.5	Effect of Full Span Spoiler Deployment	301
14.1.1	Rolling Moment with Four Engine Thrust	313
14.1.2	Roll due to Outboard Engine Failure	314
14.1.3	Roll due to Outboard Engine Failure	315
14.1.4	Effect of Outboard Engine Failure on Lift	316
14.1.5	Inboard Versus Outboard Engine Failure Rolling Moment Comparison	317
14.1.6	Inboard Versus Outboard Engine Failure Rolling Moment Comparison	318
14.1.7	Rolling Moment with Four Engine Thrust	319
14.1.8	Roll due to Outboard Engine Failure	320
14.1.9	Roll due to Outboard Engine Failure	321
14.1.10	Roll due to Engine Failure Versus Powered Lift	322
14.1.11	Center of Pressure of Load due to Engine Failure	323
14.1.12	Center of Pressure of Load due to Engine Failure	324
14.2.1	Effect of Tail on Rolling Moment with Outboard Engine Inoperative	325
14.2.2	Effect of Tail on Rolling Moment with Outboard Engine Inoperative	326
14.3.1	Effect of Long Slotted Krueger on Roll with an Outboard Engine Failure	327
14.3.2	Effect of Vane Spoiler on Roll due to Main Spoilers	328
14.4.1	Roll Increment due to Aileron	329
14.4.2	Roll Increment due to Spoiler Panel #5 and Aileron	330
14.4.3	Roll Increments due to Outboard Spoiler (#5)	331
14.4.4	Roll Increment due to Spoiler Panels 3 - 14	332
14.4.5	Roll Increment due to Spoiler Panels #3 and 5 With/Without Aileron	333
14.4.6	Roll Increments due to Spoiler Panels 3, 4 and 5	334
14.4.7	Effect of Spoiler on Three Engine Lift	335
14.4.8	Roll Capability of the Tip Spoiler Plus Aileron When Used with #3 and #4 Spoiler Panels	336
14.4.9	Roll Increment due to Spoiler Panels 1 and 2	337
14.4.10	Roll Increment due to Spoiler Panels (#1 through #5)	338
14.4.11	Roll Increment due to Various Spoiler Panels	339

Figure		Page
14.4.12	Roll Increment due to Various Spoiler Panels	340
14.4.13	Roll Increment due to Various Spoiler Panels	341
14.4.14	Roll Increment due to Various Spoiler Panels	342
14.4.15	Roll due to Various Spoilers Versus Symmetric Lift	343
14.4.16	Roll due to Spoiler plus Aileron Versus Symmetric Lift	344
14.4.17	Roll due to Various Spoilers Versus Three Engine Lift	345
14.4.18	Effect of Angle of Attack on Spoiler C.P.	346
14.4.19	Effect of Blowing on Spoiler C.P.	347
14.4.20	Effect of Blowing on Spoiler C.P.	348
14.4.21	Rolling Moment due to Spoiler Panel #3→#5 with Ailerons Deflected	349
14.4.22	Rolling Moment Coefficient due to Spoiler and Aileron Deflection	350
14.5.1	Roll due to Blowing on Aileron (One Side) Four Engine Thrust	351
14.5.2	Roll due to Blowing on Aileron (One Side) Four Engine Thrust	352
14.5.3	Roll due to Blowing on Aileron (One Side) Four Engine Thrust	353
14.5.4	Roll due to Blowing on Aileron	354
14.5.5	Rolling Moment due to Blown Aileron	355
14.5.6	Aileron Thrust versus Gross Thrust Four Engine Operation	356
14.6.1	Spoiler Effectiveness with Outboard Engine Out	357
15.1.1	Power Effects on Flaps Down Directional Stability	362
15.1.2	Change in Flaps Down Directional Stability due to Power Effects	363
15.1.3	Power Effects on Flaps Down Dihedral Effect	364
15.1.4	Change in Flaps Down Dihedral Effect due to Power Effect	365
15.1.5	Power Effects on Flaps Down Side Force Derivative	366
15.1.6	Change in Flaps Down Side Force Derivative due to Power Effects	367
15.1.7	Directional Stability - Flaps Up	369
15.1.8	Directional Stability - Flaps Down	371
15.2.1	Dorsal Optimization and Directional Stability - Flaps Down	373
15.2.2	Dorsal Optimization	375
15.2.3	Dorsal Optimization	377
15.3.1	Yaw Characteristics with Engine Failure	379
15.3.2	Yaw Characteristics with Engine Failure	381
15.3.3	Directional Characteristics for Symmetric and Asymmetric Engine Operation	383

Figure		Page
15.3.4	Yaw Characteristics with Engine Failure	385
15.3.5	Yaw Characteristics with Engine Failure	387
15.3.6	Yaw Characteristics with Engine Failure	389
15.3.7	Directional Characteristics Critical (#1) Engine Out . . .	391
15.3.8	Directional Characteristics Critical (#1) Engine Out, Tail On	392
15.4.1	Yaw Characteristics with Deflected Rudder	393
15.4.2	Yaw Characteristics with Deflected Rudder	395
15.4.3	Control Capability of Vertical Tail with Deflected Rudder	397
15.4.4	Control Efficiency of Vertical Tail with Deflected Rudder	398

LIST OF SYMBOLS

A.E.O.	All engines operating
AR	Wing aspect ratio, b^2/S
b	Span, feet or inches
c	Local chord, feet or inches
\bar{c}	Mean aerodynamic chord, feet or inches
c.g.	Center of gravity, percent
C_D	Total drag coefficient, includes thrust and ram drag, D/qS
\bar{c}	Centerline
C_L	Total lift coefficient, L/qS
C_{LMAX}	Maximum total lift coefficient, L_{max}/qS
C_l	Rolling moment coefficient, \mathcal{L}/qSb
$C_{l\psi}$	Dihedral effect derivative, $\partial \mathcal{L} / \partial \psi \frac{1}{qSb}$, per degree
C_m	Total pitching moment coefficient, includes thrust and ram drag, $M/qS\bar{c}$
C_{D_R}	Ram drag coefficient, D_R/qS
C_n	Yawing moment coefficient, N/qSb
$C_{n\psi}$	Directional stability derivative, $\partial N / \partial \psi \frac{1}{qSb}$, per degree
c.p.	Center of pressure
C_T, C_{μ}	Total engine gross blowing coefficient, T_G/qS
$C_{y\psi}$	Side force derivative, $\partial Y / \partial \psi \frac{1}{qS}$, per degree
D	Total drag, pounds
E.O.	Engine out
F	Force, pounds

LIST OF SYMBOLS - Cont.

i_t, i_H	Incidence angle of horizontal tail, positive is leading edge up, degrees
L	Total lift, pounds
\mathcal{L}	Total rolling moment, foot-pounds
l	Tail arm, distance from $0.25\bar{c}$ to $0.25\bar{c}_H$ or V, feet or inches
M	Total pitching moment, foot-pounds
MAC	Mean aerodynamic chord, feet or inches
M.H.B.	Maximum half breadth
N	Total yawing moment, foot-pounds
N.O.P.	Normal engine operation
O.E.I.	One engine inoperative
q	Freestream dynamic pressure, pounds per square foot
S	Wing reference area, ft^2
T	Thrust, pounds
\bar{V}	Tail volume
x_a	Distance from center of gravity to aerodynamic center, positive direction is rearward, feet or inches
Y	Total side force, pounds
Y_{INBD}, Y_{OUTBD}	Spanwise engine locations, inches
α	Angle of attack, degrees
α_T	Angle of attack of horizontal tail, degrees
Δ	Change or increment
δ_a	Aileron deflection angle, degrees

LIST OF SYMBOLS - Cont.

δ_E, δ_e	Elevator deflection angle, positive is trailing edge down, degrees
δ_f	Flap deflection angle, positive is trailing edge down, degrees
δ_j	Jet plume deflection angle, degrees
δ_n, δ_{noz}	Engine nozzle deflection angle, positive with nozzle pointing up, degrees
δ_r	Rudder deflection angle, positive with trailing edge left, degrees
δ_{sp}	Spoiler deflection angle, positive with trailing edge up, degrees
γ	Flight path angle, degrees
ϵ	Downwash angle, degrees
η	Turning efficiency
Λ	Sweep angle of wing quarter chord, degrees
ψ	Wind tunnel yawing angle, positive is nose right, degrees

LIST OF SYMBOLS - Cont.

SUBSCRIPTS

a	Aileron
A	Axial
AR	Due to aspect ratio
AR=7.0	Due to aspect ratio equals seven
AR=10.0	Due to aspect ratio equals ten
Δb	Due to change in span
BLC	Boundary layer control
Corr.	Inflow angle and tunnel wall corrected
C_{μ}	Due to engine power
FRL	Fuselage reference line
G	Gross
H, Hor.	Horizontal tail
i_t	Due to incidence angle of horizontal tail
Λ	Lambda, sweep angle of wing quarter chord
le	Leading edge
N	Normal
O	Zero angle of attack
PE	Per engine
\mathcal{P}	Power off
Ψ	Due to tunnel yaw angle
s	Stability axis
$\overline{\mathcal{P}}$	Tail off

LIST OF SYMBOLS - Concluded

SUBSCRIPTS

V,V.T.	Vertical tail
1	Forward rudder segment
2	Aft rudder segment

Section I

INTRODUCTION

The data contained in this report represents a partial analysis of all the data obtained by wind tunnel testing of a 0.07183 scale STOL transport model in the Lockheed-Georgia Company's 16 by 23-foot low speed STOL wind tunnel. It is not the intent of this report to present a complete analysis of the tunnel data as a great amount of data was collected and any attempt at such an endeavor would take considerable time; only the predominant elements of each particular model geometry that was tested has been analyzed in order to accomplish the objectives set forth in the North American report NA-71-1121 (Wind Tunnel Test Plan for a Research Model of an Externally Blown Flap STOL Transport).

Included in this report is a three-view drawing showing the general arrangement of the basic configuration, a definition of areas and sizes of the model hardware that was tested including model dimensional data and a wind tunnel test run log summary. Throughout the report the symbols C_T and C_{μ} are used indiscriminately and in either case they mean total engine gross blowing coefficient with momentum drag not included. The drag coefficient (C_D) used herein is total drag with power effects and ram drag included unless otherwise noted. Tests were conducted at dynamic pressures of 0 psf, 16 psf and 100 psf corresponding to Reynolds numbers of 0 per foot, 0.74×10^6 per foot and 1.84×10^6 per foot respectively.

The compressed air for the engine simulators was supplied by the GELAC facility through the model rear mounting strut which was an air bearing strut and on into the model internal plenum chamber. The high pressure air was then directed from the plenum chamber through wing ducts to each engine pylon and then down through the pylons to the ejector nozzles. At each wing/pylon juncture an orifice adjusting valve (manually set) was utilized to balance the engine gross thrust output symmetrically.

The downwash probes used in the rake survey of the horizontal tail flow field environment measured inflow angles in the vertical plane and sidewash flows in the horizontal plane.

Pylons of two distinct cross-sectional shapes were tested. The "fixed" pylon which was used only with the 24-degree sweep wing and the "swivel" pylon which was tested on all three separate wing sweeps because as its name implies it can be swiveled streamwise on any of the three sweeps that were tested. Comparisons of these two pylons can be found in Section XI.

Two flap systems were tested, a double slotted and a triple slotted configuration. Both configurations were tested on the same wing and were immersed in the same high energy powered flow field. The wing used was the AR 7.0 wing with its quarter chord swept to 24 degrees. All detail flap testing was conducted tail-off and at a wind tunnel freestream dynamic pressure of 16 psf with the exception of the static turning angles which were tested at maximum engine thrust and $q_{\infty} = 0$ psf. The span for both flap systems was identical as well as the number and location of the flap bracket attach points.

The high energy flow field was generated by blowing high velocity exhaust gases from the four powered nacelles directly on the lower surfaces of the flaps.

Included in this report is the analysis of wing spoilers when used as DLC and roll control devices, various other roll control devices such as ailerons and asymmetric trailing edge blowing and combinations of various roll control devices and power and flap deflection effects on directional stability parameters.

Ground effects data was not obtained during this test due to a GELAC equipment failure which prevented NR from utilizing the moving ground plane.

The test itself ran for 509 hours during which 549 runs were completed for an overall run rate of 1.08 runs per hour. In general, five power settings were used during the test. At a tunnel freestream dynamic pressure of 16 psf, total engine gross thrust levels of 0 lbs., 165.4 lbs., 330.5 lbs., 496.0 lbs., and 543.0 lbs. were set yielding C_{μ} 's of 0, 1.0, 2.0, 3.0, and 3.28 respectively. The reasoning behind the maximum C_{μ} of 3.28 is that GELAC's air supply had reached its maximum flow capability at that point.

Each nacelle inlet and nozzle was instrumented with total and static pressure probes so that the engine simulator flow through characteristics would be determinable. From these the ram drag was prepared.

The AR 7 left hand wing was pressure instrumented at six chordwise wing stations, upper and lower surfaces, and at one spanwise chord element, also at upper and lower surfaces. This wing pressure data is presented in tabular form in Rockwell report NA-72-670, Appendix E, Volumes 7 through 12 inclusive.

All data presented in this report is in the stability axis system unless otherwise noted.

Section II

MODEL DIMENSIONS, NOMENCLATURE, AND PHOTOGRAPH

Illustration 1 of this section shows the relative location of various model components with respect to each other in the basic configuration. Butt planes for the alternate or "spread engine" location is also shown. The fuselage reference plane (FRP) is at water plane (W.P.) 0.000 and the fuselage nose is at fuselage station (F.S.) 0.000.

The MAC's of the wing, horizontal tail and vertical tail are also located in three dimensions. The moment reference center is taken about the wing MAC and is located vertically in the plane of the wing on the wing reference plane (WRP).

The model nomenclature defines all the model configuration symbols and model component geometry that is called out in the wind tunnel test run log summary.

A photograph of the model as a whole is presented in Illustration 2.2. Double slotted flap detail is shown in the photograph in Illustration 2.3, and similarly, triple slotted flap details are pictured in Illustrations 2.4 and 2.5. The standard upward deflection of the nacelle exhaust nozzle is photographed in Illustration 2.6. This illustration shows also the Type II (fixed) pylon, whereas Type I (swiveling) pylon is shown in Illustration 2.7. Krueger flap details are pictured in Illustration 2.8. Photographs of the tip spoiler with the double slotted flaps are given in Illustration 2.9, and with the single slotted flap for BLC in Illustration 2.10. Pictures of the horizontal tail and a large dorsal are presented in Illustration 2.11, and of the downwash rake and a smaller dorsal in Illustration 2.12.

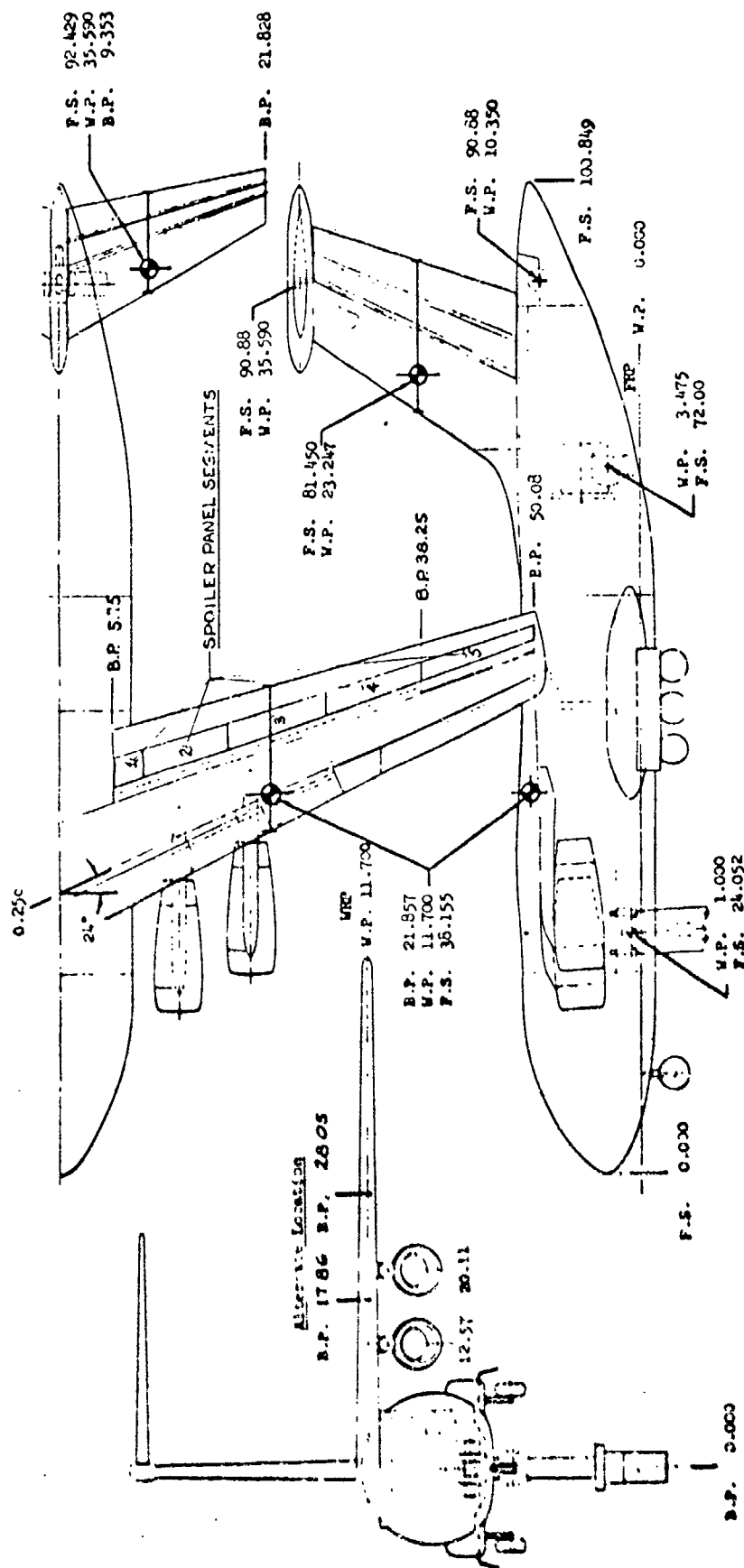
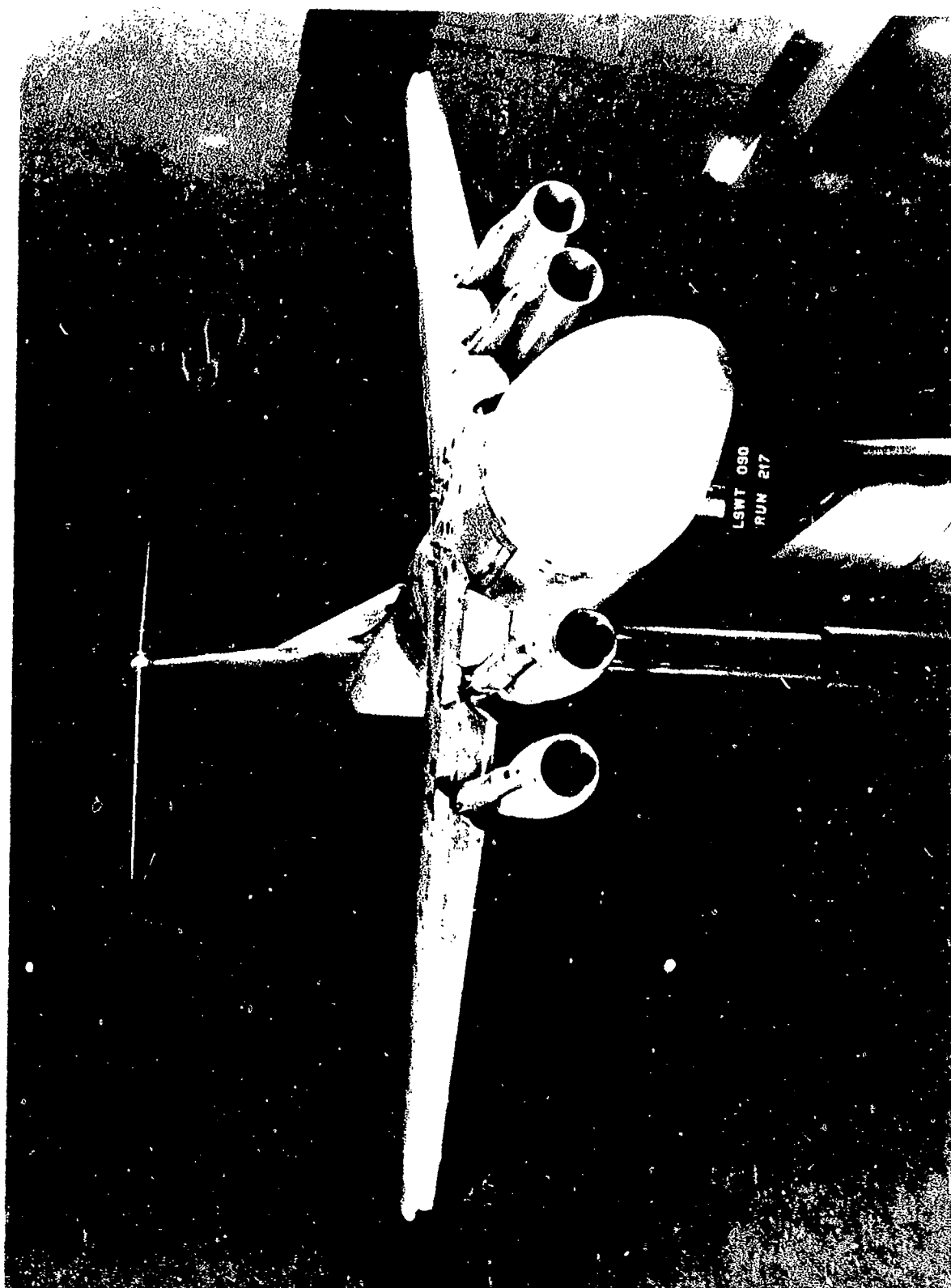


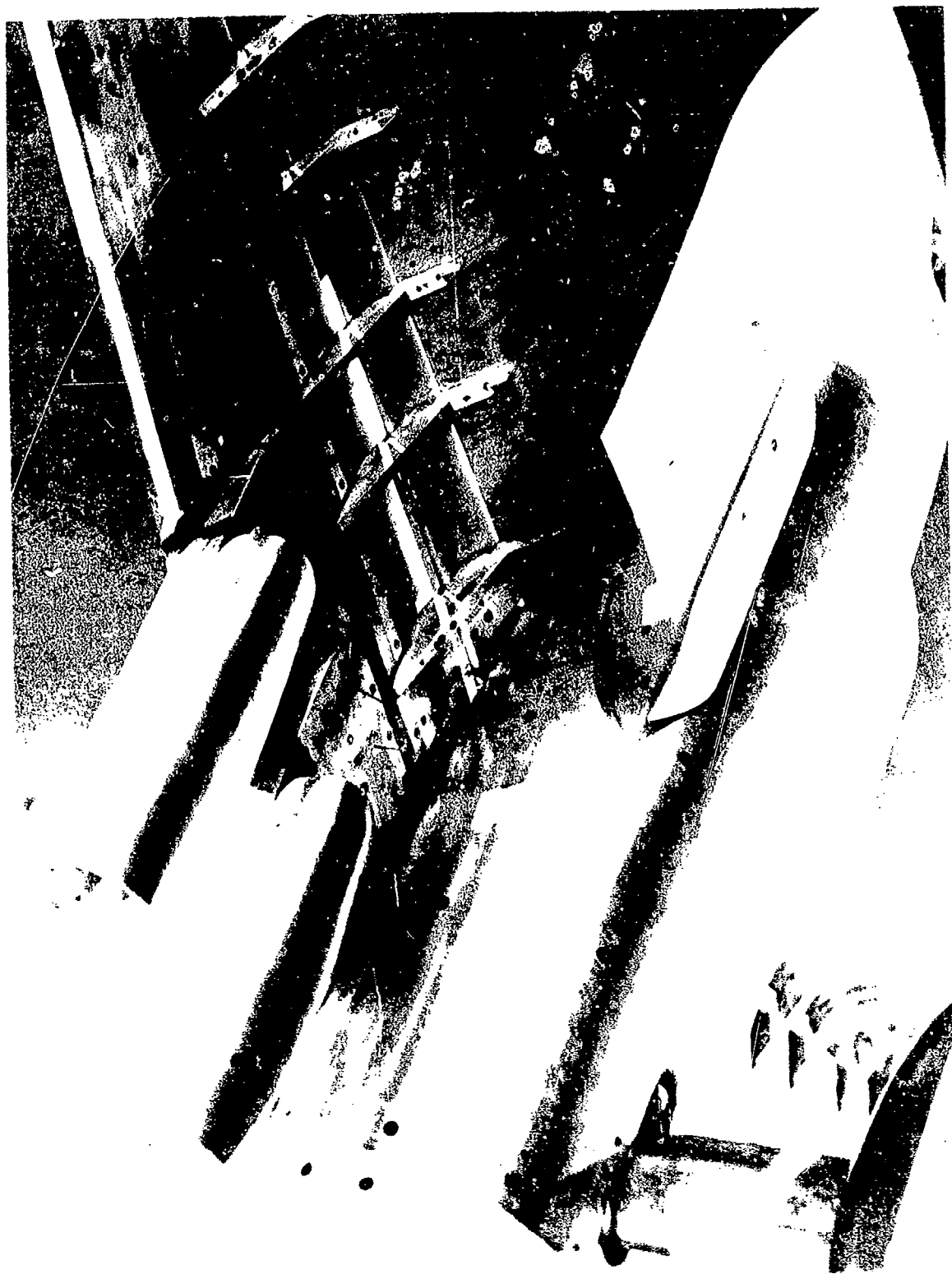
FIG 7, A = 24° Wing Shown

Free View, 0.07183-Size SIX Transport Model

5 ILLUSTRATION 2.1
(The reverse side of this page is blank)



Preceding page blank



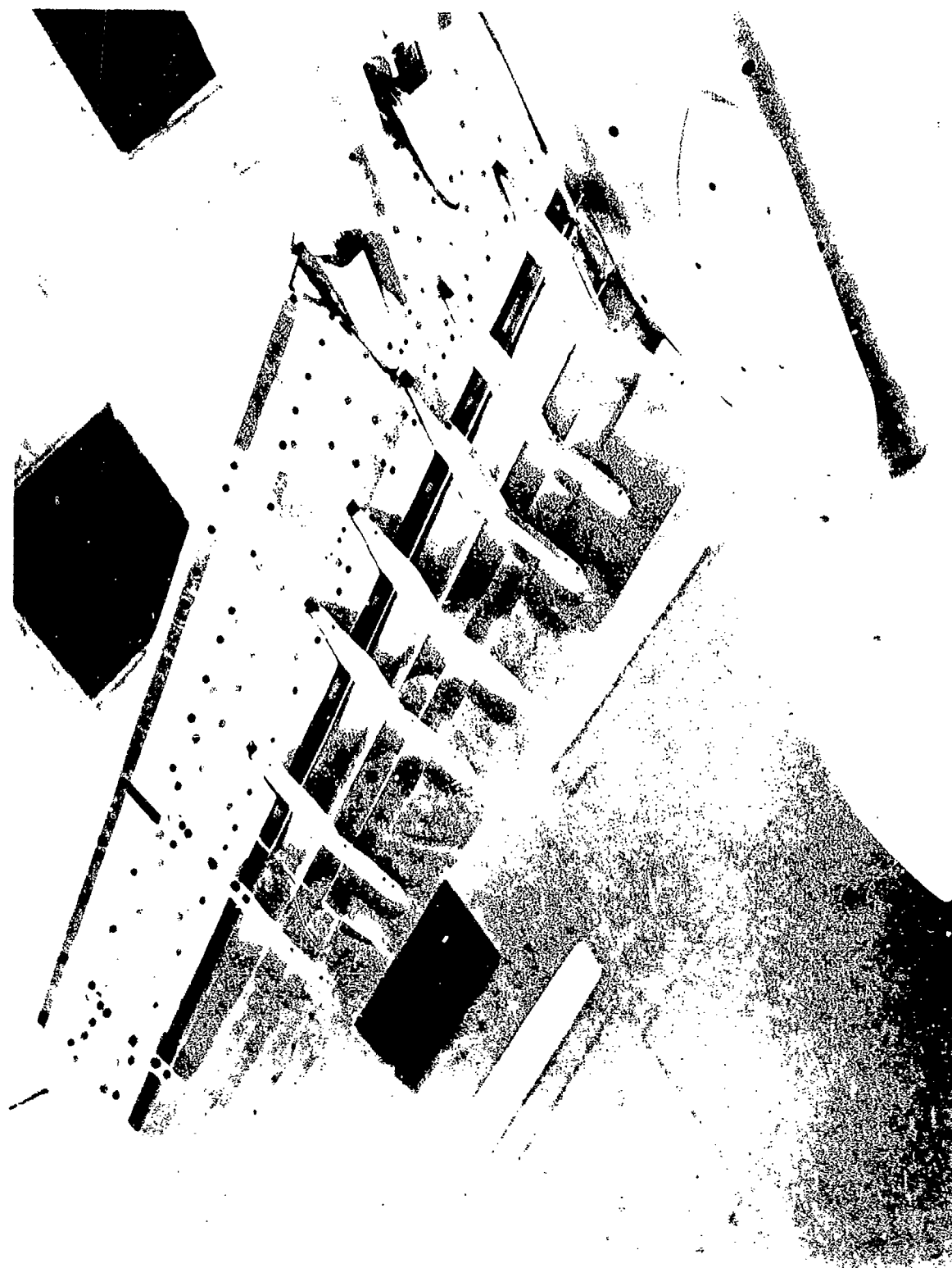


Illustration 2.1 Triple-dotted Lip Detail



Illustration 2.5 - Armle Slotted Flap Upper Surface Detail



Illustration of the Blade Configuration Up Deflected Position with
 Case II Pylon



Illustration 2.7 Basic Configuration Up Deflected Nozzle With Type 1 Pylon



SWT 090 - 453 - 100 - 100

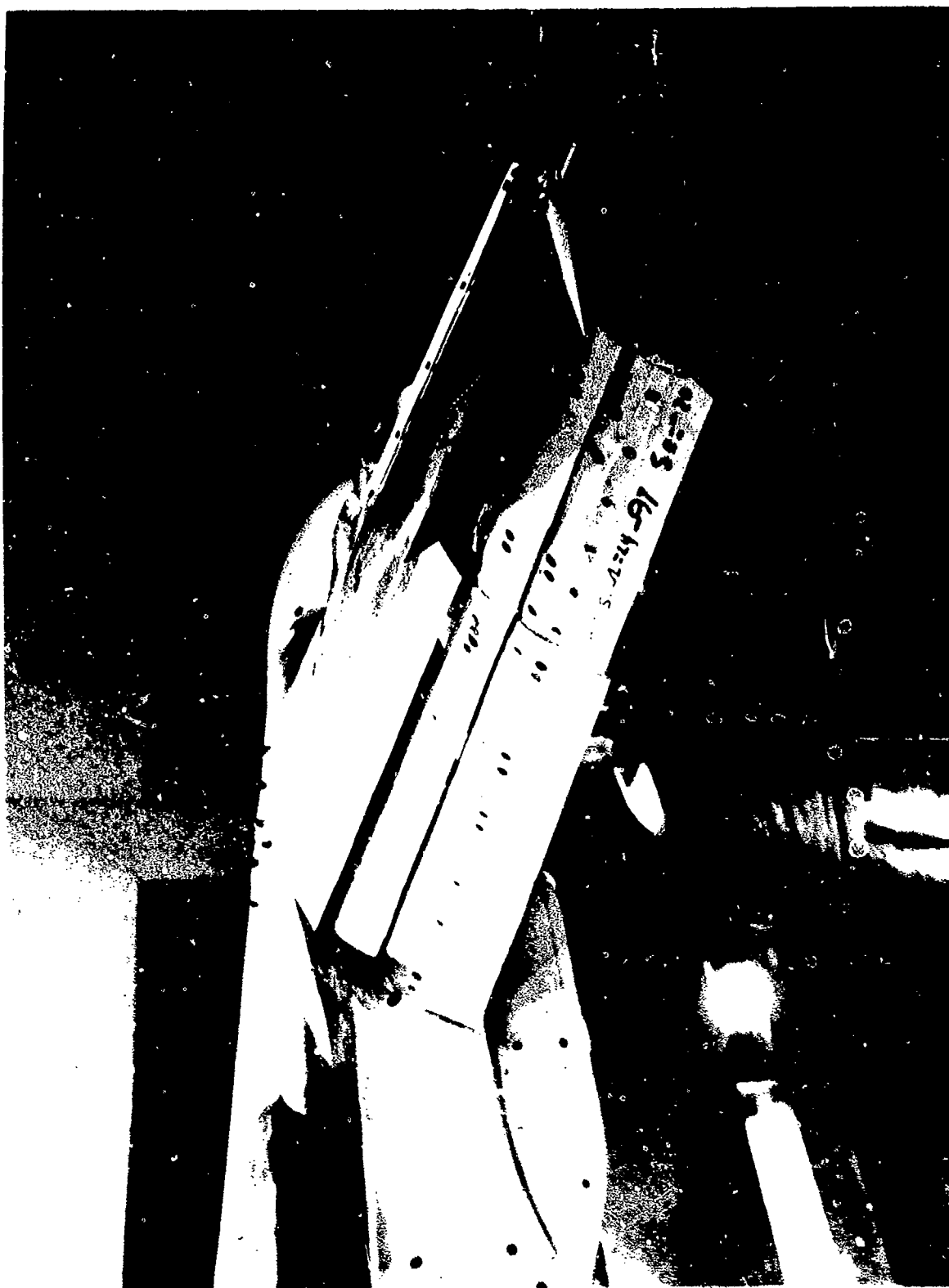


Illustration 2.9 Tip Spoiler with Double Slotted Flap



Illustration 2.10 Tip Spoiler with Airfoil Type BLF



Illustration 2.11 Tail Assembly with Large Dorsal

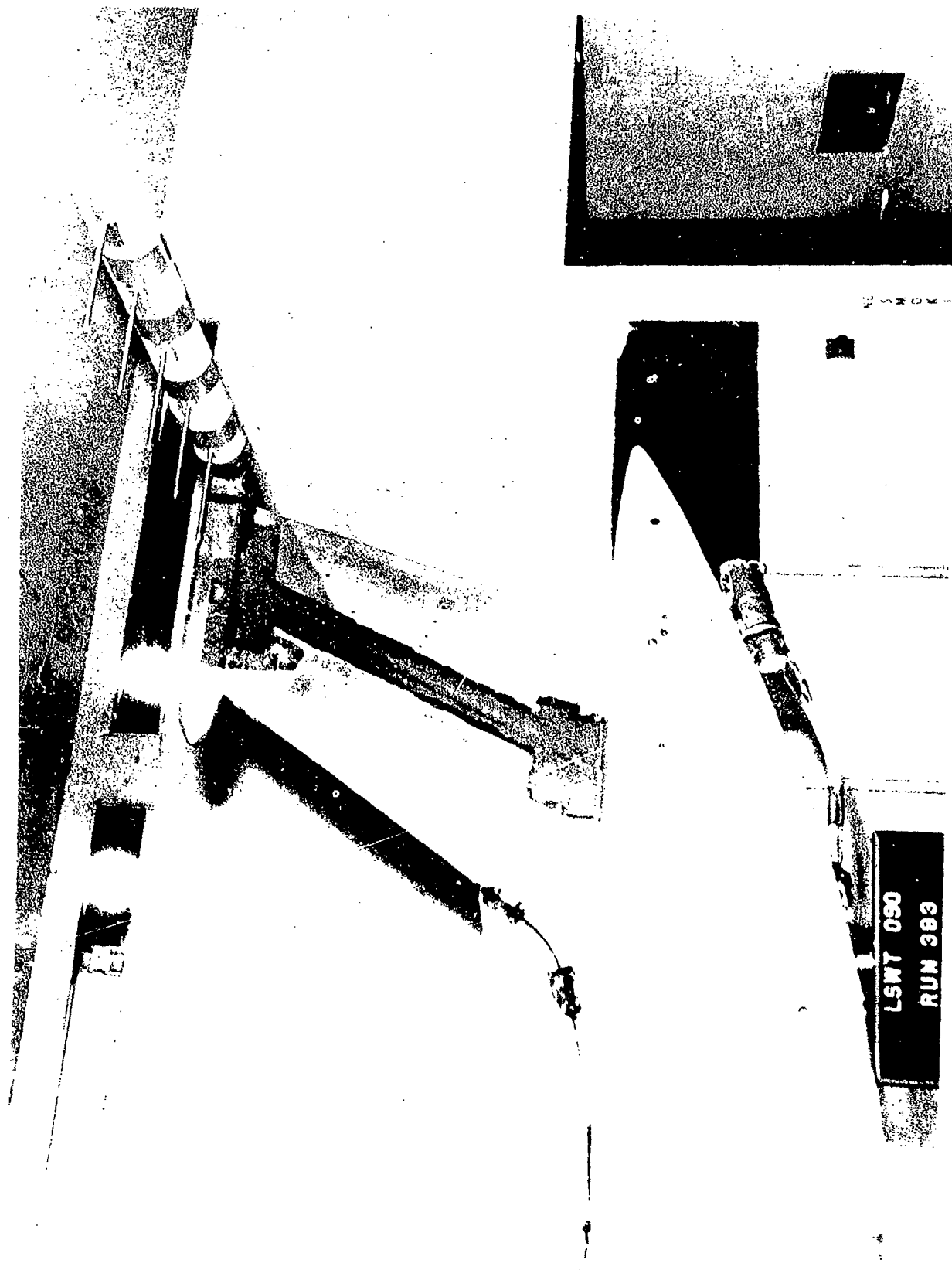


Illustration 2.12 Downwash Rake with Scatter Dorsal

MODEL DIMENSIONAL NOMENCLATURE

All dimensions are model scale unless otherwise noted.

BODY, B

Description: Fuselage simulating the D505-8 configuration. Includes landing gear pods, different wing/fuselage blocks for different wing sweeps and nose/windshield. Enclosed within the fuselage are the supply air duct, plenum chamber, splice plate, engine shut off valves and instrumentation bay.

Drawing No.: S-1002, -1025, -1041, -1042, -1043, -1054, -1055, -1056, -1057

Dimensions:

Length	100.849 in.
Maximum Depth	13.90 in.
Maximum Width	17.70 in.
Maximum X-Sectional Area	188.24 in. ²

WING, W

Description: Basic AR 7 wing spar attached to S-1015-1 splice plate on top of fuselage plenum. Wing sweep is controlled by hole pattern in splice plate. Contains internal air ducts for inboard engine, outboard engine, LE BLC and TE BLC.

Drawing No.: S-1004, -1015, -1027, -1028, -1032, -1044, -1048, -1051

Dimensions:

Area	10.321 ft ²
Span	102.00 in.
Root Chord (B.P. 0.00)	20.816 in.
Tip Chord (B.P. 51.00)	8.326 in.
MAC, \bar{c}_w (B.P. 21.857)	15.464 in.
Fus. Sta. of 0.25 \bar{c}_w	38.155 in.
Aspect Ratio	7.0
Taper Ratio	0.40
Sweep Angle (0.25 c_w)	24.0 deg.
Dihedral	0.0 deg.
Incidence	1.0 deg.
Airfoil	NASA 641A212.5

WING, W2

Description: Basic AR 10 wing spar attached to S-1016-1 splice plate. Contains internal air ducts for inboard engine, outboard engine, LE BLC and TE BLC.

Drawing No.: S-1005, -1016, -1027, -1028, -1032, -1045, -1049, -1052

Dimensions:

Area	10.321 ft ²
Span	121.91 in.
Root Chord (B.P. 0.00)	17.416 in.
Tip Chord (B.P. 60.957)	6.966 in.
MAC, \bar{c}_w (B.P. 26.124)	12.938 in.
Fus. Sta. of 0.25 \bar{c}_w	38.155 in.
Aspect Ratio	10.0
Taper Ratio	0.40
Sweep Angle (0.25 c_w)	24.0 deg.
Dihedral	0.0 deg.
Incidence	1.0 deg.
Airfoil	NASA 641212.5

WING, W4

Description: AR 7 wing spar used with the S-1015-4 splice plate.

Drawing No.: S-1004, -1015, -1027, -1028, -1032, -1044, -1048, -1051

Dimensions:

Area	10.445 ft ²
Span	109.43 in.
Root Chord (B.P. 0.00)	19.660 in.
Tip Chord (B.P. 54.716)	7.828 in.
MAC, \bar{c}_w (B.P. 23.432)	14.593 in.
Fus. Sta. of 0.25 \bar{c}_w	38.155 in.
Aspect Ratio	7.96
Taper Ratio	0.40
Sweep Angle (0.25 c_w)	(9°20') 9.33 deg.
Dihedral	0.0 deg.
Incidence	1.0 deg.

WING, W5

Description: AR 7 wing spar used with S-1015-2 splice plate.

Drawing No.: S-1004, -1015, -1027, -1028, -1032, -1044, -1048, -1051

Dimensions:

Area	9.964 ft ²
Span	97.52 in.
Root Chord (B.P. 0.00)	21.821 in.
Tip Chord (B.P. 48.762)	7.605 in.
MAC, \bar{c}_w (B.P. 20.454)	15.857 in.
Fus. Sta. of 0.25 \bar{c}_w	38.155 in.
Aspect Ratio	6.63
Taper Ratio	0.35
Sweep Angle (0.25 c_w)	30.0 deg.
Dihedral	0.0 deg.
Incidence	1.0 deg.

PYLON, *p

Description: Type II pylons (fixed) in basic position, used with wing (W) only. Smooth fairing with wax and tuff-fill into wing LE. Pylon extends to LE of each nacelle, P.S. 0.00 equals N.S. 0.34. Contains duct to supply air to ejector simulators. Duct length is measured from engine plenum face to wing spar face.

Drawing No.: S-1018, -1019, -1020, -1022

Dimensions:

Air Duct Area	0.985 in. ²
Duct Length, Inboard	12.16 in.
Duct Length, Outboard	11.73 in.
Inboard Pylon B.P.	12.57 in.
Outboard Pylon B.P.	20.11 in.

PYLON, *P2

Description: Type II pylons (fixed) shortened to move nacelles aft 2.38 inches, used with wing (W) only. Other descriptions are the same as (*P).

Drawing No.: S-1018, -1019, -1020, -1022

Dimensions:

Air Duct Area	0.985 in. ²
Duct Length, Inboard	9.82 in.
Duct Length, Outboard	9.40 in.
Inboard Pylon B.P.	12.57 in.
Outboard Pylon B.P.	20.11 in.

PYLON, *P3

Description: Type II pylons (fixed) vertically displaced upward to move nacelles 1.47 inches, used with wing (W) only. Other descriptions are the same as (*P).

Drawing No.: S-1018, -1019, -1020, -1022

PYLON, *P3 - Continued

Dimensions:

Air Duct Area	0.985 in. ²
Duct Length, Inboard	11.68 in.
Duct Length, Outboard	11.31 in.
Inboard Pylon B.P.	12.57 in.
Outboard Pylon B.P.	20.11 in.

PYLON, *P4

Description: Type I pylons (swivel) in basic spanwise location, used with wing (W) only. Other descriptions are the same as (*P).

Drawing No.: S-1017, -1018, -1022

Dimensions:

Air Duct Area	0.985 in. ²
Duct Length (Inboard and Outboard)	13.73 in.
Inboard Pylon B.P.	12.57 in.
Outboard Pylon B.P.	20.11 in.

PYLON, *P5

Description: Type I pylons (swivel) in alternate spanwise location, used with wing (W) only. Other descriptions are the same as (*P).

Drawing No.: S-1017, -1018, -1022

Dimensions:

Air Duct Area	0.985 in. ²
Duct Length (Inboard and Outboard)	13.73 in.
Inboard Pylon B.P.	17.86 in.
Outboard Pylon B.P.	28.05 in.

PYLON, *P8

Description: Type I pylons (swivel) in basic spanwise location, used with wing (W4) only. Other descriptions are the same as (*P).

Drawing No.: S-1017, -1018, -1022

PYLON, *P8 - Continued

Dimensions:

Air Duct Area	0.985 in. ²
Duct Length (Inboard and Outboard)	13.73 in.
Inboard Pylon B.P.	12.57 in.
Outboard Pylon B.P.	20.80 in.

PYLON, *P10

Description: Type I pylons (swivel) in basic spanwise location, used with wing (W5) only. Other descriptions are the same as (*P).

Drawing No.: S-1017, -1018, -1022

Dimensions:

Air Duct Area	0.985 in. ²
Duct Length (Inboard and Outboard)	13.73 in.
Inboard Pylon B.P.	12.57 in.
Outboard Pylon B.P.	19.68 in.

PYLON, *P12

Description: Type I pylons (swivel) in basic spanwise location, used with wing (W2) only. Other descriptions are the same as (*P).

Drawing No.: S-1017, -1018, -1022

Dimensions:

Air Duct Area	0.985 in. ²
Duct Length (Inboard and Outboard)	13.73 in.
Inboard Pylon B.P.	12.57 in.
Outboard Pylon B.P.	20.11 in.

NACELLE, N

Description: Nacelles used with Type I and Type II pylons, two left hand and two right hand. Flow through type nacelles each enclosing a TD-530 ejector engine simulator plus inlet instrumentation. Includes a basic cowl or bellmouth for calibrations plus a variable nozzle exit deflector (Px). Nacelle centerline is three degrees nose down from FRP. In the basic pylon position the aft end on the nacelle (with nozzle at 0°) is at the same F.S. as the wing LE.

Drawing No.: S-1022

Dimensions:

Inlet Throat Area	8.314 in. ²
Nozzle Exit Area	7.895 in. ²
Length	13.383 in.
Incidence of Nacelle Centerline	-3.00 deg.

NOZZLE, P

Description: Deflectable nozzle exit used with nacelle (N) and both types of pylons. Positive deflection is up and is considered the basic condition.

Drawing No.: S-1022

Dimensions:

Incidence	+15.0 deg.
Hingeline N.S.	12.30 in.

NOZZLE, P2

Description: Same as nozzle (P) except for deflection.

Drawing No.: S-1022

Dimensions:

Incidence	0.0 deg.
-----------	----------

NOZZLE, P3

Description: Same as nozzle (P) exception for deflection.

Drawing No.: S-1022

Dimensions:

Incidence	-15.0 deg.
-----------	------------

KRUEGER FLAP, K1

Description: Inboard krueger flap used with wing (W) and basic spanwise pylon configuration (*P). Located between fuselage and inboard pylon/nacelle, 20% of local chord. Outboard edge is flush with pylon. Dimensional data are per side and do not take into account any wax fairings.

Drawing No.: S-1051

Dimensions:

Area	0.1357 ft. ²
Span (equivalent)	5.26 in.
Inboard Chord (B.P. 6.51)	3.844 in.
Outboard Chord (B.P. 11.77)	3.587 in.
Deflection	120.0 deg.

KRUEGER FLAP, K2

Description: Mid-inboard krueger flap used with wing (W) and basic spanwise pylon configuration (*P). Located between inboard pylon and outboard pylon, 20% of local chord. Outboard edge is flush with pylon. Dimensional data are per side and do not take into account any wax fairings.

Drawing No.: S-1051

Dimensions:

Area	0.1217 ft. ²
Span (equivalent)	5.24 in.
Inboard Chord (B.P. 14.12)	3.472 in.
Outboard Chord (B.P. 19.36)	3.215 in.
Deflection	120.0 deg.

KRUEGER FLAP, K3

Description: Mid-outboard krueger flap used with wing (W) and basic spanwise pylon configuration (*P). Located between outboard pylon and B.P. 34.00, 20% of local chord. Dimensional data are per side and do not take into account any wax fairings.

Drawing No.: S-1051

KRUEGER FLAP, K3 - Continued

Dimensions:

Area	0.2417 ft. ²
Span (equivalent)	12.42 in.
Inboard Chord (B.P. 21.58)	3.106 in.
Outboard Chord (B.P. 34.00)	2.498 in.
Deflection	120.0 deg.

KRUEGER FLAP, K4

Description: Outboard krueger flap used with wing (W) and located between B.P. 34.00 and the wing tip, 20% of local chord. Dimensional data are per side.

Drawing No.: S-1051

Dimensions:

Area	0.2350 ft. ²
Span (equivalent)	16.08 in.
Inboard Chord (B.P. 34.00)	2.498 in.
Outboard Chord (B.P. 50.08)	1.710 in.
Deflection	120.0 deg.

KRUEGER FLAP, K5

Description: Mid-inboard krueger flap used with wing (W) and alternate spanwise pylon configuration (*P5). Located between inboard and outboard pylons, 20% of local chord. Dimensional data are per side and do not take into account any wax fairings.

Drawing No.: S-1051

Dimensions:

Area	0.1668 ft. ²
Span (equivalent)	7.95 in.
Inboard Chord (B.P. 19.35)	3.215 in.
Outboard Chord (B.P. 27.30)	2.826 in.
Deflection	120.0 deg.

KRUEGER FLAP, K6

Description: Mid-outboard krueger flap used with wing (W) and alternate spanwise pylon configuration (*P5). Located between outboard pylon and B.P. 34.00, 20% of local chord. Dimensional data are per side and do not take into account any wax fairings.

Drawing No.: S-1051

Dimensions:

Area	0.0836 ft. ²
Span (equivalent)	4.61 in.
Inboard Chord (B.P. 29.39)	2.724 in.
Outboard Chord (B.P. 34.00)	2.498 in.
Deflection	120.0 deg.

KRUEGER FLAP, K10

Description: Mid-inboard krueger flap used with wing (W4) and basic spanwise pylon configuration (*P8). Located between inboard and outboard pylons, 20% of local chord. Dimensional data are per side and do not take into account any wax fairings.

Drawing No.: S-1051

Dimensions:

Area	0.1423 ft. ²
Span (equivalent)	6.40 in.
Inboard Chord (B.P. 13.70)	3.340 in.
Outboard Chord (B.P. 20.10)	3.063 in.
Deflection	120.0 deg.

KRUEGER FLAP, K11

Description: Mid-outboard krueger flap used with wing (W4) and basic spanwise pylon configuration (*P8). Located between outboard pylon and B.P. 35.25, 20% of local chord. Dimensional data are per side and do not take into account any wax fairings.

Drawing No.: S-1051

KRUEGER FLAP, K11 - Continued

Dimensions:

Area	0.2490 ft. ²
Span (equivalent)	13.30 in.
Inboard Chord (B.P. 21.95)	2.983 in.
Outboard Chord (B.P. 35.25)	2.408 in.
Deflection	120.0 deg.

KRUEGER FLAP, K12

Description: Outboard krueger flap used with wing (W4), located between B.P. 35.25 and wing tip, 20% of local chord. Dimensional data are per side.

Drawing No.: S-1051

Dimensions:

Area	0.2370 ft. ²
Span (equivalent)	16.67 in.
Inboard Chord (B.P. 35.25)	2.408 in.
Outboard Chord (B.P. 51.92)	1.687 in.
Deflection	120.0 deg.

KRUEGER FLAP, K13

Description: Mid-inboard krueger flap used with wing (W5) and basic span-wise pylon configuration (*P10). Located between inboard and outboard pylons, 20% of local chord. Dimensional data are per side and do not take into account any wax fairings.

Drawing No.: S-1051

Dimensions:

Area	0.1208 ft. ²
Span (equivalent)	5.10 in.
Inboard Chord (B.P. 13.83)	3.558 in.
Outboard Chord (B.P. 18.93)	3.261 in.
Deflection	120.0 deg.

KRUEGER FLAP, K14

Description: Mid-outboard krueger flap used with wing (W5) and basic span-wise pylon configuration (*PI0). Located between outboard pylon and B.P. 33.27, 20% of local chord. Dimensional data are per side and do not take into account any wax fairings.

Drawing No.: S-1051

Dimensions:

Area	0.2319 ft. ²
Span (equivalent)	12.03 in.
Inboard Chord (B.P. 21.24)	3.126 in.
Outboard Chord (B.P. 33.27)	2.425 in.
Deflection	120.0 deg.

KRUEGER FLAP, K15

Description: Outboard krueger flap used with wing (W5). Located between B.P. 33.27 and wing tip, 20% of local chord. Dimensional data are per side.

Drawing No.: S-1051

Dimensions:

Area	0.2149 ft. ²
Span (equivalent)	15.74 in.
Inboard Chord (B.P. 33.27)	2.425 in.
Outboard Chord (B.P. 49.01)	1.507 in.
Deflection	120.0 deg.

KRUEGER FLAP, K17

Description: Mid-inboard krueger flap used with wing (W2) and basic span-wise pylon configuration (*PI2). Located between inboard and outboard pylons, 20% of local chord. Dimensional data are per side and do not take into account any wax fairings.

Drawing No.: S-1052

KRUEGER FLAP, K17 - Continued

Dimensions:

Area	0.1048 ft. ²
Span (equivalent)	5.19 in.
Inboard Chord (B.P. 14.17)	2.997 in.
Outboard Chord (B.P. 19.35)	2.820 in.
Deflection	120.0 deg.

KRUEGER FLAP, K18

Description: Mid-outboard krueger flap used with wing (W2) and basic span-wise pylon configuration (*PI2). Located between outboard pylon and B.P. 40.84, 20% of local chord. Dimensional data are per side and do not take into account any wax fairings.

Drawing No.: S-1052

Dimensions:

Area	0.3226 ft. ²
Span (equivalent)	19.25 in.
Inboard Chord (B.P. 21.59)	2.743 in.
Outboard Chord (B.P. 40.84)	2.083 in.
Deflection	120.0 deg.

KRUEGER FLAP, K19

Description: Outboard krueger flap used with wing (W2). Located between B.P. 40.84 and wing tip, 20% of local chord. Dimensional data are per side.

Drawing No.: S-1052

Dimensions:

Area	0.2358 ft. ²
Span (equivalent)	19.40 in.
Inboard Chord (B.P. 40.84)	2.083 in.
Outboard Chord (B.P. 60.24)	1.418 in.
Deflection	120.0 deg.

KRUEGER FLAP, K25

Description: Outboard krueger flap (long chord) used with wing (W). Located between B.P. 34.00 and wing tip, 30% of local chord. Dimensional data are per side.

Drawing No.: S-1051

Dimensions:

Area	0.3524 ft. ²
Span (equivalent)	16.08 in.
Inboard Chord (B.P. 34.00)	3.747 in.
Outboard Chord (B.P. 50.08)	2.565 in.
Deflection	135.0 deg.

KRUEGER FLAP, K26

Description: Outboard slotted krueger flap (long chord) used with wing (W). Located between B.P. 34.00 and wing tip, 30% of local chord. Dimensional data are per side.

Drawing No.: S-1053

Dimensions:

Area	0.3294 ft. ²
Span (equivalent)	16.08 in.
Inboard Chord (B.P. 34.00)	3.50 in.
Outboard Chord (B.P. 50.08)	2.40 in.
Deflection	135.0 deg.
Slot Gap	1.5%

KRUEGER FLAP, K28

Description: Asymmetrical krueger flap used with wing (W). Consists of (K26) krueger on left wing panel and (K25) krueger on right hand wing.

Drawing No.: S-1051, -1053

Dimensions:

Same as for K25 and K26.

FLAP, F

Description: Double-slotted trailing edge flap used with wing (W) and flap (F7). Located between fuselage and B.P. 38.25. Different flap deflections require different flap to fuselage end pieces which add to or subtract from the basic flap dimensions ($\delta_V = 25^\circ$, $\delta_F = 50^\circ$). Also includes flap entry fairing. Dimensions are per side.

Drawing No.: S-1029, -1044

Dimensions:

Vane

Area	0.5978 ft. ²
Span (Equivalent)	32.30 in.
Inboard Chord (B.P. 5.95)	3.349 in.
Outboard Chord (B.P. 38.25)	1.981 in.
Deflection	25.0 deg.

Flap

Area	0.9921 ft. ²
Span (Equivalent)	31.19 in.
Inboard Chord (B.P. 7.06)	5.726 in.
Outboard Chord (B.P. 38.25)	3.435 in.
Deflection	50.0 deg.

Flap Entry Fairing

Area	0.3969 ft. ²
Span	32.50 in.
Inboard Chord (B.P. 5.75)	2.212 in.
Outboard Chord (B.P. 38.25)	1.305 in.

VANE			FLAP		
δ_V	GAP	O.H.	δ_F	GAP	O.H.
25	3.5	2.5	30	2.0	3.7
			50		
	2.5		70		
	4.5		50		
35	3.5		50		
			40		
			60		
			80		

Gaps and overhangs (O.H.) are in $\frac{1}{8}$ of wing chord.

Vane gap is the distance between the T.E. of the -10 degree spoiler and the vane upper surface.

Flap gap is the distance between the T.E. of the vane and the flap upper surface.

FLAP, F2

Description: Double-slotted trailing edge flap used with wing (W2) and flap (F8). Located between fuselage and B.P. 48.41. Does not include a flap entry fairing. Only the basic deflections were tested ($\delta_v = 25^\circ$, $\delta_f = 50^\circ$). Dimensions are per side.

Drawing No.: S-1029, -1045

Dimensions:

Vane

Area	0.6547 ft. ²
Span (Equivalent)	42.66 in.
Inboard Chord (B.P. 5.75)	2.842 in.
Outboard Chord (B.P. 48.41)	1.578 in.
Gap (% C_w)	3.5%
Overhang (% C_w)	2.5%
Deflection	25.0 deg.

Flap

Area	1.0936 ft. ²
Span (Equivalent)	41.43 in.
Inboard Chord (B.P. 6.98)	4.866 in.
Outboard Chord (B.P. 48.41)	2.736 in.
Gap (% C_w)	2.0%
Overhang (% C_w)	3.7%
Deflection	50.0 deg.

FLAP, F4

Description: Double-slotted trailing edge flap used with wing (W4) and flap (F10). Located between fuselage and B.P. 37.0. Includes a flap entry fairing, same as flap (F) except for bracket cut-outs. Dimensions are based on wing (W) B.P.'s and are per side.

Drawing No.: S-1029, -1046

Dimensions:

Vane

Area	0.6435 ft. ²
Span (Equivalent)	33.85 in.
Inboard Chord (B.P. 3.46)	3.455 in.
Outboard Chord (B.P. 37.31)	2.020 in.
Gap (% C_w)	3.5%
Overhang (% C_w)	2.5%

FLAP, F4 - Continued

Vane - Continued

Deflection

25.0 deg.

Flap

Area

1.0746 ft.²

Span (Equivalent)

32.65 in.

Inboard Chord (B.P. 4.16)

5.939 in.

Outboard Chord (B.P. 36.81)

3.540 in.

Gap (% C_w)

2.0%

Overhang (% C_w)

3.7%

Deflection

50.0 deg.

FLAP, F5

Description: Double-slotted trailing edge flap used with wing (W5) and flap (F11). Located between fuselage and B.P. 38.25. Includes a flap entry fairing, same as flap (F) except for bracket cutouts. Dimensions are based on wing (W) B.P.'s and are per side.

Drawing No.: S-1029, -1046

Dimensions:

Vane

Area

0.5786 ft.²

Span (Equivalent)

31.47 in.

Inboard Chord (B.P. 6.78)

3.314 in.

Outboard Chord (B.P. 38.25)

1.981 in.

Gap (% C_w)

3.5%

Overhang (% C_w)

2.5%

Deflection

25.0 deg.

Flap

Area

0.9385 ft.²

Span (Equivalent)

29.83 in.

Inboard Chord (B.P. 8.42)

5.626 in.

Outboard Chord (B.P. 38.25)

3.435 in.

Gap (% C_w)

2.0%

Overhang (% C_w)

3.7%

Deflection

50.0 deg.

FLAP, F7

Description: Double-slotted trailing edge flap used with wing (W), flap (F) and aileron (A). Located between B.P. 38.25 and wing tip. Includes a flap entry fairing. Dimensions are per side.

Drawing No.: S-1030, -1048

Dimensions:

Vane	
Area	0.1356 ft. ²
Span	11.83 in.
Inboard Chord (B.P. 38.25)	1.990 in.
Outboard Chord (B.P. 50.08)	1.312 in.
Gap (% C _w)	3.5%
Overhang (% C _w)	3.12%
Deflection	25.0 deg.
Flap	
Area	0.2464 ft. ²
Span	11.83 in.
Inboard Chord (B.P. 38.25)	3.435 in.
Outboard Chord (B.P. 50.08)	2.565 in.
Gap (% C _w)	2.0%
Overhang (% C _w)	3.65%
Deflection	50.0 deg.
Flap Entry Fairing	
Area	0.0938 ft. ²
Span	11.83 in.
Inboard Chord (B.P. 38.25)	1.307 in.
Outboard Chord (B.P. 50.08)	0.976 in.

FLAP, F8

Description: Double-slotted trailing edge flap used with wing (W2) and flap (F2). Located between B.P. 48.41 and wing tip. Includes a flap entry fairing. Dimensions are per side.

Drawing No.: S-1030, -1049

FLAP, F8 - Continued

Dimensions:

Vane

Area	0.1157 ft. ²
Span	11.83 in.
Inboard Chord (B.P. 48.41)	1.585 in.
Outboard Chord (B.P. 60.24)	1.232 in.
Gap (% C _w)	3.5%
Overhang (% C _w)	3.12%
Deflection	25.0 deg.

Flap

Area	0.1998 ft. ²
Span	11.83 in.
Inboard Chord (B.P. 48.41)	2.736 in.
Outboard Chord (B.P. 60.24)	2.127 in.
Gap (% C _w)	2.0%
Overhang (% C _w)	3.65%
Deflection	50.0 deg.

Flap Entry Fairing

Area	0.0561 ft. ²
Span	11.83 in.
Inboard Chord (B.P. 48.41)	0.768 in.
Outboard Chord (B.P. 60.24)	0.597 in.

FLAP, F10

Description: Double-slotted trailing edge flap used with wing (W4) and flap (F4). Located between B.P. 38.25 and wing tip. Includes a flap entry fairing. Dimensions are per side and referenced to wing (W) B.P.'s.

Drawing No.: S-1048

Dimensions:

Vane

Area	0.1524 ft. ²
Span (Equivalent)	12.33 in.
Inboard Chord (B.P. 37.02)	2.042
Outboard Chord (B.P. 49.35)	1.517 in.
Gap (% C _w)	3.5%
Overhang (% C _w)	3.12%
Deflection	25.0 deg.

FLAP, F10 - Continued

Dimensions - Continued

Flap

Area	0.2688 ft. ²
Span (Equivalent)	12.46 in.
Inboard Chord (B.P. 36.49)	3.564 in.
Outboard Chord (B.P. 48.95)	2.648 in.
Gap (% C _w)	2.0%
Overhang (% C _w)	3.65%
Deflection	

Flap Entry Fairing

Area	0.0970 ft. ²
Span (Equivalent)	12.13 in.
Inboard Chord (B.P. 37.78)	1.321 in.
Outboard Chord (B.P. 49.91)	0.981 in.

FLAP, F11

Description: Double-slotted trailing edge flap used with wing (W5) and flap (F5). Located between B.P. 38.25 and wing tip. Includes a flap entry fairing. Same dimensions as flap (F7) except for wing sweep.

Drawing No.: S-1048

Dimensions:

See Flap (F7).

FLAP, F13

- Description: Triple-slotted trailing edge flap used with wing (W) and flap (F14). Located between B.P. 5.75 and B.P. 38.25. Includes same flap entry fairing as flap (F). Dimensions are per side.

Drawing No.: S-1050

FLAP, F13 - Continued

Dimensions:

Vane

Area 0.6319 ft.²
 Span 32.50 in.
 Inboard Chord (B.P. 5.75) 3.522 in.
 Outboard Chord (B.P. 38.25) 2.078 in.
 Gap (% C_w) 3.0%
 Overhang (% C_w) 1.45%

Fore Flap

Area 0.7226 ft.²
 Span 32.50 in.
 Inboard Chord (B.P. 5.75) 4.027 in.
 Outboard Chord (B.P. 38.25) 2.376 in.
 Gap (% C_w) 2.0%
 Overhang (% C_w) 1.55%

Flap

Area 0.8337 ft.²
 Span (Equivalent) 31.21 in.
 Inboard Chord (B.P. 7.04) 4.809 in.
 Outboard Chord (B.P. 38.28) 2.884 in.
 Gap (% C_w) 2.5%
 Overhang (% C_w) 2.92%

Flap Entry Fairing
 Same as flap (F)

VANE			FOREFLAP			FLAP		
δ _V	GAP	O.H.	δ _{FF}	GAP	O.H.	δ _F	GAP	O.H.
2.5°	3.0%	1.45%	20°	2.0%	1.55%	25°	2.5%	2.92%
↓	↓	↓	↓	↓	↓	45°	↓	↓
			30°			65°		
			↓			35°		
						55°		
						75°		

FLAP, F14

Description: Triple-slotted trailing edge flap used with wing (W) and flap (F13). Located between B.P. 38.25 and B.P. 50.08. Includes same flap entry fairing as flap (F7). Dimensions are per side.

Drawing No.: S-1050

FLAP, F14 - Continued

Dimensions:

Vane

Area	0.1491 ft. ²
Span	11.83 in.
Inboard Chord (B.P. 38.25)	2.078 in.
Outboard Chord (B.P. 50.08)	1.552 in.
Gap (% C _w)	3.0%
Overhang (% C _w)	1.45%
Deflection	2.5 deg.

Fore Flap

Area	0.1705 ft. ²
Span	11.83 in.
Inboard Chord (B.P. 38.25)	2.376 in.
Outboard Chord (B.P. 50.08)	1.774 in.
Gap (% C _w)	2.0%
Overhang (% C _w)	1.55%
Deflection	20.0 deg.

Flap

Area	0.2069 ft. ²
Span	11.83 in.
Inboard Chord (B.P. 38.25)	2.884 in.
Outboard Chord (B.P. 50.08)	2.154 in.
Gap (% C _w)	2.5%
Overhang (% C _w)	2.92%
Deflection	45.0 deg.

Flap Entry Fairing

Same as flap (F7)

FLAP, F15

Description: Double-slotted, long chord trailing edge flap used with wing (W) and flap (F16). Same as flap (F13) except gap between fore flap and flap has been closed. Includes same flap entry fairing as flap (F). Dimensions are per side.

Drawing No.: None

FLAP, F15 - Continued

Dimensions:

Vane

Area	0.6319 ft. ²
Span	32.50 in.
Inboard Chord (B.P. 5.75)	3.522 in.
Outboard Chord (B.P. 38.25)	2.078 in.
Gap (% C _w)	3.0%
Overhang (% C _w)	1.45%
Deflection	2.5 deg.

Flap (44.5% C_w)

Area	1.5083 ft. ²
Span (Equivalent)	31.70 in.
Inboard Chord (B.P. 6.55)	8.608 in.
Outboard Chord (B.P. 38.25)	5.095 in.
Gap (% C _w)	2.0%
Overhang (% C _w)	1.55
Deflection	39.0 deg.

FLAP, F16

Description: Double-slotted, long chord trailing edge flap used with wing (W) and flap (F15). Same as flap (F14) except gap between fore flap and flap has been closed. Includes same flap entry fairing as flap (F7). Dimensions are per side.

Drawing No.: None

Dimensions:

Vane

Area	0.1491 ft. ²
Span	11.83 in.
Inboard Chord (B.P. 38.25)	2.078 in.
Outboard Chord (B.P. 50.08)	1.552 in.
Gap (% C _w)	3.0%
Overhang (% C _w)	1.45%
Deflection	2.5 deg.

Flap (44.5% C_w)

Area	0.3656 ft. ²
Span	11.83 in.
Inboard Chord (B.P. 38.25)	5.095 in.
Outboard Chord (B.P. 50.08)	3.805 in.
Gap (% C _w)	2.0%
Overhang (% C _w)	1.55%
Deflection	39.0 deg.

TE SPOILER, *N

Description: Trailing edge spoiler used with wing (W) and all TE flap configurations. Consists of five panels between B.P. 5.75 and B.P. 50.08 with hingeline located at 67.5% wing chord. Capable of deflections from -12 to +50 degrees. Dimensional data are per side and aft of hingeline.

Drawing No.: S-1029, -1030, -1044, -1048

Dimensions:

First Segment	
Area	0.0655 ft. ²
Span	3.00 in.
Inboard Chord (B.P. 5.75)	3.202 in.
Outboard Chord (B.P. 8.75)	3.081 in.
Second Segment	
Area	0.1804 ft. ²
Span	8.96 in.
Inboard Chord (B.P. 8.75)	3.081 in.
Outboard Chord (B.P. 17.71)	2.719 in.
Third Segment	
Area	0.1802 ft. ²
Span	10.34 in.
Inboard Chord (B.P. 17.71)	2.719 in.
Outboard Chord (B.P. 28.05)	2.301 in.
Fourth Segment	
Area	0.1484 ft. ²
Span	10.20 in.
Inboard Chord (B.P. 28.05)	2.301 in.
Outboard Chord (B.P. 38.25)	1.889 in.
Fifth Segment	
Area	0.1356 ft. ²
Span	11.83 in.
Inboard Chord (B.P. 38.25)	1.889 in.
Outboard Chord (B.P. 50.08)	1.411 in.

TE SPOILER, *N2

Description: Trailing edge spoiler used with wing (W2) and flaps (F2 and F8). Consists of two panels between B.P. 5.75 and B.P. 60.24 with hingeline located at 67.5% of wing chord. Capable of deflections from -10 to +50 degrees. Dimensional data are per side and aft of hingeline.

TE SPOILER, *N2 - Continued

Drawing No.: S-1029, -1030, -1045, -1049

Dimensions:

Inboard Panel

Area	0.6245 ft. ²
Span	42.66 in.
Inboard Chord (B.P. 5.75)	2.711 in.
Outboard Chord (B.P. 48.41)	1.505 in.

Outboard Panel

Area	0.1099 ft. ²
Span	11.83 in.
Inboard Chord (B.P. 48.41)	1.505 in.
Outboard Chord (B.P. 60.24)	1.170 in.

TE SPOILER, *N4

Description: Trailing edge spoiler used with wing (W4) and flaps (F4 and F10). Consists of five panels between B.P. 4.05 and B.P. 49.72 with hingeline located at 67.5% of wing chord. Same as spoiler (*N) except for end cuts on first, fourth and fifth panels. Deflections available are -10 and +50 degrees. All B.P.'s are referenced to wing (W). Dimensional data are per side and aft of hingeline.

Drawing No.: S-1044, -1046, -1048

Dimensions:

First Segment

Area	0.1037 ft. ²
Span	4.70 in.
Inboard Chord (B.P. 4.05)	3.271 in.
Outboard Chord (B.P. 8.75)	3.081 in.

Second Segment

Same as *N

Third Segment

Same as *N

Fourth Segment

Area	0.1423 ft. ²
Span	9.74 in.
Inboard Chord (B.P. 28.05)	2.301 in.
Outboard Chord (B.P. 37.79)	1.908 in.

TE SPOILER, *N4 - Continued

Dimensions - Continued

Fifth Segment

Area	0.1381 ft. ²
Span	11.93 in.
Inboard Chord (B.P. 37.79)	1.908 in.
Outboard Chord (B.P. 49.72)	1.426 in.

TE SPOILER, *N5

Description: Trailing edge spoiler used with wing (W5) and flaps (F5 and F11). Consists of five panels between B.P. 6.49 and B.P. 50.08 with hingeline located at 67.5% of wing chord. Same as spoiler (*N) except for first panel. Deflections available are -10 and +50 degrees. All B.P.'s are referenced to wing (W). Dimensional data are per side and aft of hingeline.

Drawing No.: S-1044, -1046, -1048

Dimensions:

First Segment

Area	0.0490 ft. ²
Span	2.26 in.
Inboard Chord (B.P. 6.49)	3.170 in.
Outboard Chord (B.P. 8.75)	3.081 in.

Second thru Fifth Segments

Same as *N

VANE SPOILER, *S

Description: Vane spoiler used with flap (F7) and wing (W). Located on RH vane of flap assembly between B.P. 28.05 and B.P. 38.25. Hingeline of spoiler is located on the upper surface and the vane and at 23.5% of vane chord. Dimensional data are for RH spoiler only.

Drawing No. S-1032, -1044

Dimensions:

Area	0.0360 ft. ²
Span	10.20 in.
Inboard Chord (B.P. 28.05)	0.558 in.
Outboard Chord (B.P. 38.25)	0.458 in.
Hingeline (% Wing Chord)	85.55%
Deflection	90.0 deg.

LE SPOILER, *J

Description: Leading edge spoiler used with wing (W) and kruegers (K3 and K28). Spoiler is deflected 90 degrees from wing upper surface and is used on right hand wing only. Hingeline is located on upper surface and is 2% of wing chord. Dimensional data is for right hand spoiler only.

Drawing No.: S-1032, -1051

Dimensions:

Area	0.0537 ft. ²
Span	20.07 in.
Inboard Chord (B.P. 30.01)	0.471 in.
Outboard Chord (B.P. 50.08)	0.299 in.
Hingeline (% Wing Chord)	2.0%
Deflection	90.0 deg.

AILERON, A

Description: Aileron used with wing (W) and double slotted flap (F7). Chord is 15% of local wing chord and is located on trailing edge of main flap. Dimensional data are per side and aft of hingeline.

Drawing No.: S-1030, -1048

Dimensions:

Area	0.1232 ft. ²
Span	11.83 in.
Inboard Chord (B.P. 38.25)	1.717 in.
Outboard Chord (B.P. 50.08)	1.283 in.
Hingeline (% Wing Chord)	15.0%
Deflection	<u>±</u> 20.0 deg.

AILERON, A7

Description: Aileron used with wing (W) and triple slotted flap (F14). Chord is 15% of local wing chord and is located on trailing edge of main flap. Dimensional data are per side and aft of hingeline.

Drawing No.: S-1030, -1050

Dimensions:

Same as A.

AILERON, A8

Description: Drooped aileron/flap used with wing (W) and located between B.P. 38.25 and B.P. 50.08. Consists of a single flap with the aft 15% drooped 15 degrees TE down. The main flap is deflected 35 degrees from the WRP. Dimensional data are per side and aft of the hingeline.

Drawing No.: S-1031, -1048

AILERON, A8 - Continued

Dimensions:

Flap

Area	0.3040 ft. ²
Span	11.83 in.
Inboard Chord (B.P. 38.25)	4.236 in.
Outboard Chord (B.P. 50.08)	3.164 in.
Deflection	35.0 deg.

Aileron

Area	0.1232 ft. ²
Span	11.83 in.
Inboard Chord (B.P. 38.25)	1.717 in.
Outboard Chord (B.P. 50.08)	1.283 in.
Hingeline (% Wing Chord)	15.0%
Neutral Position	15.0 deg.
Deflection (From Neutral Position)	<u>±20.0 deg.</u>

DORSAL, D

Description: Dorsal fin located forward of vertical tail/fuselage intersection.

Drawing No.: S-1003

Dimensions:

Projected Side Area	0.0608 ft. ²
Intersection, Dorsal/Fuselage	
Fuselage Station	60.03 in.
Water Plane	12.41 in.
Intersection, Dorsal/Vertical Tail	
Fuselage Station	72.86 in.
Water Plane	16.09 in.

DORSAL, D2

Description: Sheet metal dorsal fin located forward of vertical tail/fuselage intersection. Larger in area than dorsal (D).

Drawing No.: None

Dimensions:

Projected Side Area	0.8418 ft. ²
Intersection, Dorsal/Fuselage	
Fuselage Station	49.05 in.
Water Plane	12.41 in.
Intersection, Dorsal/Vertical Tail	
Fuselage Station	77.05 in.
Water Plane	22.43 in.
Leading Edge Sweep Angle	71.5 deg.

DORSAL, D3

Description: Sheet metal dorsal fin located forward of vertical tail/fuselage intersection. Larger in area than dorsal (D) but smaller than dorsal (D2).

Drawing No.: None

DORSAL, D3 - Continued

Dimensions:

Projected Side Area	0.6831 ft. ²
Intersection, Dorsal/Fuselage	
Fuselage Station	47.43 in.
Water Plane	12.41 in.
Intersection, Dorsal/Vertical Tail	
Fuselage Station	74.75 in.
Water Plane	18.95 in.
Leading Edge Sweep Angle	78.5 deg.

VERTICAL, V

Description: Single centerline vertical stabilizer used with rudder (R), horizontal (H) and bullet fairing (Y). Vertical is located in the "basic" position, root chord LE at F.S. 70.762. Dimensions are for the total exposed vertical above W.P. 12.785.

Drawing No.: S-1003

Dimensions:

Area, Total	2.3969 ft. ²
Span	22.805 in.
Chords, Root (W.P. 12.785)	18.881 in.
Tip (W.P. 35.590)	11.389 in.
MAC (W.P. 23.247)	15.444 in.
Fus. Sta. of 0.25 MAC	81.450 in.
Sweepback Angles, Leading Edge	33.4 deg.
25% Element	30.0 deg.
Trailing Edge	18.3 deg.
Airfoil Section	NASA 64A010
Aspect Ratio	1.50
Taper Ratio	0.603

VERTICAL, V2

Description: Single centerline vertical stabilizer, same as vertical (V) except alternate "square" tip replaces T-tail bullet fairing (Y). Same dimensions as vertical (V).

Drawing No.: S-1003

Dimensions:

See vertical (V).

RUDDER, R

Description: Full span double-hinged rudder used with vertical (V). Hingelines are at 55% and 75% element lines of vertical tail.
Dimensions for forward segment do not include aft segment and are aft of the hingeline.

Drawing No.: S-1003

Dimensions:

Forward Segment

Area	0.4572 ft. ²
Span	21.432 in.
Inboard Chord (W.P. 12.785)	3.776 in.
Outboard Chord (W.P. 34.217)	2.368 in.
Sweepback Angle of Hingeline (55%)	25.68 deg.

Aft Segment

Area	0.5715 ft. ²
Span	21.432 in.
Inboard Chord (W.P. 12.785)	4.720 in.
Outboard Chord (W.P. 34.217)	2.960 in.
Sweepback Angle of Hingeline (75%)	22.58 deg.

BULLET FAIRING, Y

Description: T-tail bullet fairing located at horizontal stabilizer/vertical tail intersection.

Drawing No.: S-1003, -1035

Dimensions:

Projected Side Area	0.307 ft. ²
Length	19.10 in.
F.S. of Leading Edge (B.P. 0.00)	81.75 in.
Max X-Sectional Area (F.S. 87.00)	0.0303 ft. ²

HORIZONTAL, H

Description: Horizontal stabilizer which is T-tail mounted on vertical tail (V) with bullet fairing (Y). The airfoil is an inverted and modified NASA 64A210 section. The stabilizer is capable of remote actuation (+20 degrees) and also includes a double hinge elevator (E).

Drawing No.: S-1003

Dimensions:

Area, Total	2.776 ft. ²
Span	43.656 in.
Chords, Root (B.P. 0.00)	13.850 in.
Tip (B.P. 21.828)	5.532 in.
MAC (B.P. 9.353)	10.286 in.
Fus. Sta. of 0.25 MAC	92.429 in.
W.P. of 0.25 MAC	35.590 in.
Hingeline Center, F.S.	90.880 in.
W.P.	35.590 in.
Dihedral	0.0 deg.
Incidence (Basic)	0.0 deg.
Sweepback Angles, Leading Edge	31.70 deg.
25% Element Line	25.00 deg.
Trailing Edge	10.14 deg.
Airfoil Section	NASA 64A210 Modified

ELEVATOR, E

Description: Full span double-hinged elevator used with horizontal stabilizer (H). Hinge lines are at 55% and 75% element lines. Dimensions for forward segment do not include aft segment. Dimensions are per side and aft of hingeline.

Drawing No.: S-1003

Dimensions:

Forward Segment

Area	0.2915 ft. ²
Span	20.978 in.
Inboard Chord (B.P. 0.85)	2.840 in.
Outboard Chord (B.P. 21.828)	1.162 in.
Sweepback Angle of Hingeline (55%)	19.23 deg.

Aft Segment

Area	0.3643 ft. ²
Span	20.978 in.
Inboard Chord (B.P. 0.85)	3.550 in.
Outboard Chord (B.P. 21.828)	1.452 in.
Sweepback Angle of Hingeline (75%)	15.42 deg.

HORIZONTAL SLAT, S

Description: Full span leading edge slat used with horizontal stabilizer (H). The slat is mounted on the top surface of the inverted airfoil and is 14% of the horizontal chord. The slat gap is 1.25% of the horizontal chord. Dimensions are per side.

Drawing No.: S-1003

Dimensions:

Area	0.2040 ft. ²
Span	20.978 in.
Inboard Chord (B.P. 0.85)	1.988 in.
Outboard Chord (B.P. 21.828)	0.813 in.
Gap (% C_H)	1.25%
Deflection (Nose Up)	25.0 deg.
Extension (% C_H), Vertical	5.94%
Horizontal	12.65%
Control Point (% C_H , Unextended), Vertical	1.28%
Horizontal	0.30%

FEFO

Description: Flap entry fairing off; bulge hood fairing which replaces flap entry fairing used with flaps (F) and (F7).

Drawing No.: S-1044-56 & -57, S-1048

RAKE

Description: Horizontal flow survey rake used with vertical (V) and containing five conical flow angularity probes. Each probe has a conical probe with four orthogonally located surface pressure orifices and a single centerline total probe. The number 5 probe is inboard and number 1 probe is the farthest outboard. The number 4 probe is lined up to coincide with coordinates for 0.25 MAC of the horizontal stabilizer.

Drawing No.: S-1026

Dimensions:

Rake Strut, X-sectional area	0.0491 ft ²
Diameter	3.00 in.
Span	26.25 in.
Leading Edge of Probes, F.S.	92.429 in.
W.P.	35.591 in.
Probe Spacing, Number 5, B.P.	4.375 in.
Number 4, B.P.	9.375 in.
Number 3, B.P.	14.375 in.
Number 2, B.P.	19.375 in.
Number 1, B.P.	24.375 in.
Probe Diameter	0.312 in.

BELLMOUTH

Description: Bellmouth inlet cowl used with nacelle (N) during part of engine calibration. Includes inlet instrumentation to measure inlet weight flow. Purpose was to prevent possible flow separation from inlet lip on basic cowl. One bellmouth was mounted on each nacelle.

Drawing No.: S-1022

Dimensions:

Throat Diameter	3.253 in.
Throat Area	0.0578 ft ²
Lip Diameter (N.S. - 1.86)	6.506 in.
Capture Area	0.2310 ft ²

Section III

WIND TUNNEL TEST RUN LOG SUMMARY

The last column of the run log summary titled "Figure No." represents a means whereby any particular run is cross-referenced against the GELAC wind tunnel data plots (STOL Tactical Aircraft Investigation, Wind Tunnel Test Data of an Externally Blown Flap Model, Contract F33615-71-C-1760, Appendix A, Volumes 1 through 3 inclusive, 24 August 1972.)

Some runs appear without any cross referenced data plots. These were calibration runs, or single point runs for static turning angles, or have been re-run later in the test and then plotted. Any force data taken with the horizontal tail flow field survey rake installed was not plotted.

TEST NO. LIMITS AND CORRELATION TRANSMITTANCE		PAGE 1 OF 14		FIGURE NO.	
PANEL 007113					
DATE	CONCRETE	Q	A	AR	U
7 APR	BN*PND + BELL POINTS	0	24	7	0 0 1/16
1					
2					
3					
4					
5					
6					
7					
8					
9					
10					
11					
12					
13					
14					
15					
16					
17					
18	BN*PND + BELL POINTS				
19	BN*PND + BELL POINTS				
20	BN*PND + BELL POINTS				
21					
22	BN*PND (Base Case)				
23					
24					
25					
26					
27					
28					
29					
30					
31					
32					
33					
34					
35					
36					
37					
38					
39					
40					
41					
42					
43					
44					
45					
46					
47					
48					
49					
50					

[illegible]

TEST NO. LIGHT 600		PAGE 10 OF 14	
TEST NO. LIGHT 600		PAGE 10 OF 14	
DATE	TIME	TEST NO.	FIGURE NO.
15 MAY 1964	0800	100	100
16 MAY 1964	0800	101	101
17 MAY 1964	0800	102	102
18 MAY 1964	0800	103	103
19 MAY 1964	0800	104	104
20 MAY 1964	0800	105	105
21 MAY 1964	0800	106	106
22 MAY 1964	0800	107	107
23 MAY 1964	0800	108	108
24 MAY 1964	0800	109	109
25 MAY 1964	0800	110	110
26 MAY 1964	0800	111	111
27 MAY 1964	0800	112	112
28 MAY 1964	0800	113	113
29 MAY 1964	0800	114	114
30 MAY 1964	0800	115	115
31 MAY 1964	0800	116	116
1 JUN 1964	0800	117	117
2 JUN 1964	0800	118	118
3 JUN 1964	0800	119	119
4 JUN 1964	0800	120	120
5 JUN 1964	0800	121	121
6 JUN 1964	0800	122	122
7 JUN 1964	0800	123	123
8 JUN 1964	0800	124	124
9 JUN 1964	0800	125	125
10 JUN 1964	0800	126	126
11 JUN 1964	0800	127	127
12 JUN 1964	0800	128	128
13 JUN 1964	0800	129	129
14 JUN 1964	0800	130	130
15 JUN 1964	0800	131	131
16 JUN 1964	0800	132	132
17 JUN 1964	0800	133	133
18 JUN 1964	0800	134	134
19 JUN 1964	0800	135	135
20 JUN 1964	0800	136	136
21 JUN 1964	0800	137	137
22 JUN 1964	0800	138	138
23 JUN 1964	0800	139	139
24 JUN 1964	0800	140	140
25 JUN 1964	0800	141	141
26 JUN 1964	0800	142	142
27 JUN 1964	0800	143	143
28 JUN 1964	0800	144	144
29 JUN 1964	0800	145	145
30 JUN 1964	0800	146	146
1 JUL 1964	0800	147	147
2 JUL 1964	0800	148	148
3 JUL 1964	0800	149	149
4 JUL 1964	0800	150	150
5 JUL 1964	0800	151	151
6 JUL 1964	0800	152	152
7 JUL 1964	0800	153	153
8 JUL 1964	0800	154	154
9 JUL 1964	0800	155	155
10 JUL 1964	0800	156	156
11 JUL 1964	0800	157	157
12 JUL 1964	0800	158	158
13 JUL 1964	0800	159	159
14 JUL 1964	0800	160	160
15 JUL 1964	0800	161	161
16 JUL 1964	0800	162	162
17 JUL 1964	0800	163	163
18 JUL 1964	0800	164	164
19 JUL 1964	0800	165	165
20 JUL 1964	0800	166	166
21 JUL 1964	0800	167	167
22 JUL 1964	0800	168	168
23 JUL 1964	0800	169	169
24 JUL 1964	0800	170	170
25 JUL 1964	0800	171	171
26 JUL 1964	0800	172	172
27 JUL 1964	0800	173	173
28 JUL 1964	0800	174	174
29 JUL 1964	0800	175	175
30 JUL 1964	0800	176	176
31 JUL 1964	0800	177	177
1 AUG 1964	0800	178	178
2 AUG 1964	0800	179	179
3 AUG 1964	0800	180	180
4 AUG 1964			

[illegible]

71

Section IV

WING SWEEP

Three wing sweep angles were tested at three C_{μ} 's each. The AR 7 wing was tested at $\Lambda = 9.33^\circ$, 24° , and 30° . Each sweep angle was tested at $C_{\mu} = 0$, 2.0 and 3.0. All wing sweep tests were conducted tail-off and with the inboard Krueger removed from the basic configuration of $\Lambda = 24^\circ$ since no inboard Kruegers were available for the other wing sweep angles tested.

4.1 EFFECTS ON LIFT

Wing sweep effects on total powered lift coefficient are presented in Figures 4.1.1 and 4.1.2 for α 's of 0° and 8° respectively and at varying engine thrust coefficients. The reference point from which increments were taken is the basic configuration wing sweep angle of 24° .

As the wing is swept forward from $\Lambda = 24^\circ$, the lift coefficient increases and as the wing is swept further aft from $\Lambda = 24^\circ$ the lift coefficient decreases. The higher blowing coefficients always generate positive lift coefficient increments at any sweep angle over the unpowered lift coefficient increments.

Figures 4.1.3 and 4.1.4 are test data points from which the sweep effects on lift coefficient were obtained.

4.2 EFFECTS ON DRAG

As would be expected the effects of wing sweep variation on total powered drag coefficient closely parallel the lift coefficient effects as can be seen in Figures 4.2.1 and 4.2.2. Wind tunnel backup data is presented in Figures 4.2.3 and 4.2.4.

4.3 EFFECTS ON PITCHING MOMENT

Figures 4.3.1 and 4.3.2 show the stabilizing effects of sweeping the wings rearward. At any given wing sweep angle the stabilizing tendencies increase appreciably with increasing power. This is due to the rearward shift of the wing center of pressure as C_{μ} is increased.

Wind tunnel backup data is presented in Figures 4.2.3 and 4.2.4.

LSWT - 090

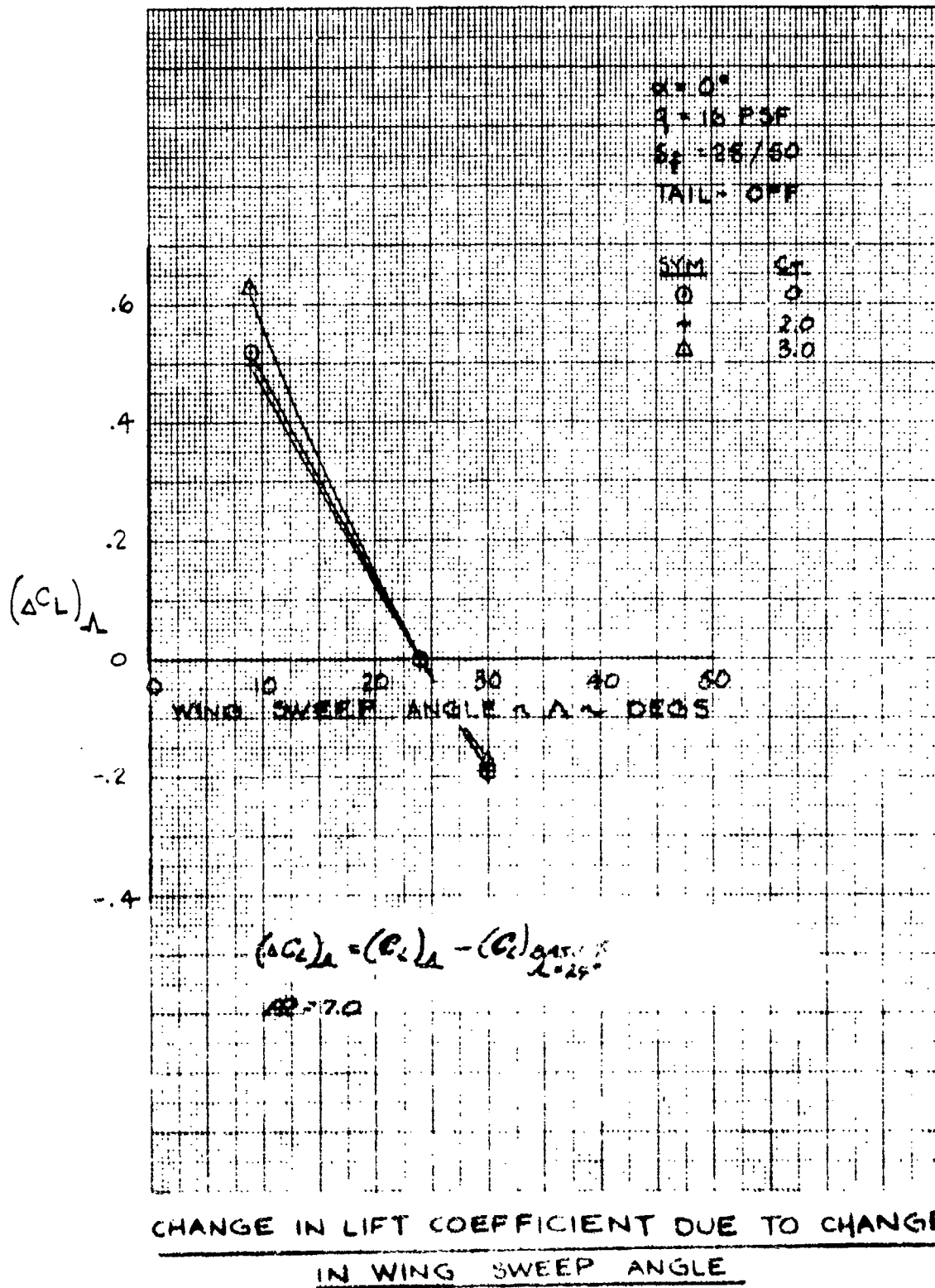
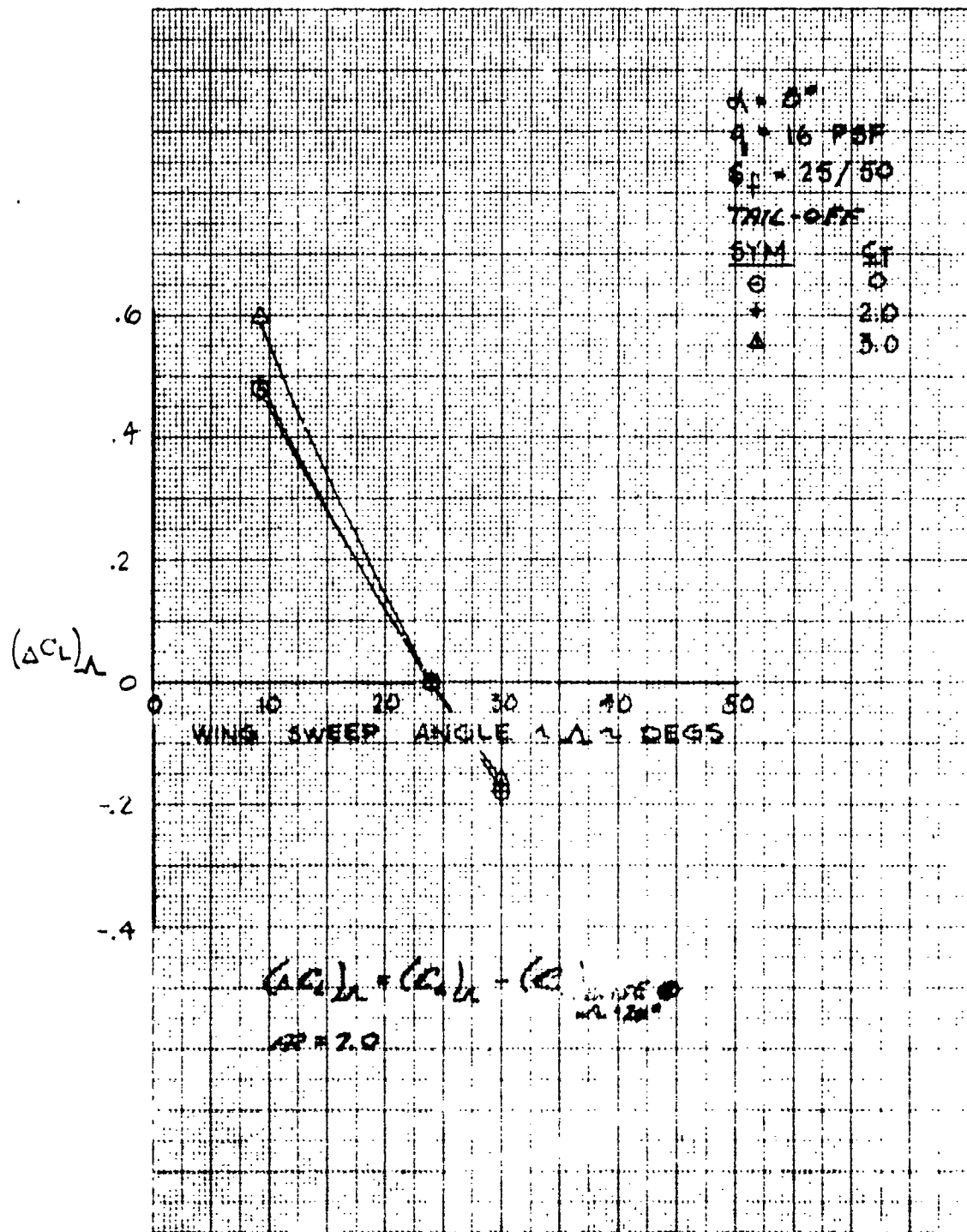


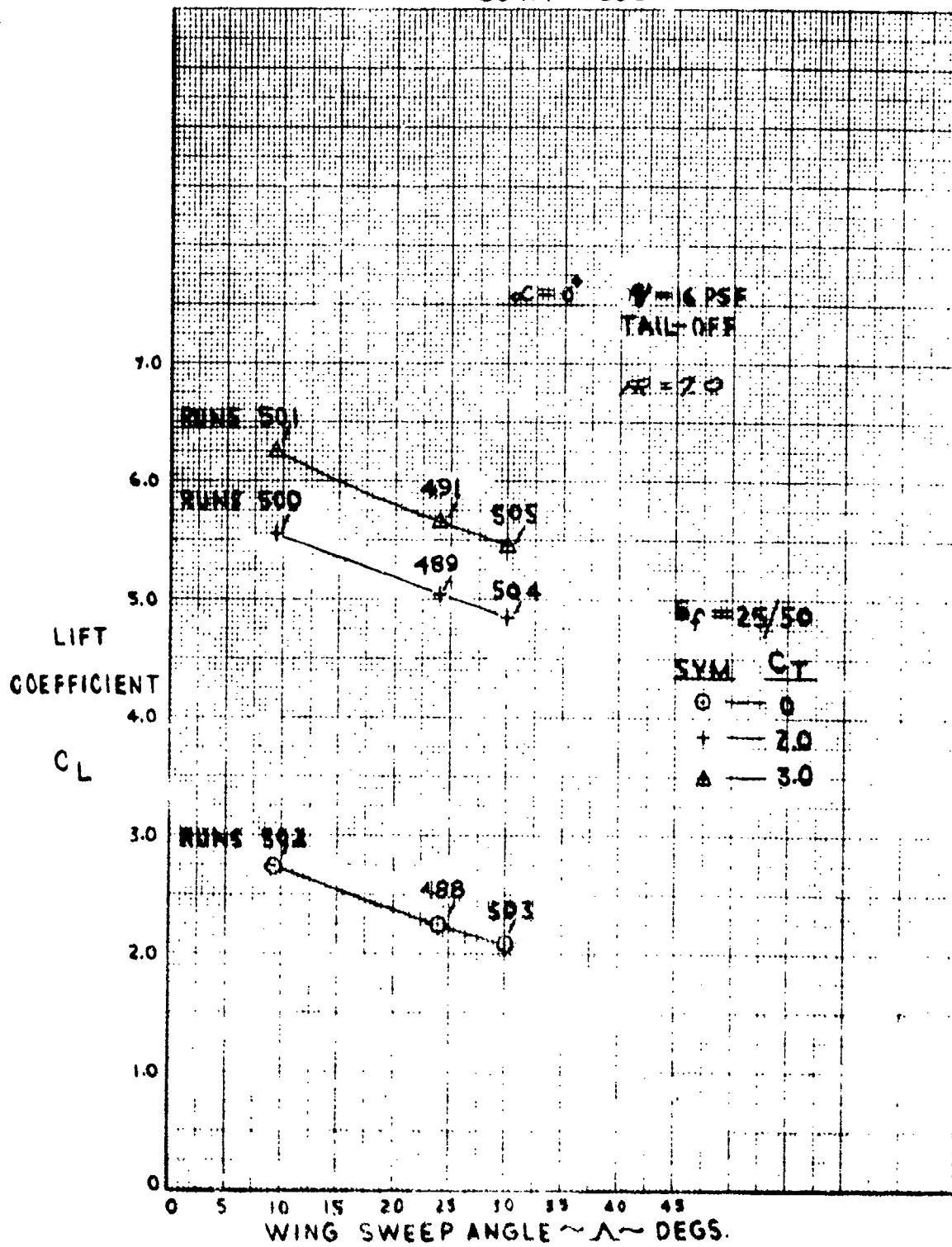
Figure 4.1.1

LSWT-090



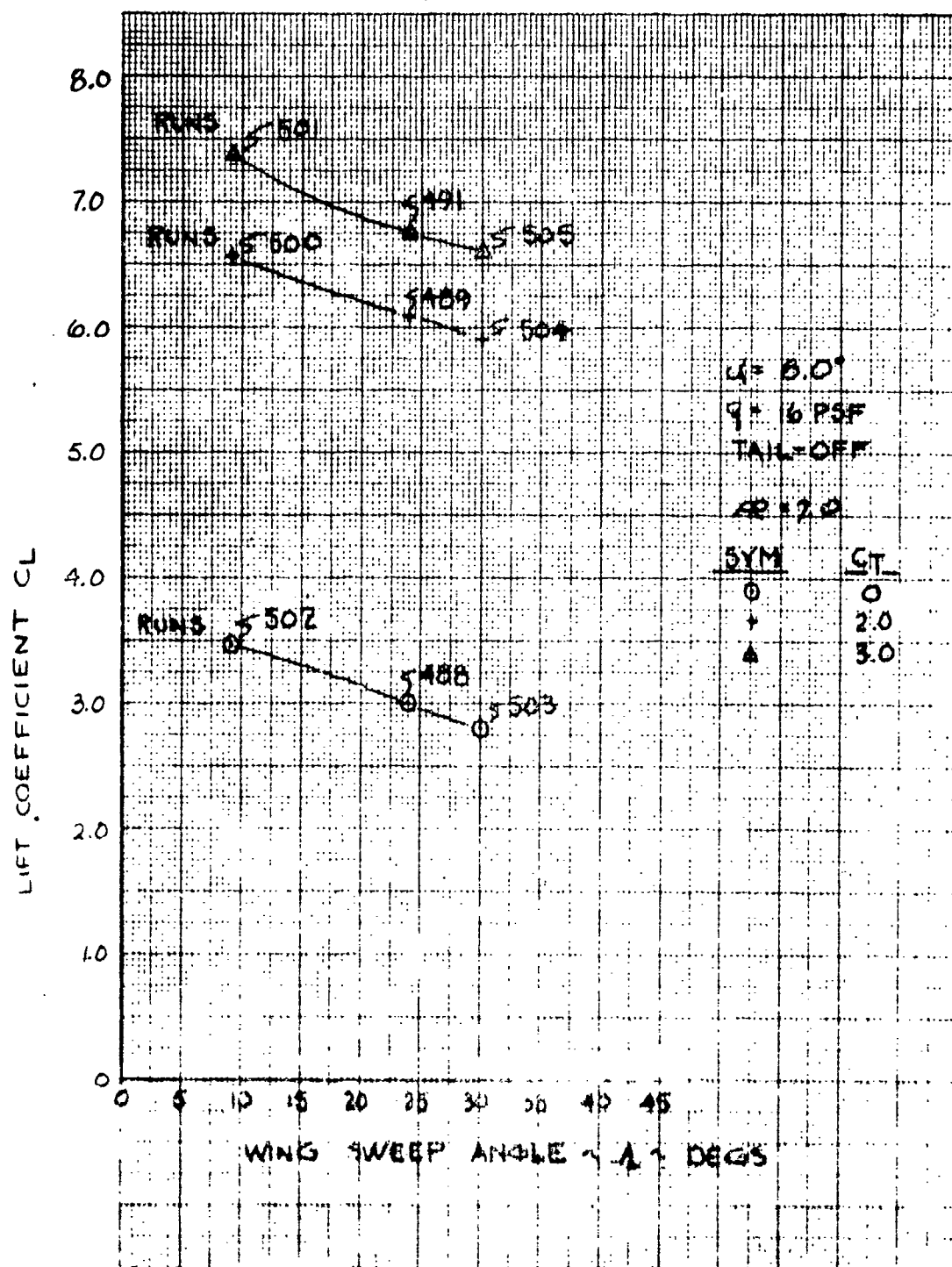
CHANGE IN LIFT COEFFICIENT DUE TO CHANGE
IN WING SWEEP ANGLE

Figure 4.1.2



WING SWEEP ANGLE EFFECT ON LIFT
COEFFICIENT AT CONSTANT ANGLE OF
ATTACK.

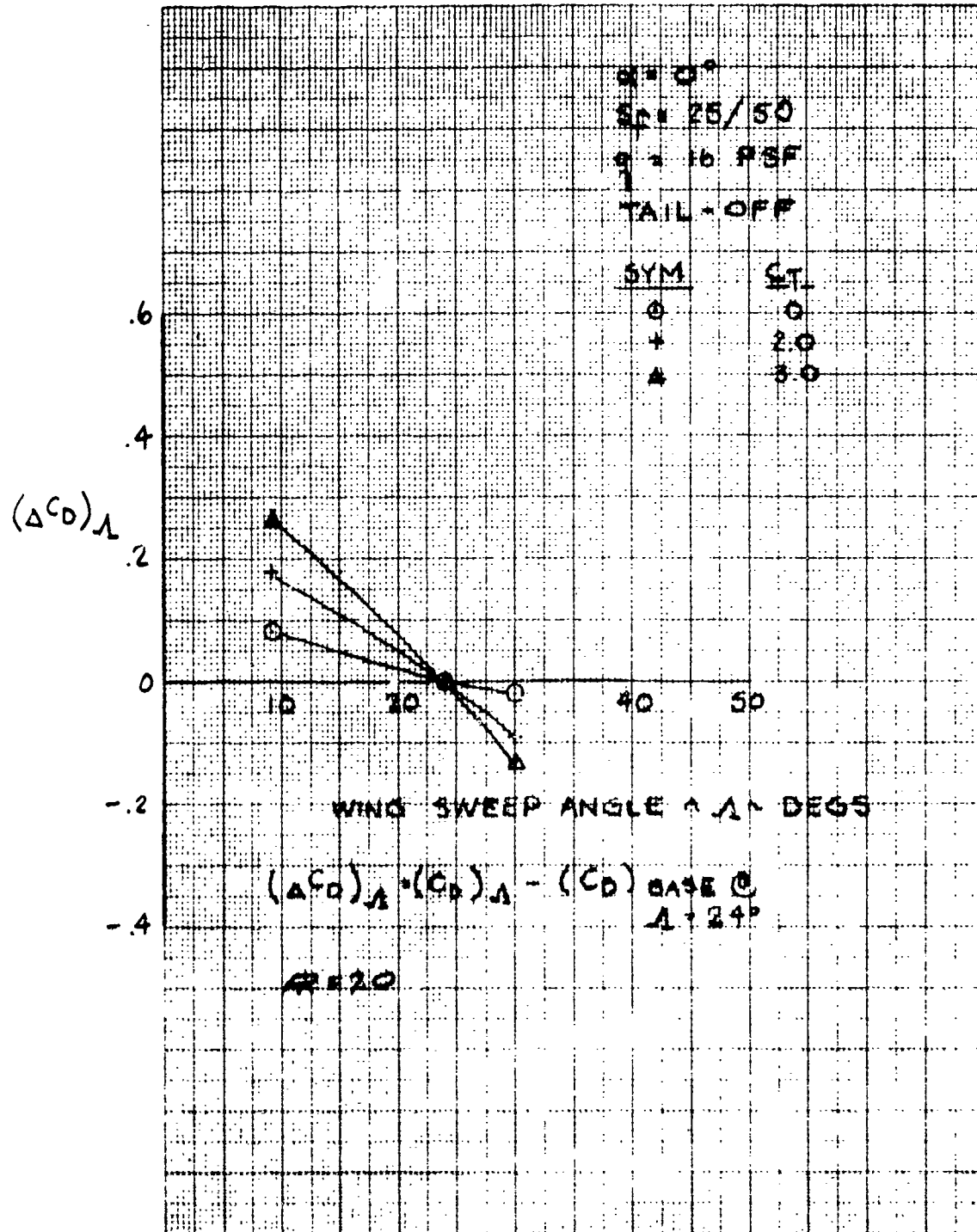
Figure 4.1.3



WING SWEEP ANGLE EFFECTS ON LIFT COEFFICIENT
AT CONSTANT ANGLE OF ATTACK

Figure 4.1.4

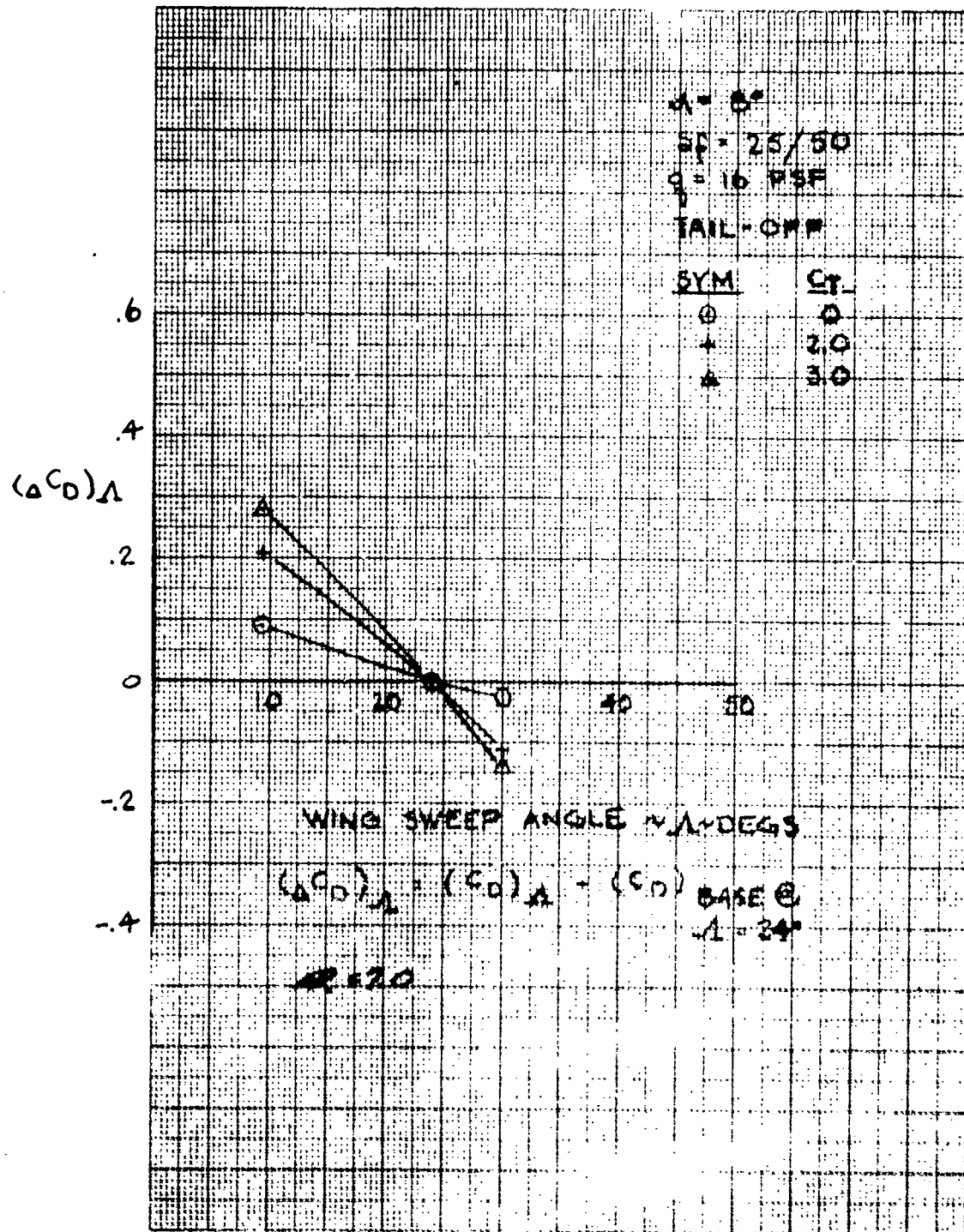
LSWT - 090



CHANGE IN TOTAL DRAG COEFFICIENT DUE
TO CHANGE IN WING SWEEP ANGLE

Figure 4.2.1

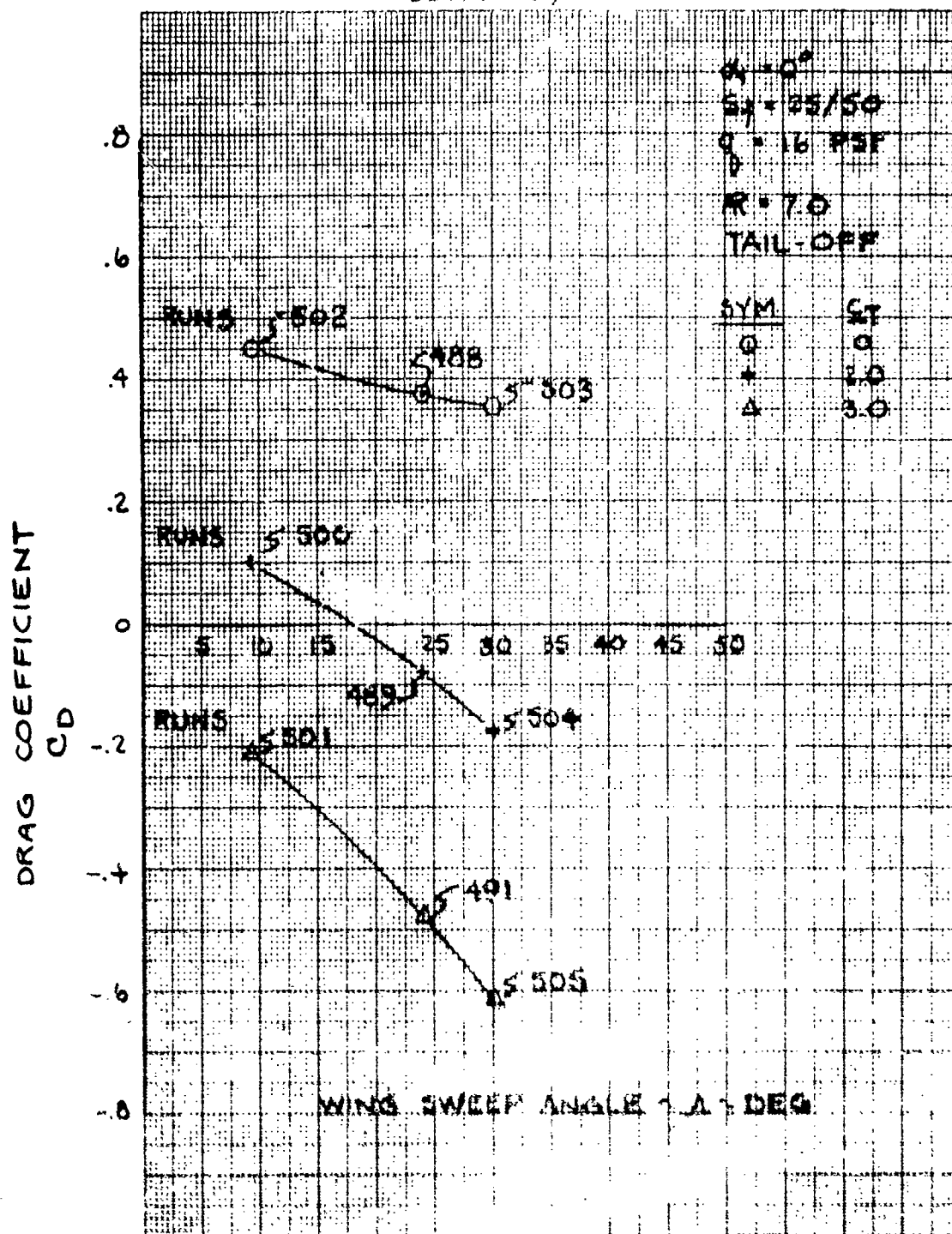
LSWT-090



CHANGE IN TOTAL DRAG COEFFICIENT DUE
TO CHANGE IN WING SWEEP ANGLE

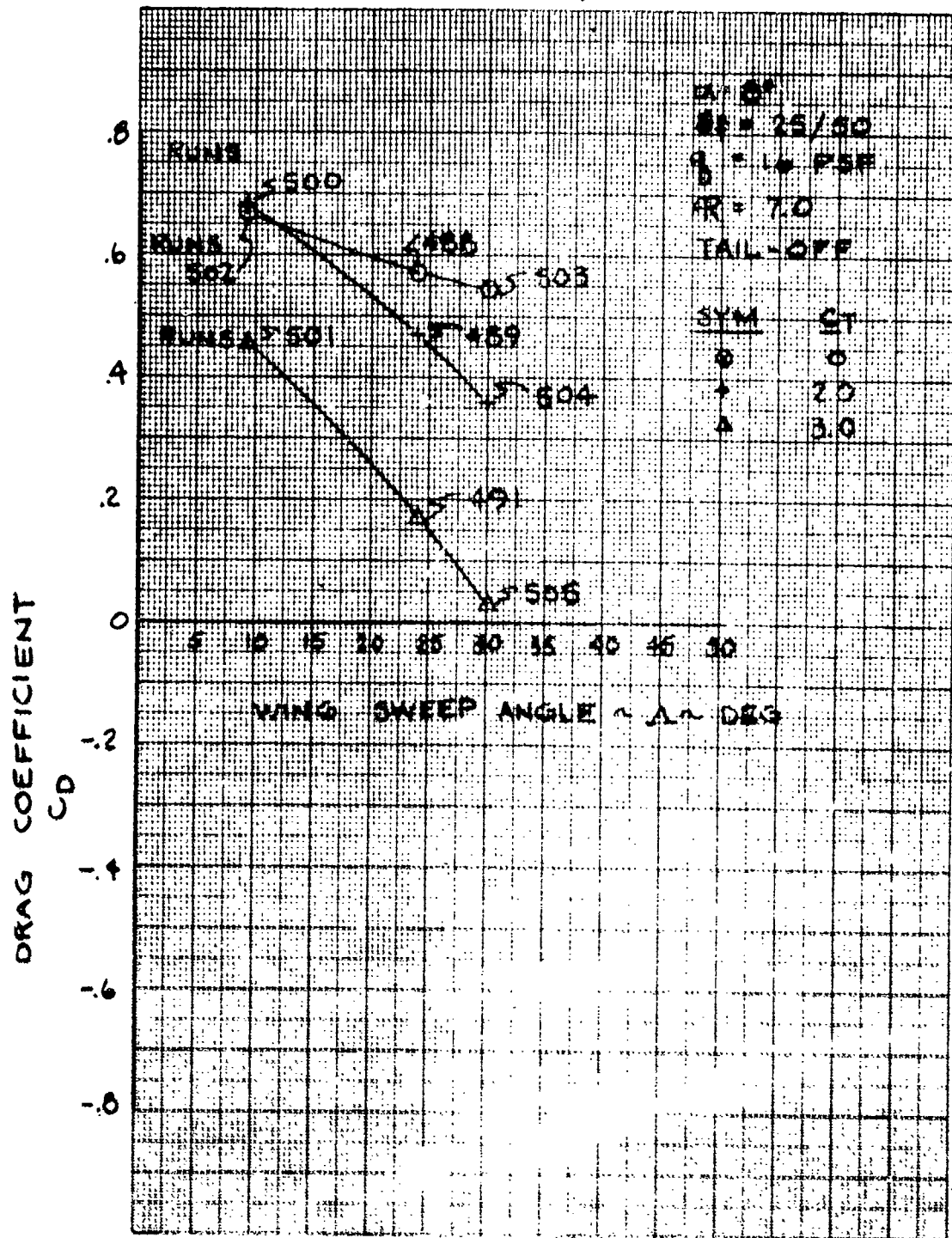
Figure 4.2.2

LSWT-390



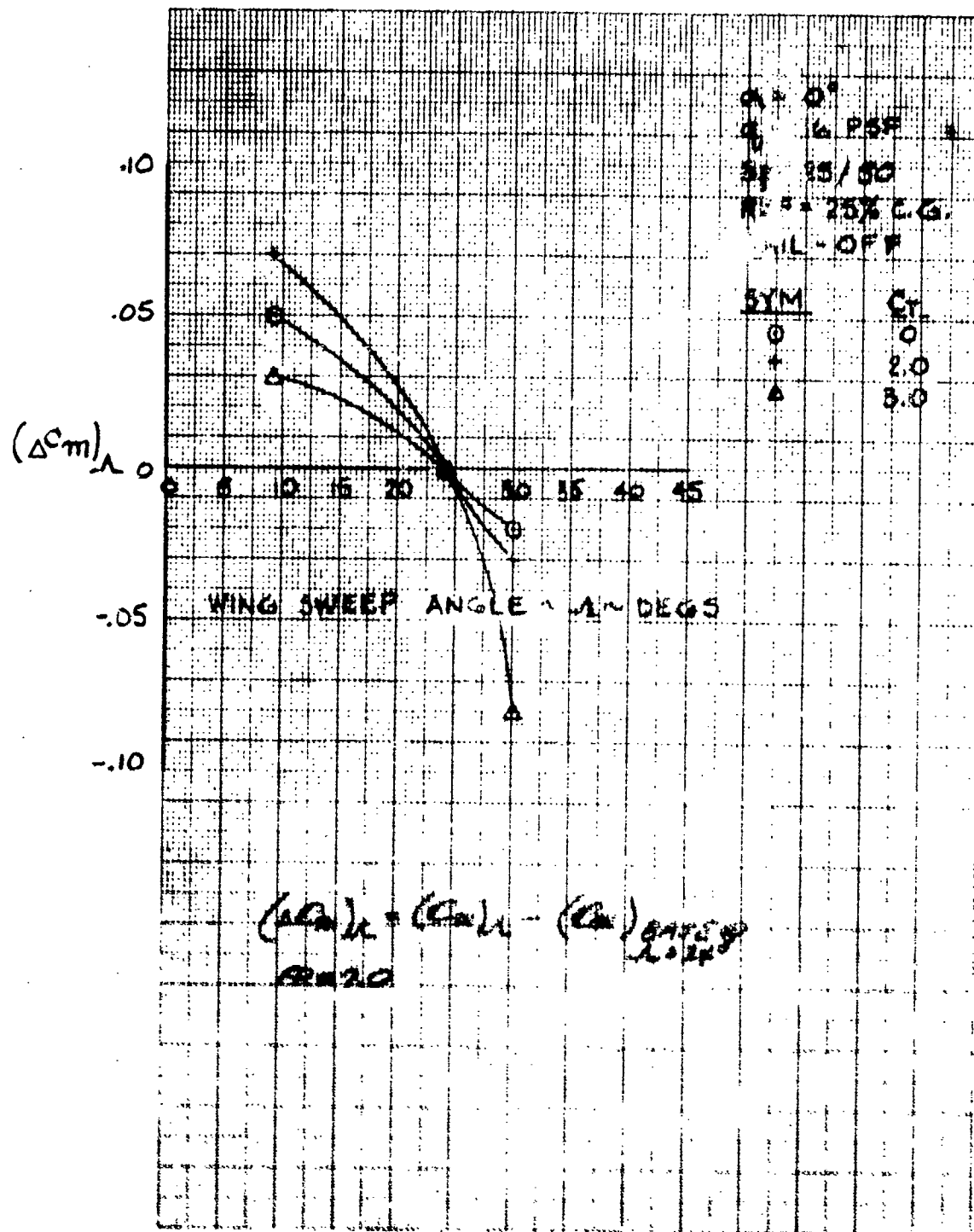
WING SWEEP ANGLE EFFECTS ON TOTAL DRAG COEFFICIENT AT CONSTANT ANGLE OF ATTACK

LSWT - 090



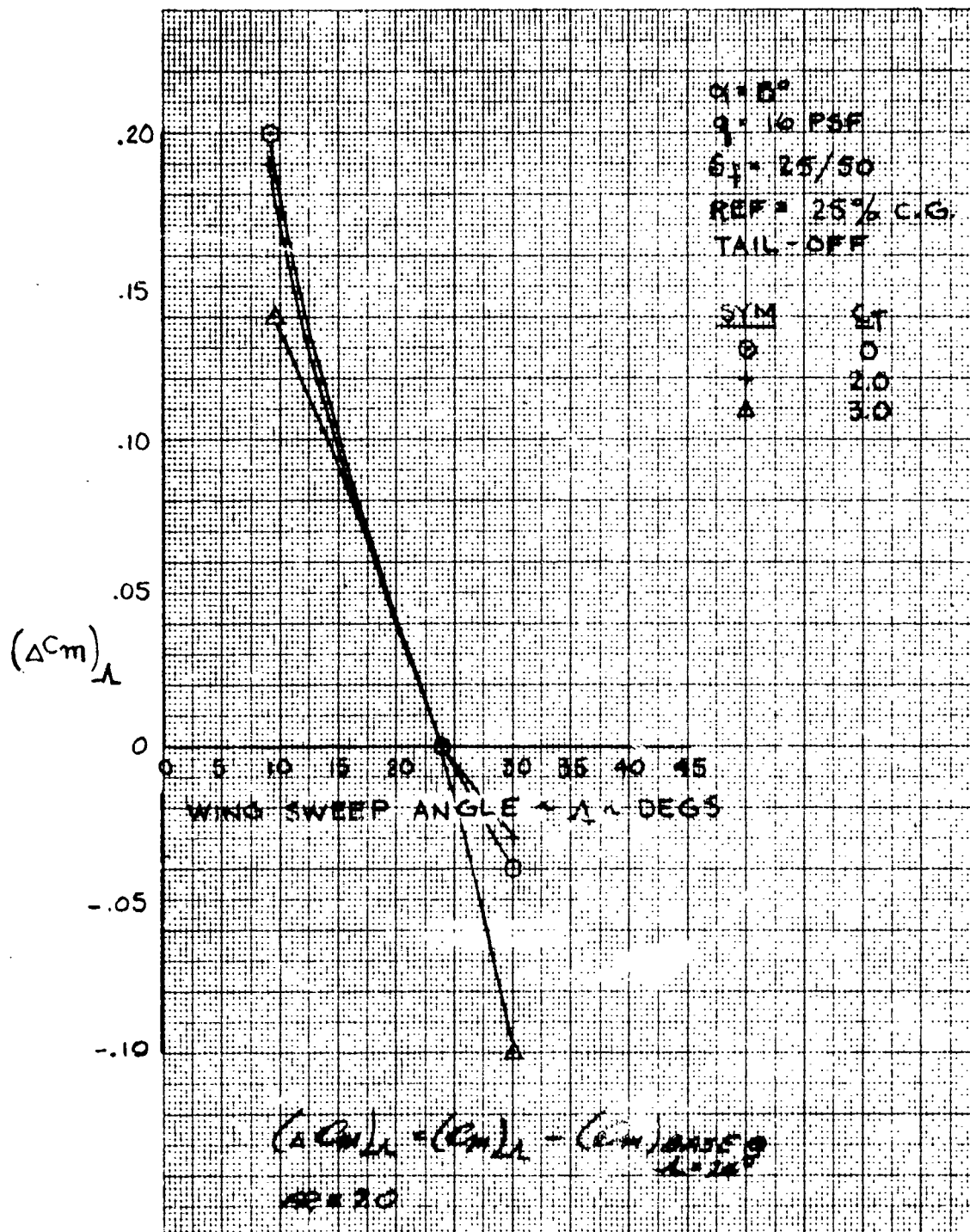
WING SWEEP ANGLE EFFECTS ON TOTAL DRAG COEFFICIENT AT CONSTANT ANGLE OF ATTACK

LSWT-090

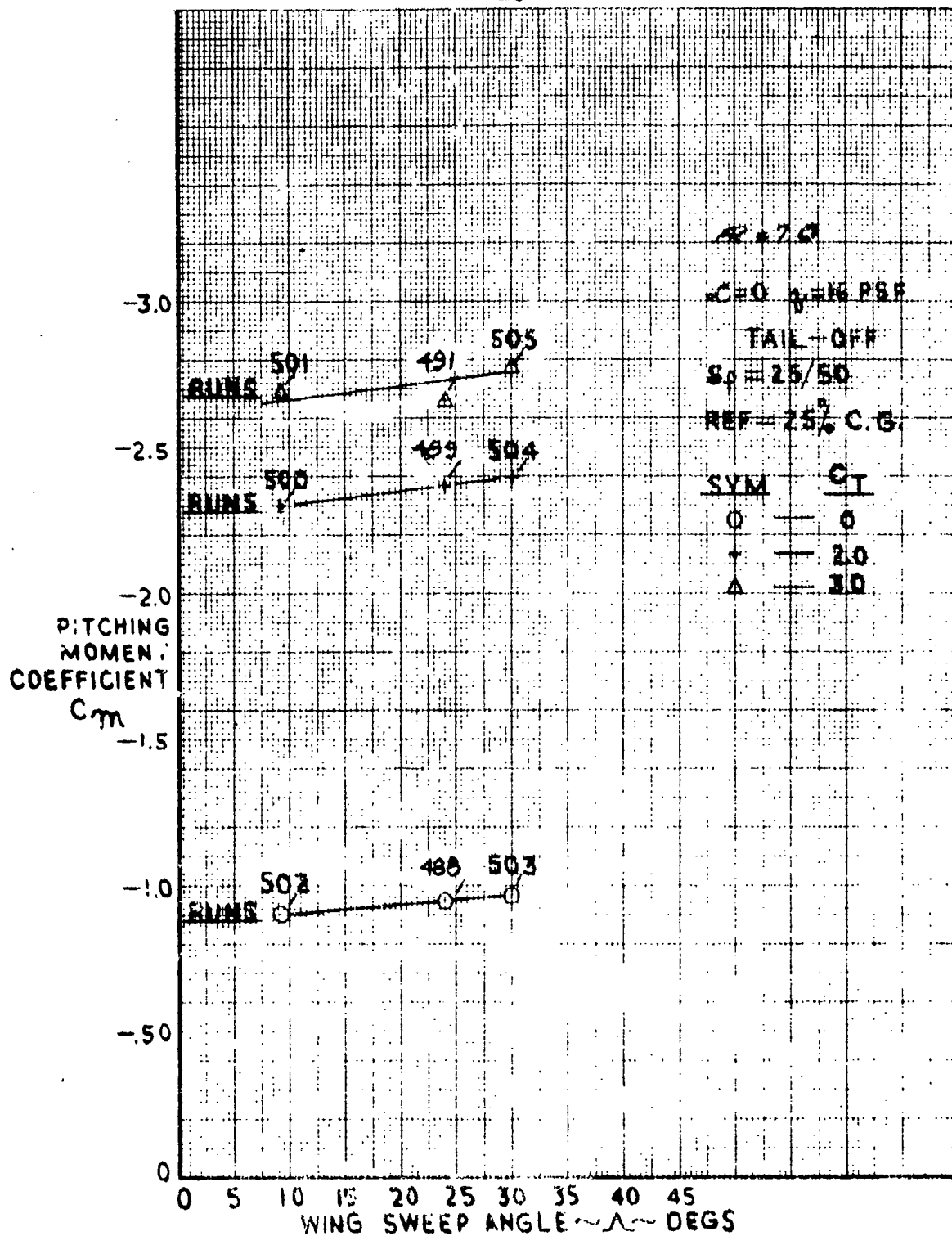


CHANGE OF PITCHING MOMENT COEFFICIENT
DUE TO CHANGE IN WING SWEEP ANGLE

LSWT - 090



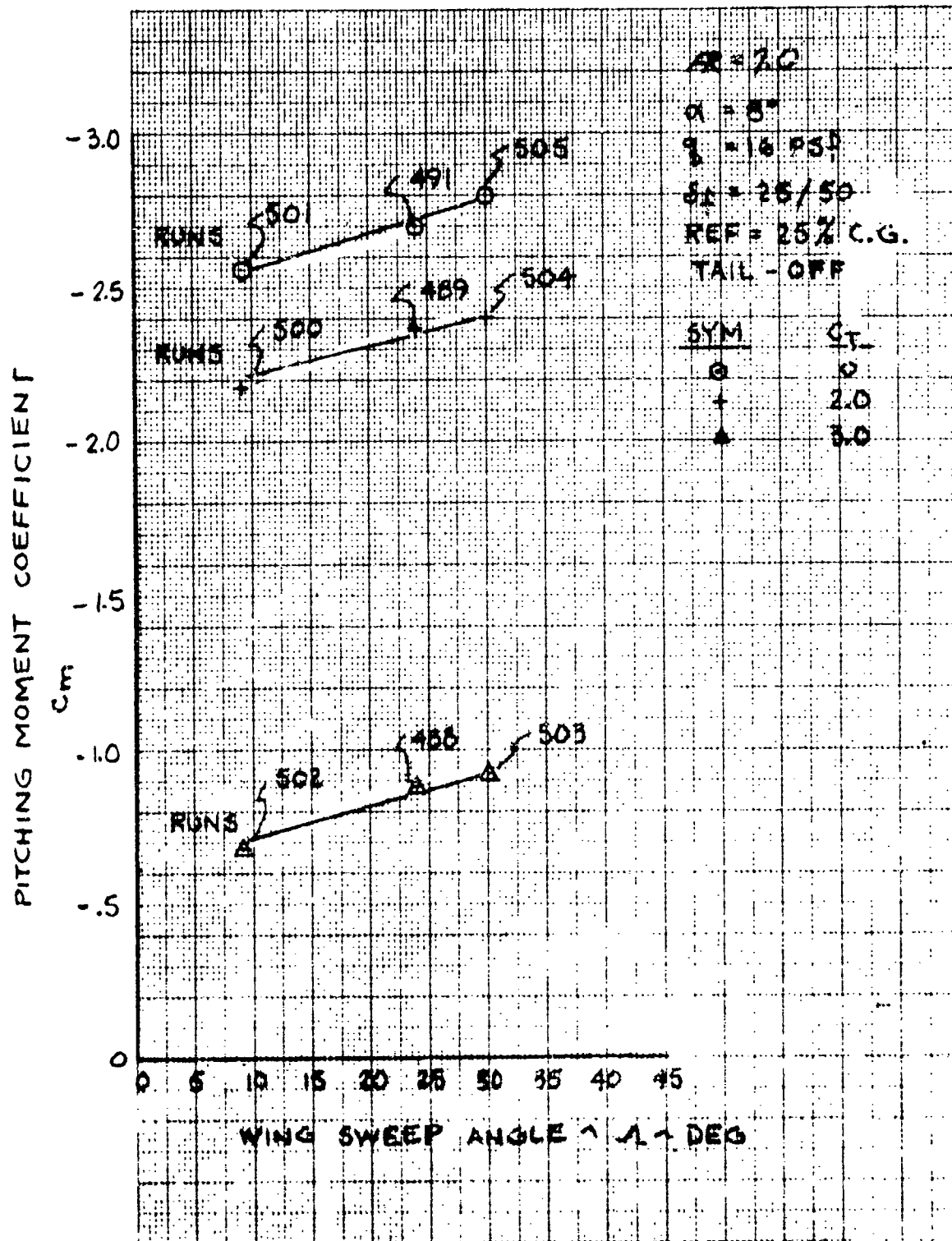
CHANGE OF PITCHING MOMENT COEFFICIENT
DUE TO CHANGE IN WING SWEEP ANGLE



WING SWEEP ANGLE EFFECTS ON PITCHING
MOMENT COEFFICIENT AT CONSTANT ANGLE
OF ATTACK.

Figure 4.3.3

LSWT-090



WING SWEEP ANGLE EFFECTS ON PITCHING
MOMENT COEFFICIENT AT CONSTANT ANGLE OF ATTACK

Section V

ASPECT RATIO

Two wings of different aspect ratio were tested by NR on the MST model. The wing of the basic configuration with an $AR = 7.0$ and an alternate wing with an $AR = 10.0$ were evaluated during the LSWT-090 wind tunnel test. Both wings were mounted to the model fuselage so as to position the quarter chord points of their respective MAC's at F.S. 38.155. Each wing was 10.3214 ft.² in total area and the quarter chord of each wing was swept to 24 degrees. The \bar{c} of the $AR = 7.0$ wing was 15.4636 inches on a 51.00-inch semi-span and the \bar{c} of the $AR = 10.0$ wing was 12.9377 inches on a 60.957-inch semi-span.

The $AR = 10.0$ wing was tested with the 25°/50° full span double slotted flaps only. The inboard Krueger section was not available for this test. This wing was tested at various C_{μ} 's tail-off and tail-on.

5.1 EFFECTS ON LIFT

Figure 5.1.2 shows that for any angle of attack less than α_{stall} the $AR = 10.0$ wing demonstrates positive lift coefficient increments when compared with the $AR = 7.0$ wing. The $AR = 10.0$ wing, however, stalls at a much lower angle of attack as can be seen in Figures 5.1.2 and 5.1.3 when both wings are blown. One reason for the sharp decay in the $AR = 10.0$ wing α_{stall} angles may be possibly a span effect. A smaller area of the $AR = 10.0$ wing is immersed in the engine exhaust plume due to the increased span than is with respect to the $AR = 7.0$ wing. Hence the phenomenon of super-circulation is experienced by a greater portion of the $AR = 7.0$ wing thereby possibly enhancing its stall characteristics over that of the $AR = 10.0$ wing.

5.2 EFFECTS ON DRAG

Due to the increase in aspect ratio of 30 percent, all drag coefficients are lower for the $AR = 10.0$ wing than for the $AR = 7.0$ wing because of an approximate 30 percent reduction in the wing induced drag. Since the wing areas are the same the wing profile drag levels are, for all practical purposes, the same. Figure 5.2.1 shows this reduction in drag coefficient and Figures 5.2.2 and 5.2.3 are the plotted wind tunnel data points except as noted.

5.3 EFFECTS ON PITCHING MOMENT

Figure 5.3.1 shows that going from an $AR = 7.0$ wing to an $AR = 10.0$ wing introduces destabilizing tendencies at high power and angle of attack settings.

As was mentioned in Section 5.1 the reduction in influence of power effects on the $AR = 10.0$ wing due to increased span will cause this wing's center of pressure to move forward on the wing's MAC for any given power level thus causing the nose-up tendencies.

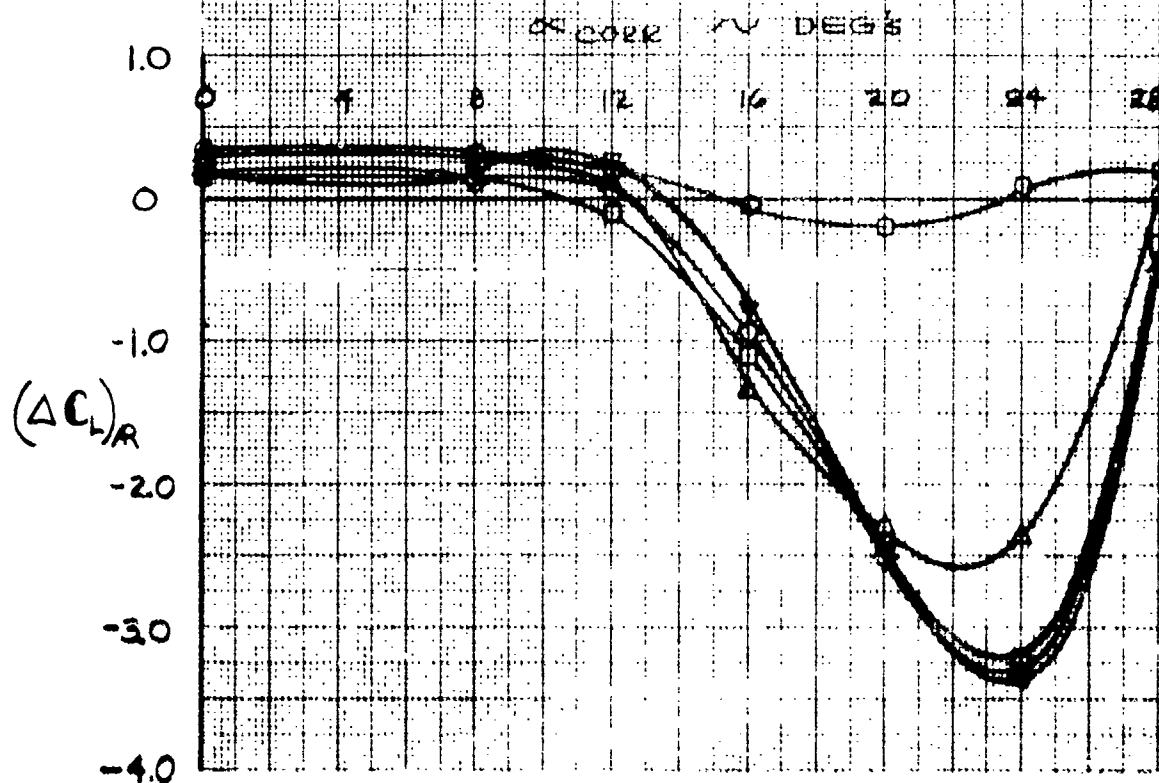
Figures 5.3.2 and 5.3.3 present plotted wind tunnel test data except as noted.

LSWT-040

$$(\Delta C_L)_R = C_{LR=10} - C_{LR=7}$$

C_L	RUNS
0	542 - 468
1.0	543 - INTERP
2.0	544 - 497/490
3.0	INTERP - 491
3.28	545 - INTERP

TAIL OFF
 $\gamma = 16^\circ$ PSF
 $\delta = 25^\circ/50^\circ$
 INSD KRUEGER REMOVED
 $\delta_{SP} = -10^\circ$
 TYPE T PYLON
 (SWIVELLING)

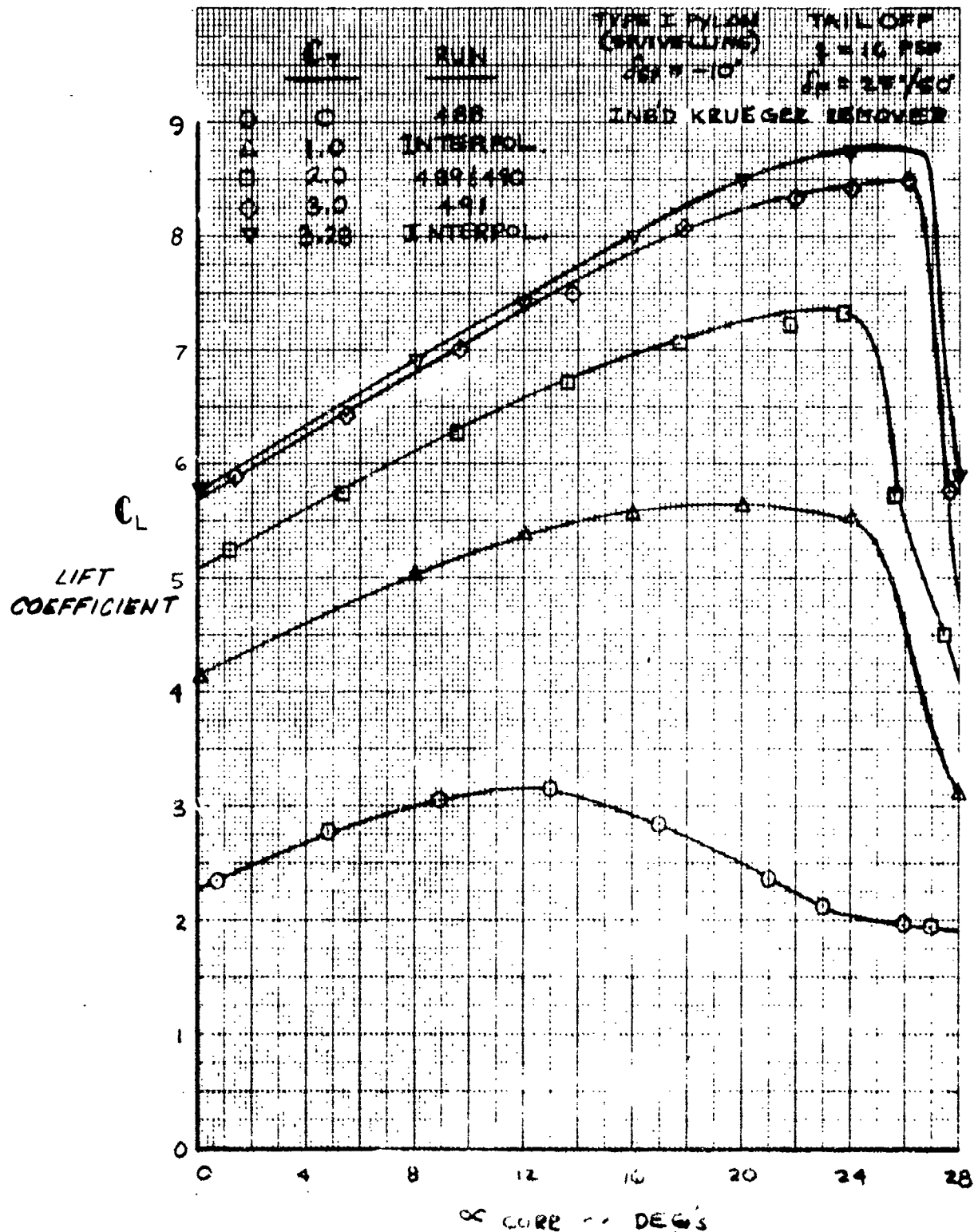


EFFECT OF ASPECT RATIO CHANGE ON LIFT

COEFFICIENT

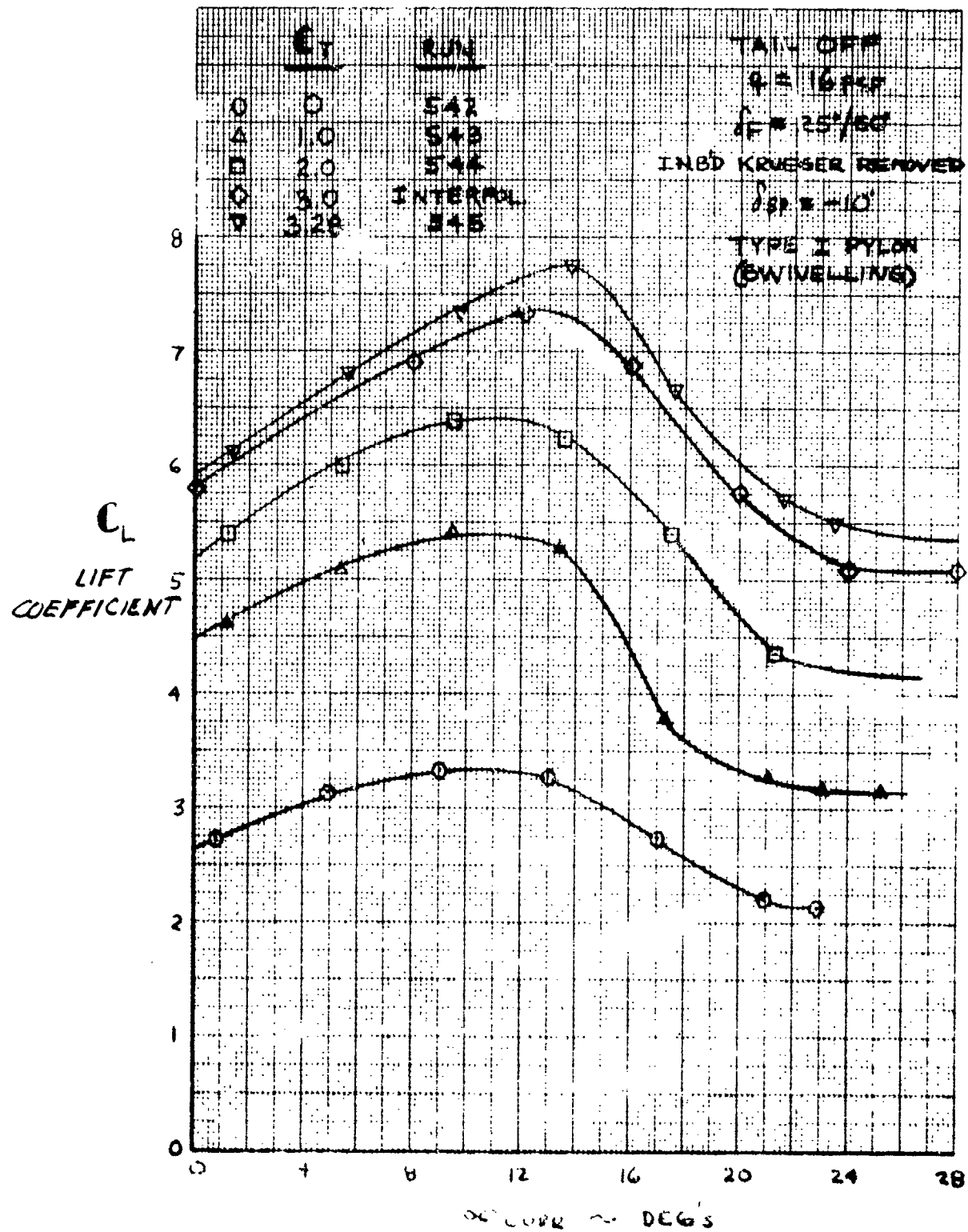
Figure 5.1.1

LSWT-090



TOTAL POWERED LIFT COEFFICIENT FOR AR:7 WING

LSWT-090



TOTAL POWERED LIFT COEFFICIENT FOR AR=10 WING

LSWT-090

$$(\Delta C_D)_R = C_{DA=10} - C_{DA=7}$$

C_T RUNS

○	0	542 - 488
△	10	543 - INTERP.
□	20	544 - 489/410
◇	30	INTERP. 411
▽	3.28	545 - INTERP.

TAIL OFF

$\frac{1}{2} = 16$ PSF

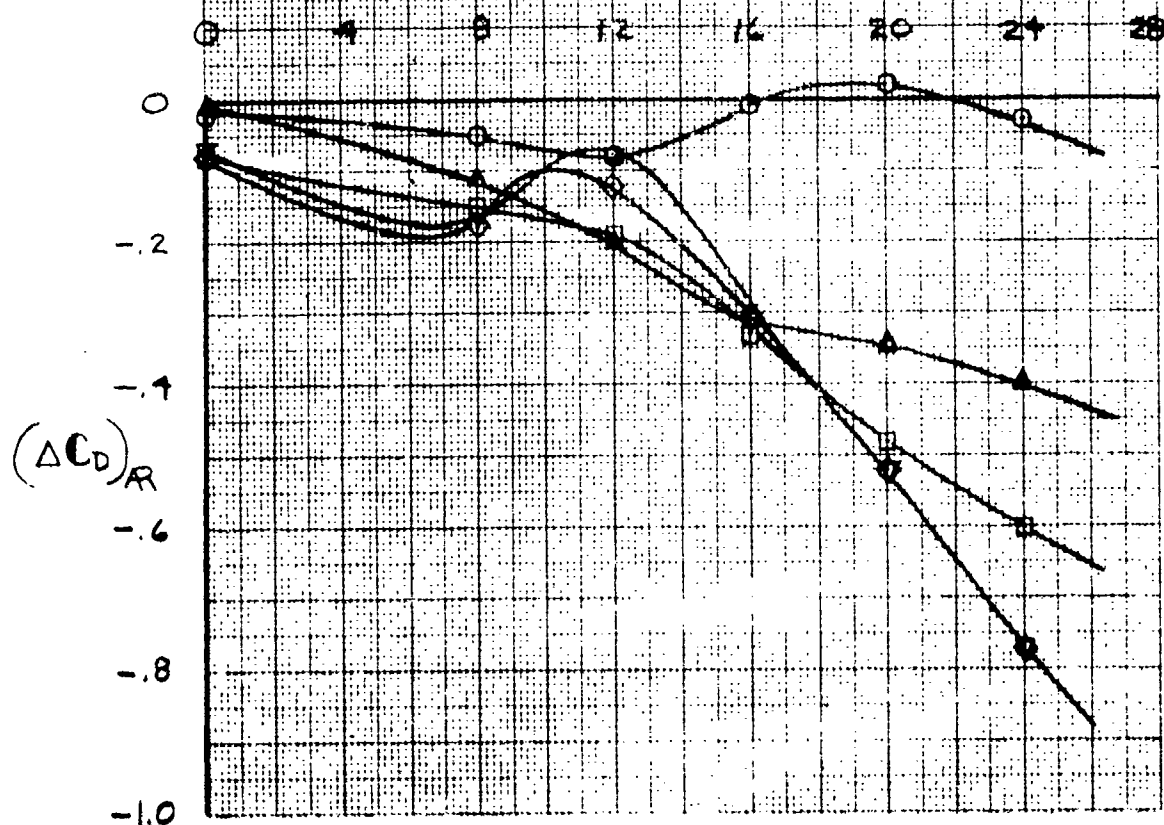
$\rho = 25/50$

INBD KRUEGER REMOVED

$\delta_{LP} = -10^\circ$

TYPE T FYLON
(SWIVELLING)

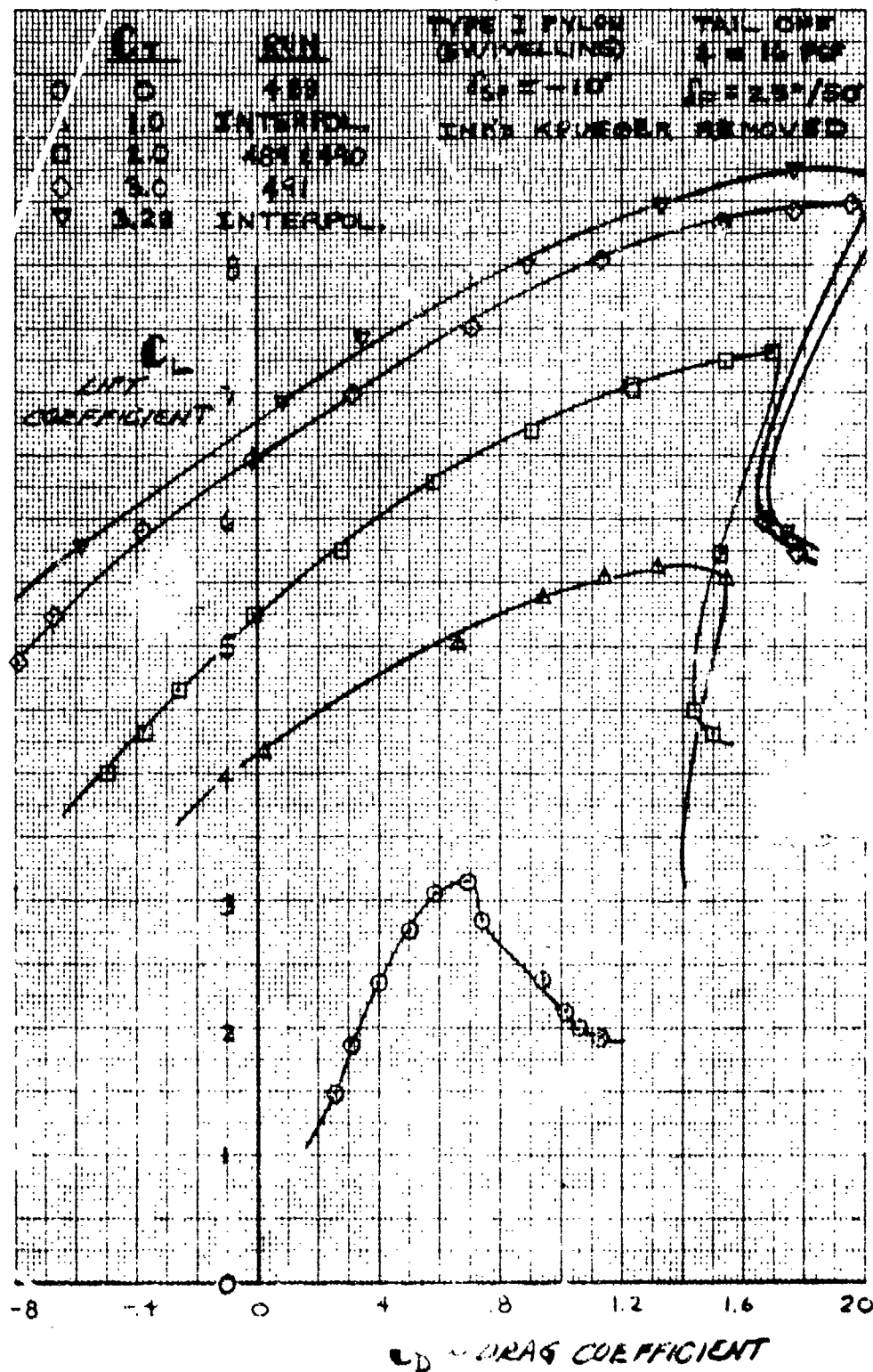
DC CORR \sim DEG $\frac{1}{2}$



EFFECT OF ASPECT RATIO CHANGE ON DRAG
COEFFICIENT

Figure 5.2.1

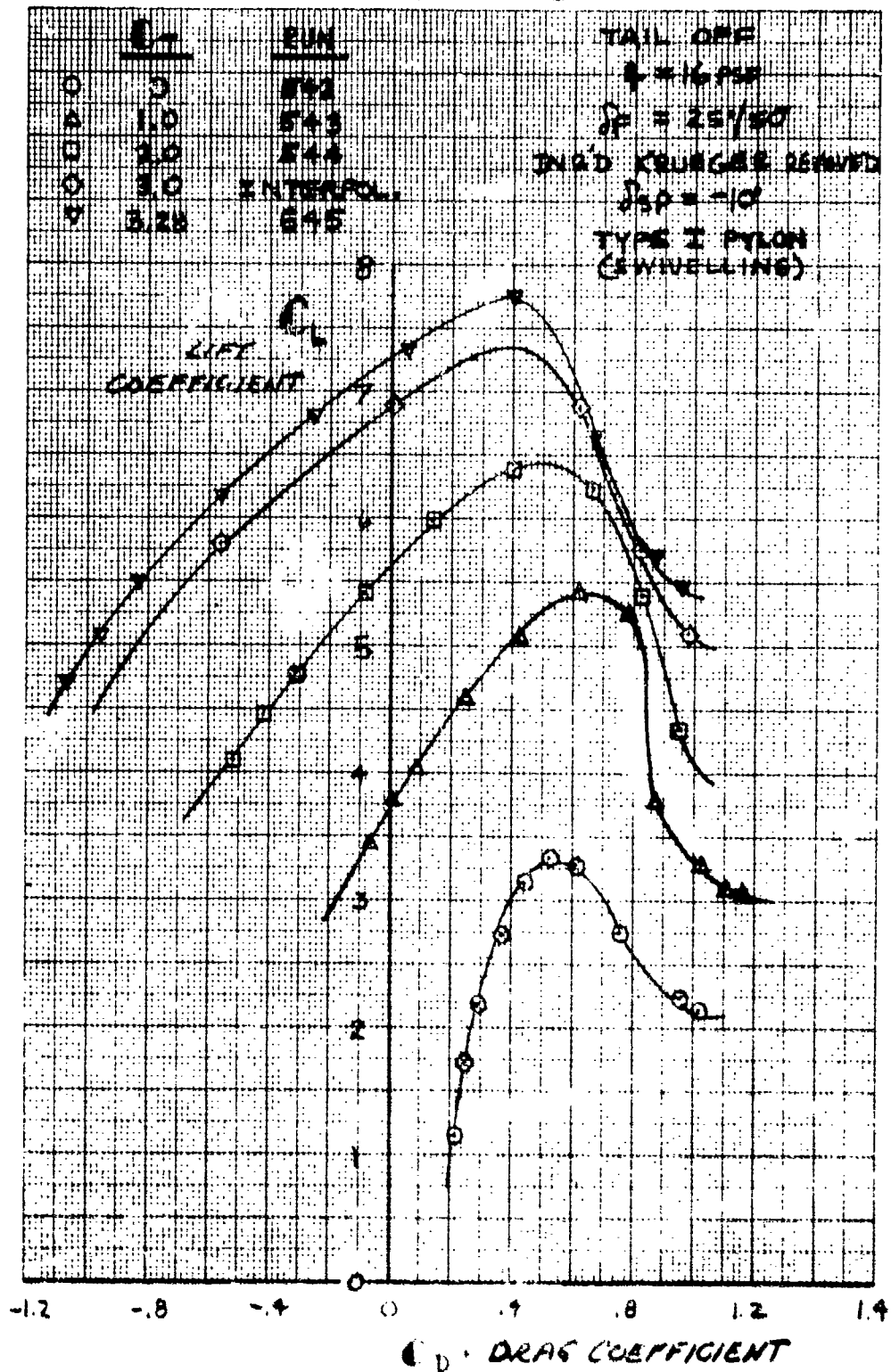
LSWT-090



TOTAL POWERED DRAG COEFFICIENT
FOR $AR=7$ WING

Figure 8.2.2

LSWT - 090



TOTAL POWERED DRAG COEFFICIENT
FOR AR=10 WING

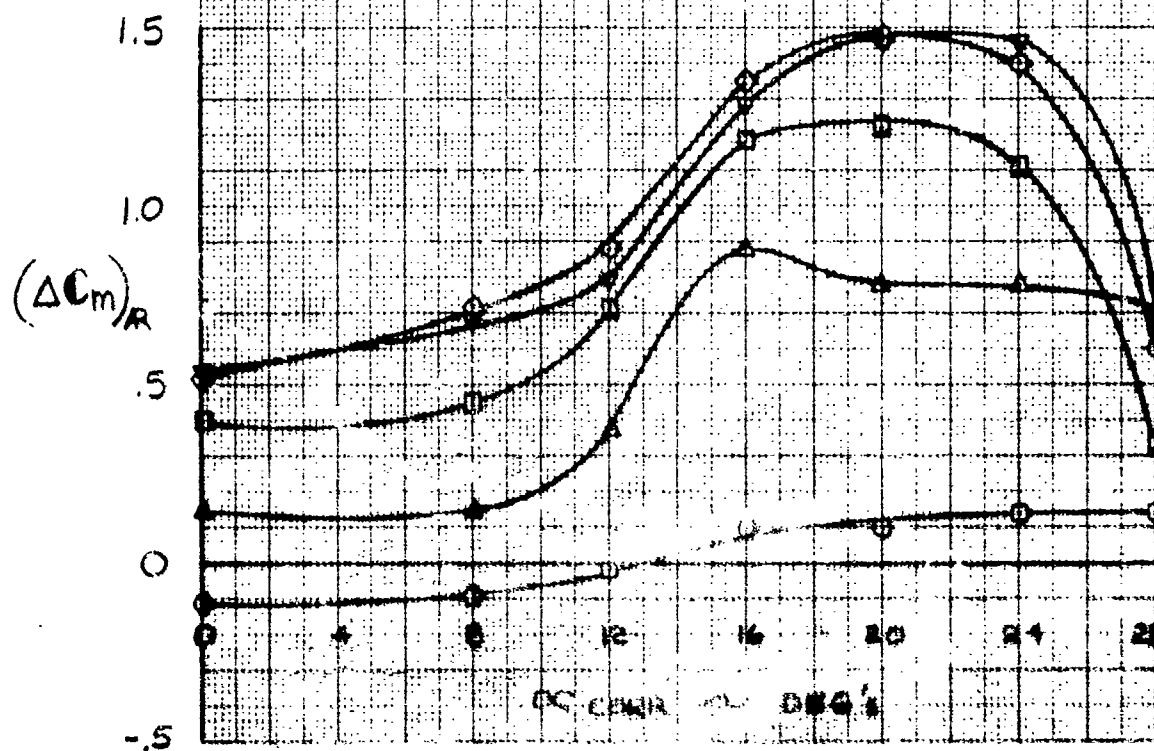
Figure 5.2.3

LSWT-090

$$(\Delta C_m)_R = C_{mR=10} - C_{mR=7}$$

	C_T	RUNS
O	0	542 - 488
A	1.0	543 - INTERP
B	2.0	544 - 481/480
C	3.0	INTERP - 481
V	3.23	545 - INTERP

TAIL OFF
 $\lambda = 1.8 \text{ REF}$
 $\delta_f = 25/50^\circ$
 INED KRUEGER REMOVED
 $\delta_s = -10^\circ$
 TYPE I PYLON
 (SYIVELLING)

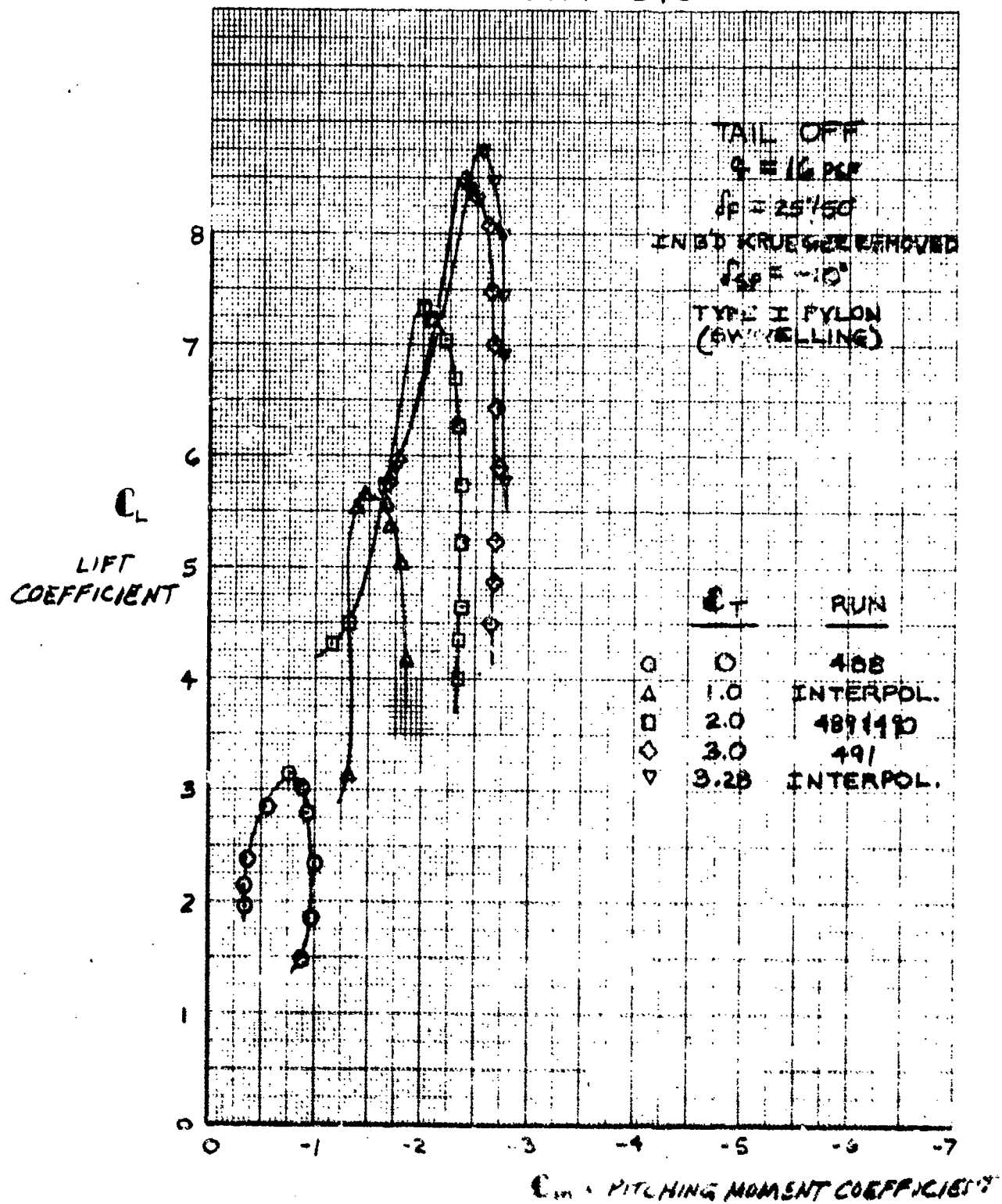


EFFECT OF ASPECT RATIO CHANGE ON PITCHING MOMENT

COEFFICIENT

Figure S.3.1

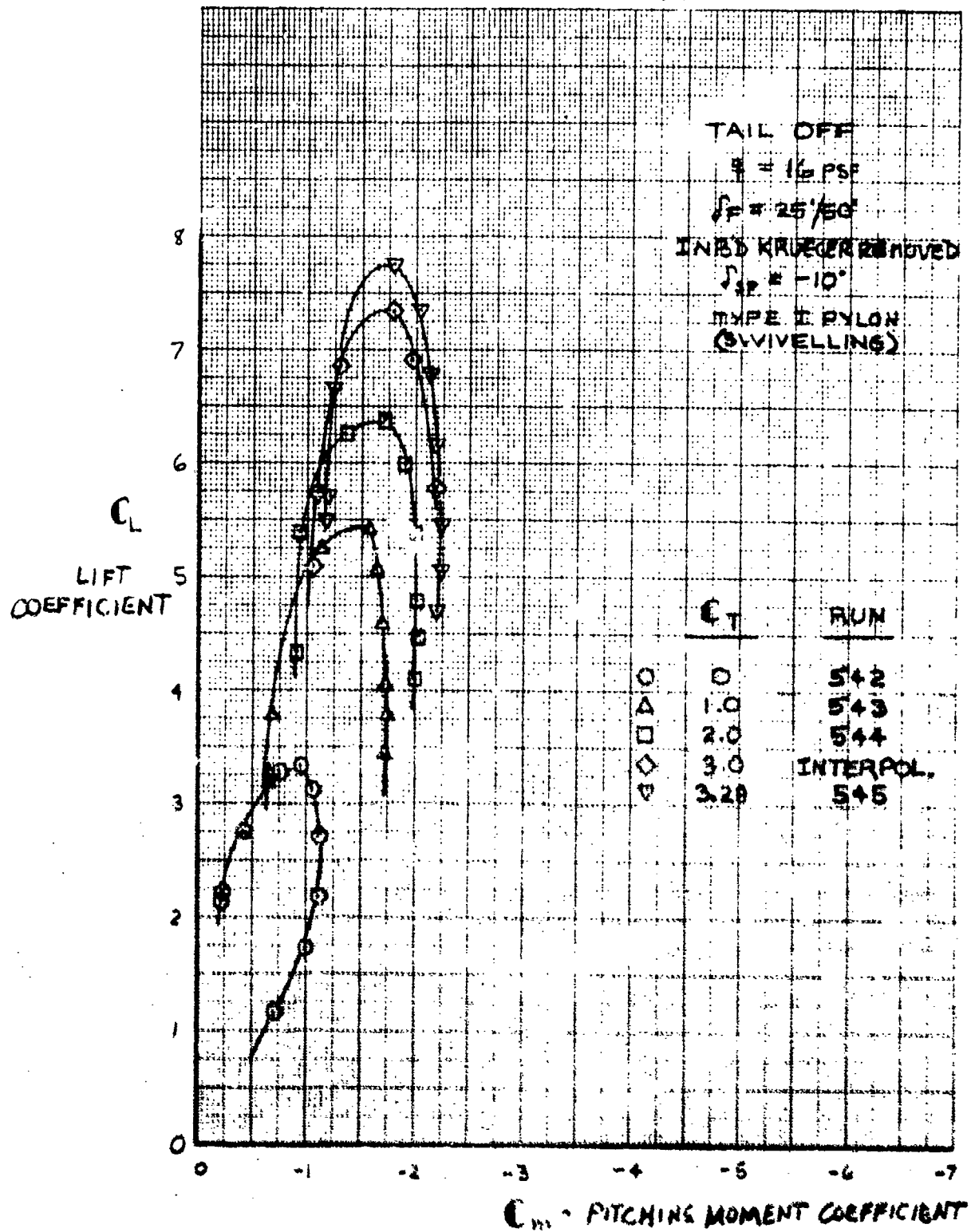
LSWT-090



TOTAL POWERED PITCHING MOMENT COEFFICIENT
FOR AR=7 WING

Figure S.3.2

LSWT-090



TOTAL POWERED PITCHING MOMENT COEFFICIENT
FOR AR=10 WING

Figure 5.3.3

Section VI

DOWNWASH

Downwash angles were determined through the use of a flow field pressure rake. The pressure rake measured the environmental in-flow angles experienced at the location of the horizontal tail as the rake was mounted on top of the vertical fin in place of the horizontal tail. It was mounted in the plane of the left hand horizontal stabilizer chord line in the "T" or high position and located axially such that the pressure sensors of the second of the five probes outboard from the fuselage centerline was congruent with the horizontal stabilizer MAC quarter chord point. The right hand horizontal stabilizer was removed for this test series. The rake was fitted with the five probes each having four orthogonally located static pressure orifices and a single center total pressure orifice. The five probes were located spanwise five inches over centers so that the outboard most probe was beyond the horizontal tip, $Y/(b_H/2) = 1.12$.

The measured in-flow angles are calibrated angles and represent local horizontal tail angles of attack (α_T) at $i_H = 0$. Averaging their spanwise readings, weighting the average in favor of the probe representing the horizontal tail MAC, the downwash factor ($1 - d\epsilon/d\alpha$) can be determined.

6.1 EFFECTS OF POWER

Power effects on downwash angle at $\alpha = 0^\circ$ are presented in Figure 6.1.1 for varying wing flap deflection and engine simulator nozzle deflection. The angle, ϵ_0 , presented in this figure is measured with respect to the ambient freestream streamlines. These data are for the clustered engine configuration. Figure 6.1.3 presents similar data but for the spread engine configuration and also shows effects on downwash at $\alpha = 0$ for various leading edges.

Figures 6.1.2 and 6.1.4 demonstrate power effects on downwash factor ($1 - d\epsilon/d\alpha$) for the clustered and spread engine configurations respectively. The clustered engine plot also includes effects of varying the wing leading and trailing edge geometries. Quantitatively the downwash factors of both engine configurations are comparable with each other.

Figures 6.1.5 through 6.1.8 inclusive are plotted wind tunnel test data points.

6.2 EFFECTS OF ENGINE NOZZLE DEFLECTION AND FLAP DEFLECTION

The effects of wing flap and engine exhaust nozzle deflections on powered downwash angle are summarized in Figure 6.2.1 at $\alpha = 0^\circ$. It is apparent that considerable scatter in the downwash angle exists.

Figures 6.2.2 through 6.2.11 inclusive are plotted wind tunnel test data points, showing unexpected trends in the effect of flap angle or considerable data scatter.

6.3 EFFECTS OF VARIOUS LEADING EDGE DEVICES

The effects of symmetrical various leading edge devices on powered downwash angle are presented in Figure 6.3.1 at $\alpha = 0^\circ$. The entire leading edge of the wing was clean with the exception of the outboard most 31.6 percent of the semispan where the various leading edges were tested. The short and long chord Kruegers as well as the blown leading edge present little influence on downwash angles at the tail.

Figures 6.3.2 through 6.3.6 inclusive are plotted wind tunnel test data points.

6.4 EFFECTS OF ENGINE SPANWISE LOCATION

The engine nacelles were perturbed in an outboard direction in order to evaluate the effects on downwash of spreading out the powered flow field over the horizontal tail. The inboard nacelles were moved from $Y/(b/2) = 0.247$ out to $Y/(b/2) = 0.350$ and the outboard nacelles were moved further out from $Y/(b/2) = 0.394$ to $Y/(b/2) = 0.550$. Figures 6.4.1 and 6.4.2

show that by spreading out the powered flow field the tail angle of attack variation with model angle of attack is dramatically improved especially at the higher C_{μ} 's.

Figures 6.4.3 and 6.4.4 show the spanwise tail angle of attack variation for the clustered and spread engine configurations.

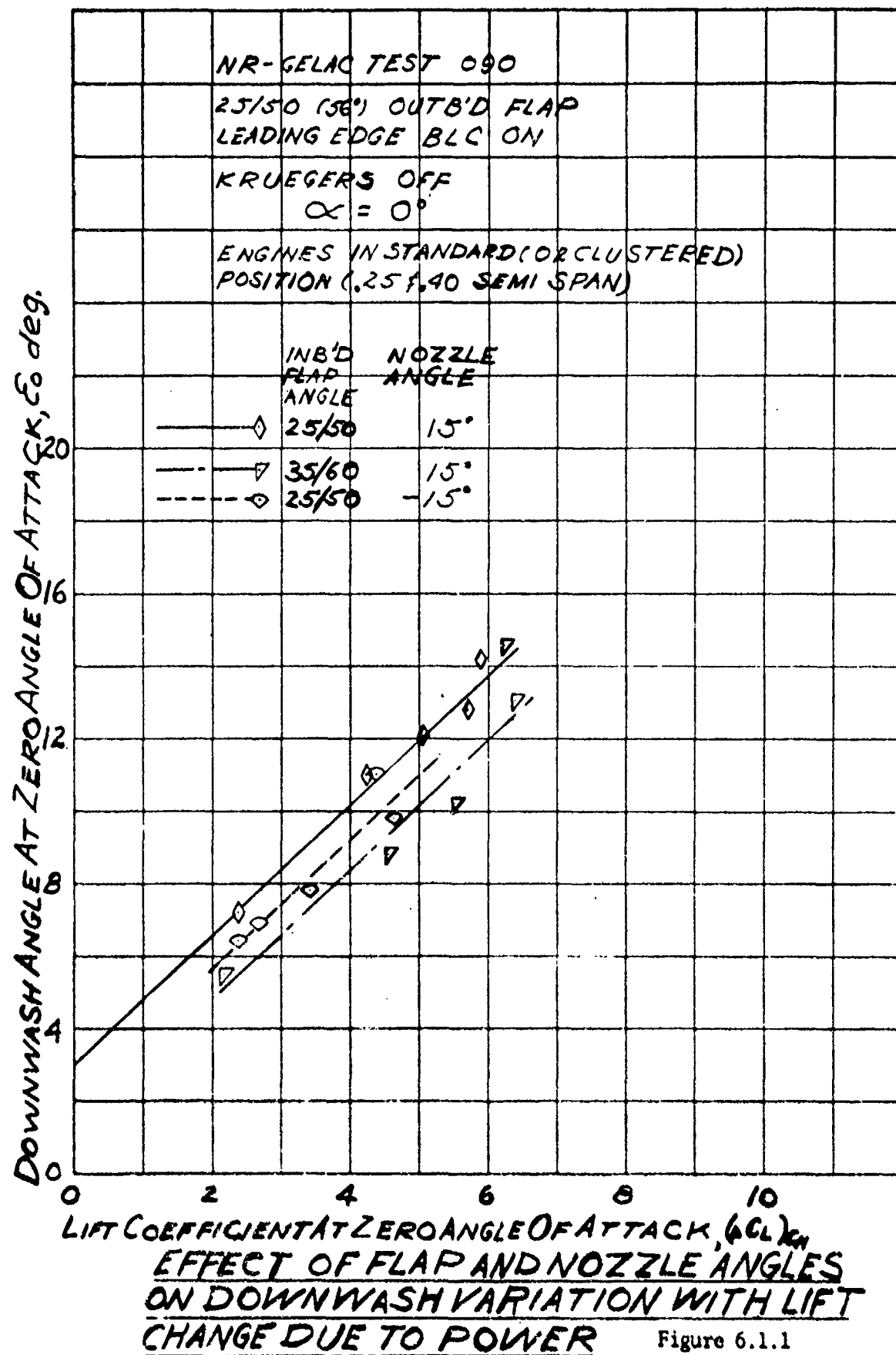


Figure 6.1.1

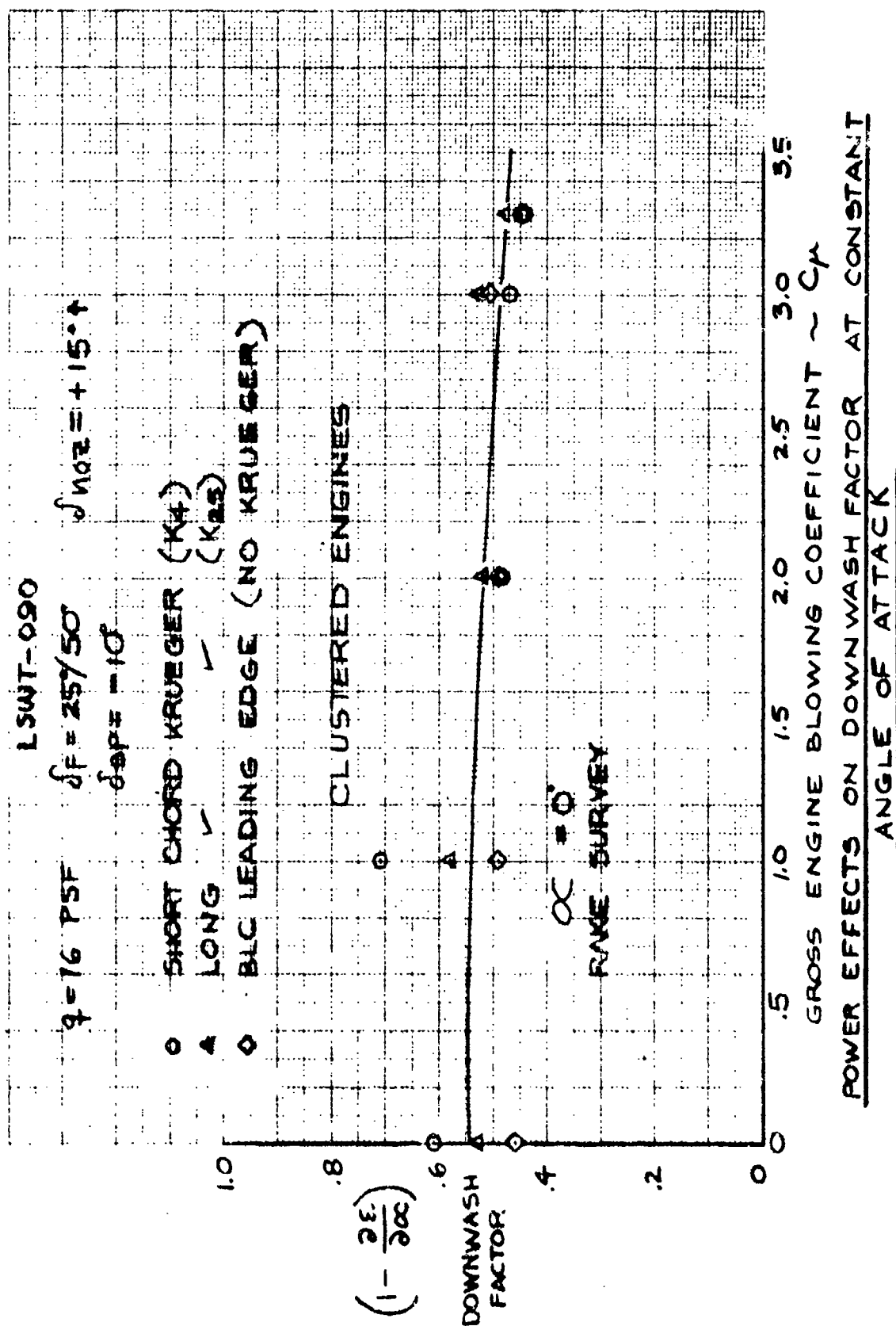


Figure 6.1.2

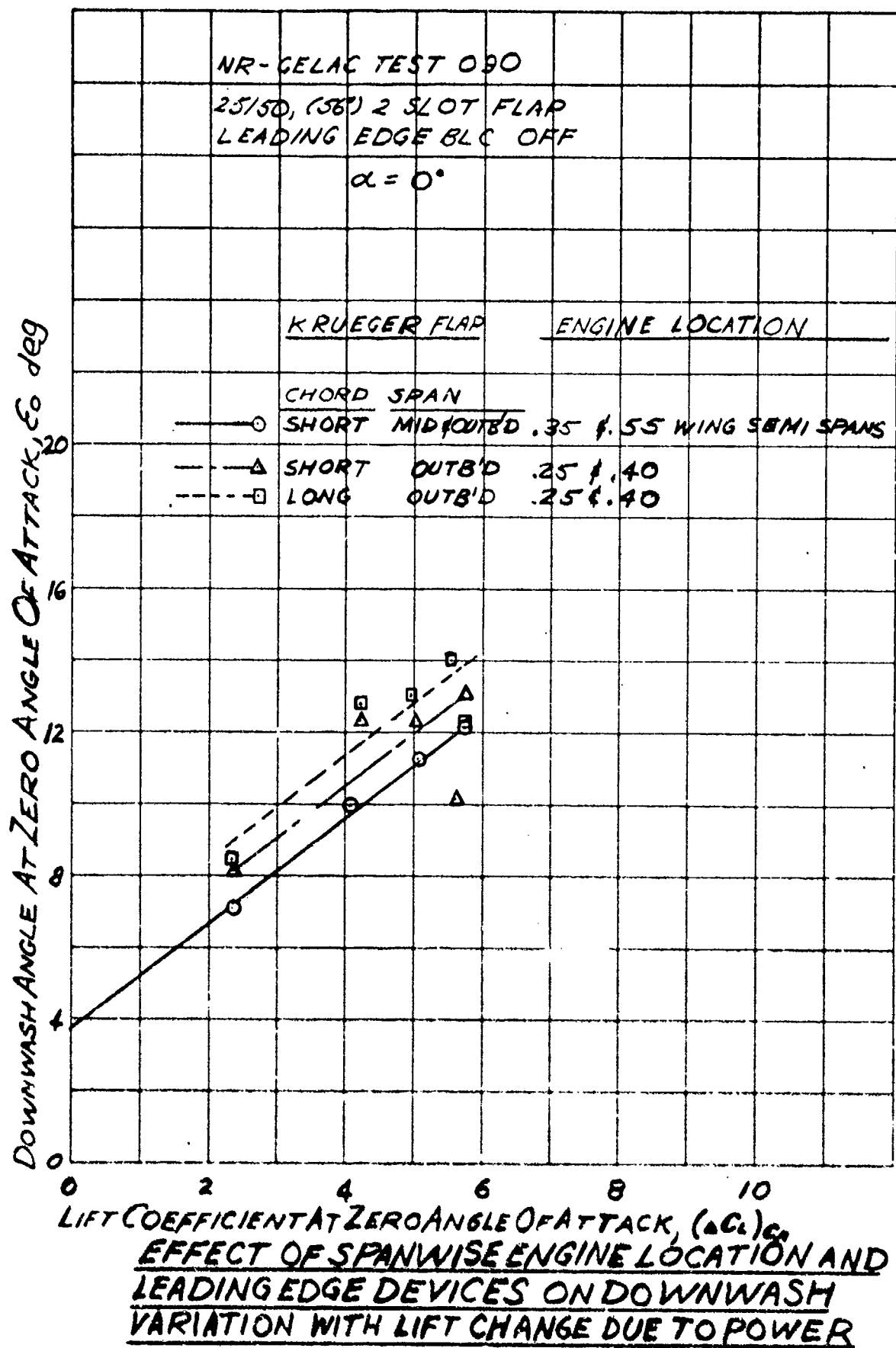


Figure 6.1.3

LSWT-090

$\beta = 16 \text{ psf}$ $\delta_F = 25^\circ/50^\circ$ $\delta_A = +15^\circ$

$\delta_{SP} = -10^\circ$

SPREAD ENGINES

INB'D SHORT CHORD KRUEGER REMOVED

$\left(1 - \frac{\partial \epsilon}{\partial \alpha}\right)$

DOWNWASH
FACTOR

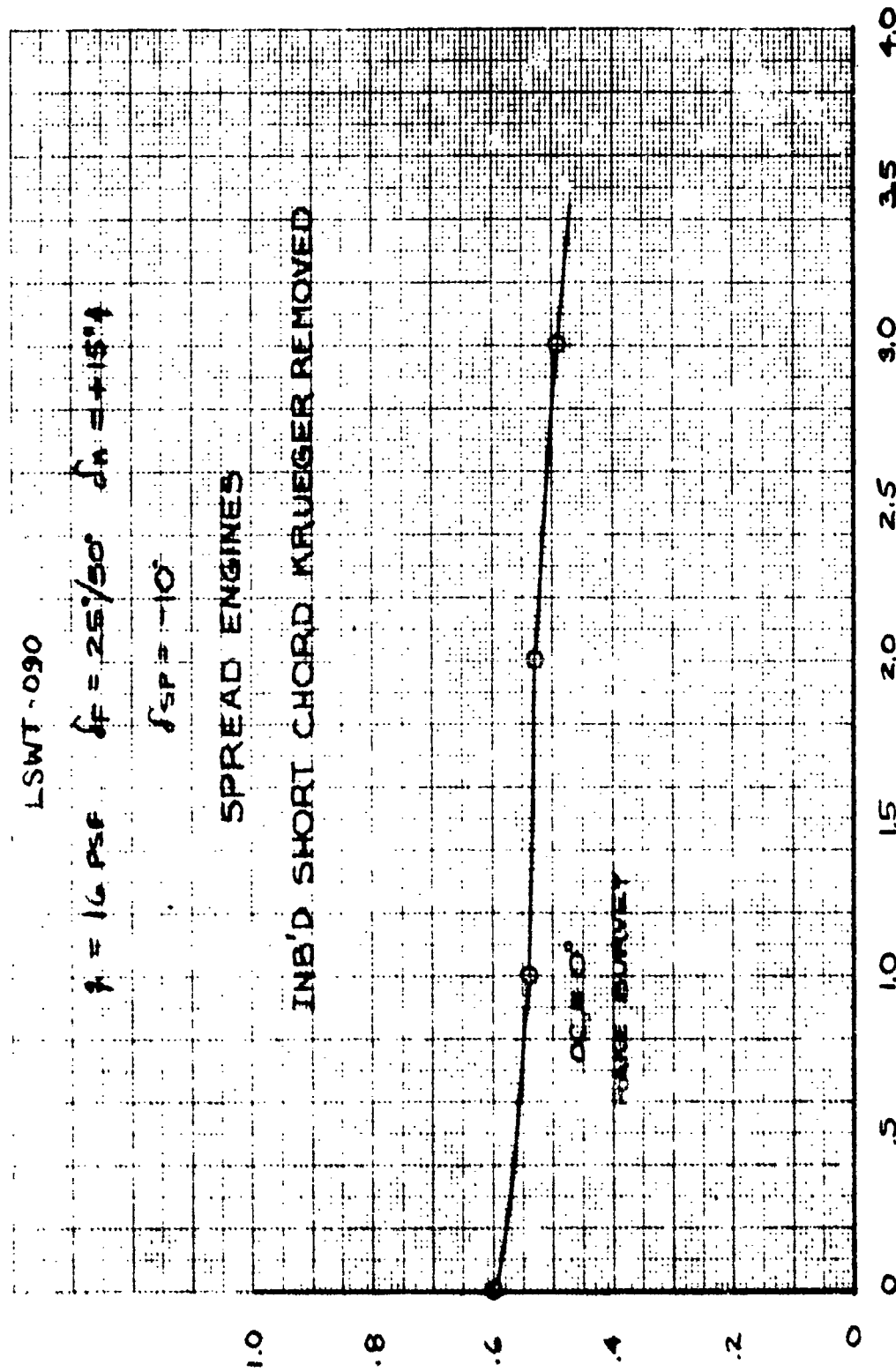


Figure 6.1.4

GROSS ENGINE BLOWING COEFFICIENT $\sim C_\mu$

POWER EFFECTS ON DOWNWASH FACTOR AT CONSTANT ANGLE OF ATTACK

LBWT-090

VARIATION OF HORIZ. TAIL ANGLE WITH ANGLE OF ATTACK EFFECTS OF POWER

SHORT
CHORD KRUEGER (K4 ONLY)

$\delta F = 25^\circ/50^\circ$

$\delta \eta = +15^\circ \uparrow$

$\delta \sigma = -10^\circ$

	RUN	C_T	η
●	396	0	55
○	397	0	16
△	398	1.0	
□	399	2.0	
◇	400	3.0	
▽	401	3.3	

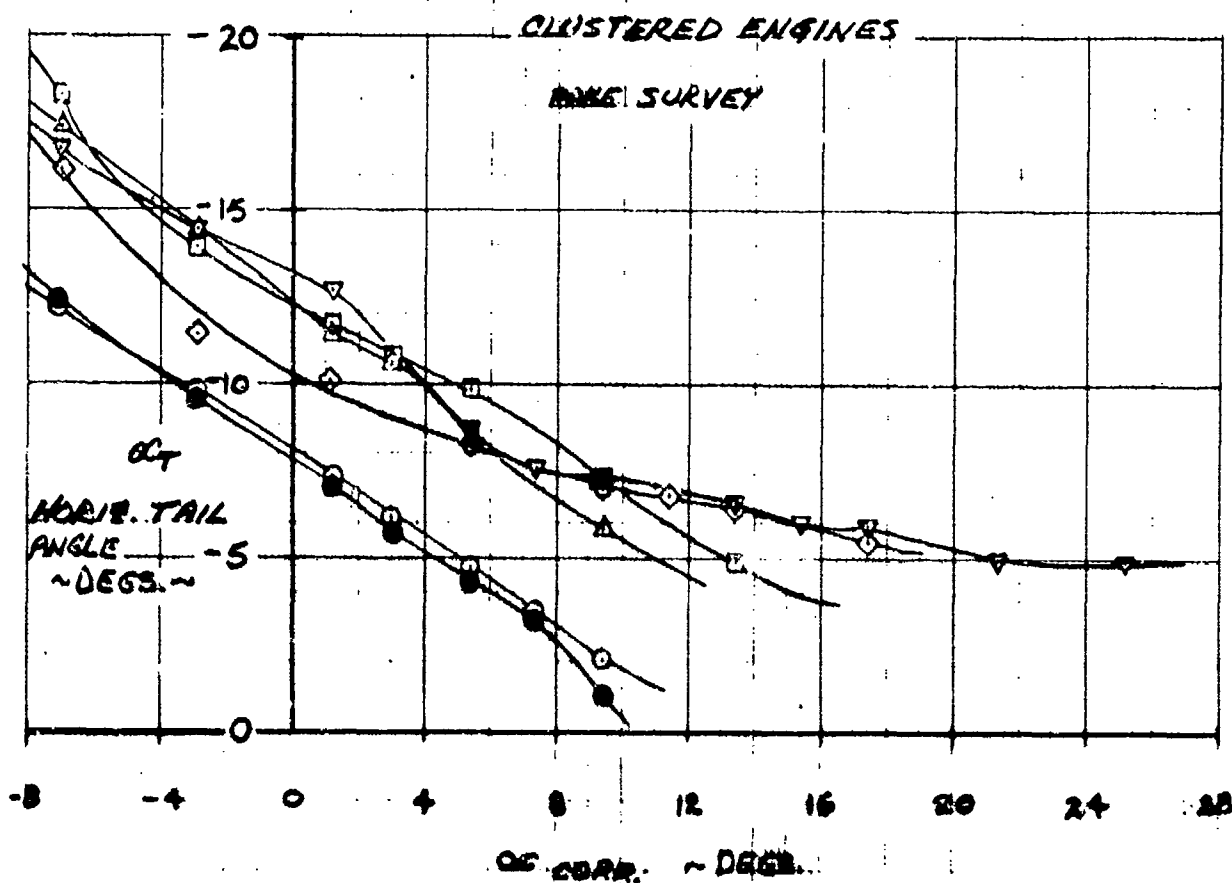


Figure 6.1.3

LSWT-070

VARIATION OF HORIZ. TAIL ANGLE WITH ANGLE OF ATTACK

EFFECTS OF POWER

LONG
CHORD KRUEGER (K₂₅ ONLY)

$$\delta_F = 25^\circ/50^\circ$$

$$\delta_H = +15^\circ \uparrow$$

$$\delta_S = -10^\circ$$

	RUN	C _T	η
○	388	0	16
△	389	1.0	
□	390	2.0	
◇	391	3.0	
▽	392	3.3	
●	393	0	55

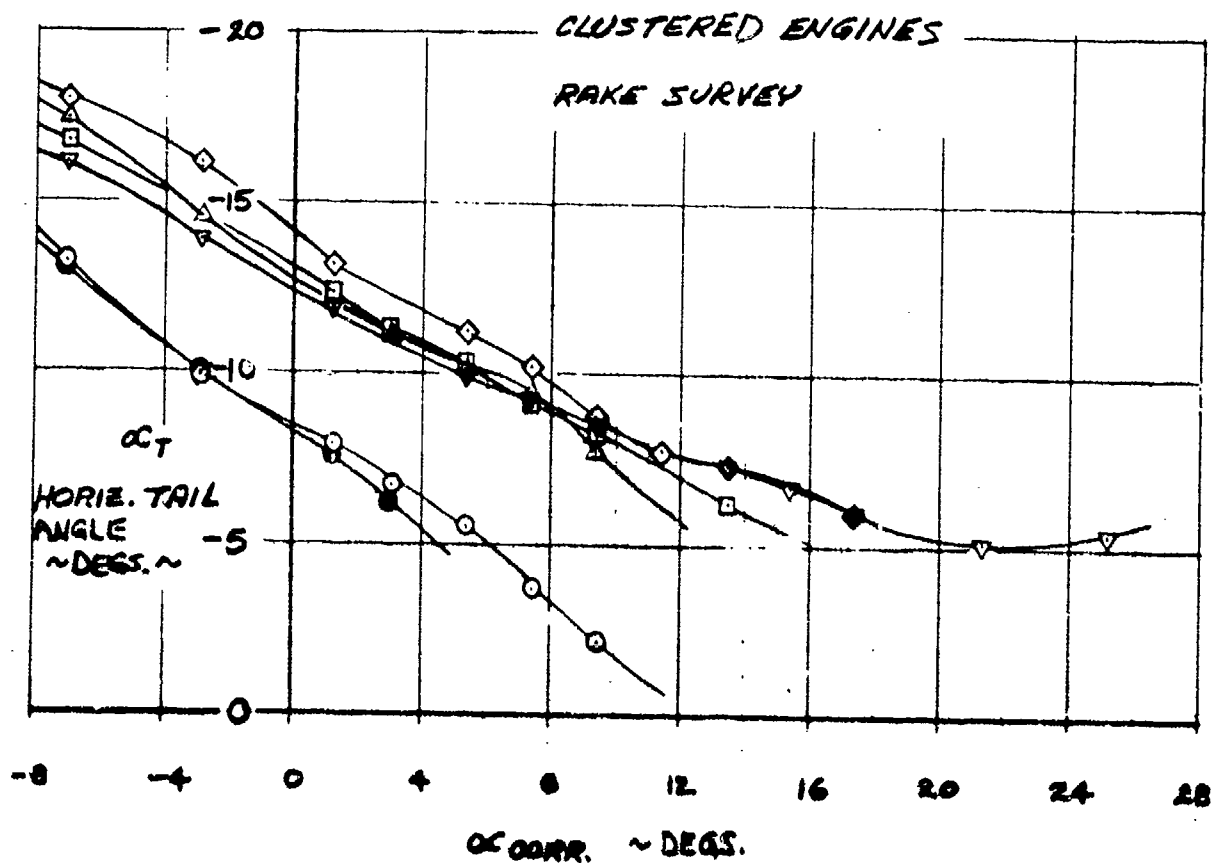


Figure 6.1.6

LSWT-090

VARIATION OF HORIZ. TAIL ANGLE WITH ANGLE OF ATTACK

EFFECTS OF POWER

L.E. BLC (NO KRUEGER)

$\delta F = 25^\circ/50^\circ$

$\delta \eta = +15^\circ \uparrow$

$\delta \text{SP} = -10^\circ$

	RUN	C_T	η
○	376 + 377	0	16
△	378	1.0	
□	379	2.0	
◇	380 + 381	3.0	
▽	382	3.3	

CLUSTERED ENGINES

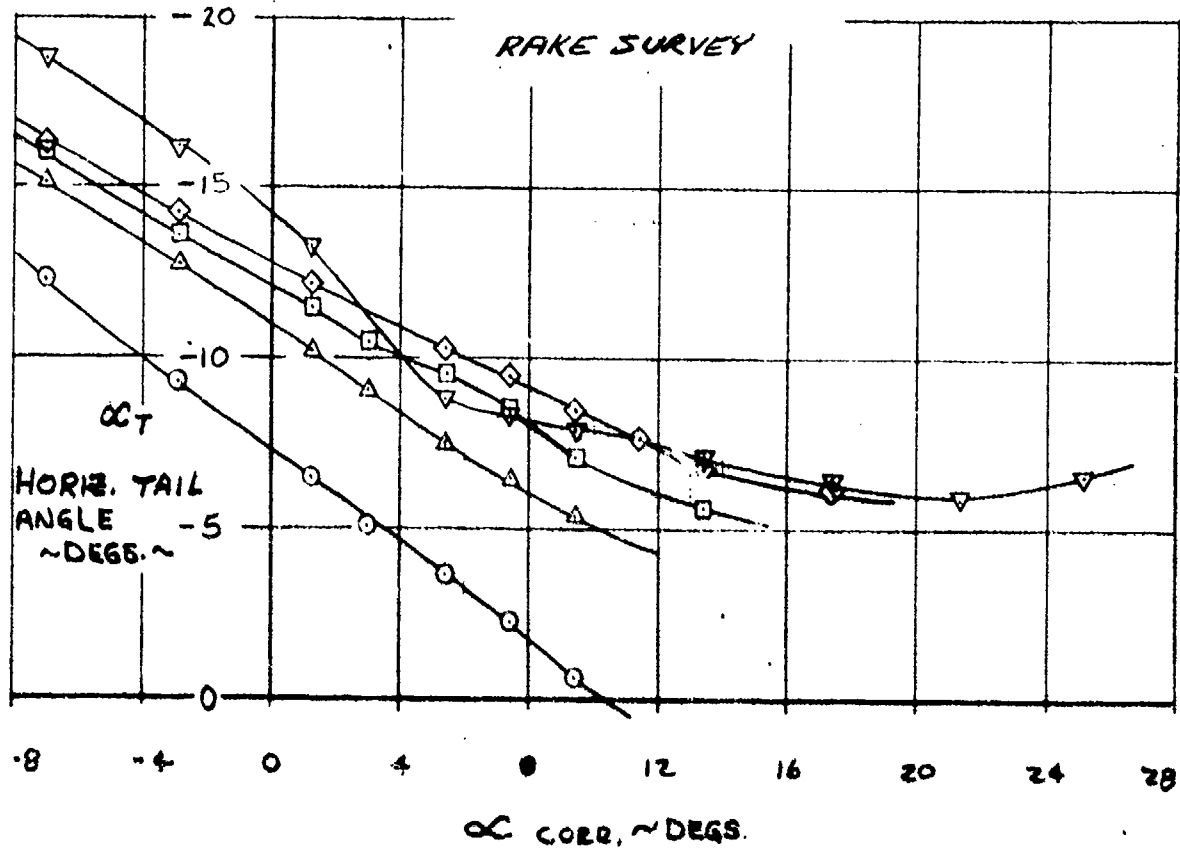
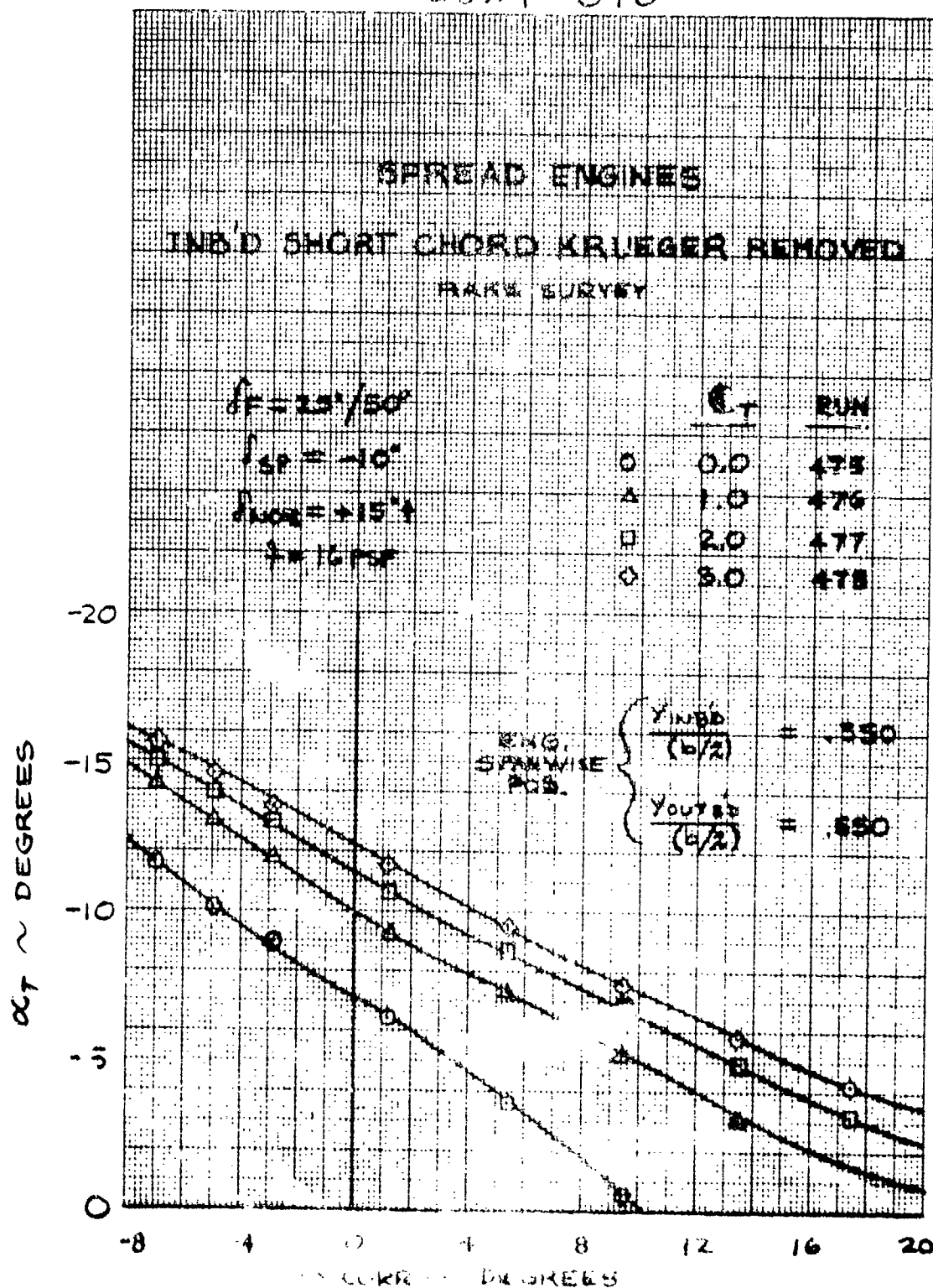
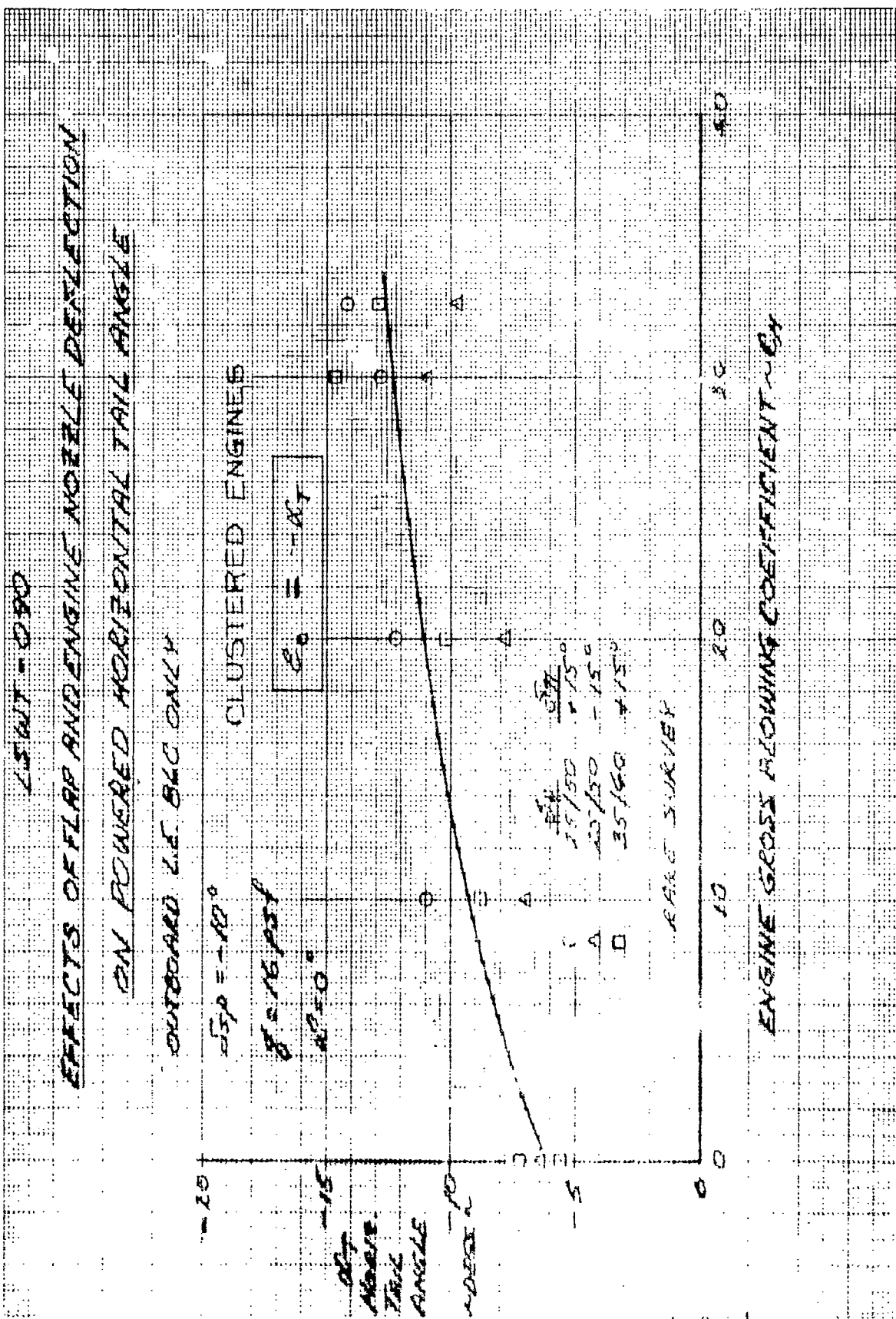


Figure 6.1.7

LSWT-090



VARIATION OF HORIZ. TAIL ANGLE WITH ANGLE OF ATTACK
- EFFECT OF POWER -



LSWT-090

HORIZ. TAIL ANGLE VS ANGLE OF ATTACK

OUTBOARD L.E. BLC ONLY

$C_T = 0$

EFFECTS OF FLAP AND ENGINE NOZZLE DEFLECTION

$q = 16 \text{ psf}$
 $\delta_{sp} = -10^\circ$

	δ_F	δ_n	RUN
○	25°/30°	+15°	376 & 377
△	25°/50°	-15°	383
□	35°/60°	+15°	402

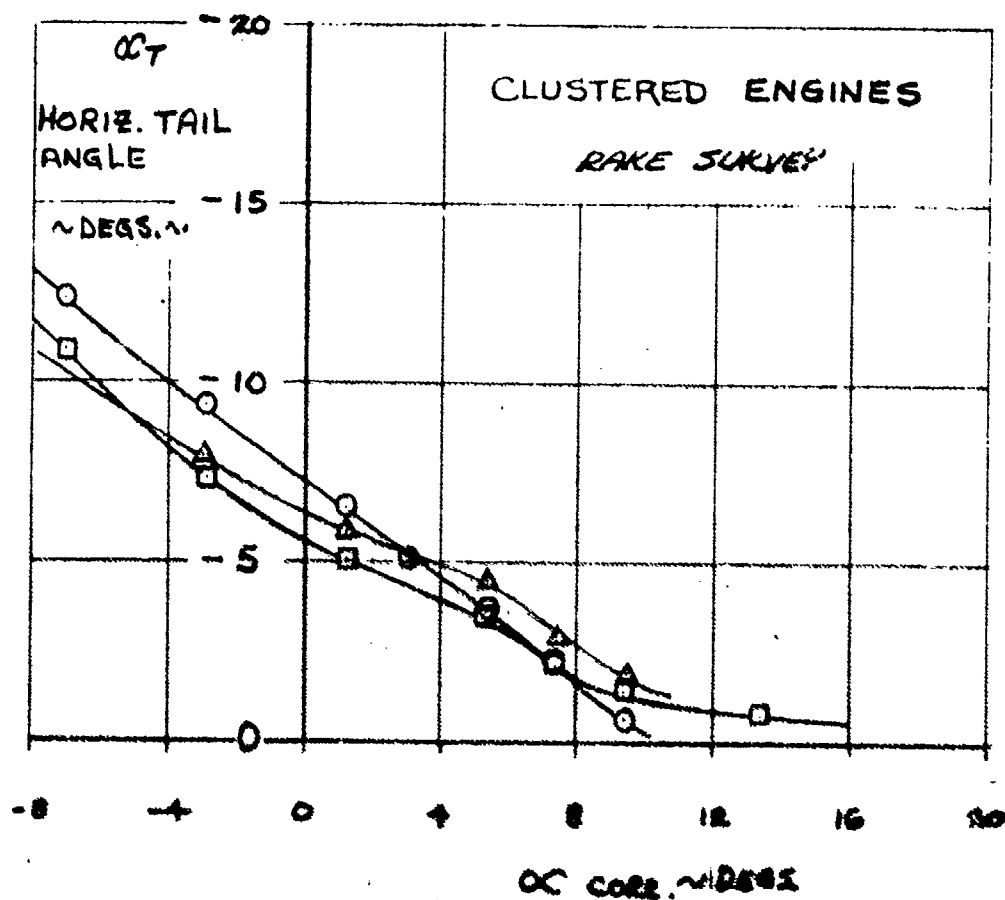


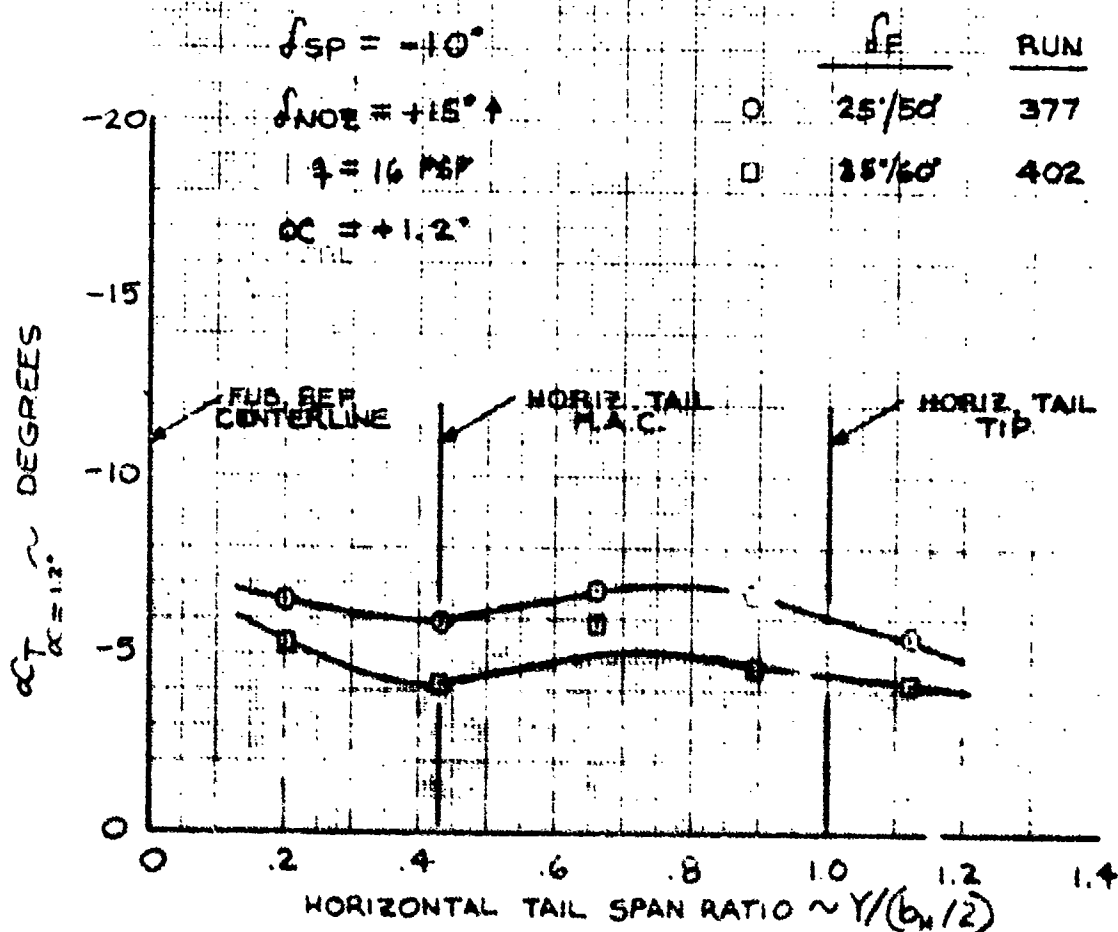
Figure 6.2.2

LSWT-080

CLUSTERED ENGINES WITH OUTBOARD I.E. BLC ONLY

RAKE SURVEY

$$C_T = 0$$



SPANWISE VARIATION OF HORIZONTAL TAIL ANGLE

AT $\alpha = +1.2^\circ$

Figure 6.2.3

LSWT-090

HORIZ. TAIL ANGLE VS. ANGLE OF ATTACK

OUTBOARD L.E. BLC ONLY

$C_T = 1.0$

EFFECTS OF FLAP AND ENGINE NOZZLE DEFLECTION

$q = 16 \text{ psf}$
 $\delta_{sp} = -10^\circ$

	δ_F	δ_n	RUN
○	25°/50°	+15°	378
△	25°/50°	-15°	384
□	35°/60°	+15°	403

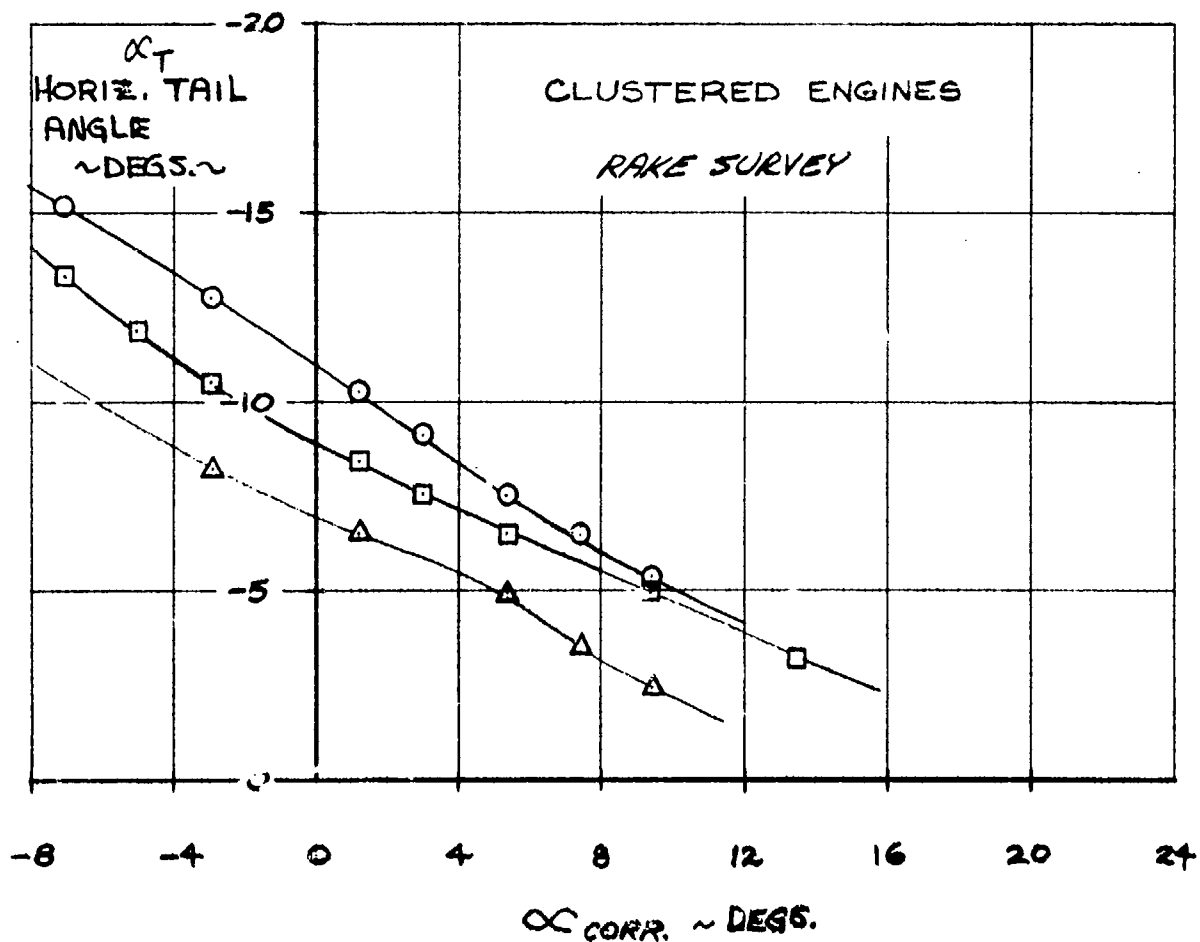


Figure 6.2.4

LSWT-090

CLUSTERED ENGINES
WITH OUTBOARD L.E. BLC ONLY

RAKE SURVEY

$C_T = 1.0$

$\delta_{SP} = -10^\circ$

$\delta_{NOZ} = +15^\circ \uparrow$

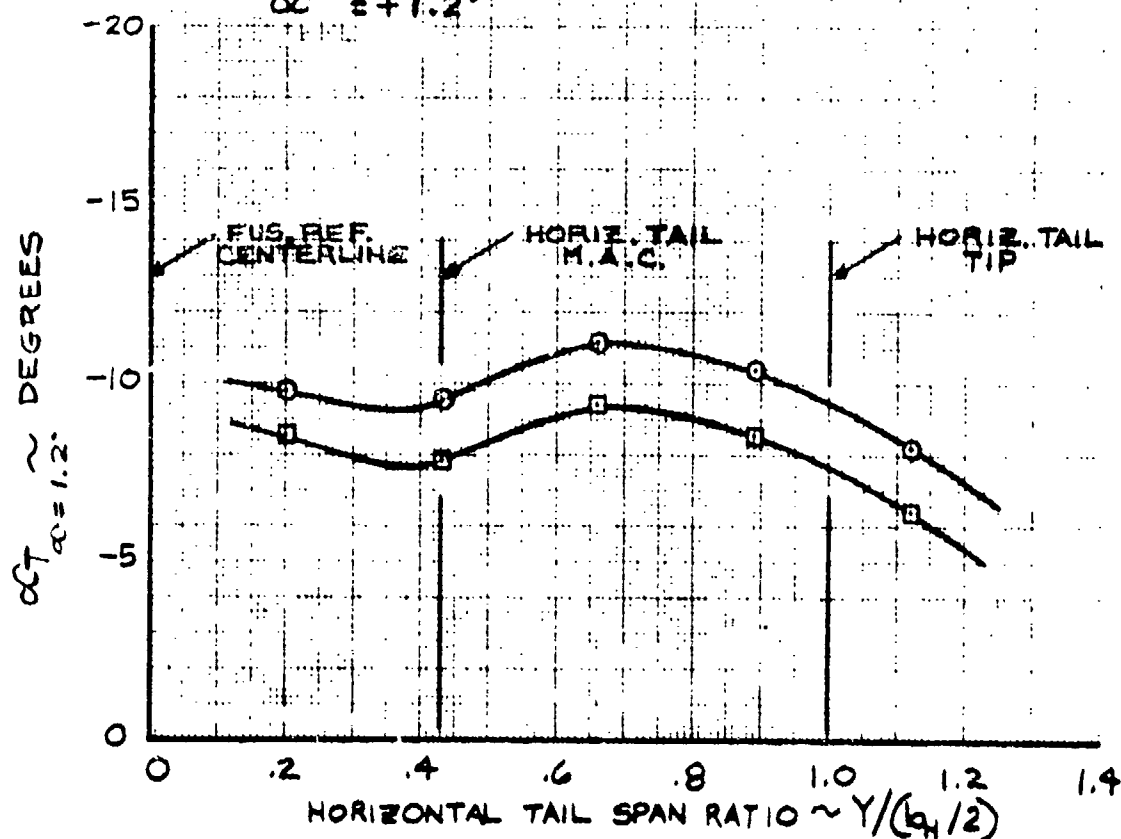
$\delta = 16 \text{ REF}$

$\alpha = +1.2^\circ$

δ_F

RUN

\circ	25/50	378
\square	35/60	403



SPANWISE VARIATION OF HORIZONTAL TAIL ANGLE
AT $\alpha = +1.2^\circ$

LSWT -090

HORIZ. TAIL ANGLE VS. ANGLE OF ATTACK

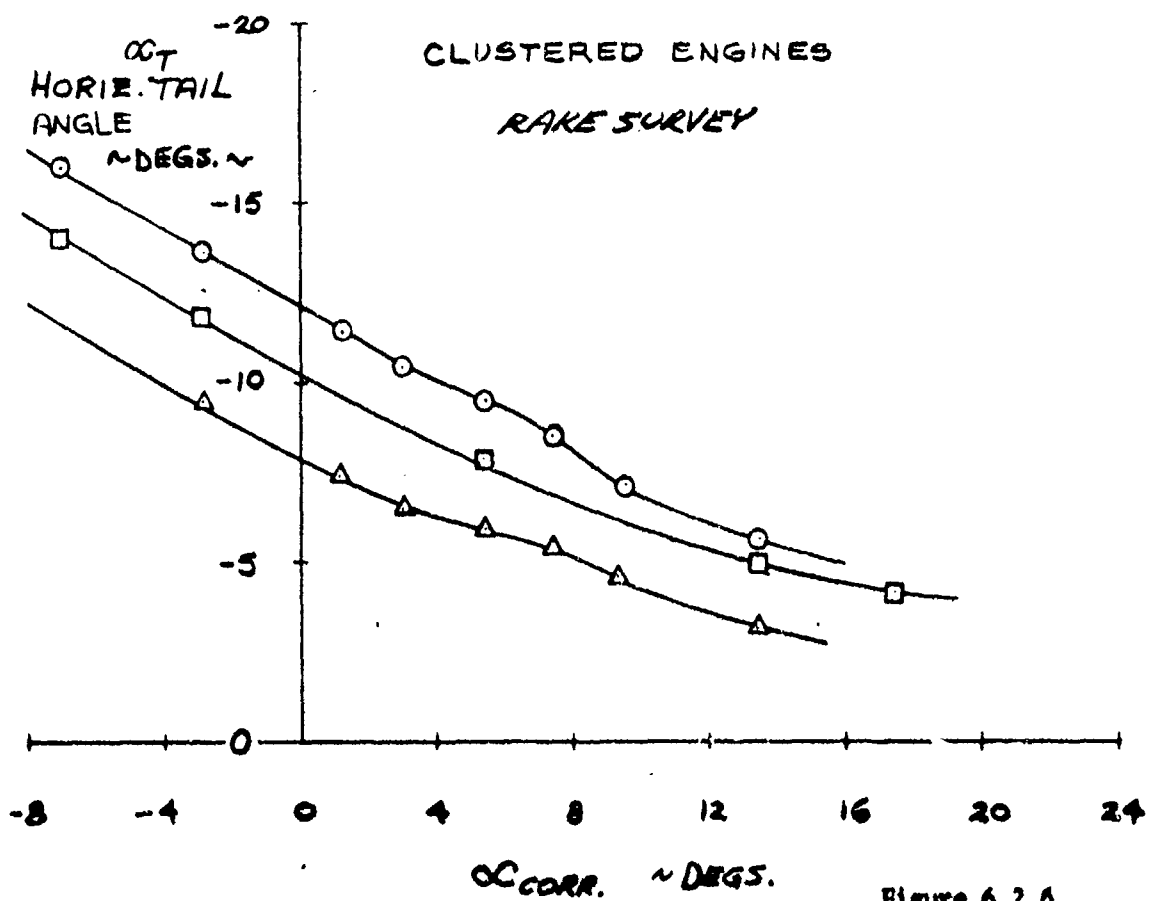
OUTBOARD L.E. BLC ONLY

$C_T = 2.0$

EFFECTS OF FLAP AND ENGINE NOZZLE DEFLECTION

$q = 16 \text{ psf}$
 $\delta_{sp} = -10^\circ$

	δ_F	δ_n	RUN
○	25°/50°	+15°	379
△	25°/50°	-15°	385
□	35°/60°	+15°	404



LSWT-090

CLUSTERED ENGINES
WITH OUTBOARD L.E. BLC ONLY

WAKE SURVEY

$C_T = 2.0$

$\int SP = -10'$

$\int NOZ = +15'$

$q = 16 \text{ PSF}$

$\alpha_c = +1.2'$

$\int P$

RUN

○

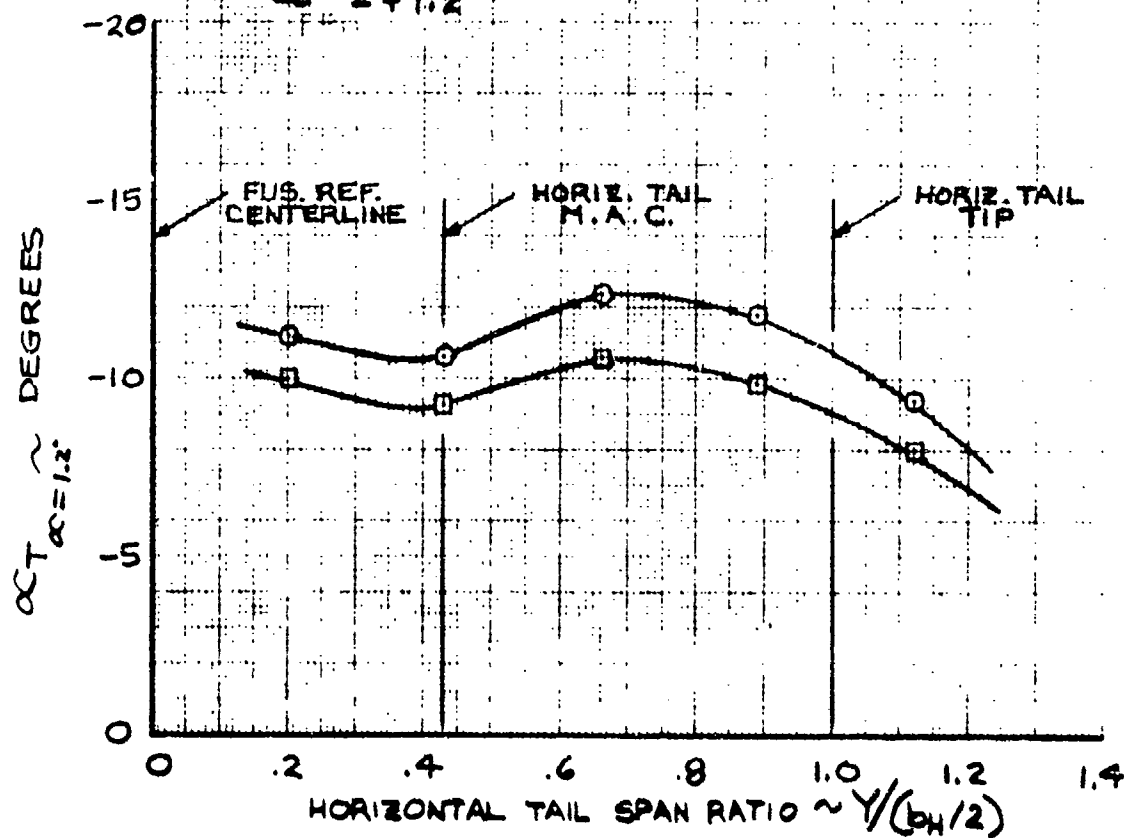
25/30

379

□

35/60

404



SPANWISE VARIATION OF HORIZONTAL TAIL ANGLE
AT $\alpha_c = +1.2'$

Figure 6.2.7

LSWT-090

HORIZ. TAIL ANGLE VS ANGLE OF ATTACK

OUTBOARD L.E. BLC ONLY

$$C_T = 3.0$$

EFFECTS OF FLAP AND ENGINE NOZZLE DEFLECTION

$$q = 16 \text{ psf}$$
$$\delta_{sp} = -10^\circ$$

	<u>δ_F</u>	<u>δ_n</u>	<u>RUN</u>
○	25°/50°	+15°	380 & 381
△	25°/50°	-15°	386
□	35°/60°	+15°	405

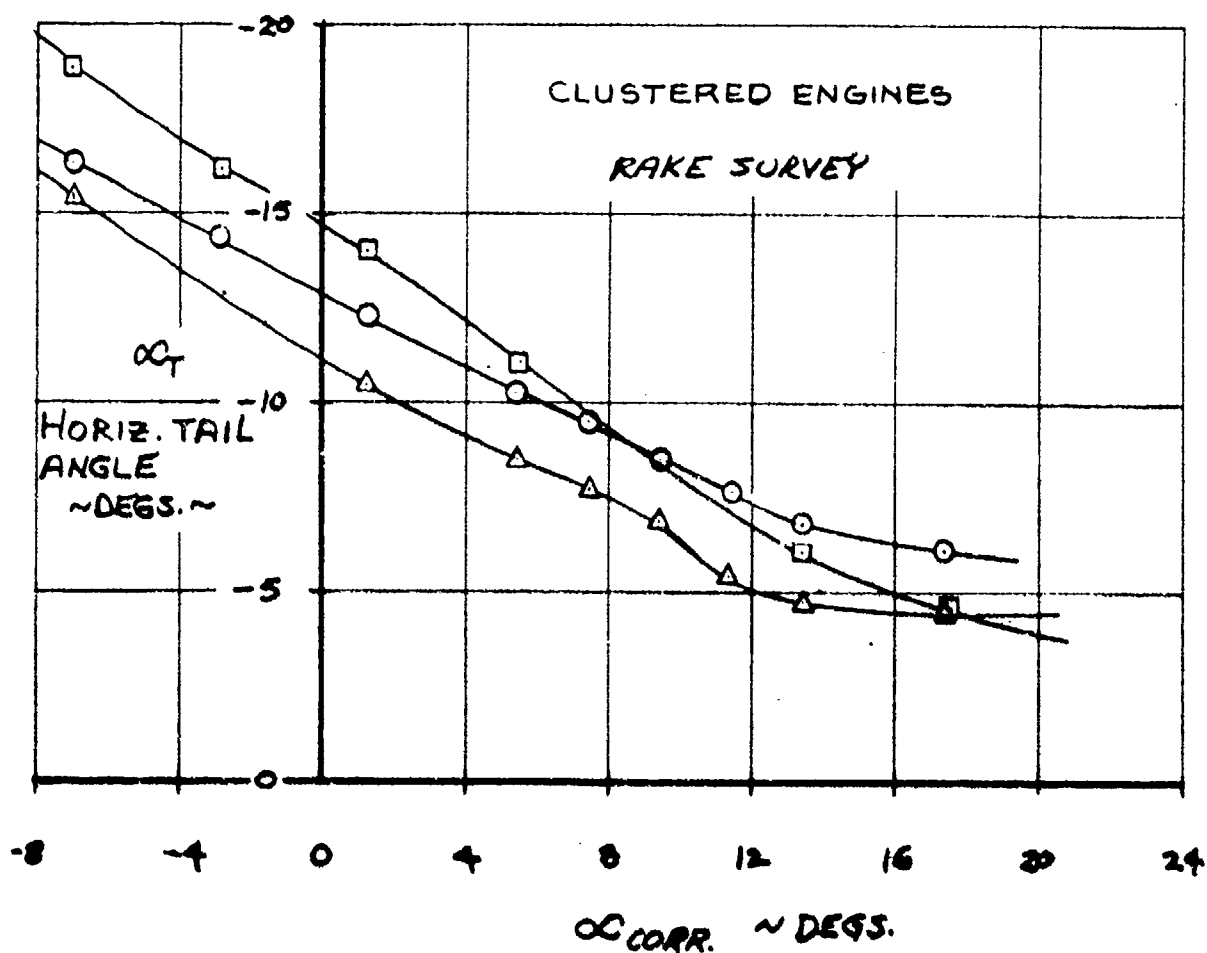


Figure 6.2.8

LSWT-090

CLUSTERED ENGINES
WITH OUTBOARD L.E. BLC ONLY

PAKE SURVEY

$$C_T = 3.0$$

$$\int_{SP} = -10^\circ$$

$$\int_{NOZ} = +15^\circ \uparrow$$

$$\rho = 16 \text{ PSF}$$

$$\alpha_c = +1.2^\circ$$

\int_F

RUN

○

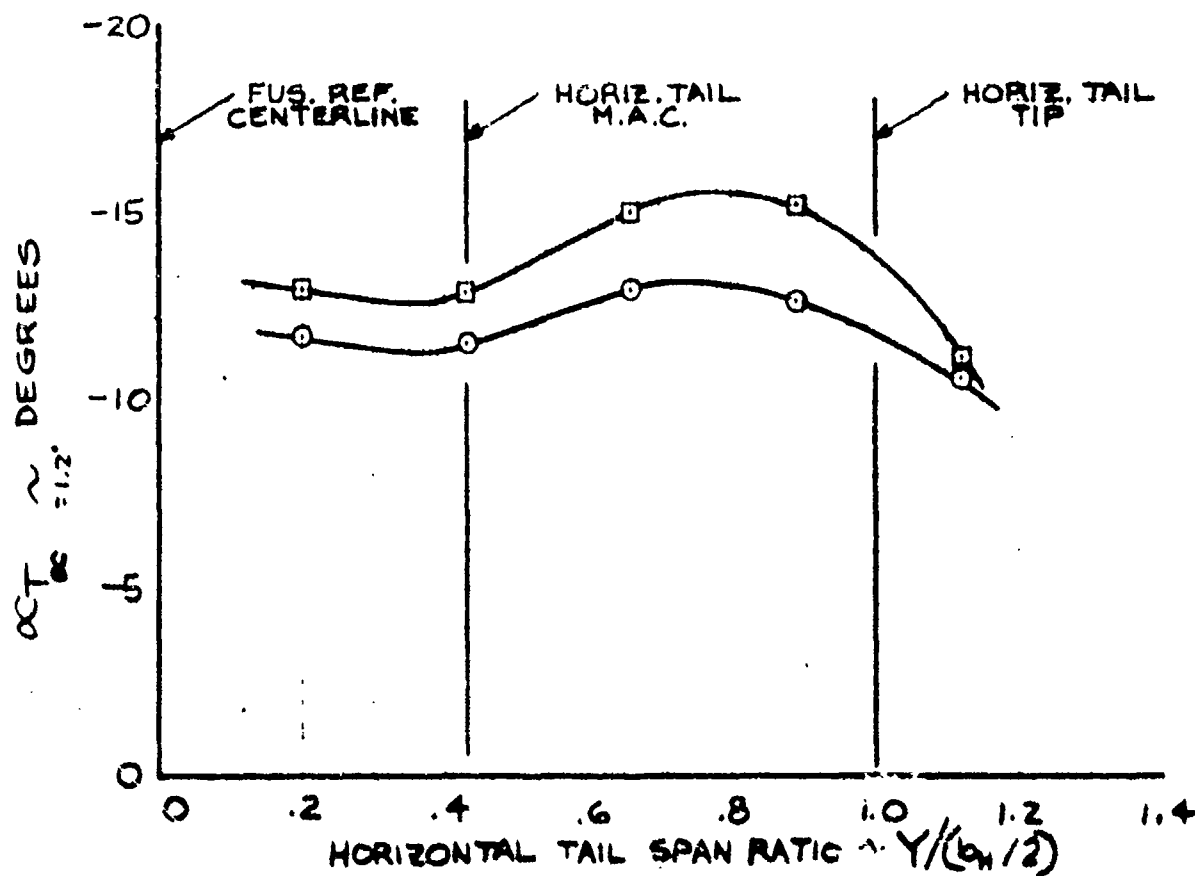
25°/50°

380

□

35°/60°

405



SPANWISE VARIATION OF HORIZONTAL TAIL ANGLE

AT $\alpha_c = +1.2^\circ$

Figure 6.2.9

LSWT-090

HORIZ. TAIL ANGLE VS. ANGLE OF ATTACK

OUTBOARD L.E. BLC ONLY

$C_T = 3.3$

EFFECTS OF FLAP AND ENGINE NOZZLE DEFLECTION

$q = 16 \text{ psf}$
 $\delta_{SP} = -10^\circ$

	δ_F	δ_n	RUN
○	25°/50°	+15°	382
△	25°/50°	-15°	387
□	35°/60°	+15°	407/408

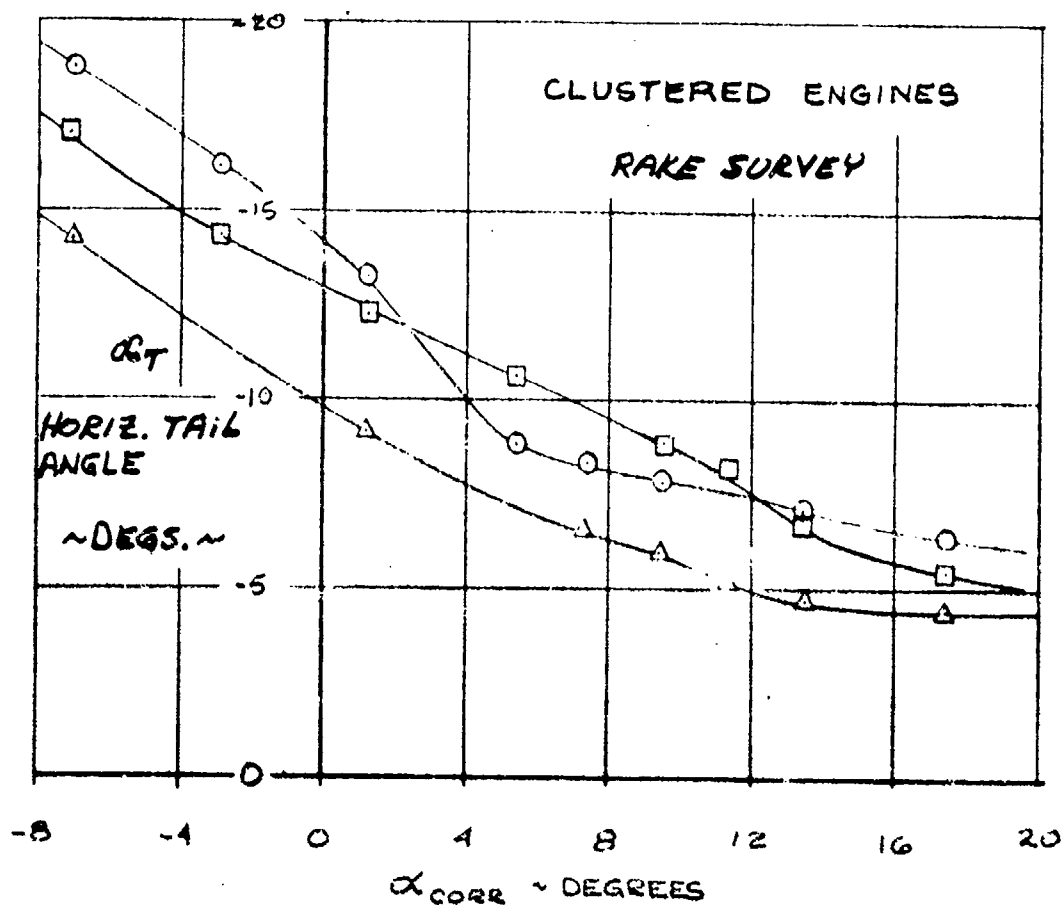


Figure 6.2.10

LSWT-090

CLUSTERED ENGINES
WITH OUTBOARD L.E. BLC ONLY

RAKE SURVEY

$C_T = 3.3$

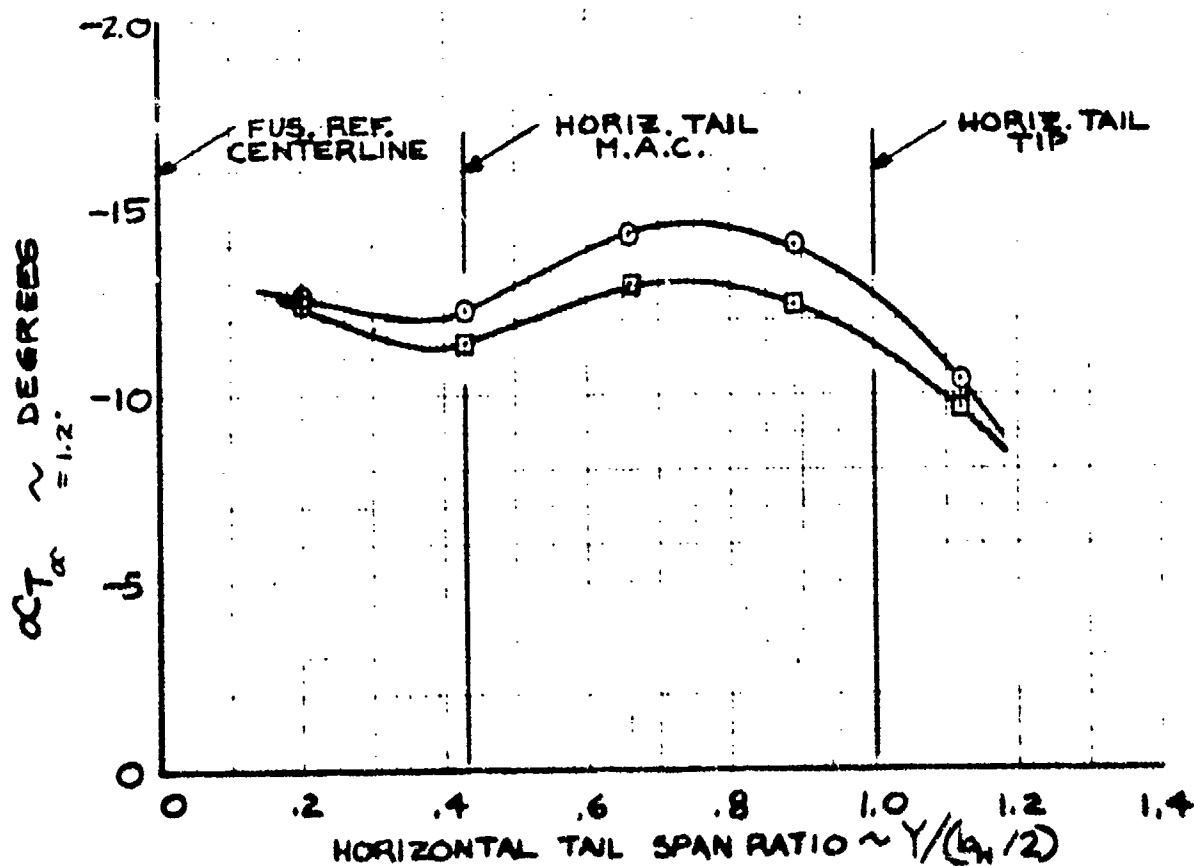
$\delta SP = -10^\circ$

$\delta NOZ = +15^\circ$

$q = 16 \text{ PSF}$

$\alpha_c = +1.2^\circ$

	δF	RUN
○	25/50	382
□	35/60	408



SPANWISE VARIATION OF HORIZONTAL TAIL ANGLE
AT $\alpha_c = +1.2^\circ$

Figure 6.2.11

LSINT-090

EFFECTS OF VARIOUS LEADING EDGE DEVICES

ON POWERED AIRBORNE TRAIL AIRBLE

$\delta_f = 25/50$

$\alpha = 0$

CLUSTERED ENGINES

$\delta_{30} = -10^\circ$

$\delta_{70} = +15^\circ$

$\delta = 16 \text{ psf}$

$C_D = -0.7$

107
10012
TRAIL
AIRBLE

WAGON

SHORT CHORD AIRBORNE, A
LONG
C.E. BLE (NO IN VEEER)

RAKE SURVEY

ENGINE GROSS BLOWING COEFFICIENT C_D

Figure 0.1

LSWT-090

HORIZ. TAIL ANGLE VS. ANGLE OF ATTACK

VARIAION OF OUTBOARD L.E. DEVICES

$$C_T = 0$$

EFFECTS OF LEADING EDGE DEVICES

	<u>SF</u>		<u>L.E. DEVICE</u>	<u>RUN</u>
$\delta h = +15^\circ \uparrow$	25/50	①	SHORT CHORD KRUEGER, K_4	397
$q = 16 \text{ psf}$	✓	△	LONG ✓, K_{25}	388
$\delta_{SP} = -10^\circ$	35/60	□	L.E. BLC (NO KRUEGER)	402
	25/50	◇	✓ ✓ ✓	376 & 377

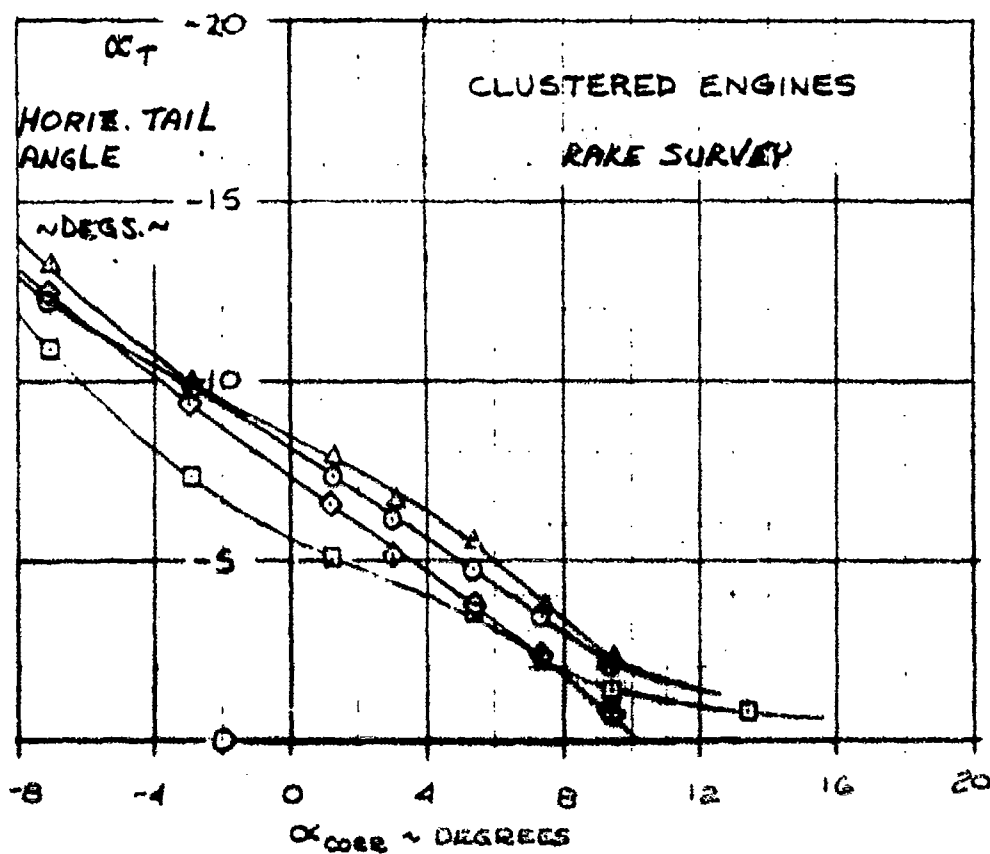


Figure 6.3.2

LSWT-090

HORIZ. TAIL ANGLE VS ANGLE OF ATTACK

VARIATION OF OUTBOARD L.E. DEVICES

$C_T = 1.0$

EFFECTS OF LEADING EDGE DEVICES

	<u>St</u>		<u>L.E. DEVICE</u>	<u>RUN</u>
$\delta n = +15^\circ \uparrow$	25/50	O	SHORT CHORD KRUEGER, K_4	398
$q = 16 \text{ psf}$	✓	Δ	LONG ✓	389
$\delta sp = -10^\circ$	35/60	□	L.E. BLC (NO KRUEGER)	403
	25/50	◇	✓ / ✓ ✓	378

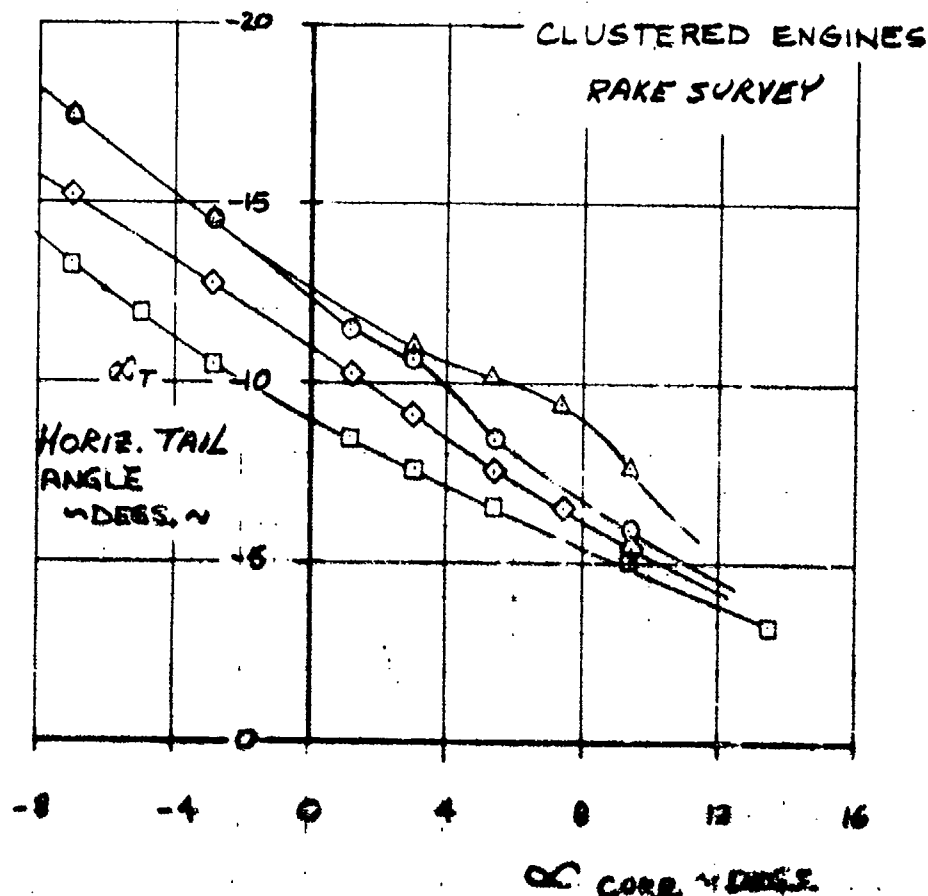


Figure 5.3.3

LSWT-090

HORIZ. TAIL ANGLE Vs. ANGLE OF ATTACK

VARIATION OF OUTBOARD L.E. DEVICES

$C_T = 2.0$

EFFECTS OF LEADING EDGE DEVICES

	δ_f		L.E. DEVICE	RUN
$\delta_n = +15^\circ \uparrow$	25/50	○	SHORT CHORD KRUEGER, K4	399
$q = 16 \text{ psf}$	✓	△	LONG ✓, K25	390
$\delta_{sp} = -10^\circ$	35/60	□	L.E. BLC (NO KRUEGER)	404
	25/50	◇	✓ ✓ ✓	379

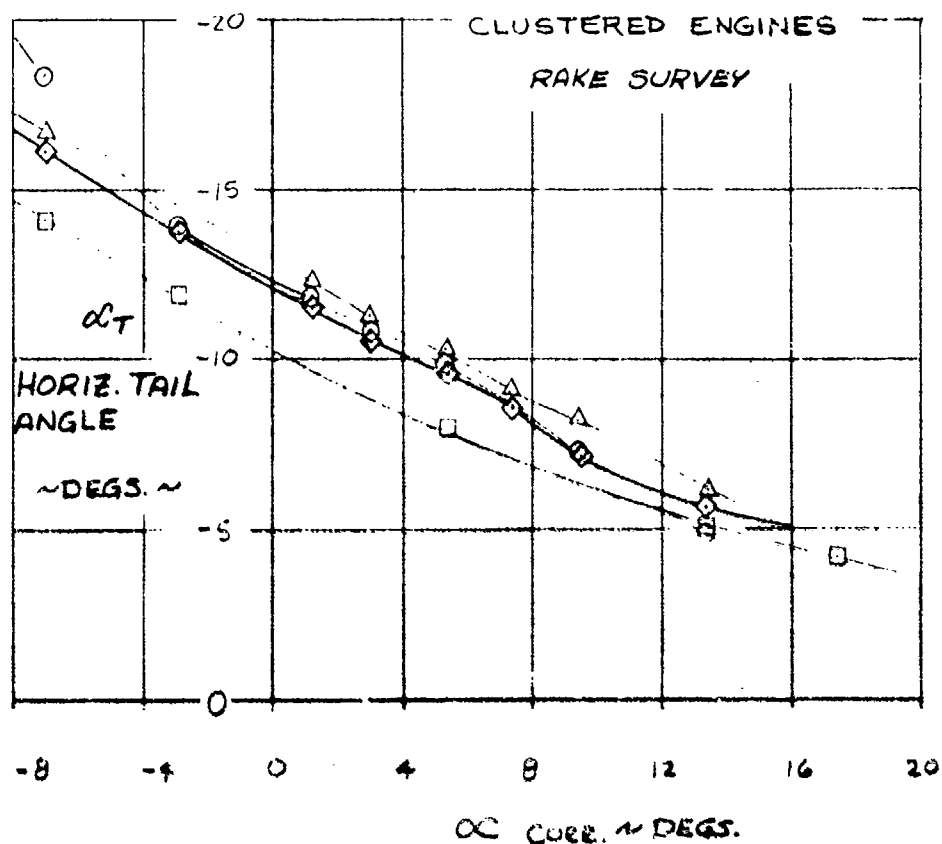


Figure 6.3.4

LSWT-090

HORIZ. TAIL ANGLE VS ANGLE OF ATTACK

VARIATION OF OUTBOARD LE. DEVICES

$$C_T = 3.0$$

EFFECT OF LEADING EDGE DEVICES

	<u>δ_f</u>		<u>L. E. DEVICES</u>	<u>RUN</u>
$\delta_h = +15^\circ \uparrow$	25/50	○	SHORT CHORD KRUEGER, K_4	400
$q = 16 \text{ psf}$	✓	△	LONG ✓ K_{25}	391
$\delta_{SP} = -10^\circ$	35/60	□	L. E. BLC (NO KRUEGER)	405
	25/50	◇	✓ ✓ ✓	580 & 581

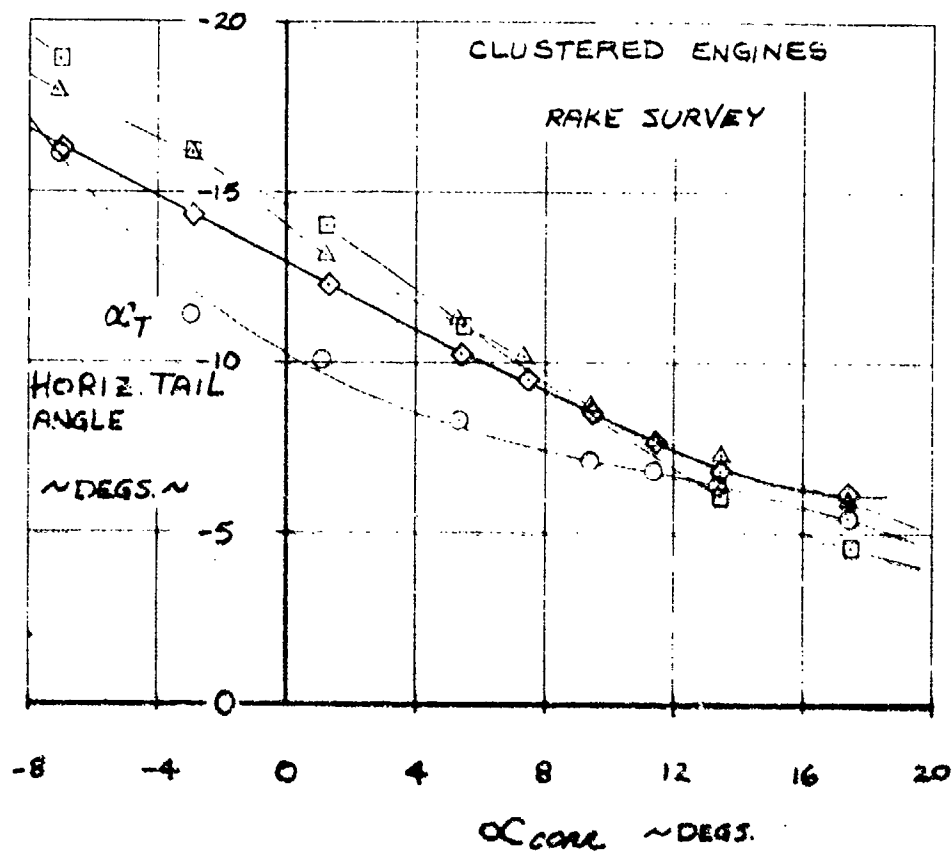


Figure 6.3.5

LSWT-090

HORIZ. TAIL ANGLE VS ANGLE OF ATTACK

VARIATION OF OUTBOARD L.E. DEVICES

$$C_T = 3.3$$

EFFECTS OF LEADING EDGE DEVICES

	<u>δf</u>		<u>L.E. DEVICE</u>	<u>RUN</u>
$\delta_{Y_1} = +15^\circ \uparrow$	25/50	O	SHORT CHORD KRUEGER, K_4	401
$\eta = 16 \text{ ps}$	✓	Δ	LONG ✓, K_{25}	392
$\delta_{SP} = -10^\circ$	35/60	□	L.E. BLC (NO KRUEGER)	407 & 408
	25/50	◇	✓ ✓ ✓	382

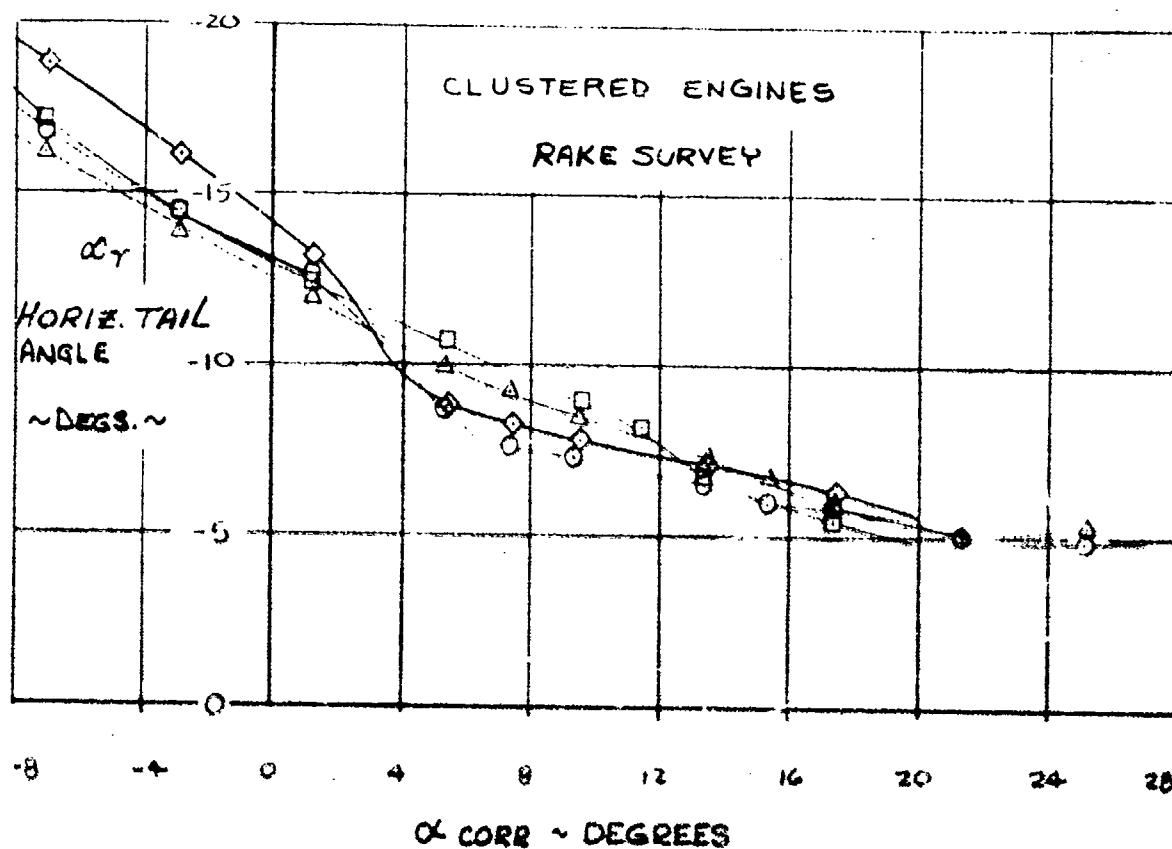
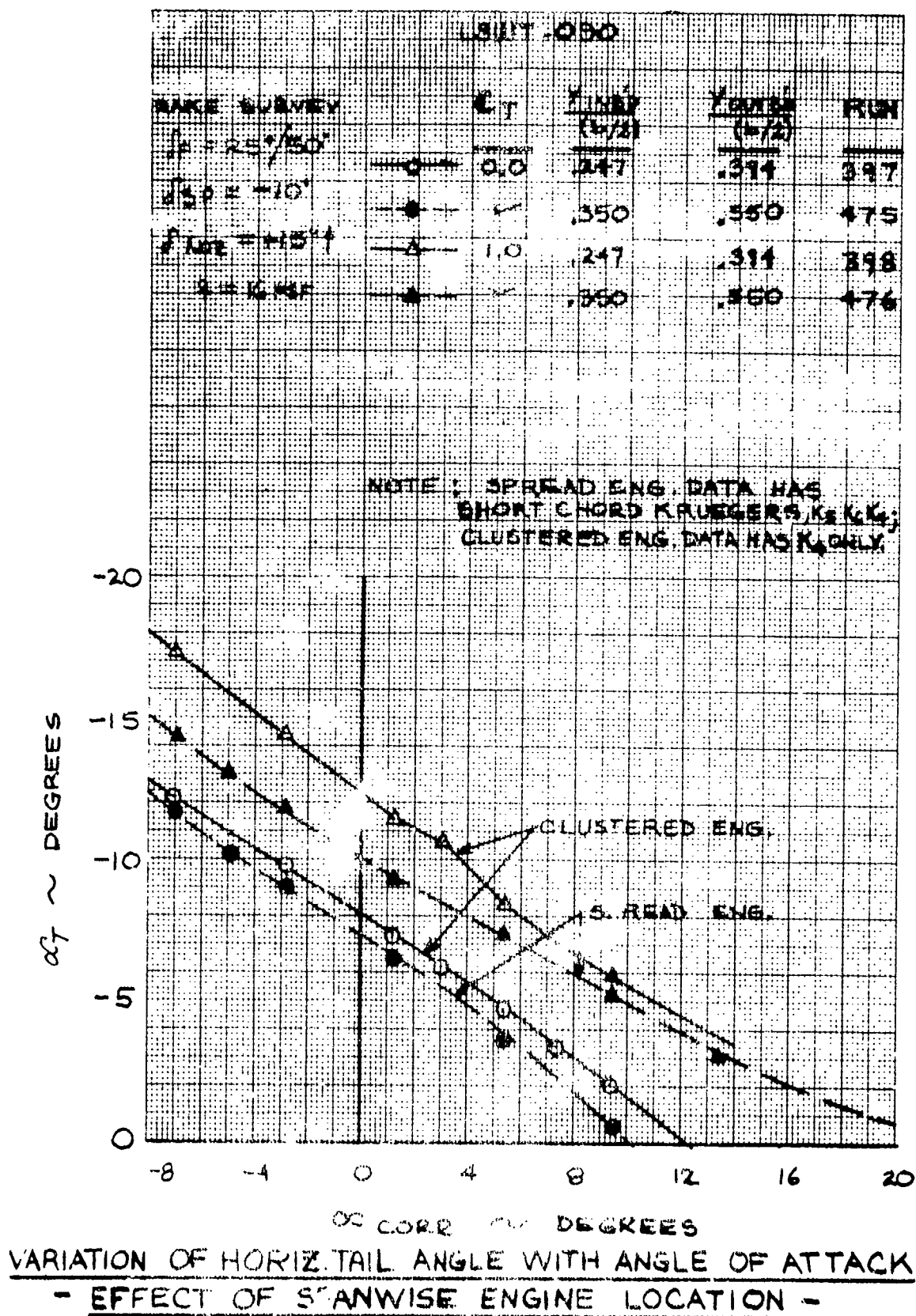
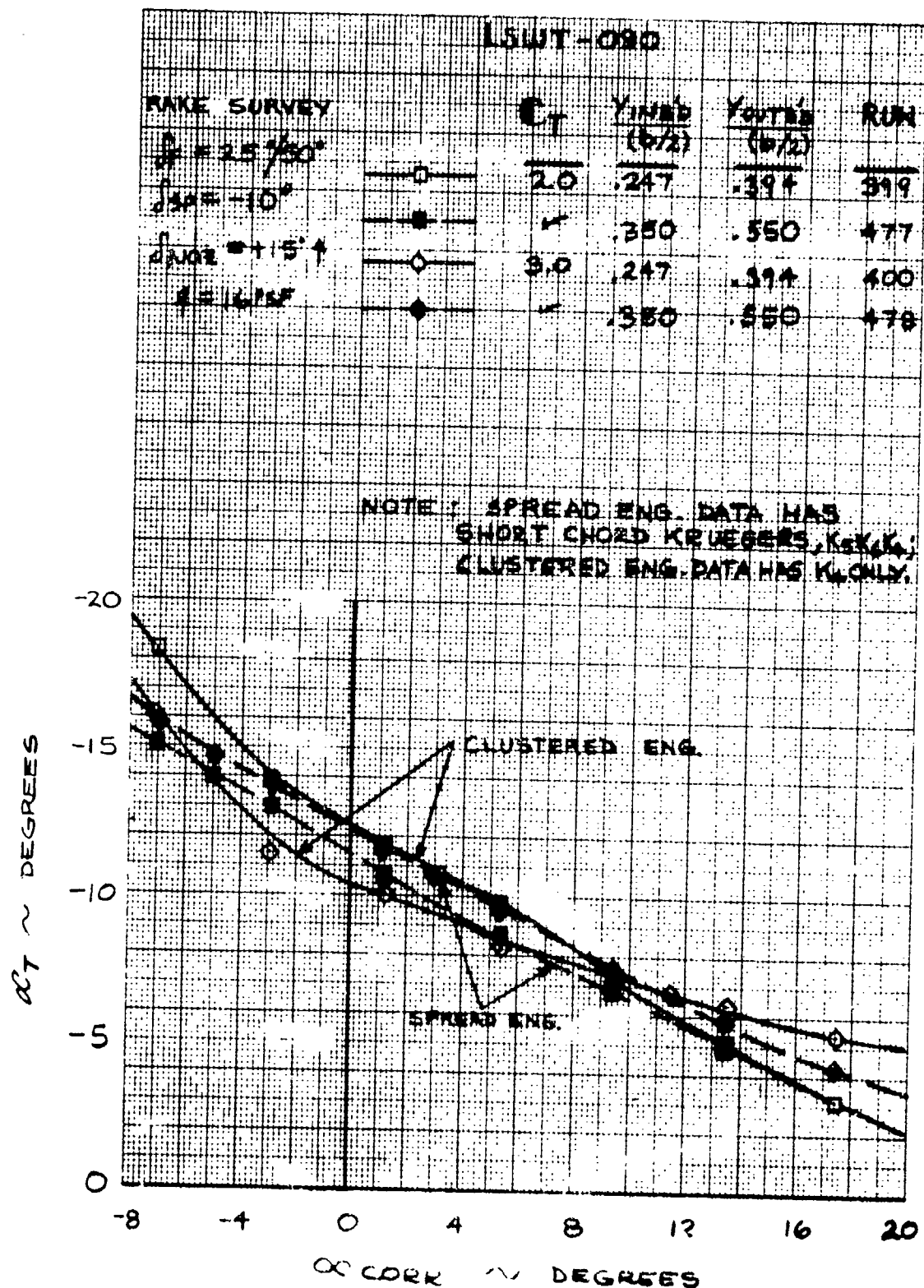


Figure 6.3.6



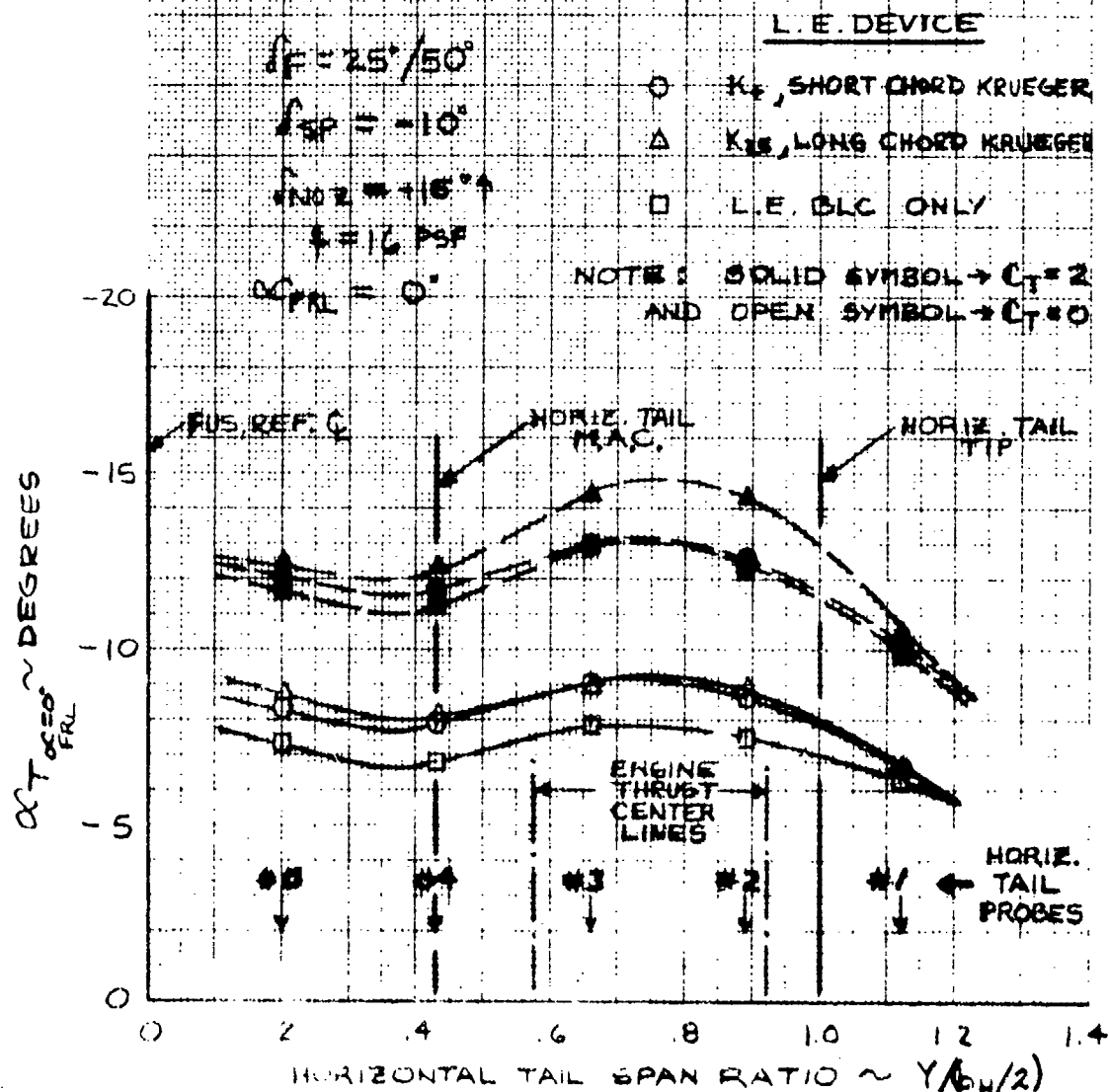


VARIATION OF HORIZ. TAIL ANGLE WITH ANGLE OF ATTACK
- EFFECT OF SPANWISE ENGINE LOCATION -

Figure 6.4.2

LSWT-090

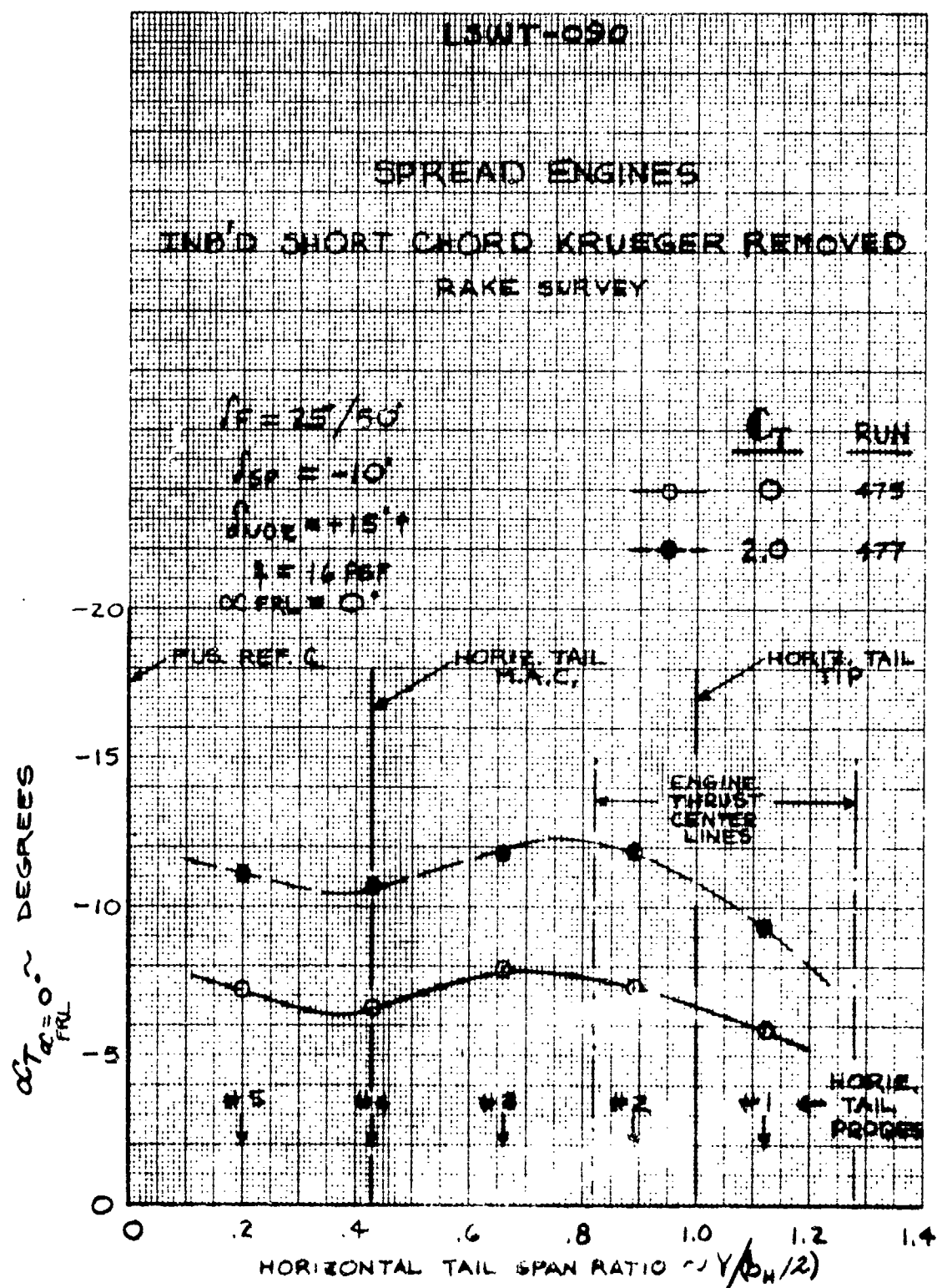
CLUSTERED ENGINES
WITH VARIOUS OUTBD L.E. DEVICES
RAKE SURVEY



SPANWISE VARIATION OF HORIZONTAL TAIL ANGLE

AT $\alpha_{FRL} = 0^\circ$

Figure 0.4.5



SPANWISE VARIATION OF HORIZONTAL TAIL ANGLE

AT $\alpha_{FRL} = 0^\circ$

Figure 6.4.4

Section VII

REYNOLDS NUMBER

Since the GELAC tunnel is a single return tunnel not having variable density capabilities, the only way to increase Reynolds number was to increase tunnel speed. As was mentioned in the introduction, three tunnel speeds were run corresponding to tunnel q 's of 0 psf, 16 psf and 100 psf.

7.1 EFFECTS ON LONGITUDINAL AERODYNAMIC PARAMETERS

Figures 7.1.1, 7.1.2, and 7.1.3 show the effects of Reynolds number on the power-off lift, drag and pitching moment coefficients. Along with Reynolds number effects a high lift configuration buildup is presented beginning with clean wing, then adding full span leading edge Kruegers and finally mounting trailing edge double slotted flaps.

7.2 EFFECTS ON LATERAL-DIRECTIONAL AERODYNAMIC PARAMETERS

Figures 7.2.1 and 7.2.2 present the effects of Reynolds number on dihedral effect for $\alpha_{FRL} = 0^\circ$ and 12° respectively. At $\alpha_{FRL} = 0^\circ$ practically no effects of Reynolds number are seen on $C_{l\psi}$ but in sharp contrast at $\alpha_{FRL} = 12^\circ$, severe flow separation existing at 16q are completely eliminated with an increase in Reynolds number at 100q.

Reynolds number effects on directional stability are presented in Figures 7.2.3 and 7.2.4. As can be seen little change in either stability level or vertical tail stall angles are affected by increasing Reynolds number.

7.3 EFFECTS ON HORIZONTAL TAIL ANGLE OF ATTACK

Figures 7.3.1 and 7.3.2 show the effects of Reynolds number on horizontal tail angle for two different leading edge configurations.

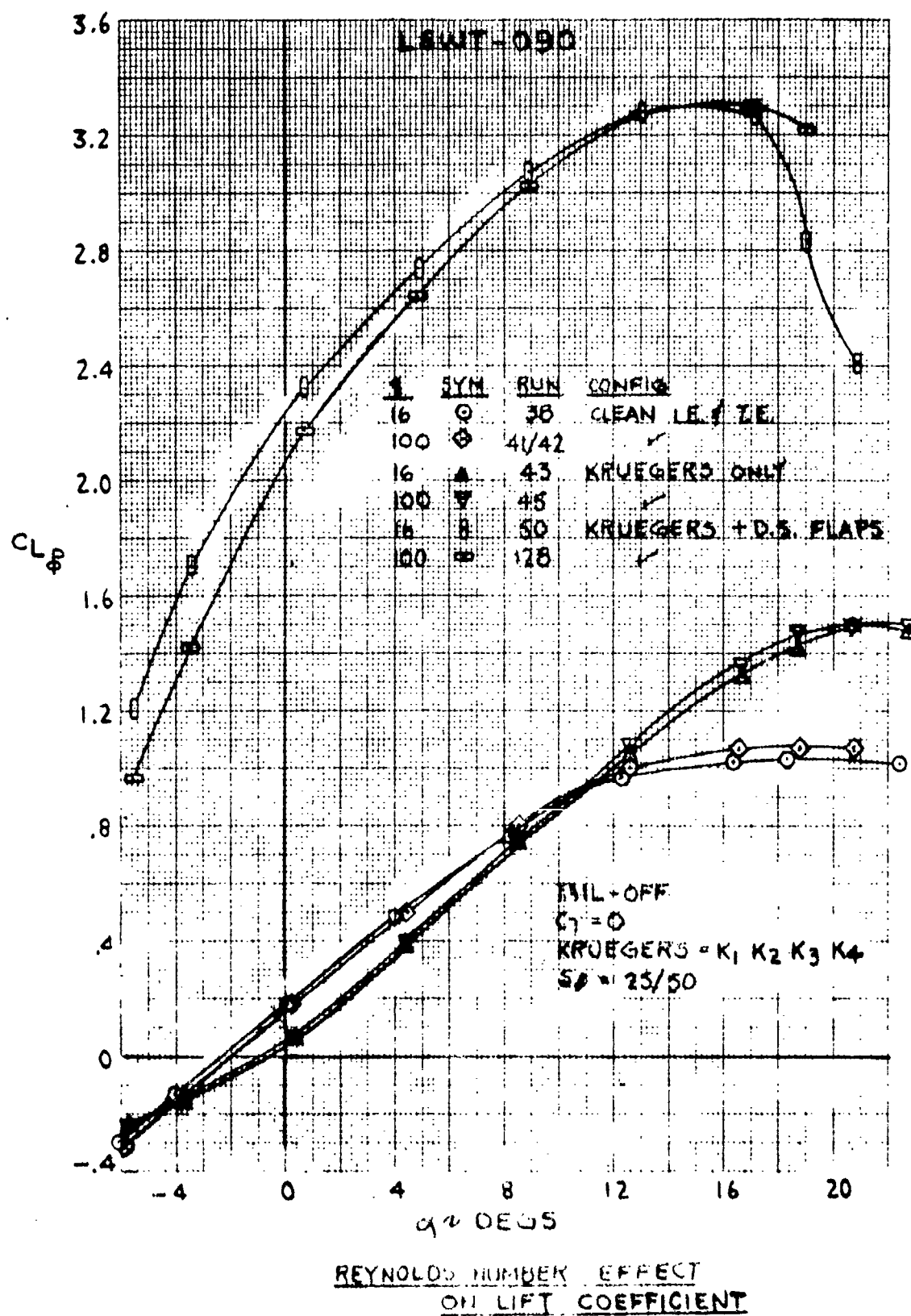
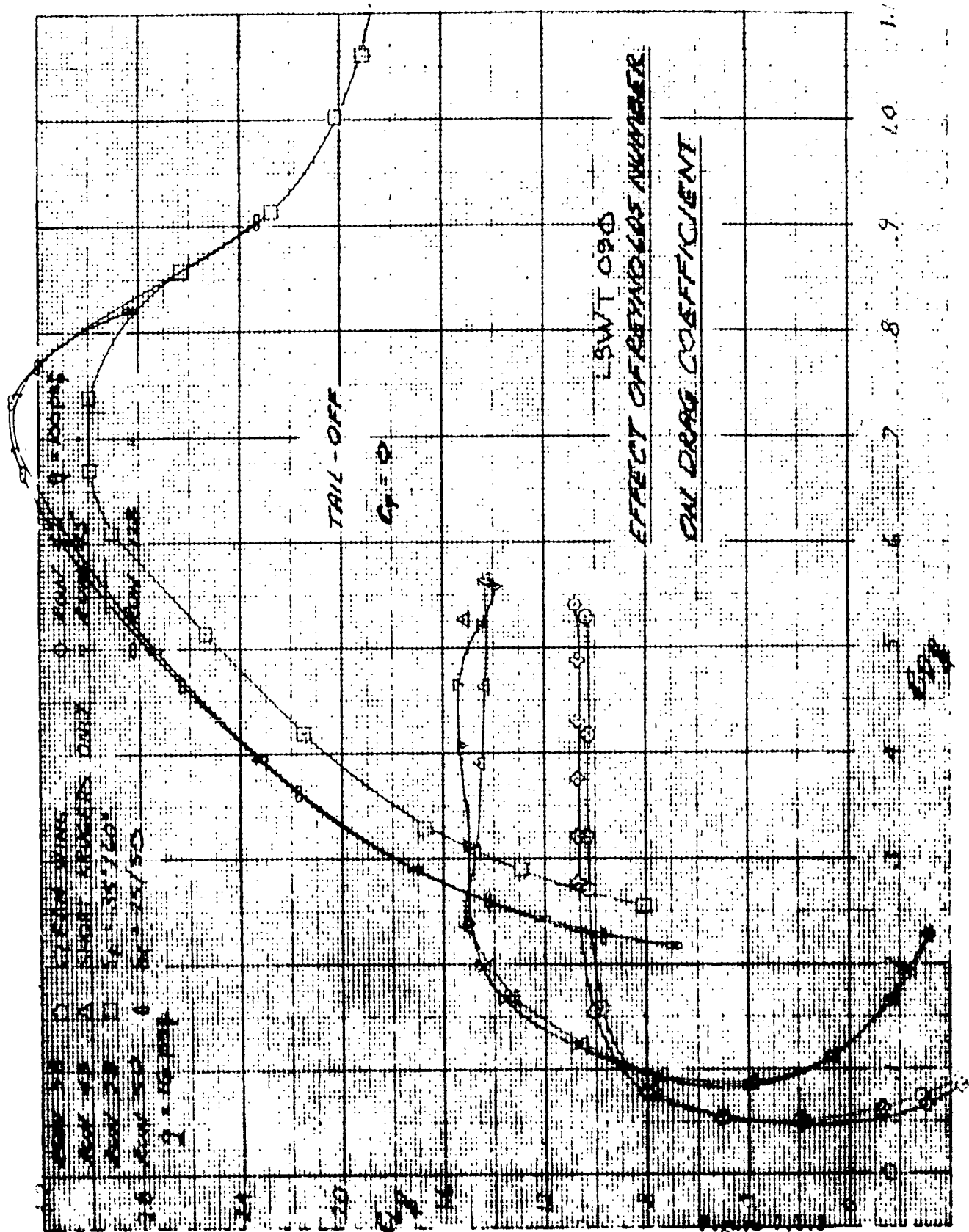


Figure 7.1.1



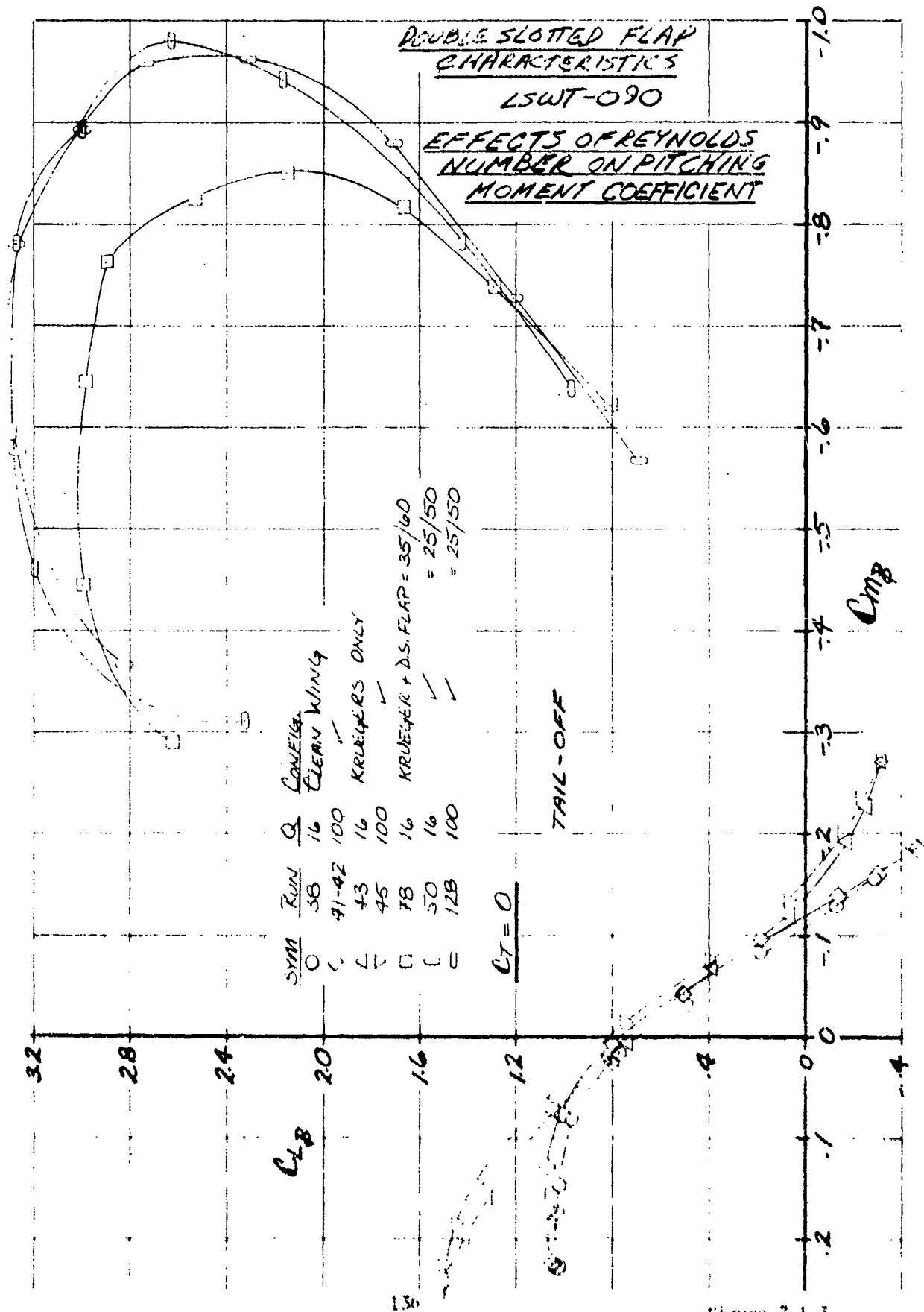
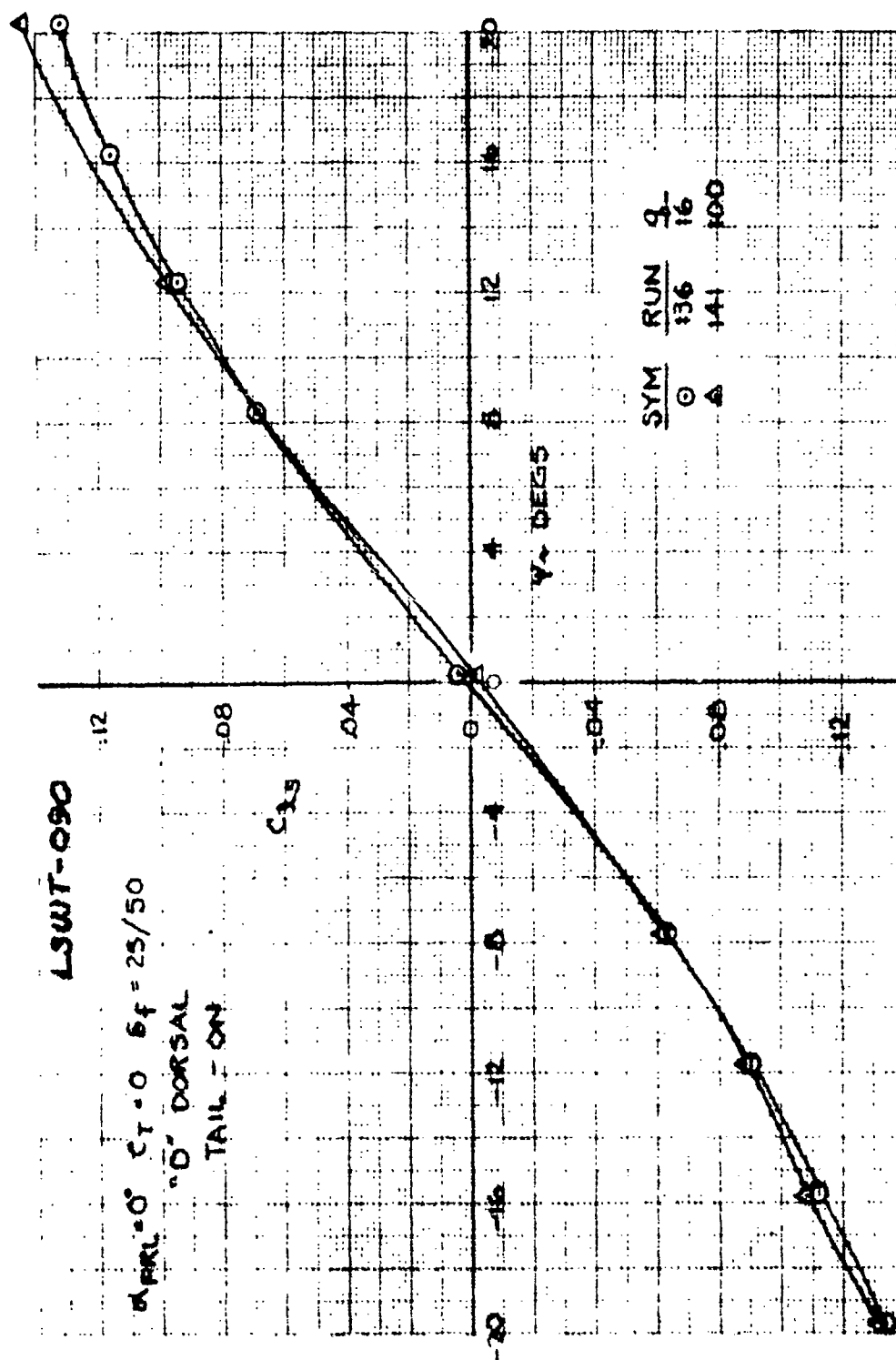
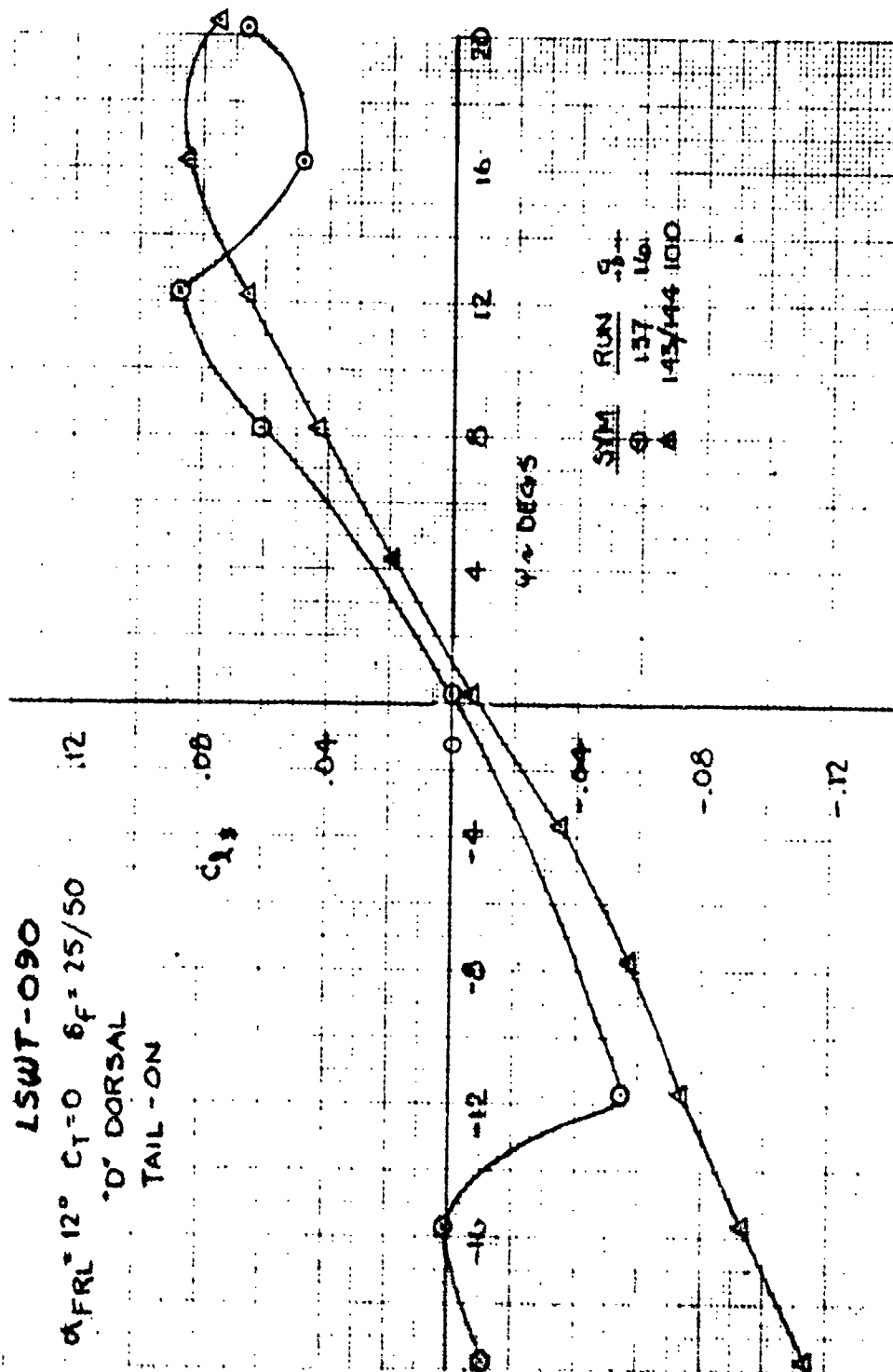


Figure 7.1.3

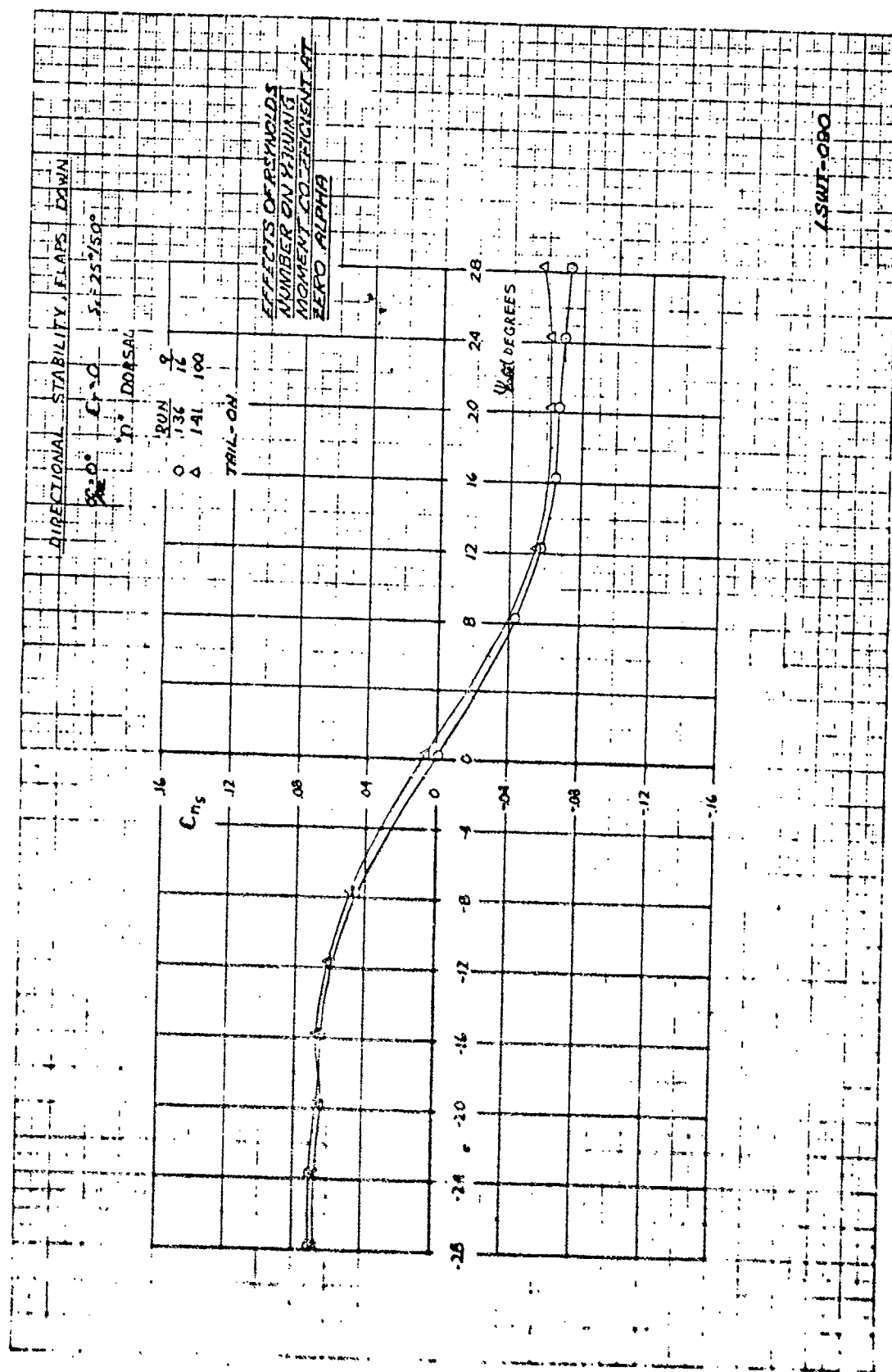


EFFECT OF REYNOLDS NUMBER ON
 DIHEDRAL EFFECT

Figure 7.2.1



EFFECT OF REYNOLDS NUMBER ON
 DIHEDRAL EFFECT



139
 Figure 7.2.3
 (The reverse side of this page is blank)

DIRECT /NAL STABILITY, FLAPS DOWN

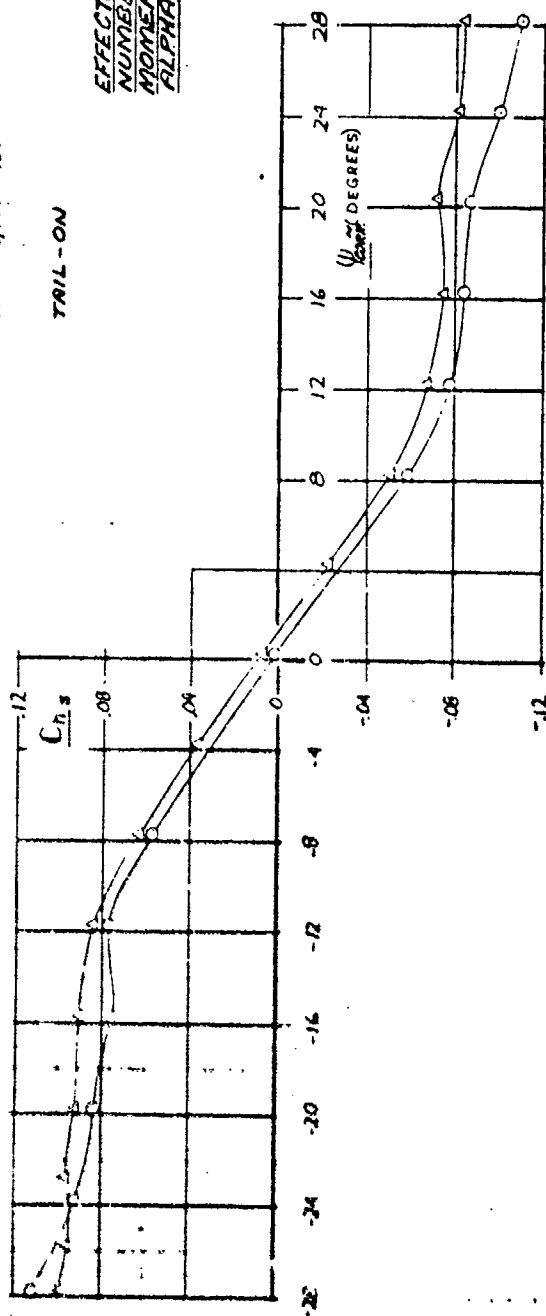
$\alpha_{FL} = 14^\circ$ $C_T = 0$ $S_F = 25^\circ/50^\circ$

"D" DORSAL

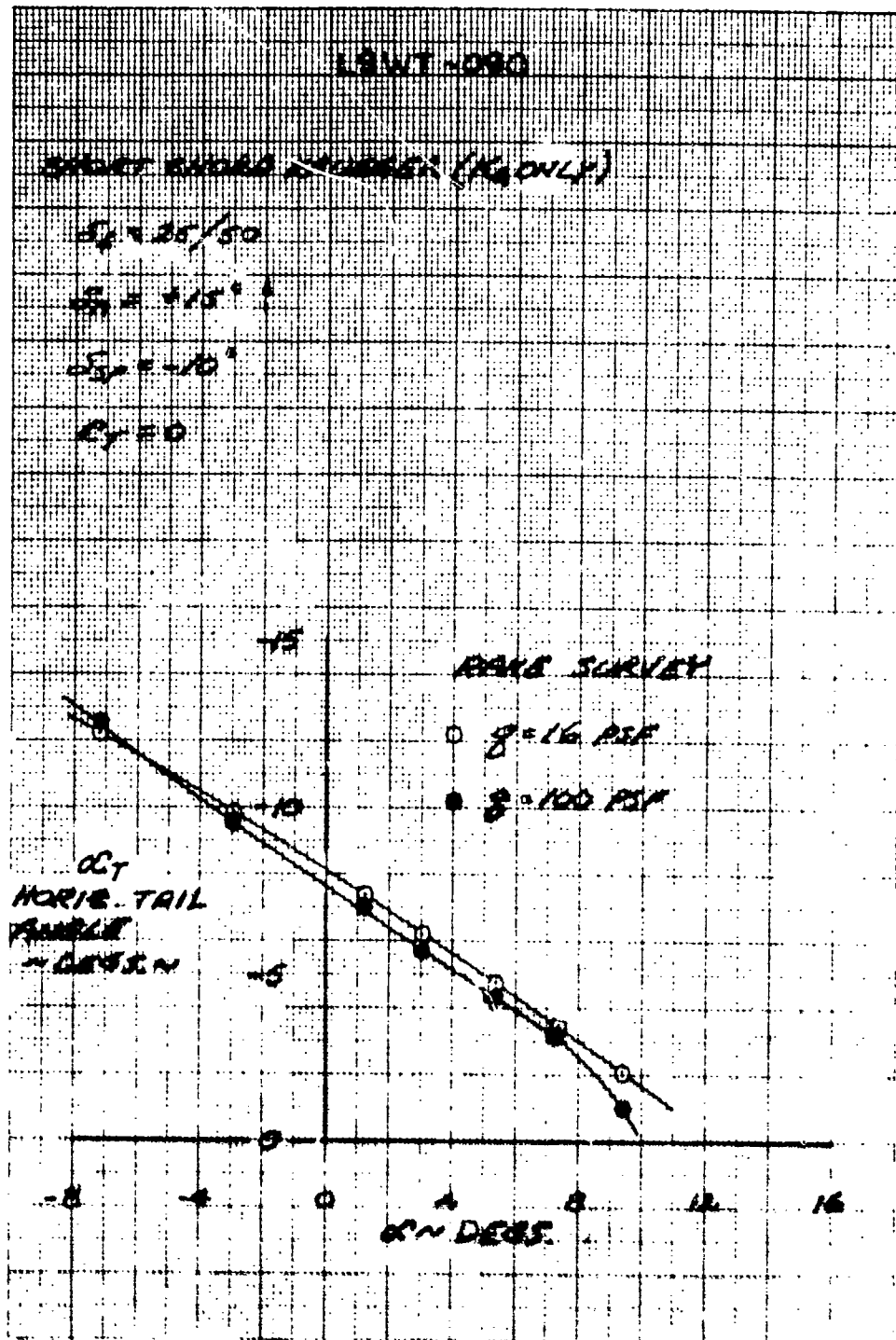
RUN $\frac{q}{100}$
 O 137 16
 Δ 143/144 100

TAIL-ON

EFFECTS OF REYNOLDS
 NUMBER ON YAWING
 MOMENT COEFFICIENT AT
 ALPHA OF 12 DEGREES

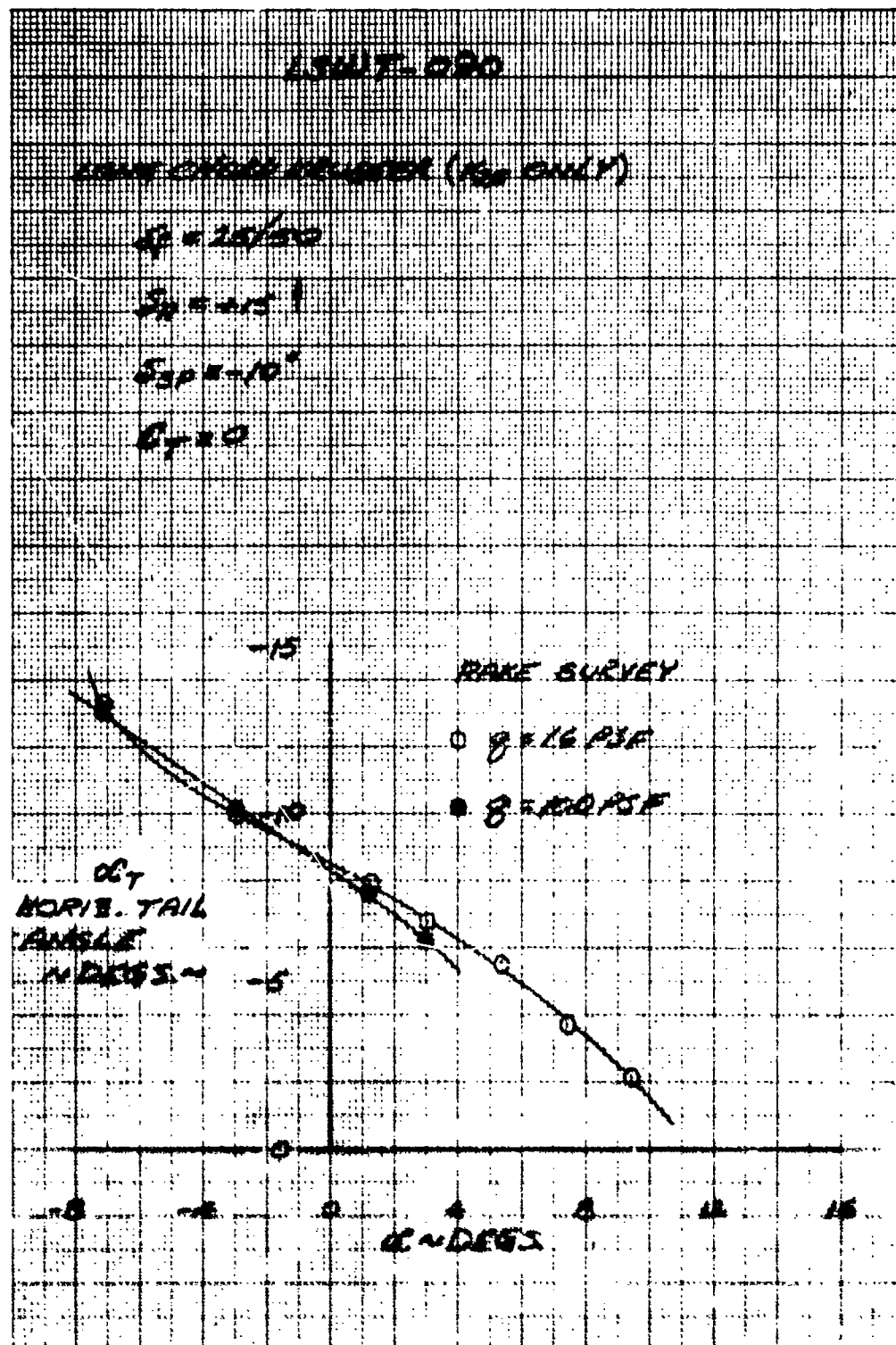


LSWT-090



REYNOLDS NUMBER EFFECTS ON HORIZONTAL TAIL
ANGLE

Figure 7.3.1



REYNOLDS NUMBER EFFECTS ON HORIZONTAL TAIL ANGLE

Figure 7.3.2

Section VIII

FLAP SPAN

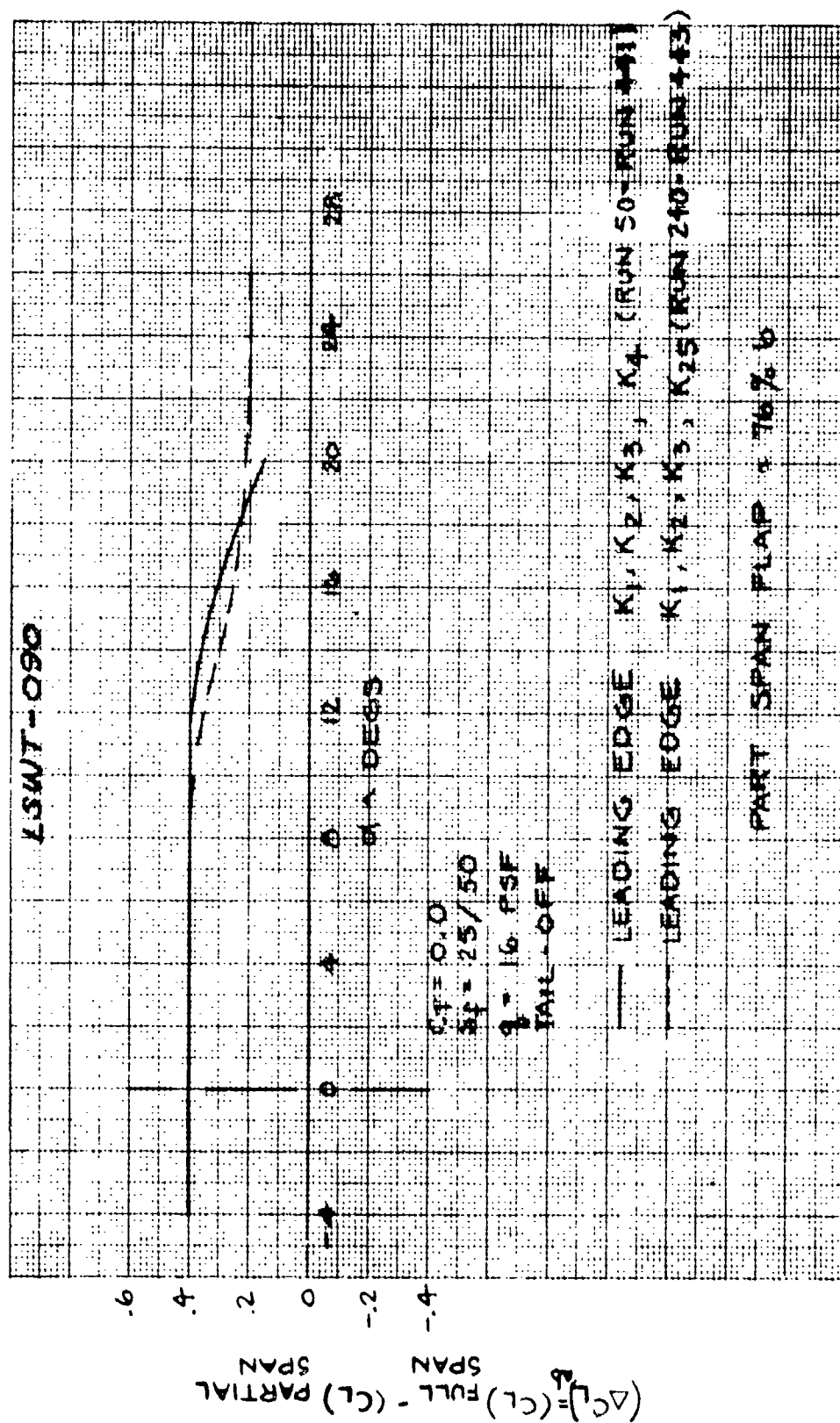
The model was equipped with inboard and outboard flap sections. The inboard flap section extends from the fuselage out to 76 percent semi-span and the outboard flap section continues from 76 percent semispan out to the tip of the wing. The outboard flap section was available only with the one double slotted flap deflection of 25/50 degrees.

8.1 EFFECTS ON LONGITUDINAL AERODYNAMIC PARAMETERS

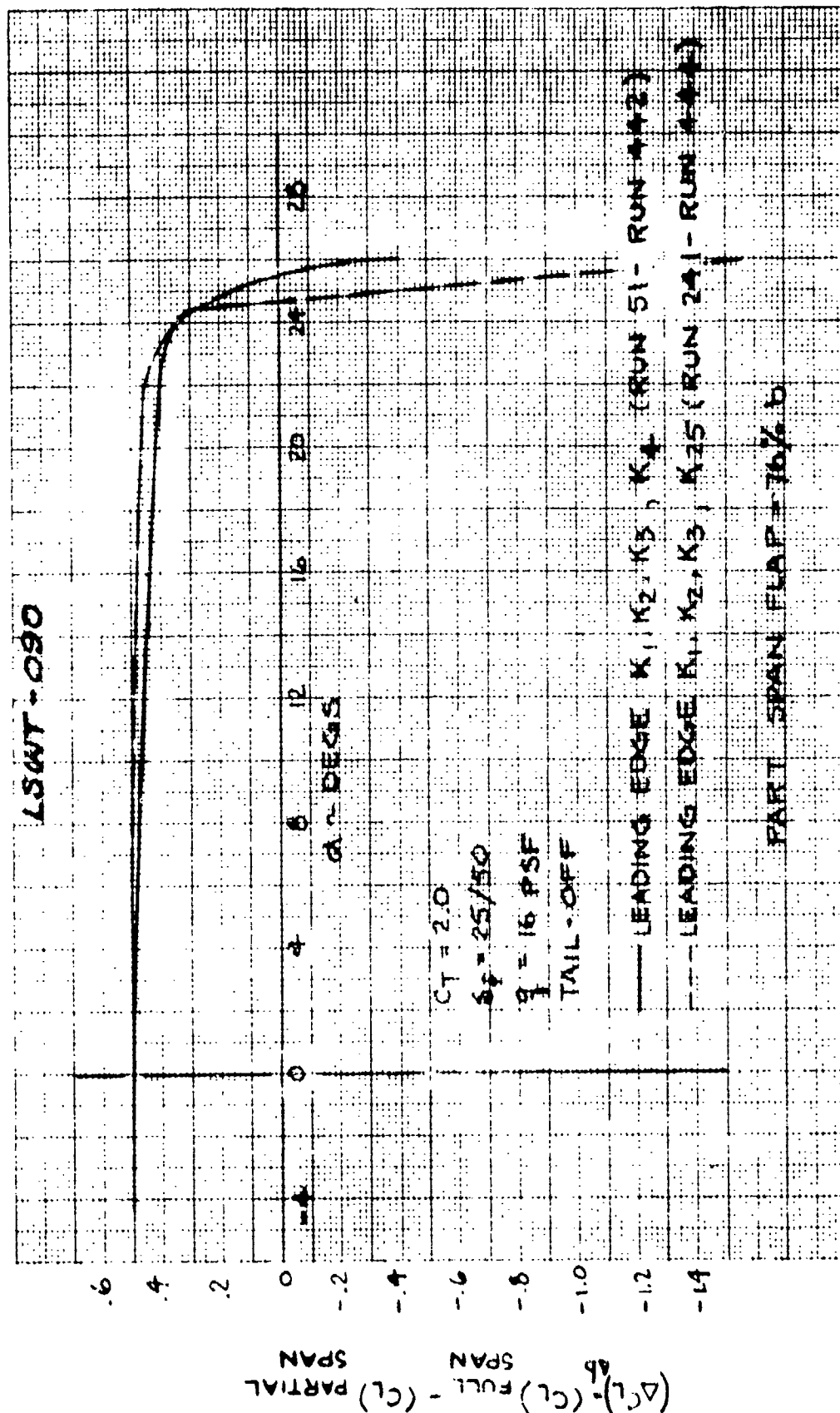
Flap span effects on power-off and power-on lift coefficient are shown in Figures 8.1.1 and 8.1.2 respectively for two different leading edge configurations.

Flap span effects on power-off and power-on drag coefficient are shown in Figures 8.1.3 and 8.1.4 respectively.

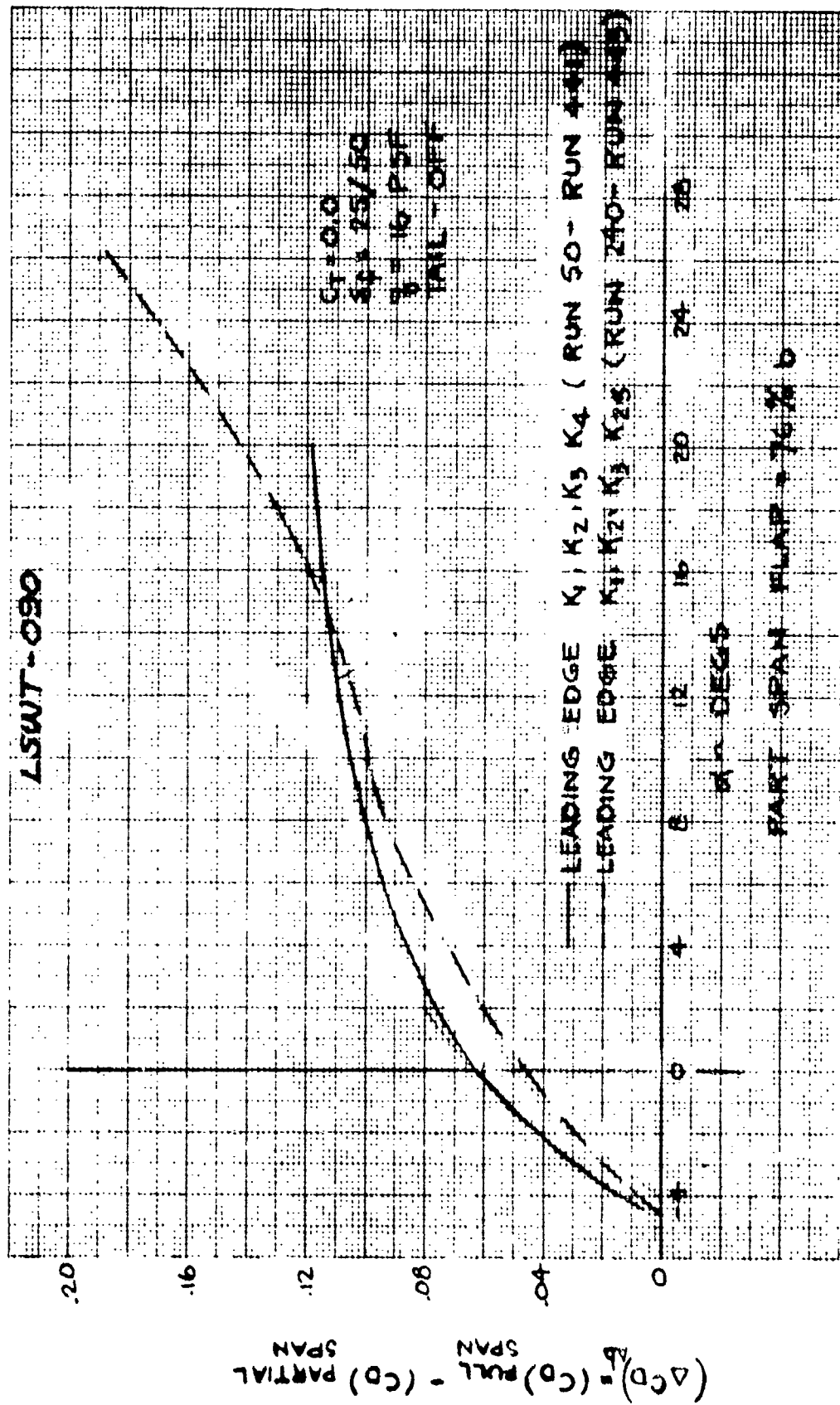
Flap span effects on power-off and power on pitching moment coefficient are shown in Figures 8.1.5 and 8.1.6 respectively.



FLAP SPAN EFFECTS ON LIFT COEFFICIENT

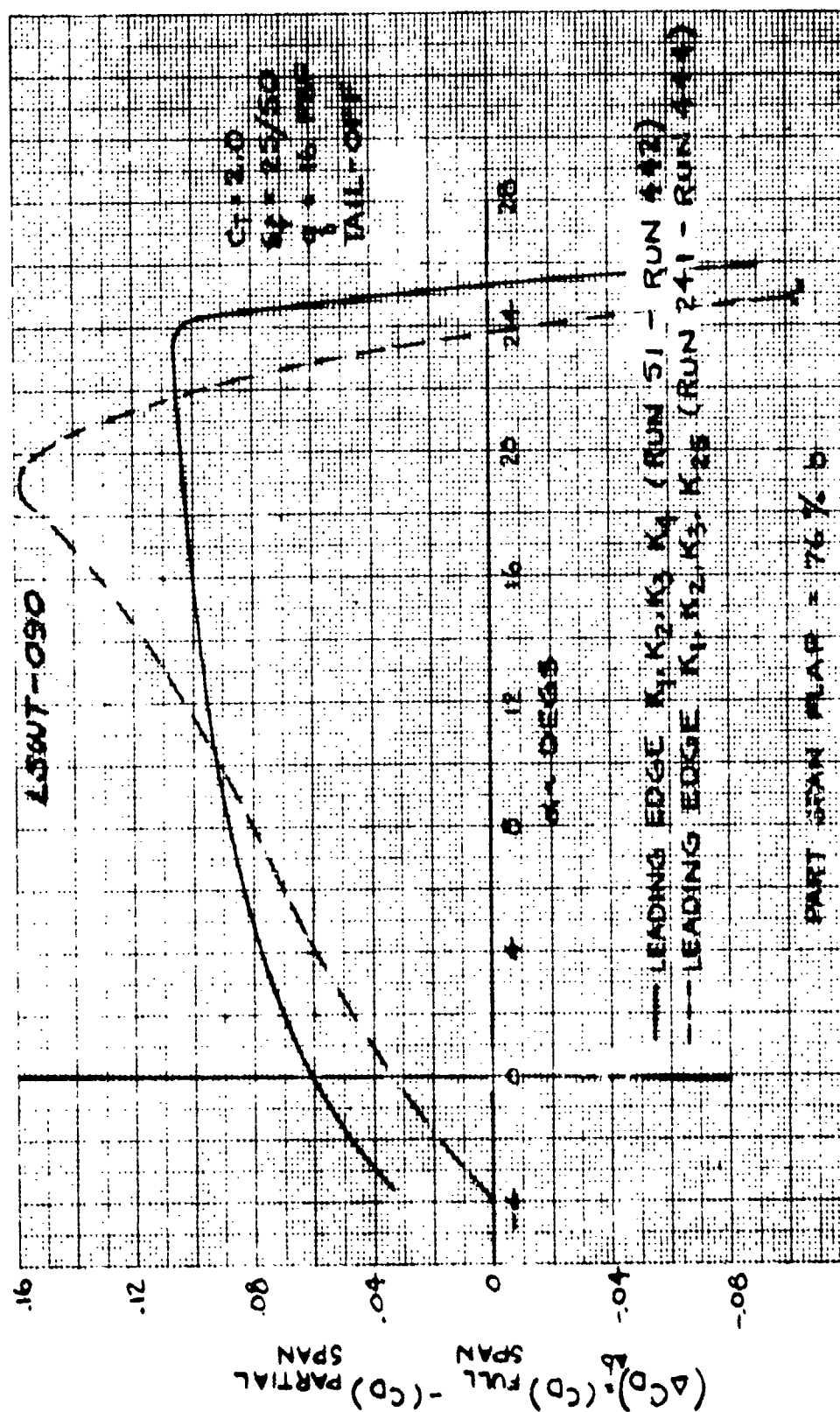


FLAP SPAN EFFECTS ON LIFT COEFFICIENT



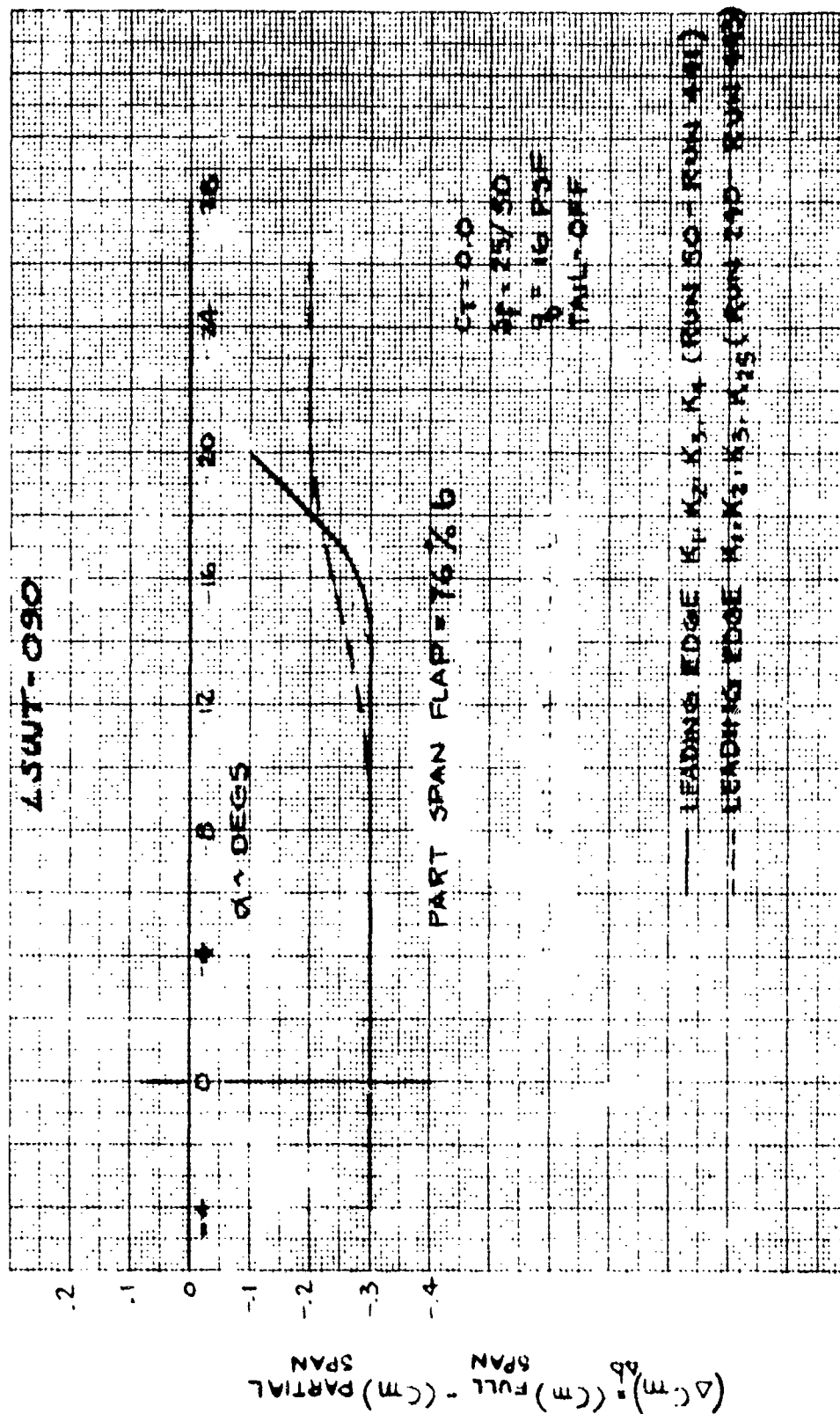
FLAP SPAN EFFECTS ON DRAG COEFFICIENT

Figure 8.1.3



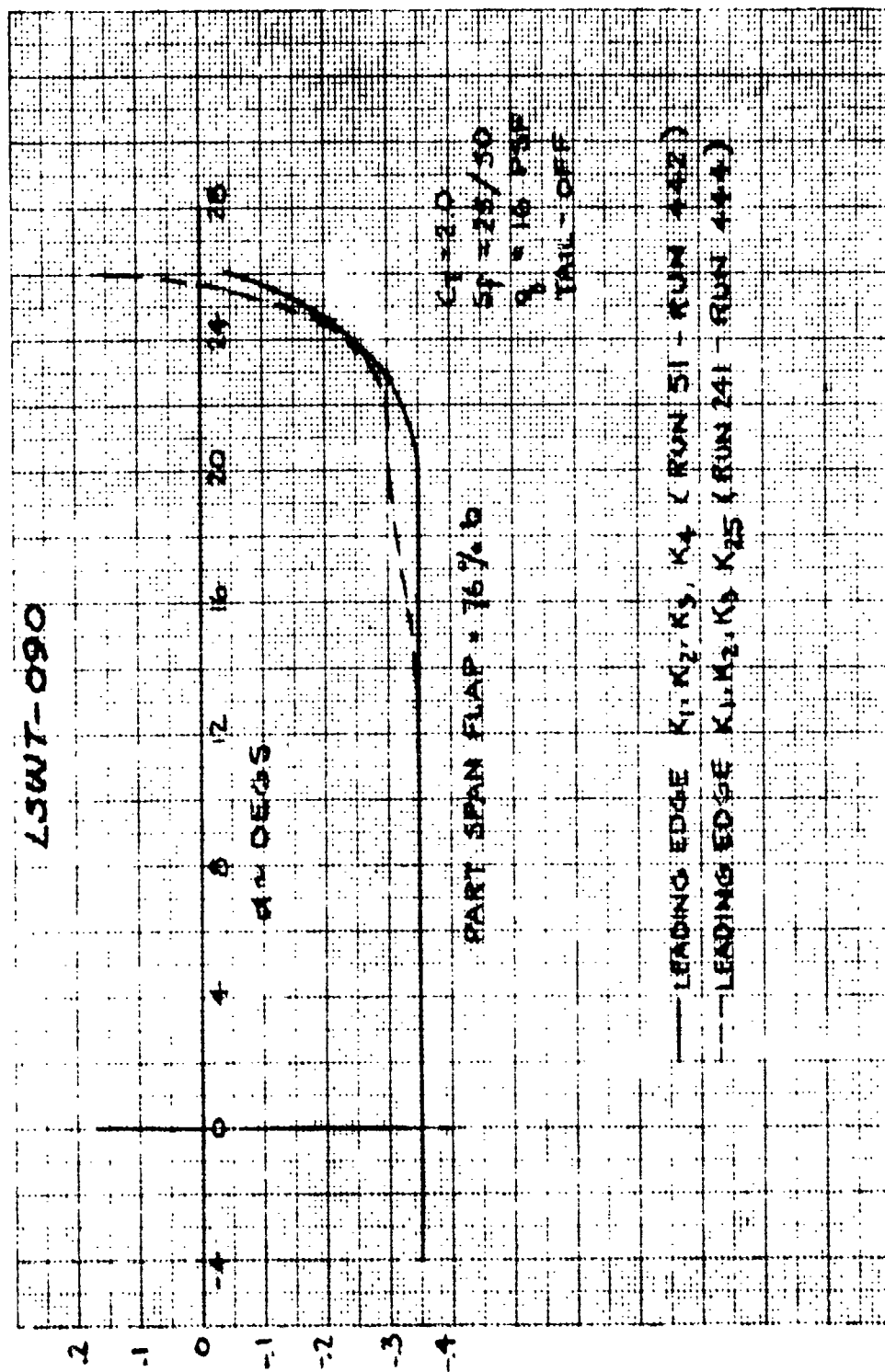
FLAP SPAN EFFECTS ON DRAG COEFFICIENT

Figure 8.1.4



FLAP SPAN EFFECT ON PITCHING MOMENT COEFFICIENT

Figure 8.1.5



FLAP SPAN EFFECT ON PITCHING MOMENT COEFFICIENT

Figure 8.1.6

Section IX

HORIZONTAL TAIL AND ELEVATOR EFFECTIVENESS

The horizontal tail was tested in the high or "T" tail position only at $q = 16$ psf and at $q = 100$ psf. The elevators were tested at $q = 100$ psf only with varying horizontal tail incidence angle. This test series was conducted with a clean wing trailing edge and engine power off to assess the effects of the horizontal tail leading edge slat and effectiveness of the deflected elevator in a virtually nondisturbed wing flow. The tail volume of the horizontal tail tested was $\bar{V}_H = 0.942$.

The horizontal tail trim capability was determined with zero elevator setting at $q = 16$ psf, with wing trailing edge flaps at 25/50 and at 35/60 degrees for varying engine power levels.

9.1 HORIZONTAL TAIL EFFECTIVENESS

With the horizontal tail incidence angle set at $i_H = 0^\circ$ and $\alpha_{FRL} = 0^\circ$, engine power effects on tail contribution to pitching moment of the model is presented in Figure 9.1.1. The leading edge slat is extended and data points for two flap deflections are spotted on the curve which represents a reasonable fairing through obviously wide data scatter.

Figure 9.1.2 shows the engine power effects on tail contribution to model pitch stability levels at $\alpha_{FRL} = i_H = 0^\circ$.

Horizontal tail effectiveness for two flap deflections is shown in Figures 9.1.3 and 9.1.4 versus gross engine blowing coefficient.

9.2 EFFECT OF HORIZONTAL TAIL LEADING EDGE FLAP

Figure 9.2.1 shows the effects of installing a leading edge slat on the horizontal tail. The slat is demonstrated with and without elevators deflected, power off and at $q = 100$ psf. A dramatic increase in Cl_{max} of the tail is readily apparent. The slat was .14c in length, deflected 25° upward with a gap of 0.0125c and a zero percent overhang. The slat was deflected upward because the horizontal tail was mounted inverted.

9.3 ELEVATOR EFFECTIVENESS

The elevator was a double hinged device with its forward hinge at 0.55c and its aft hinge at 0.75c.

Figures 9.3.1, 9.3.2, and 9.3.3 show the effects of elevator deflection on model lift, drag and pitching moment coefficients respectively for varying horizontal tail incidence angles. The wing flaps were at 0/0 degree and power was off. The data was analyzed at $\alpha = 0^\circ$.

Figures 9.3.4, 9.3.5, and 9.3.6 present the change in model lift, drag and pitching moment coefficients respectively due to elevator deflections at various horizontal tail incidence angles.

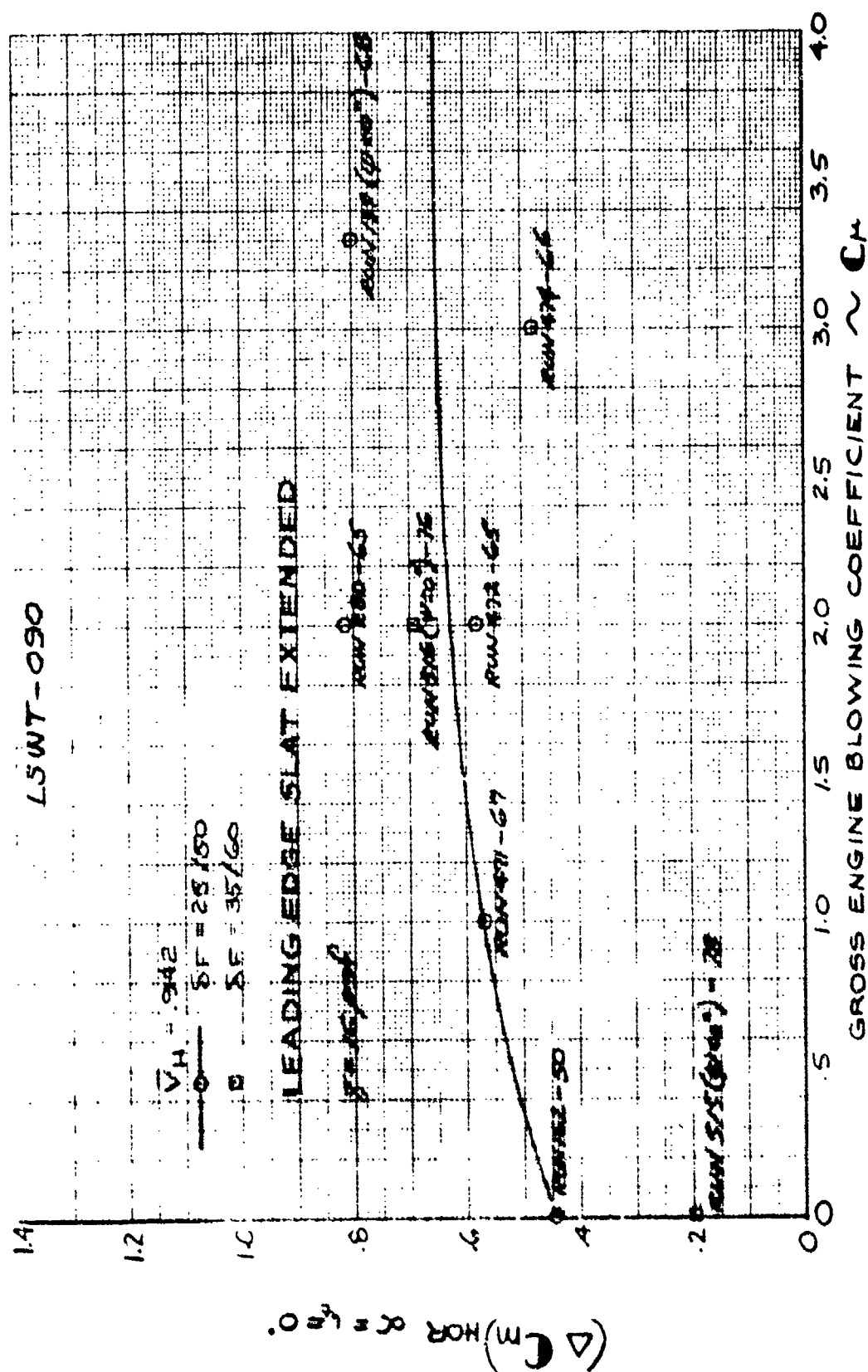
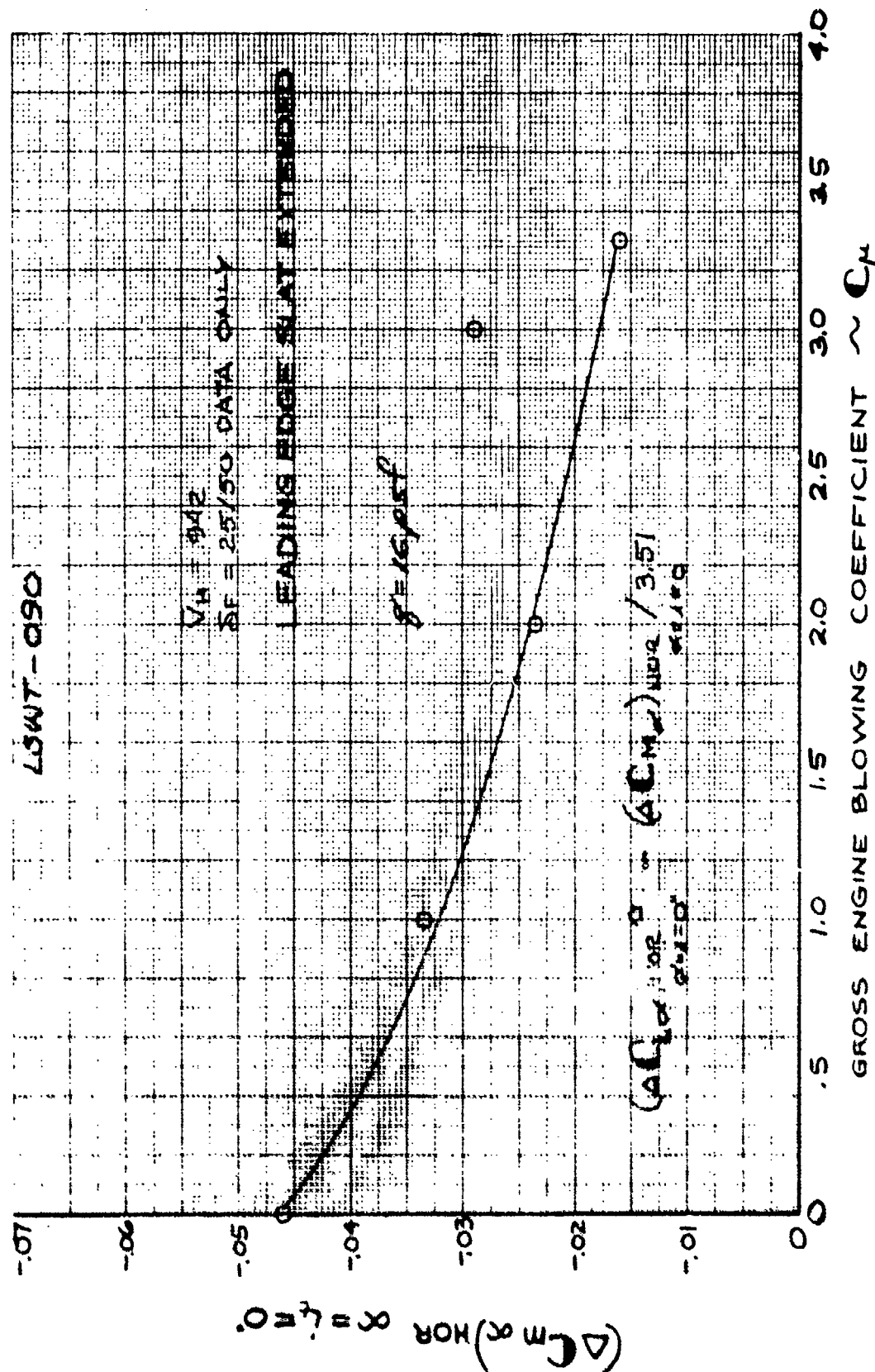


Figure 9.1.1



GROSS ENGINE BLOWING COEFFICIENT $\sim C_\mu$

CHANGE IN HORIZONTAL TAIL ANGLE -OF- ATTACK STATIC STABILITY
 DUE TO ENGINE POWER EFFECTS AT $i_t = 0^\circ$

Figure 9.1.2

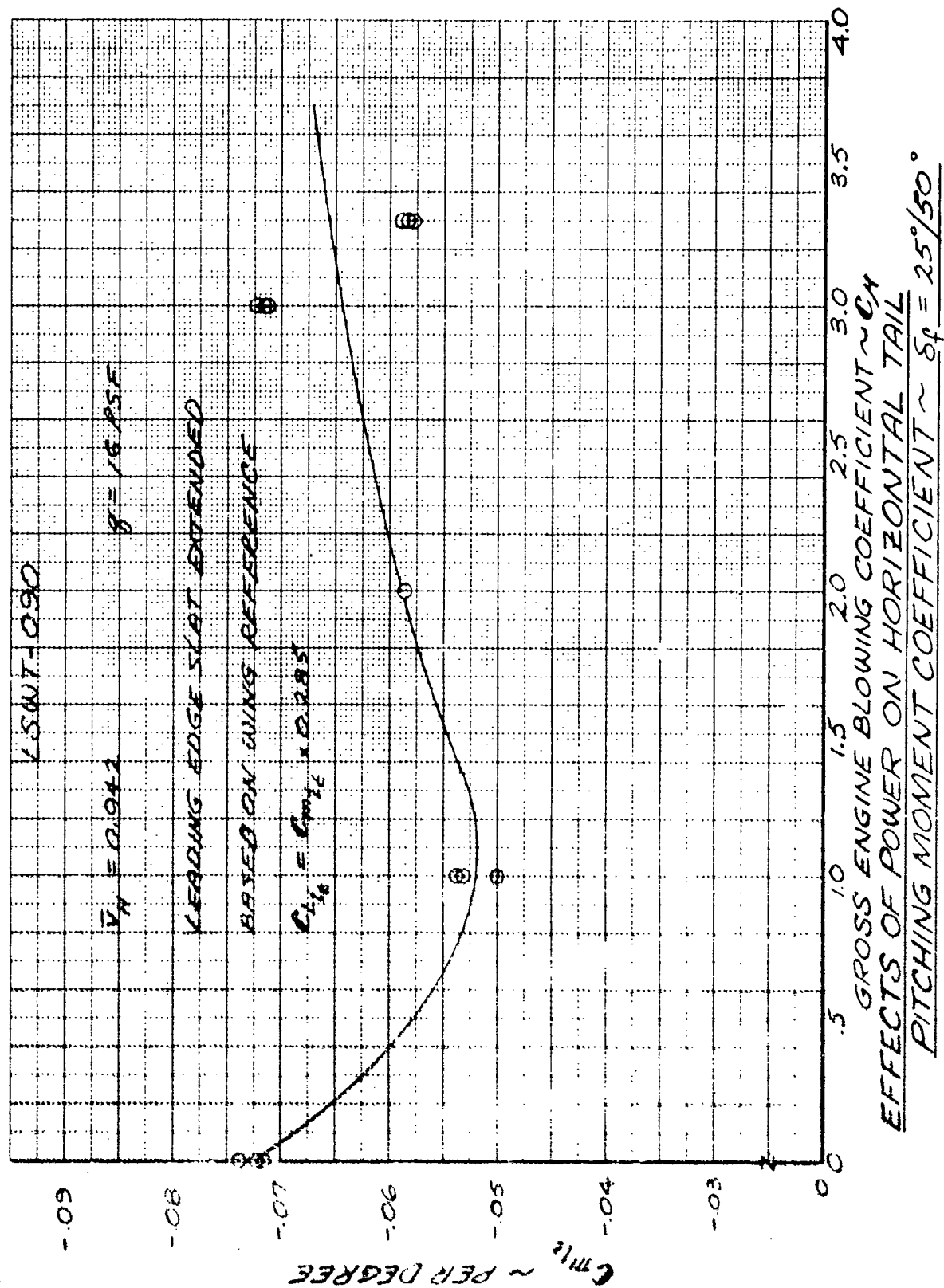


Figure 9.1.3

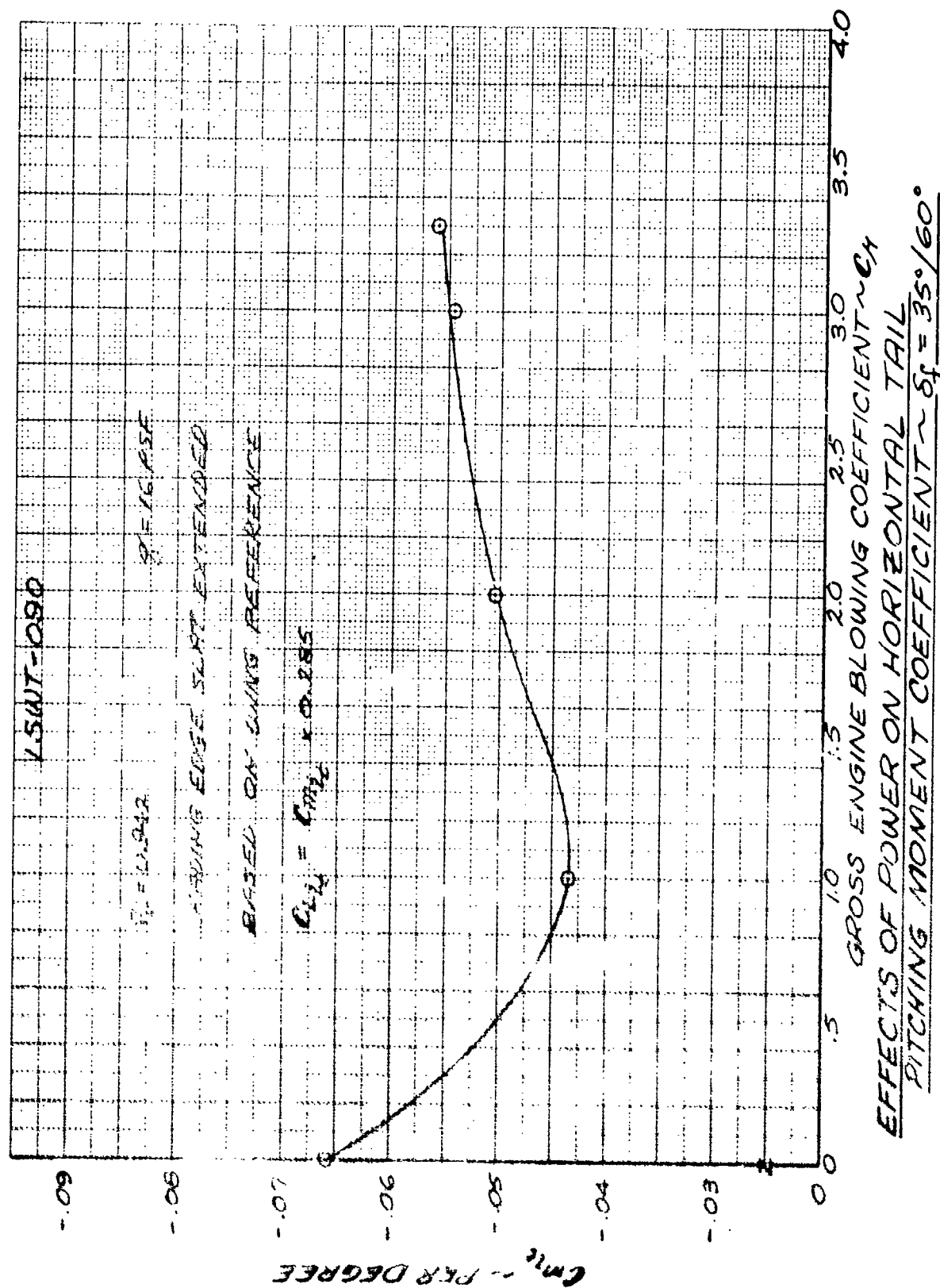


Figure 9.1.4

ELEVATION CONTROL EFFECTIVENESS

$V_H = 0.942$

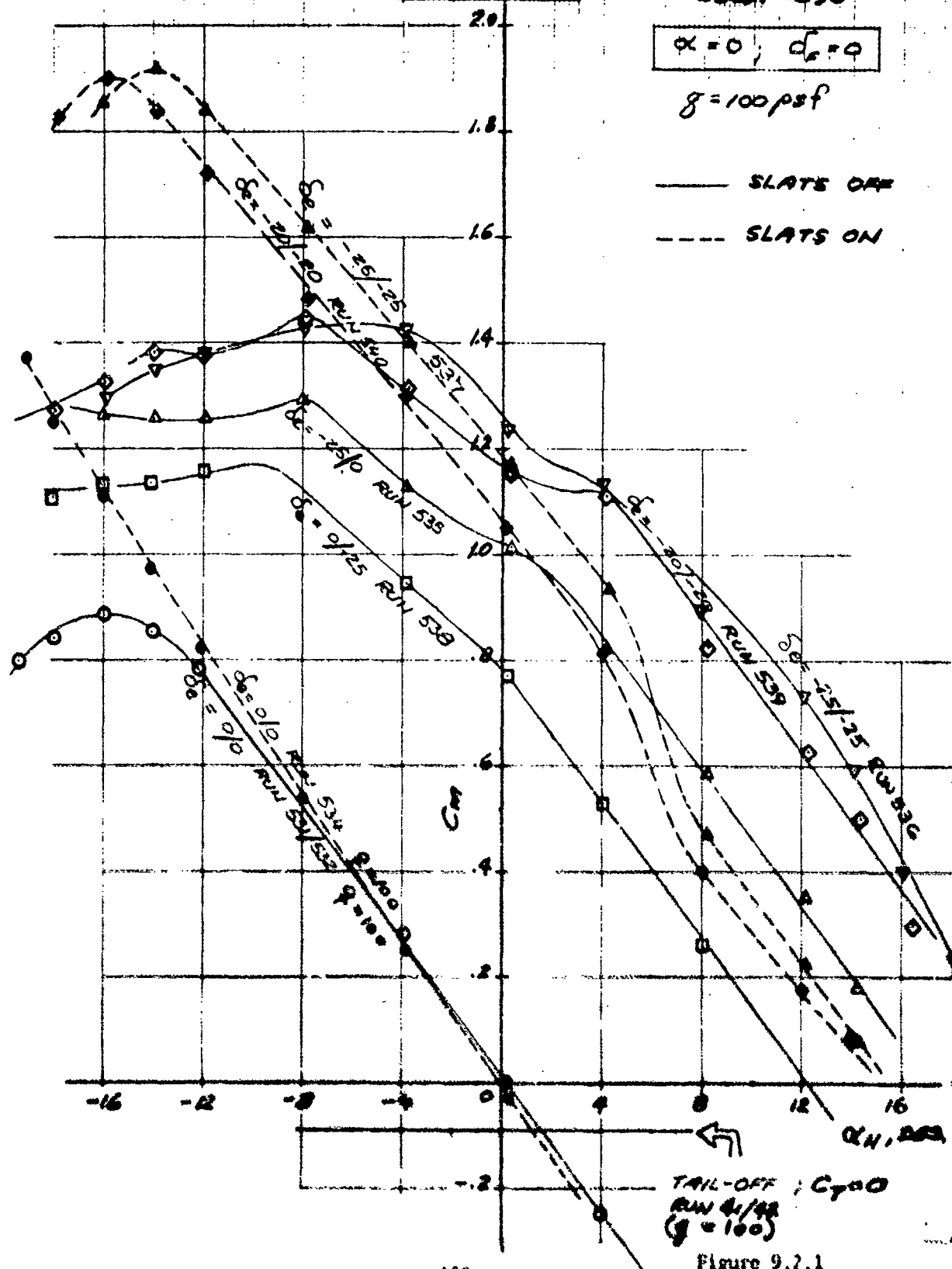
LSWT-090

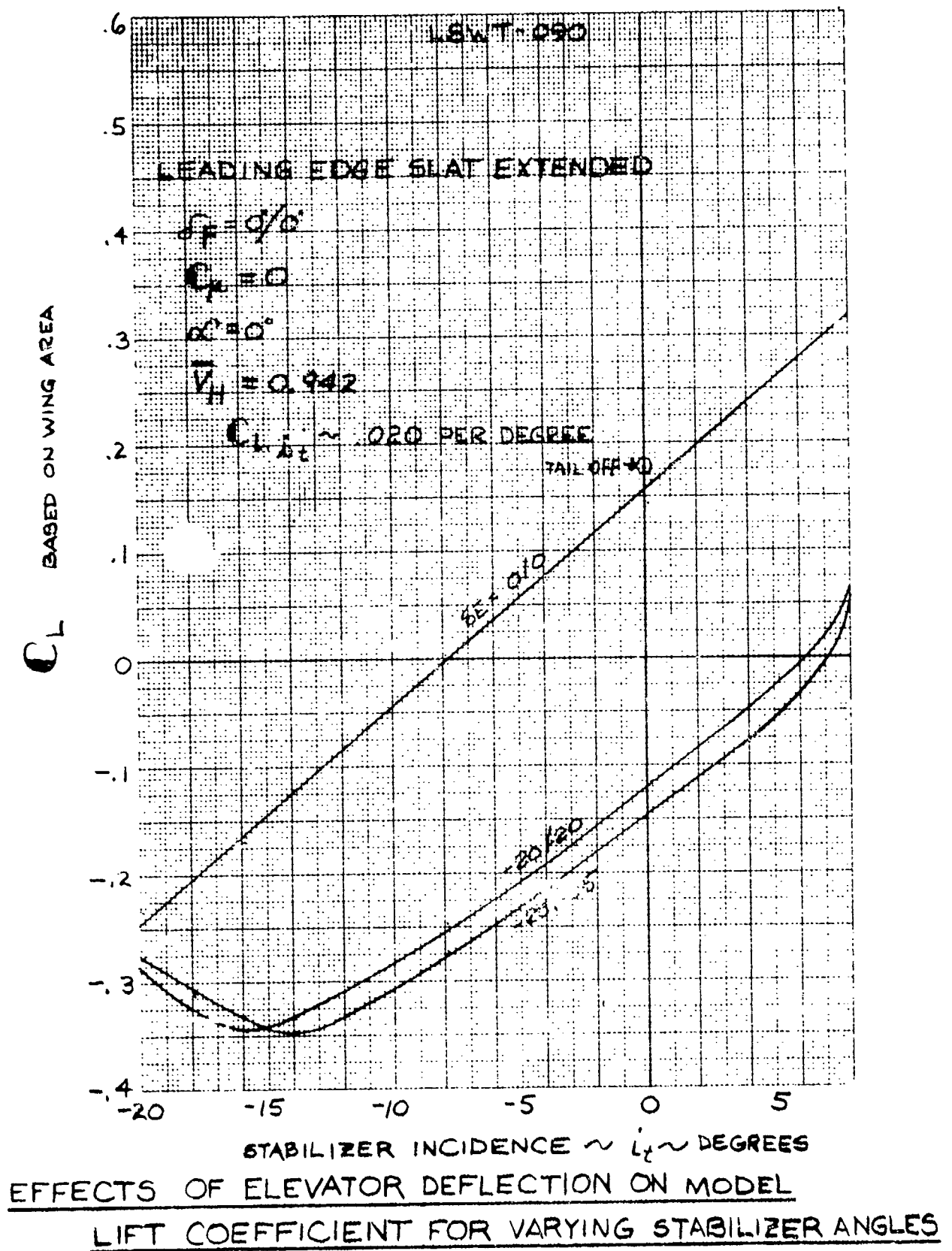
$\alpha = 0; \sigma_c = 0$

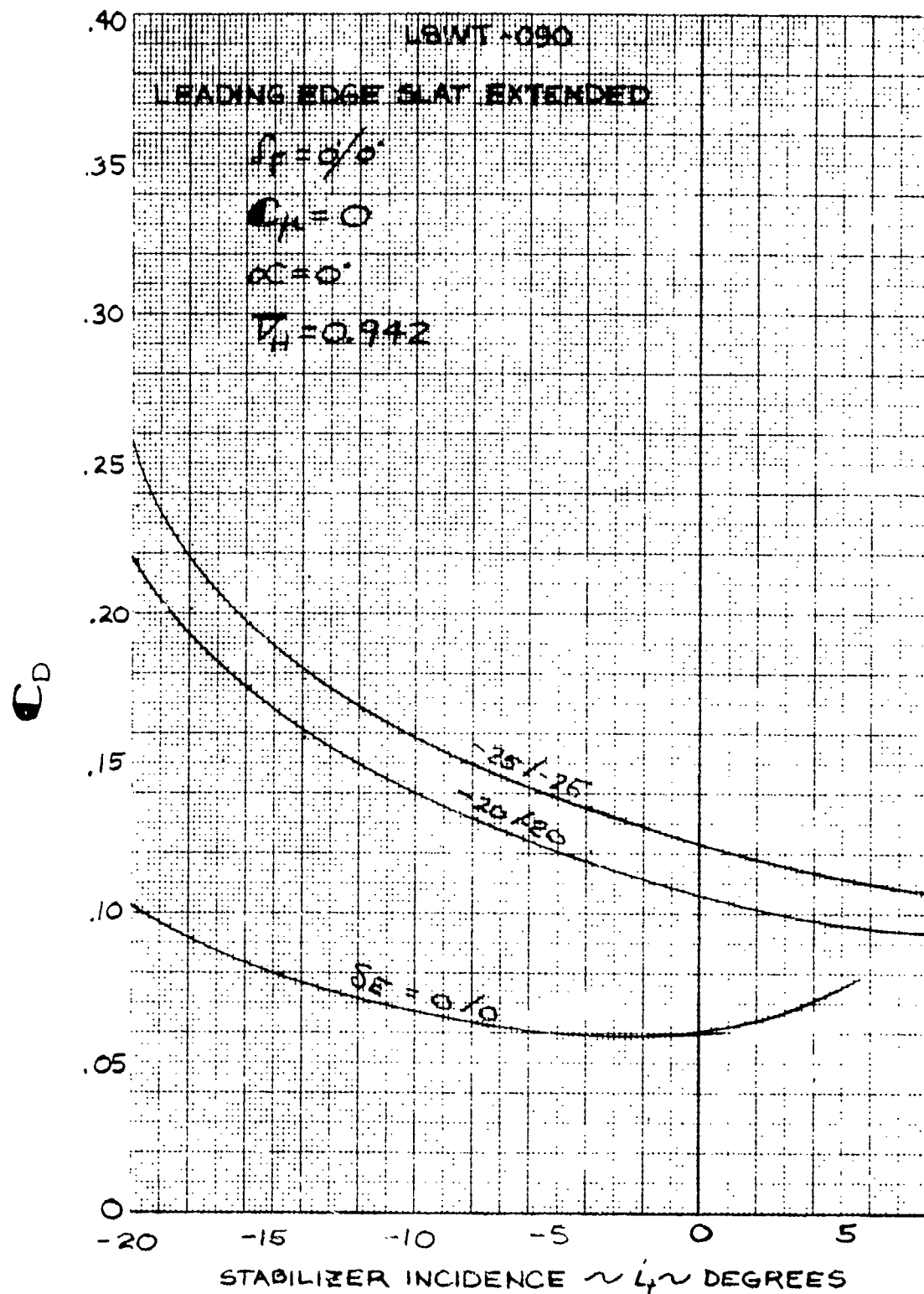
$g = 100 \text{ psf}$

— SLATS OFF

- - - SLATS ON







EFFECTS OF ELEVATOR DEFLECTION ON MODEL
 DRAG COEFFICIENT FOR VARYING STABILIZER ANGLES

Figure 9.3.2

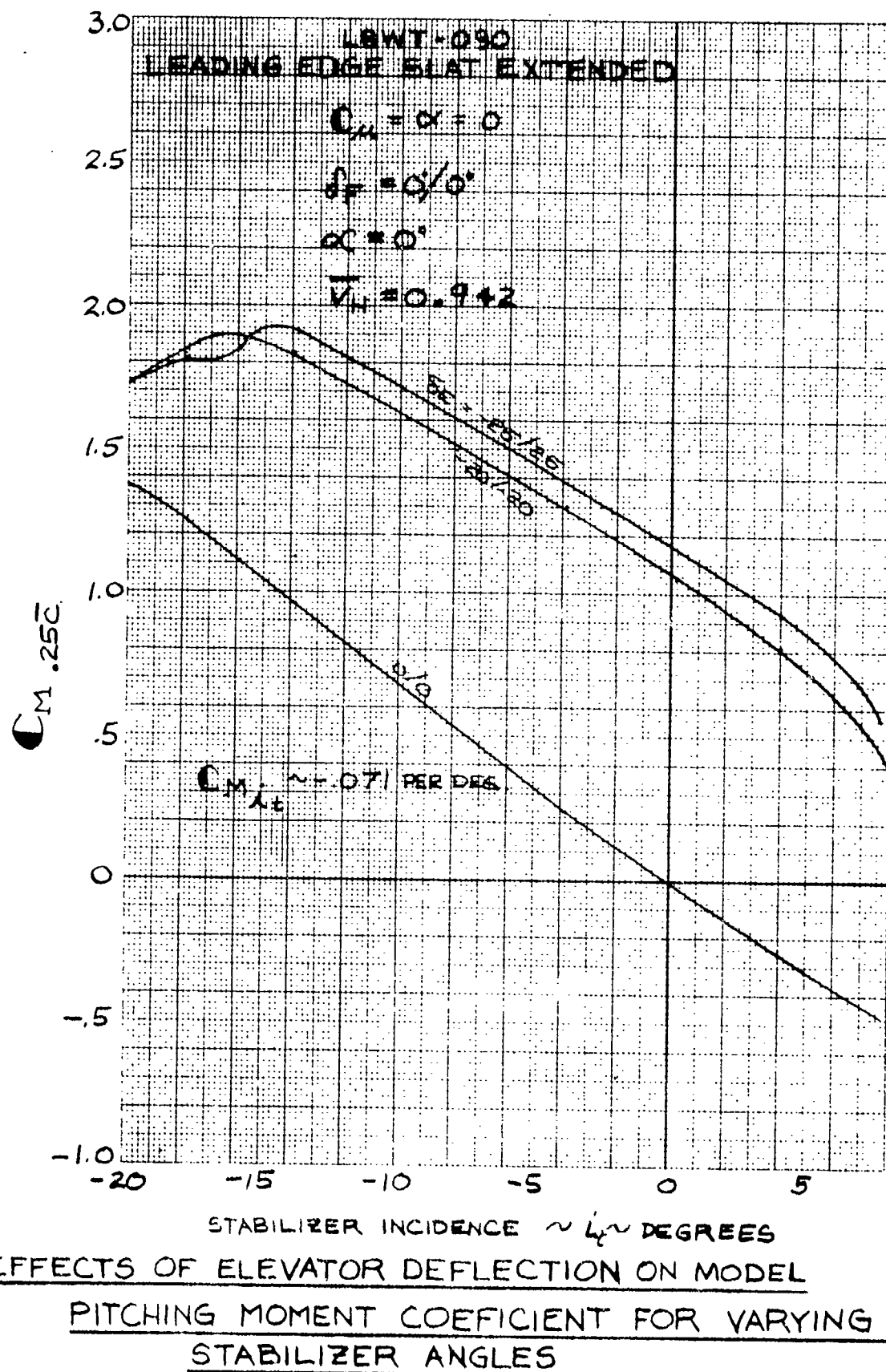


Figure 9.3.3

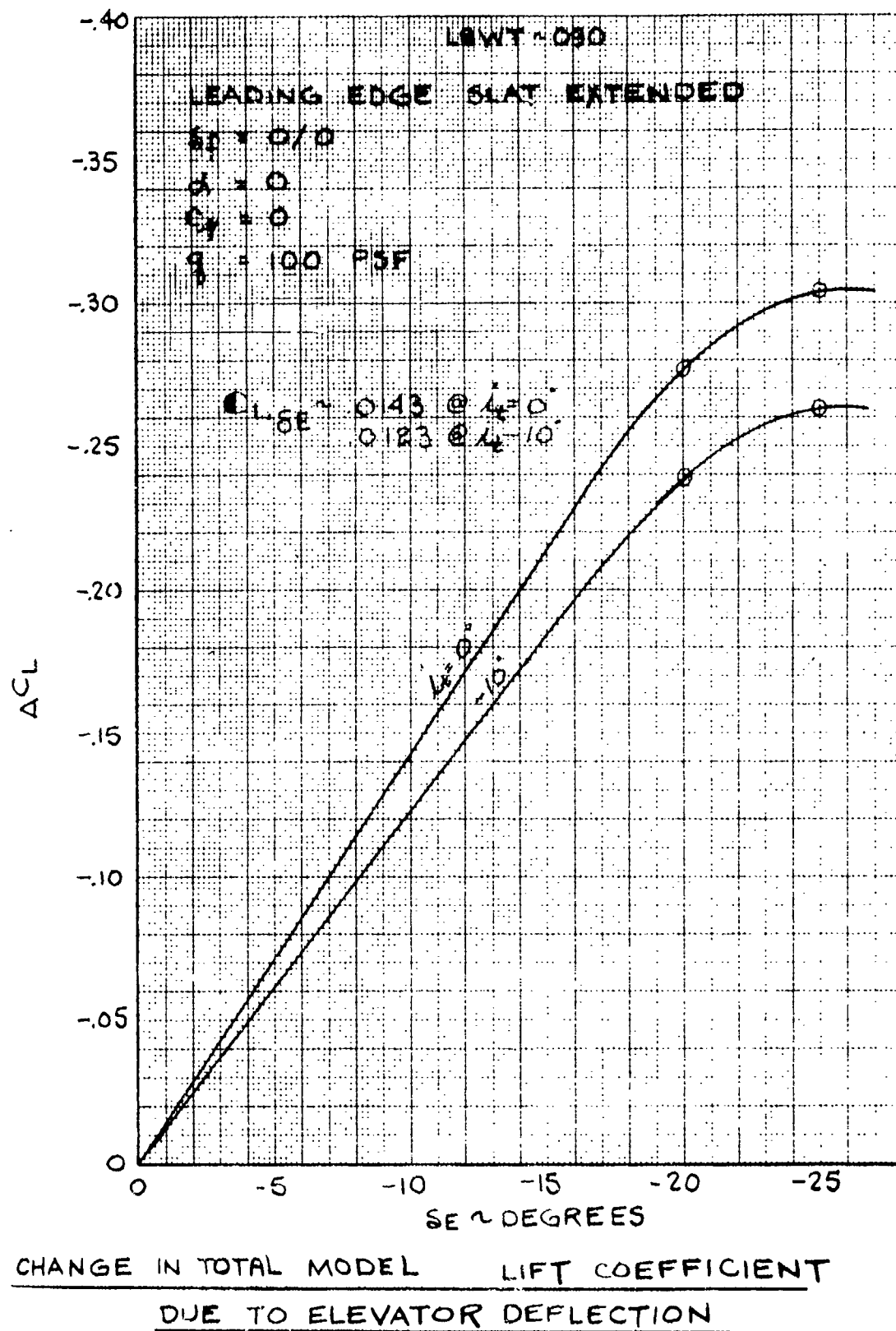
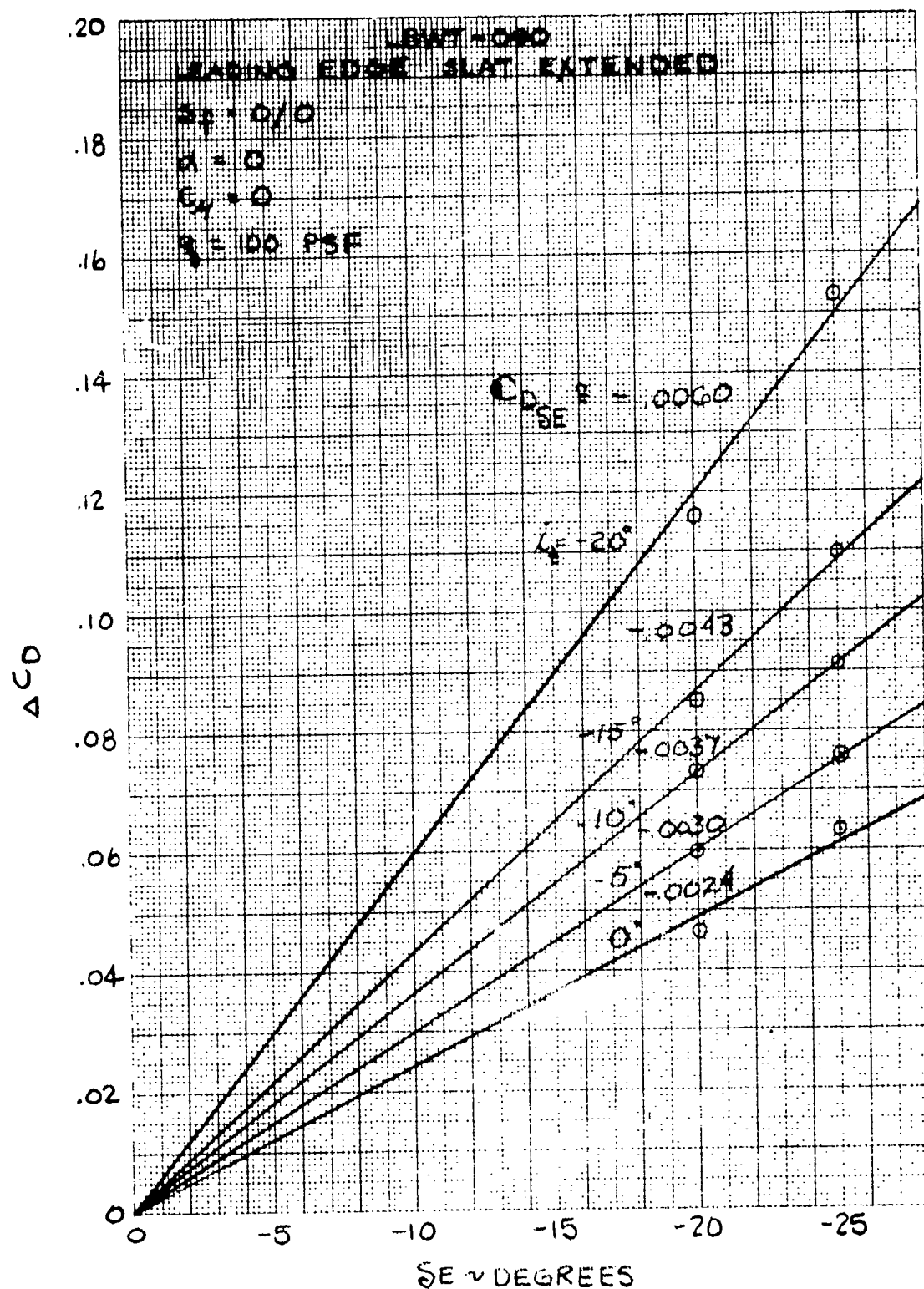


Figure 9.3.4



CHANGE IN TOTAL MODEL DRAG COEFFICIENT
DUE TO ELEVATOR DEFLECTION

Figure 9.3.5

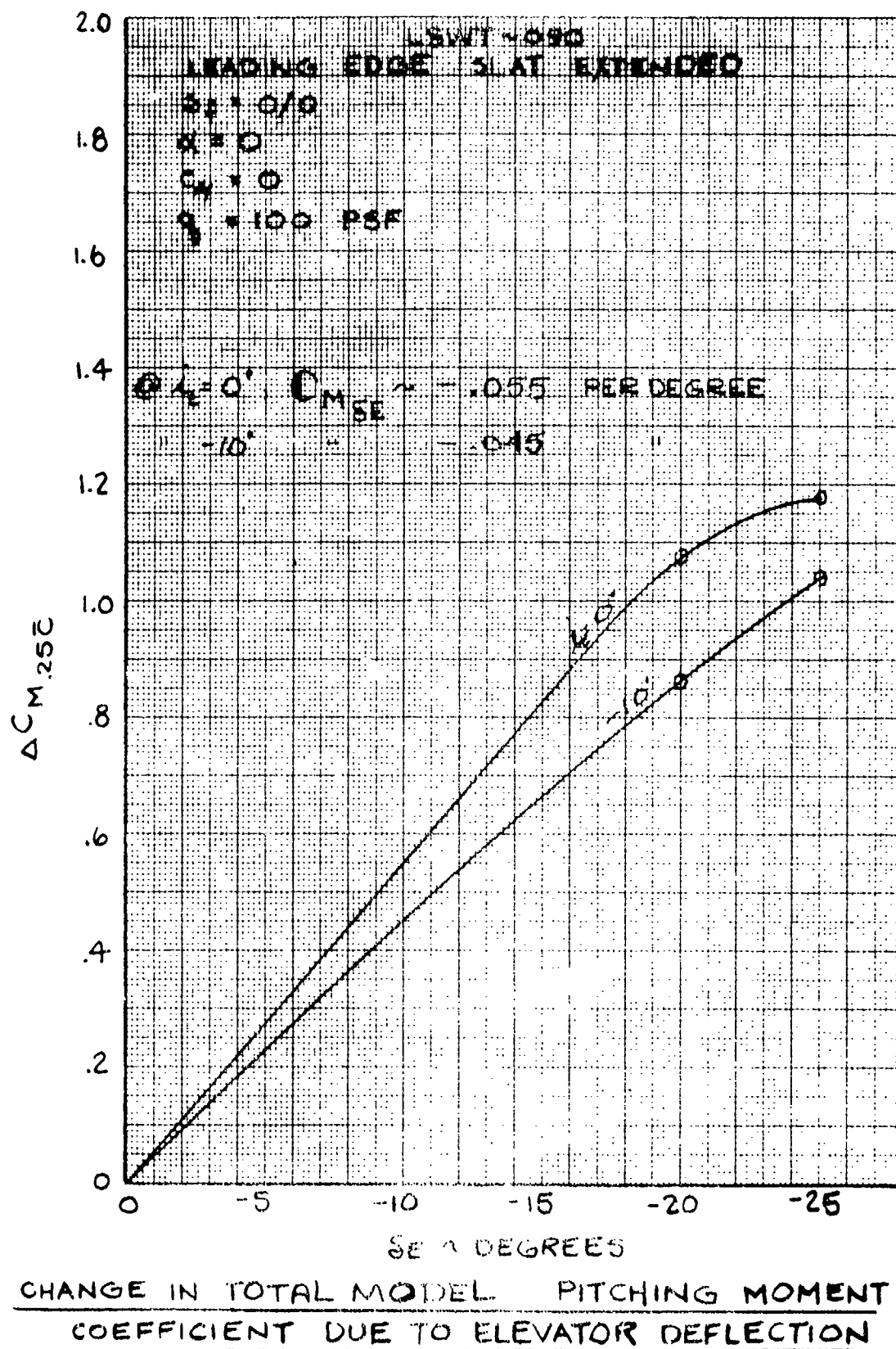


Figure 9.3.6

Section X

LEADING EDGE DEVICES

The leading edge Kruegers were installed in four separate segments consisting of the inboard segment which was mounted between the fuselage and the inboard engine pylon, the mid-pylon Krueger segment which was mounted between the inboard and outboard engine pylons, the outboard Krueger segment which was mounted just outboard of the outboard engine pylon and finally the tip Krueger which was mounted on the outboard most 16 percent of the wing semi-span.

10.1 EFFECT OF LEADING EDGE KRUEGERS

In order to be able to determine individual Krueger segment effects a leading edge buildup was tested whereby each Krueger segment was added one at a time and tested. In order to evaluate the effects of wing sweep the inboard Krueger on the basic configuration had to be removed once since no inboard Krueger was available for the other wing sweeps tested. Figure 10.1.1 shows the effects of removing the inboard Krueger from the basic configuration on the longitudinal aerodynamic parameters with power-off.

Figure 10.1.3 represents the same test results and for the same purposes as does Figure 10.1.1 with the exception that Figure 10.1.3 is powered.

Figure 10.1.2 shows the effects of performing a leading edge slat build-up on longitudinal aerodynamic parameters with power off. The build-up begins with the tip Krueger only installed and continues adding each segment working inboard until a full span configuration is realized.

Figures 10.1.4 and 10.1.5 represent the same test results as does Figure 10.1.2 with the exception that the tests of Figures 10.1.4 and 10.1.5 are powered.

10.2 COMPARISON OF LEADING EDGE BLC WITH LEADING EDGE KRUEGERS

In this test the leading edge was clean with the exception of the tip segment where the three different leading edges were tested. They were tested at a $C\mu = 2.0$ so that leading edge blowing would be available. Figure 10.2.1 shows the effects of the three different leading edges on powered $C_{L_{max}}$ and α_{stall} . Leading edge blowing was a direct function of engine blowing level and was mechanically adjusted so that maximum engine blowing coefficient will produce a maximum leading edge blowing coefficient of approximately 6 percent per side and total maximum leading edge blowing was 12 percent ($C\mu_{1e} = 0.12$).

The variation of $C_{L_{max}}$ with power is presented in Figure 10.2.2 for the three leading edges tested.

ASWT-090

EFFECT OF INBOARD KRUEGER

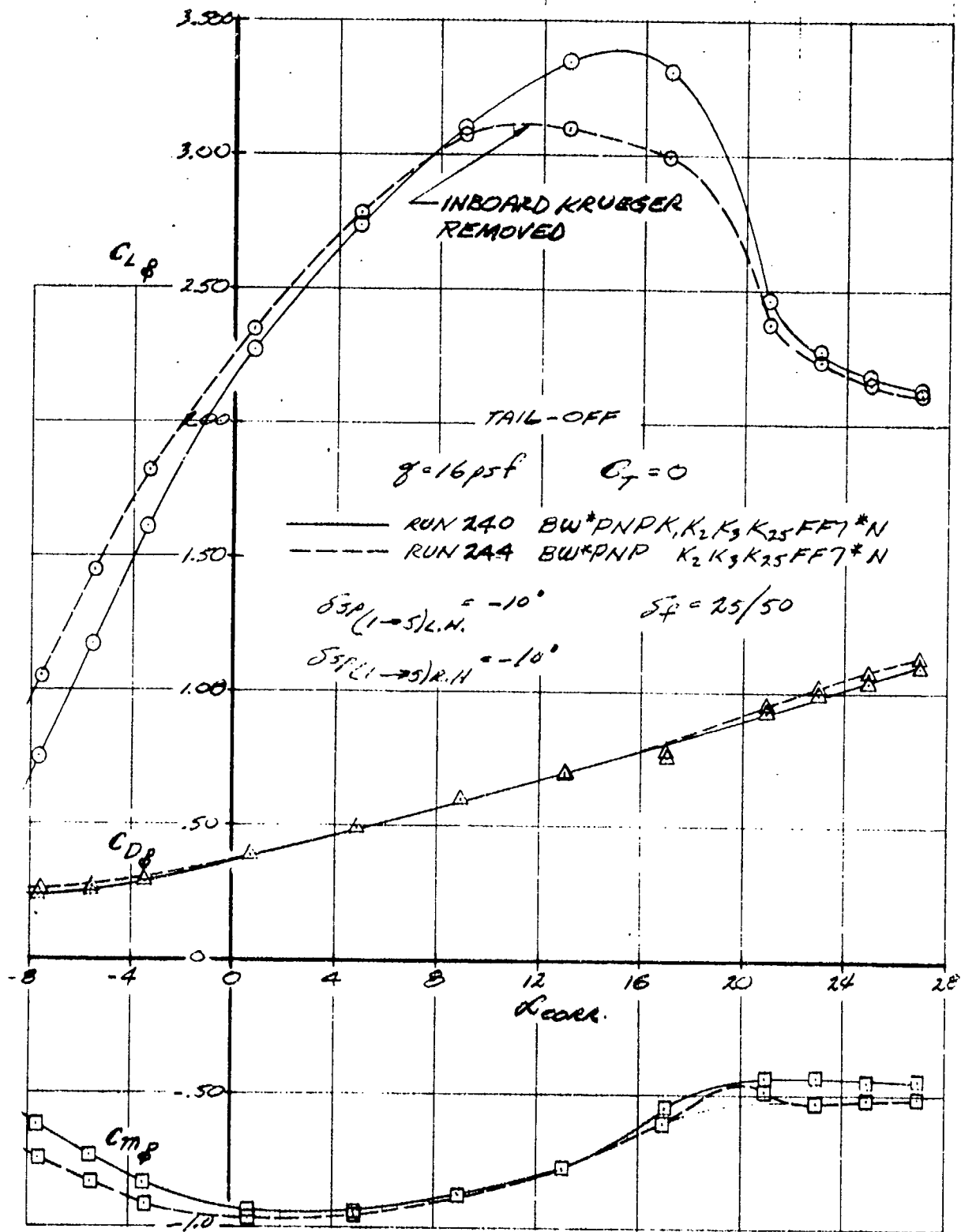


Figure 10.1.1

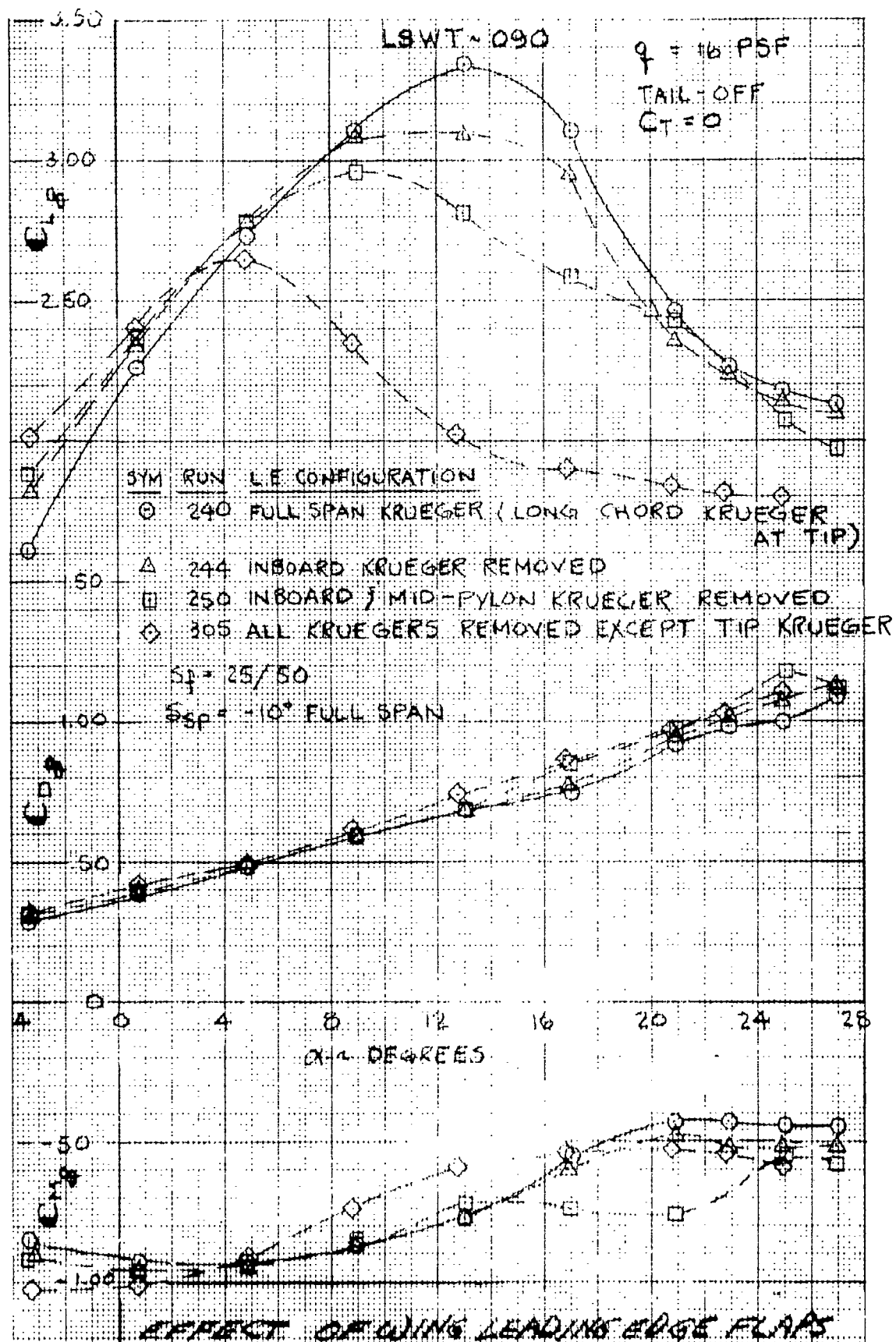


Figure 10.1.2

ASWT-090
EFFECT OF INBOARD KRUEGER

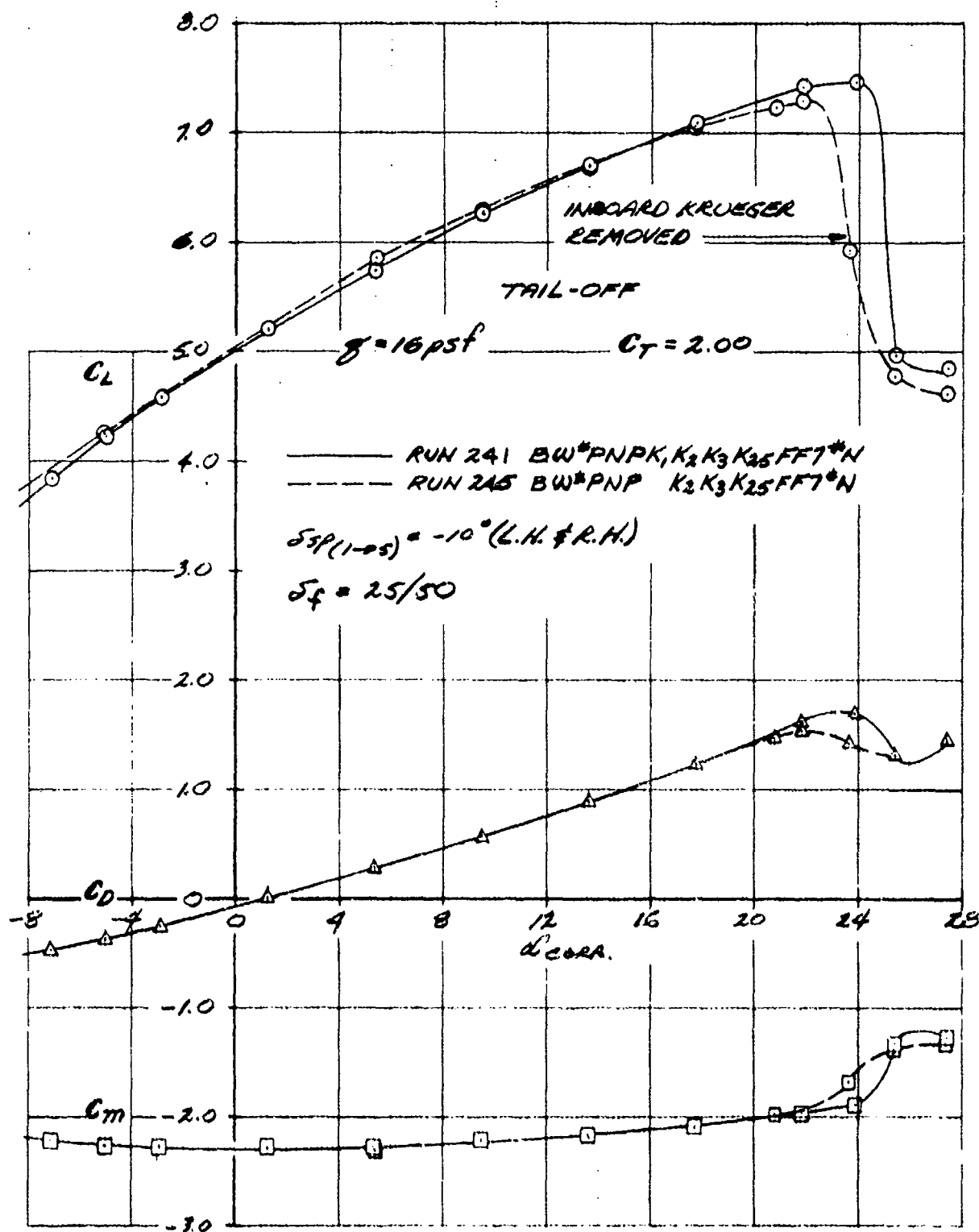
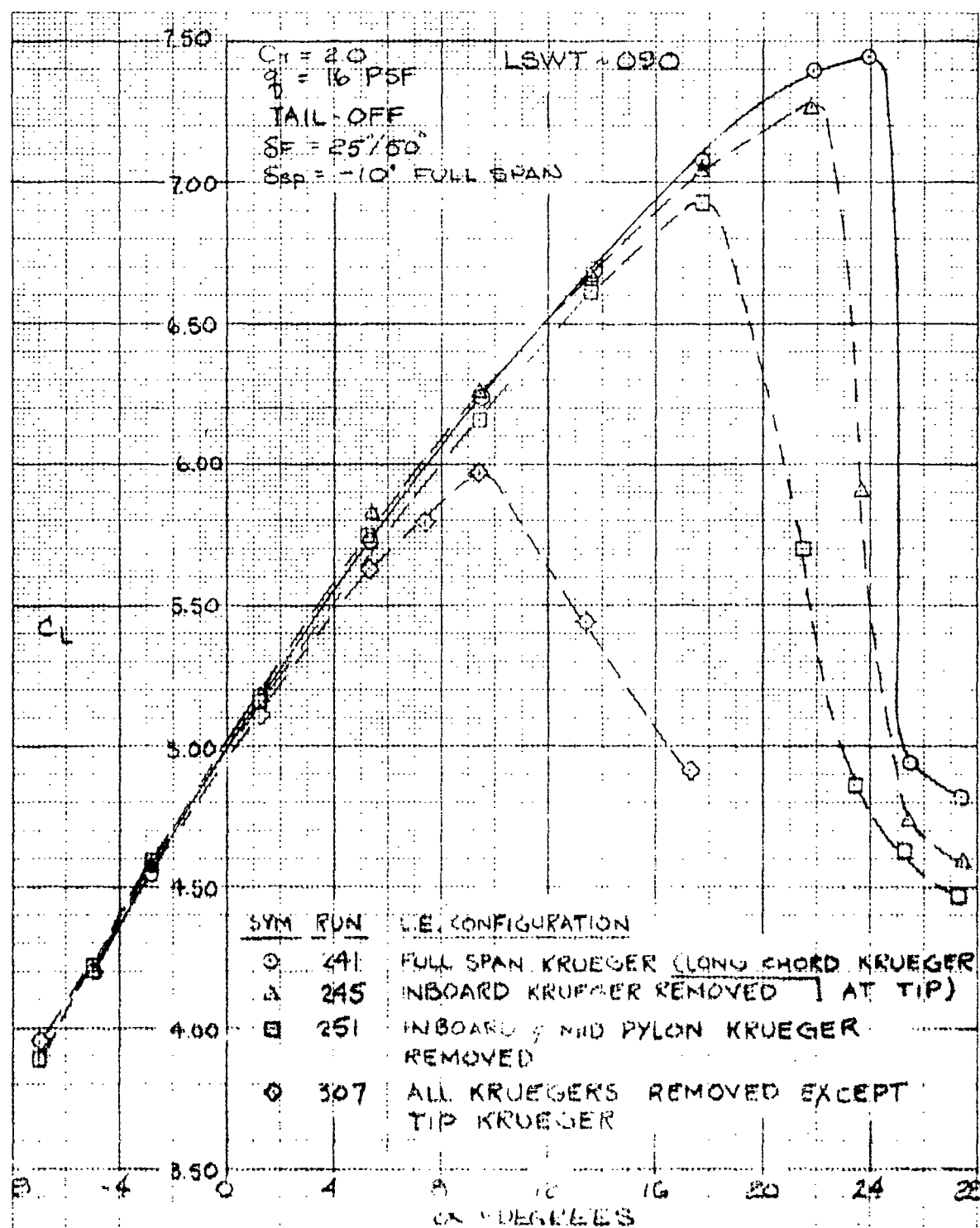


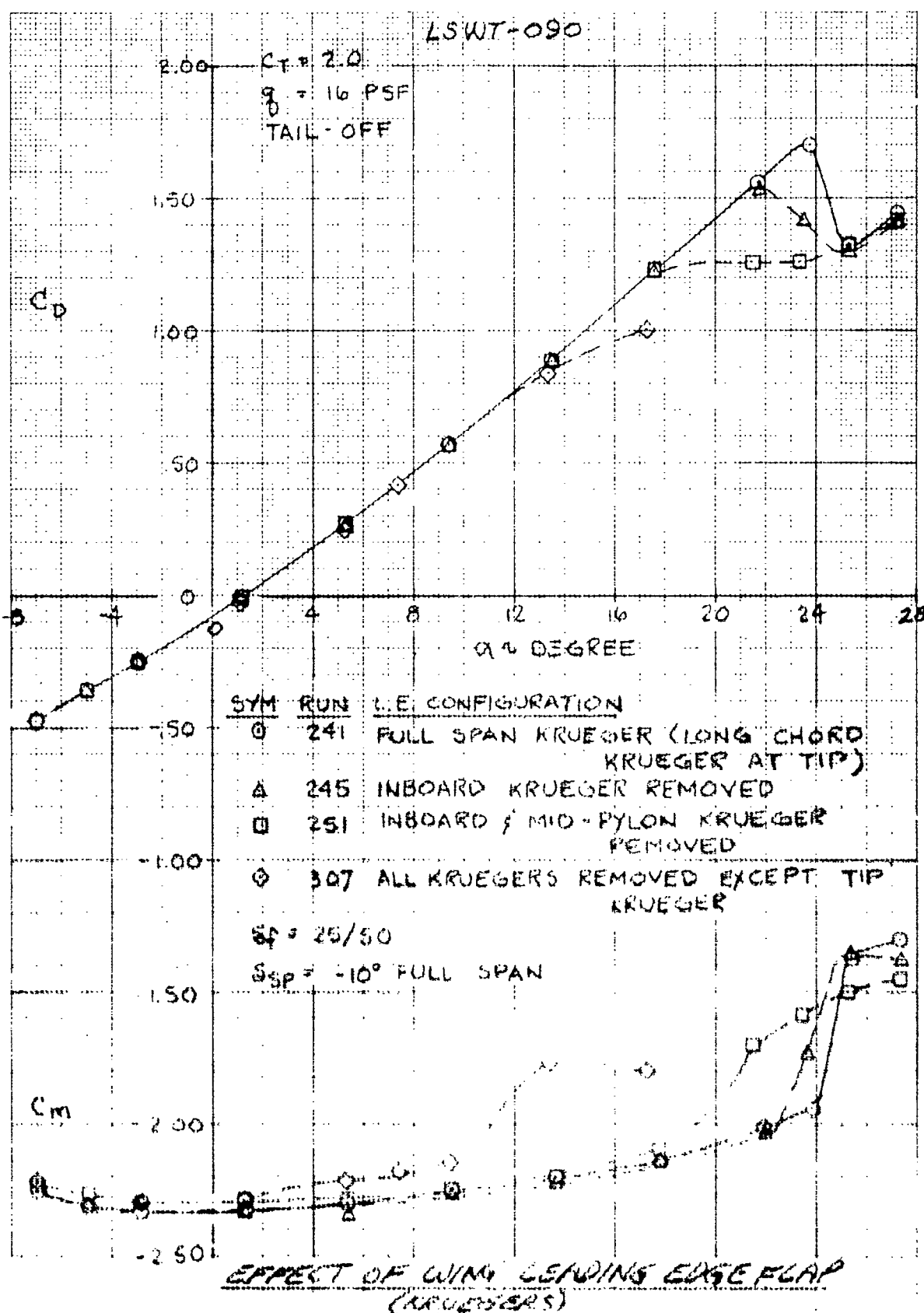
Figure 10.1.3

FOR 10 TO THE CENTIMETER 46 1513
 10 6 25 24
 ALUFEL & ESSER CO



EFFECT OF WING LEADING EDGE FLAP
 (KRUEGERS)

W-E 10 X 10 TO THE CENTIMETER 46 1513
 10 X 10 IN. 10 X 10 IN. 10 X 10 IN.
 10 X 10 IN. 10 X 10 IN. 10 X 10 IN.



LSWT - 090

COMPARISON OF OUTBOARD L.E. DEVICES

$C_T = 2.0$

$\delta_F = 25^\circ/50'$

$q = 16 \text{ psf}$

$\delta_{SP} = -10^\circ$

$\delta_H = +15^\circ$

RUN

LE. DEVICE

—○—

297

K_4 , BASIC KRUEGER

—△—

307

K_{25} , LONG CHORD

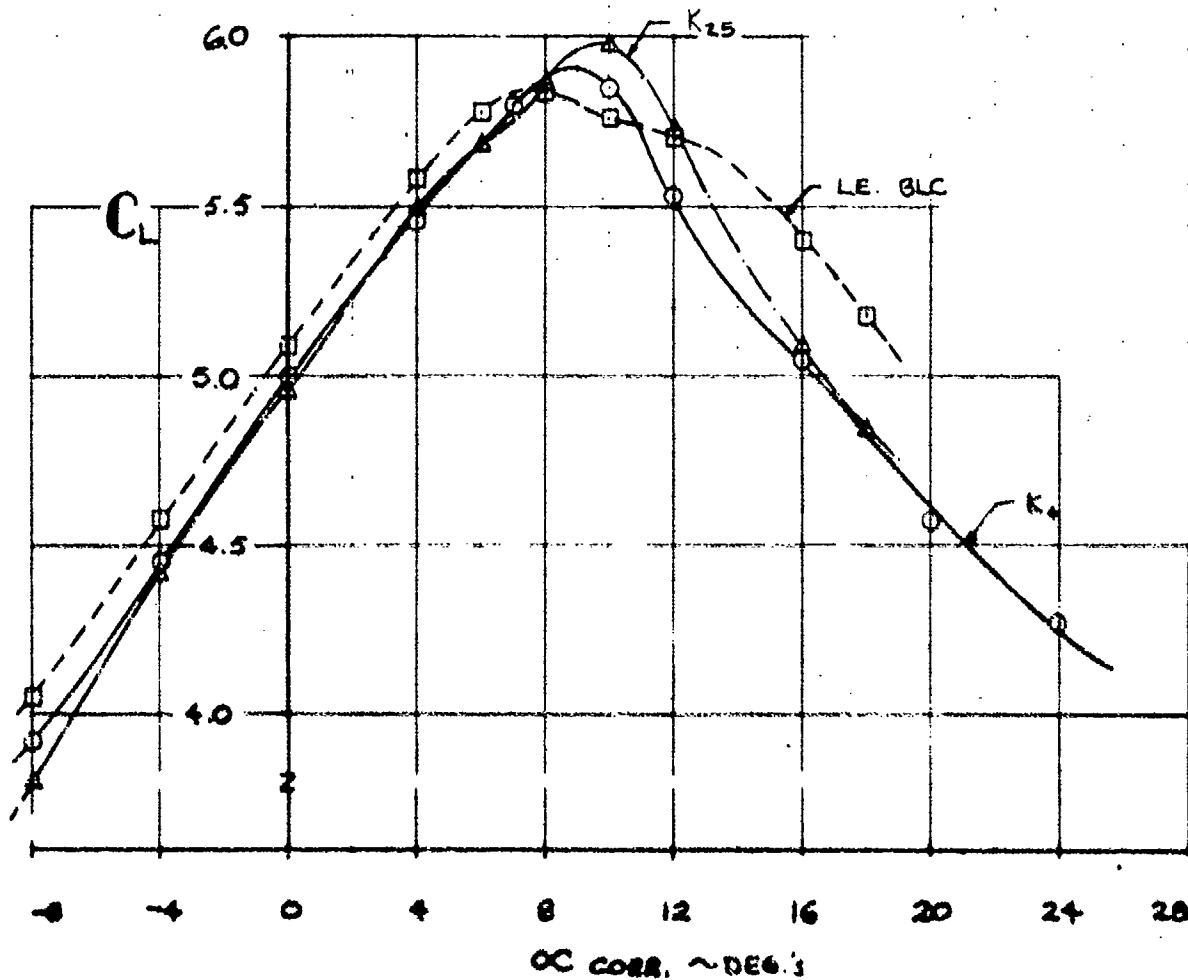
KRUEGER

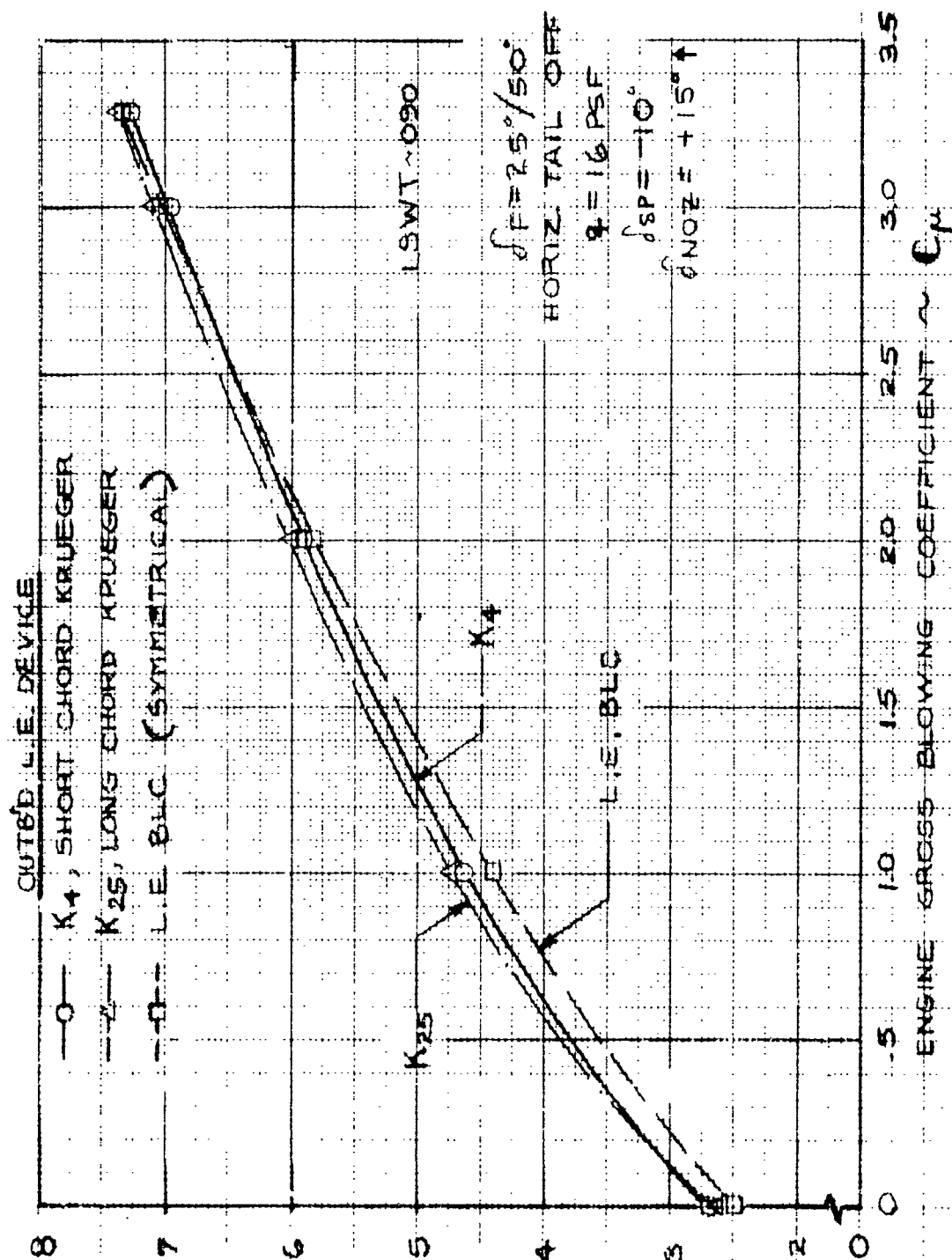
---□---

317

L.E. BLC

TAIL-OFF





EFFECT OF POWER ON MAXIMUM LIFT COEFFICIENT
 FOR VARIOUS OUTBOARD LEADING EDGE DEVICES

Figure 10.2.2

Section XI

NACELLE LOCATION VARIATION

The engine nacelles were moved vertically and fore- and-aft to two locations other than that defined in the basic configuration. The centerline of thrust in the plane of each exhaust nozzle is located vertically (Z/C) and axially (X/C) with respect to the wing leading edge. In this test, at the basic spanwise location, the nacelles were moved aft from an $X/C = 0$ to an $X/C = 0.15$ in the horizontal plane of $Z/C = 0.27$ (basic configuration) and they were moved up from a $Z/C = 0.27$ to a $Z/C = 0.19$ in the vertical plane of $X/C = 0$ (basic configuration).

Lateral relocations were carried out with the nacelles mounted in the basic configuration ($X/C = 0$ and $Z/C = 0.27$) with respect to the wing leading edge and the nacelles were moved outboard along the span. The inboard nacelles were moved from $Y/(b/2) \approx 25$ percent to $Y/(b/2) \approx 35.6$ percent and the outboard nacelles were moved further outboard from $Y/(b/2) \approx 40$ percent to $Y/(b/2) \approx 56$ percent based upon a semispan of 50.08 inches.

11.1 EFFECTS OF LONGITUDINAL AND VERTICAL ENGINE LOCATION PERTURBATION ON LONGITUDINAL AERODYNAMIC PARAMETERS

The effects of axial and vertical engine nacelle relocation are presented in Figures 11.1.1 to 11.1.6 inclusive. The increments in the total lift, drag and pitching moment coefficients are shown for $C_T = 0$ and 2.0 and at $\alpha = 0^\circ, 4^\circ$, and 8° . Figures 11.1.1 through 11.1.3 show the effects of a rearward nacelle shift and Figures 11.1.4 through 11.1.6 show the effects of a vertical nacelle shift.

11.2 EFFECTS OF ENGINE SPANWISE PERTURBATION

Figures 11.2.1 through 11.2.3 inclusive show the effects of the spanwise engine perturbation on incremental lift, drag and pitching moment coefficients due to power. The increments were taken at $\alpha = 0^\circ$ with tail off.

Figures 11.2.4 through 11.2.6 inclusive present the effects of engine spanwise relocation on the lateral-directional derivatives. These data were taken at $\alpha = 0^\circ$ with tail on and at C_{μ} 's of 0 and 2.0 only.

11.3. COMPARISON OF "FIXED" AND "SWIVEL" PYLONS

Figures 11.3.1 and 11.3.2 represents the increments in the longitudinal aerodynamic parameters at $C_T = 0$ and 2.0 respectively involved when changing from the fixed to the swiveling pylon. As can be seen at $C_T = 0$ practically no differences exist in going from the fixed to the swiveling pylon. However at $C_T = 2.0$ and at angles of attack greater than 2.0° significant drag coefficient penalties are incurred with the use of the swiveling pylon. The fixed pylon is called "Type II pylon" and the swiveling pylon is called "Type I" pylon.

LSWT-090

$$(\Delta C_L)_{NAC} = (C_L)_{NEW LOC.} - (C_L)_{BASIC LOC.}$$

$$\delta \alpha = 25^\circ / 50^\circ$$

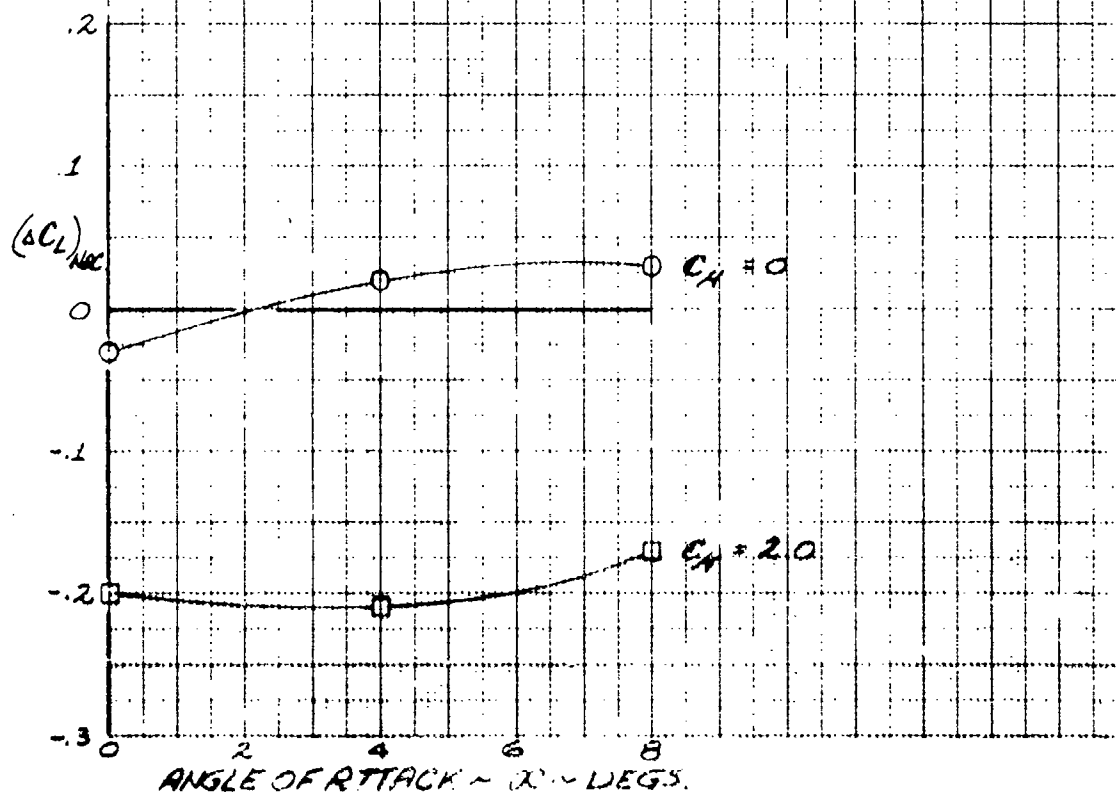
$$\rho = 16 \text{ PSF}$$

$$\delta \alpha_{sp} = -10^\circ \text{ FULL SPAN}$$

TAIL-OFF

$$\delta \alpha_{noz} = +15^\circ$$

NOTE: THE NACELLE WAS SHIFTED AFT FROM AN $X/C = 0$ TO AN $X/C = 0.14$ AT A CONSTANT $Z/C = 0.27$.



CHANGE IN LIFT COEFFICIENT DUE TO A REARWARD SHIFT IN ENGINE NACELLE LOCATION FROM THE BASIC CONFIGURATION

Figure 11.1.1

LSWT-090

$$(\Delta C_D)_{NAC.} = (C_D)_{NEW LOC.} - (C_D)_{BASIC LOC.}$$

$$\delta\alpha = 25^\circ/50^\circ$$

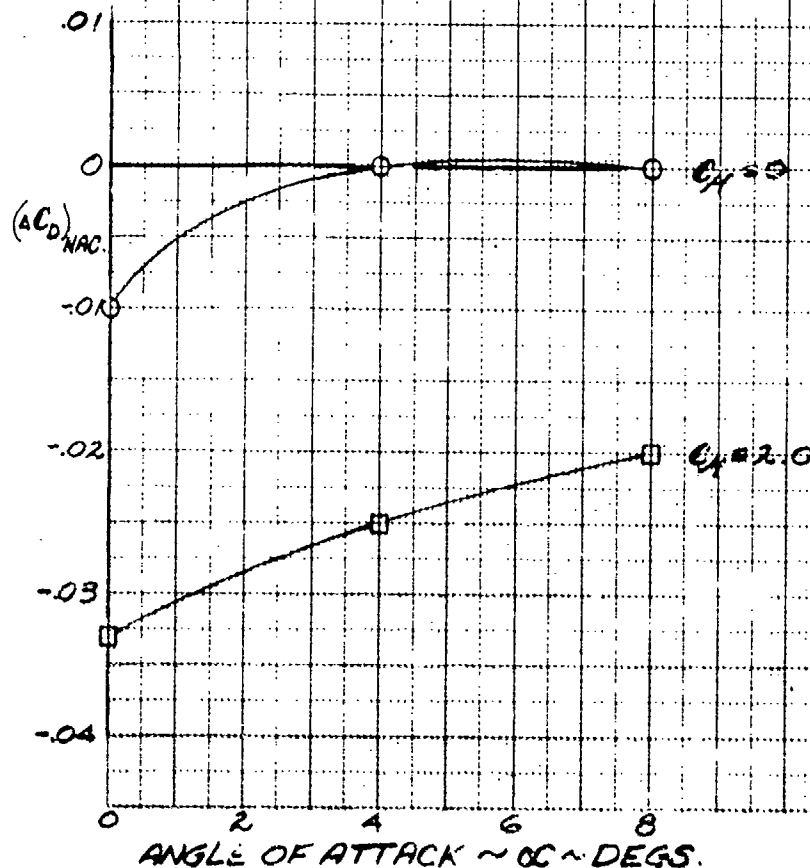
$$\rho = 16 \text{ PSF}$$

$$\delta\delta p = -10^\circ \text{ FULL SPAN}$$

TAIL-OFF

$$\delta\alpha_{NOZ} = +15^\circ$$

NOTE: THE NACELLE WAS SHIFTED AFT FROM AN $X/C = 0$ TO AN $X/C = 0.14$ AT A CONSTANT $Z/C = 0.27$.



CHANGE IN DRAG COEFFICIENT DUE TO A REARWARD SHIFT IN ENGINE NACELLE LOCATION FROM THE BASIC CONFIGURATION

Figure 11.1.2

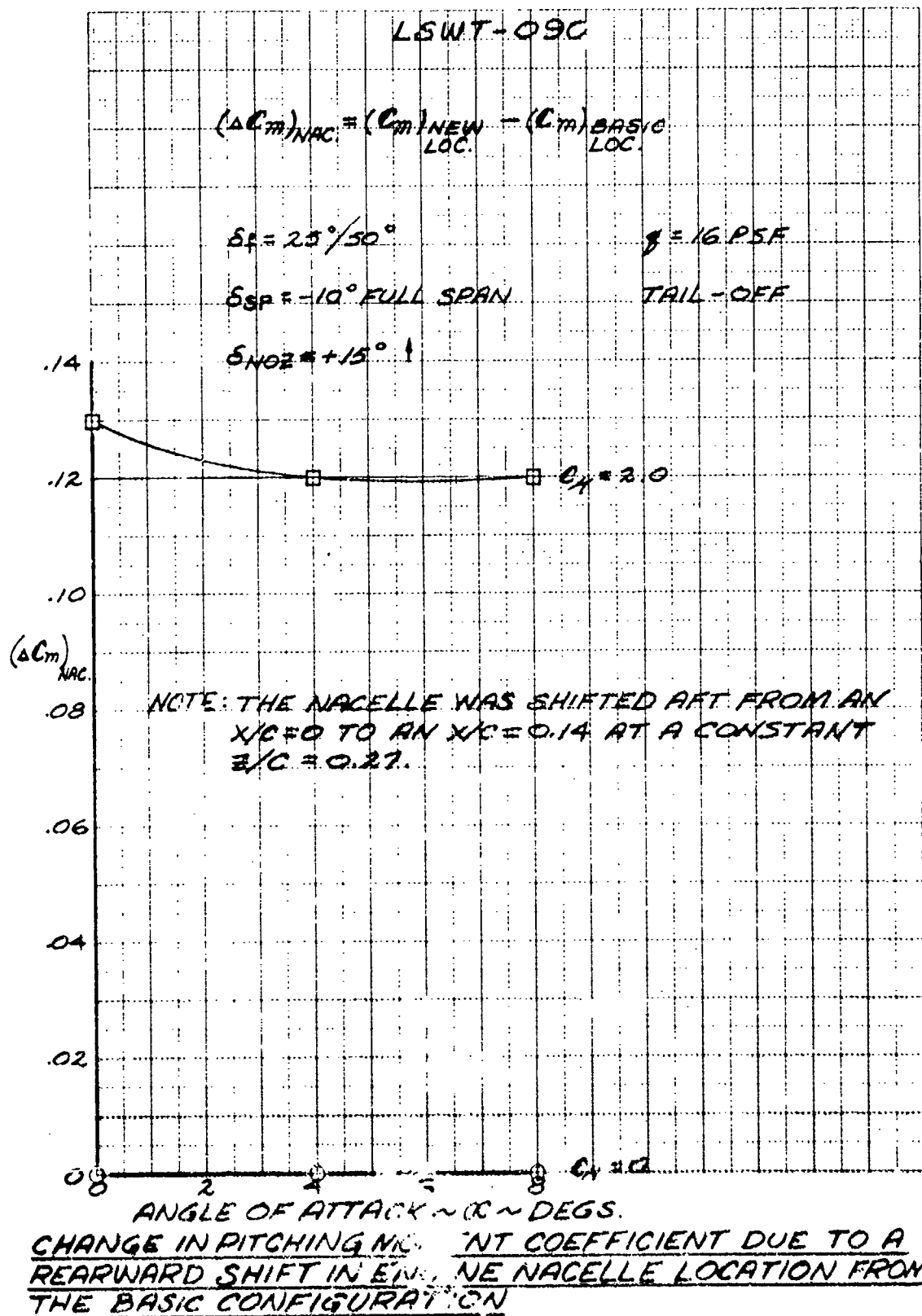


Figure 11.1.3

LSWT-090

$$(\Delta C_L)_{NAC} = (C_L)_{NEW LOC.} - (C_L)_{BASIC LOC.}$$

$$\delta \alpha = 25^\circ / 30^\circ$$

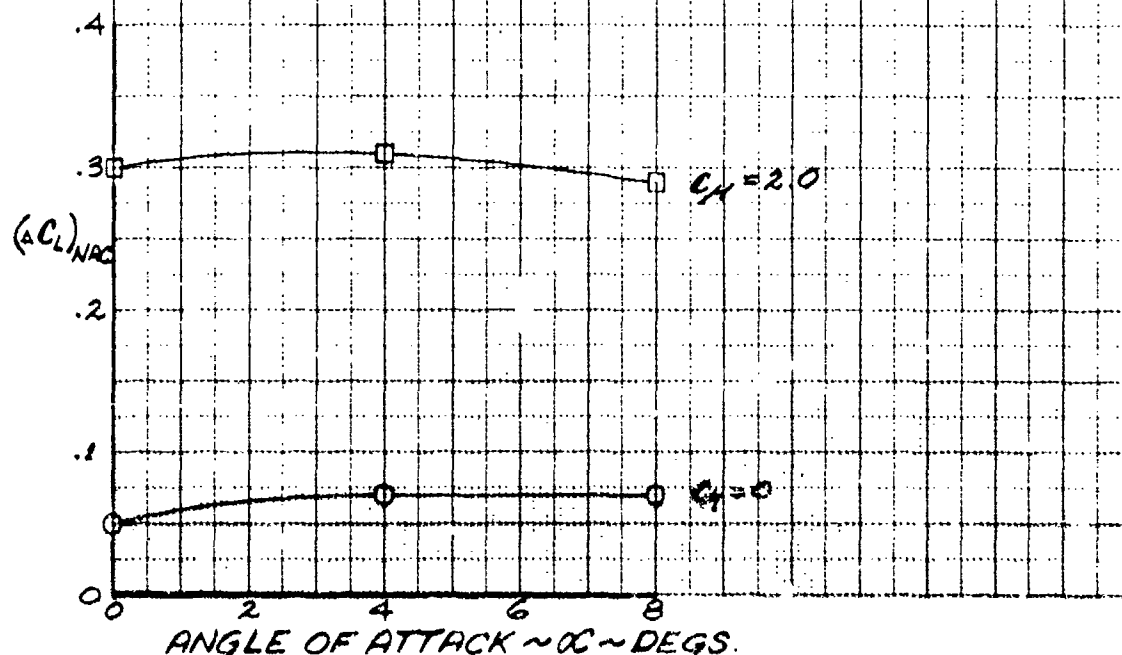
$$\rho = 16 \text{ PSF}$$

$$\delta \beta = -10^\circ \text{ FULL SPA.V}$$

TAIL-OFF

$$\delta \text{NOZ} = +13^\circ$$

NOTE: THE NACELLE WAS SHIFTED UPWARD FROM A $z/c = 0.27$ TO A $z/c = 0.19$ AT A CONSTANT $x/c = 0$.



CHANGE IN LIFT COEFFICIENT DUE TO A VERTICAL SHIFT IN ENGINE NACELLE LOCATION FROM THE BASIC CONFIGURATION

Figure 11.1.4

LSWT-090

$$(\Delta C_D)_{NAC.} = (C_D)_{NEW LOC.} - (C_D)_{BASIC LOC.}$$

$$\delta \alpha = 25^\circ/50^\circ$$

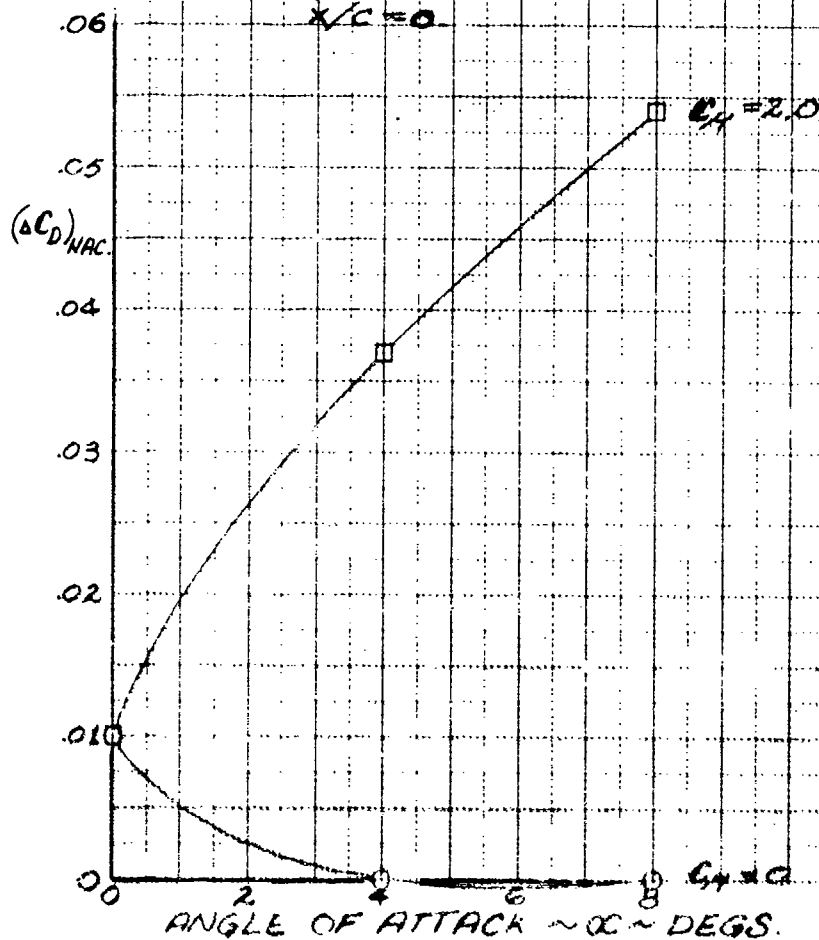
$$q = 16 \text{ PSF}$$

$$\delta \delta \alpha = -10^\circ \text{ FULL SPAN}$$

TAIL-OFF

$$\delta \text{NOZ} = +15^\circ \uparrow$$

NOTE: THE NACELLE WAS SHIFTED UPWARD FROM A $z/c = 0.27$ TO A $z/c = 0.19$ AT A CONSTANT $x/c = 0$.



CHANGE IN DRAG COEFFICIENT DUE TO A VERTICAL SHIFT IN ENGINE NACELLE LOCATION FROM THE BASIC CONFIGURATION

Figure 11.1.5

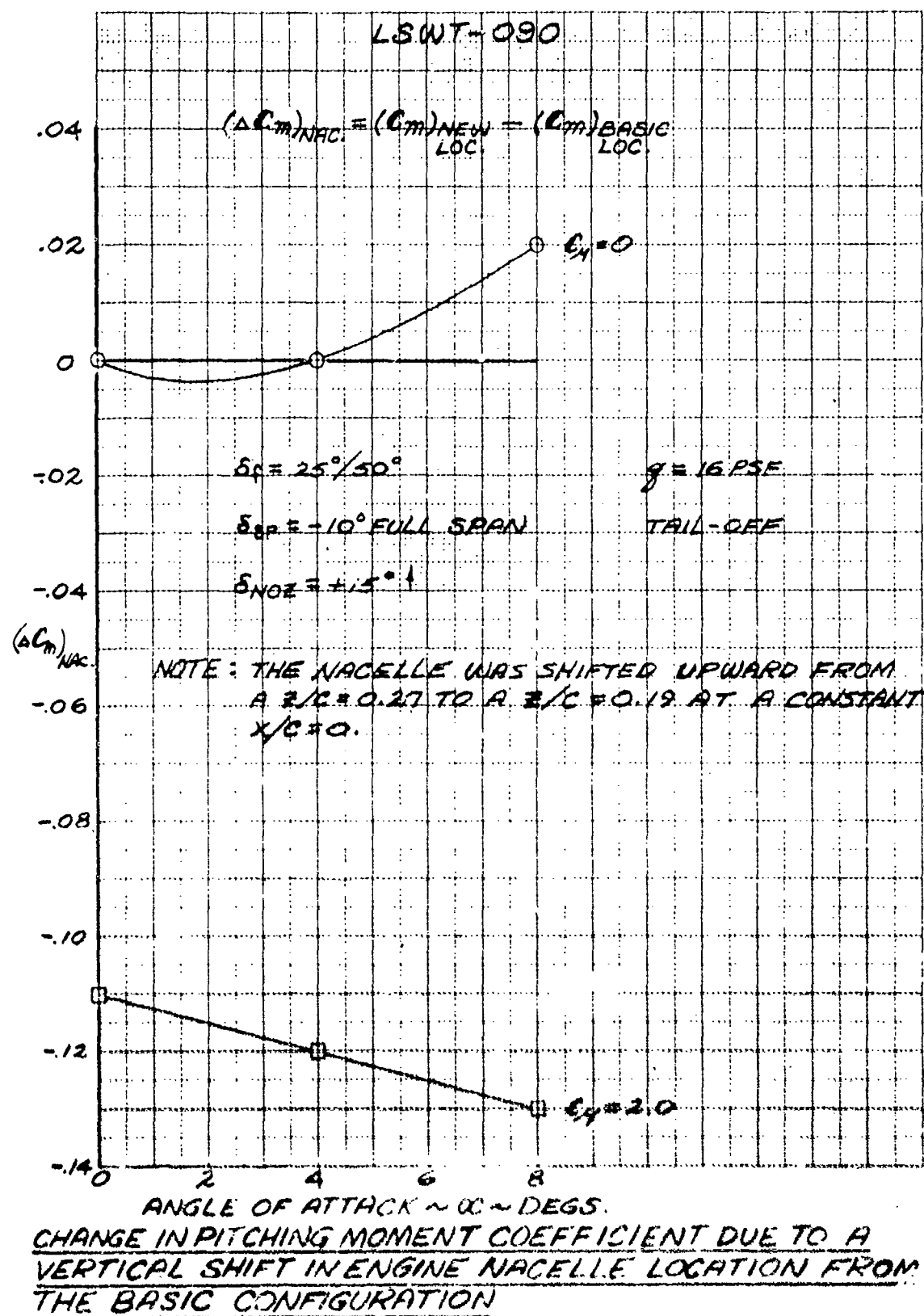
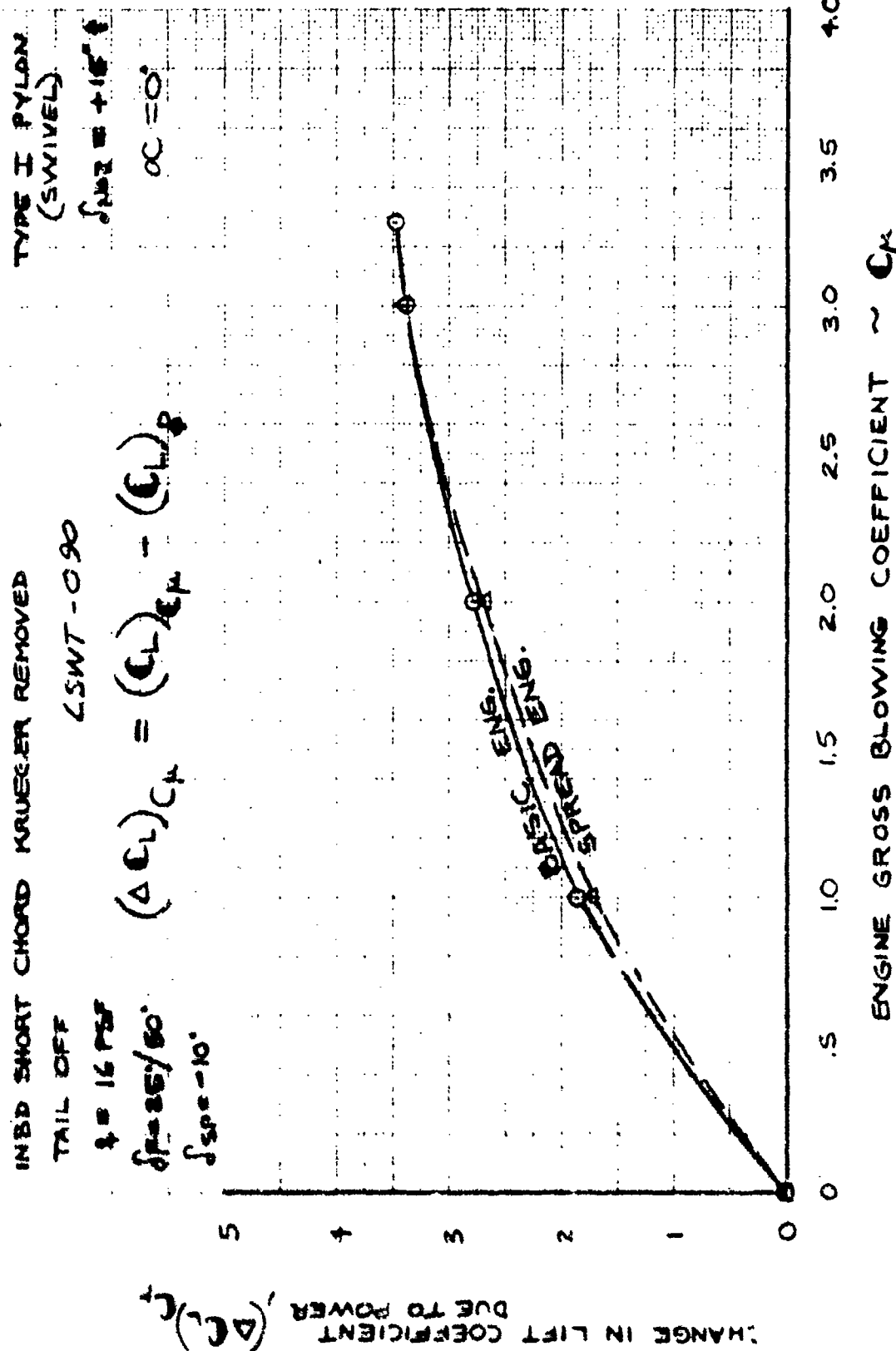
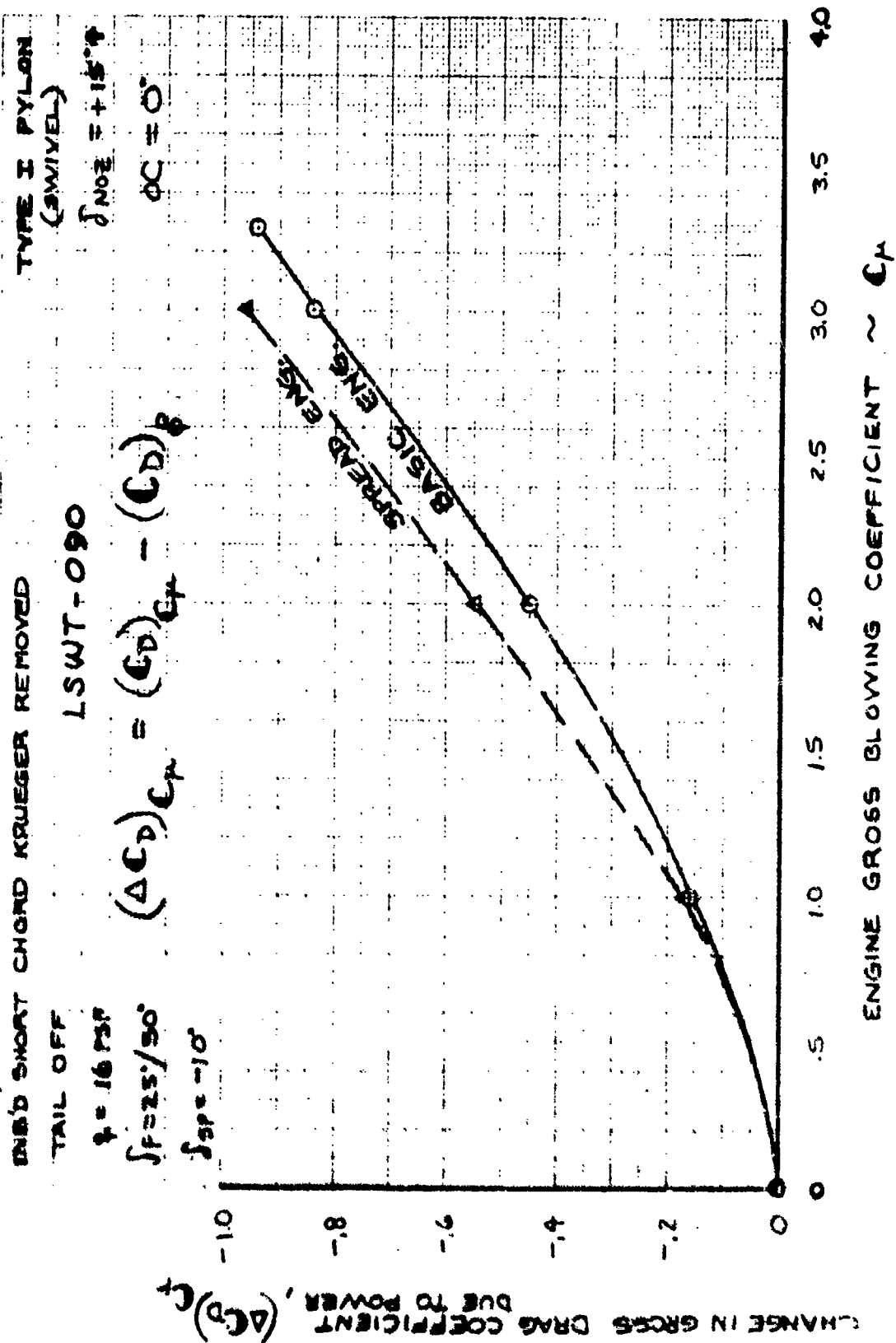


Figure 11.1.6





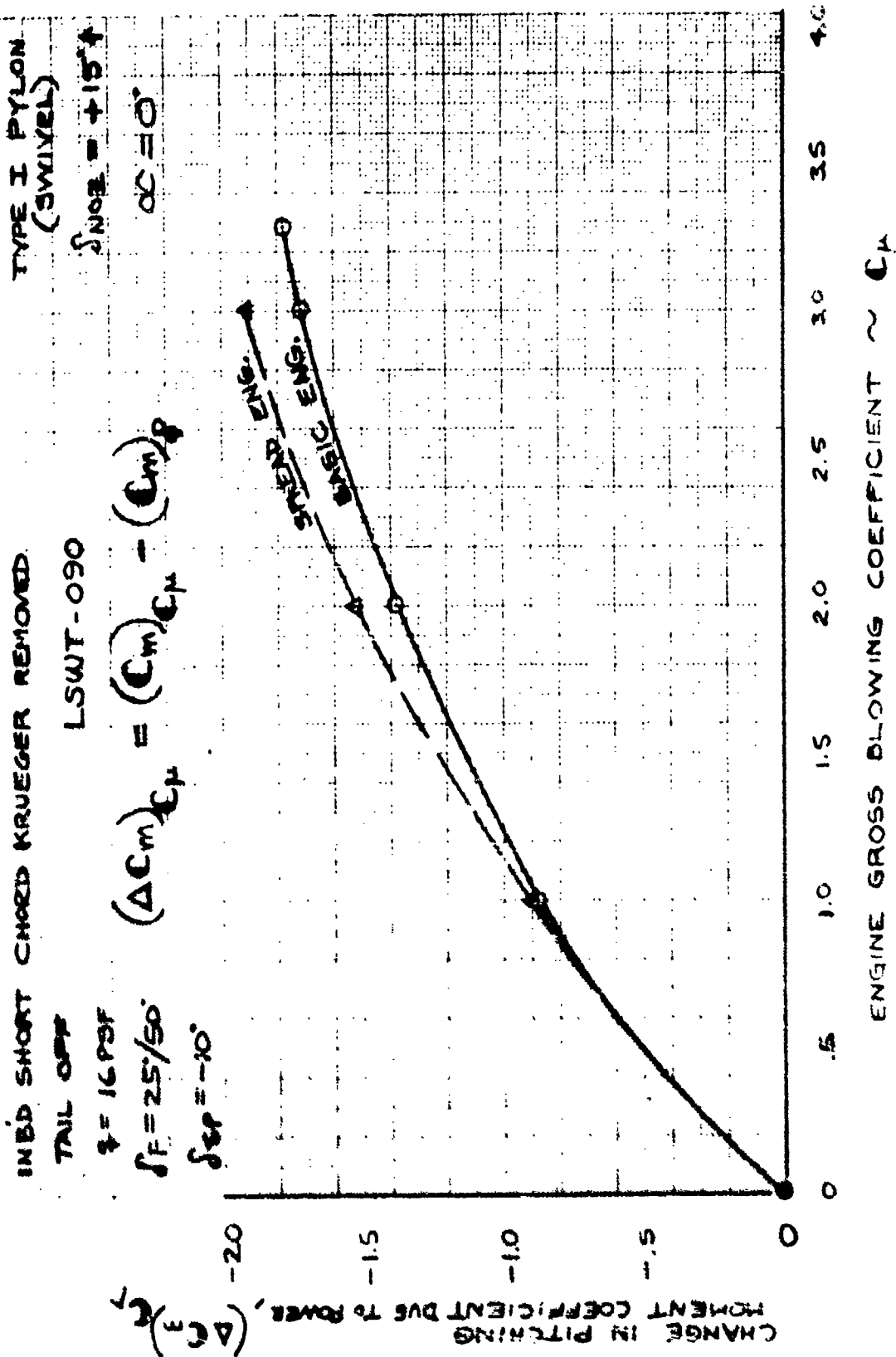
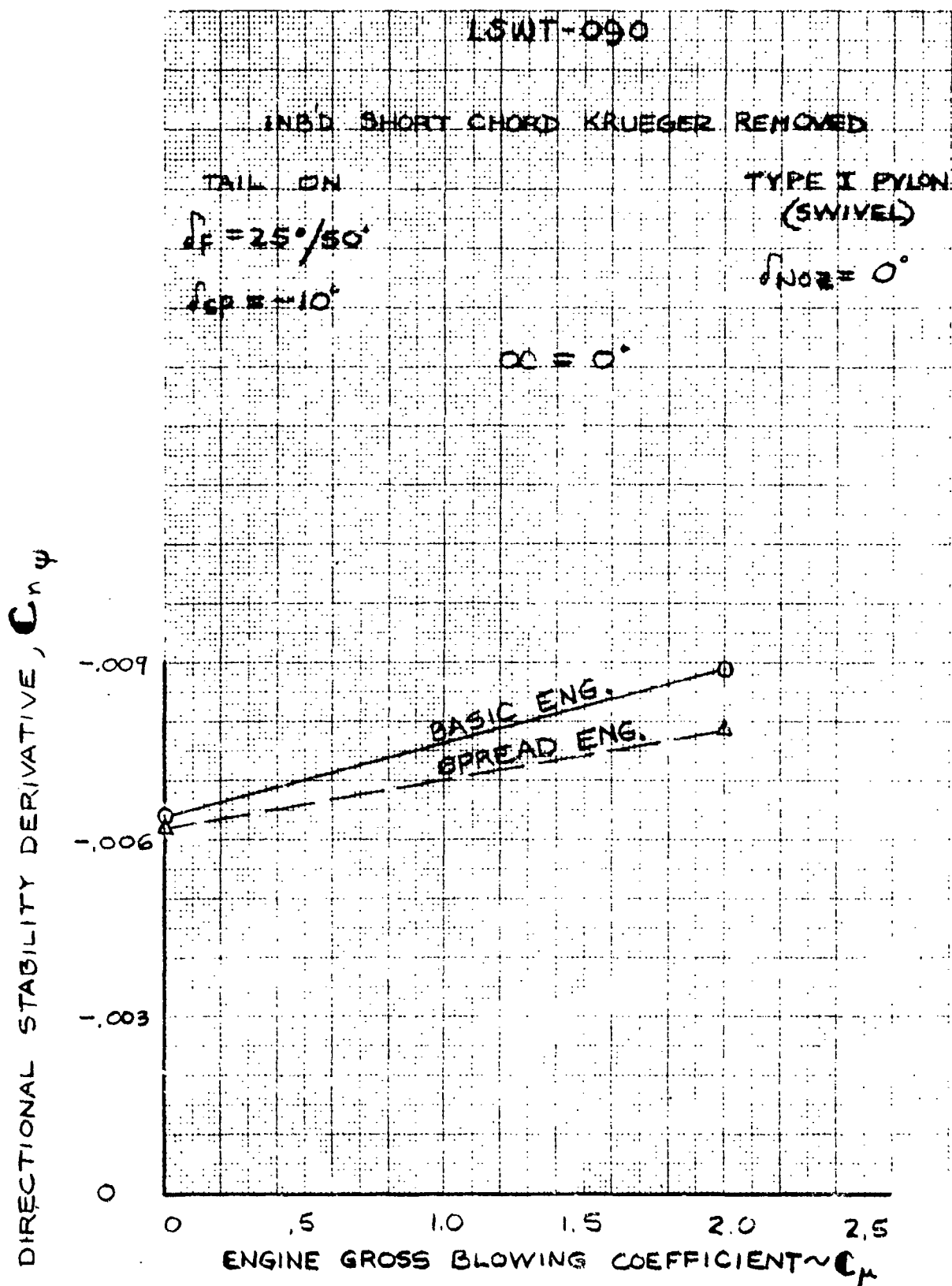
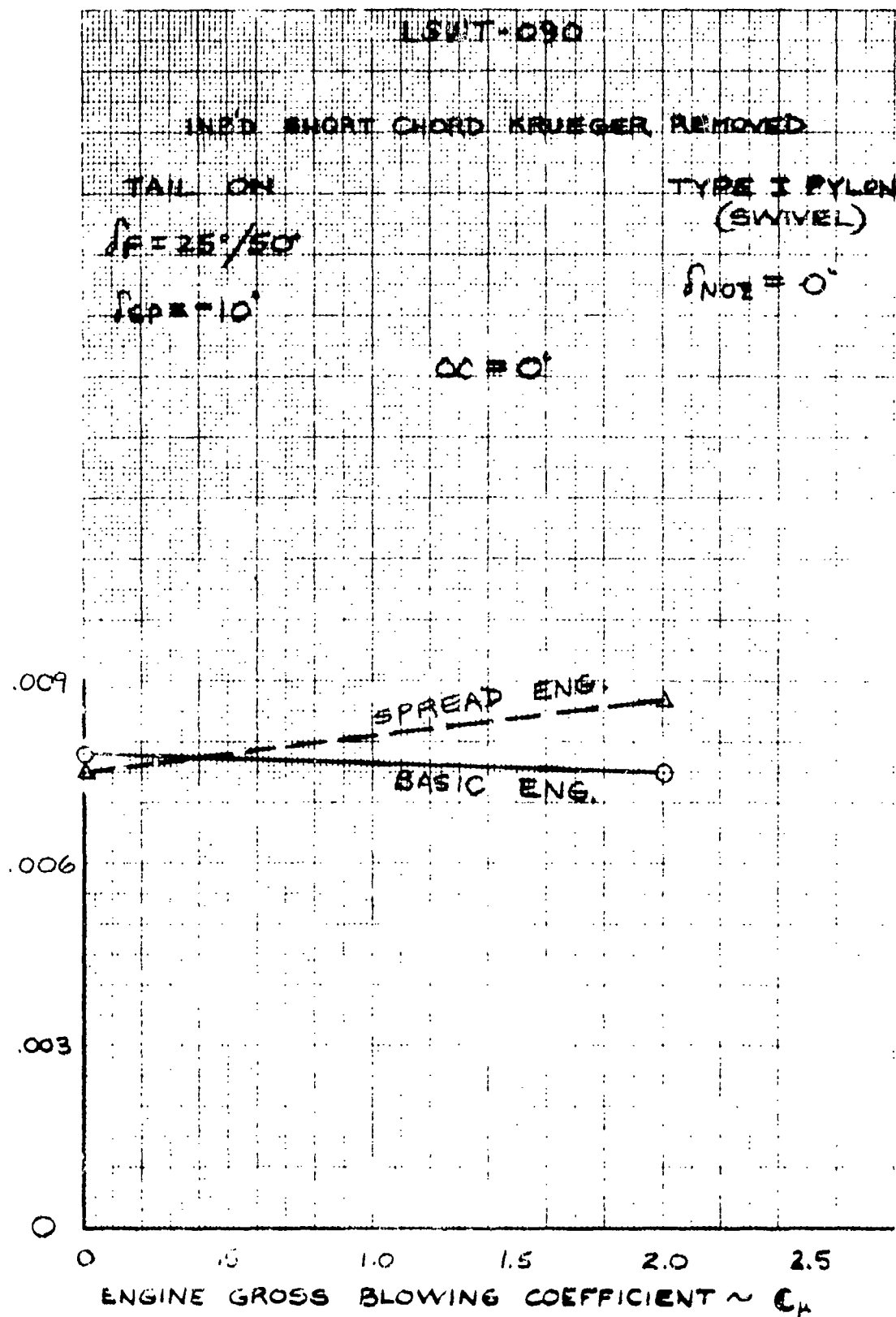


Figure 11.2.3



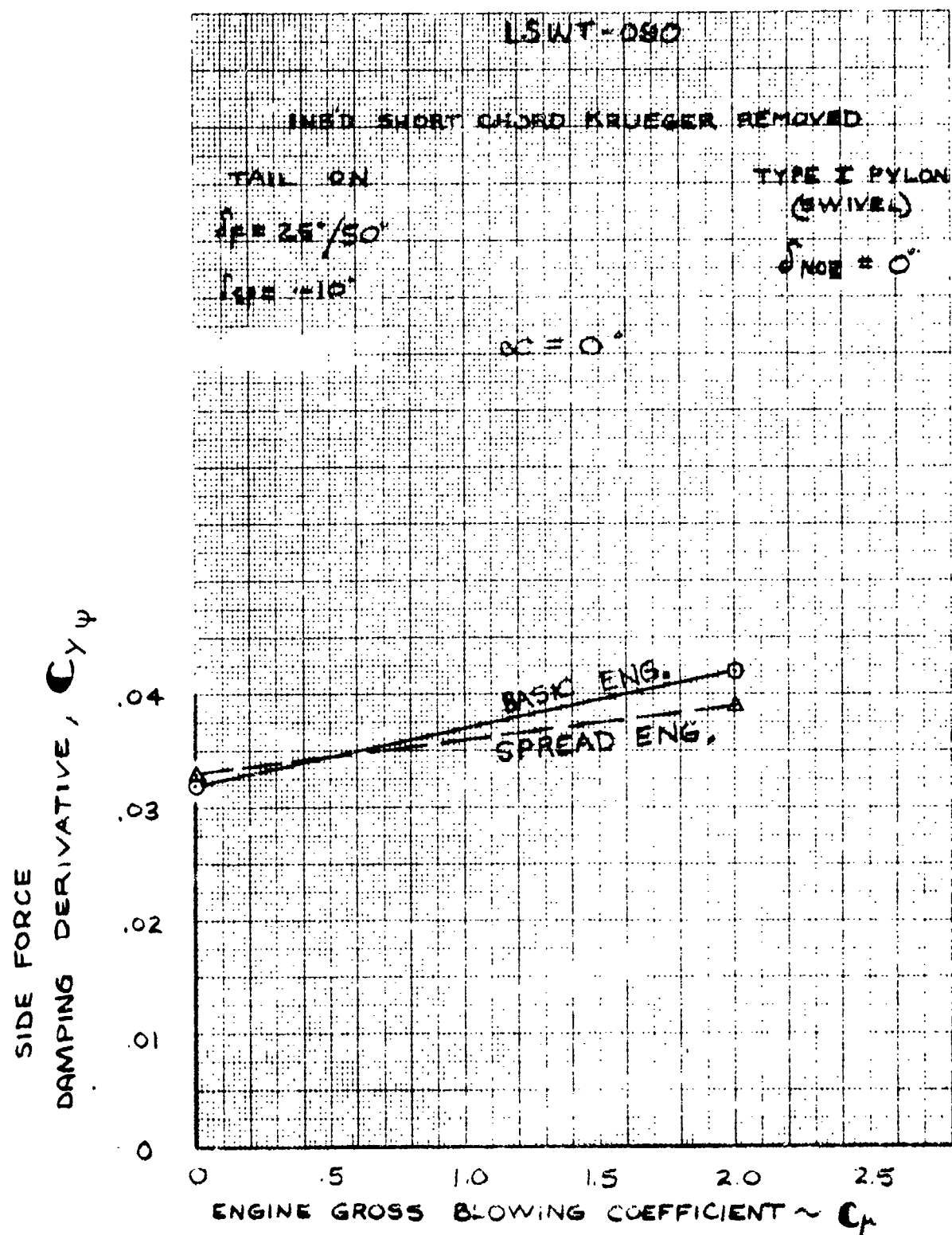
EFFECT OF ENGINE SPANWISE LOCATION
ON DIRECTIONAL STABILITY DERIVATIVE

DIHEDRAL EFFECT DERIVATIVE C_{L4}



EFFECT OF ENGINE SPANWISE LOCATION
ON DIHEDRAL EFFECT DERIVATIVE

Figure 11.2.5



EFFECT OF ENGINE SPANWISE LOCATION
ON SIDE FORCE DERIVATIVE

LSWT-090 EFFECT OF PYLON (SWIVEL vs. FIXED)

TYPE I - TYPE II

(SWIVELLING PYLON - FIXED PYLON)

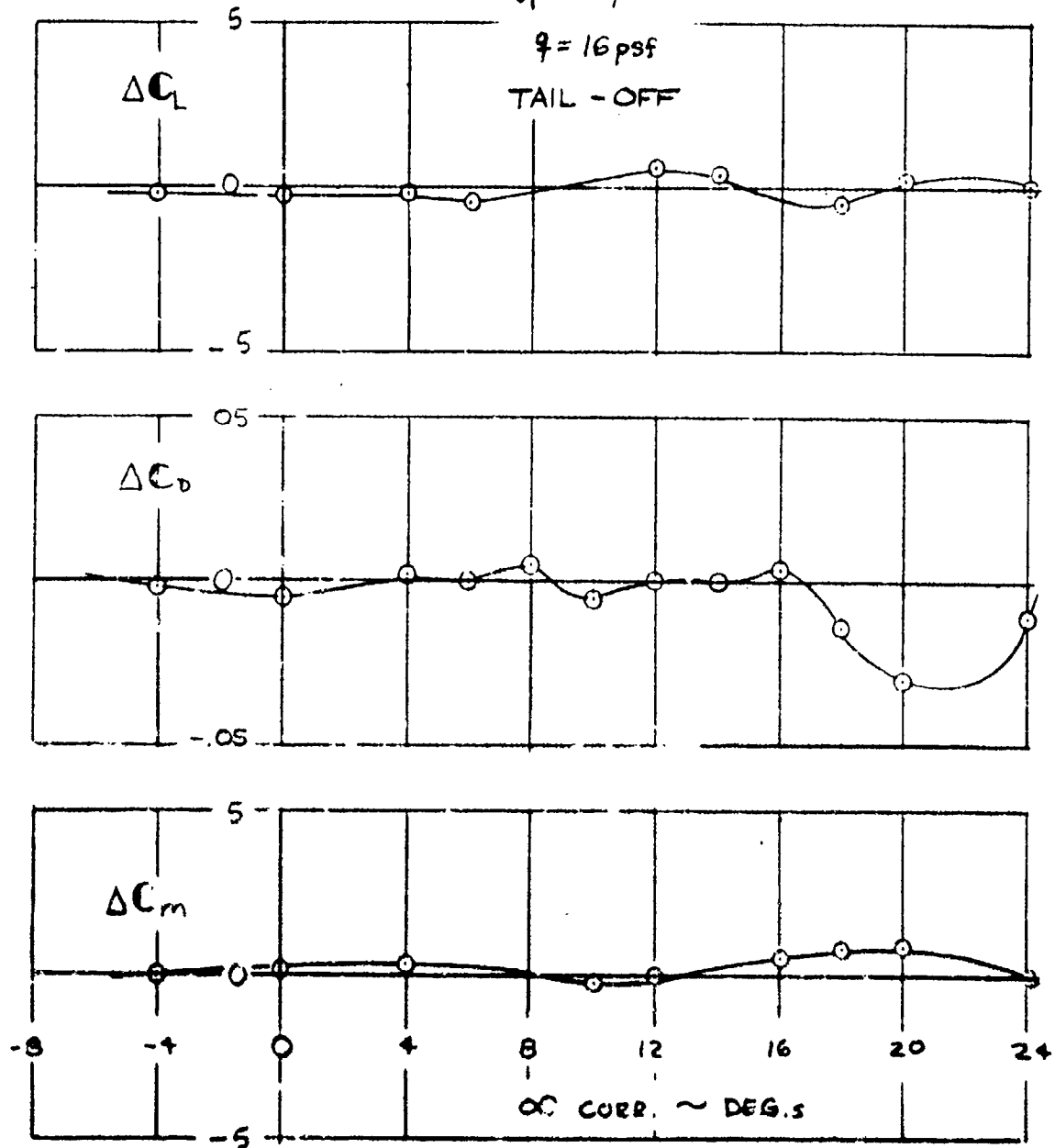
RUNS 488 + (240 - 244) = 415

$$C_T = 0$$

$$\delta F = 25/50^\circ$$

$$q = 16 \text{ psf}$$

TAIL - OFF



LSWT - 090

EFFECT OF PYLON (SWIVEL VS. FIXED)

TYPE I - TYPE II

(SWIVELLING PYLON - FIXED PYLON)

RUNS 489 + (241 - 245) - 417

$C_T = 2.0$

$\delta F = 25' / 50'$

$q = 16 \text{ psf}$

TAIL - OFF

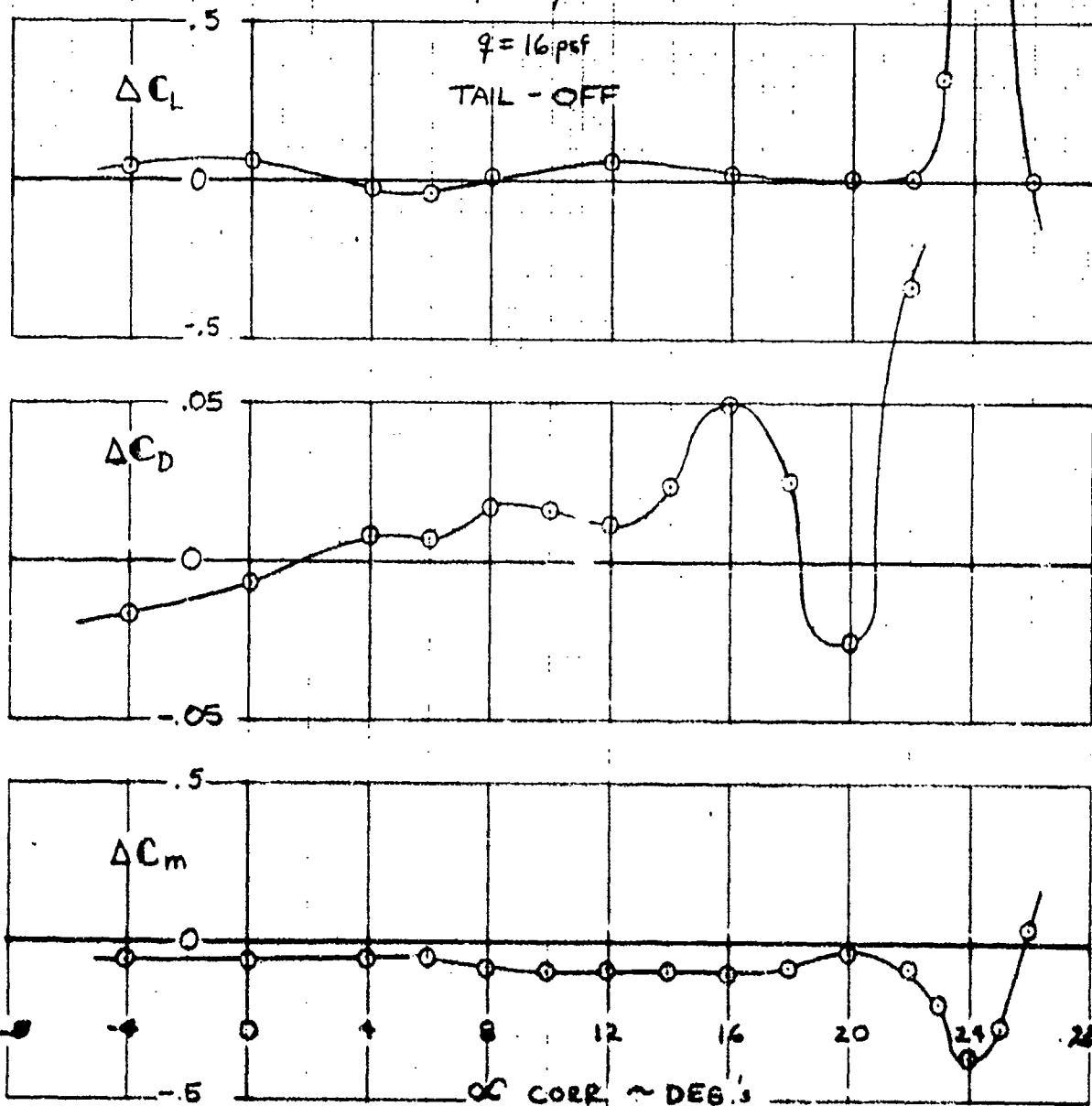


Figure 11.3.2

Section XII

FLAP CHARACTERISTICS

A cross sectional view of both flap systems tested, the double slotted and triple slotted flap, can be seen in Illustrations 12.1 and 12.2 respectively. The double slotted flap illustration also shows the vane flap spoiler which was used for roll control testing in conjunction with both flaps and will be discussed in Section XIV.

12.1 POWER-OFF LIFT CAPABILITY

This subsection is arranged so as to show a high lift system systematic buildup. Power-off lift coefficient for a clean wing is shown in Figure 12.1.1. A full span short chord Krueger is added to the leading edge with the trailing edge still clean. Power-off lift coefficient for this configuration is presented in Figure 12.1.2. The increase in maximum lift coefficient due to addition of the Krueger only is 0.46 (1.51-1.05) while the stall angle increases 4.6° (21° - 16.4°). With the full span short chord Krueger extended, the double slotted trailing edge flaps are extended to 25/30 degrees. The power-off lift coefficient for this configuration is presented in Figure 12.1.3. The power-off maximum lift coefficient now increases an additional 1.57 (3.08-1.51) and the stall angle is reduced 4.2° . Figures 12.1.4 and 12.1.5 present power-off lift coefficient vs angle of attack plots for various double and triple slotted flap deflections. All above data is tail-off and untrimmed.

Figure 12.1.6 presents the power-off trimmed lift coefficients for the same flap configurations as presented in Figure 12.1.4. The trim lift coefficients were determined analytically by multiplying the corresponding tail off, power-off pitching moment coefficient by the inverse of the non-dimensionalized horizontal tail arm. The horizontal tail arm length was taken as the distance from the wing MAC to the horizontal tail MAC (see Illustration 2.1).

12.2 STATIC TURNING ANGLES AND EFFICIENCIES

A summary of all the static turning angles tests that were conducted in test LSWT-090 for double and triple slotted flaps are presented in Figure 12.2.1.

12.3 FLAP GAP OPTIMIZATION FOR DOUBLE AND TRIPLE SLOTTED FLAPS

The flap gap was optimized for both the double and triple slotted flaps by varying the wing trailing edge spoiler which controlled the gap between its trailing edge and the leading edge upper surface of the flap vane (see Illustrations 12.1 and 12.2). In the case of the double slotted flap ($\delta_f = 25^\circ/50^\circ$) with the wing spoilers at -10° , the optimization testing was conducted on the 3.5 percent gap bracket. Figure 12.3.1 shows the actual measured flap gaps for each flap gap bracket for given spoiler deflections.

Figures 12.3.2 and 12.3.3 show the effects of flap gap variation on power-off and power-on lift coefficients respectively. Figure 12.3.4 presents cross plots of the two preceding figures at $\alpha = 0^\circ$ and $\alpha = \max$. for both the powered and unpowered conditions. The objective of this plot was to determine at what spoiler deflection an optimum C_L would be reached. It appears that optimum C_L is being approached at a spoiler deflection of -12° .

Unpowered and powered drag polars were plotted and are presented in Figures 12.3.5 and 12.3.6 respectively for a variation of flap gaps. Figures 12.3.7 and 12.3.8 are the unpowered and powered cross plots of the two preceding respective plots. The drag polars have been plotted for constant lift coefficients to determine if a definitive drag "bucket" exists for any given spoiler deflection and if so, whether it is the same spoiler deflection at which the optimum lift coefficient appeared. As can be seen in these two plots a "bucket" is hardly definitive but one might suggest a drag bucket at approximately -10.5° of spoiler deflection.

Figure 12.3.9 shows a plot of powered lift coefficient for varying spoiler deflection angles. The lift coefficients were taken at $C_p = 0$ for each spoiler deflection from Figure 12.3.6 which represents $\delta^* = 0^\circ$ since the axial drag balance read thrust and drag and C_p is as mentioned previously is total drag balance readout, thrust included. This plot again shows a spoiler deflection angle of approximately -12° (3.05 percent gap) to be optimum.

The same type of study was made for the triple slotted flap. The triple slotted flap deflection used for the gap optimization was $\delta_f = 2.5^\circ/20^\circ/45^\circ$. Figure 12.3.10 shows the actual measured flap gaps for each available spoiler deflection.

As can be seen in Figures 12.3.11 and 12.3.12 the unpowered and powered lift coefficients of the triple slotted flap are exceedingly less sensitive to gap variation than are those of the double slotted flap. Figure 12.3.13 shows an optimum lift coefficient of approximately -7° spoiler deflection at $\alpha = 0^\circ$ and approximately -4° spoiler deflection at $\alpha = \text{max}$.

The drag coefficient polars for the unpowered and powered conditions are presented in Figures 12.3.14 and 12.3.15 respectively and show further evidence of the insensitivity of the triple slotted flap system to flap gap variation.

An attempt at cross plotting figures (12.3.14) and (12.3.15) was made and the results appear in Figures 12.3.16 and 12.3.17. One may suggest the presence of a drag bucket at approximately -4° spoiler deflection.

Once again as with the double slotted flap, a triple slotted flap optimum powered lift coefficient at $\delta = 0^\circ$ has been sought and Figure 12.3.18 shows that at -4° spoiler deflection (2.00 percent gap) the optimum powered lift coefficient is realized.

12.4 POWERED LIFT CAPABILITY

The increment in lift coefficient due to power is shown in Figure 12.4.1 for the double slotted flap deflections of $25^\circ/50^\circ$ and $35^\circ/60^\circ$ at two angles of attack ($\alpha = 0^\circ$ and 8°). These are based on Figures 12.4.4 through 12.4.8 inclusive which are basic wind tunnel lift coefficient data plots for the double slotted $25^\circ/\text{XX}$ and $35^\circ/\text{XX}$ series flap systems.

Figures 12.4.2 and 12.4.3 present the effects of the double slotted flap deflection on total powered lift coefficient. These data are presented for two angles of attack and two-engine blowing coefficients ($C_{\mu} = 2.0$ and 3.28).

The increment in lift coefficient due to power is shown in Figure 12.4.9 for the triple slotted flap deflections of $2.5^\circ/20^\circ/45^\circ$ and $2.5^\circ/30^\circ/55^\circ$ at two angles of attack ($\alpha = 0^\circ$ and 8°).

Figures 12.4.10 and 12.4.11 show the effects of the $2.5^\circ/20^\circ/XX$ series triple slotted flap direct lift control system on total powered lift coefficient. The difference between the plots is spoiler deflection. Figure 12.4.10 has full span spoilers at -7° and Figure 12.4.11 has spoiler segments 1 through 4 inclusive raised to $+10^\circ$ and spoiler segment 5 at -7° . For a definition of spoiler segments see Illustration 2.1.

Similarly, Figure 12.4.12 shows the effects of the triple slotted flap configuration on powered lift coefficient for a 10° larger flap deflection ($2.5^\circ/30^\circ/XX$). All three triple slotted flap direct lift control system plots present data at two angles of attack ($\alpha = 0^\circ$ and 8°) and at two engine gross blowing coefficients ($C_{\mu} = 2.0$ and 3.28).

Some basic wind tunnel lift coefficient data plots for the triple slotted $2.5^\circ/20^\circ/XX$ and the $2.5^\circ/30^\circ/XX$ series flap systems are found in Figures 12.4.13 through 12.4.16 inclusive.

12.5 POWER EFFECTS ON DRAG

The increment in drag coefficient as effected by an application of power to the double slotted flap deflections of $25^\circ/50^\circ$ and $35^\circ/60^\circ$ for two angles of attack ($\alpha = 0^\circ$ and 8°) are shown in Figure 12.5.1.

The effects of the double slotted $25^\circ/XX$ and $35^\circ/XX$ flap direct drag control systems, or flap angle change, on total powered drag coefficient for two angles of attack and two engine gross blowing coefficients ($C_{\mu} = 2.0$ and 3.28) are presented in Figures 12.5.2 and 12.5.3.

Figures 12.5.4 through 12.5.6 represent basic wind tunnel drag coefficient polars for the double slotted $25^\circ/XX$ and $35^\circ/XX$ flap series.

Similarly, for triple slotted flaps, the increment in drag coefficient as effected by power is shown in Figure 12.5.7 for $\delta_f = 2.5^\circ/20^\circ/45^\circ$ and $2.5^\circ/30^\circ/35^\circ$ and at two angles of attack ($\alpha = 0^\circ$ and 8°).

The effects of the 2.5°/20°/XX series triple slotted flap direct drag control system on total powered drag coefficient are shown in Figures 12.5.8 and 12.5.9 for two angles of attack and two-engine gross blowing coefficients. Larger flap angles are shown in Figure 12.5.10 presenting the effects of the 2.5°/30°/XX series triple slotted flap direct drag control system on total powered drag coefficient.

Figures 12.5.11 through 12.5.14 inclusive present some basic wind tunnel drag coefficient data plots from which some of the analysis data points were extracted.

Figure 12.5.15 represents the average ram drag coefficient per engine variation with total simulated engine blowing coefficient. These data were collected by the use of simulated engine nacelle inlet static and total pressure probes mounted in rake fashion and these data were reduced per subsections 6.2.1.2 through 6.2.1.11 inclusive of NR MST pretest report NA-72-107.

12.6 POWER EFFECTS ON PITCHING MOMENT

The increment in pitching moment coefficient due to power as effected by the double slotted flap deflections of 25°/50° and 35°/60° are shown in Figure 12.6.1. The pitching moment increments are insensitive to angle of attack variation between $\alpha = 0^\circ$ and 8° .

The effects of the double slotted 25°/XX and 35°/XX flap series' last flap segment deflection on total powered pitching moment coefficient are shown in Figures 12.6.2 and 12.6.3. As can be seen there is little angle of attack effects at the high engine gross blowing coefficient ($C_{\mu} = 3.28$).

Figures 12.6.4 through 12.6.9 inclusive present unpowered and powered basic wind tunnel pitching moment coefficient data plots. The moment reference center was about the wing MAC quarter chord.

The increment, in pitching moment coefficient due to power as effected by the triple slotted flap deflections of 2.5°/20°/45° and 2.5°/30°/55° are shown in Figure 12.6.10. An angle of attack variation (between 0° and 8°) can only be detected with the 2.5°/30°/55° triple slotted flap.

The effects of the 2.5°/20°/XX series triple slotted flap last flap segment articulation on total powered pitching moment coefficient are shown in Figures 12.6.11 and 12.6.12. These data are shown for two engine gross blowing coefficients and are independent of variations in angle of attack between $\alpha = 0^\circ$ and 8° . As in the powered lift subsection 12.4 the only configuration difference in these two plots is the wing trailing edge spoiler angles.

The effects of the 2.5°/30°/XX series triple slotted flap last flap segment perturbation on total powered pitching moment coefficient is shown in Figure 12.6.13 for two-engine gross blowing coefficients ($C_{\mu} = 2.0$ and 3.28) and also is α independent between 0° and 8° .

Figure 12.6.14 is a zero power wind tunnel pitching moment data plot.

12.7 FLAP DEFLECTION AND POWER EFFECTS ON AERODYNAMIC CENTER LOCATION

Flap deflection effects on the aerodynamic center location for double and triple slotted flaps at varying engine gross blowing coefficients are presented in Figures 12.7.1 through 12.7.3 inclusive. The a.c. locations plotted are all referenced from a 25 percent c.g. and all data presented is tail off. The negative values represent a forward movement of the a.c. or a de-stabilizing shift and the positive values represent a rearward movement of the a.c. or a stabilizing shift.

It can be seen that for the full range of engine gross blowing coefficients evaluated the triple slotted flap consistently demonstrates better stability gradients than does the double slotted flap. The triple slotted flap also shows increasing stability levels to much higher flap deflections than does the double slotted flap because of its capability of delaying flow separation as a result of the added slot.

The effect on aerodynamic center location of directing a high energy flow field on to the lower surface of the double and triple slotted flap configurations is presented in Figure 12.7.4. The data was obtained with the tail off and at constant flap deflections for the double and triple slotted configurations while engine gross blowing coefficients were varied.

Here, again, the triple slotted flap shows to be more stable than the double slotted flap. However, as power was increased the a.c. location of the double slotted flap moved rearward in a stabilizing direction and the a.c. location of the triple slotted flap moved forward in a destabilizing direction.

12.8 EFFECTS OF FLAP INLET FAIRING ON LONGITUDINAL AERODYNAMIC PARAMETERS

The flap inlet fairing was a device mounted on the wing lower surface ahead of the flap vane and was used to control the direction of the stream flow attacking the flap vane (see Illustration 12.1). Although it was used with all flap deflections tested, its effects were only determined with the 25°/50° double slotted flap.

The effects of the removal of the flap entry fairing on lift, drag and pitching moment coefficients are presented in Figures 12.8.1, 12.8.2 and 12.8.3 respectively. These data are presented for engine gross blowing coefficients of $C_{\mu} = 0$ and 2.0. An obvious lift loss is encountered with the fairing removed when under engine power influences therefore the fairing was left in place for all testing.

LSWT-090

$\rho = 16 \text{ psf}$

$C_T = 0$

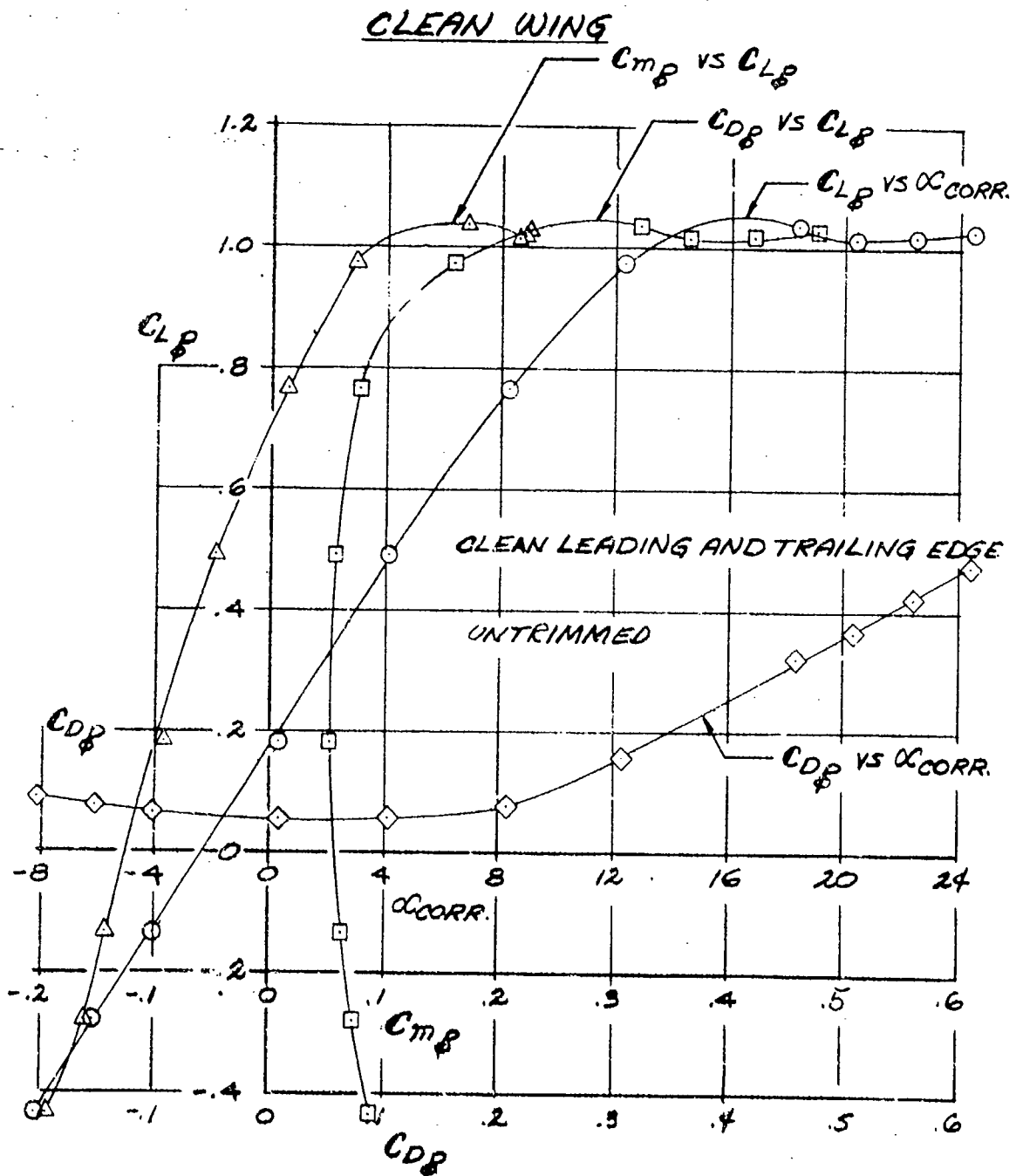
TAIL-OFF

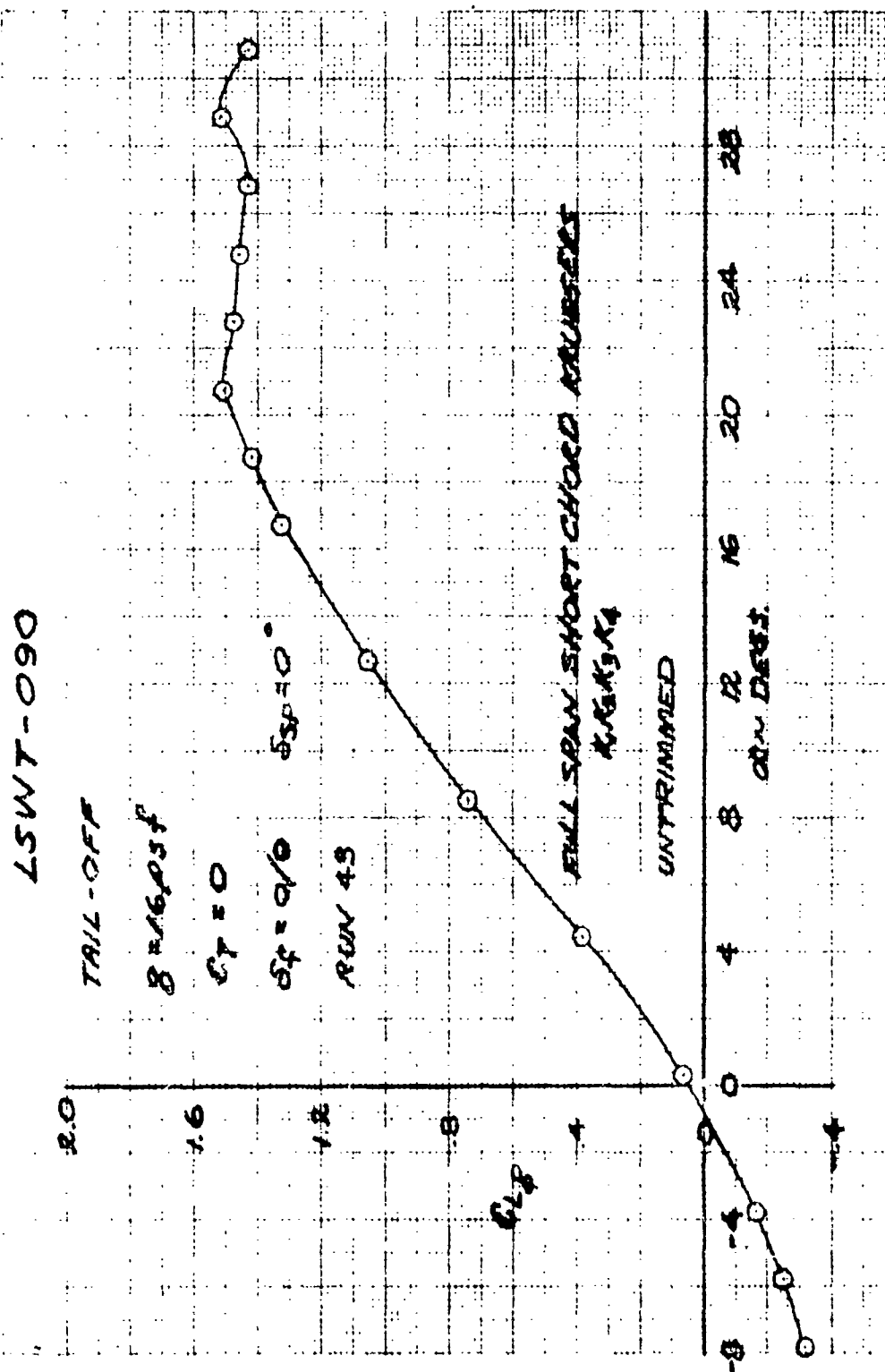
RUN 36

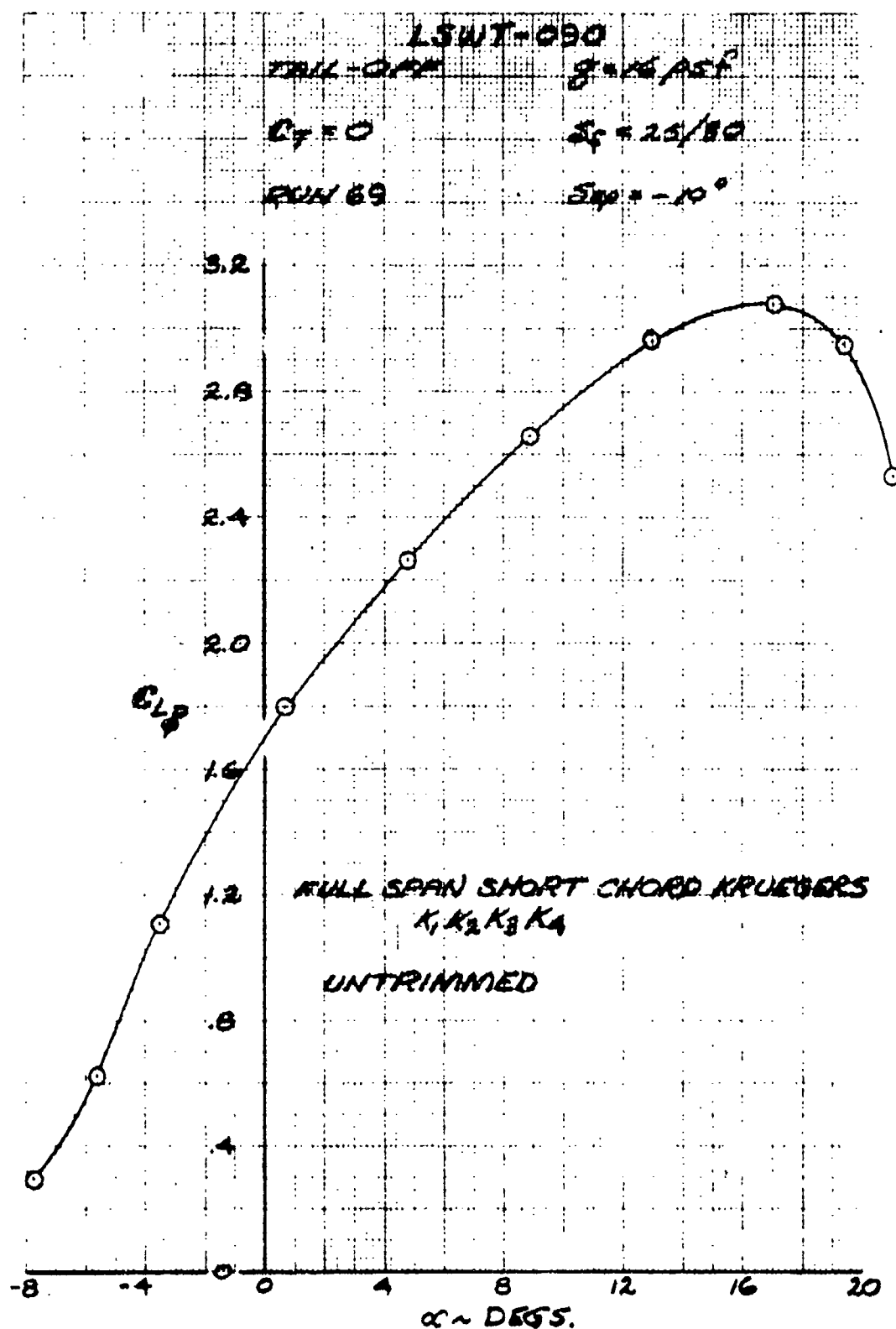
C.G. = 25% \bar{c}

$\delta_{sp} = 0^\circ$

POWER OFF LONGITUDINAL CHARACTERISTICS



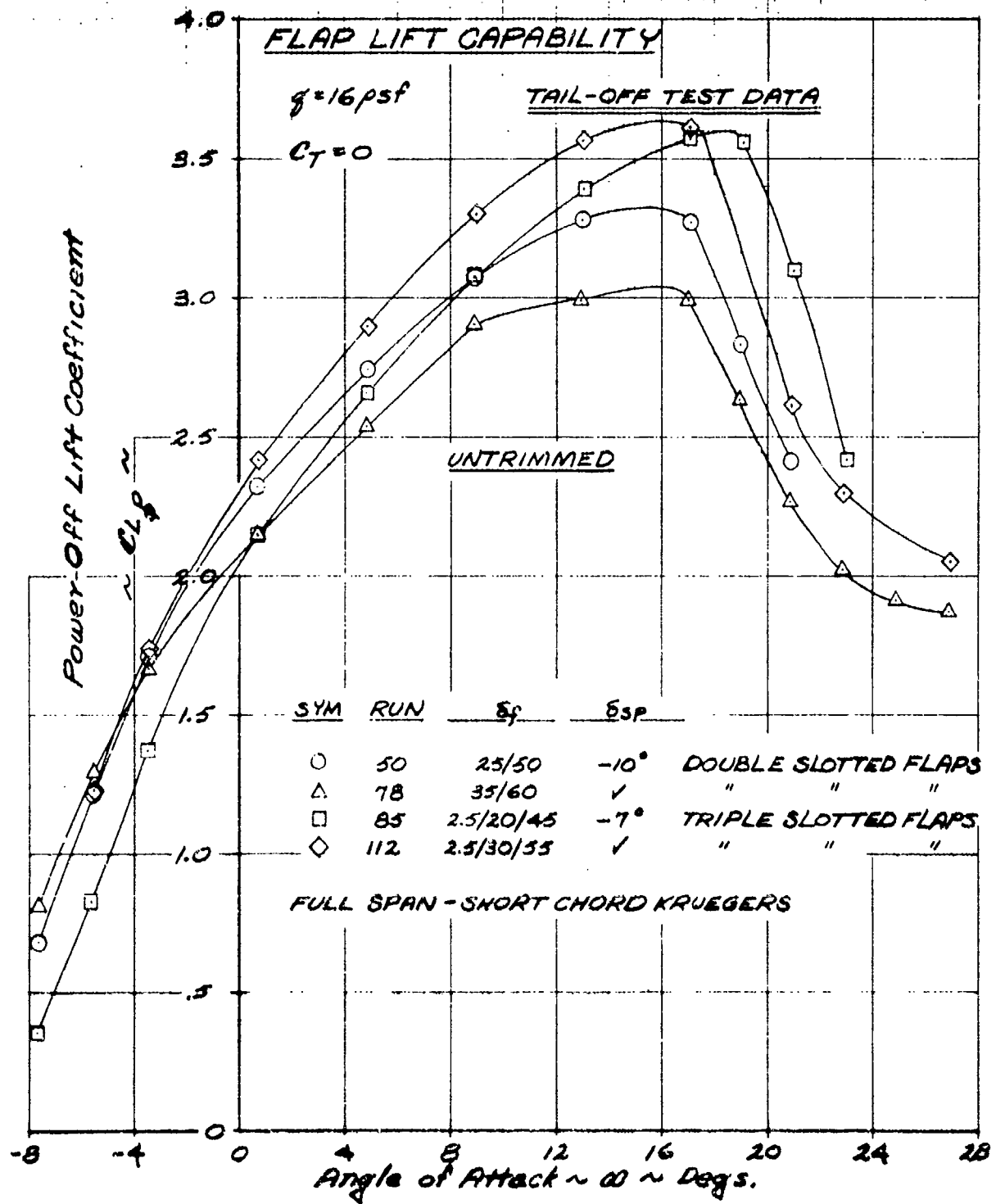




POWER OFF LIFT CAPABILITY
— DOUBLE SLOTTED FLAP —

LSWT-090

POWER-OFF DOUBLE AND TRIPLE SLOTTED



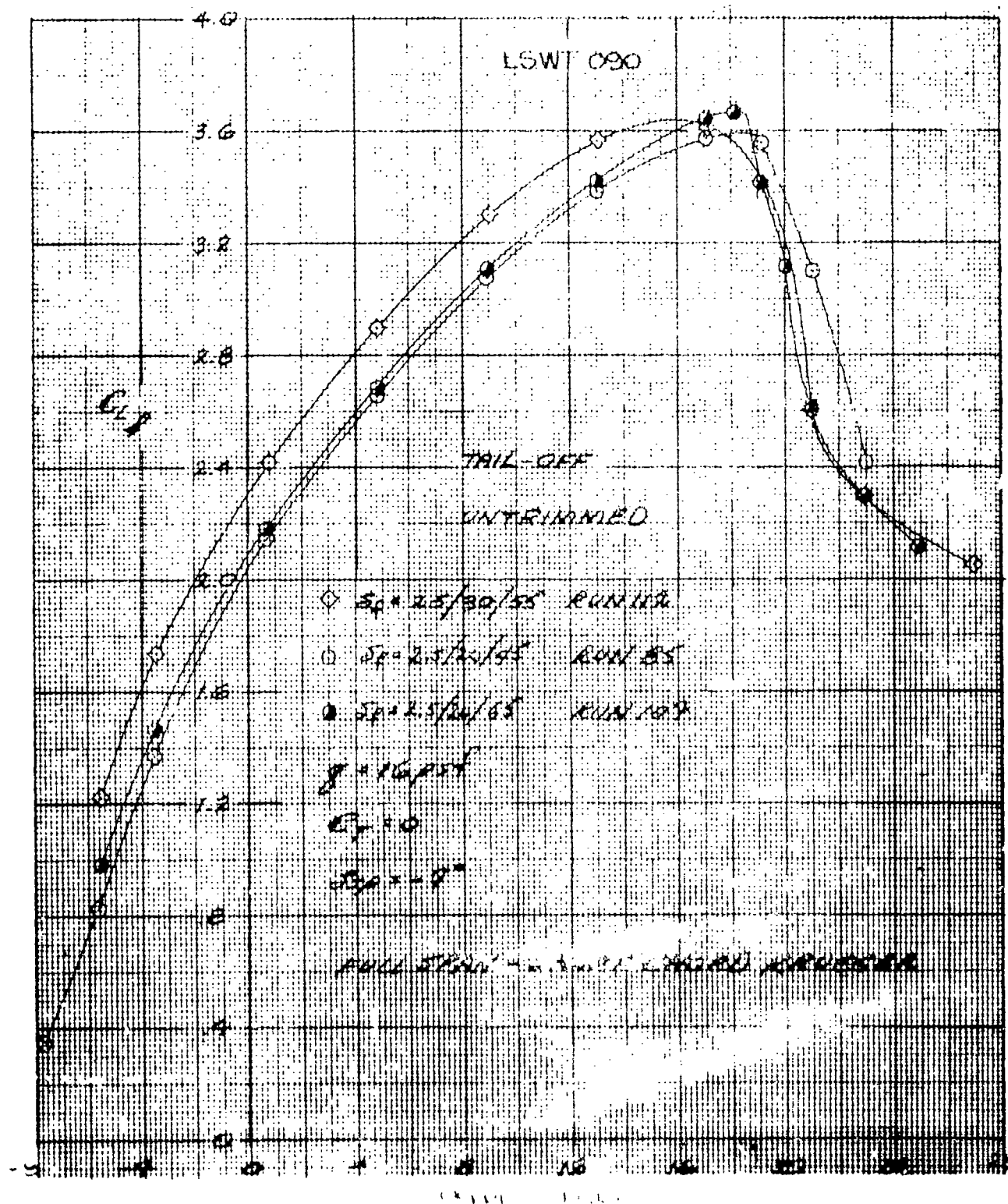
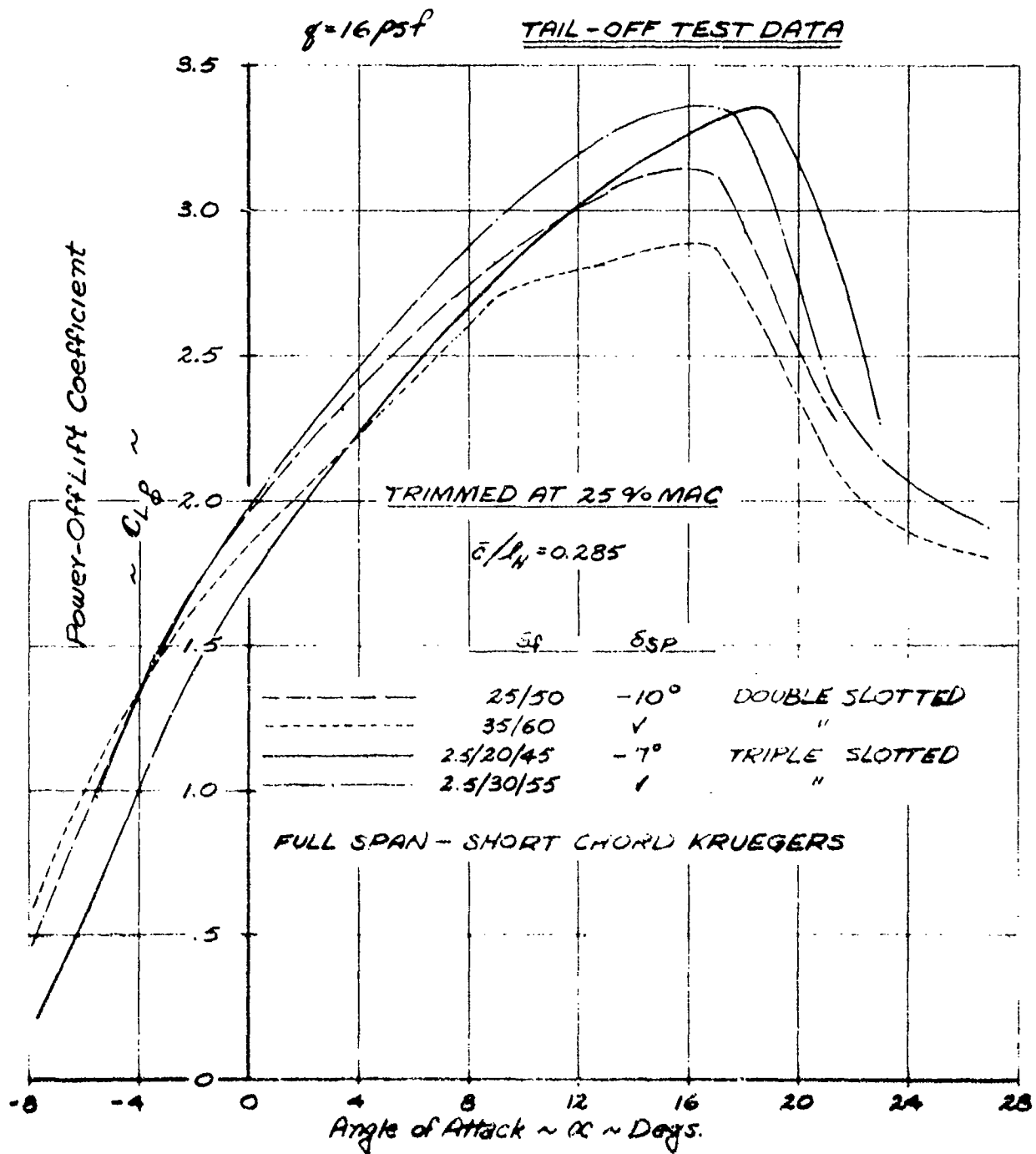


Figure 12.1.5

LSWT-090

POWER-OFF DOUBLE AND TRIPLE SLOTTED
FLAP LIFT CAPABILITY (TRIMMED)



LSNT-0-0

SUMMARY OF TURNING EFFICIENCY AND TURNING ANGLES

BODY AXIS DATA

MAXIMUM AVAILABLE THRUST

TAIL-OFF

$\delta = 0$

NOZZLE DEFLECTOR $\pm 15^\circ$ UP

* \blacksquare = FILLED FLAP GAP

\angle OF $Q/A = 24^\circ$

$\delta_j = 90^\circ$

$\delta_j = 75^\circ$

$\delta_j = 60^\circ$

TRIPLE SLOTTED FLAP

$\delta_j = 45^\circ$

DOUBLE SLOTTED FLAPS

$\delta_j = 30^\circ$

$\delta_j = 15^\circ$

$\delta_j = 0^\circ$

F_N/T

$-F_A/T$

$\eta = 0.8$

$\eta = 0.4$

$\eta = 0.2$

$\eta = 0$

FR

SYM

δ_j

RUN NO.

7

\square

25/50

64

\triangle

35/60

73

\blacksquare

2.5/20/45

91

\blacklozenge

2.5/30/55

110

∇

2.5/20/45*

117

\mid

2.5/20/25

521

\boxplus

25/50

541

FIGURE 1.2.1

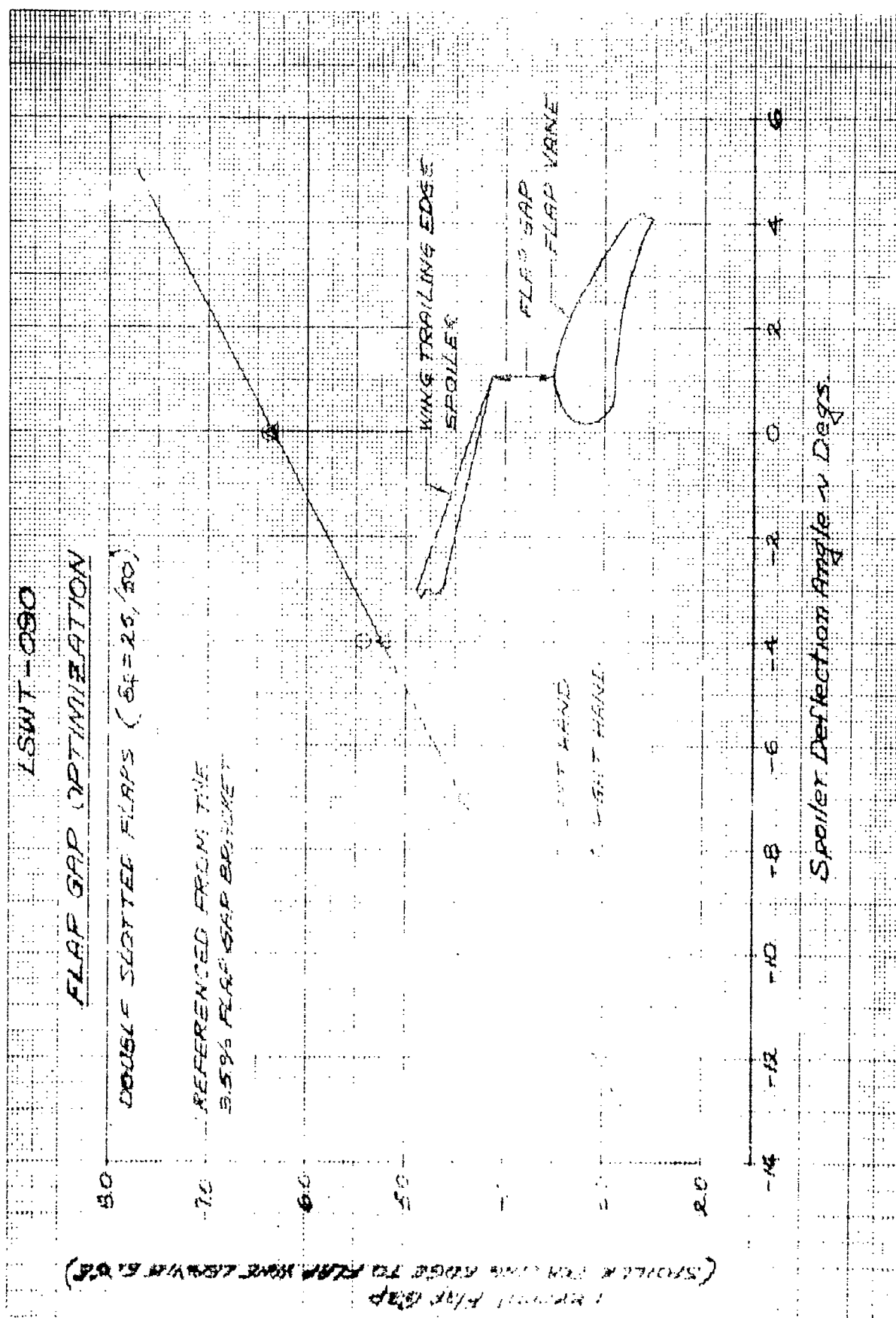
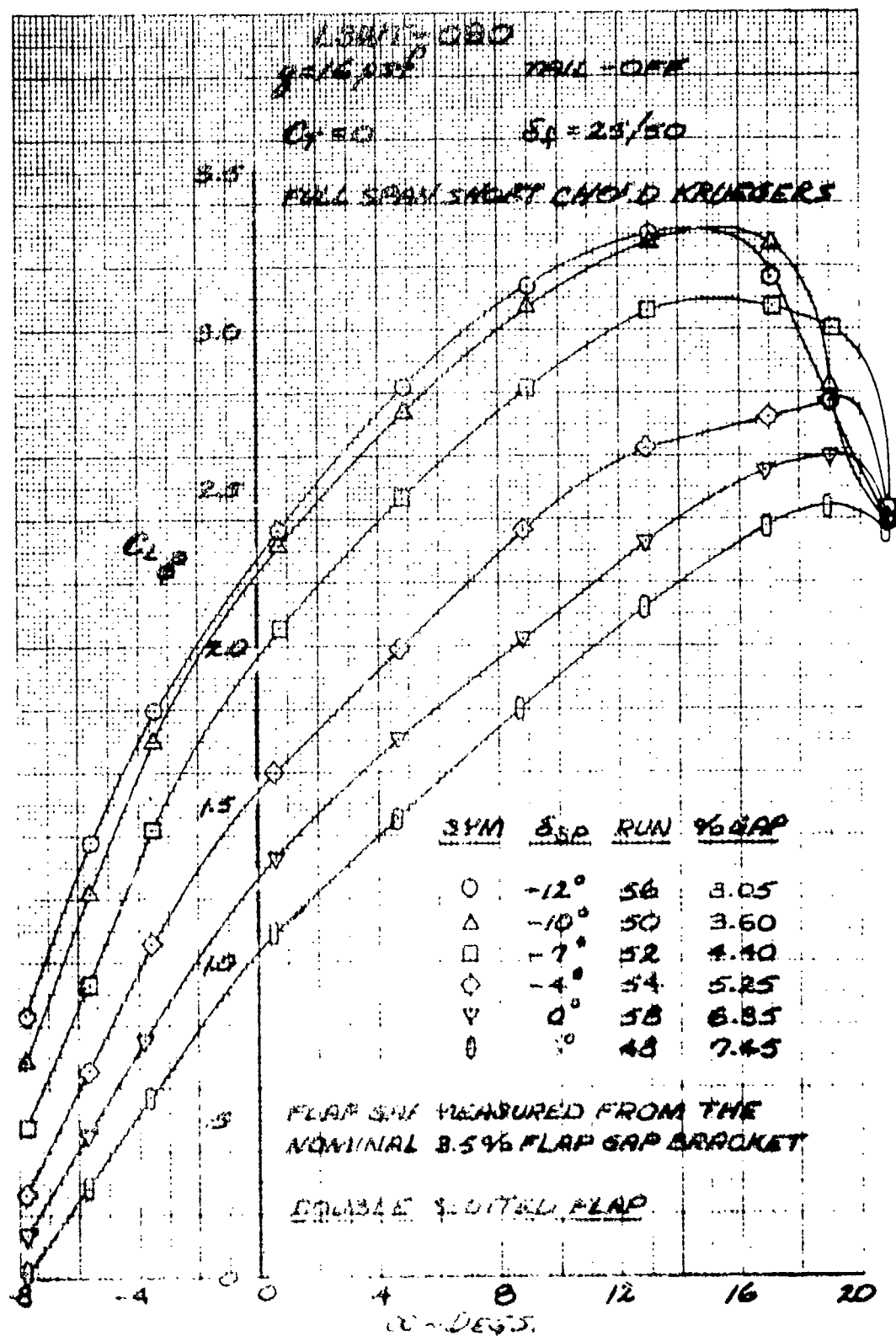


Figure 12.3.1



EFFECTS OF FLAP GAP VARIATION ON POWER-OFF
 LIFT COEFFICIENT

Figure 12.3.2

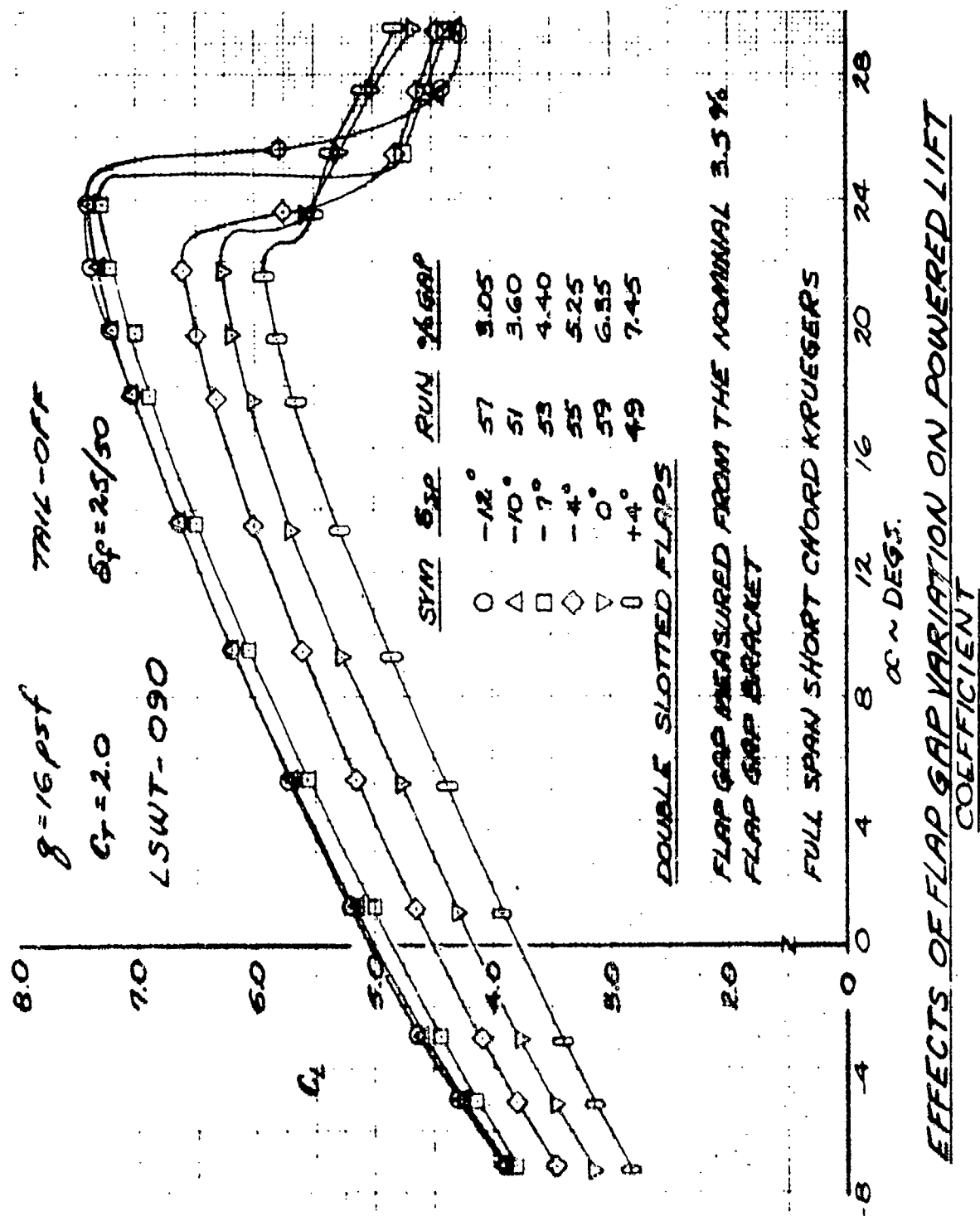
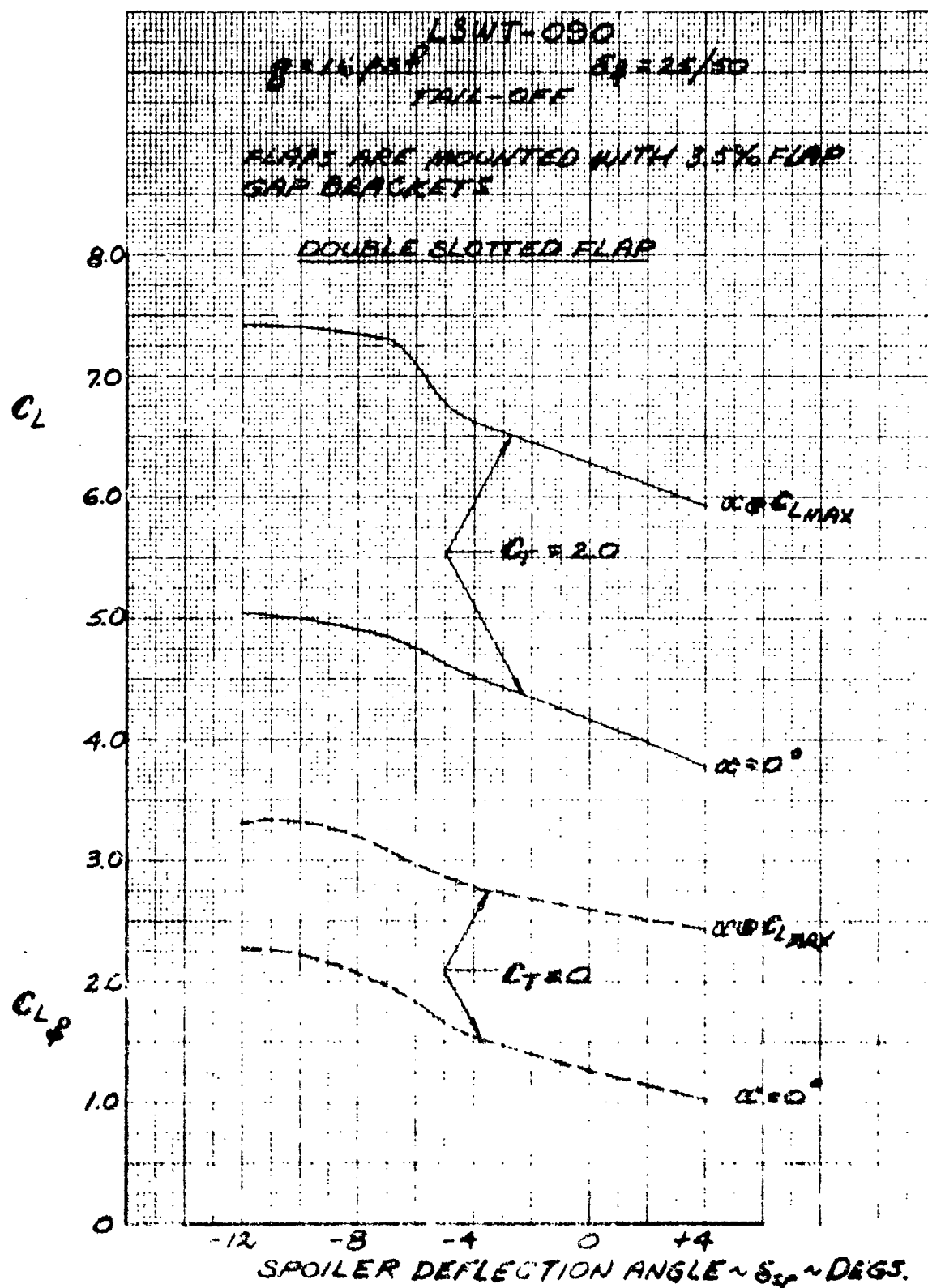
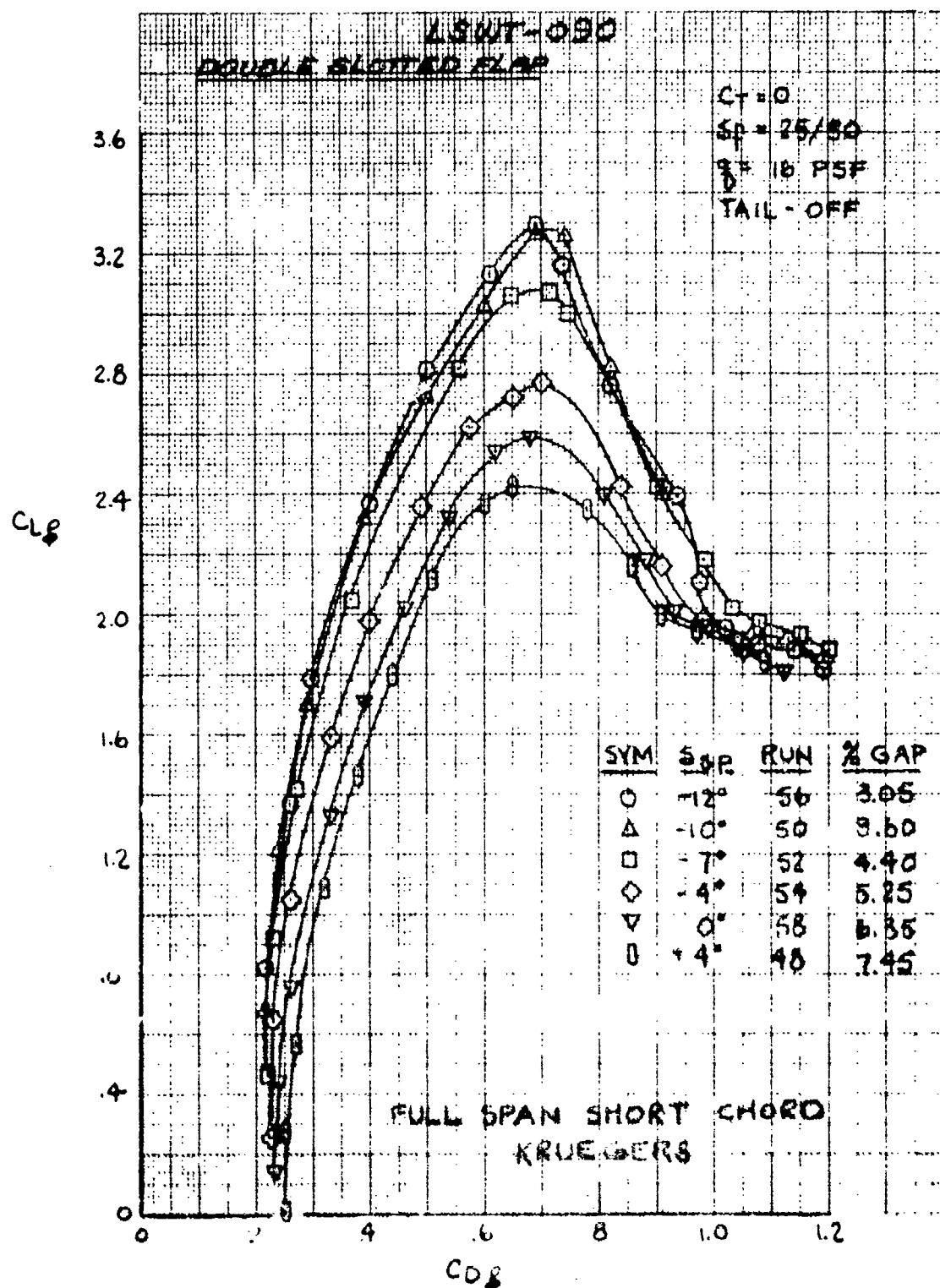


Figure 12.3.3

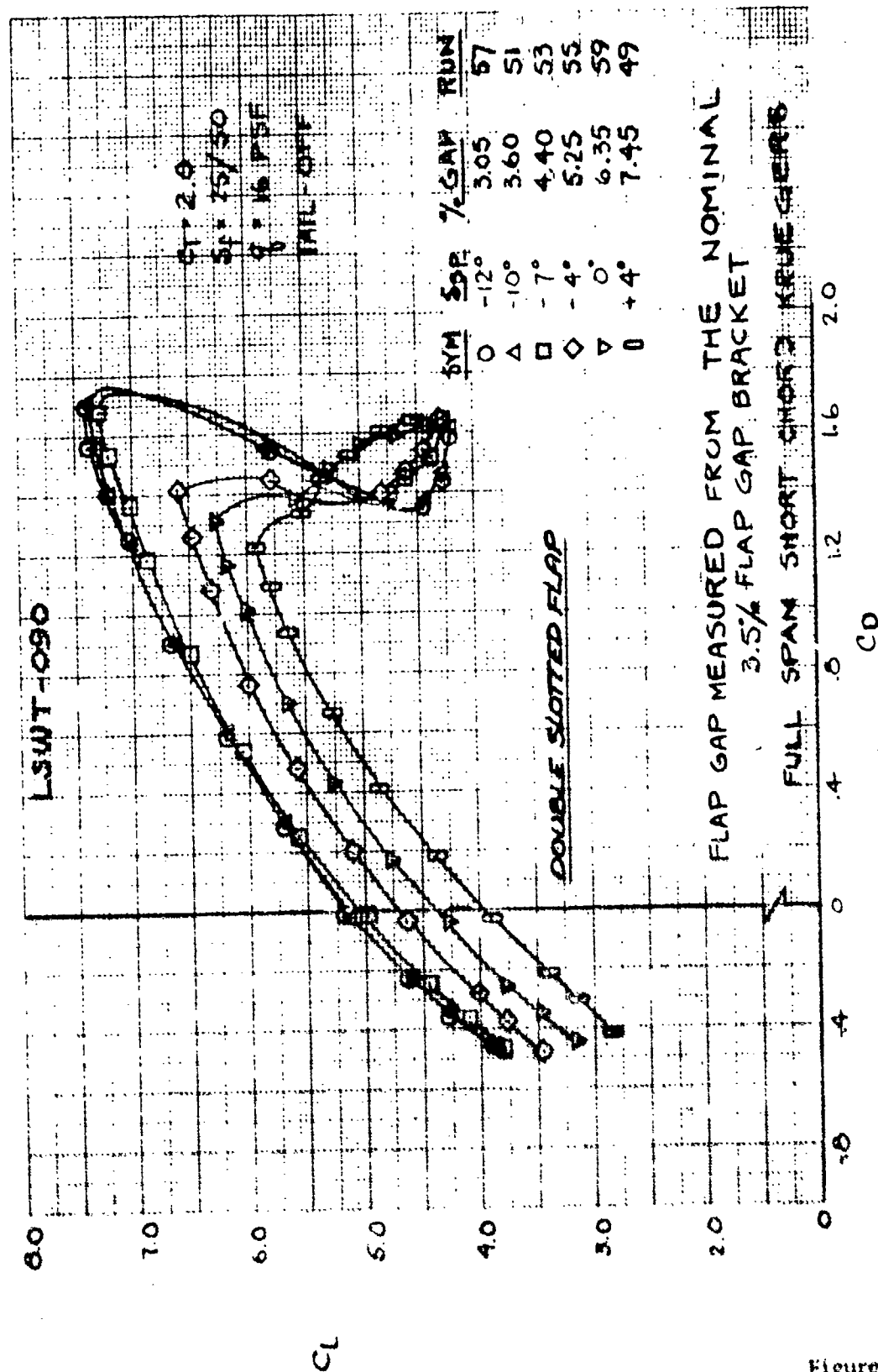


LIFT COEFFICIENT VARIATION VS. SPOILER DEFLECTION
 ANGLE AT $\alpha = 0^\circ$ AND $\alpha = C_{LMAX}$



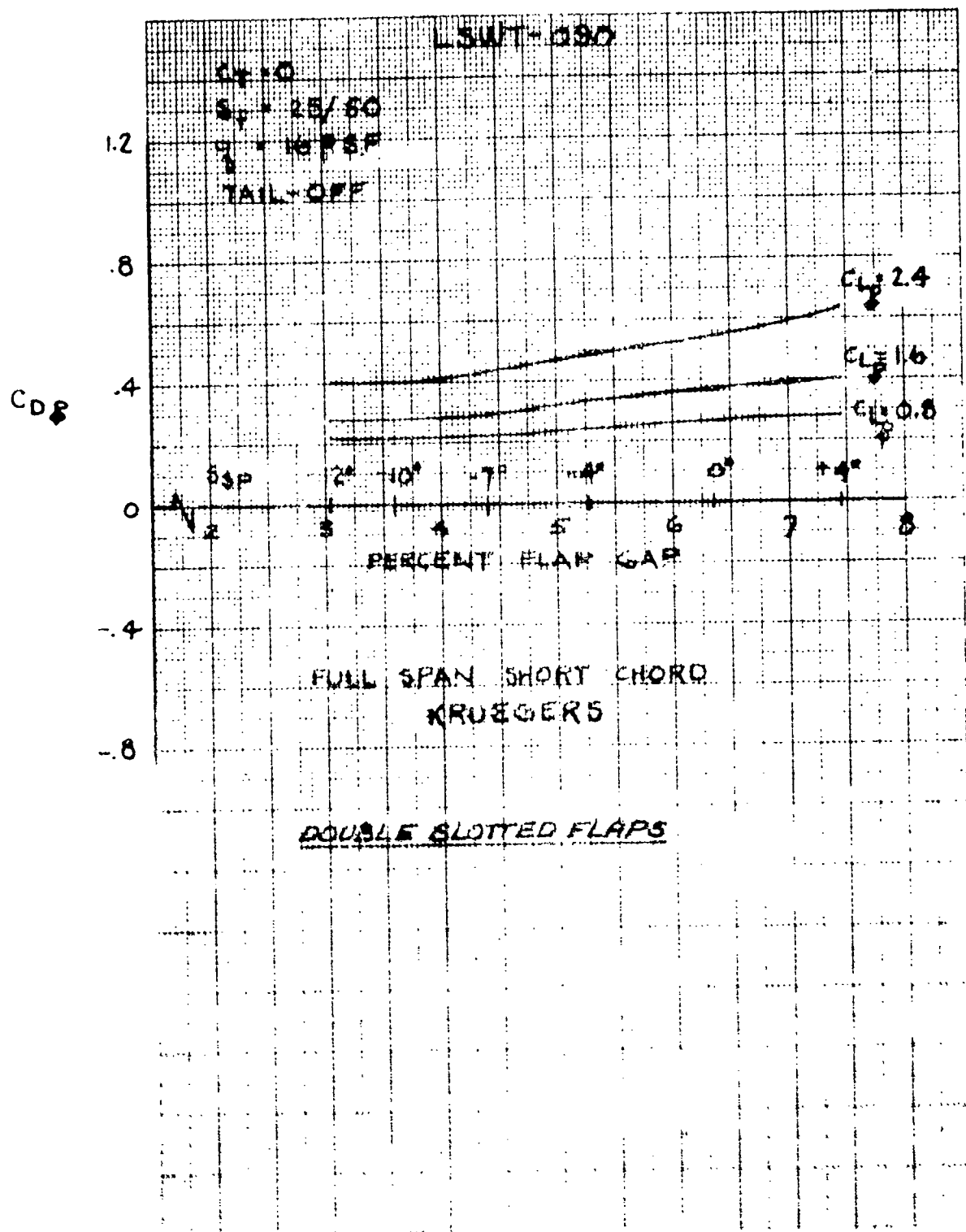
**EFFECTS OF FLAP GAP VARIATION
ON POWER-OFF DRAG COEFFICIENT**

Figure 12.3.5

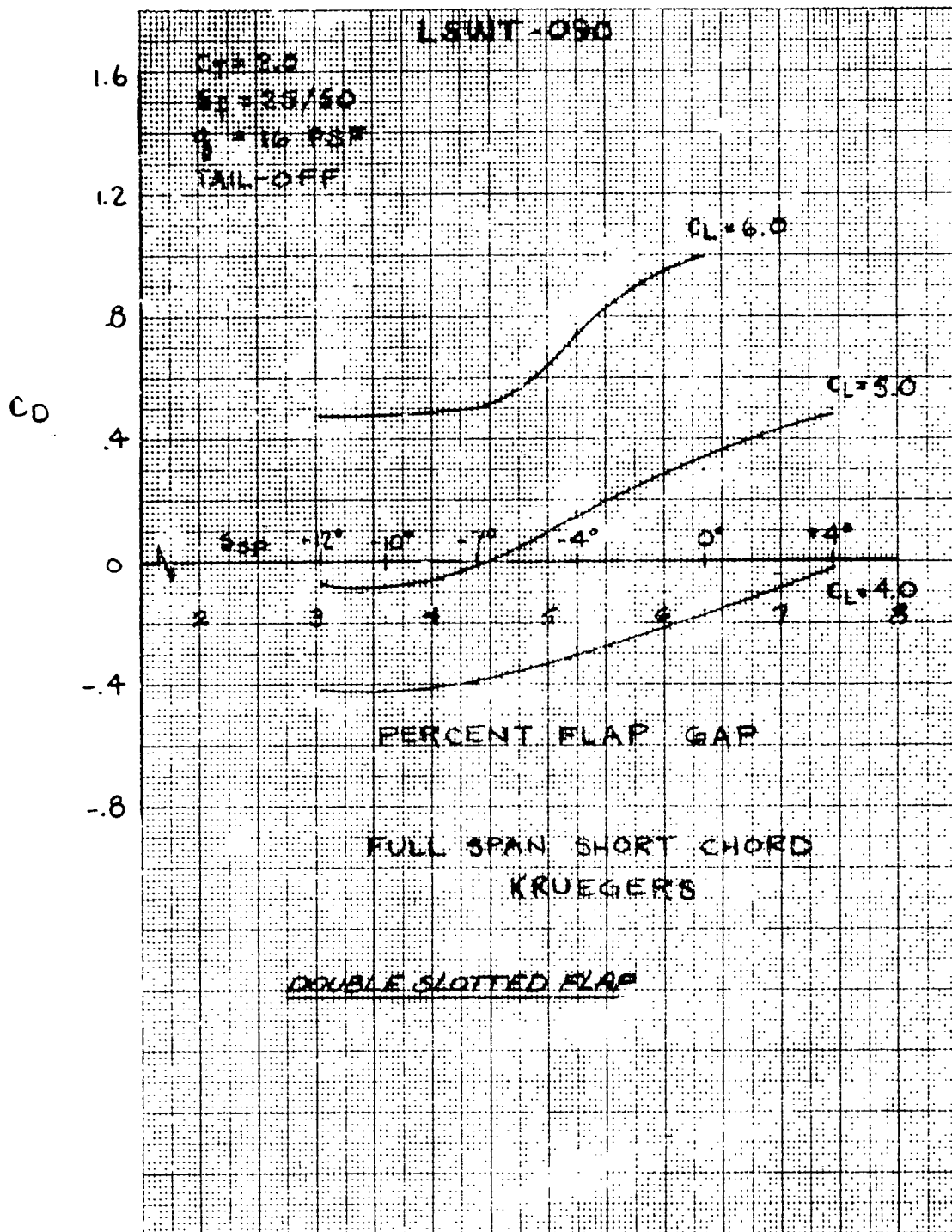


EFFECTS OF FLAP GAP VARIATION ON POWERED DRAG COEFFICIENT

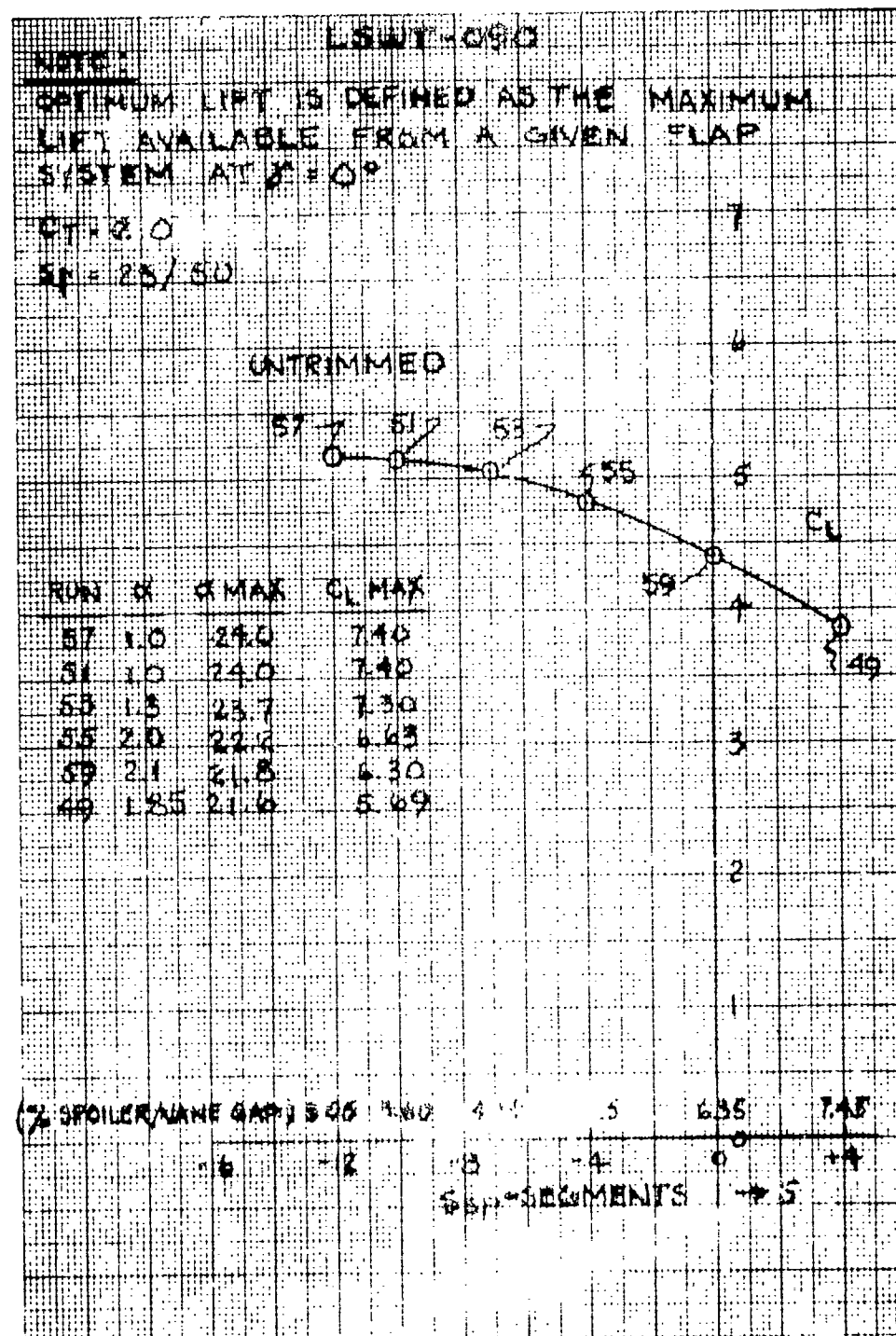
Figure 12.3.6



POWER OFF DRAG VS PERCENT FLAP GAP
VARIATION FOR LINES OF CONSTANT LIFT



POWERED DRAG VS. PERCENT FLAP GAP
VARIATION FOR LINES OF CONSTANT LIFT



EFFECT OF FLAP GAP ON OPTIMUM LIFT
OF DOUBLE SLOTTED FLAPS AT $\delta = 0^\circ$

Figure 12.3.9

K-E 10 X 10 TO THE CENTIMETER 46 1513
10 X 25 CM
KEUFFEL & ESSER CO.

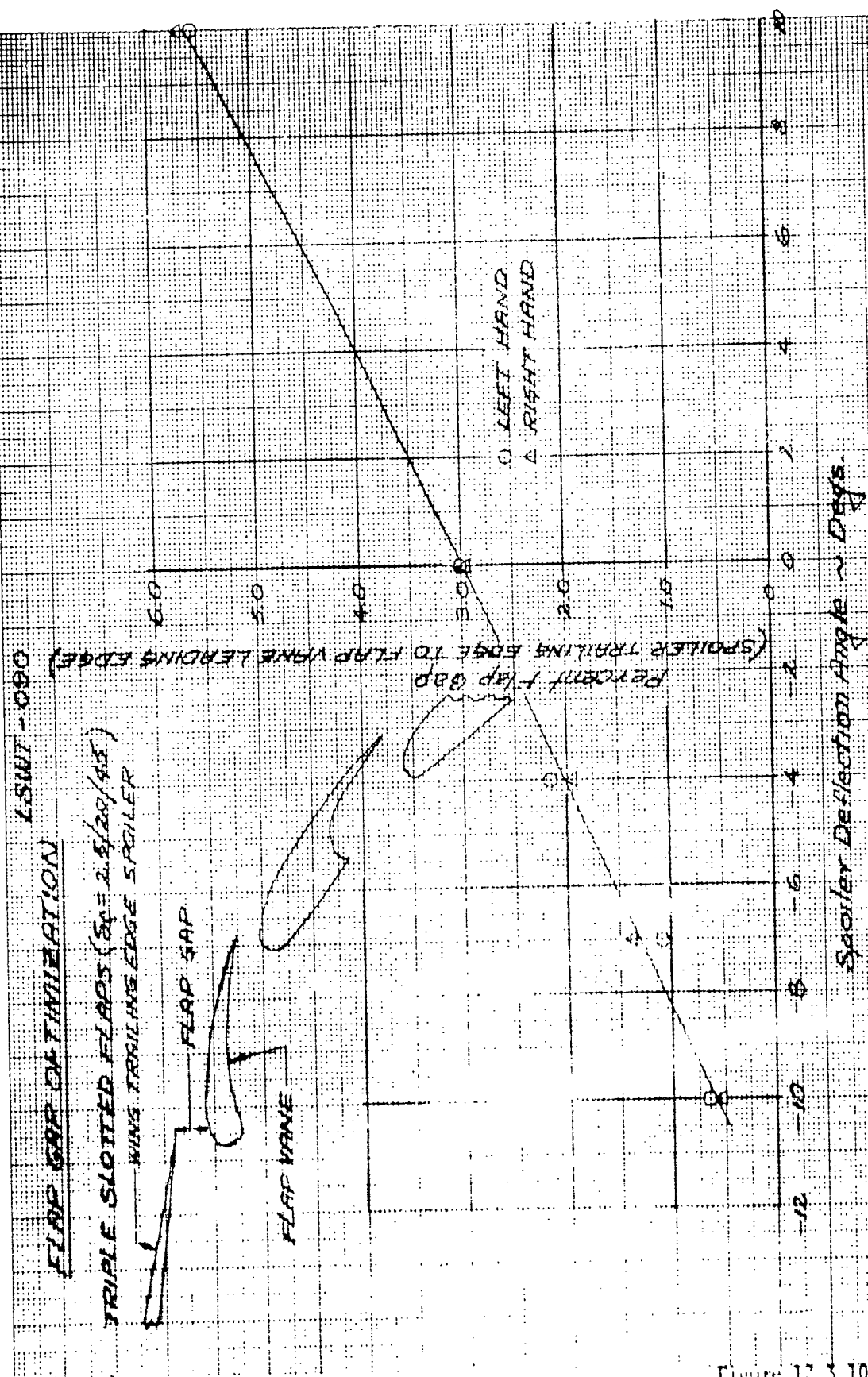
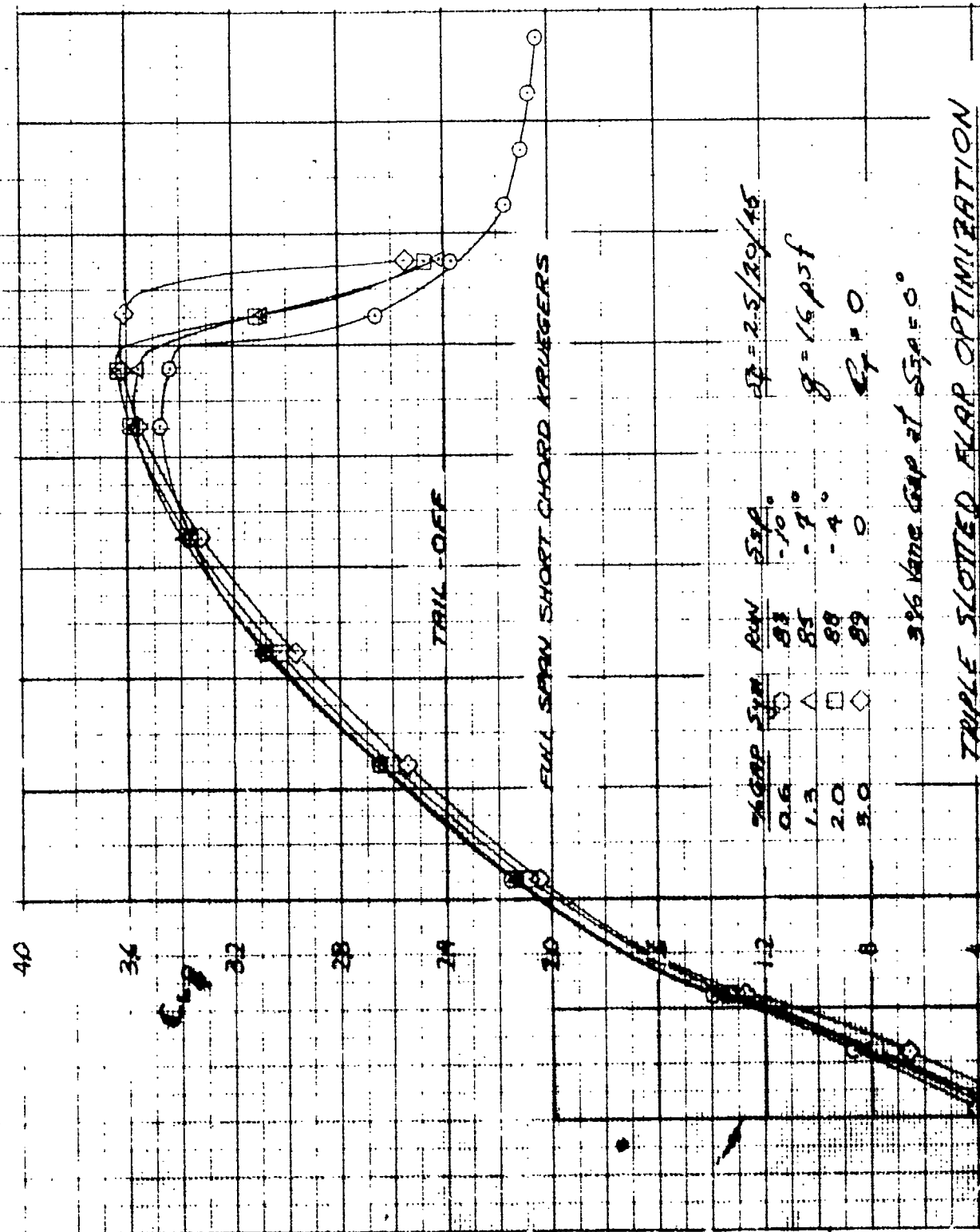
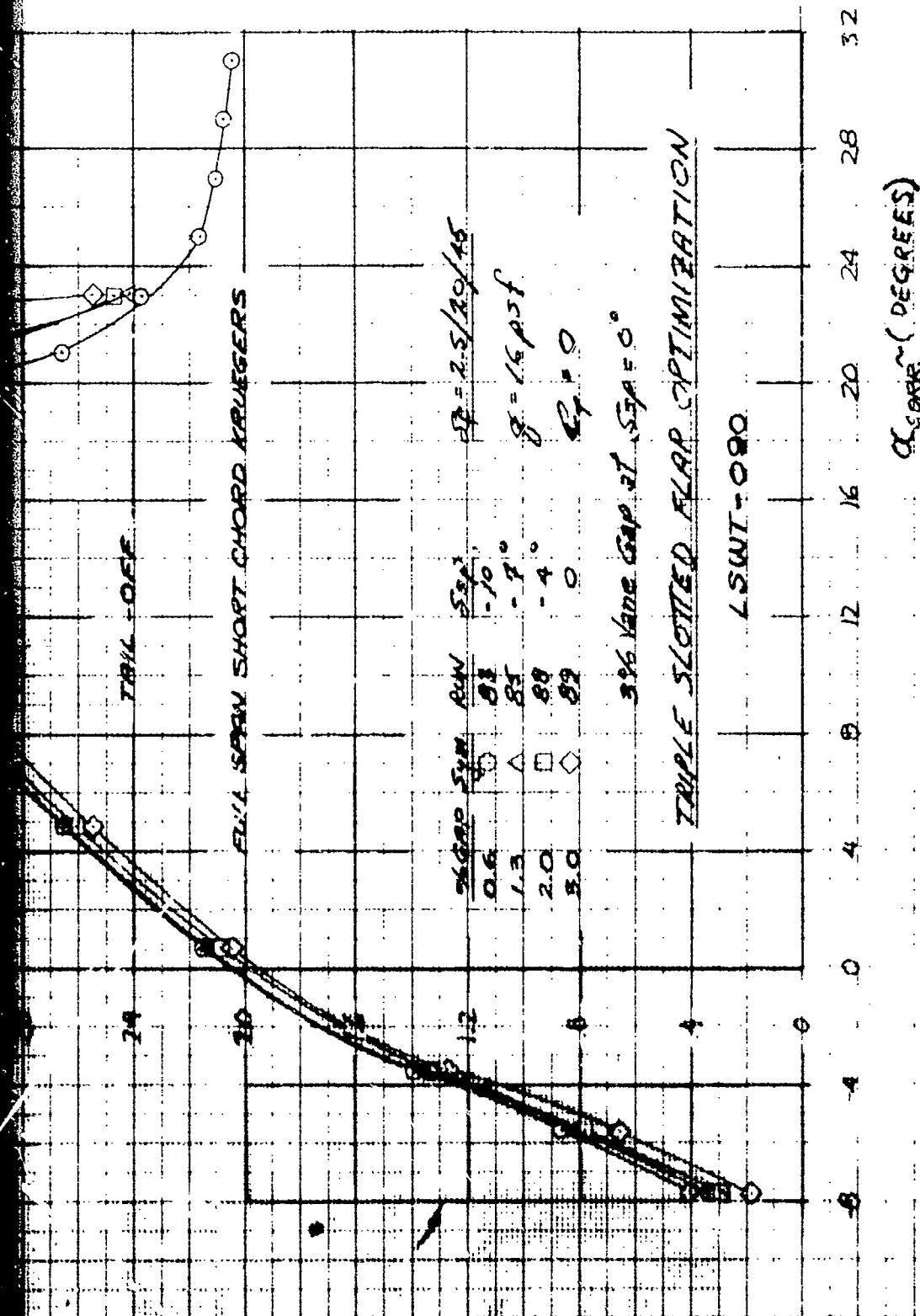


Figure 12.3.10

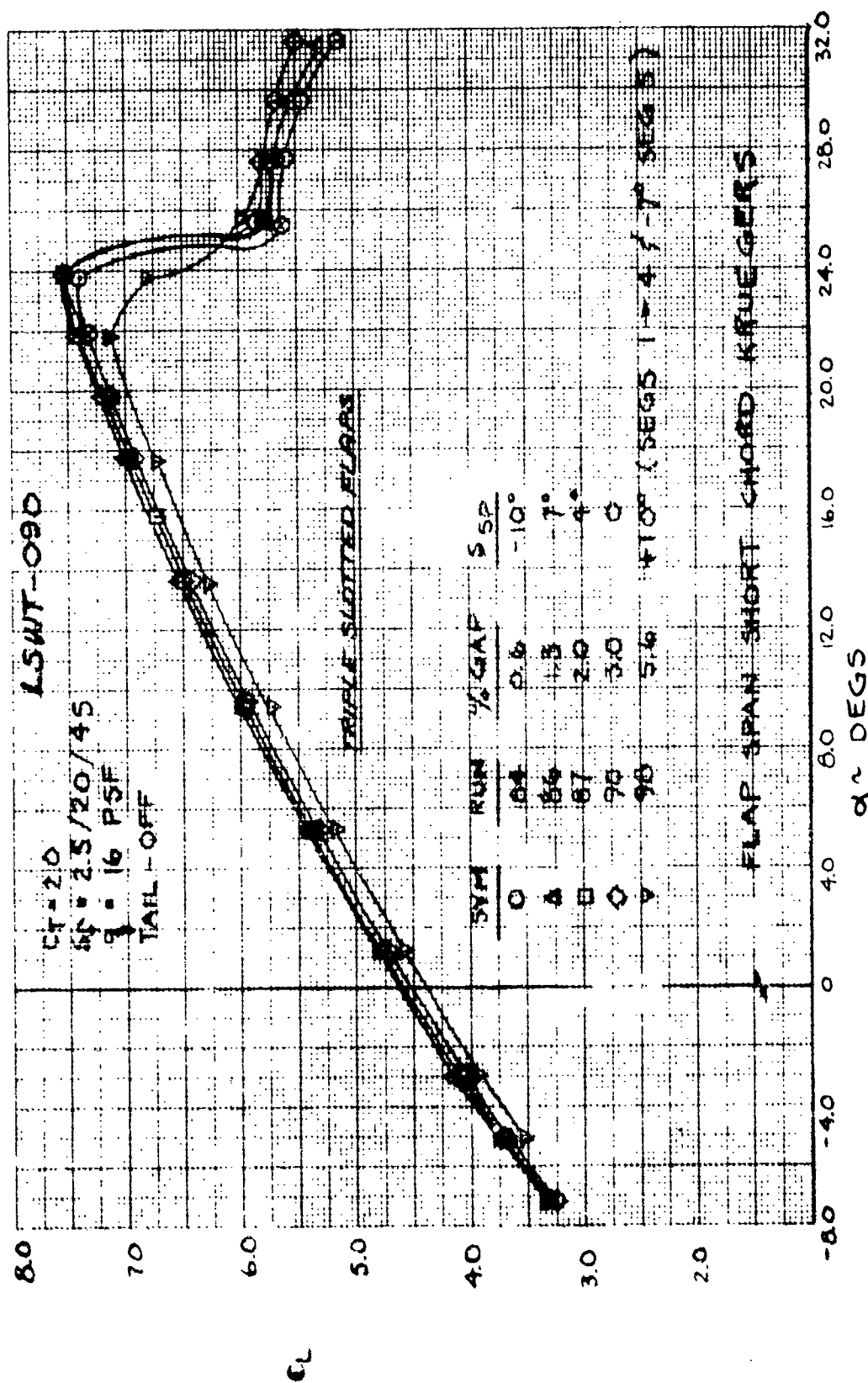


TRIPLE SLOTTED FLAP OPTIMIZATION



EFFECTS OF FLAP GAP VARIATION ON POWER-OFF LIFT COEFFICIENT

Figure 12.3.11
 (The reverse side of this page is blank)



EFFECTS OF FLAP GAP VARIATION ON POWERED LIFT COEFFICIENT

Figure 12.3.12

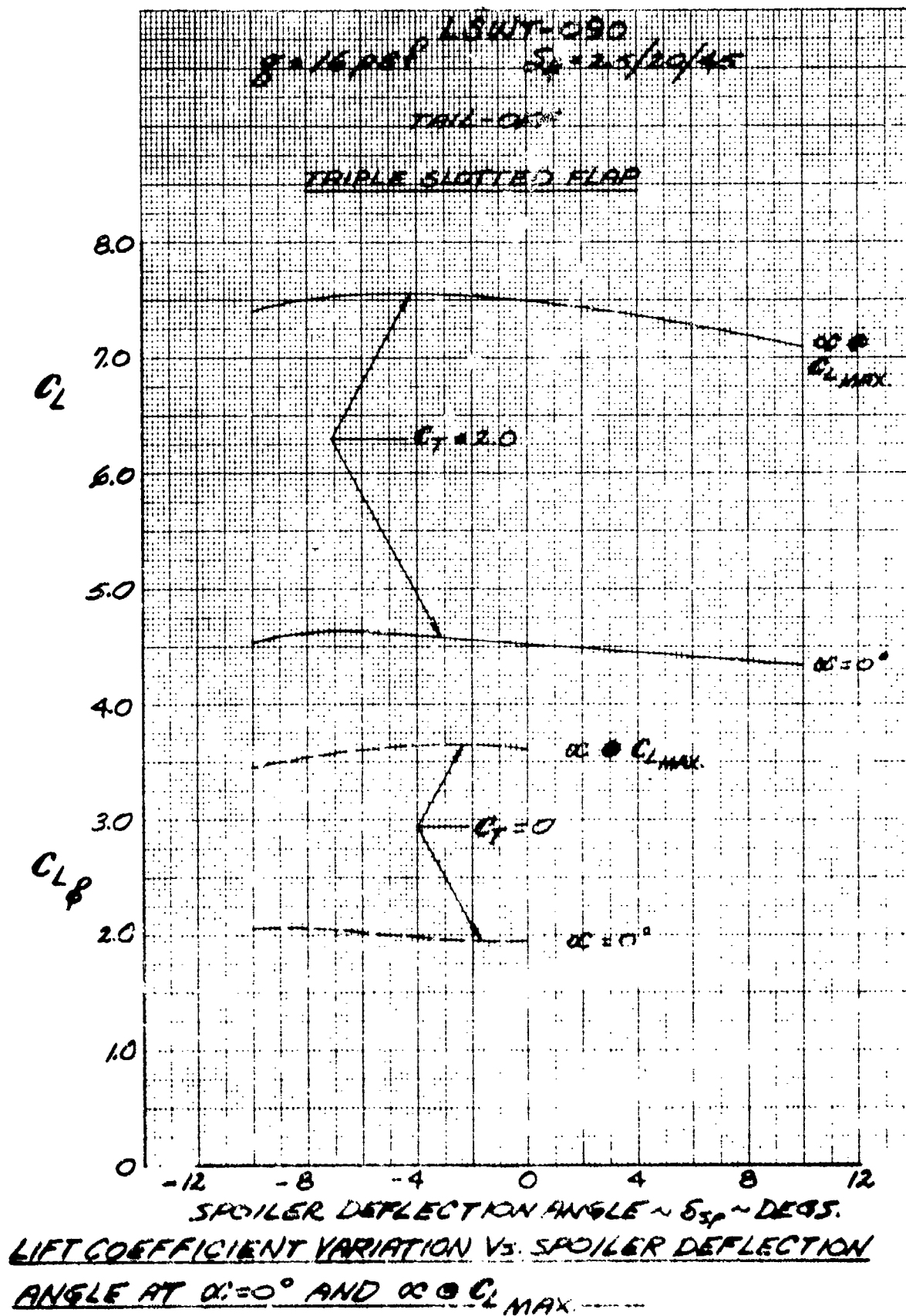
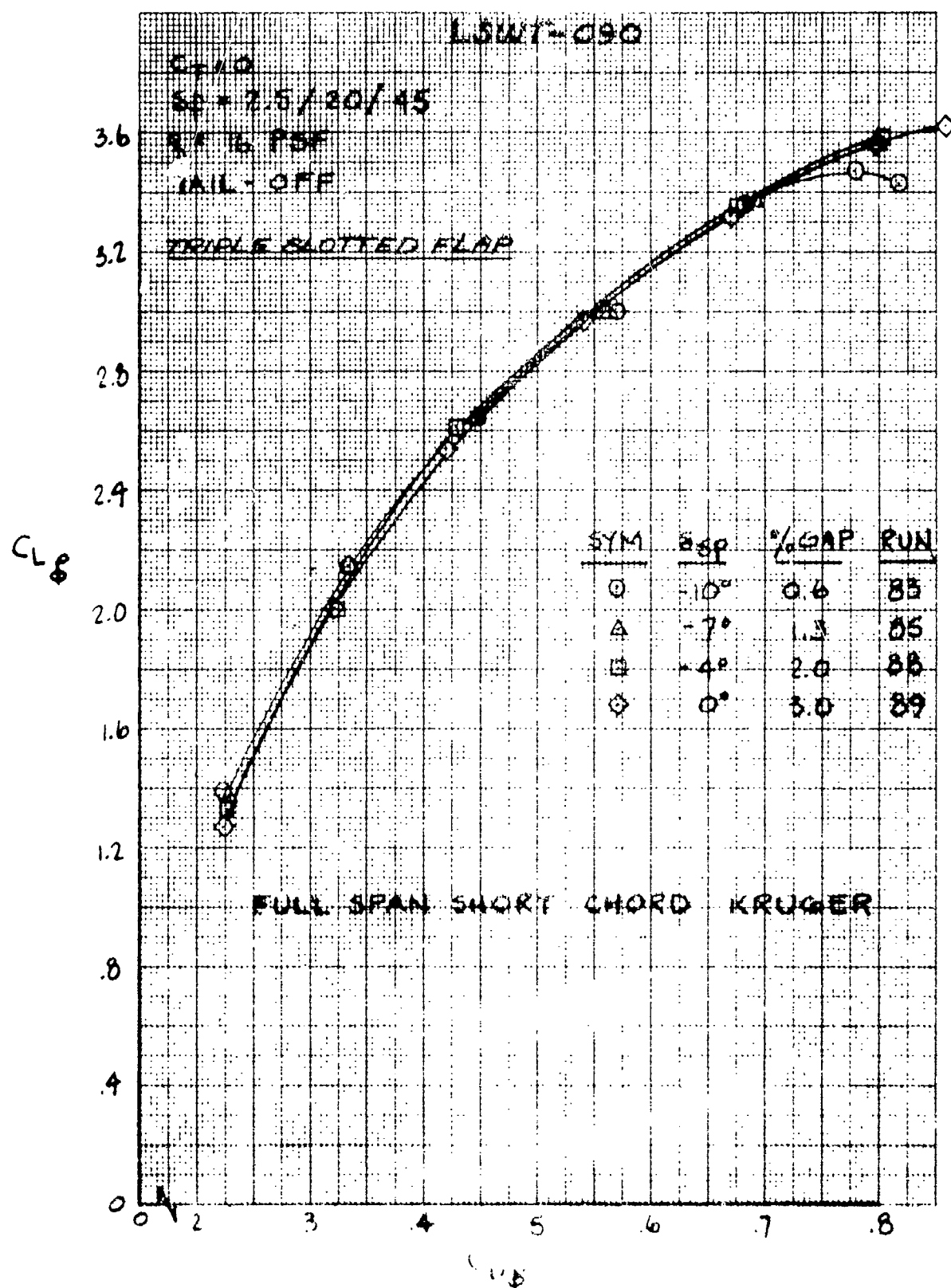
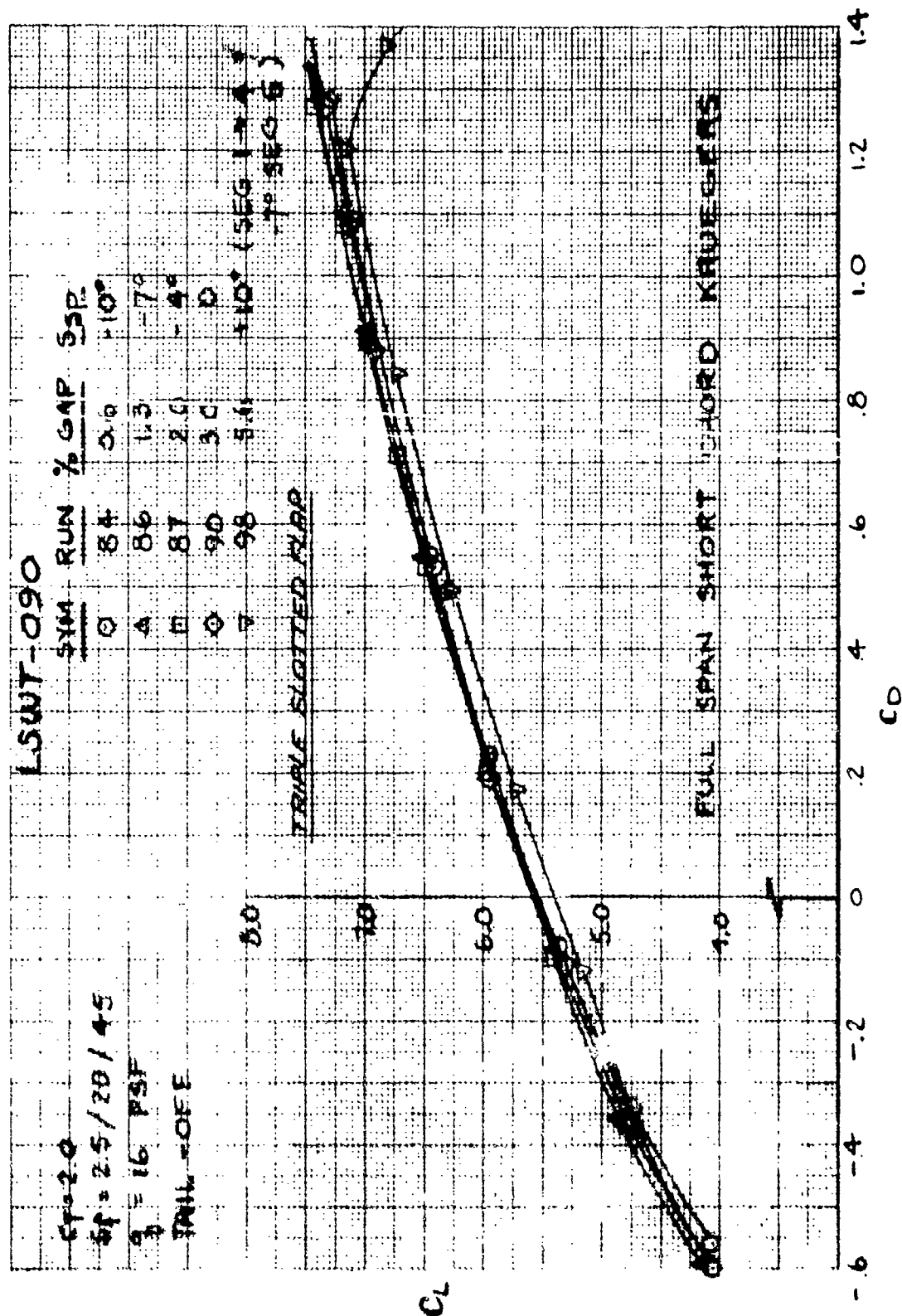


Figure 12.3.13



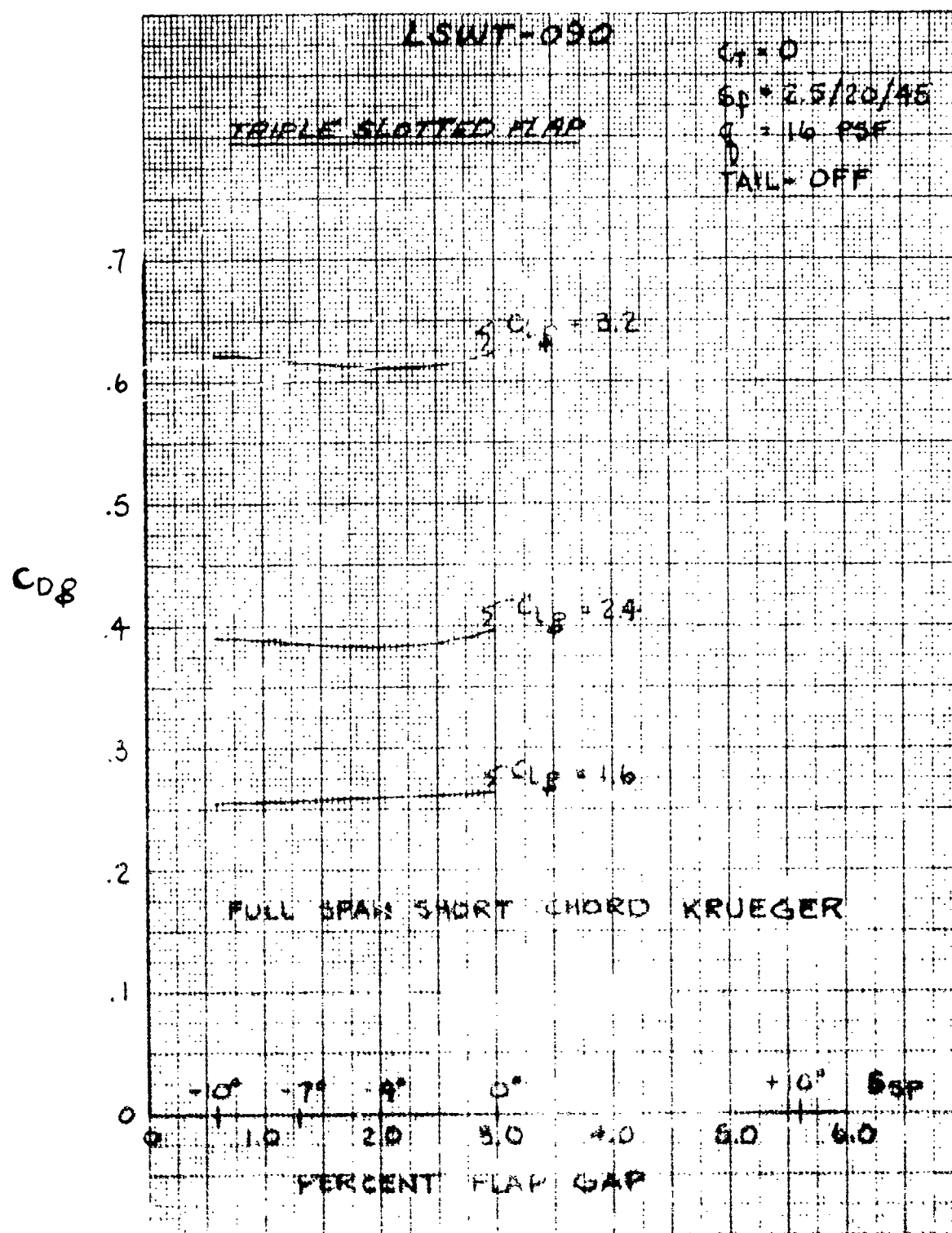
EFFECTS OF FLAP GAP VARIATION ON
POWER-OFF DRAG COEFFICIENT

Figure 12.3.14



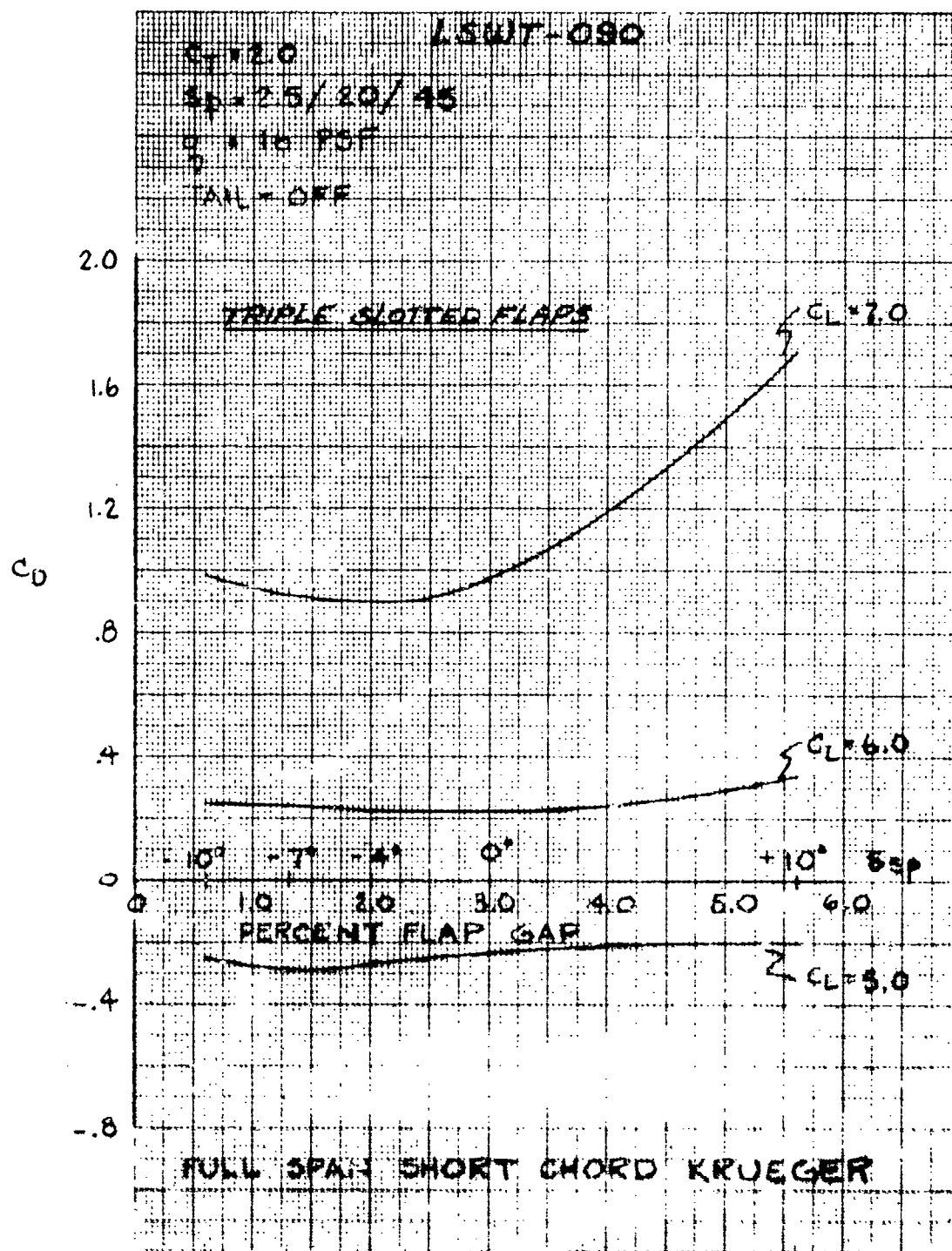
EFFECTS OF FLAP GAP VARIATION ON POWERED
DRAG COEFFICIENT

Figure 12.3.15

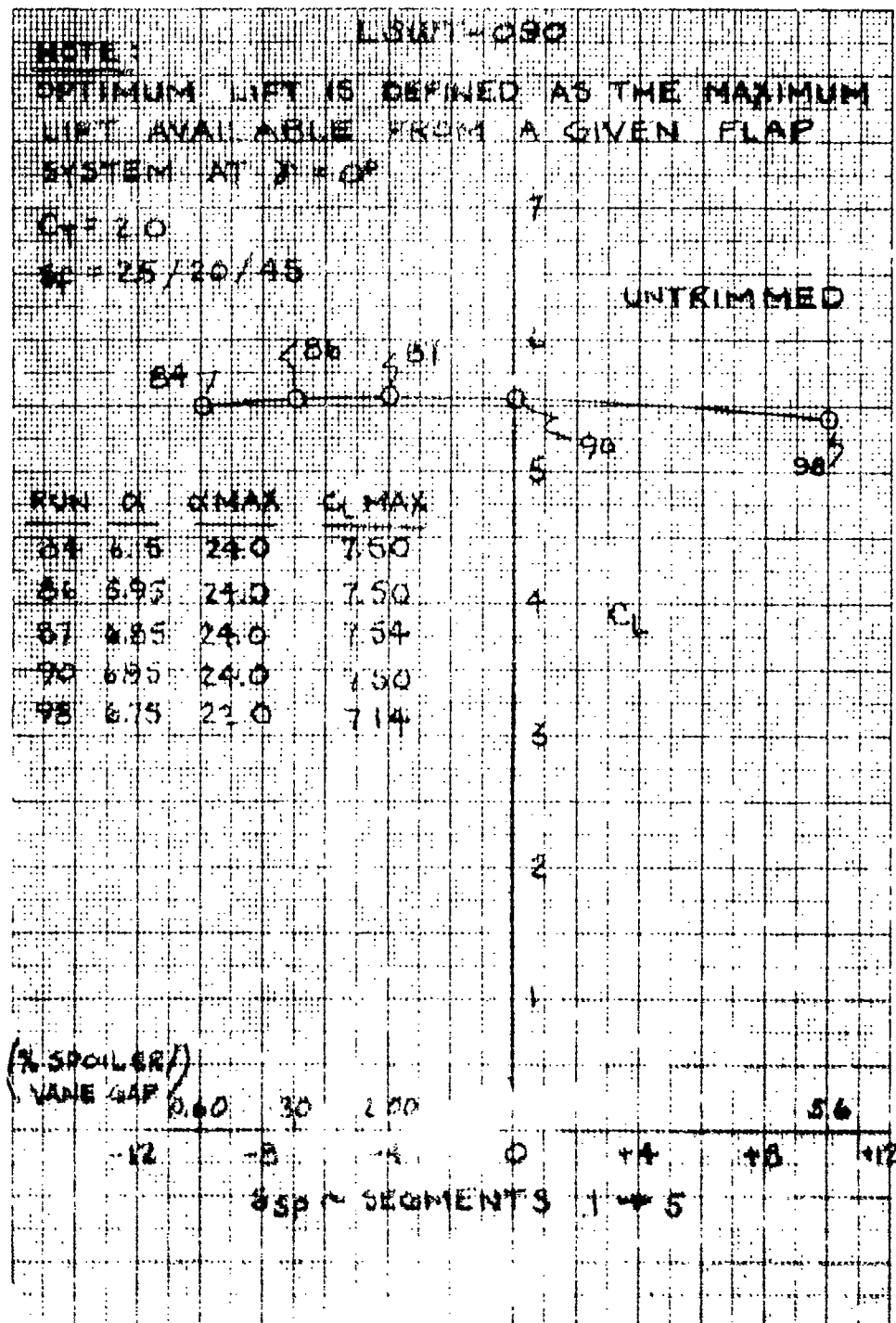


POWER-OFF DRAG COEFFICIENT VS. PERCENT
 FLAP GAP VARIATION FOR LINES OF
 CONSTANT LIFT COEFFICIENT

Figure 12.3.1b

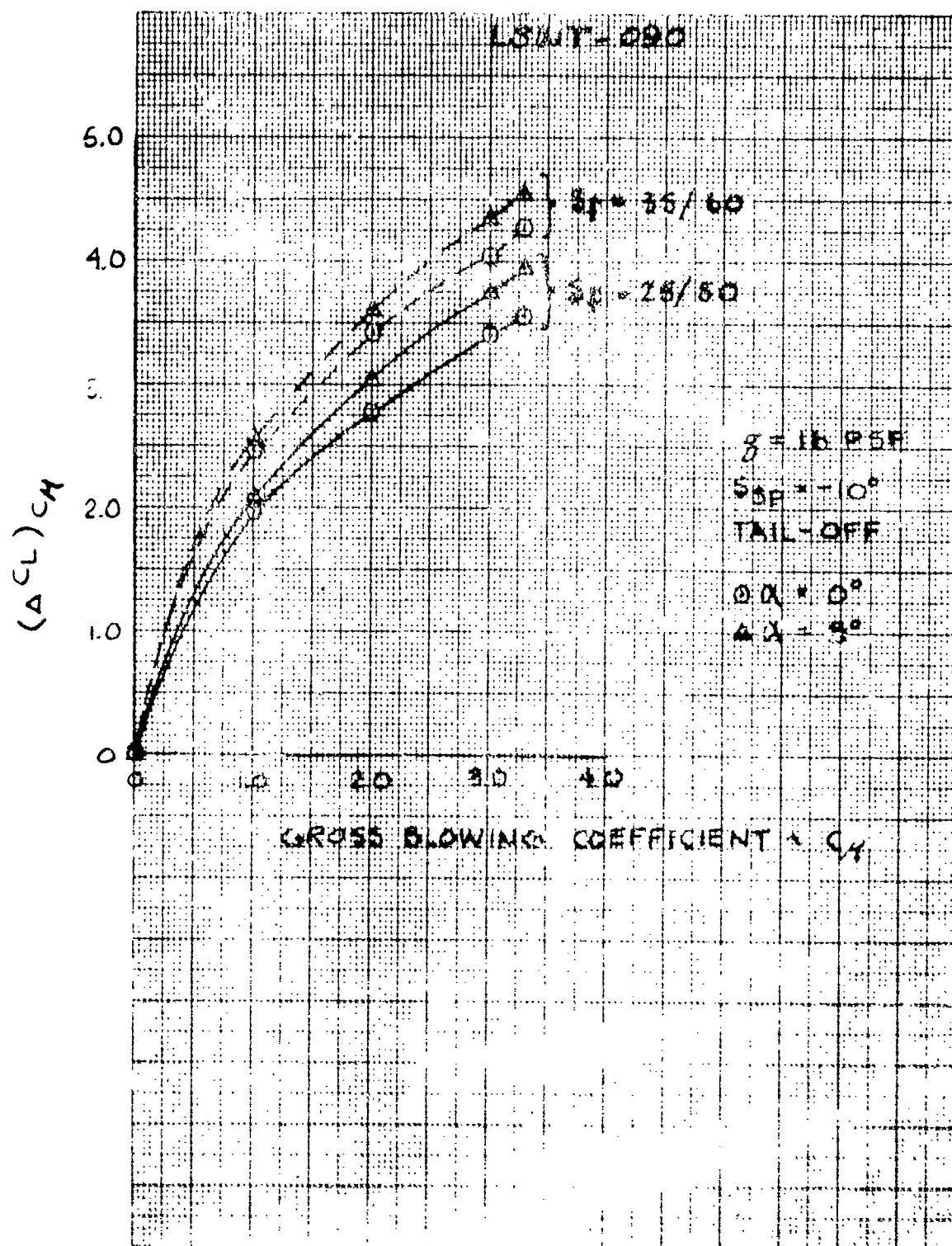


POWERED DRAG COEFFICIENT VS. PERCENT FLAP GAP VARIATION FOR LINES OF CONSTANT POWERED LIFT COEFFICIENT



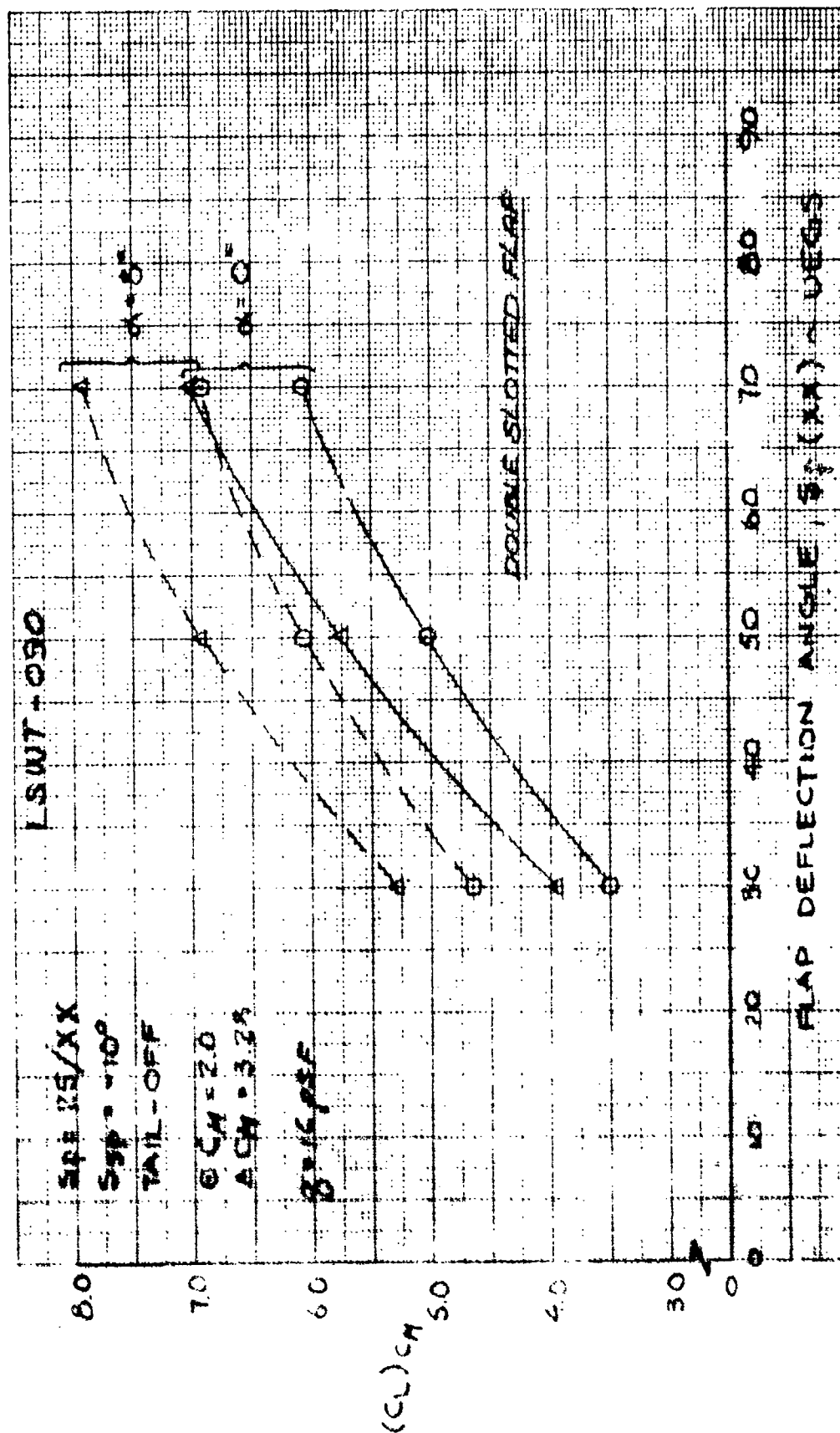
OPTIMUM LIFT OF
TRIPLE SLOTTED FLAPS AT $\delta = 0^\circ$

Figure 12.3.18



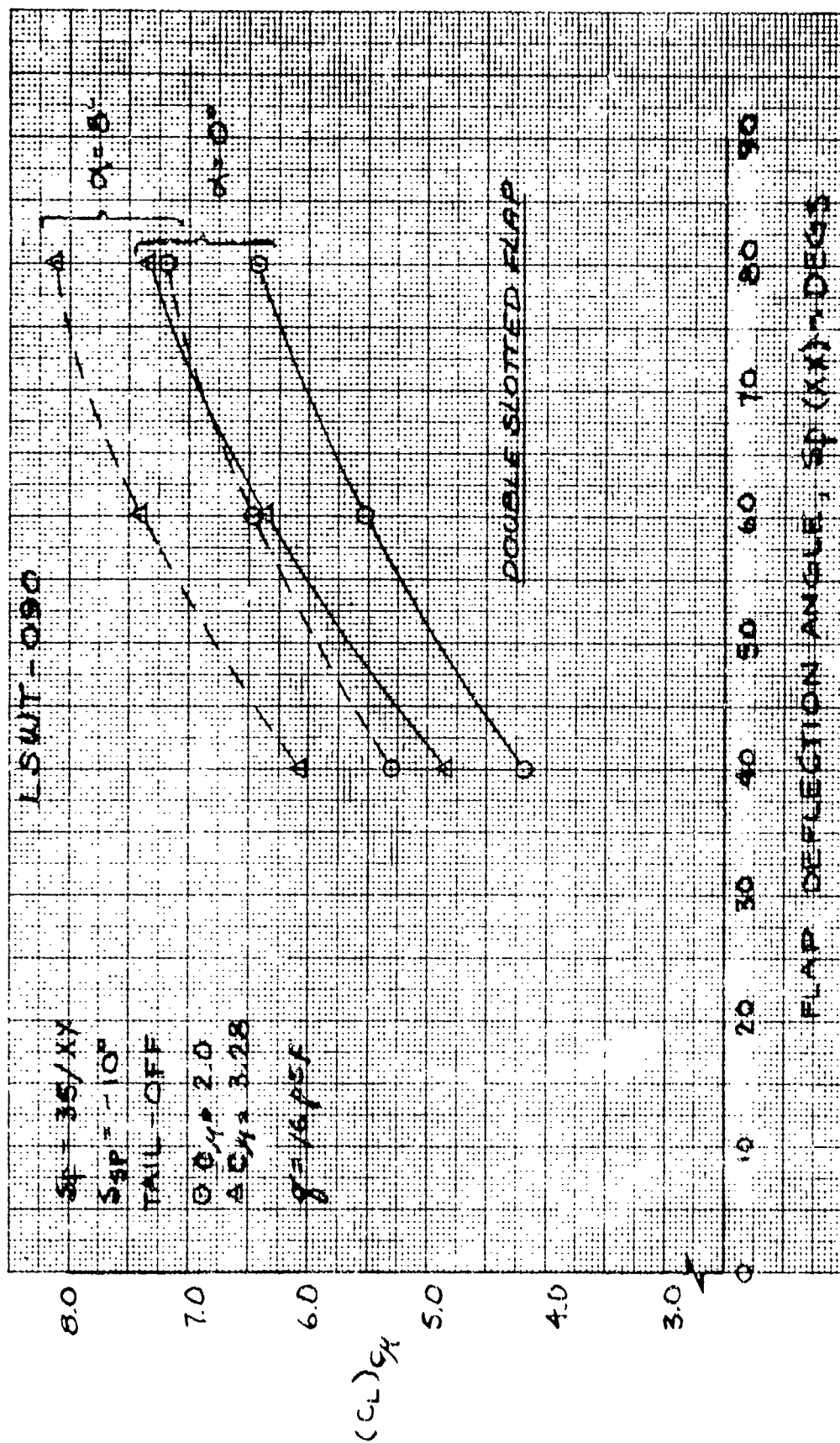
FLOWER EFFECTS ON DOUBLE SLOTTED
FLAP LIFT CAPABILITY

Figure 12.4.1

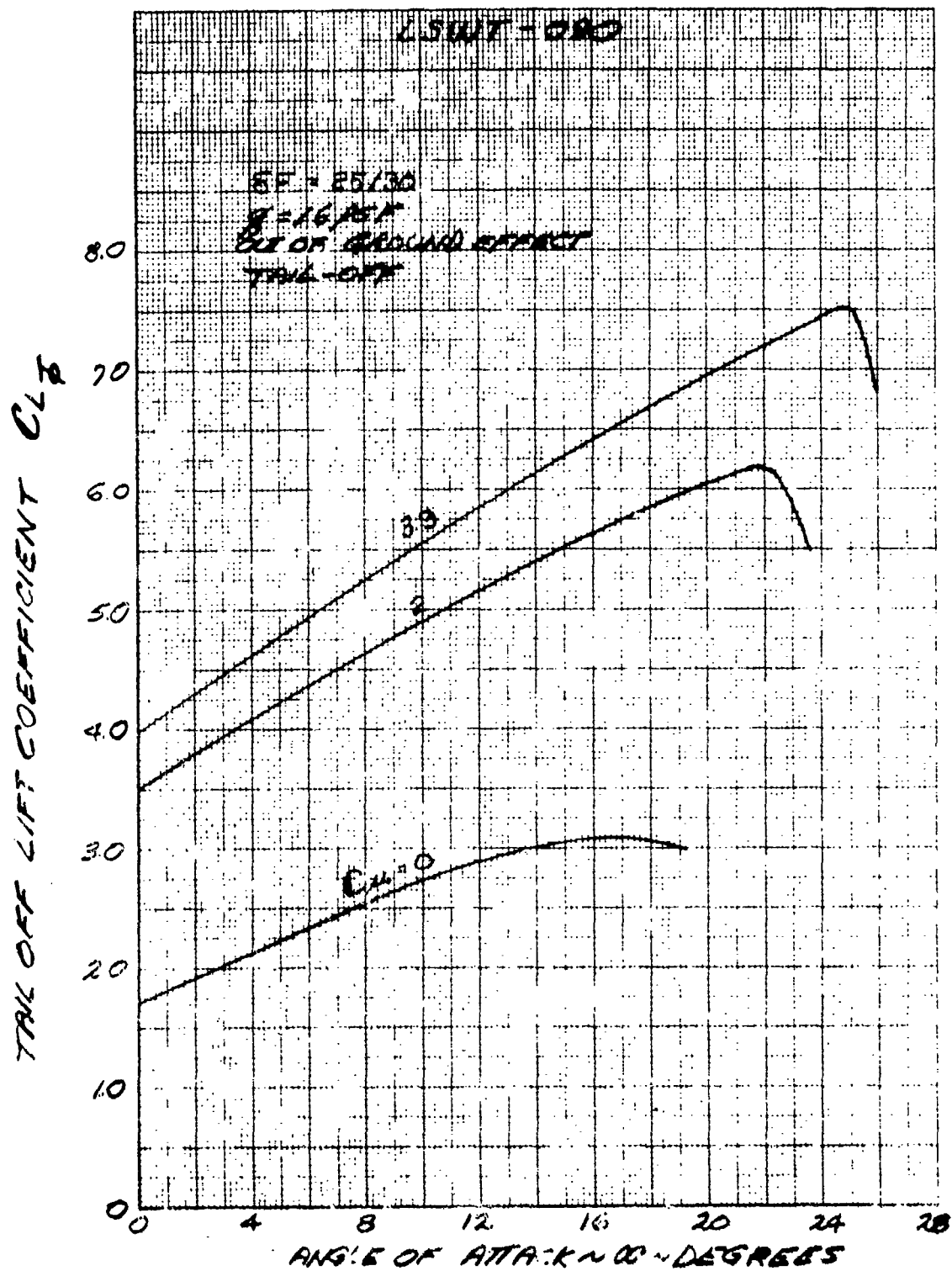


EFFECTS OF FLAP DEFLECTION ON
 POWERED LIFT COEFFICIENT

Figure 12.4.2



EFFECTS OF FLAP DEFLECTION ON
 POWERED LIFT COEFFICIENT



EFFECT OF POWER ON LIFT COEFFICIENT
- DOUBLE SLOTTED FLAP -

Figure 12.4.4

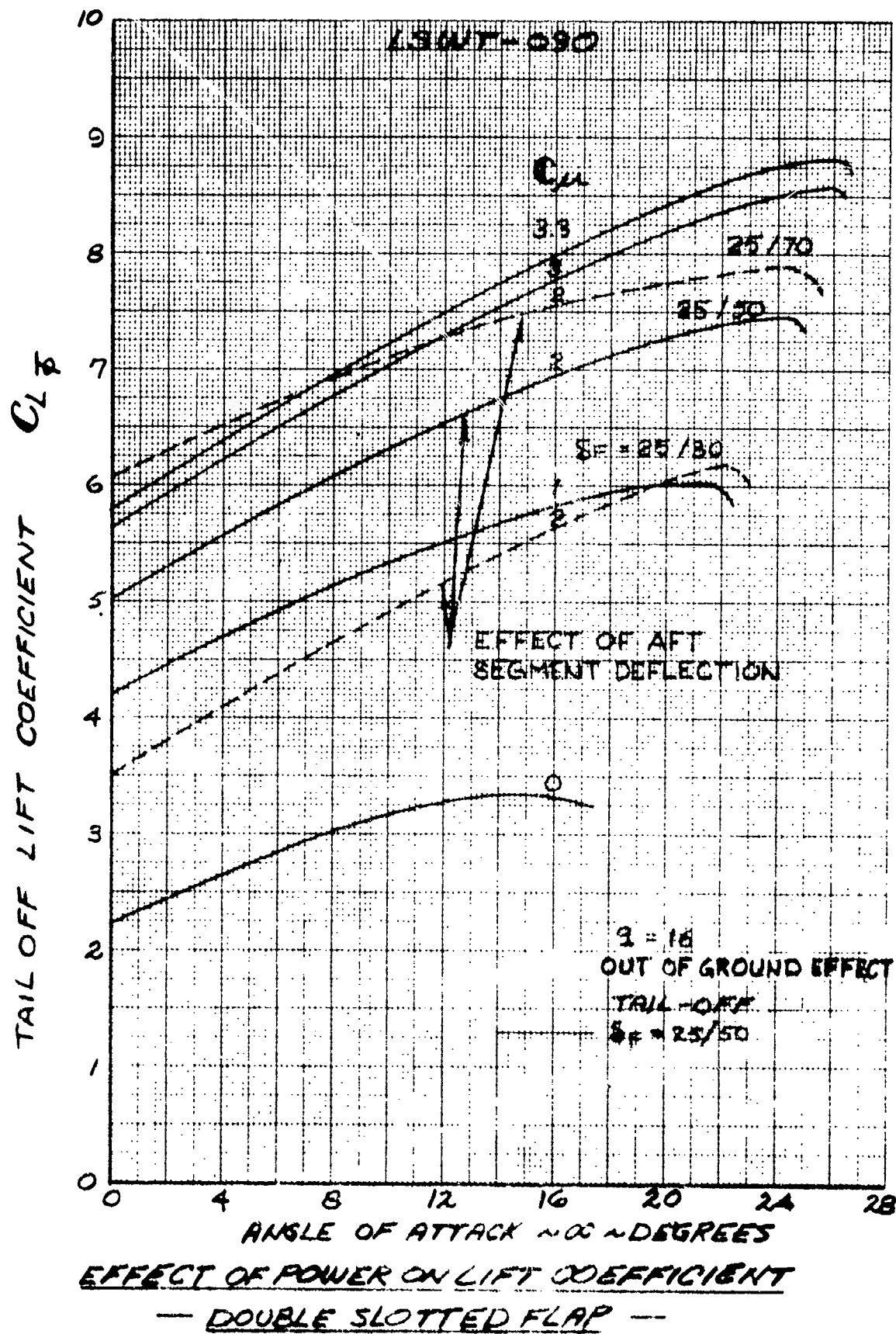
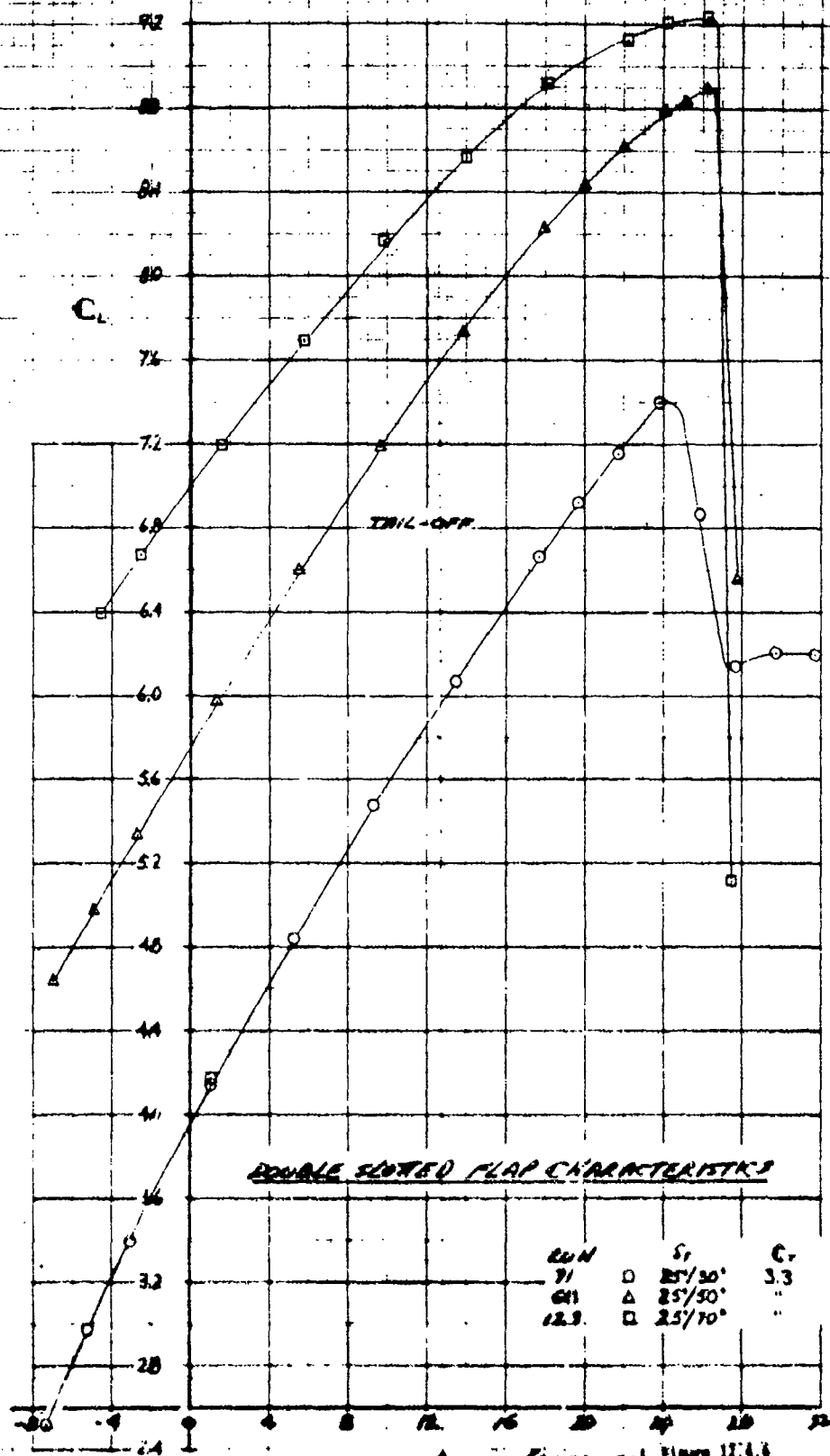
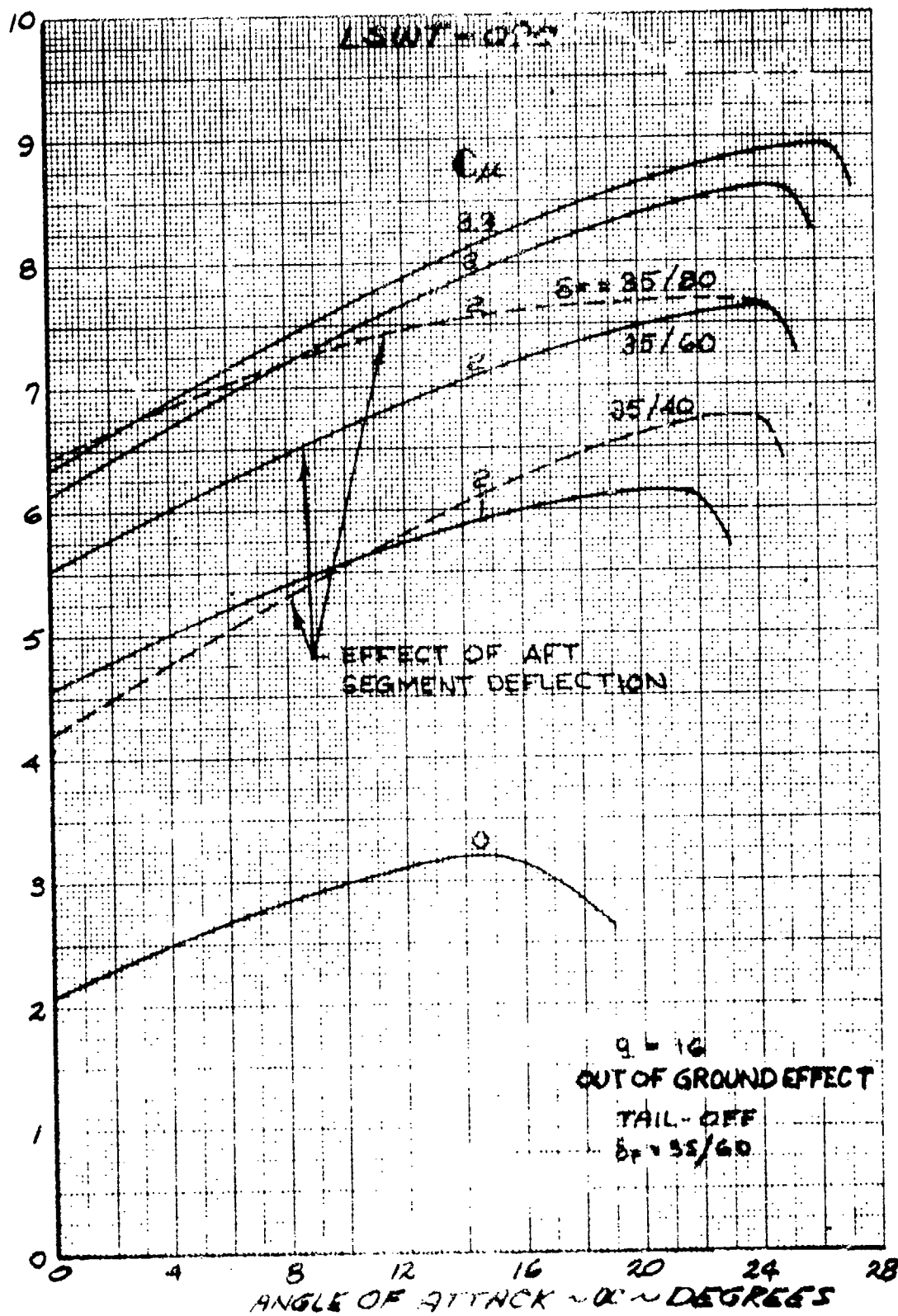


Figure 12.4.5

L5WT-090



TAIL OFF LIFT COEFFICIENT $\sim C_{L\delta}$

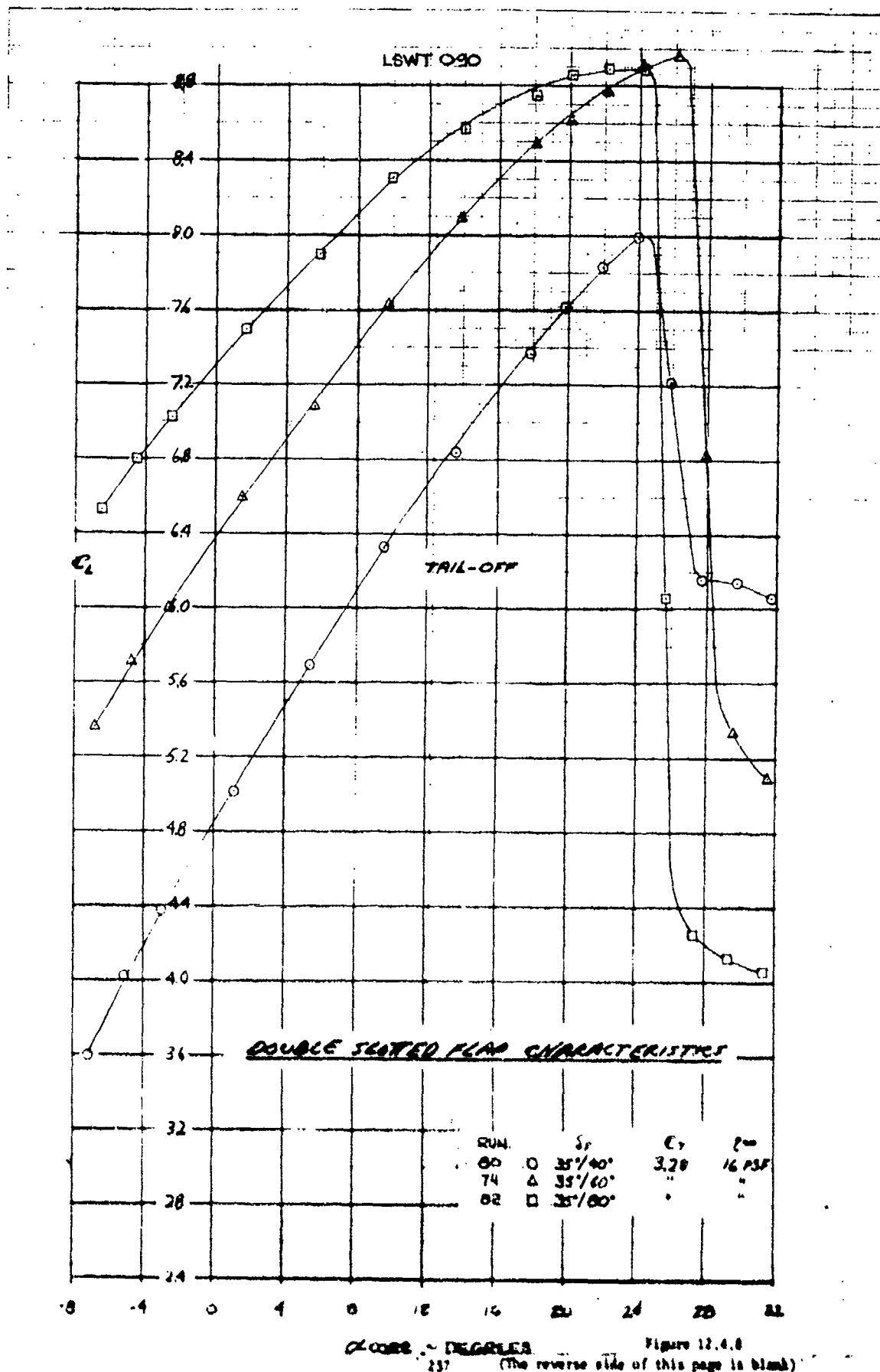


EFFECT OF POWER ON LIFT COEFFICIENT
— DOUBLE SLOTTED FLAP —

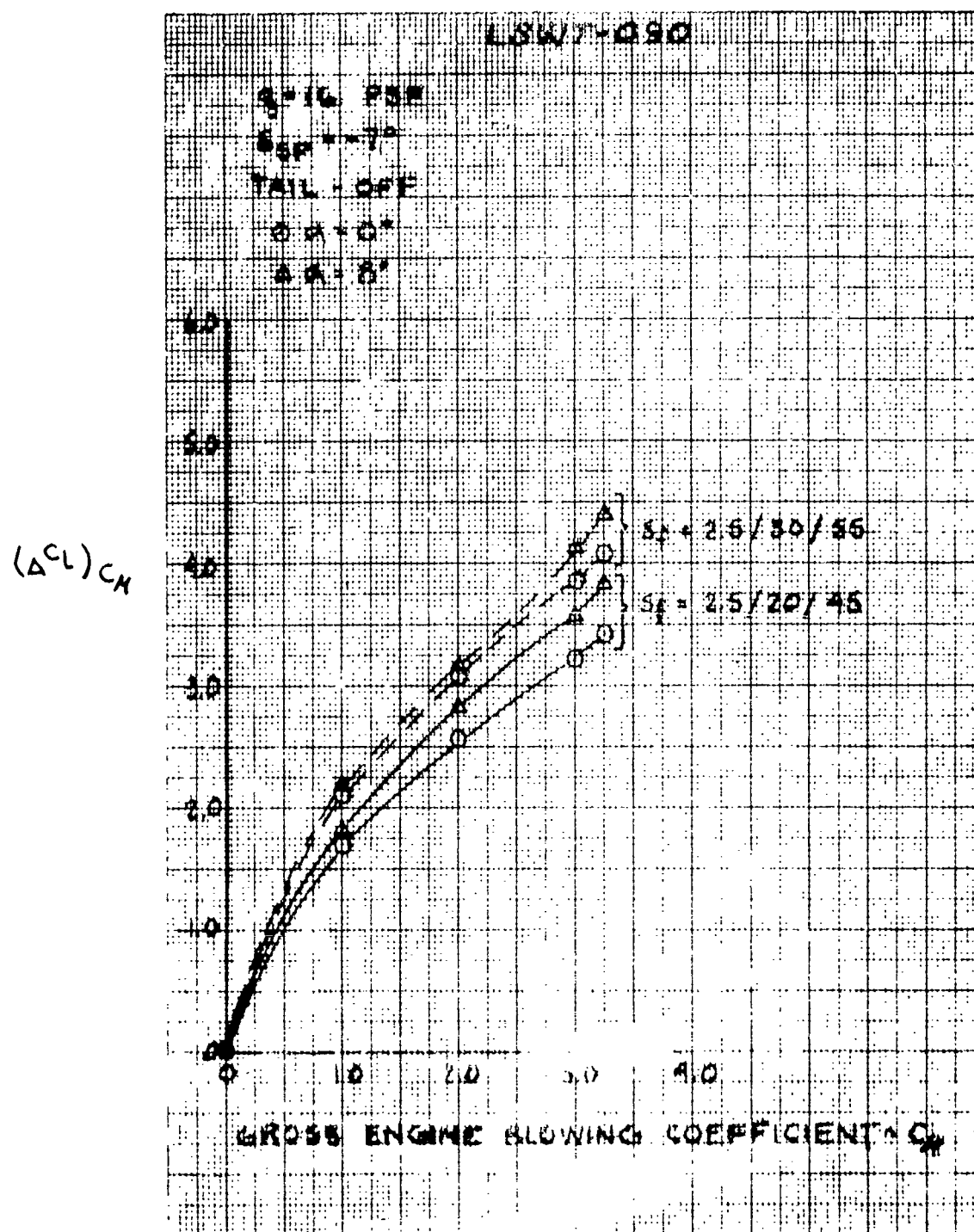
Figure 12.4.7

The reverse side of this page is blank)

Preceding page blank



Preceding page blank



POWER EFFECTS ON TRIPLE SLOTTED
FLAP LIFT CAPABILITY

Figure 12.4.9

Preceding page blank

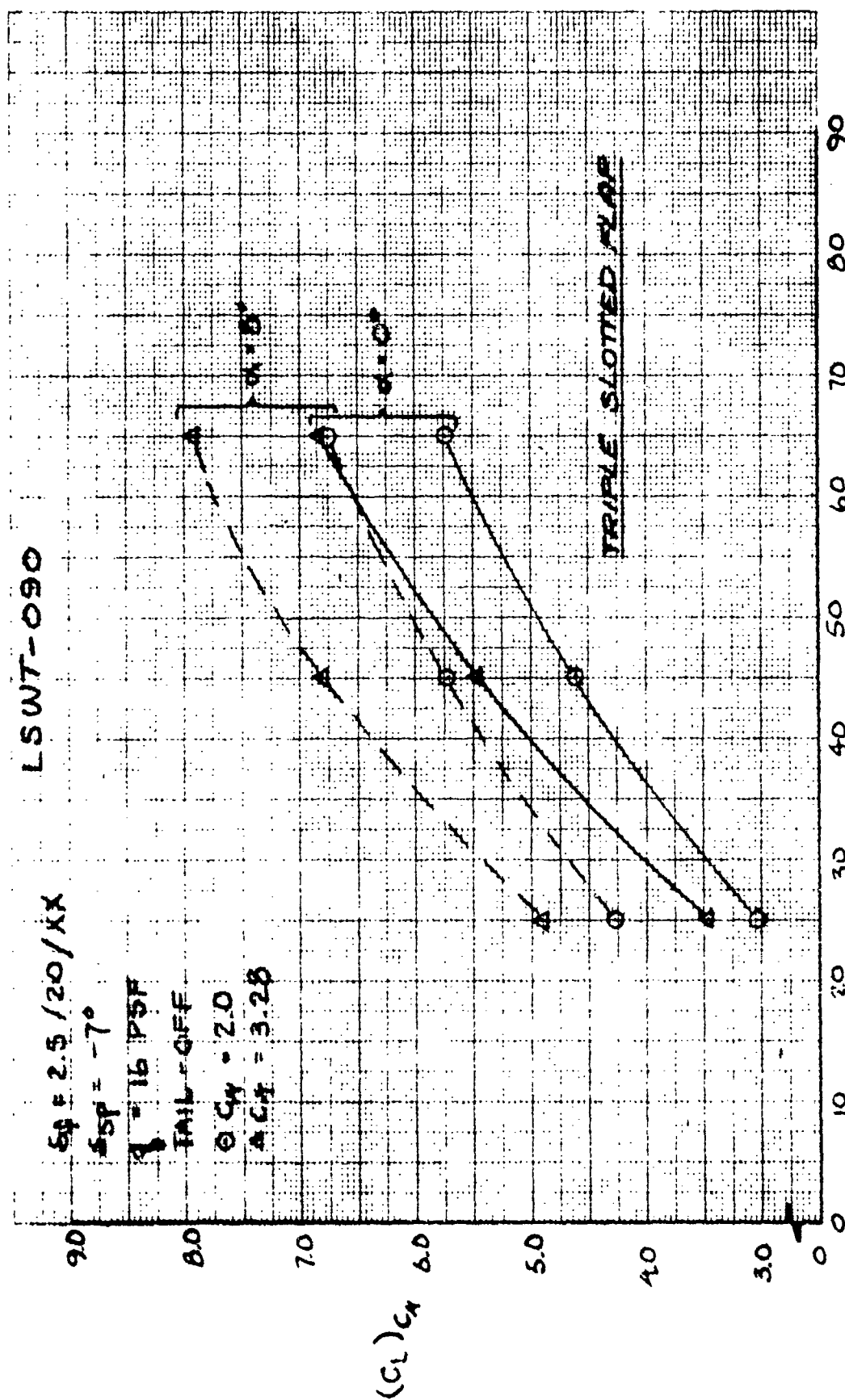


Figure 12.4.10

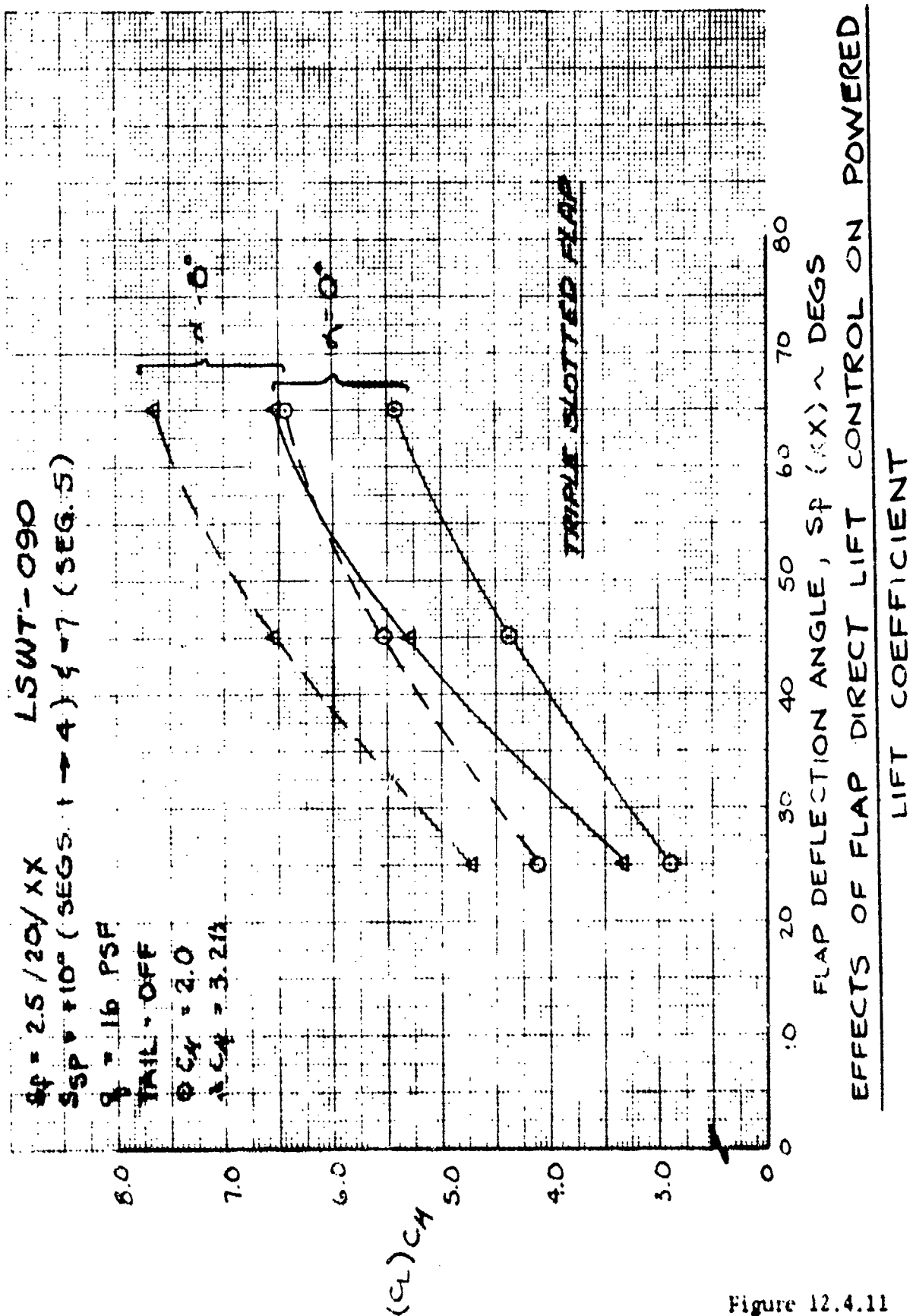


Figure 12.4.11

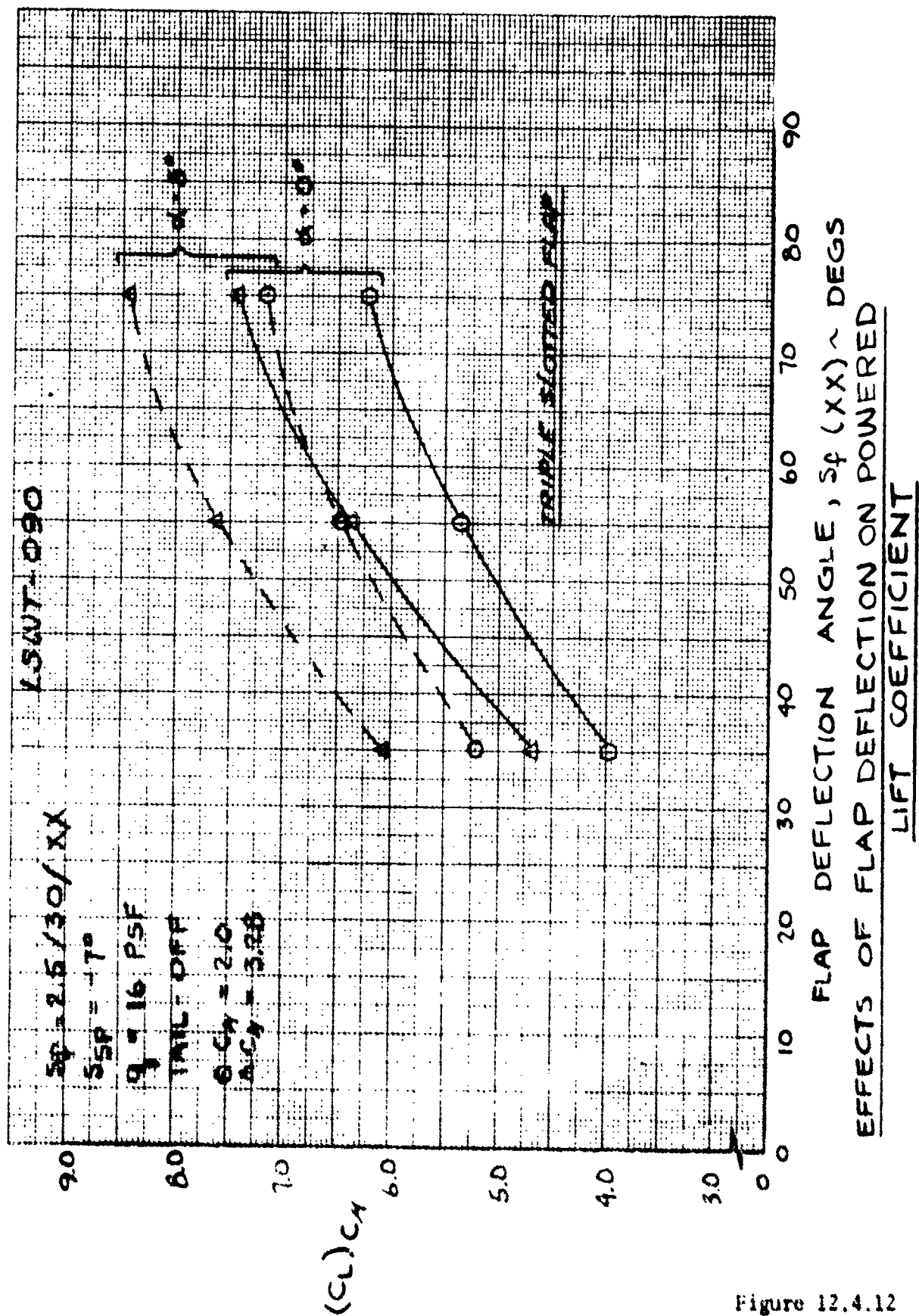


Figure 12.4.12

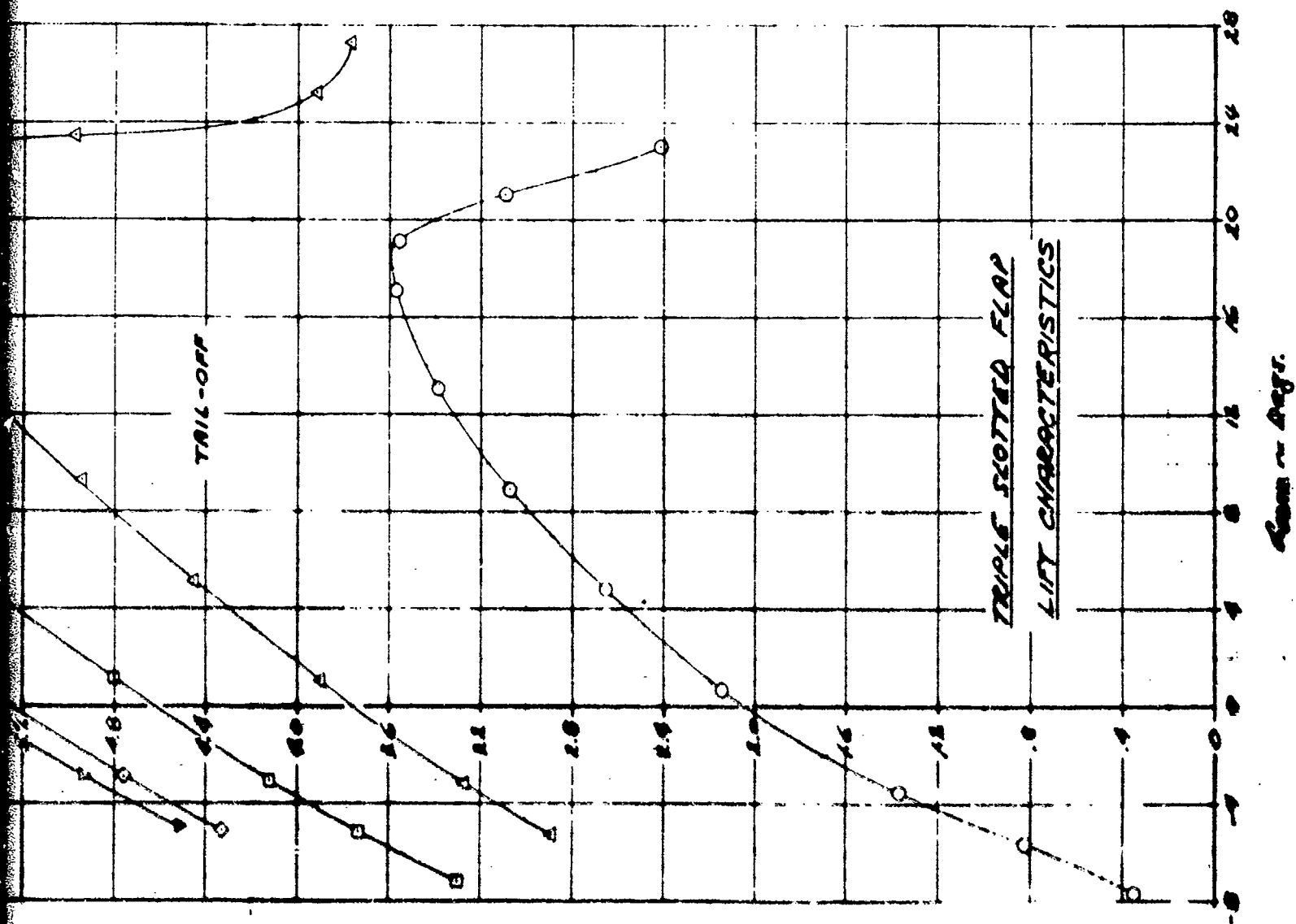


Figure 12.0.13

(The reverse side of the page is blank)

LSWT-030

TRIPLE SLOTTED FLAP CHARACTERISTICS

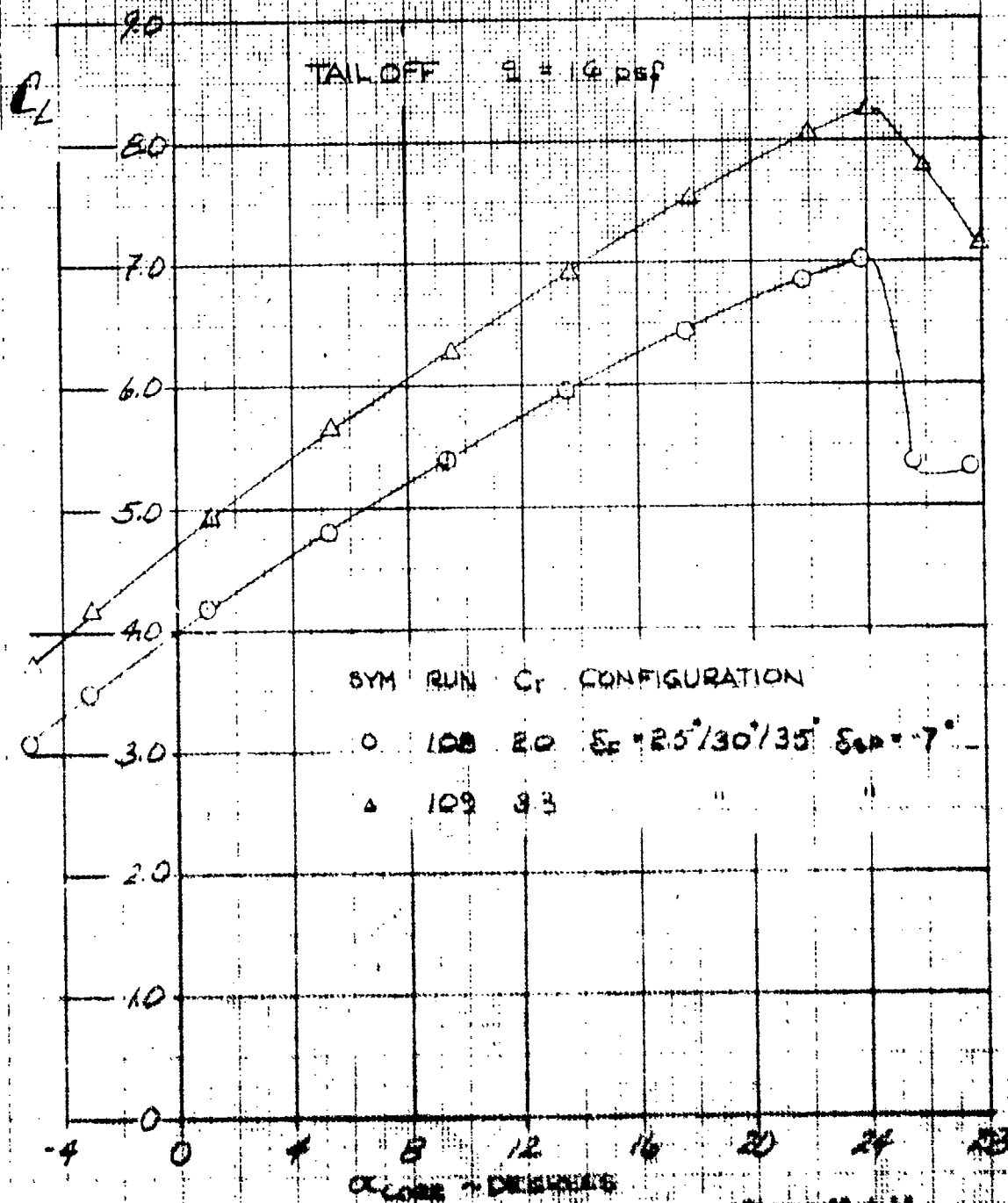


Figure 12.11

TRIPLE SLOTTED FLEET CHARACTERISTICS

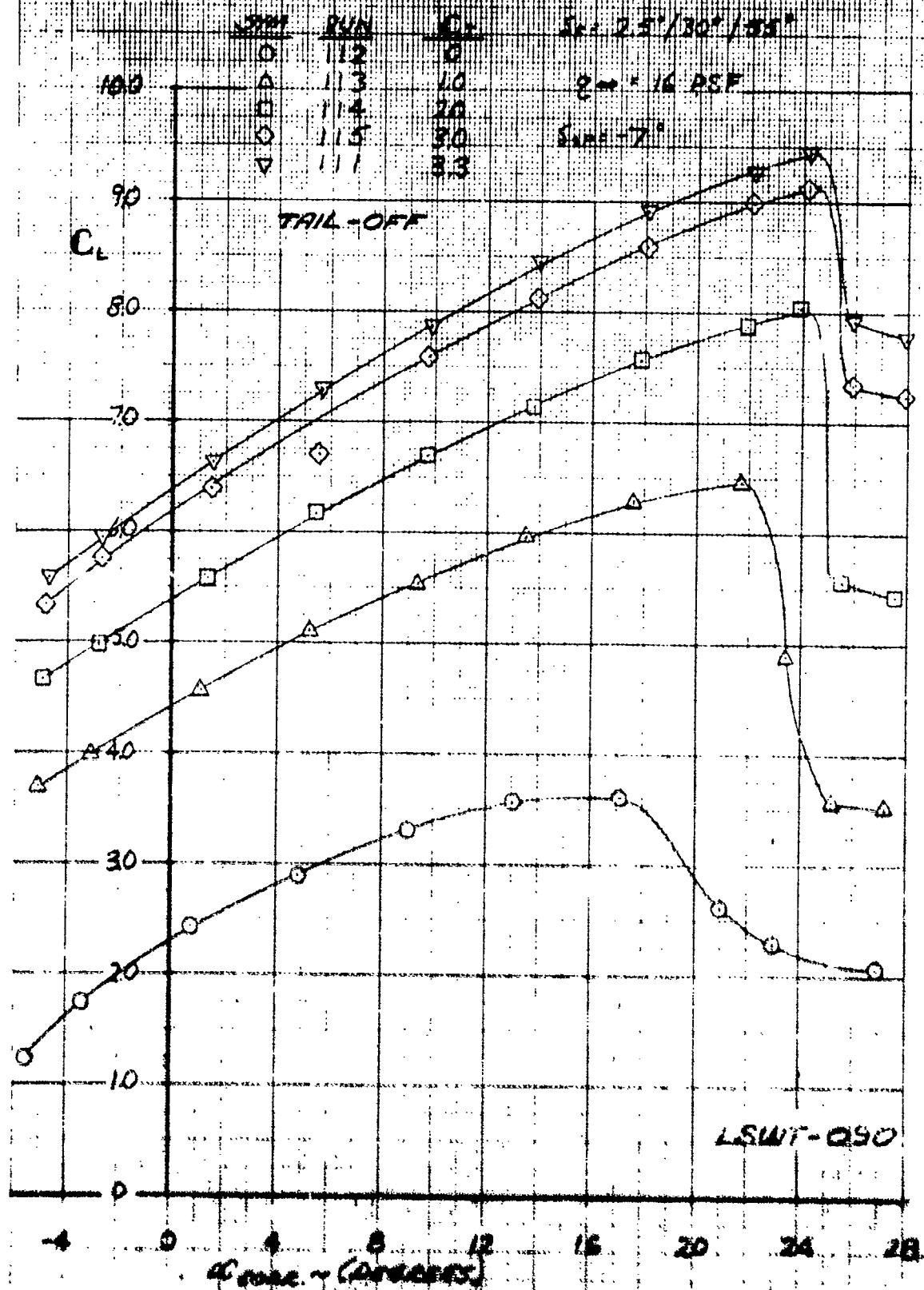


Figure 12.4.15

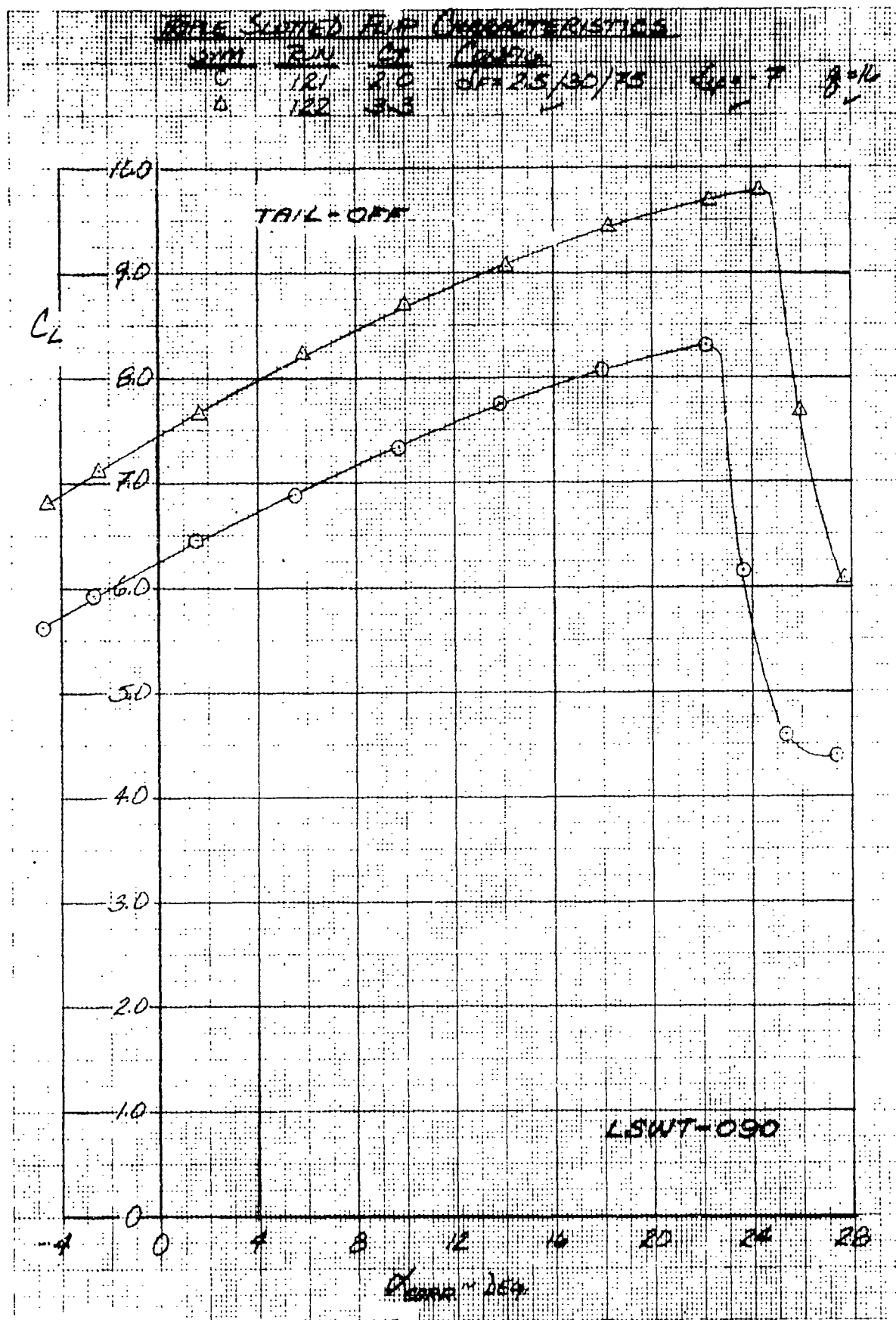
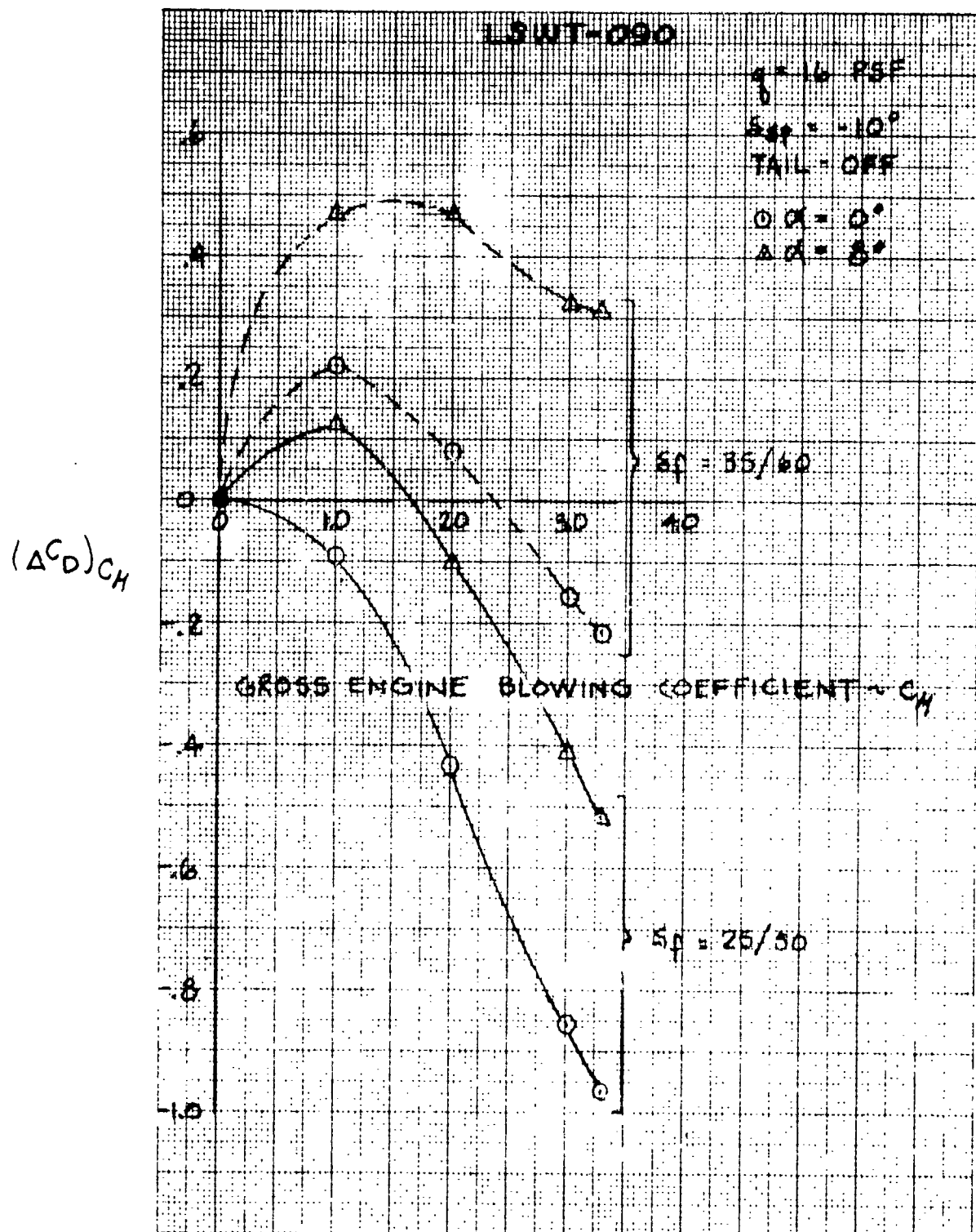
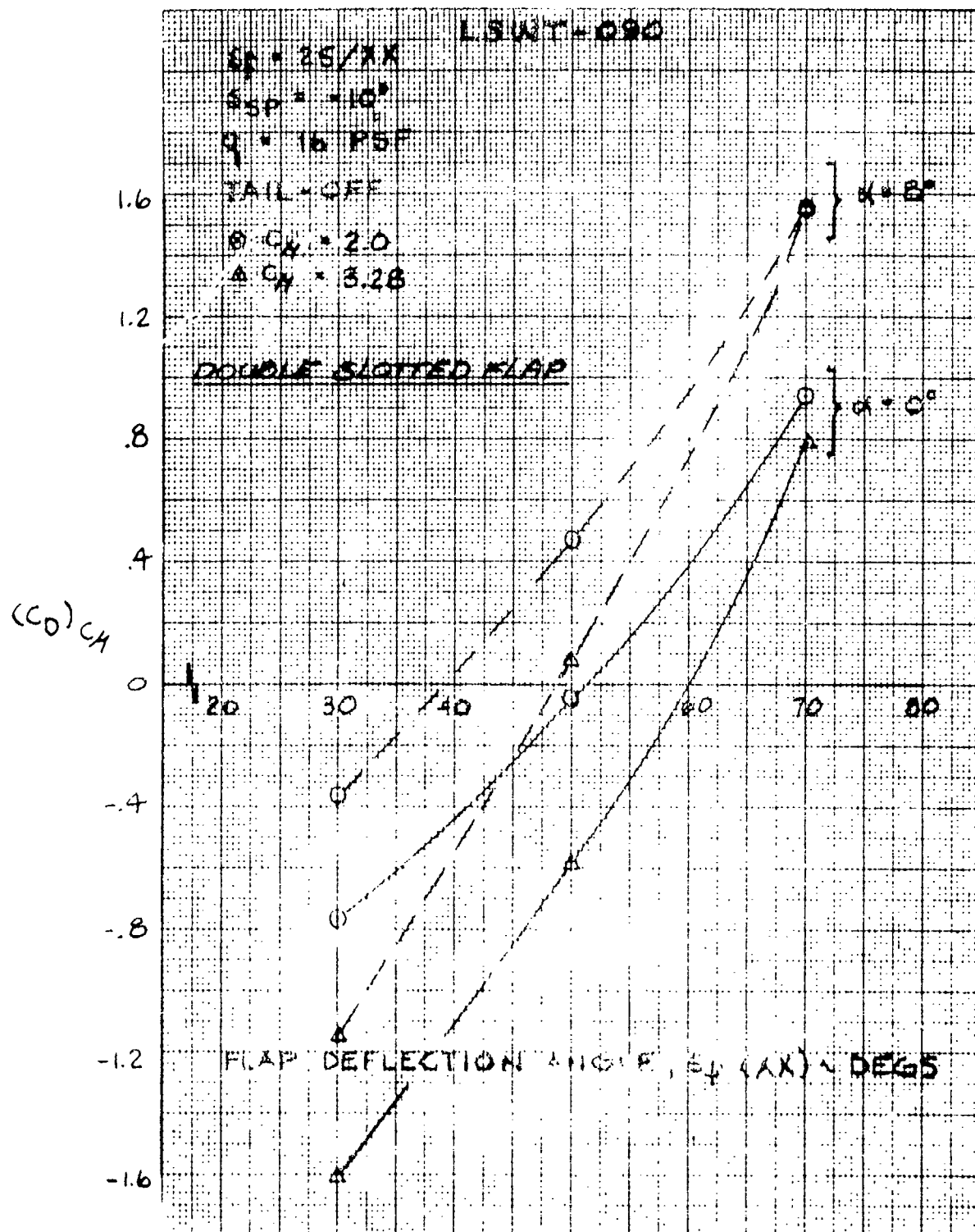


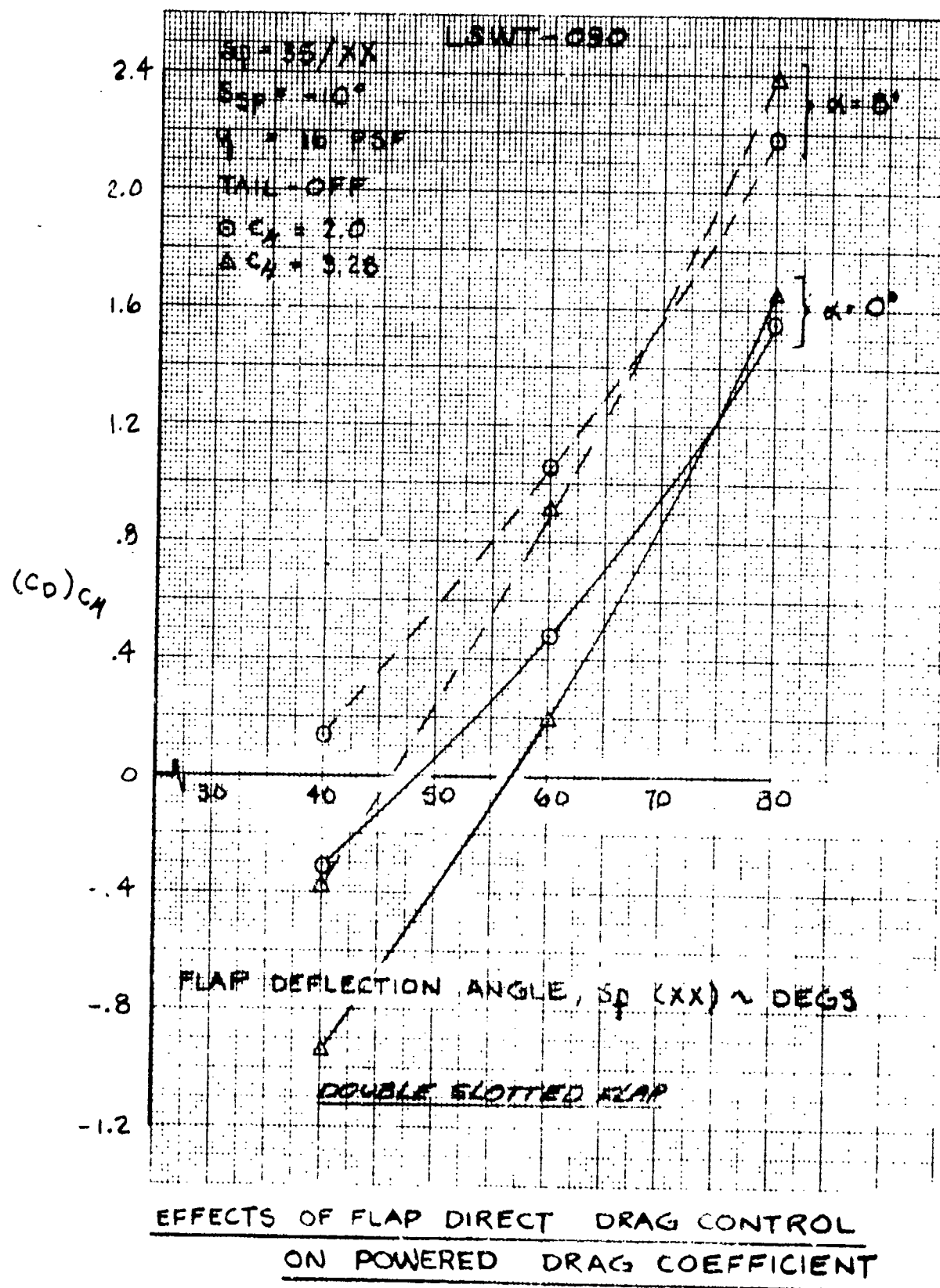
Figure 12.4.16



POWER EFFECTS ON DOUBLE SLOTTED
FLAP DRAG COEFFICIENT



EFFECTS OF FLAP DIRECT DRAG CONTROL
ON POWERED DRAG COEFFICIENT



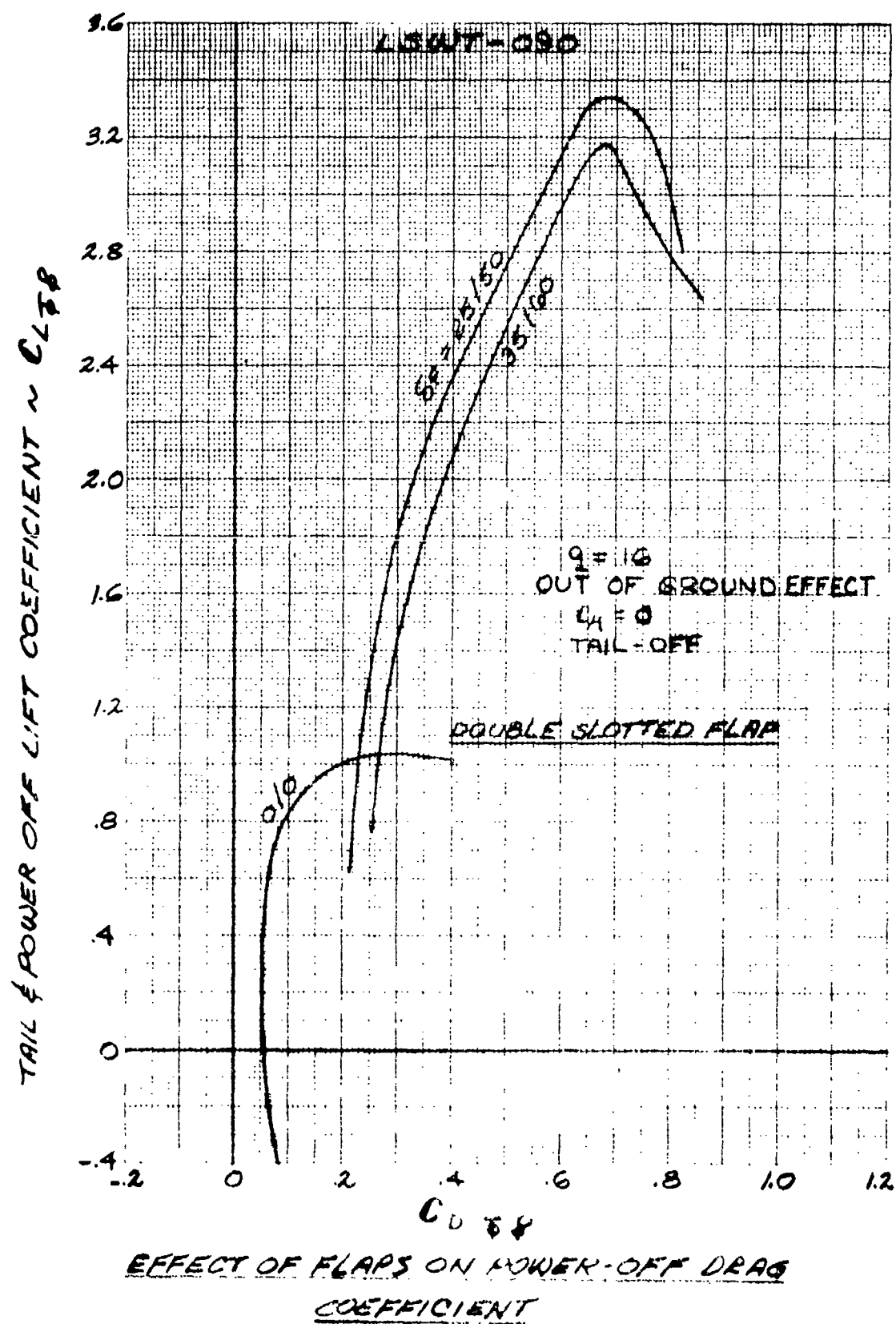


Figure 12.5.4

LSWT-090

DOUBLE SLOTTED FLAP CHARACTERISTICS

TAIL-ON

$\rho = 16 \text{ pcf}$

$\delta \rho = -10^\circ$

$\delta \rho = 25/50$

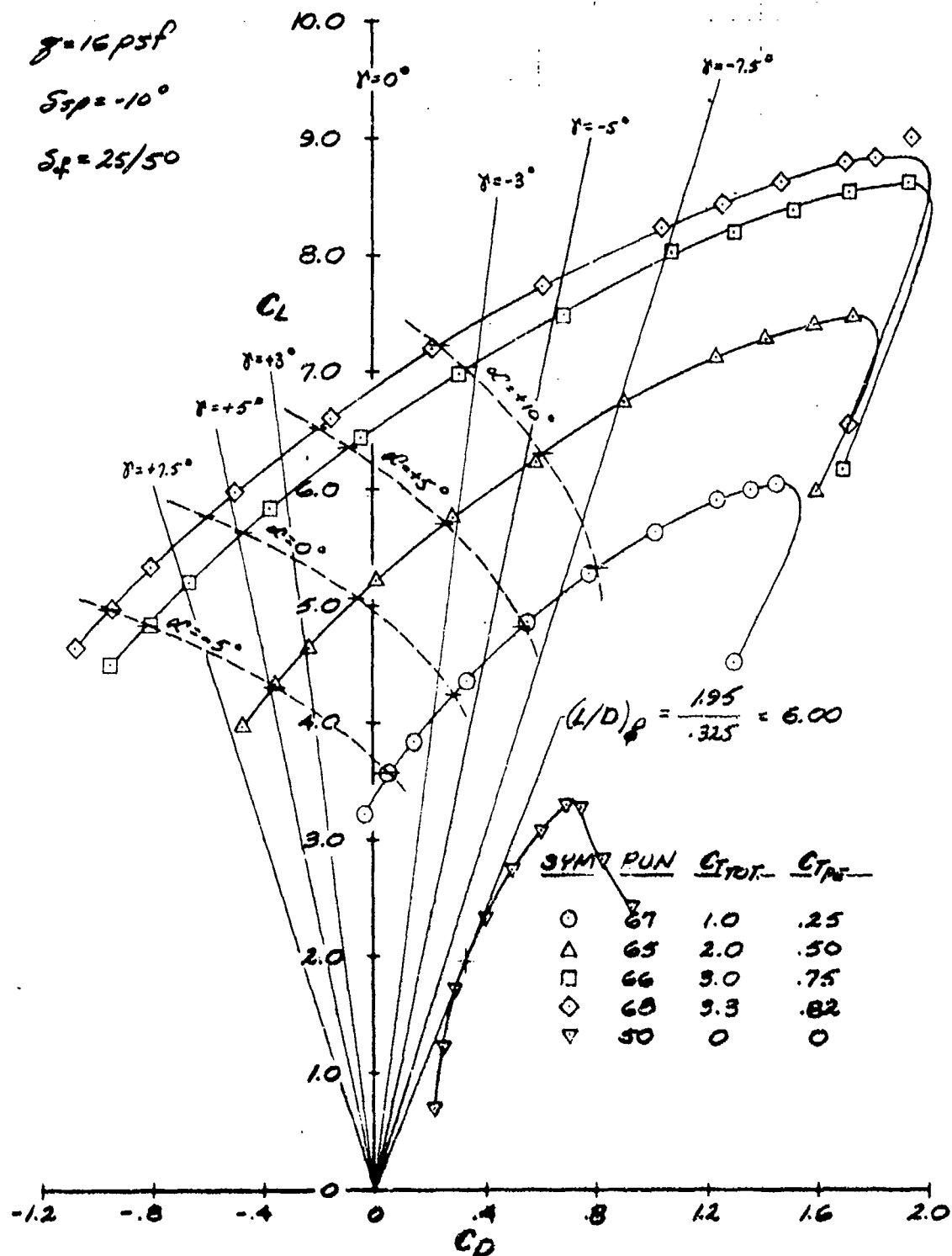


Figure 12.5.5

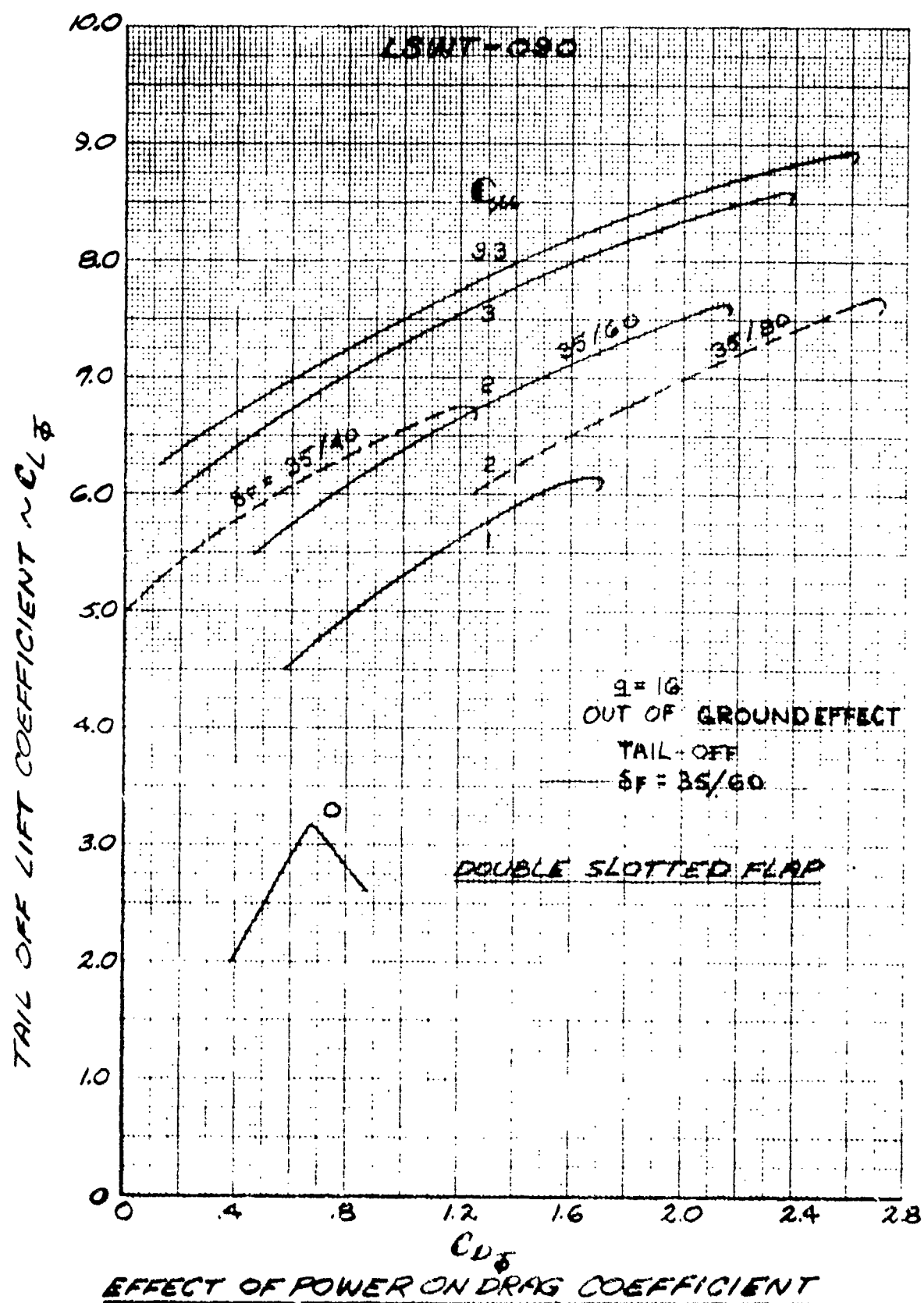
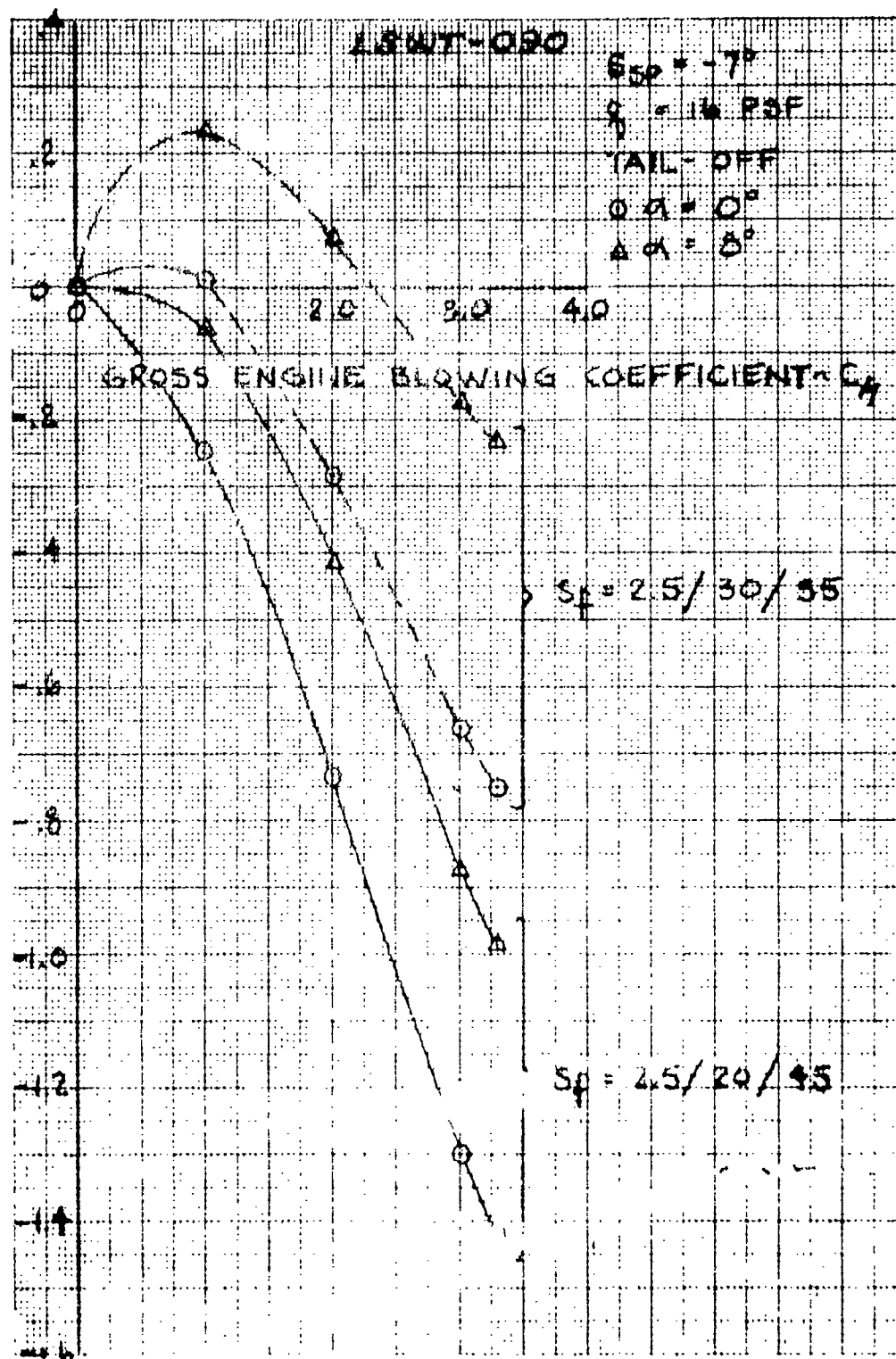


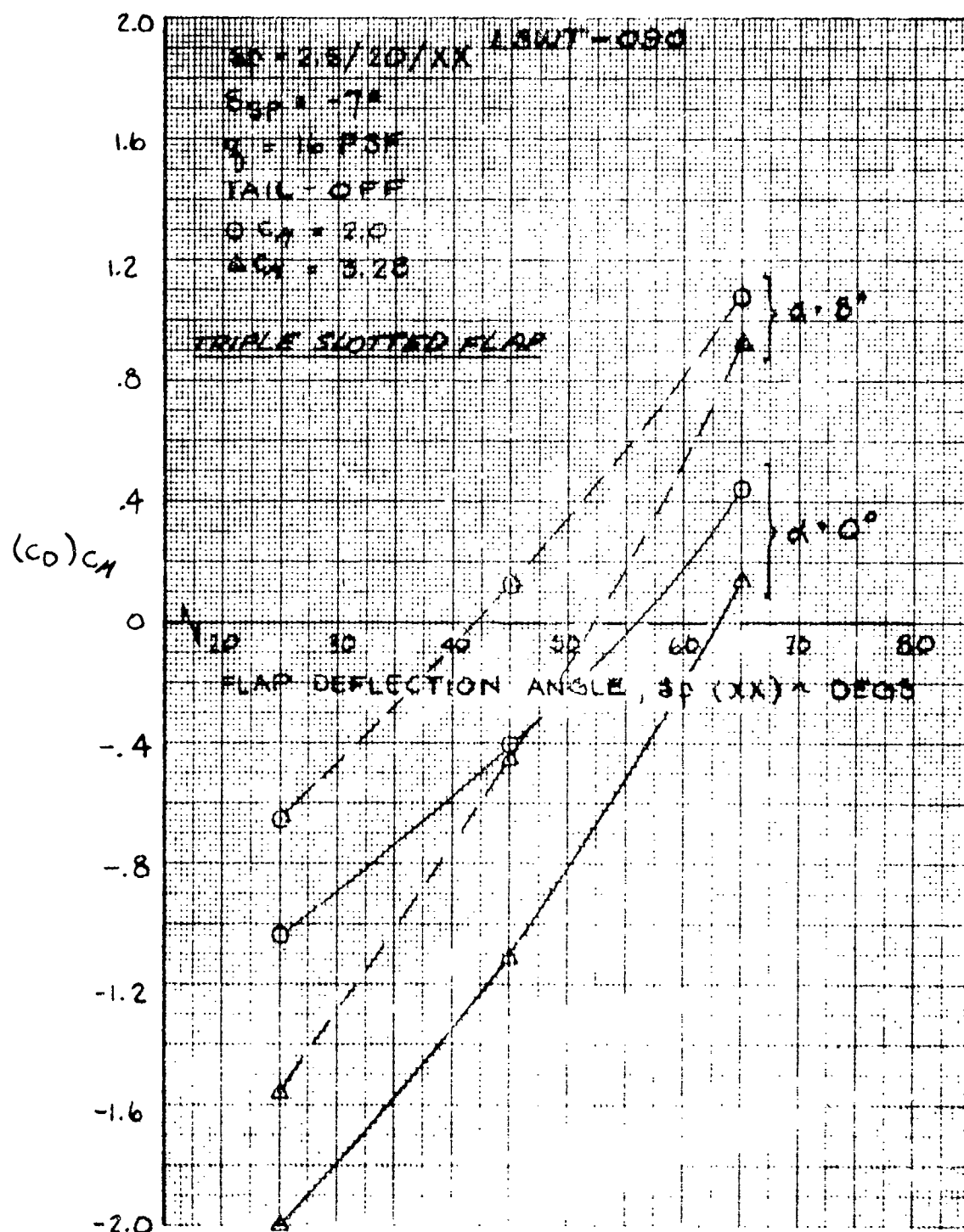
Figure 12.5.6

$(\Delta C_D)_{CH}$



POWER EFFECT ON TRIPLE SLOTTED
 FLAP DRAG COEFFICIENT

Figure 12.5.7



EFFECTS OF FLAP DIRECT DRAG CONTROL
 ON POWERED DRAG COEFFICIENT

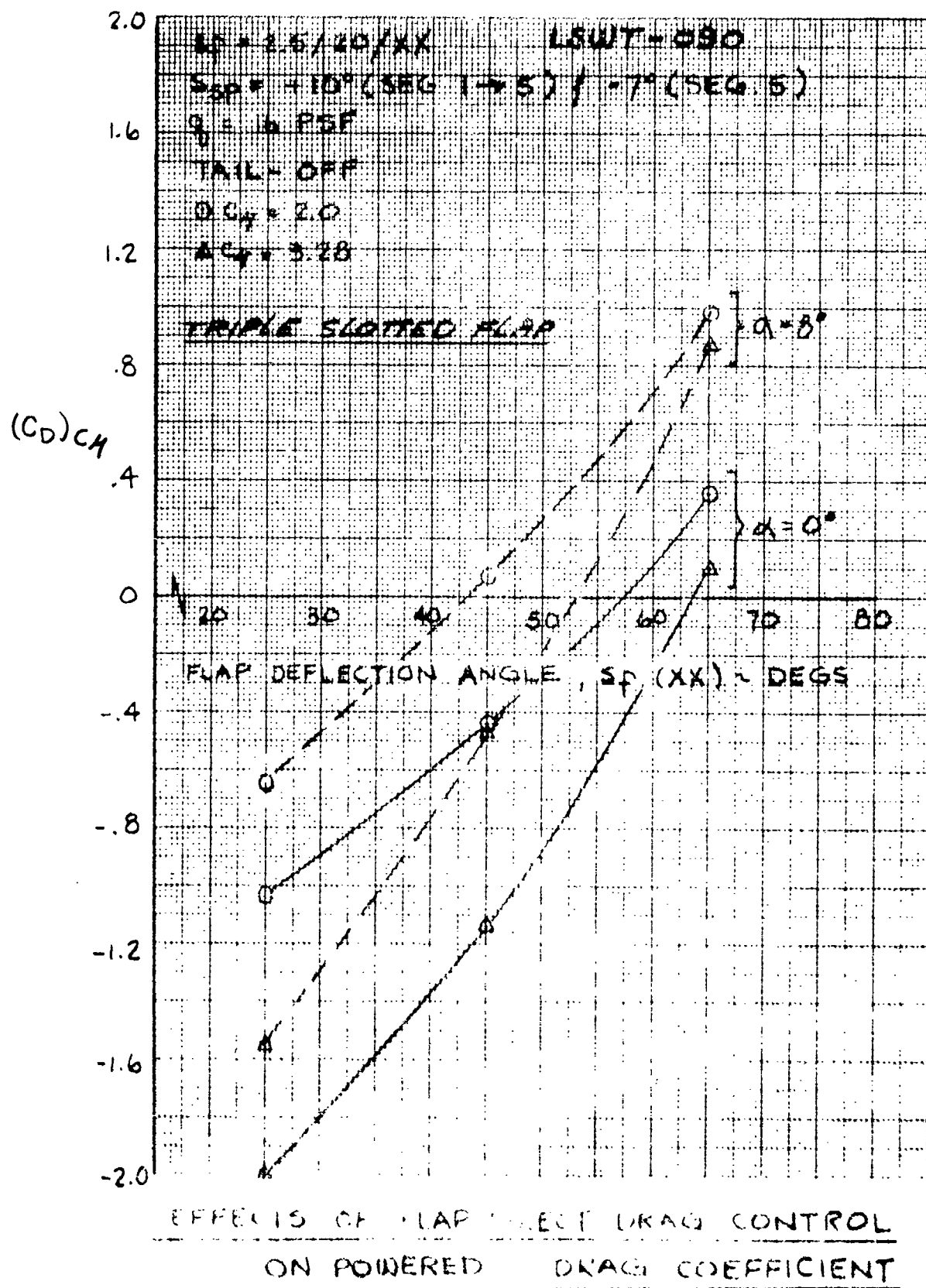
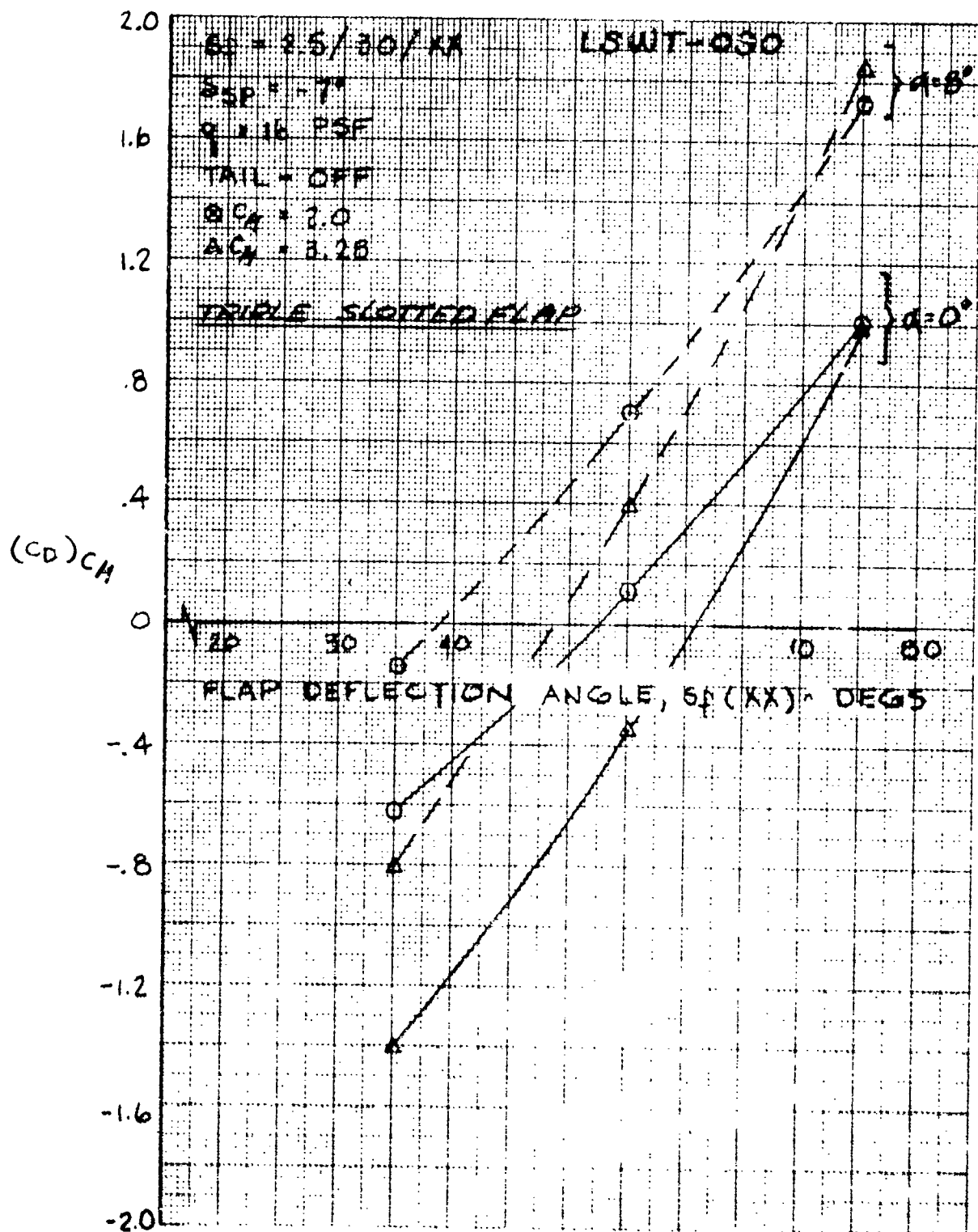
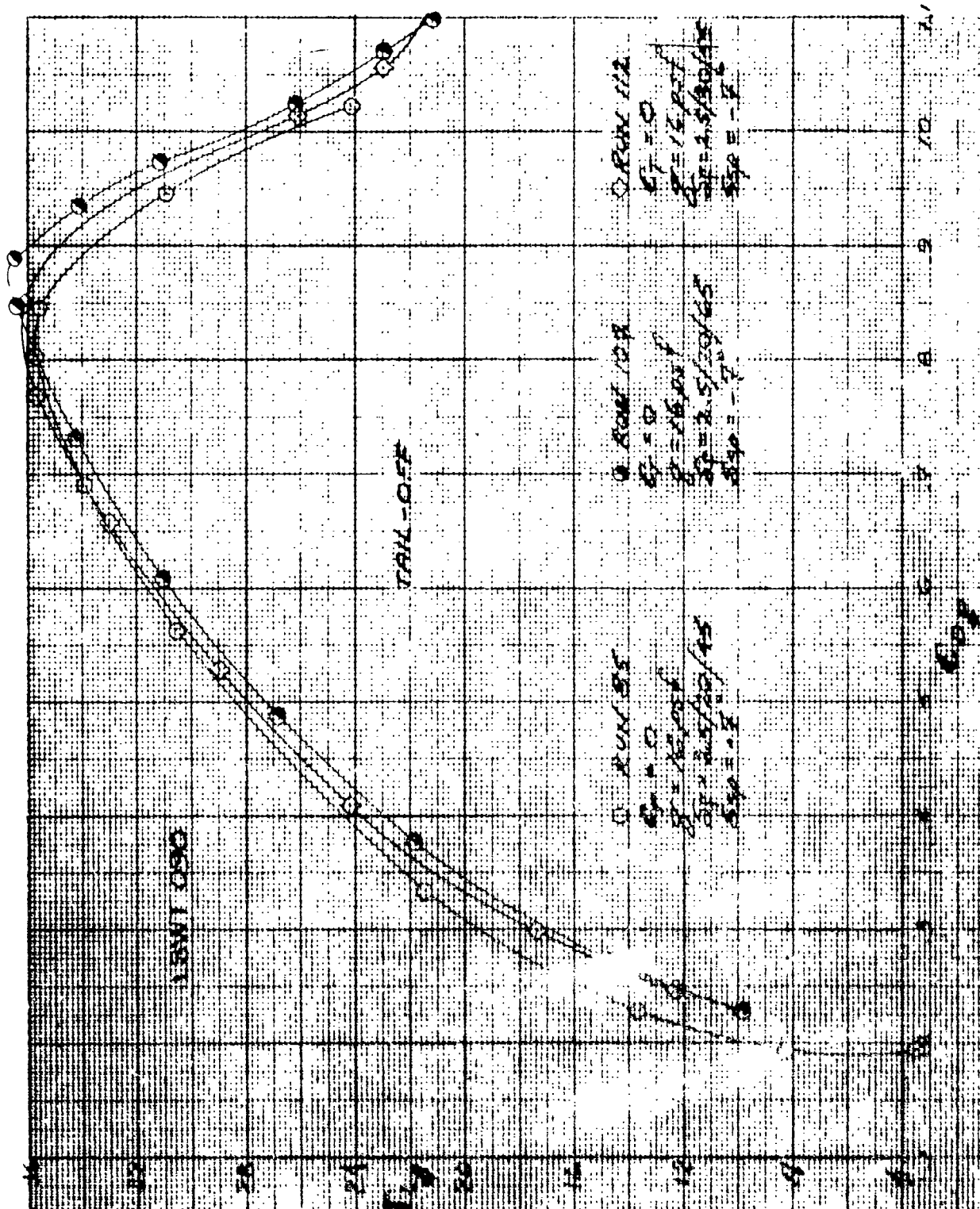


Figure 12.5.9



EFFECTS OF FLAP DIRECT DRAG CONTROL
ON POWERED DRAG COEFFICIENT

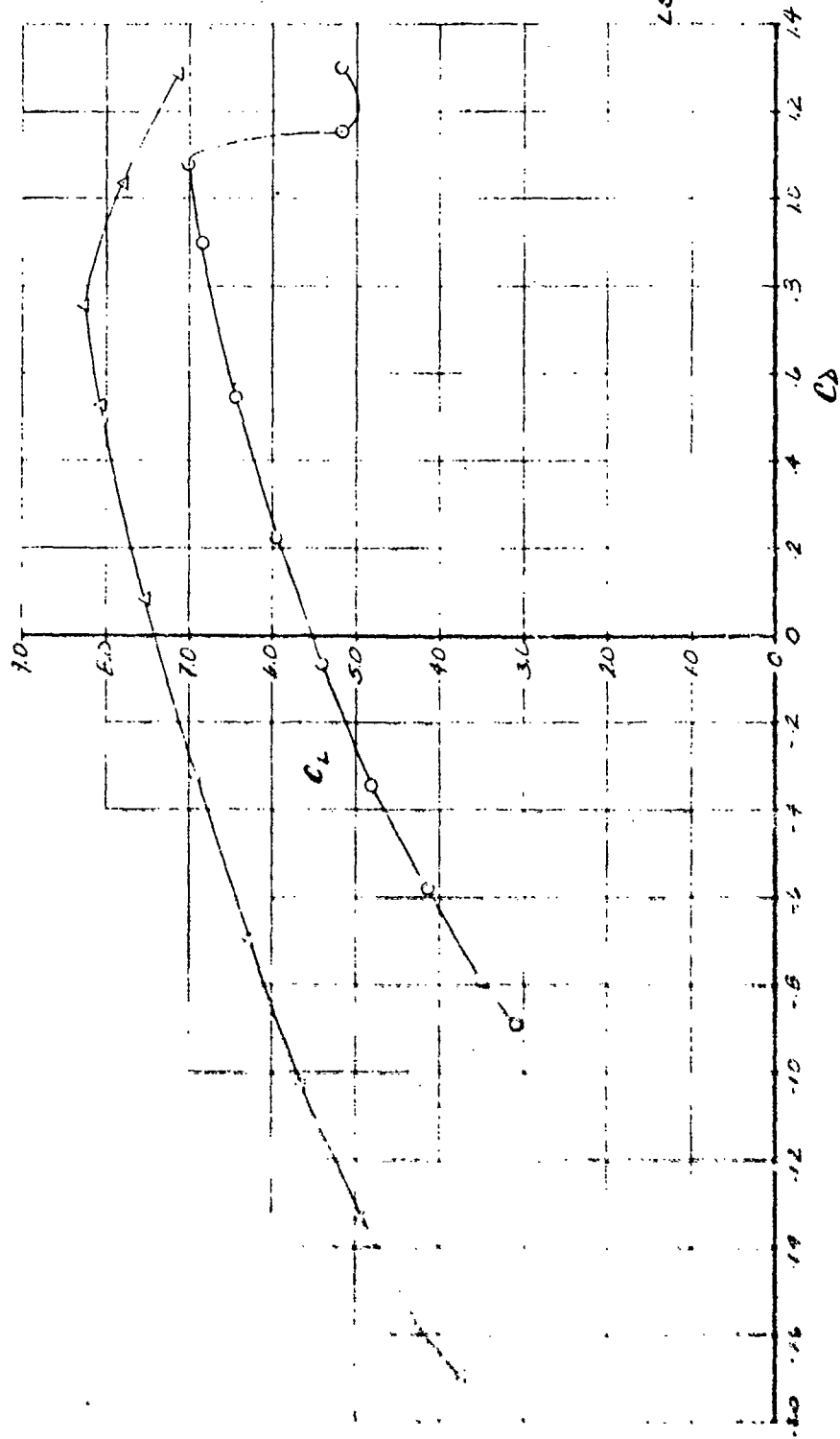


TEST REPORT 1001

1001

TRIPLE SLOTTED FLAP CHARACTERISTICS
 2000 100 2.0 2.5/30/35 60°-7° 8-16
 C L 10.1 3.3

TAIL-OFF



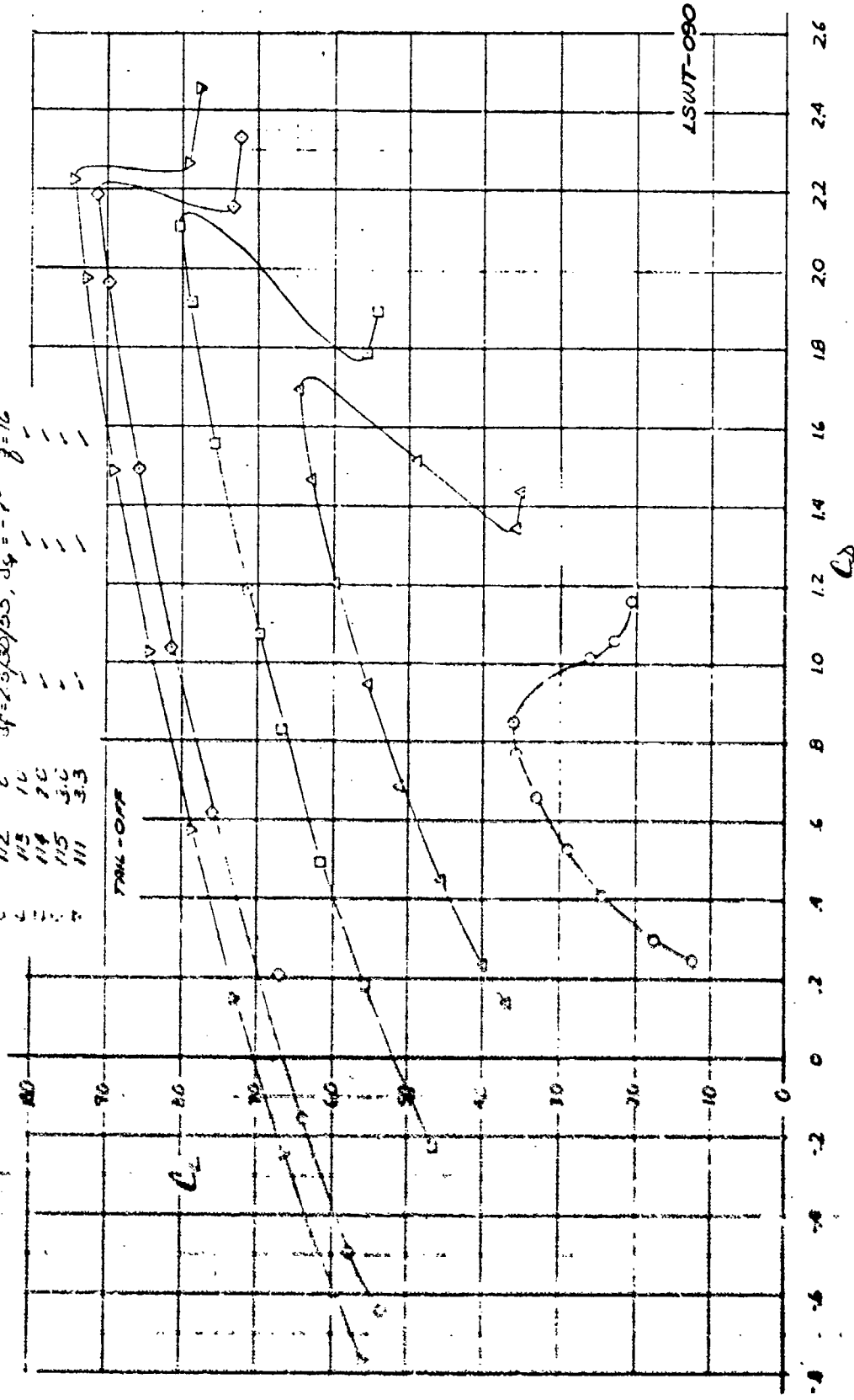
LSWT-090

Figure 12.5.12

(The reverse side of this page is blank)

THE SELECTED FLAT CHARACTERISTICS

$\frac{1}{\lambda}$	$\frac{1}{\lambda^2}$	$\frac{1}{\lambda^3}$	$\frac{1}{\lambda^4}$	$\frac{1}{\lambda^5}$	$\frac{1}{\lambda^6}$
1	1	1	1	1	1
2	4	8	16	32	64
3	9	27	81	243	729
4	16	64	256	1024	4096
5	25	125	625	3125	15625
6	36	216	1296	7776	46656
7	49	343	2401	16807	117649
8	64	512	4096	32768	262144
9	81	729	6561	59049	531441
10	100	1000	10000	100000	1000000



(The reverse side of this page is blank)

TRIPLE SLOTTED FLAP CHARACTERISTICS
 DATA RUN AT C_{Lmax}
 121 2.0 OF 2.5/30/75 $\alpha_{cr} = 7^\circ$
 122 3.3

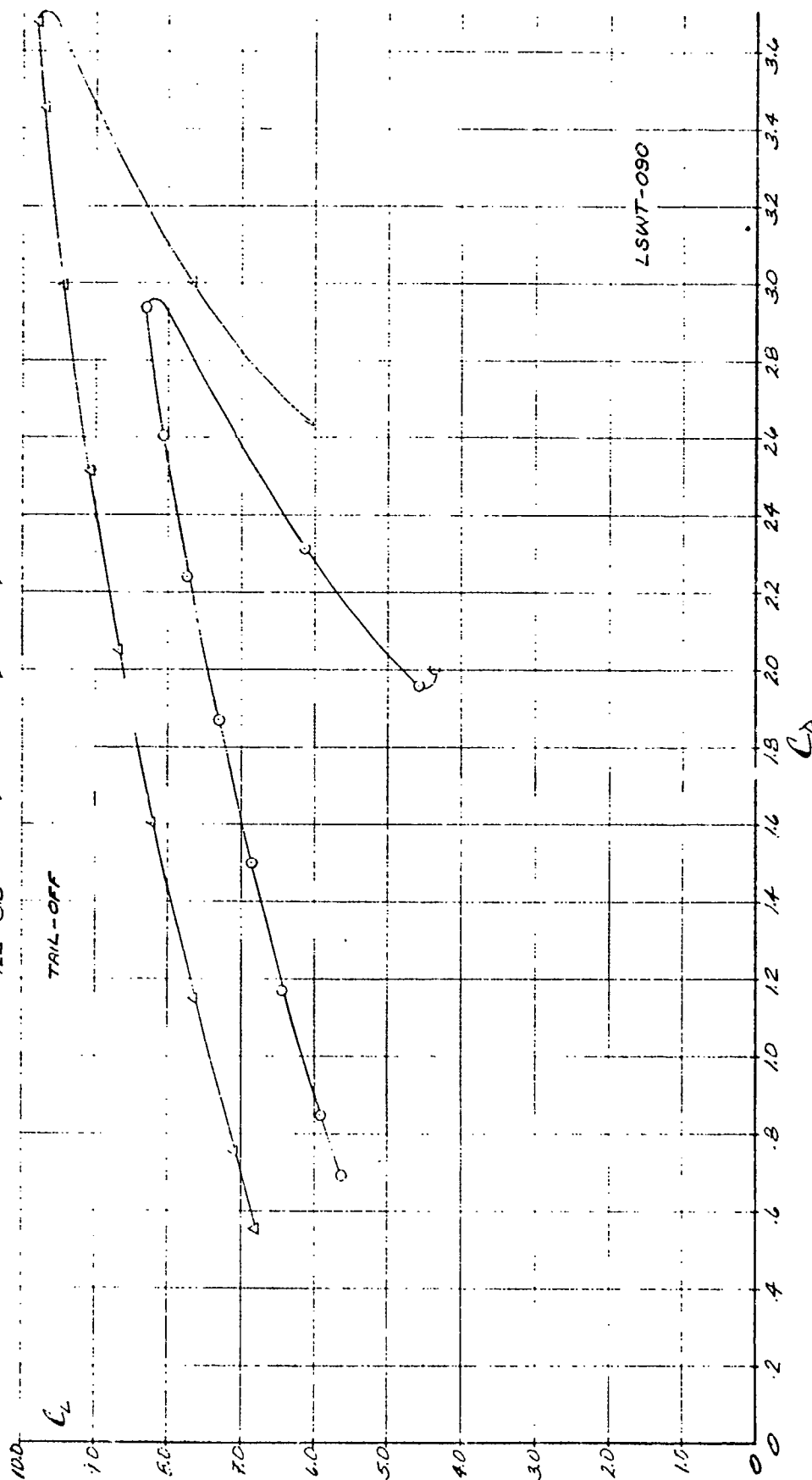


Figure 12.5.14
 264. (The reverse side of this page is blank)

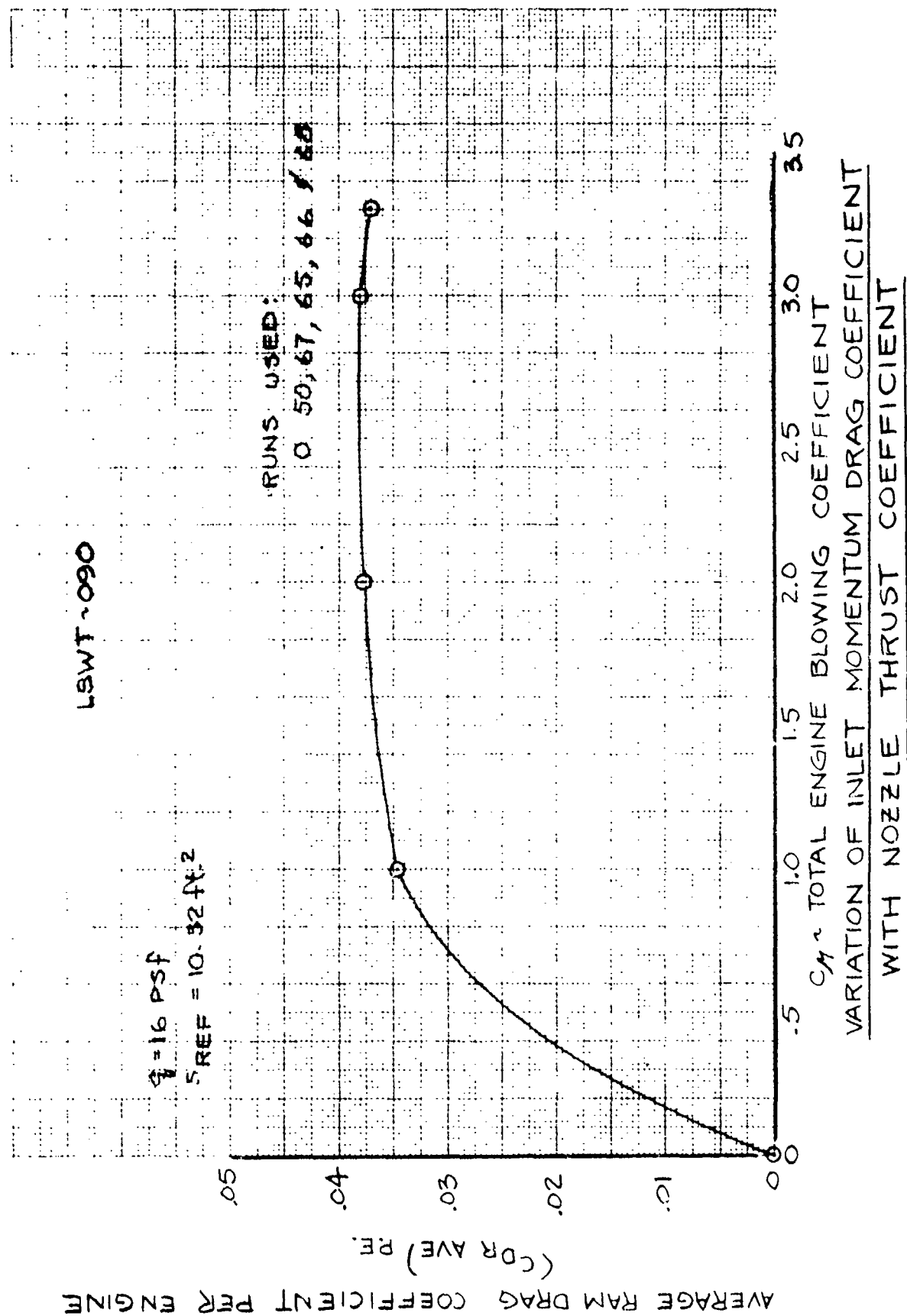
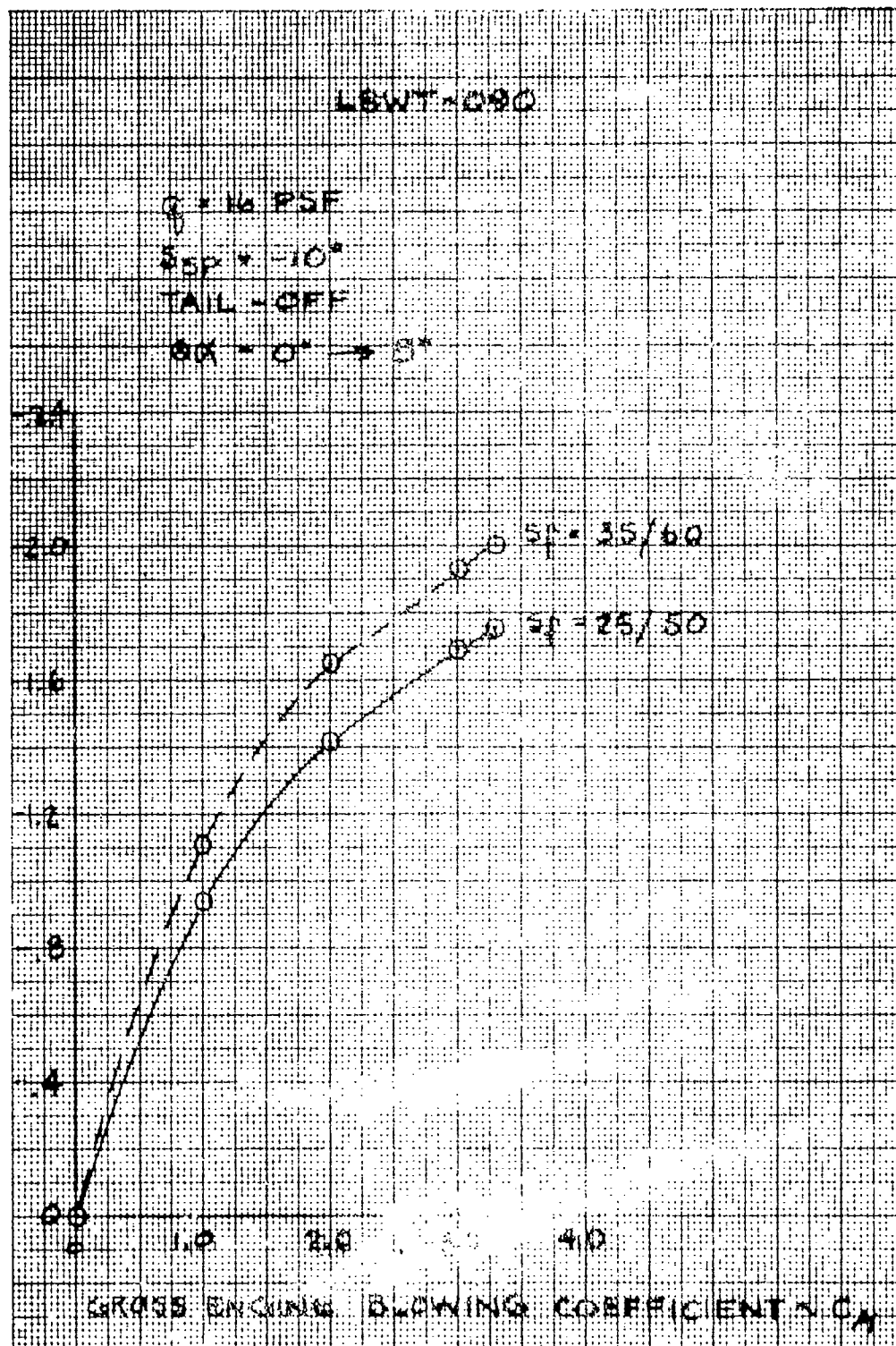


Figure 12.5.15

$(\Delta C_m)_{CH}$



POWER EFFECTS ON DOUBLE SLOTTED FLAP
 PITCHING MOMENT COEFFICIENT

LSWT-090

DOUBLE SLOTTED FLAP

$S_F = 25/XX$

$\delta S_F = -10^\circ$

$q = 16 \text{ PSF}$

TAIL - OFF

$OCX = 2.0$

$ACX = 3.28$

-4.0

-3.0

-2.0

-1.0

0

$(C_m)_{CH}$

$\alpha = 0^\circ$

$\alpha = 8^\circ$

20 30 40 50 60 70 80

FLAP DEFLECTION ANGLE, $S_F(XX) \sim \text{DEGS}$

EFFECTS OF LAST FLAP SEGMENT DEFLECTION ON

POWERED PITCHING MOMENT COEFFICIENT

LBWT-090

DOUBLE SLOTTED FLAP

$s_f = 35/XX$

$SSP = -10^\circ$

$q = 16 \text{ PSF}$

TAIL-OFF

$\odot C_H = 2.0$

$\Delta C_H = 3.28$

$\alpha = 0^\circ$

$\alpha = 5^\circ$

$(C_m)_{C_H}$

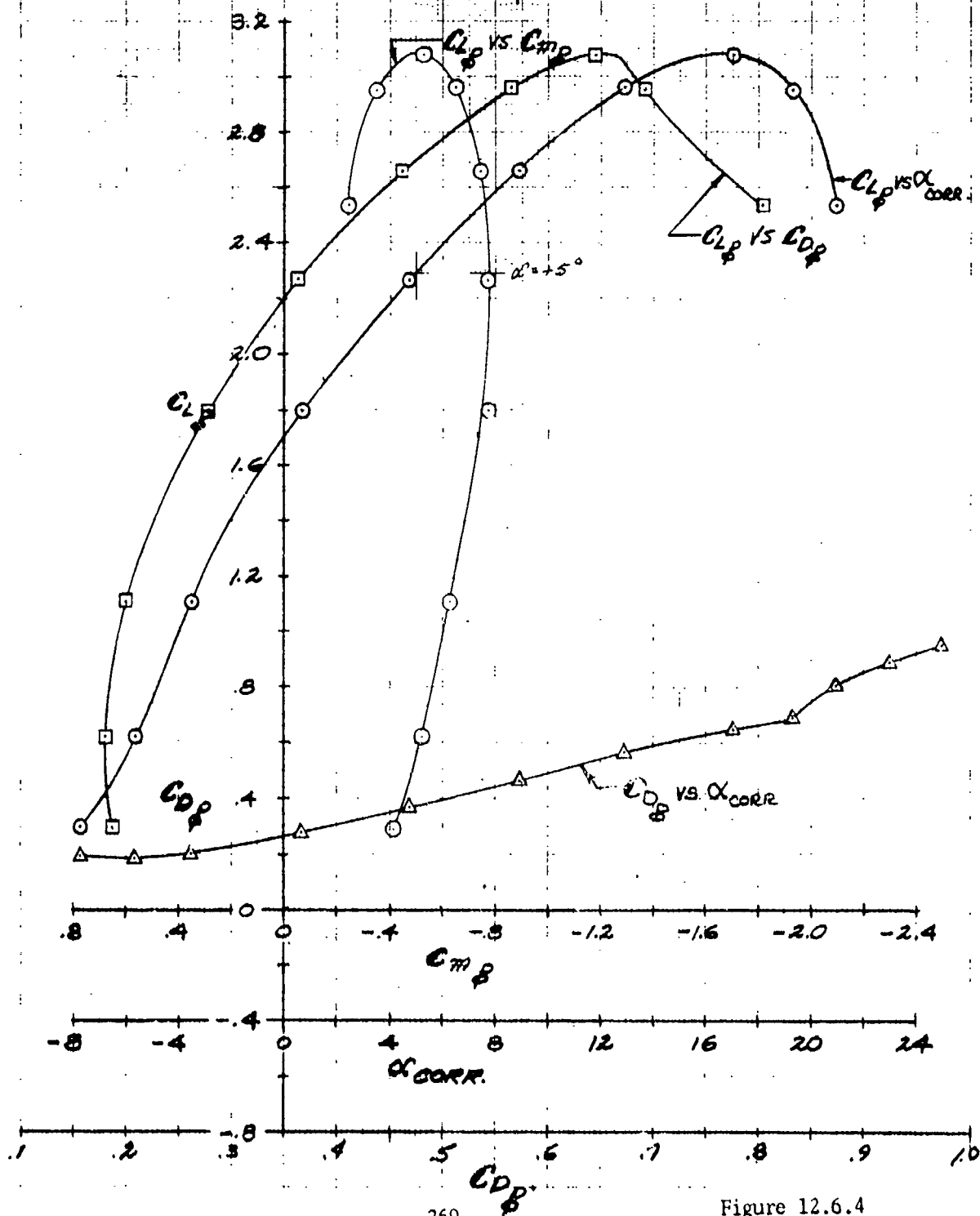
FLAP DEFLECTION ANGLE, $s_f(XX)^\circ$ DEG

EFFECTS OF LAST FLAP SEGMENT DEFLECTION ON
POWERED PITCHING MOMENT COEFFICIENT

Figure 12.6.3

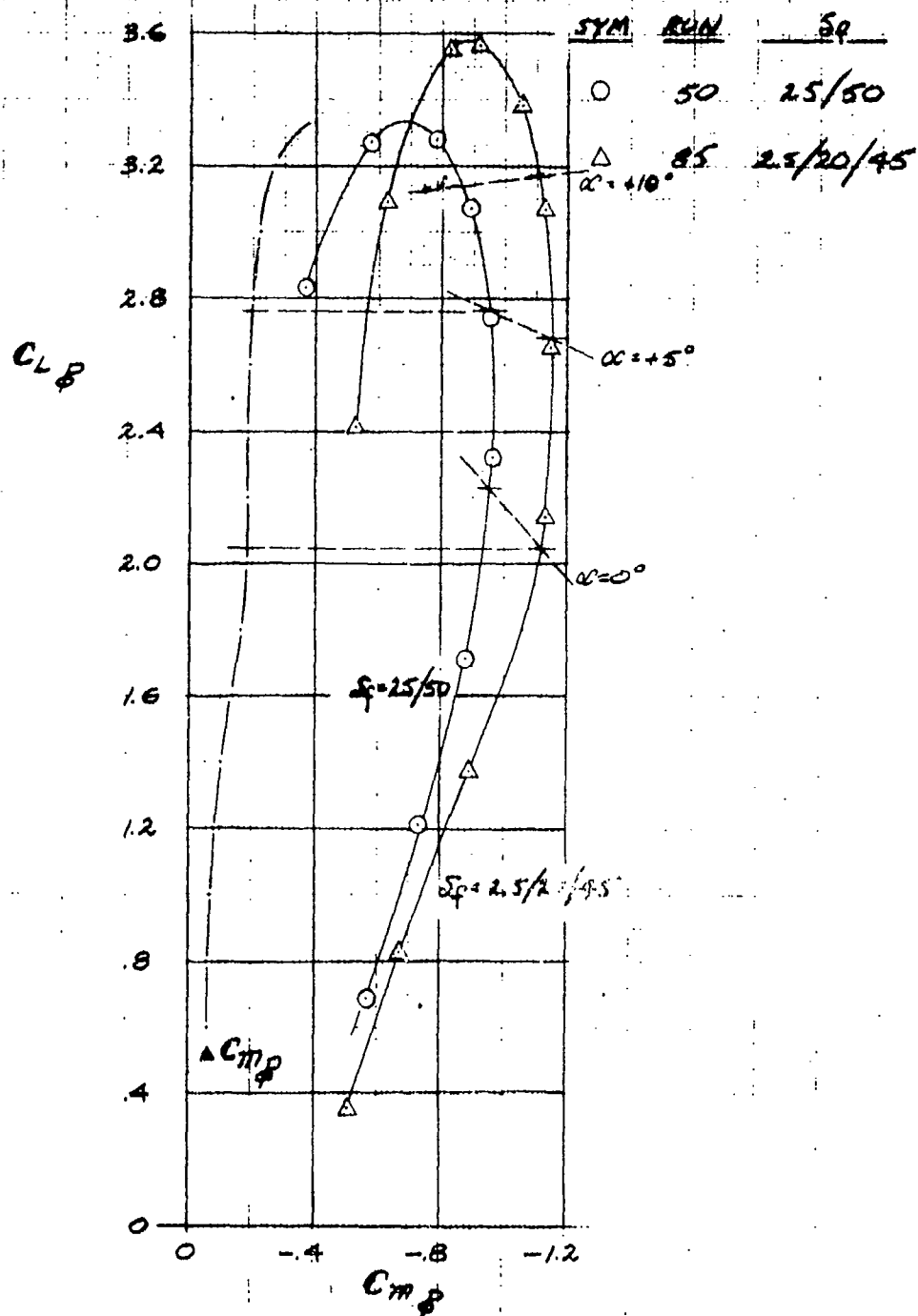
LSWT-090
DOUBLE SLOTTED FLAP LIFT & PITCHING MOMENT
CHARACTERISTICS

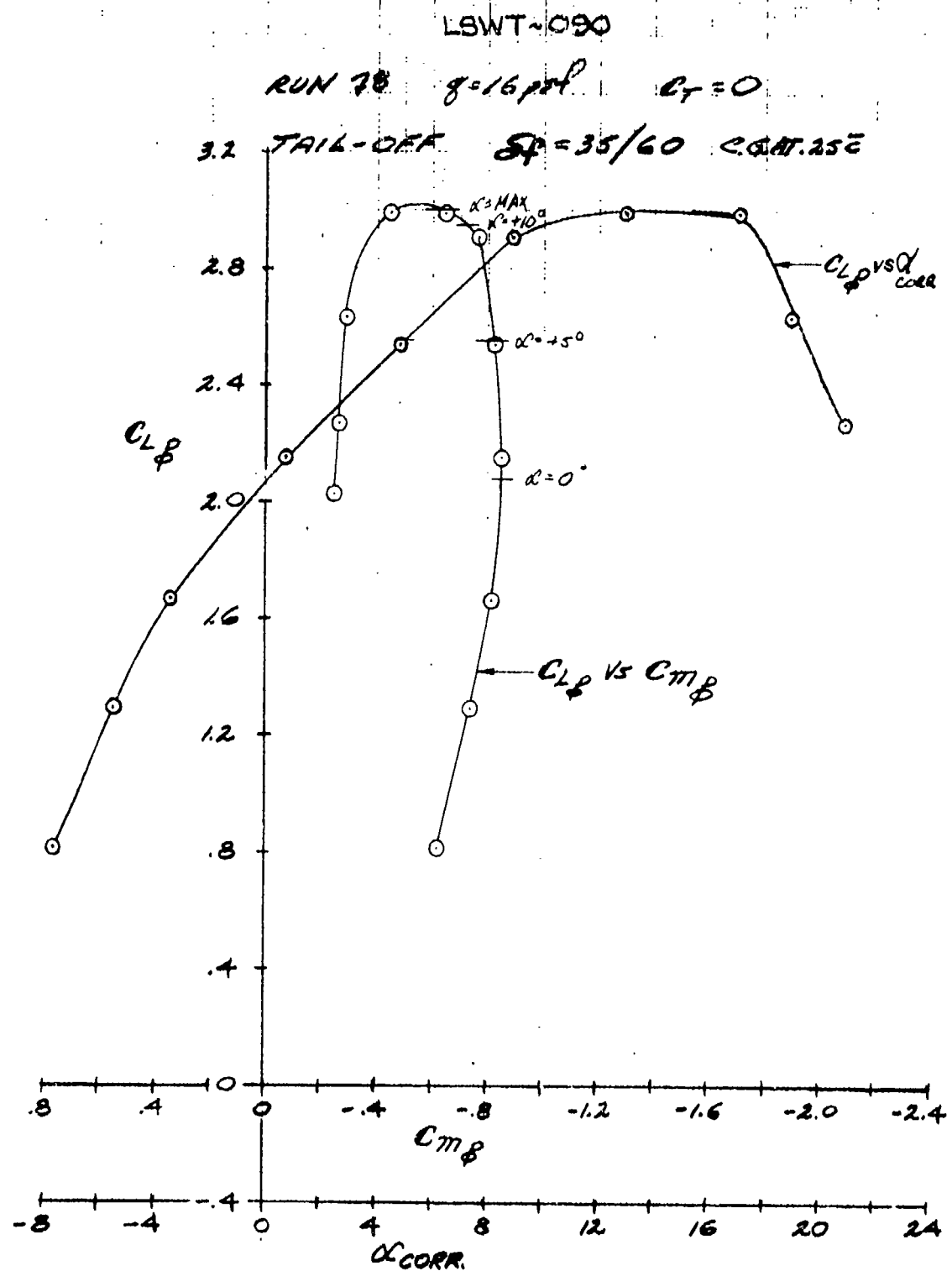
RUN 69 $\gamma = 16.5^\circ$ $C_f = 0$
 TAIL-OFF $S_f = 25/30$ C.G. AT $.25\bar{c}$



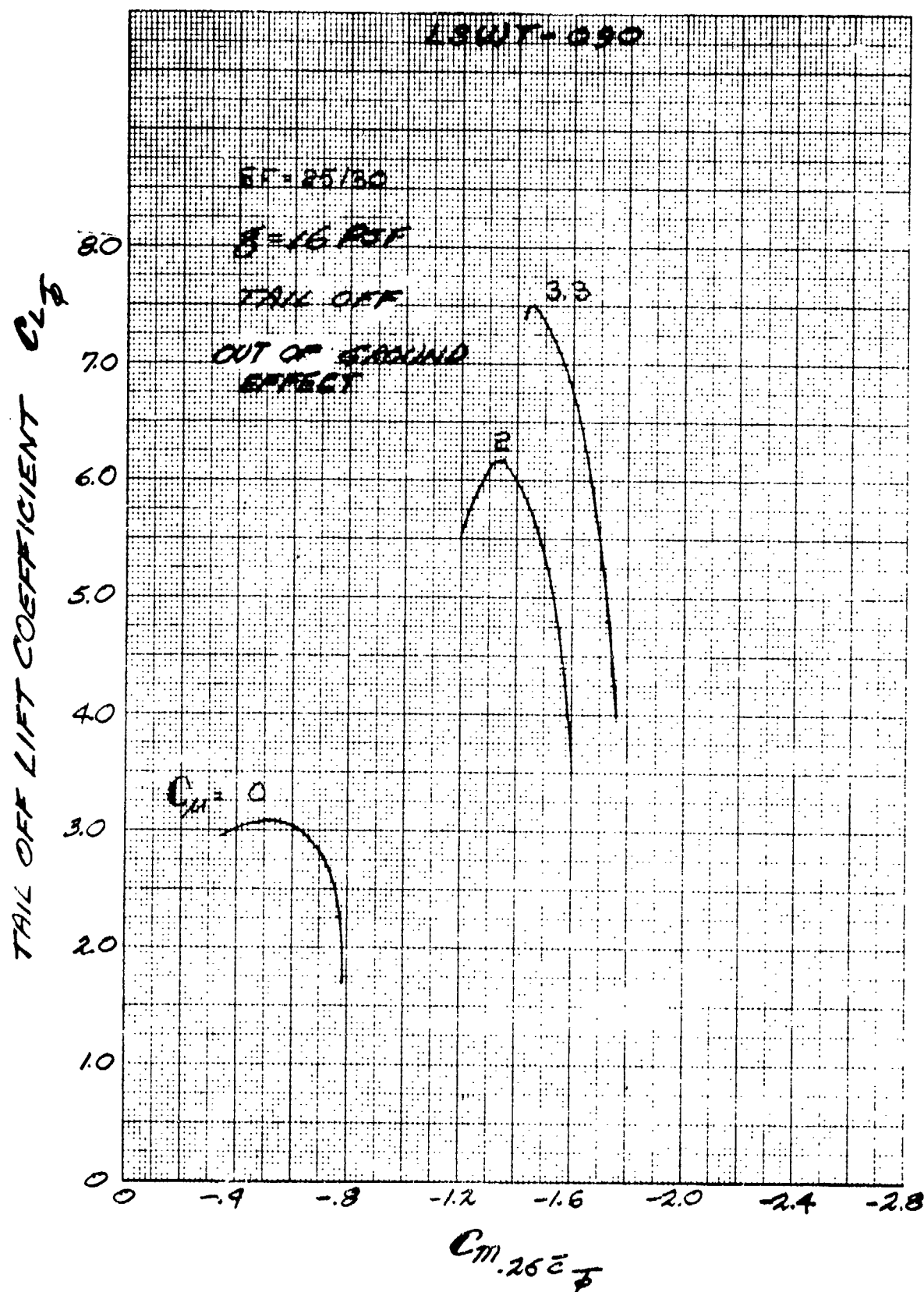
LSWT-080
DOUBLE & TRIPLE SLOTTED FLAP PITCHING MOMENT
COMPARISON

$\delta = 16.25^\circ$ $C_f = 0$
 TAIL-OFF
 C.G. AT 25% $1/C_{15} = \infty$



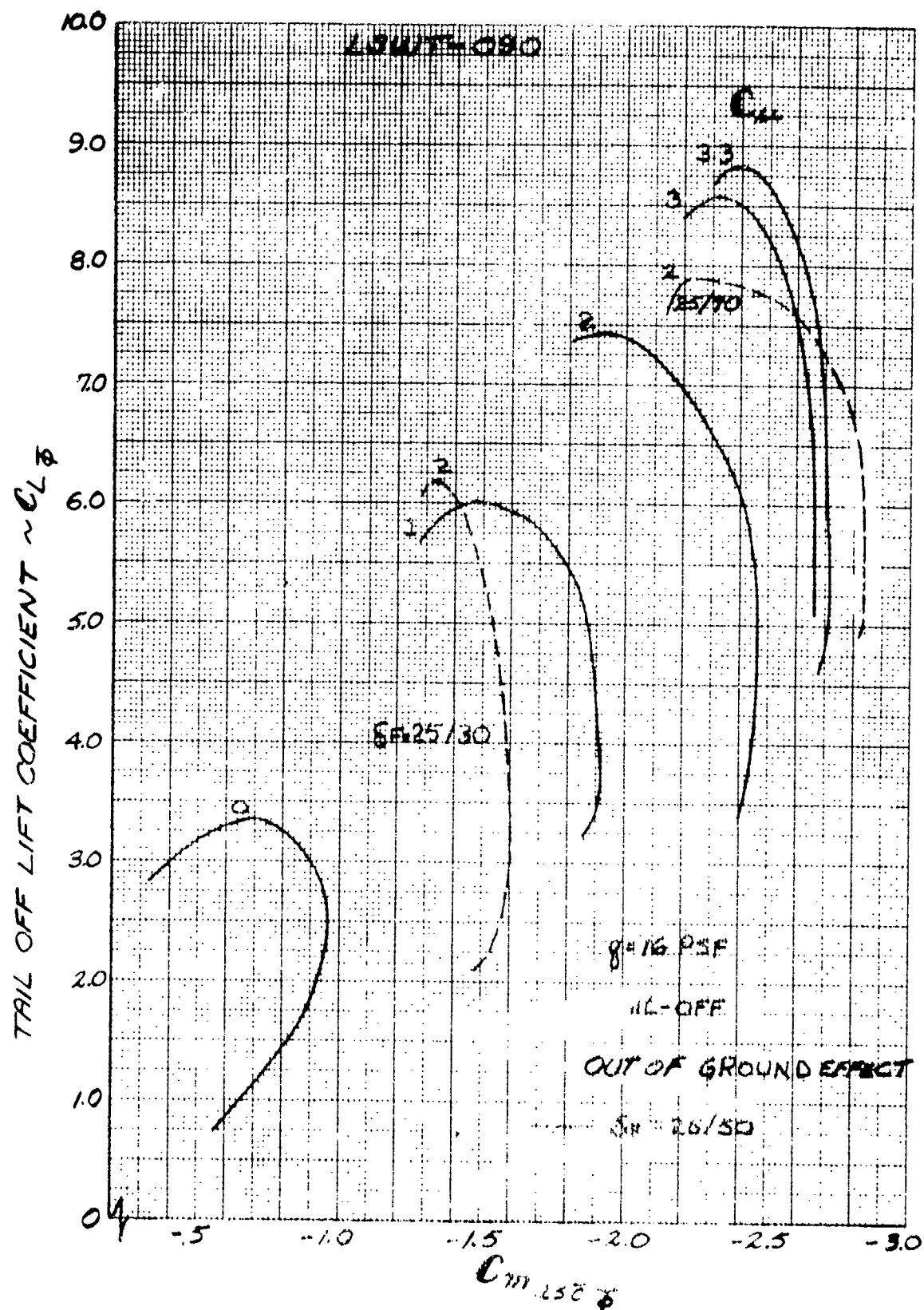


DOUBLE SLOTTED FLAP LIFT & PITCHING MOMENT CHARACTERISTICS



EFFECT OF POWER ON PITCHING MOMENT COEFFICIENT
— DOUBLE SLOTTED FLAP —

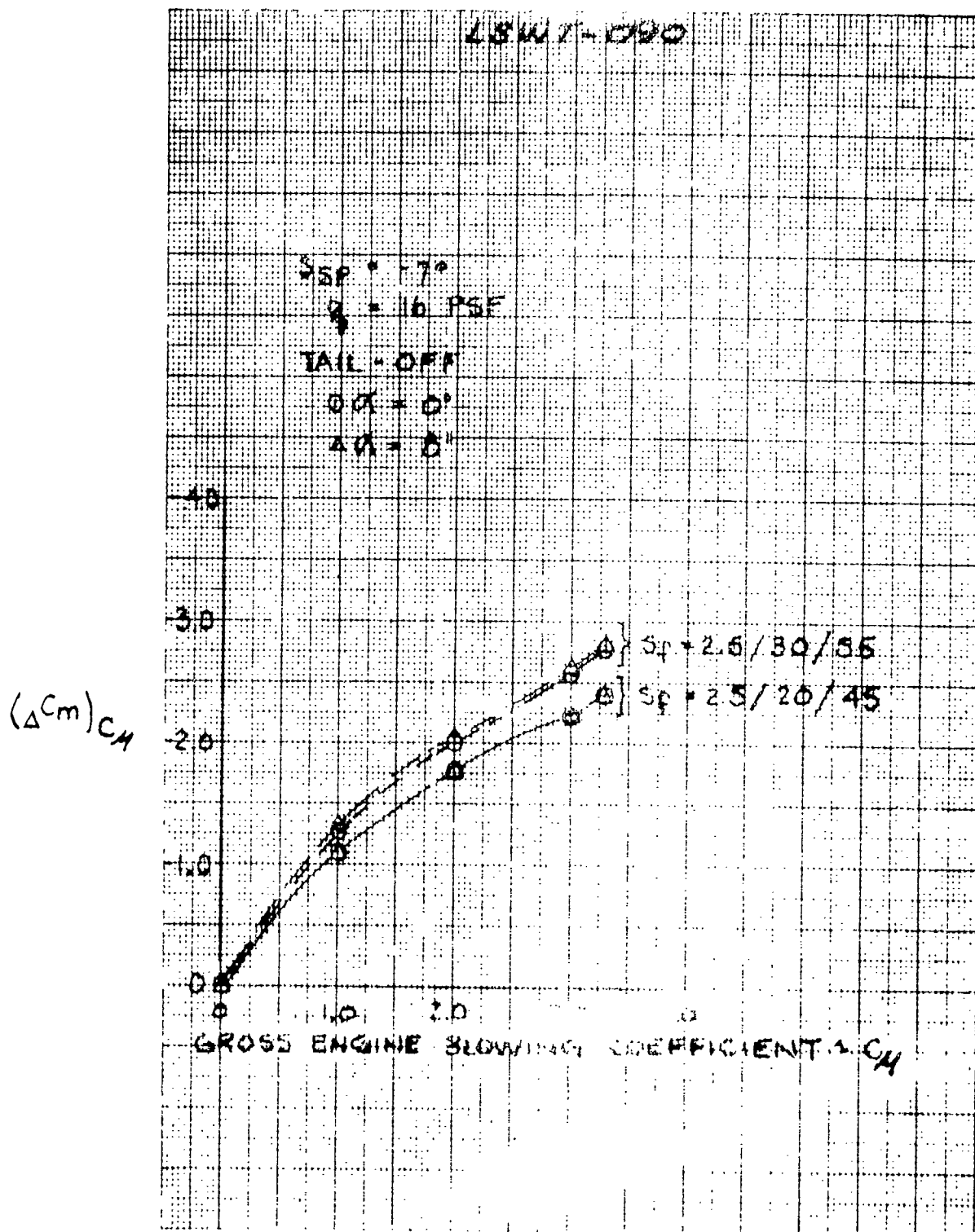
Figure 12.6.7



EFFECT OF POWER ON PITCHING MOMENT COEFFICIENT

--- DOUBLE SLOTTED FLAP ---

Figure 12.6.8



POWER EFFECTS ON TRAIL-FOOTED FLAP
PITCHING MOMENT COEFFICIENT

Figure 12.6.10

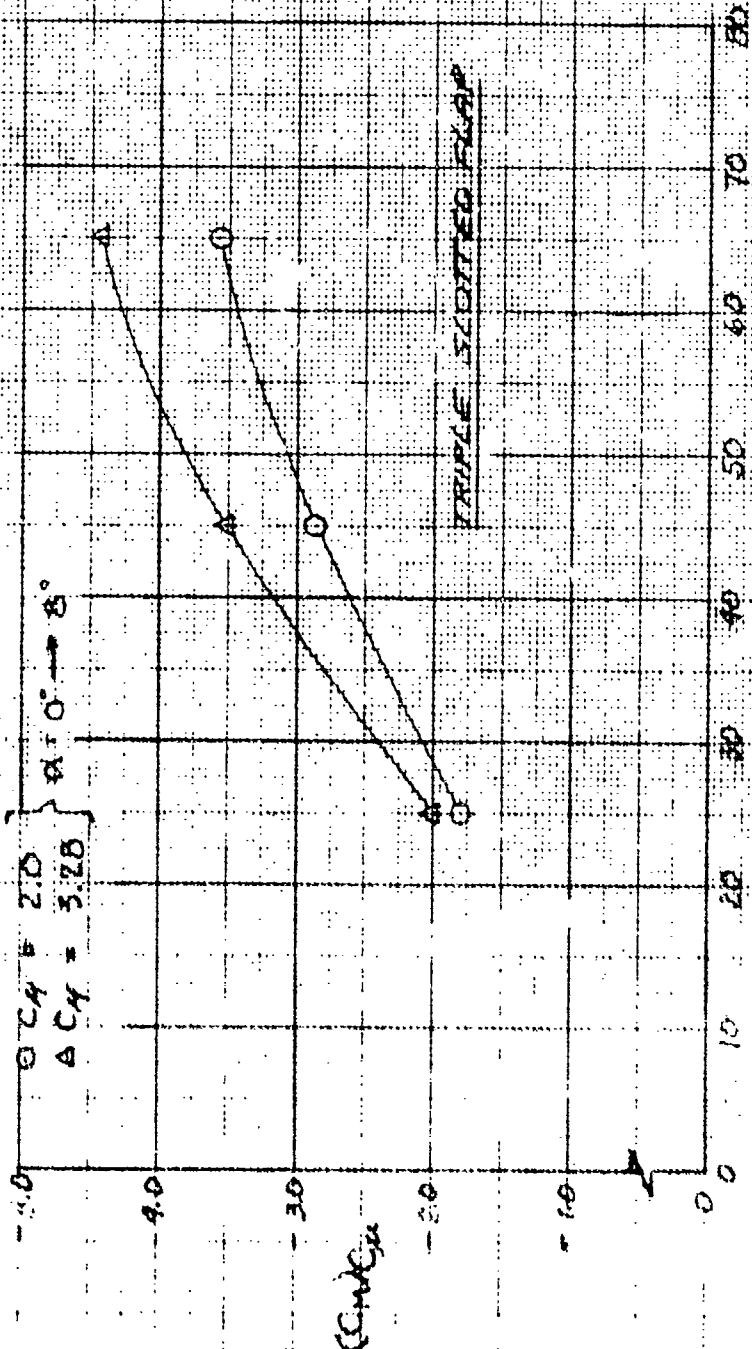
LEWT-080

$s_f = 2.5/20/XX$ $s_{sp} = 7^\circ$

$q = 10$ PSF

TAIL-OFF

$OCY = 2.0$ $\alpha = 0^\circ \rightarrow 8^\circ$
 $ACY = 3.28$



$(C_m)_{C_p}$

TRIPLE SCOTTED FLAP

FLAP DEFLECTION ANGLE, $s_f(XX)$ - DEGS

EFFECTS OF LAST FLAP SEGMENT DEFLECTION ON
 POWERED PITCHING MOMENT COEFFICIENT

LSWT-090

$SP = 2.5730 / XX$

$DEF = -70$

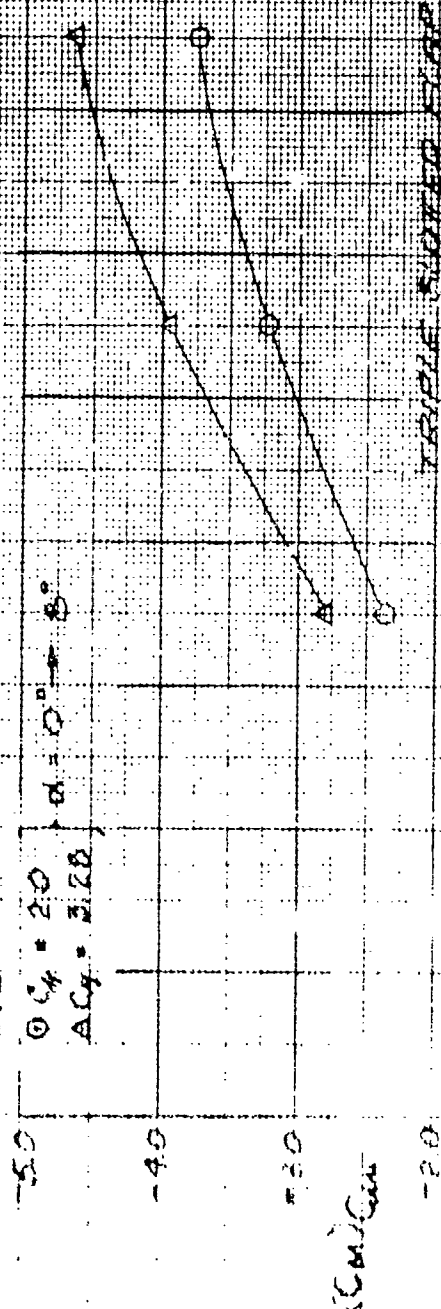
$Q = 16$ PSF

TAIL-OFF

$C_{L4} = 2.0$

$\alpha = 0^\circ \rightarrow 8^\circ$

$AC4 = 3.28$



TRIPLE SLOTTED FLAP

FLAP DEFLECTION ANGLE - δ (deg)

EFFECTS OF LAST FLAP SEGMENT DEFLECTION ON

POWERED PITCHING MOMENT COEFFICIENT

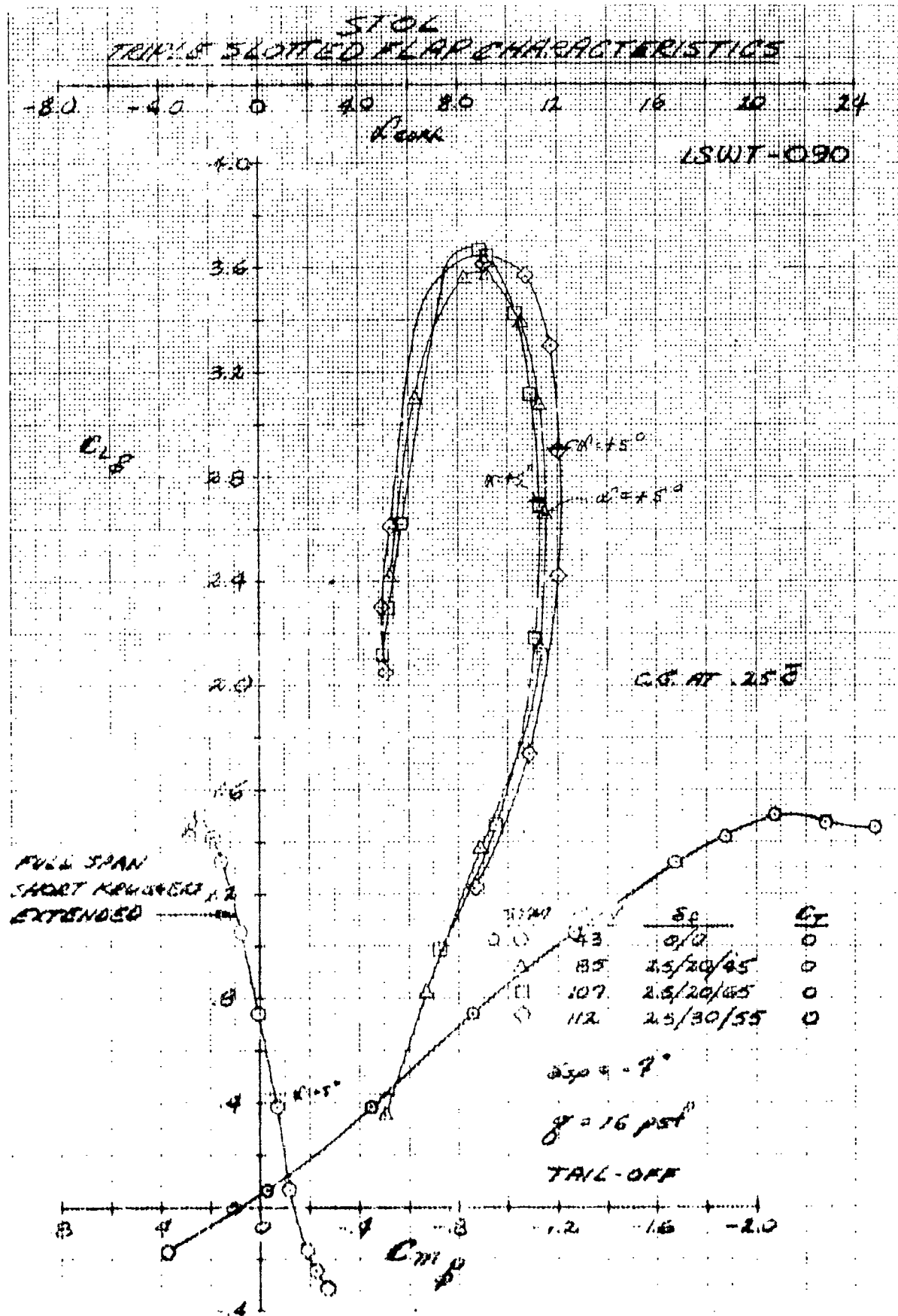


Figure 12.6.14

LSWT-090

FLAP DEFLECTION EFFECT ON AERODYNAMIC
CENTER LOCATION FOR DOUBLE AND TRIPLE
SLOTTED FLAP CONFIGURATIONS

$q = 16 \text{ psf}$

$C_T \approx 0$

TAIL-OFF

SYM δ_f

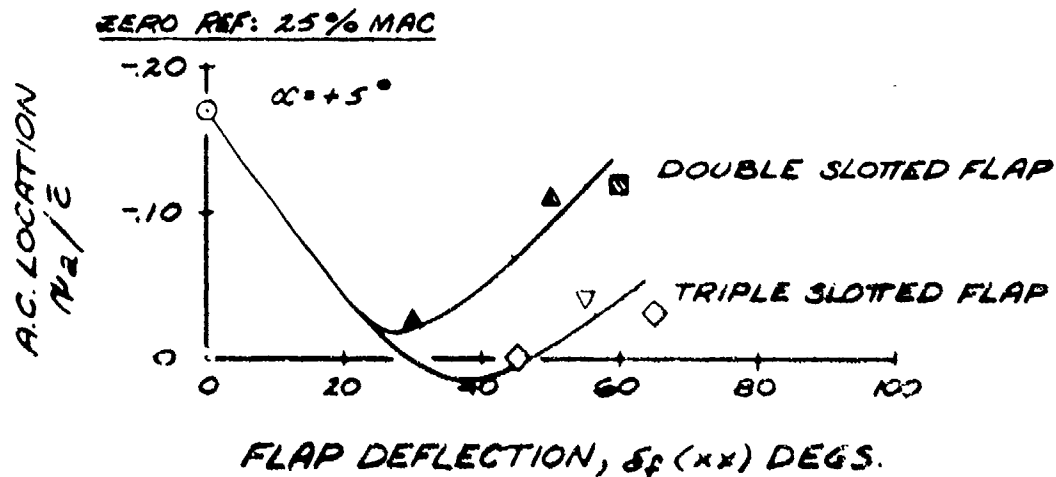
○ CLEAN LEADING & TRAILING EDGES

▲ KRUEGERS* + 25/XX

■ ✓ + 33/XX

◇ ✓ + 2.5/20/XX

▽ ✓ + 2.5/30/XX



* FULL SPAN - SHORT CHORD

Figure 12.7.1

LSWT-090

FLAP DEFLECTION EFFECT ON AERODYNAMIC
CENTER LOCATION FOR DOUBLE AND TRIPLE
SLOTTED FLAP CONFIGURATIONS

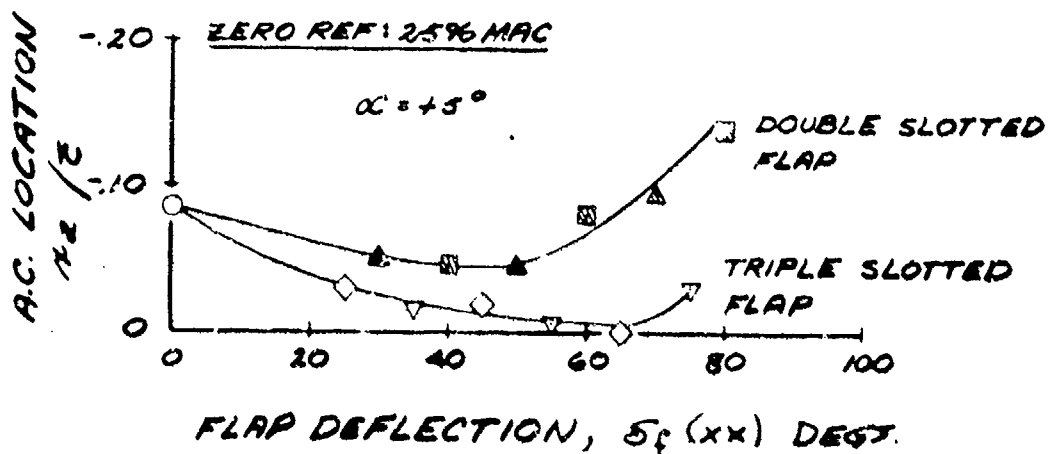
$g = 16 \text{ psf}$

$C_T = 2.00$

TAIL - OFF

SYM δ_c

- CLEAN LEADING & TRAILING EDGES
- △ KRUGGERS* + 25/XX
- ▣ ✓ + 35/XX
- ◇ ✓ + 2.5/20/XX
- ▽ ✓ + 2.5/30/XX



* FULL SPAN - SHORT CHORD

LSWT-090

FLAP DEFLECTION EFFECT ON AERODYNAMIC
CENTER LOCATION FOR DOUBLE AND TRIPLE
SLOTTED FLAP CONFIGURATIONS

$q = 16 \text{ psf}$

$C_T = 3.28$

TAIL-OFF

<u>SYM</u>	<u>δ_f</u>	
Δ	KRUEGERS*	+ 25/XX
\square	\checkmark	+ 35/XX
\diamond	\checkmark	+ 2.5/20/XX
∇	\checkmark	+ 2.5/30/XX

* FULL SPAN - SHORT CHORD

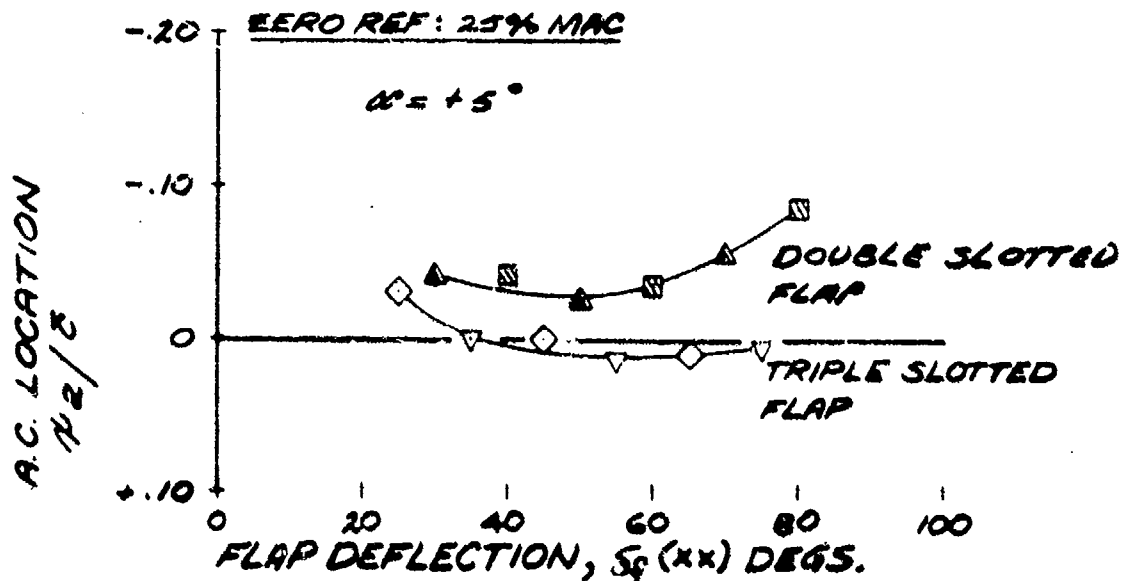


Figure 12.7.3

LSWT-080

ENGINE BLOWING EFFECT ON AERODYNAMIC
CENTER LOCATION FOR DOUBLE AND TRIPLE
SLOTTED FLAP CONFIGURATION

$\delta = 16 \text{ psf}$

TAIL-OFF

$\alpha = +5^\circ$ REF: 25% MAC

$\circ \delta_f = 25/50$

$\Delta \delta_f = 2.5/20/45$

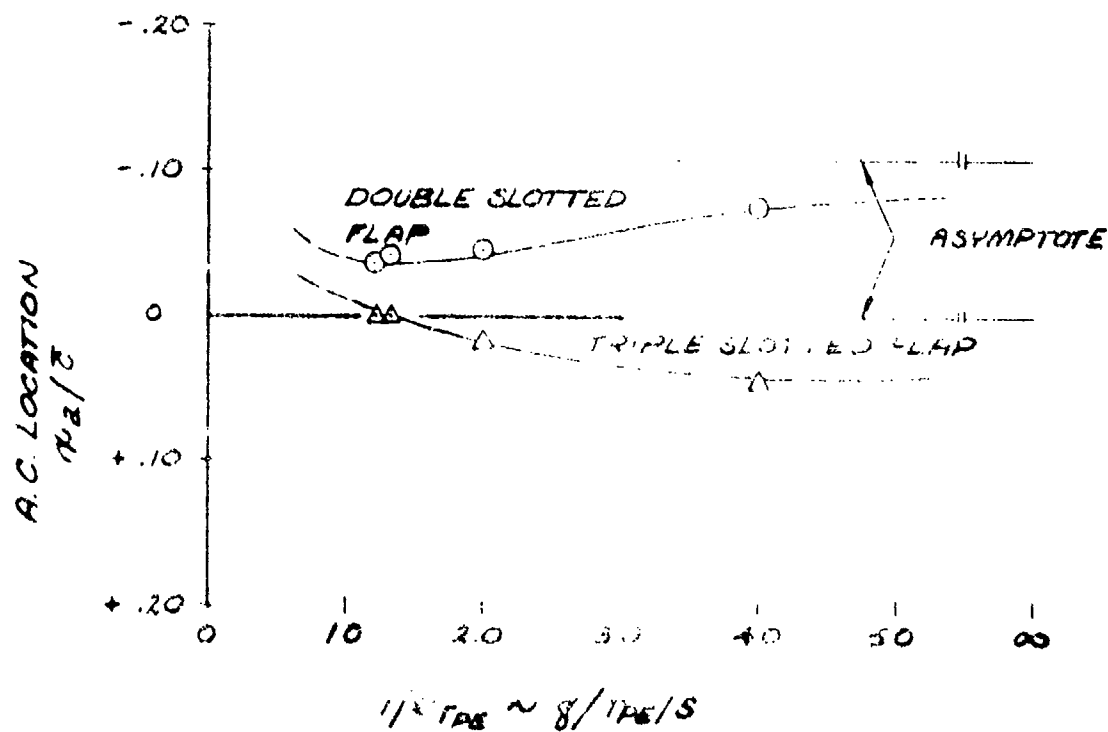


Figure 12.7.4

LSWT-090
EFFECT OF FLAP ENTRY FAIRING

$\delta_f = 25^\circ/50^\circ$

$q_\infty = 16 \text{ PSF}$

	RUN	FLAP ENTRY FAIRING	C.T.
○	50	ON	0
△	126	OFF	✓
□	65	ON	2.0
◇	127	OFF	✓

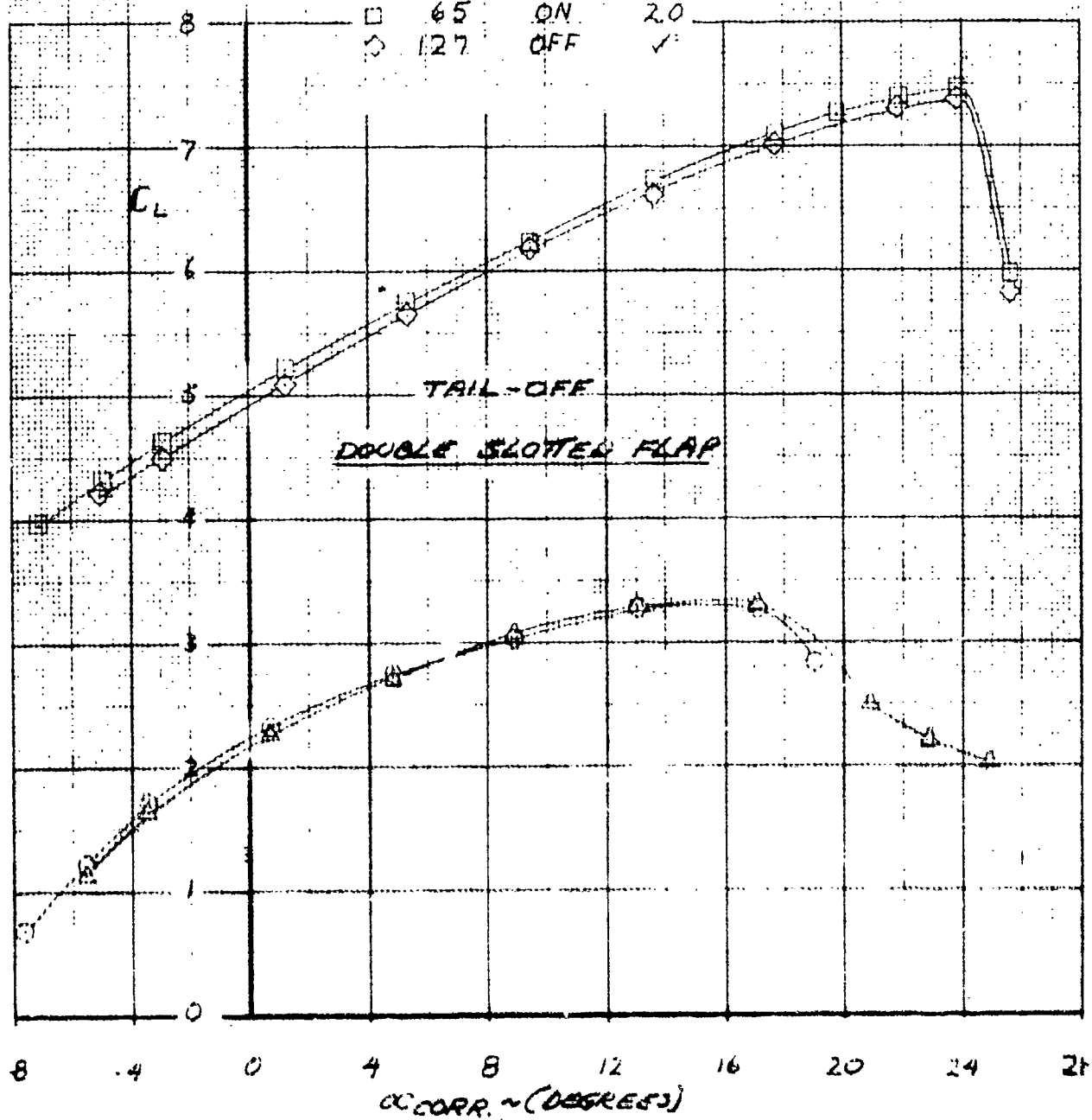
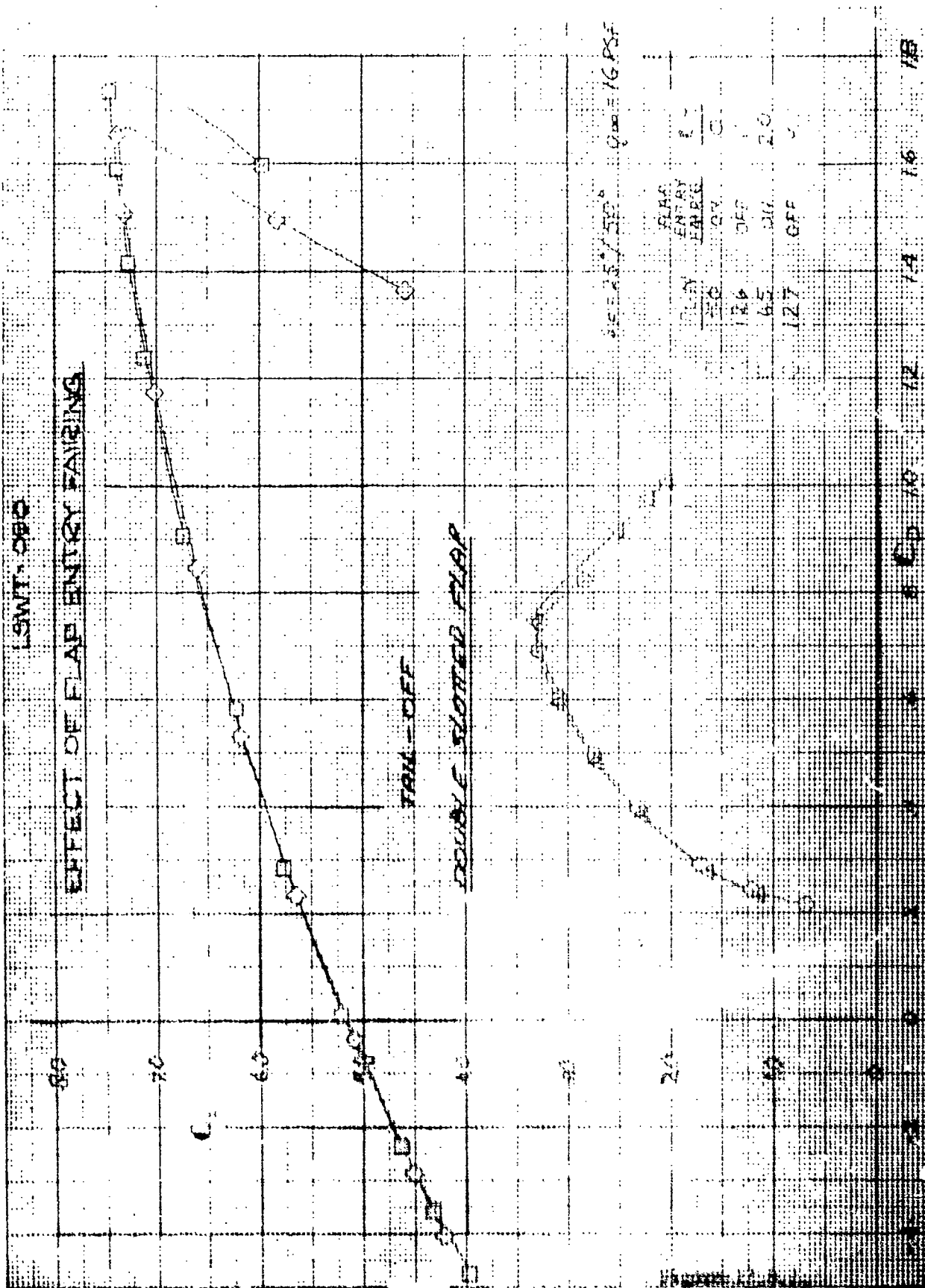
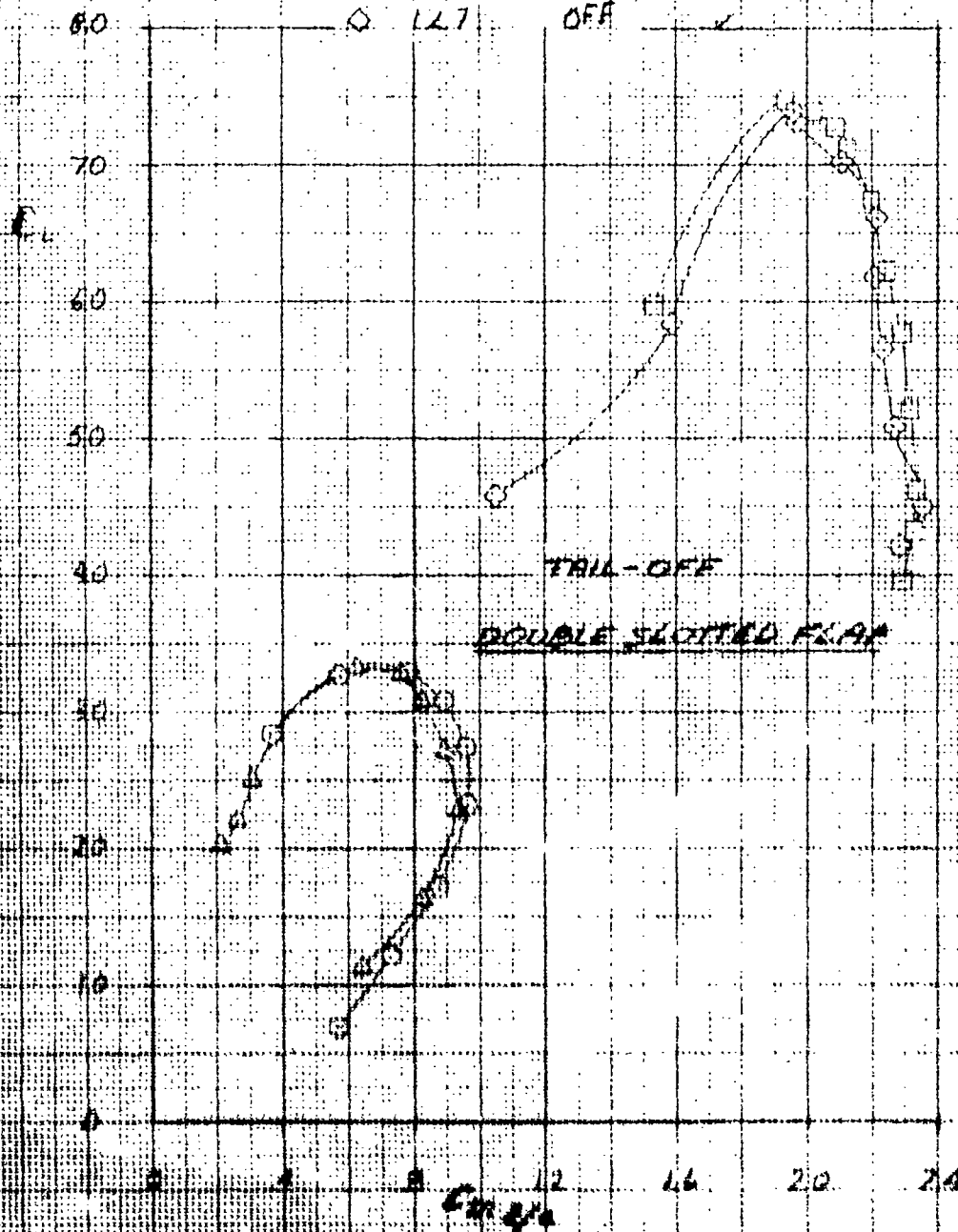


Figure 12.8.1



LSWT-090
 $\delta F = 25^\circ / 50^\circ$ $q_\infty = 16 \text{ PSF}$

	RUN	FLAP ENTRY FAIRING	C_L
○	50	ON	0
△	126	OFF	✓
□	65	ON	2.0
◇	127	OFF	✓



EFFECT OF FLAP ENTRY FAIRING

Section XIII

WING SPOILERS

Wing spoiler numerical designation and panel segmentation are defined in the general arrangement three view of Illustration 2.1. In general the only other symmetrical spoiler deflections tested other than those of the flap gap optimization program were $\delta_{sp} = +10^\circ$ and $+50^\circ$.

13.1 DLC EFFECTS ON LONGITUDINAL AERODYNAMIC PARAMETERS

Figures 13.1.1 and 13.1.2 show the effects of full span spoiler deployment for the unpowered and powered configurations respectively. These data were evaluated at $\alpha = 0^\circ$ and the basic configuration spoiler deflection of -10° is the zero reference from which all increments were taken.

The effects on lift and drag coefficients due to partial span spoiler deployment are presented in Figures 13.1.3 through 13.1.6 inclusive. These increments are presented for two-engine gross blowing coefficients ($C_{\mu} = 2.0$ and 3.28).

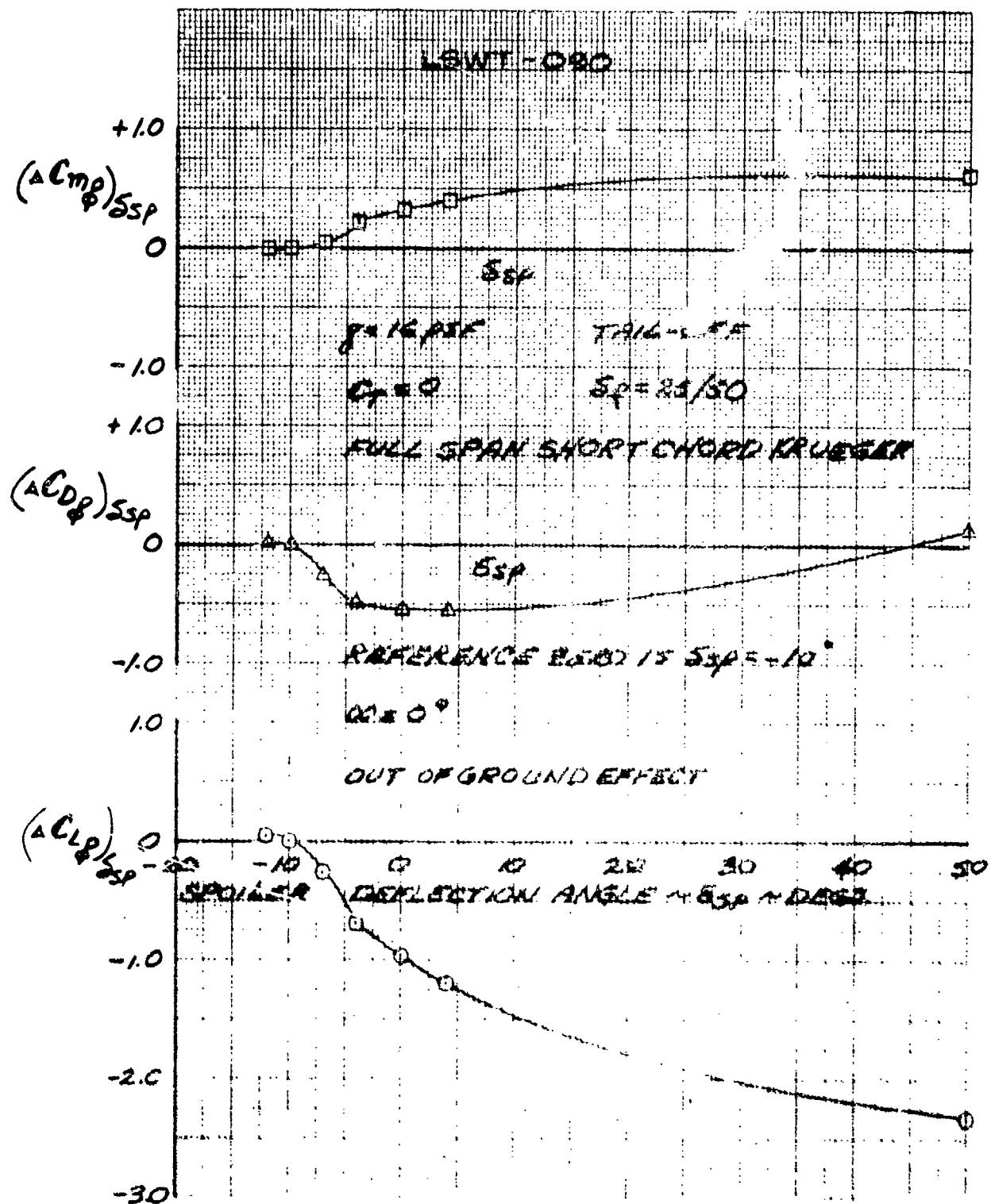
Figures 13.1.7 and 13.1.8 are the basic wind tunnel longitudinal coefficients from which the spoiler increments on the preceding figures were taken.

13.2 EFFECTS ON LONGITUDINAL AERODYNAMIC PARAMETERS WHEN USED AS AERO-DYNAMIC BRAKING DEVICES

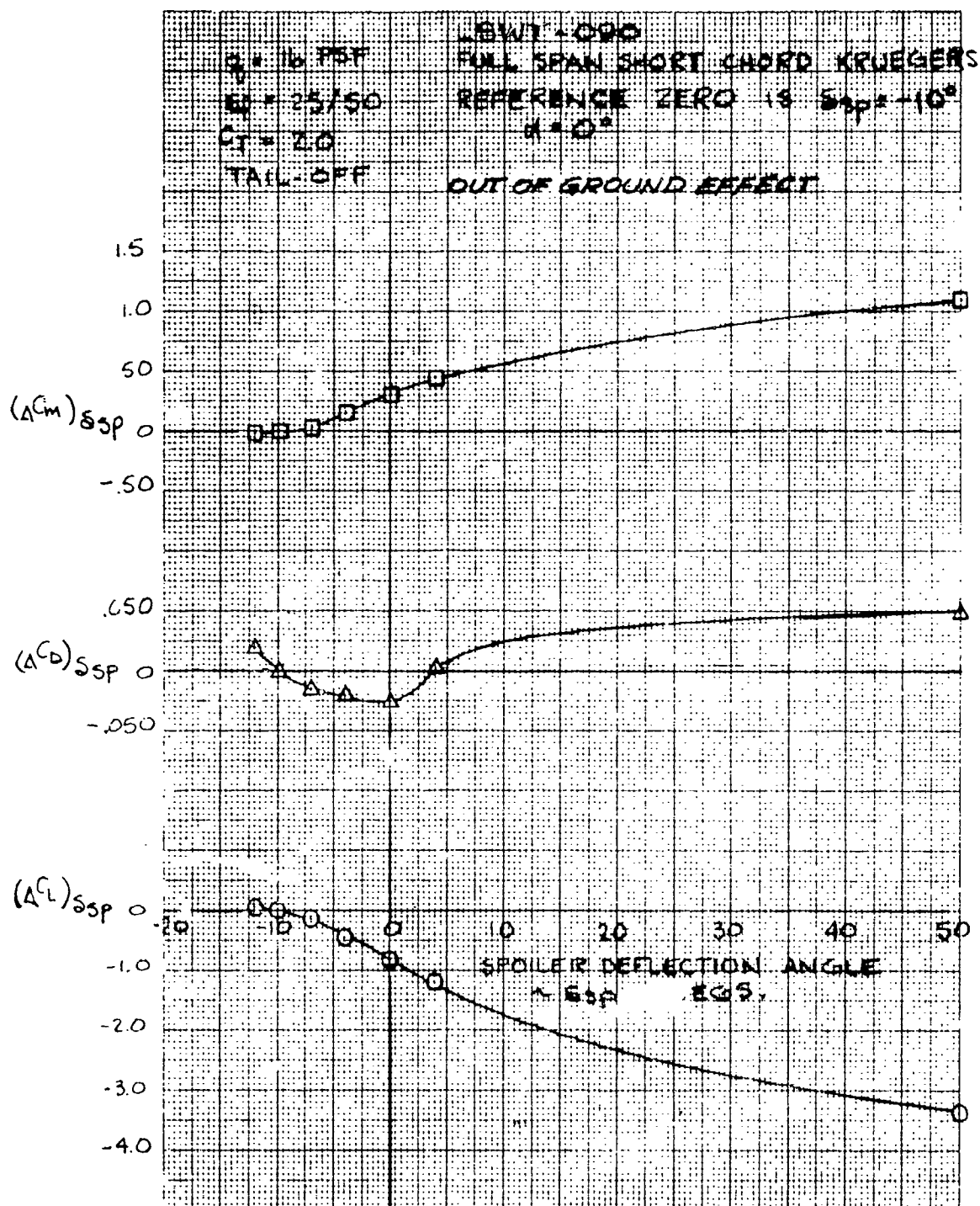
This subsection deals only with the maximum spoiler deflection available which is $+50^\circ$. A full span $\delta_{sp} = +50^\circ$ was not run during test ISWT 090. However, a $\delta_{sp} = +50^\circ$ half span test was run at $C_{\mu} = 0$ and 2.0 . Therefore the full span data was obtained by doubling the half span increments.

Figure 13.2.1 shows the effects of raising a half span spoiler to $+50^\circ$ at $C_T = 0$. Figure 13.2.2 presents the increments of Figure 13.2.1 and doubled to simulate the effects of a full span spoiler deflected to $+50^\circ$ at $C_T = 0$.

• Figure 13.2.3 shows the effects of raising a half span spoiler to +50° at $C_T = 2.0$. Figures 13.2.4 and 13.2.5 presents the increments obtained from Figure 13.2.3 and doubled to simulate the effects of a full span spoiler deflected to +50° at $C_T = 2.0$.



EFFECTS OF WING TRAILING EDGE, FULL SPAN
SPOILER DEFLECTION POWER 2.5%



EFFECTS OF WING TRAILING EDGE, FULL SPAN
SPOILER DEFLECTION - POWERED

Figure 13.1.2

L3WT - 090

EFFECT OF PARTIAL SPAN SPOILER DEPLOYMENT

$$\delta_{SP(1,2)} = +10^\circ \text{ (L.H. \& R.H.)}$$

$$\delta_{SP(3 \rightarrow 5)} = -10^\circ \text{ (L.H. \& R.H.)}$$

RUNS 234-65

OUT OF GROUND EFFECT

$$G = 2.0$$

$$\delta F = 25' / 50'$$

$$q = 16 \text{ psf}$$

TAIL-OFF

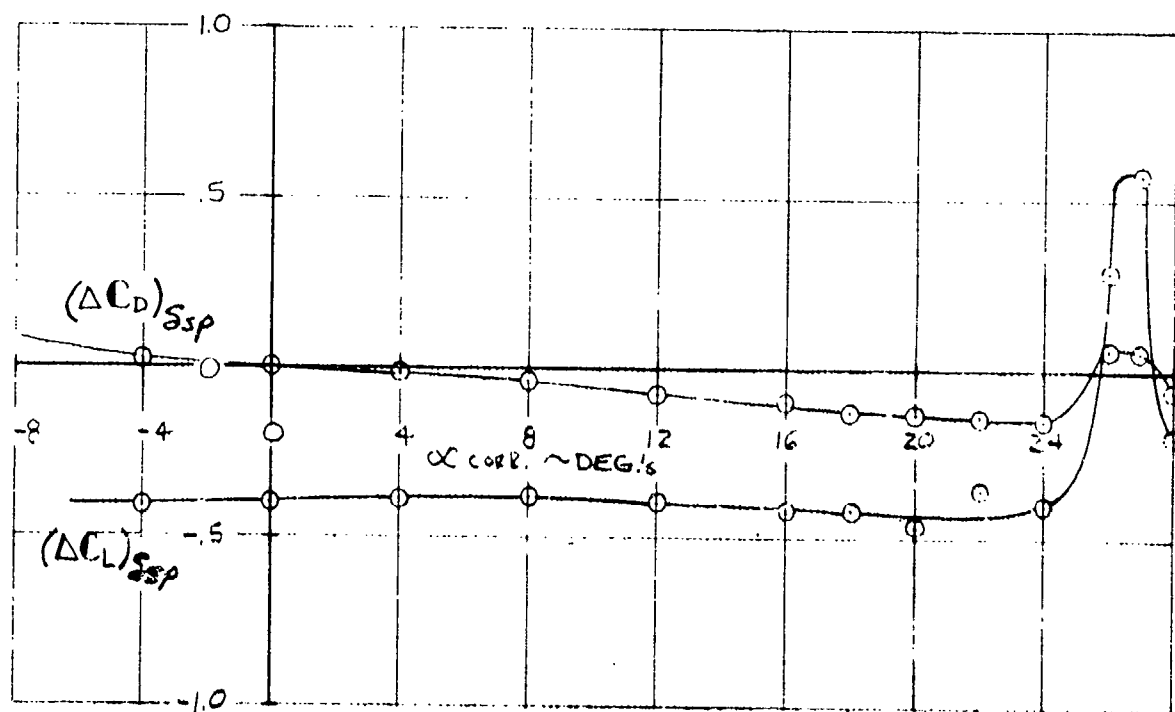


Figure 13.1.3

LSWT - 090

EFFECT OF PARTIAL SPAN SPOILER DEPLOYMENT

$$\delta_{SP(1,2)} = +10^\circ \text{ (L.H. \& R.H.)}$$

$$\delta_{SP(3 \rightarrow 5)} = -10^\circ \text{ (L.H. \& R.H.)}$$

RUNS 235 - 68

OUT OF GROUND EFFECT

$$G = 3.28$$

$$\dot{\delta} = 25^\circ/\text{sec}$$

$$q = 16 \text{ psf}$$

TAIL-OFF

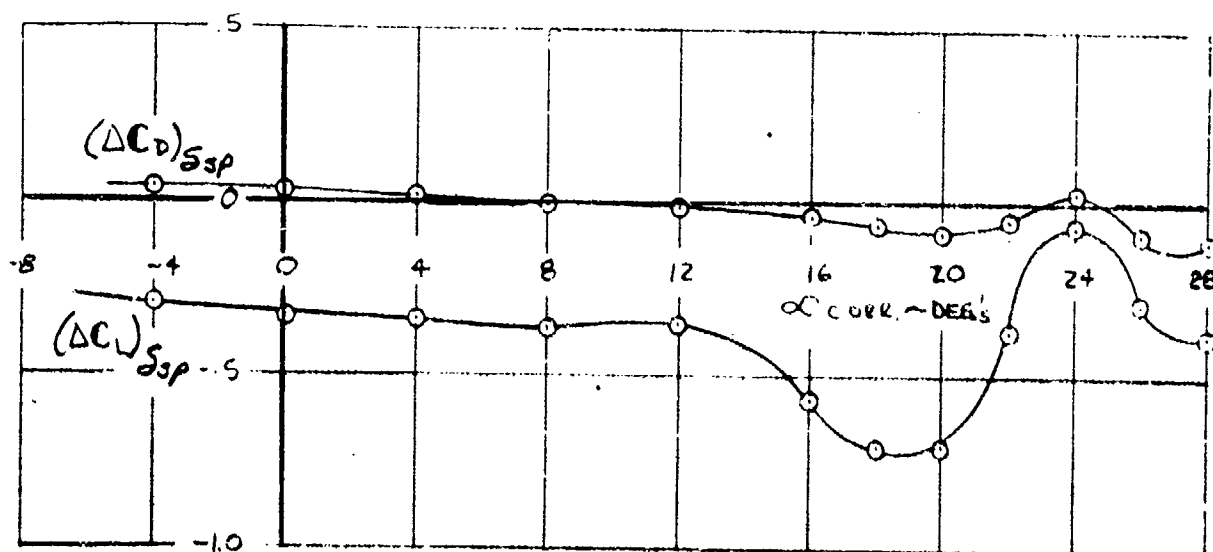


Figure 13.1.4

LSWT - 090

EFFECT OF PARTIAL SPAN SPOILER DEPLOYMENT

$$\delta_{SP(1 \rightarrow 4)} = +10' \text{ (L.H. \& R.H.)}$$

$$\delta_{SP(5)} = -10' \text{ (L.H. \& R.H.)}$$

RUNS 232-65

$$C_T = 2.0$$

$$\delta F = 25^\circ / 50'$$

$$q = 16 \text{ psf}$$

TAIL-OFF

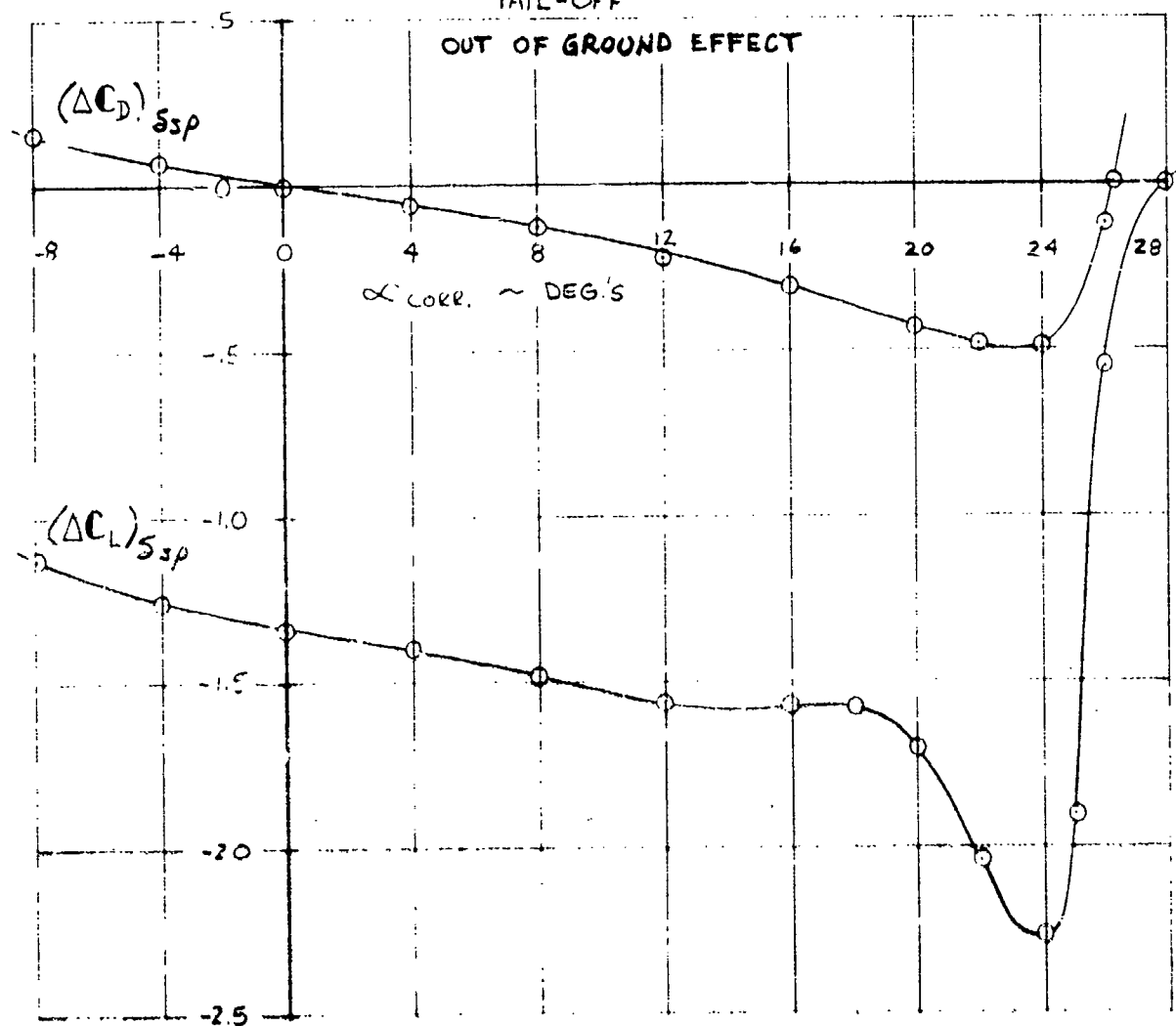


Figure 13.1.5

LSWT - 090

EFFECT OF PARTIAL SPAN SPOILER DEPLOYMENT

$$\delta_{SP(1 \rightarrow 4)} = +10' \text{ (L.H. \& R.H.)}$$

$$\delta_{SP(5)} = -10' \text{ (L.H. \& R.H.)}$$

RUNS 233 - 68

$$C_T = 3.28$$

$$\delta_f = 25^\circ/50'$$

$$q = 16 \text{ psf}$$

TAIL-OFF

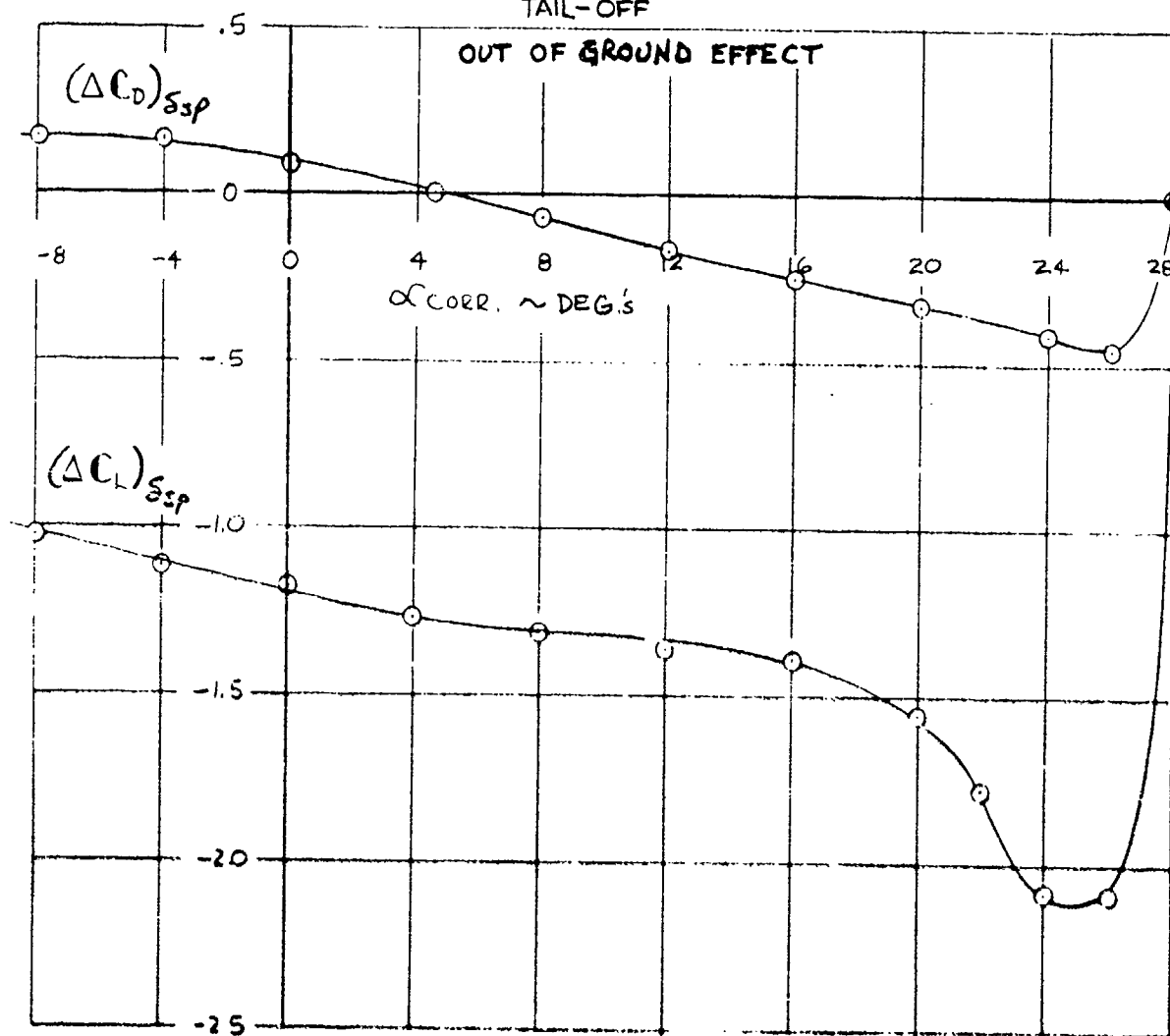
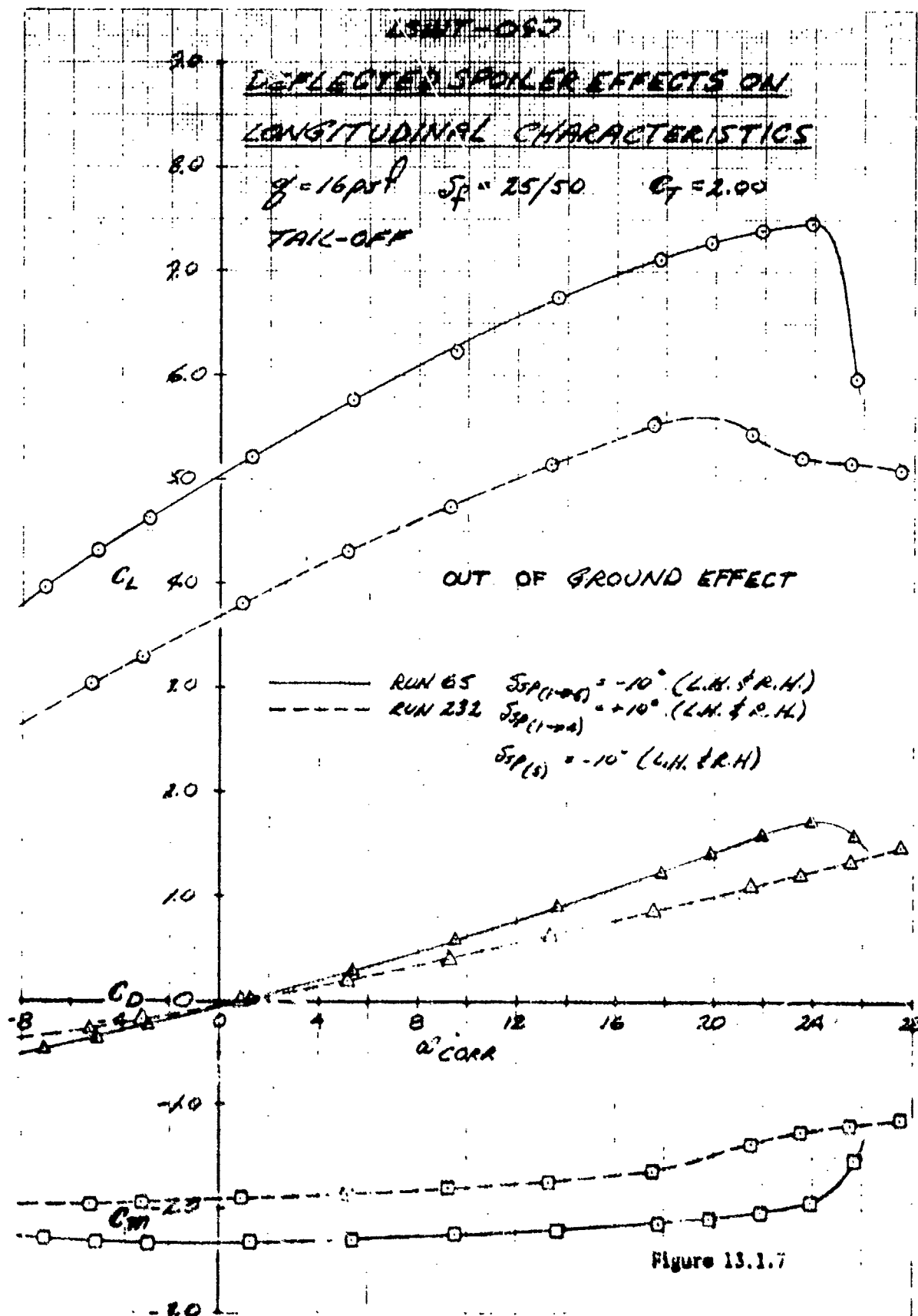
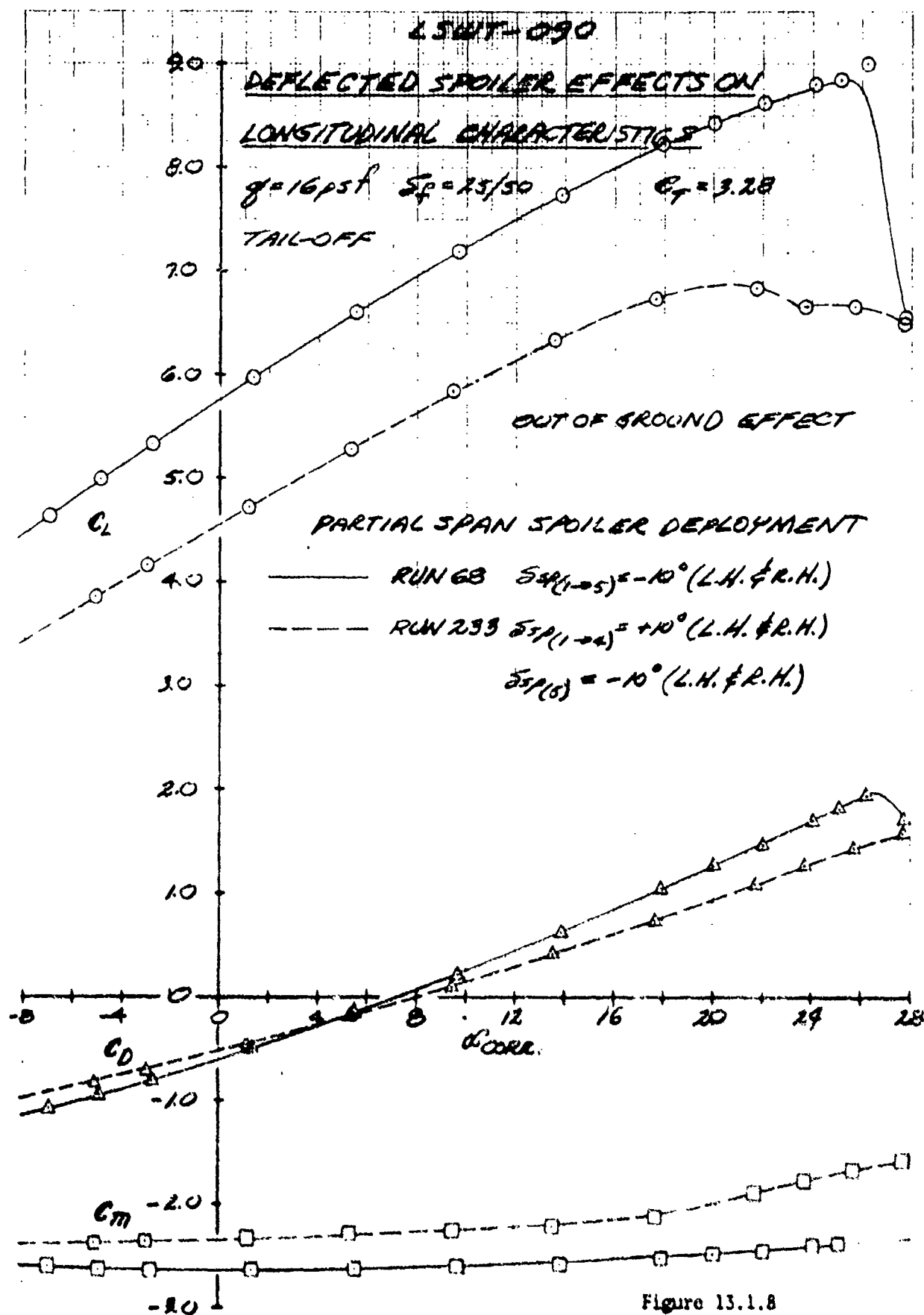


Figure 13.1.6





LSWT-090

EFFECT OF RAISING FIVE SPOILER PANELS TO

50°, RIGHT WING ONLY

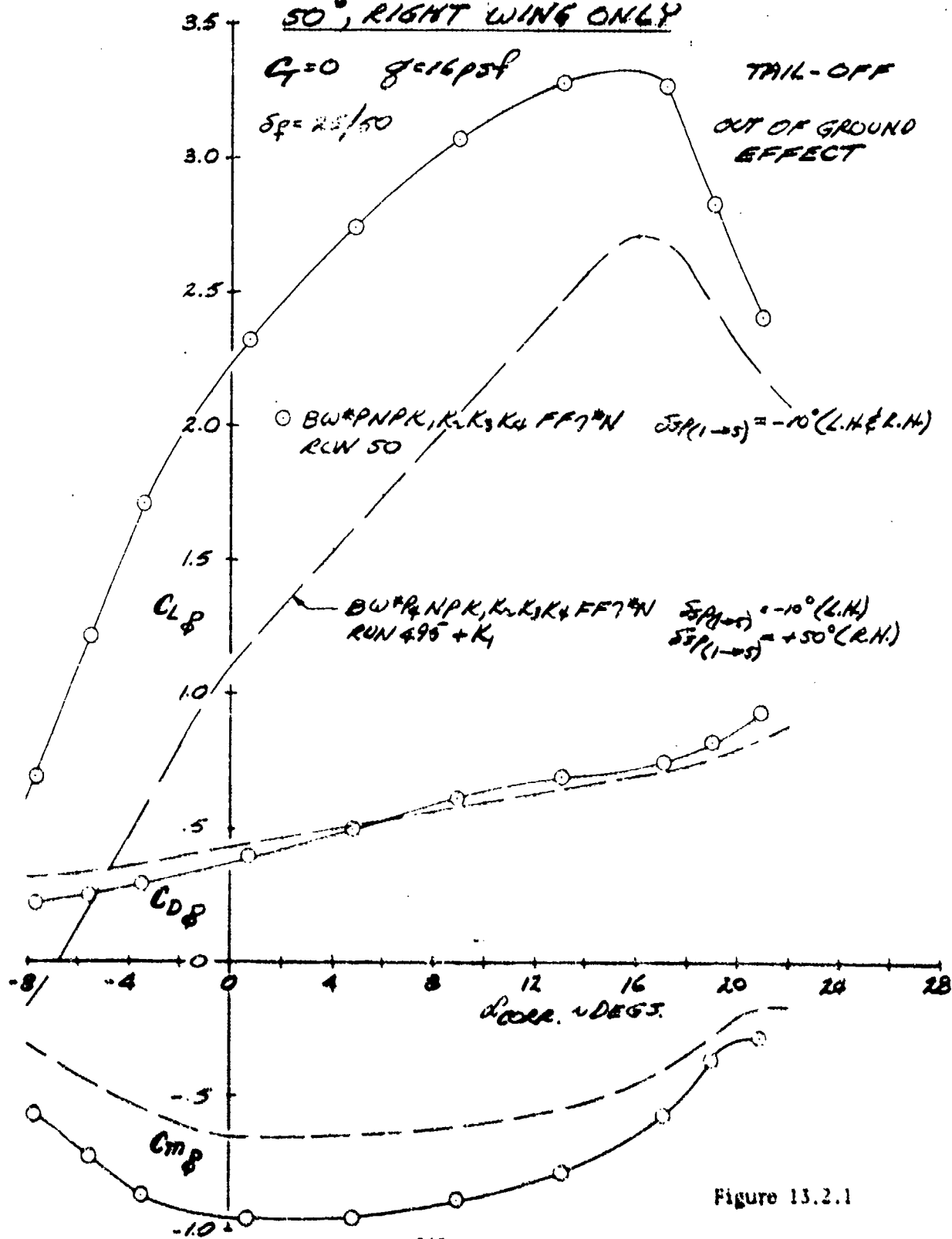


Figure 13.2.1

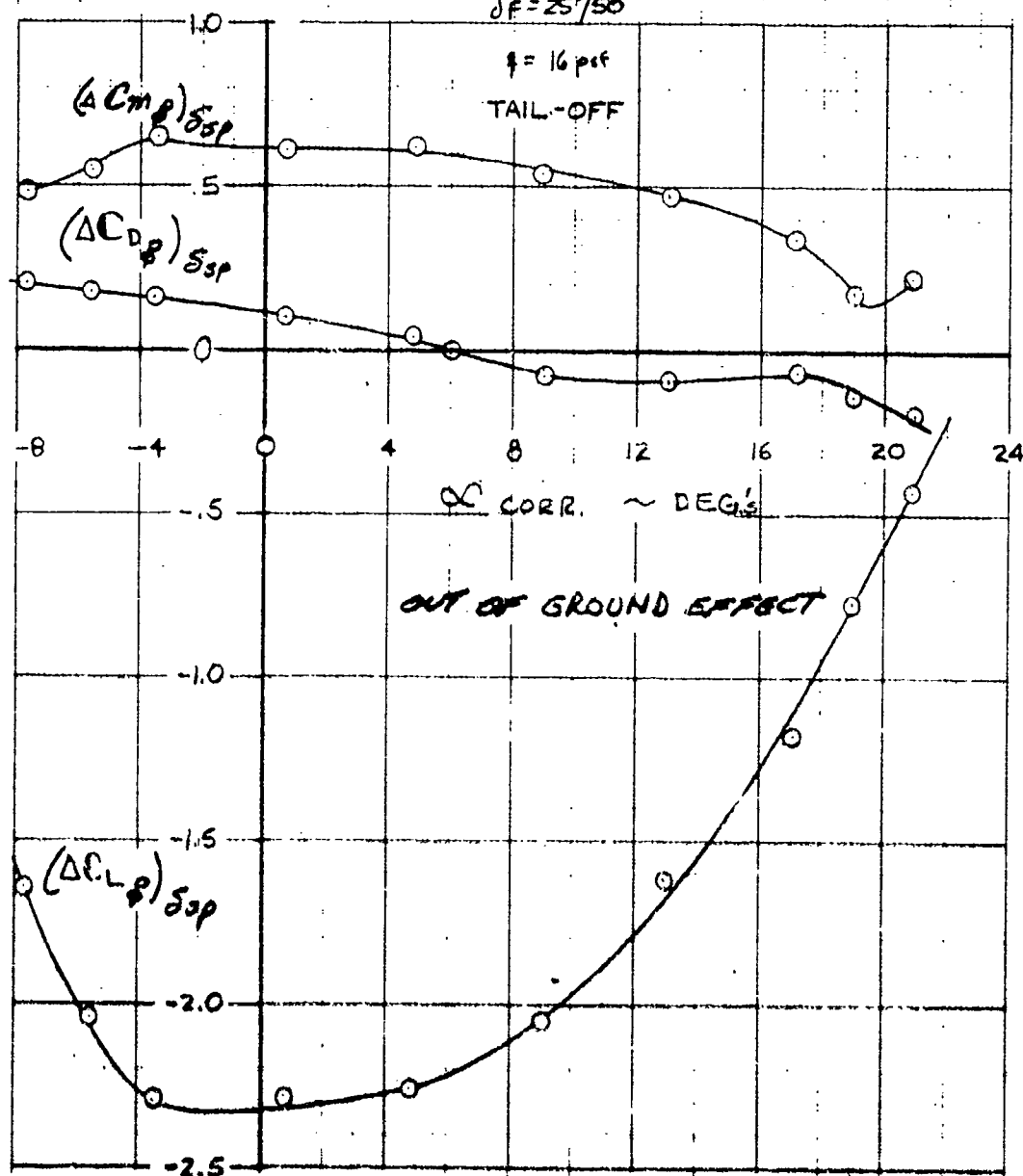
LBWT - 090
EFFECT OF FULL SPAN SPOILER DEPLOYMENT

$\delta_{sp} = 50^\circ$

RUNS 495+ (240-244) - 50

$C_T = 0$

$\delta_F = 25^\circ/50^\circ$



EFFECT OF RAISING FIVE SPOILER PANELS TO 50°, RIGHT WING ONLY

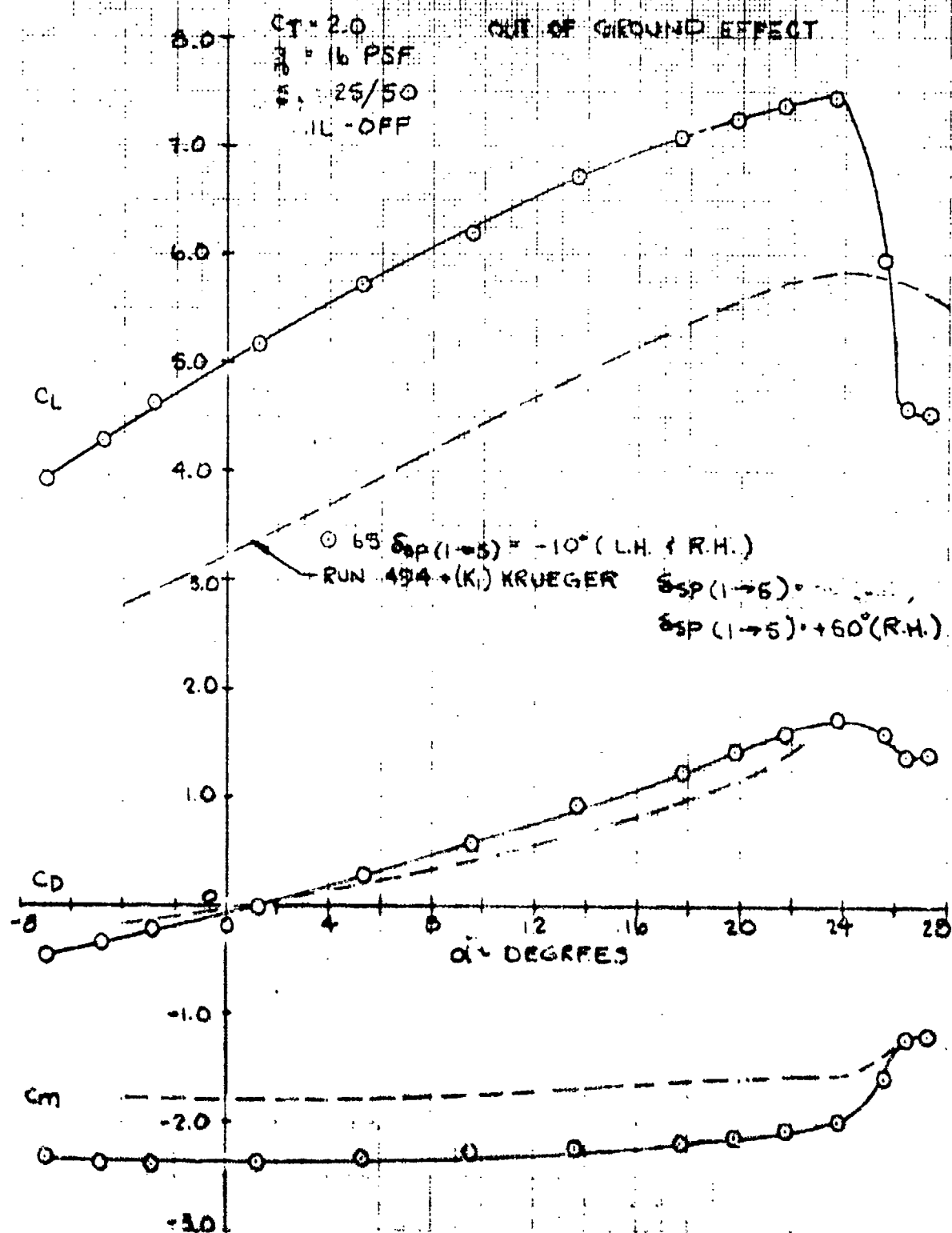


Figure 13.2.3

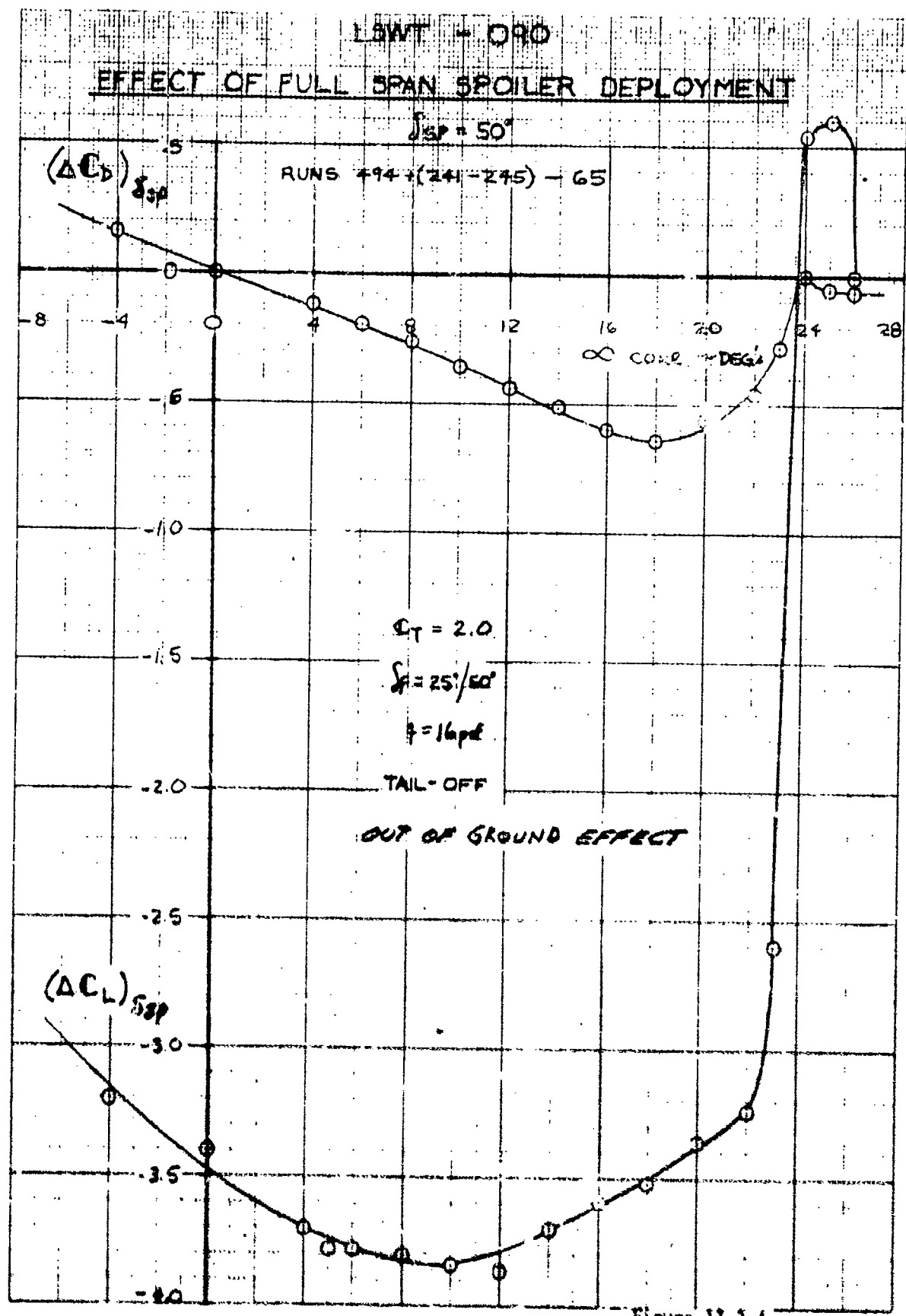


Figure 13.2.4

LSWT - 090
EFFECT OF FULL SPAN SPOILER DEPLOYMENT

$\delta_{SP} = 50^\circ$

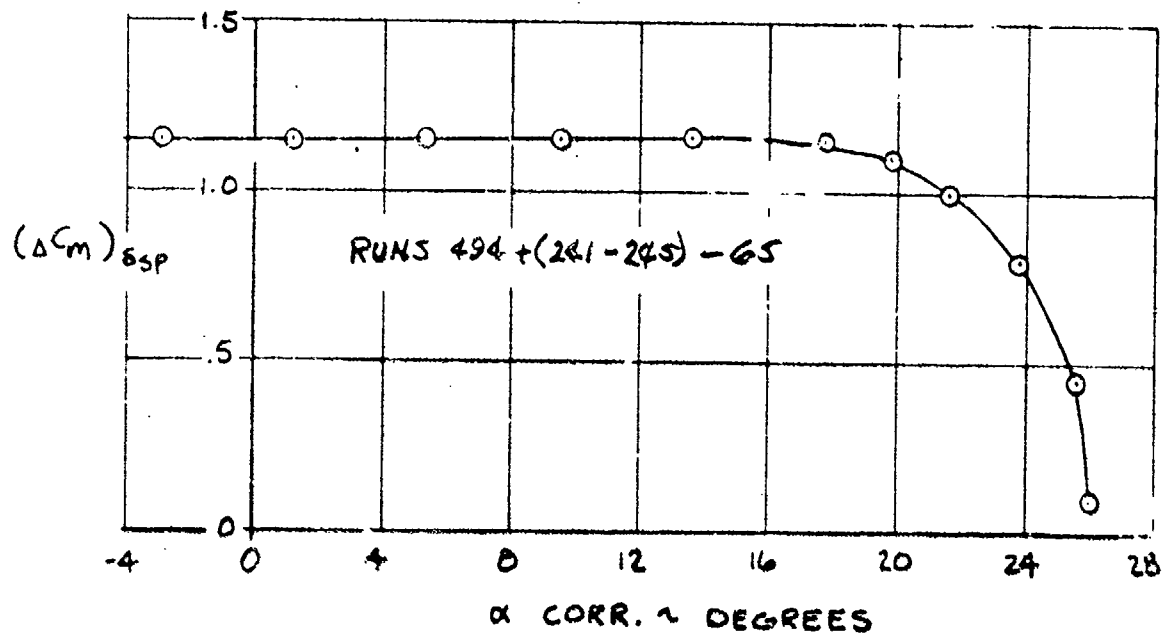
$C_T = 2.0$

$\delta_f = 25^\circ/50^\circ$

$q = 16 \text{ PSF}$

TAIL-OFF

OUT OF GROUND EFFECT



• Figure 13.2.5

Section XIV

ROLL CONTROL

The various roll control devices tested in LSWT-090 are shown in cross-section in Illustrations 14.1 through 14.4 inclusive. Methods tested for obtaining roll control were aileron deflection, spoiler deflection, aileron plus spoiler deflections, blown aileron deflection; asymmetric flap vane spoiler and asymmetric leading edge devices such as the outboard short chord Krueger, the outboard long chord Krueger, the outboard long chord slotted Krueger and leading edge boundary layer control. All roll control devices were tested on the AR 7 wing at $\alpha = 24^\circ$ and with double slotted flaps ($\delta_f = 25^\circ/50^\circ$ and $35^\circ/60^\circ$) unless otherwise noted. The spoiler panels are numbered per Illustration 2.1. Stability axis data is used throughout this subsection.

14.1 ROLL DUE TO FAILED ENGINE

Rolling moment coefficients for four-engine thrusts are presented in Figures 14.1.1 and 14.1.7 for the two basic double slotted flap configurations (50° and 60° flaps). This data shows the effects of model hardware including engine power non-uniformity.

Total rolling moment coefficients with an outboard engine failed, $(C_{l_s})_{EO}$ for $\delta_f = 25^\circ/50^\circ$ and $35^\circ/60^\circ$ at two thrust per engine coefficients are presented in Figures 14.1.2 and 14.1.8 as functions of angle of attack. Incremental rolling moment coefficients due to one engine out $(\Delta C_{l_s})_{EO}$, are obtained by subtracting the four-engine rolling moment coefficients from the engine-out rolling moment coefficients and are presented in Figures 14.1.3 and 14.1.9 for their respective flap deflections and thrust per engine coefficient. These figures indicate that power has a relatively small effect on engine-out rolling moment coefficient when analyzed on this basis.

Effects of outboard engine failure on powered lift are shown in Figure 14.1.4 and Figure 14.1.5 presents a comparison of total rolling moment coefficients of the outboard and inboard engine failures. Incremental rolling moment coefficients for outboard and inboard engine failures are presented in Figure 14.1.6.

Rolling moment coefficient due to outboard engine failure is plotted against four engine powered trim lift and three-engine powered trim lift at $\alpha = 16^\circ$ and is presented in Figure 14.1.10. This plot demonstrates that the amount of rolling moment associated with engine failure is proportional to the loss in lift when uncorrected data is used.

Figure 14.1.11 shows the centers of pressure of span loading for the inboard and outboard failed engine conditions. These centers of pressure were determined by using absolute wind tunnel data and appear questionable. In Figure 14.1.12 an increment in spanwise load centers was obtained by subtracting out the four-engine spanwise load centers which increases the credibility considerably.

14.2 EFFECT OF TAIL ON ROLLING MOMENT

The effect of the tail on total rolling moment with outboard engine inoperative is plotted as a function of angle of attack and is presented in Figure 14.2.1. Incremental rolling moment coefficient due to engine failure is plotted in Figure 14.2.2 as a function of angle of attack. As can be seen in both figures, the tail has little effect on outboard engine failed rolling moment coefficient.

14.3 EFFECT OF SLOTTED KRUEGERS AND FLAP VANE SPOILER ON ROLLING MOMENT

The effect of slotting the long chord Krueger on total rolling moment is presented in Figure 14.3.1 as a function of angle of attack. It is apparent from the plot that essentially no benefits are gained from slotting the long chord Krueger either symmetrically or asymmetrically.

Figure 14.3.2 shows the effects of adding a spoiler to the right hand vane flap on the inboard flap segment and corresponding spanwise to the fourth spoiler segment. The objective was to cause a right wing down rolling moment by spoiling the flow over the vane flap. Only minimal results were achieved.

14.4 ROLL INCREMENT DUE TO AILERONS AND SPOILER DEFLECTION

An unpowered rolling moment coefficient increment for aileron only ($\delta_a = 20^\circ/-20^\circ$) is shown in Figure 14.4.1 as a function of angle of attack. The aileron power goes to zero at α_{stall} . The aileron is located behind the open number 5 spoiler panel and therefore is of only limited effectiveness.

Rolling moment coefficient increments due to deflection of ailerons and spoiler panel No. 5 are shown in Figures 14.4.2 and 14.4.3 as functions of angle of attack for symmetrical four-engine power, asymmetrical three-engine power and the power off configurations. It is apparent that the spoiler panel No. 5 is very effective at the full 50° up deflection.

Three engine incremental spoiler data is permitted to be interspersed with four-engine incremental spoiler data since the failed engine is on the wing opposite to that on which the spoiler panels are being evaluated and as such does not change incremental spoiler effectiveness.

Figures 14.4.4 through 14.4.6 inclusive show incremental rolling moment coefficients as functions of angle of attack for the unpowered and powered configurations (three and four engines operating) for various combinations of spoiler panel deflections with and without aileron deflection.

It will be noted that an abrupt increase in rolling moment is introduced at or very near the stall angle when spoiler panels are deflected. This is attributed to the decrease in wing local α_{stall} when a spoiler panel is raised thus causing the spoiled wing to stall first and causing what appears to be this large increase in roll effectiveness.

The effect of spoiler deflection on three engine lift is presented, tail on, as a function of angle of attack in Figure 14.4.7.

The roll effectiveness of spoiler panels Nos. 3 and 4 are presented in Figure 14.4.8 for unpowered and powered conditions with and without the use of tip spoilers and ailerons. When the tip spoiler and aileron is used in conjunction with spoiler panels Nos. 3 and 4 the resultant interference causes a decay in roll effectiveness of spoiler panels Nos. 3 and 4 of approximately 33 percent unpowered and 18 percent powered. Very small power effects are seen in the roll effectiveness of the tip spoiler plus aileron combination because they are located almost beyond the influence of engine blowing. The roll effectivity of spoiler panels Nos. 3 and 4

alone is approximately 50 percent greater than the roll effectivity of the tip spoiler and aileron combination by itself unpowered and approximately 69 percent greater when powered.

Figures 14.4.9 and 14.4.10 present incremental rolling moment coefficients of spoiler panels Nos. 1 and 2 and of spoiler panels Nos. 1 through 5 as functions of angle of attack for the unpowered and powered configurations.

Incremental rolling moment coefficients due to various spoiler panel combinations are plotted as functions of spoiler panel deflection for $C_T = 0$ and 2.0 and at $\alpha = 0^\circ$ and 8° and are presented, tail on, in Figures 14.4.11 through 14.4.14 inclusive. These plots demonstrate the maximum roll capability of the various spoiler panel combinations.

Since the available rolling moment is a function of the wing lift, Figures 14.4.15 and 14.4.16 present plots of incremental rolling moment coefficient due to spoiler deflection as a function of symmetrically powered unspoiled total wing lift. At low angles of attack the $(\Delta C_{l_s})_{\delta_{sp}}$ is a linear function of C_L and is independent of power influences, other than those of C_L .

Similar analysis of the three-engine data for roll control is made and incremental rolling moment coefficients due to spoiler deflections are plotted against three-engine unspoiled total wing lift and presented in Figure 14.4.17.

The location of centers of pressure due to spoiler deflections were obtained by dividing the rolling moment increment by a corresponding lift loss. Figure 14.4.18 shows the effects of α on c.p. locations with spoiler panel No. 5 only deflected. Figure 14.4.19 shows the effects of engine blowing on the c.p. locations of spoiler panels Nos. 3 and 4 as well as α effects. This shows that the application of power moves the c.p. locations inboard. The effects of power and angle of attack on the c.p. locations of all five spoiler panels raised is shown in Figure 14.4.20. The application of power to this configuration, in contrast with the previous figure, moves the c.p. locations outboard for α 's in excess of 4° .

Rolling moment coefficient for spoiler panel Nos. 3, 4, and 5 plus aileron deflection is plotted against angle of attack for the triple slotted flap ($\delta_f = 2.5^\circ/20^\circ/25^\circ$) at two engine gross blowing coefficients ($C_{\mu} = 2.0$ and 3.28). A unique phenomenon appears here in that more roll

is available at $C_T = 2.0$ than at $C_T = 3.28$. It is suggested that because of the additional slot in the triple slotted flap system followed by the main flap segment, powered lift is being generated with spoilers deployed due to flow being directed through a slot and causing a flow reattachment to the main flap segment behind the spoiler action. This flow reattachment then could be developing more lift than the spoiler is capable of destroying resulting in a lesser roll capability at a higher C_{μ} .

A comparison of double and triple slotted roll capability is presented in Figure 14.4.22 where it is apparent that the double slotted flap is more than twice as powerful as the triple slotted flap at $\alpha = 0^\circ$.

14.5 ROLLING MOMENTS DUE TO BLOWN AILERON

The wing trailing edge or aileron blowing was treated the same as the leading edge blowing in that the aileron BLC was also a direct function of engine blowing level. It was mechanically adjusted so as to give the thrust at the BLC nozzles for the thrust of the simulated jet engine nozzles as presented in Figure 14.5.6.

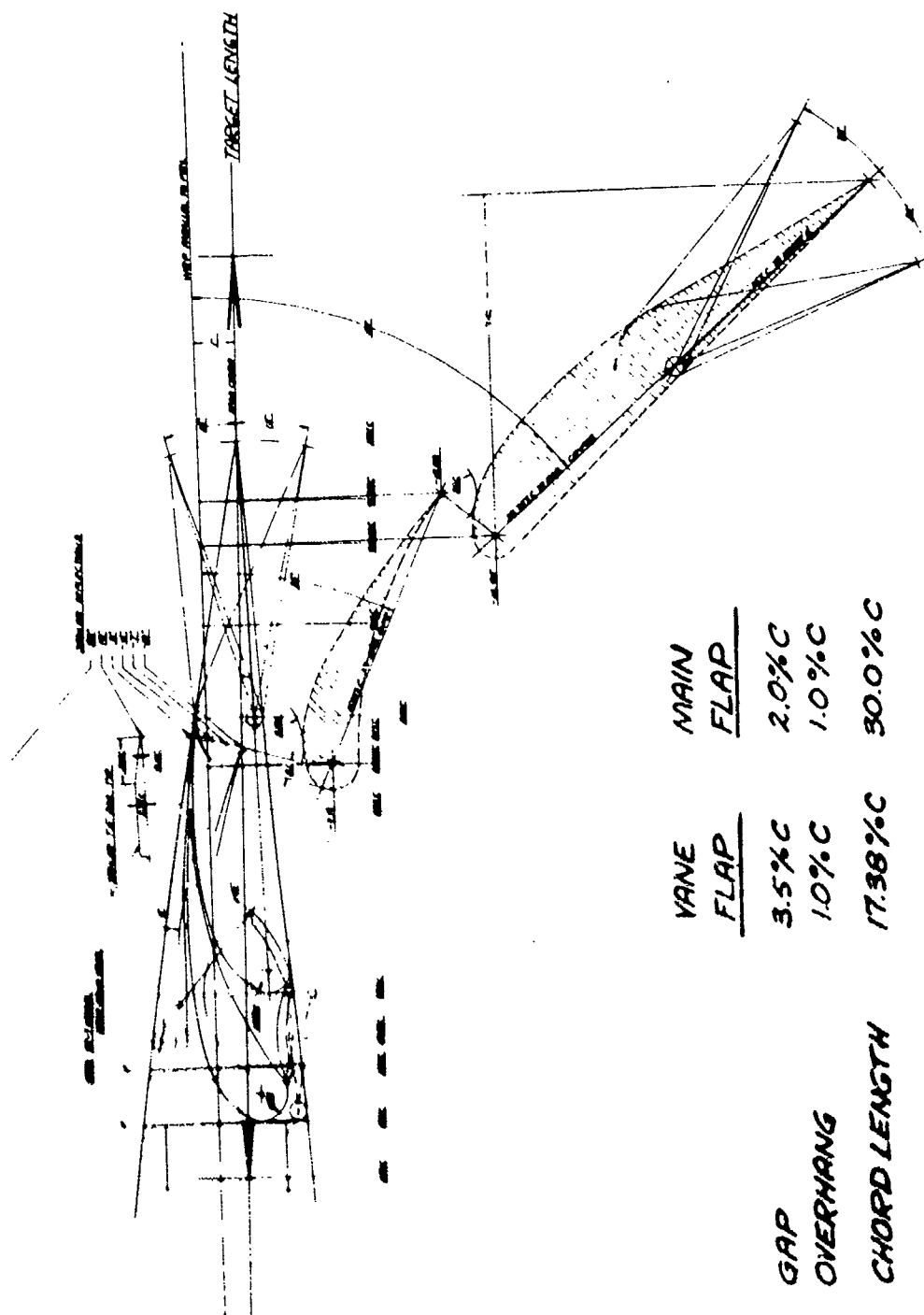
Figures 14.5.1 through 14.5.3 inclusive show the effects of blowing on the aileron on one side only at three symmetrical aileron deflections ($\delta_a = 35^\circ/30^\circ$, $35^\circ/50^\circ$ and $35^\circ/70^\circ$) as functions of angle of attack. The plots at the bottom of these figures are cross plots at the indicated α 's of the curves at the top of the figures. An obvious decay in roll capability is recognizable for C_{μ} 's greater than 2.0. It is suggested that this loss in aileron BLC effectiveness above $C_{\mu} = 2.0$ is possibly due to model asymmetries as was found in Figures 14.1.1 ($\delta_f = 25^\circ/50^\circ$) and 14.1.7 ($\delta_f = 35^\circ/60^\circ$). In both of these cases, a reduction in four engine rolling moment coefficient was observed when C_{μ} was increased from 2.0 to 3.0.

Figure 14.5.4 represents a summary of the bottom plots of each of the three preceding figures. This plot points out that a reduction in aileron effectiveness also exists as a function of angle of attack whereby the $\delta_a = 35^\circ/30^\circ$ is the least effective at $\alpha = 0^\circ$, and it becomes the most effective at $\alpha = 16^\circ$.

Figure 14.5.5 presents the incremental rolling moment coefficient due to blown aileron corrected for model asymmetries in the upper family of curves and blown aileron incremental rolling moment coefficients due to engine blowing coefficient in the lower family of curves. Since there are no directly comparable runs for the blown aileron deflections of $35^\circ/30^\circ$, $35^\circ/50^\circ$, and $35^\circ/70^\circ$, the $\delta_f = 25^\circ/50^\circ$ full span flaps are used as the base four engine run. Note that the decay in roll effectiveness above $C_{\mu} = 2.0$ previously experienced in Figures 14.5.1 through 14.5.4 inclusive does not occur in Figure 14.5.5. The family of curves at the bottom of Figure 14.5.5 not only shows data with corrections applied for power asymmetries in the base run, but also model asymmetries in the power off case.

14.6 SPOILER EFFECTIVENESS WITH FAILED ENGINE

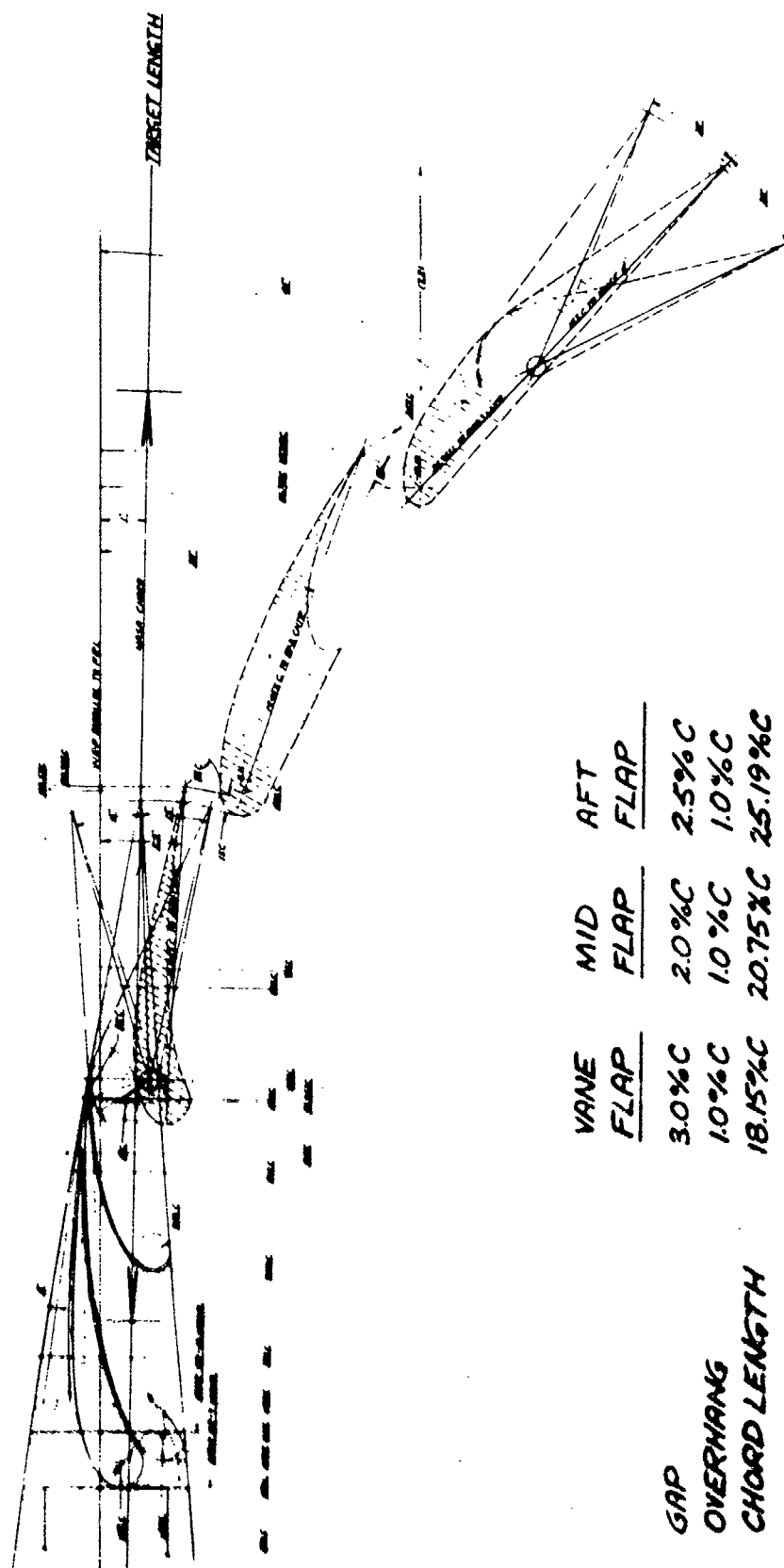
Figures 14.6.1 shows that deployment of spoiler panels Nos. 3, 4, and 5 in conjunction with aileron deflection are quite sufficient throughout the power range to trim out the rolling moment caused by an outboard engine failure up to α_{stall} . However, this combination of roll control devices is not adequate to maintain control of the large asymmetric wing stall characteristics associated with an engine failure.



	VANE	MAIN
	FLAP	FLAP
GAP	3.5% C	2.0% C
OVERHANG	1.0% C	1.0% C
CHORD LENGTH	17.38% C	30.0% C

C - LOCAL WING CHORD LENGTH
 WING CHORD = $20.8163 - (.2449 \times X_F)$
 WHERE X_F IS ANY WING STATION MEASURED
 FROM THE FUSELAGE CENTERLINE.

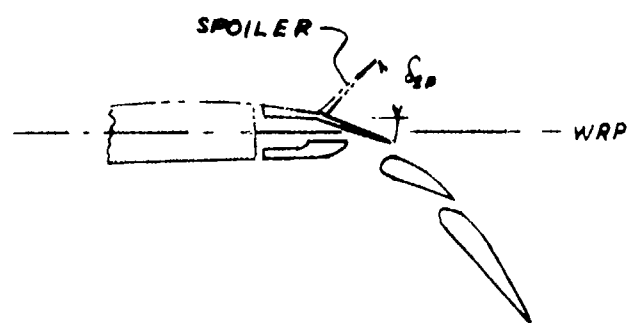
AILERON - OUTBOARD
WING FLAP - DOUBLE
SLOTTED - MST W.T. MODEL



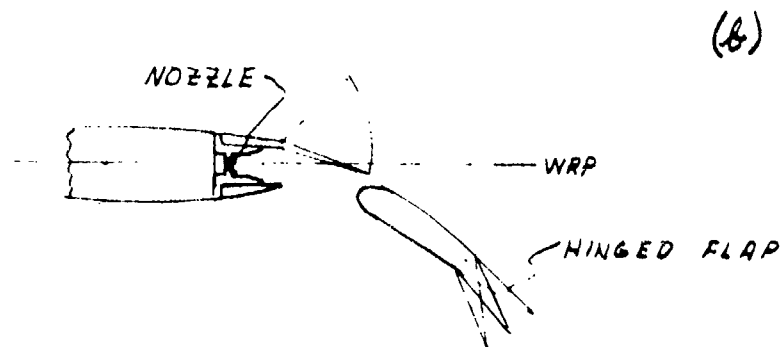
	VANE FLAP	MID FLAP	AFT FLAP
GAP	3.0% C	2.0% C	2.5% C
OVERHANG	1.0% C	1.0% C	1.0% C
CHORD LENGTH	18.15% C	20.75% C	25.19% C

C=LOCAL WING CHORD LENGTH
 WING CHORD = 20.8163 - (.2449 * X_F)
 WHERE X_F IS ANY WING STATION
 MEASURED FROM THE FUSELAGE
 CENTERLINE.

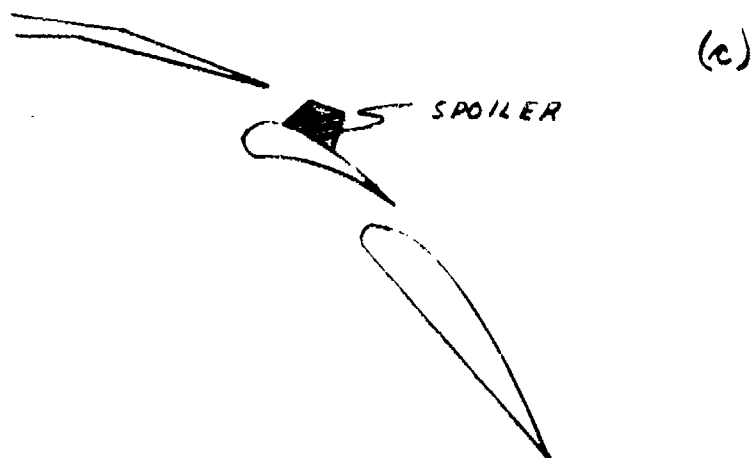
AILERON - OUTBOARD
WING FLAP - TRIPLE
SLOTTED - MST W.T. MODEL



DOUBLE-SLOTTED FLAP

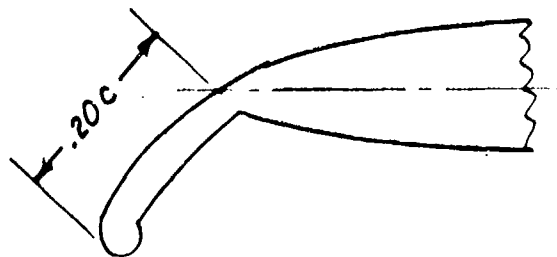


BLOWN AILERON



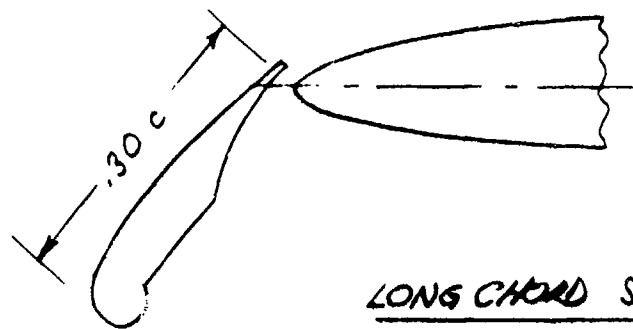
VANE SPOILER

(a)



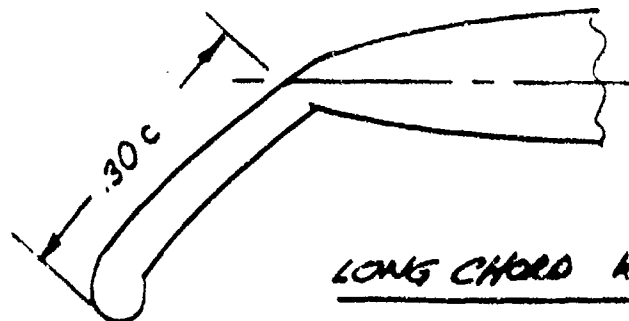
SHORT CHORD KRUEGER

(b)



LONG CHORD SLOTTED KRUEGER

(c)



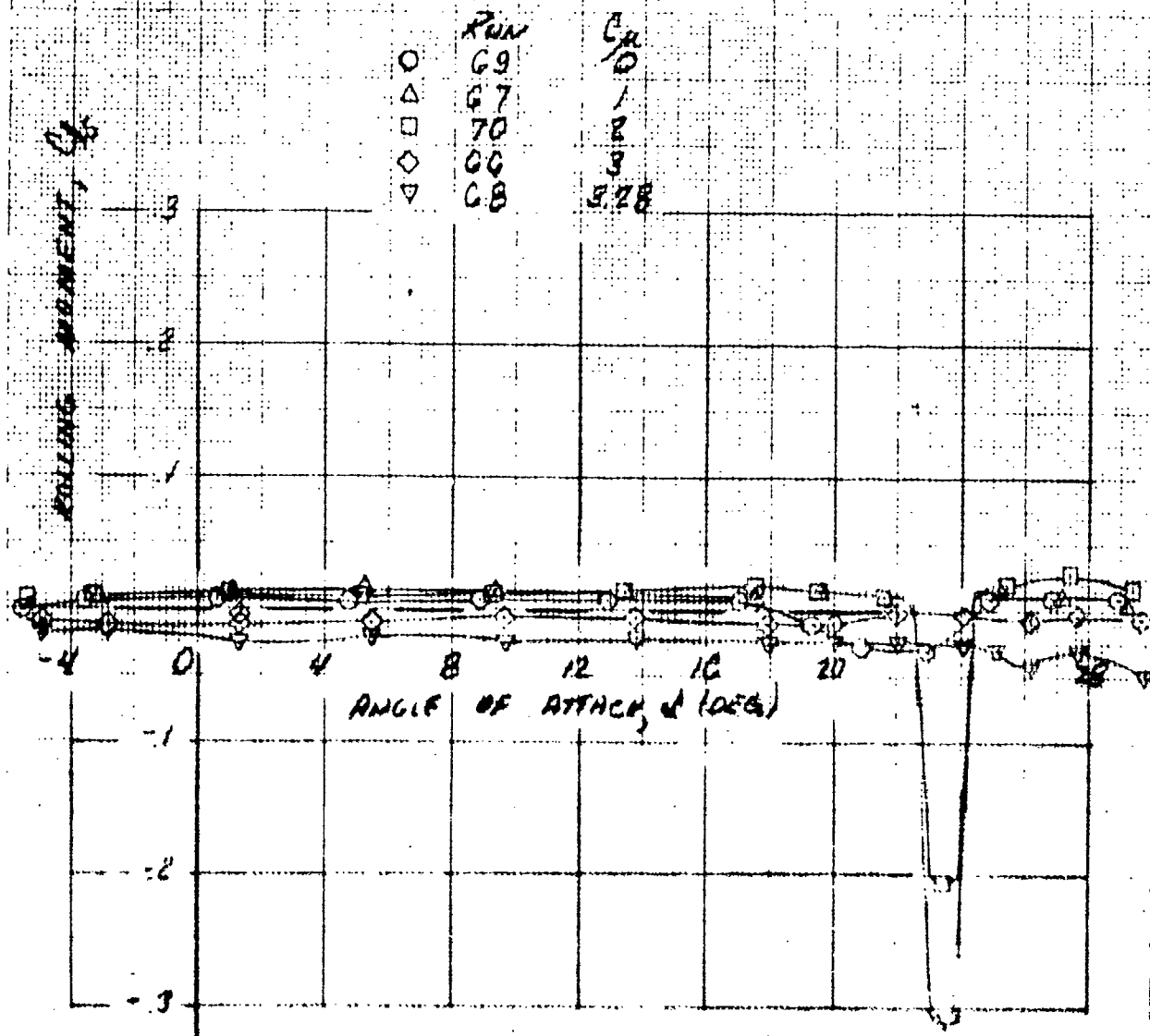
LONG CHORD KRUEGER

LSWT-090

ROLLING MOMENT WITH FOUR ENGINE THRUST

$S_F = 25/50$

TAIL OFF



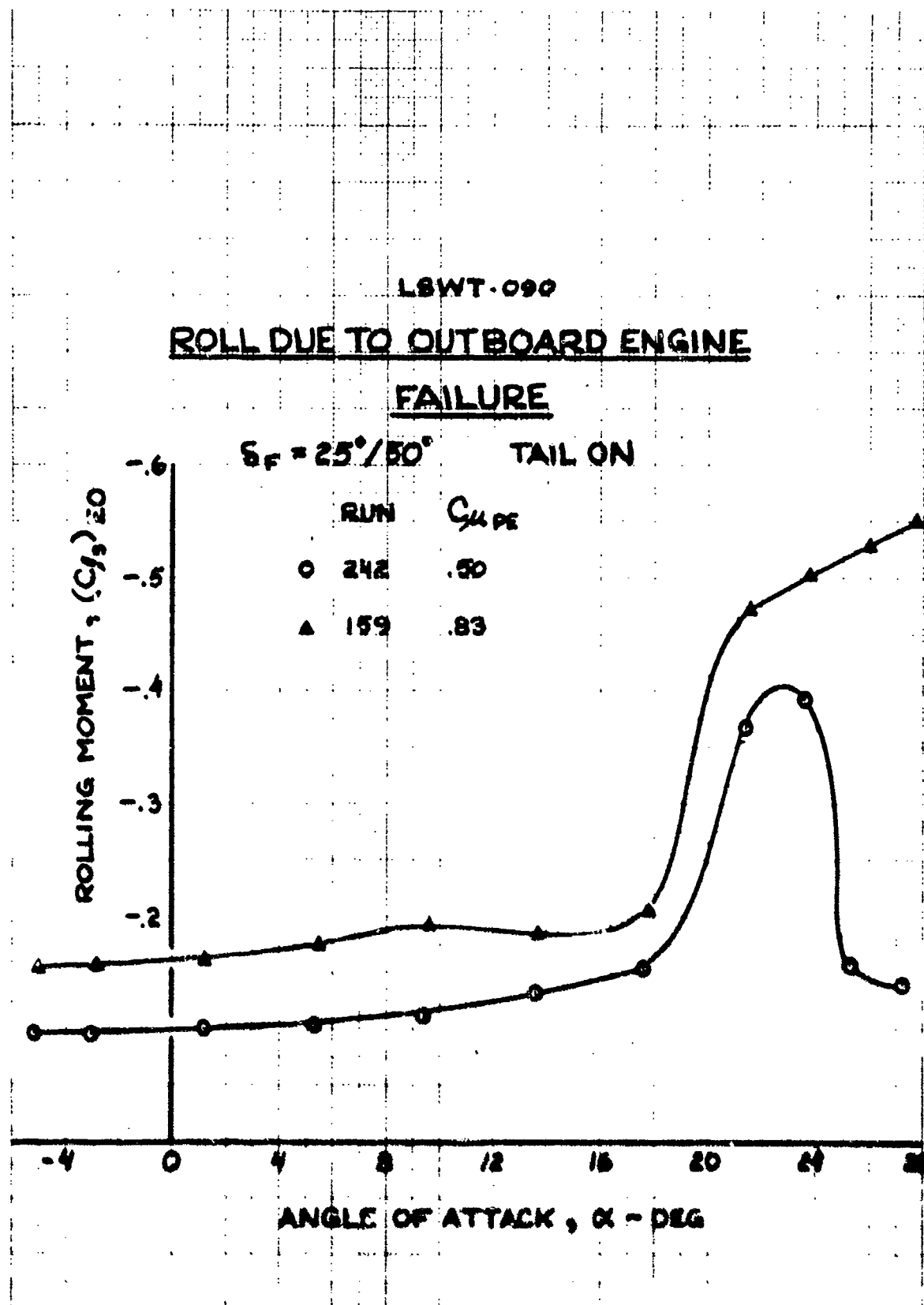
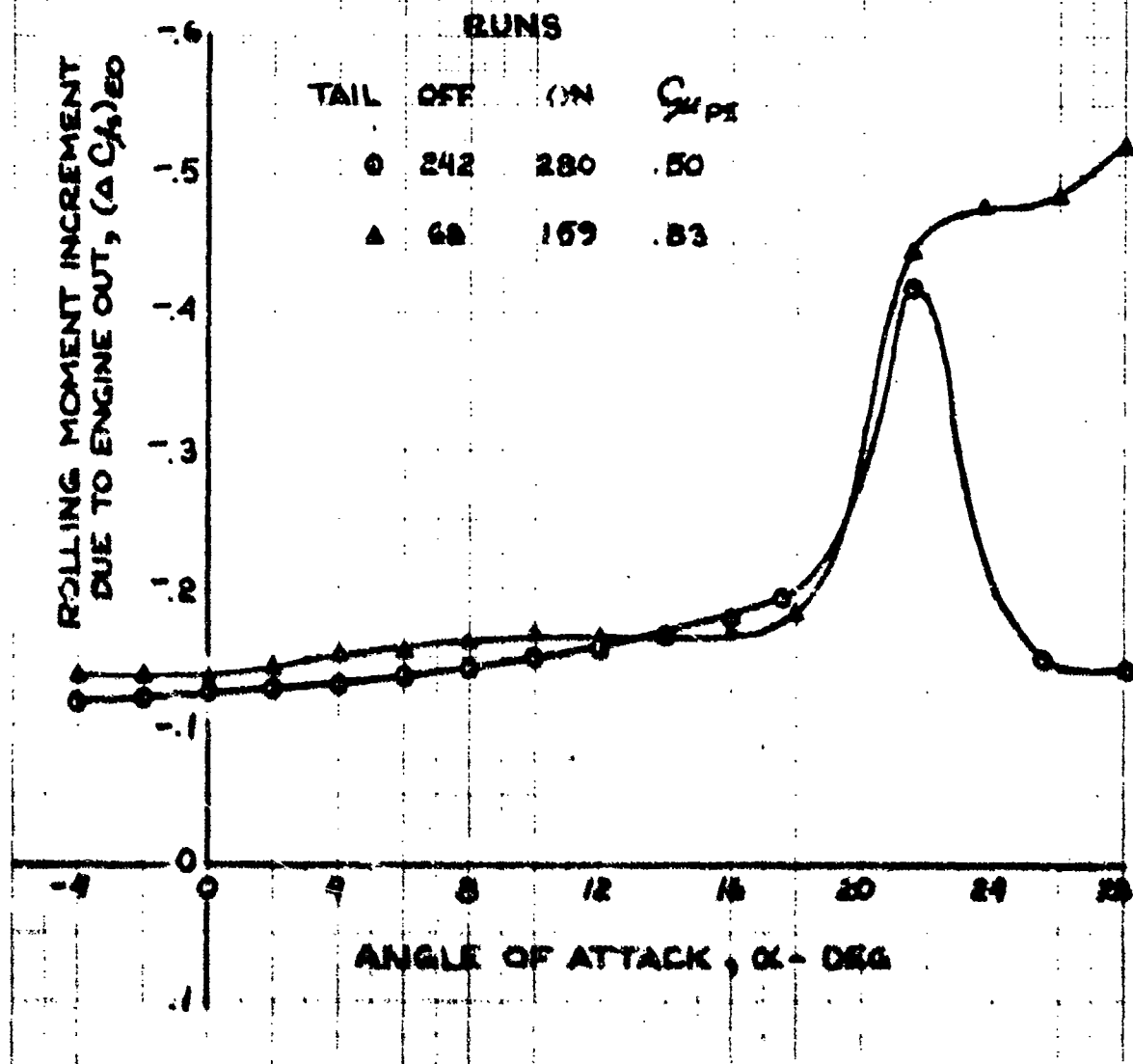


Figure 14.1.2

LSWT-090

ROLL DUE TO OUTBOARD ENGINE FAILURE

$\delta_F = 25^\circ/50^\circ$



LSWT-090

EFFECT OF OUTBOARD ENGINE FAILURE ON LIFT

$\delta_F = 25^\circ/50^\circ$ - TAIL OFF - LONG KRUEGERS

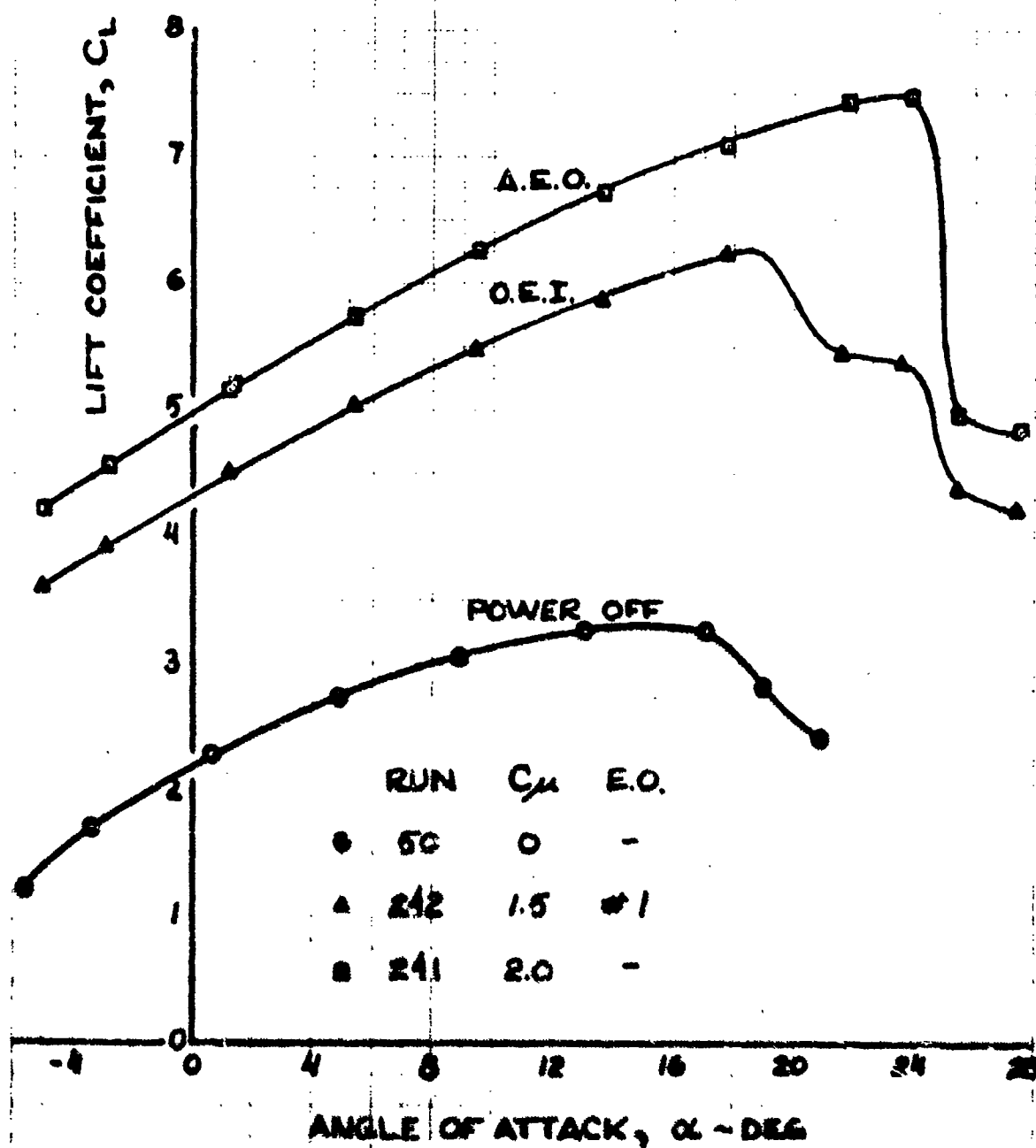


Figure 14.1.4

LSWT-090
INBOARD VERSUS OUTBOARD ENGINE FAILURE
ROLLING MOMENT COMPARISON

$\delta_e = 25^\circ/50^\circ$

TAIL OFF

LONG KRUEGERS INSTALLED

	RUNS	CH	E.O.
○	243	1.5	#3
△	242	✓	#4

NOTE: SIGN OF ROLLING MOMENT FOR
 RUN 242 CHANGED TO REFLECT
 #4 ENGINE FAILURE

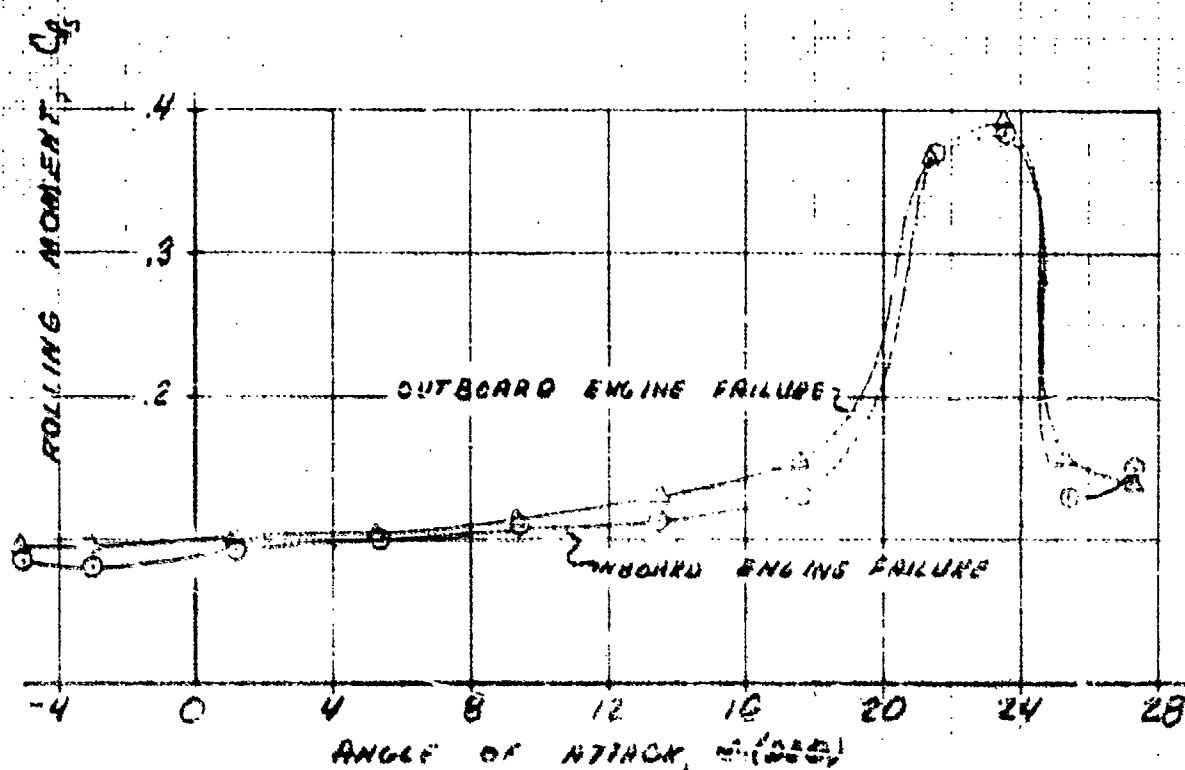
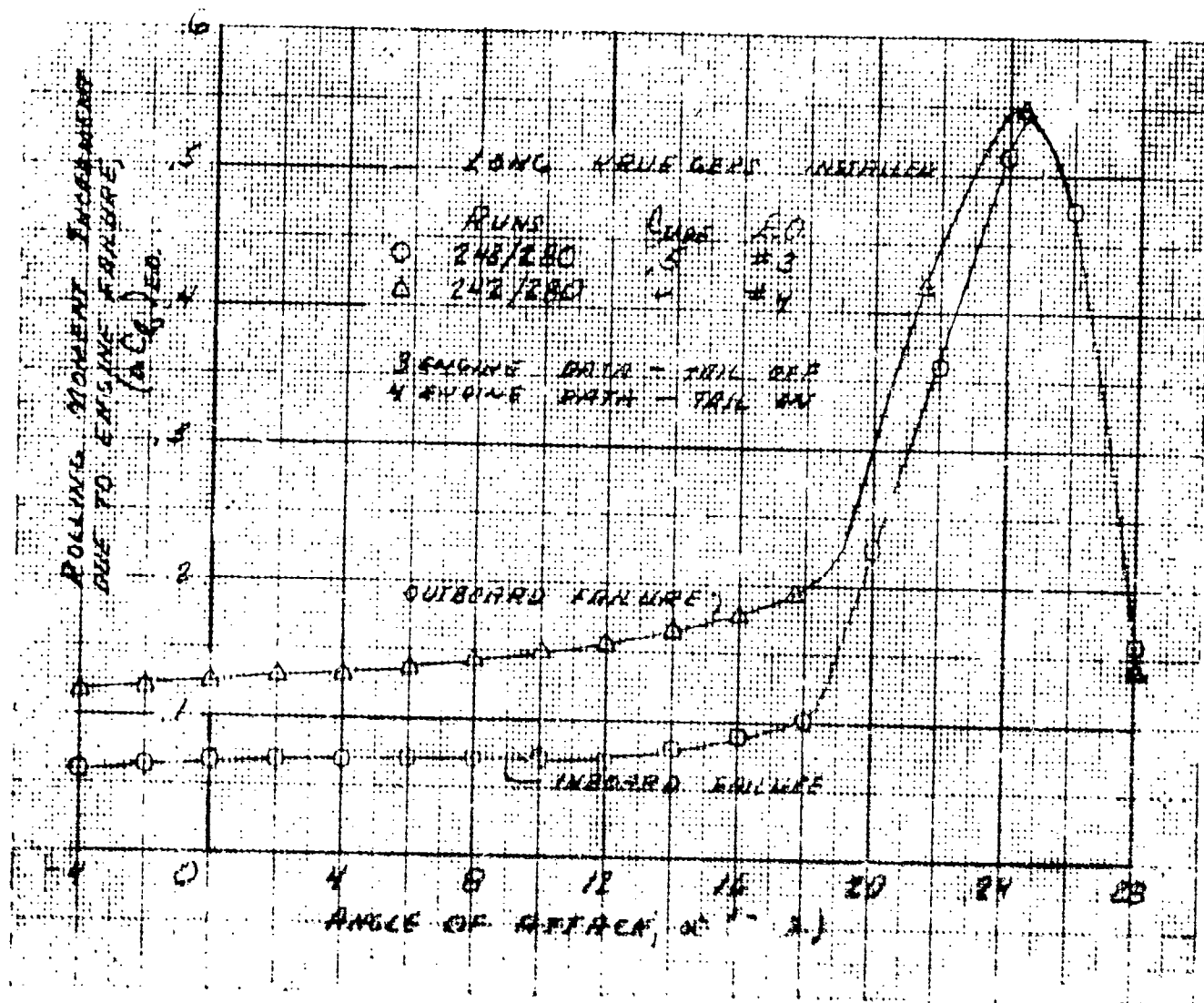


Figure 14.1.5

LSWT 0.00

$\delta_f = 25^\circ, 50^\circ$



ROLLING MOMENT INBOARD DUE TO ENGINE FAILURE (ACG) ED.

ANGLE OF ATTACK, α (°)

11.1.0

LSWT-090
ROLLING MOMENT WITH FOUR ENGINE THRUST

$\phi = 35^\circ / 60^\circ$

TAIL OFF

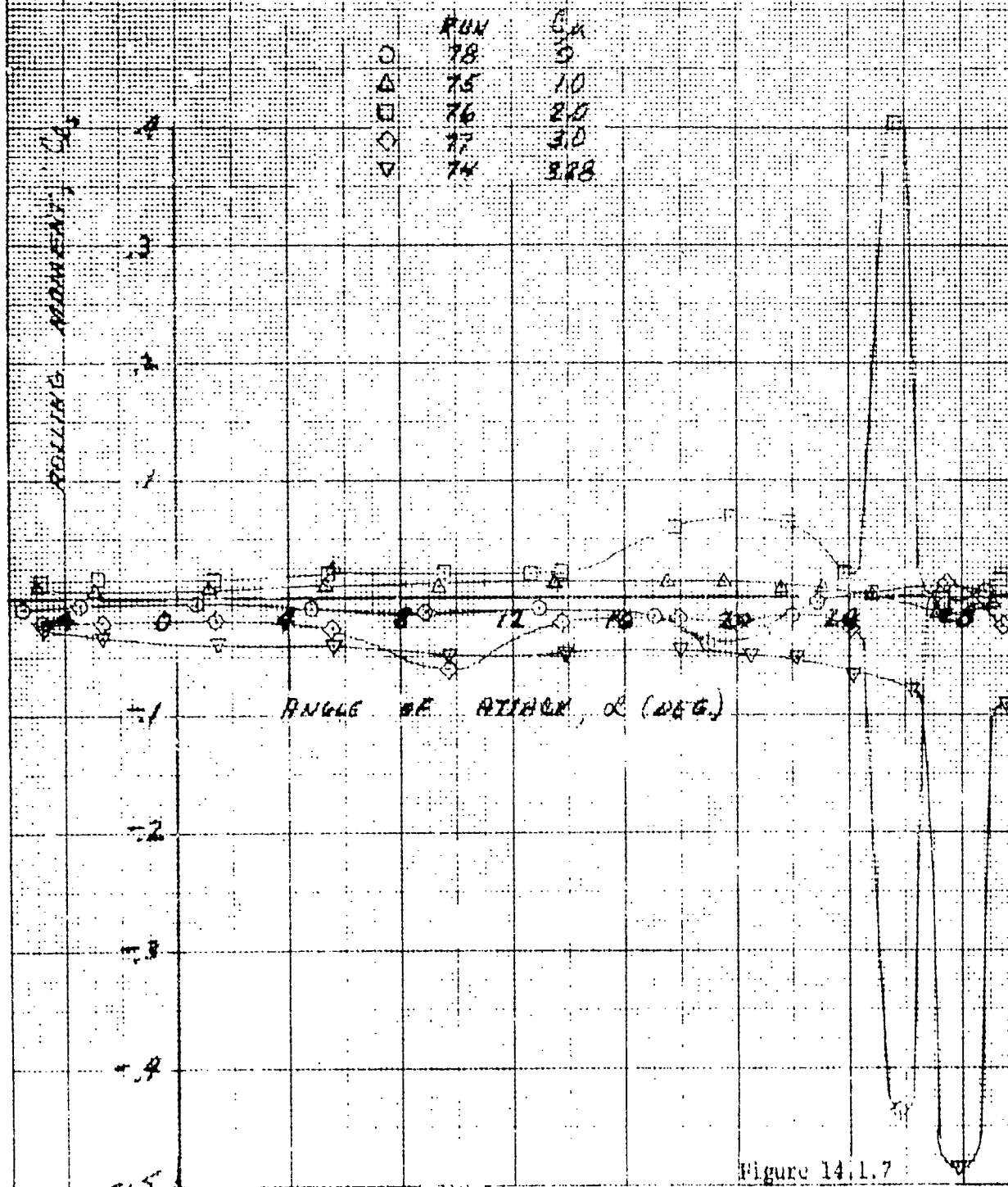


Figure 14.1.7

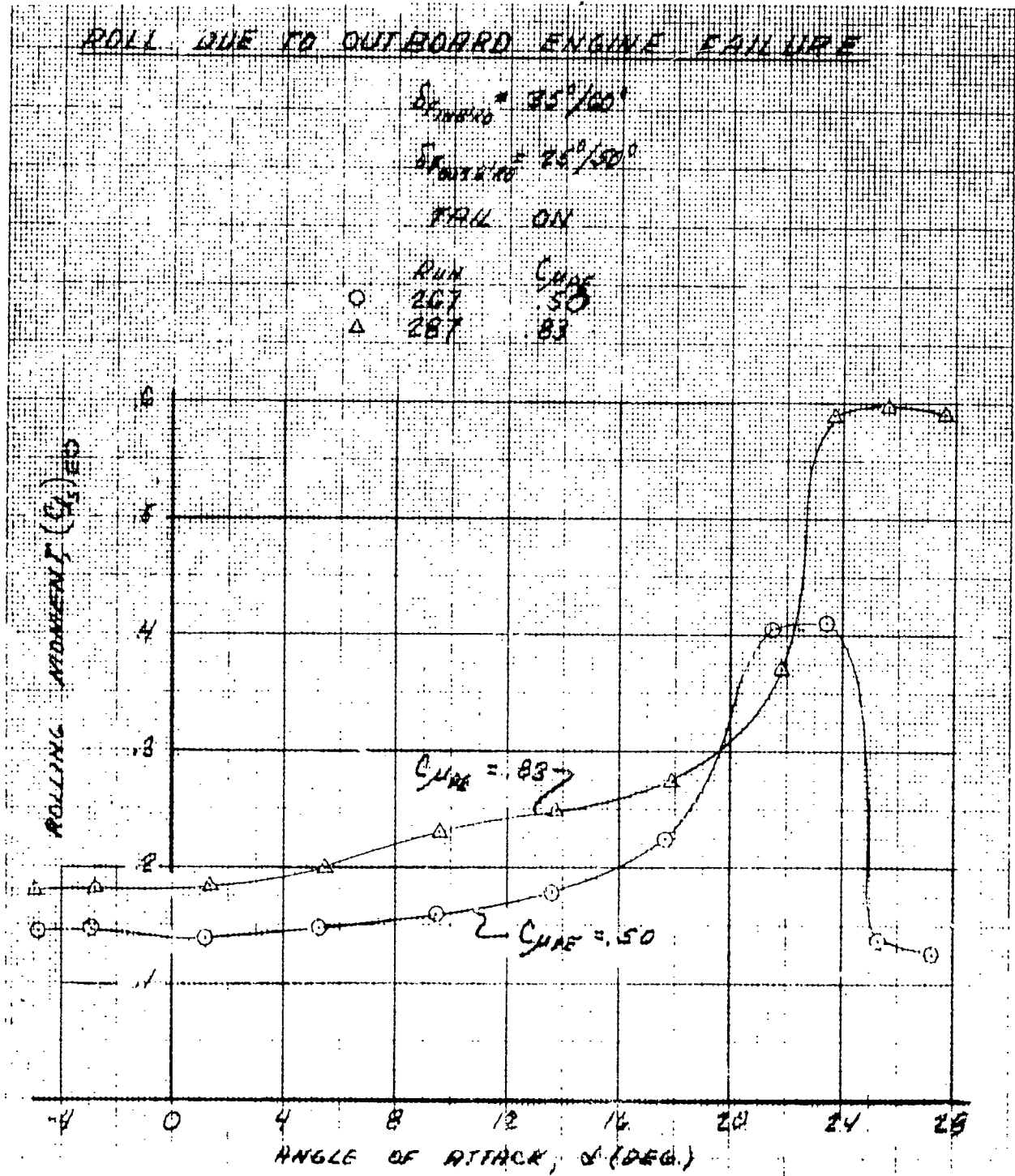
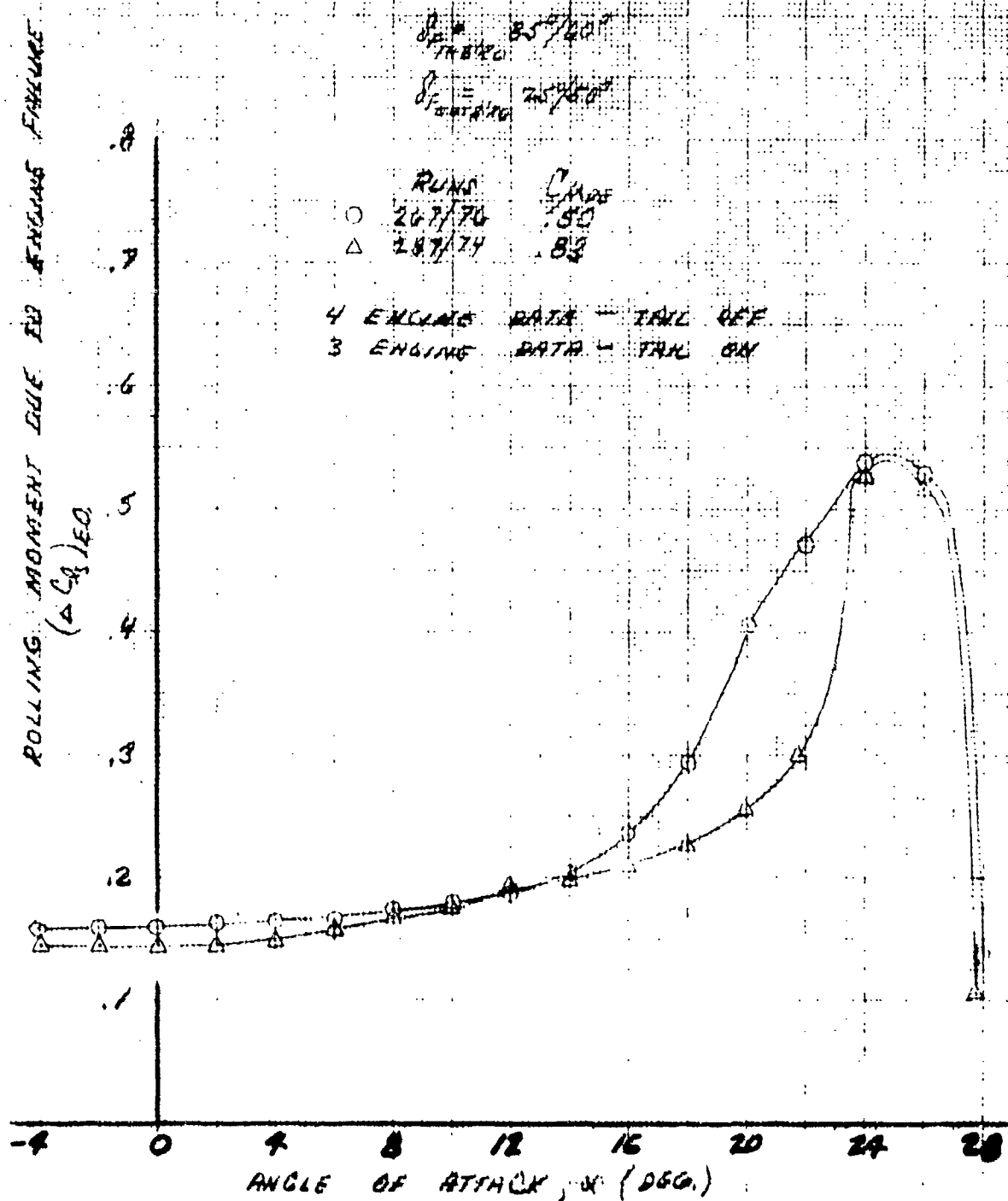


Figure 14.1.8

LSWT-090 ROLL DUE TO OUTBOARD ENGINE FAILURE

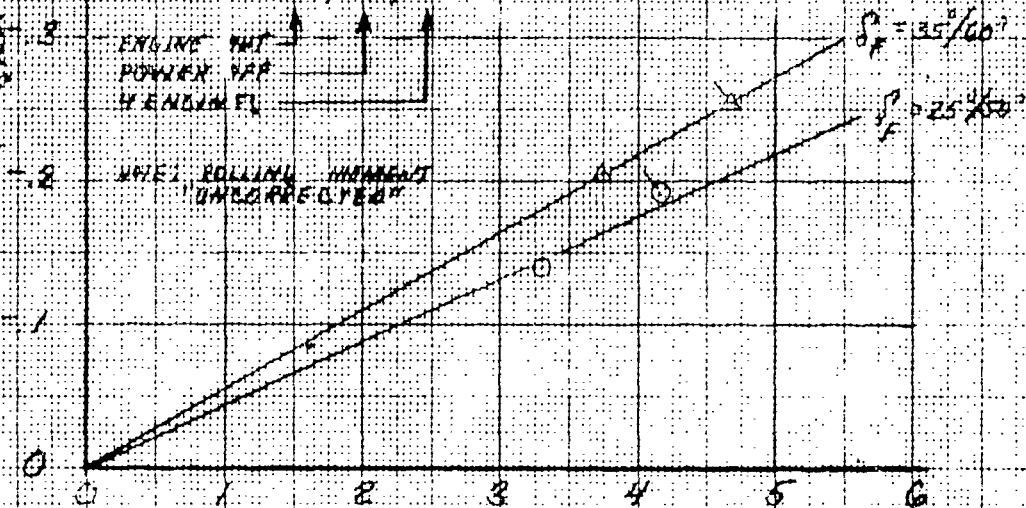


ROLL DUE TO ENGINE FAILURE VERSUS POWERED LIFT (OUTBOARD ENGINE)

($\alpha = 16^\circ$)

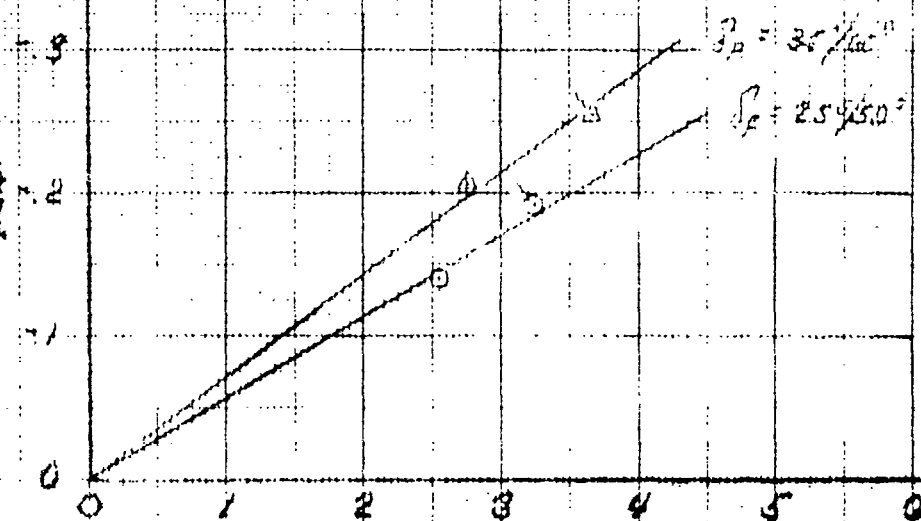
	PLANS	δ_F	C_{LTP}
○	254/257/280	$25^\circ/50^\circ$.50
○	24/102/48	—	.83
○	207/78/76	$35^\circ/60^\circ$.50
△	287/78/74	—	.83

ROLLING MOMENT DUE
TO ENGINE FAILURE,
(C_{LTP})



($\Delta C_{L TRIM}$) POWER 4 ENG.

ROLLING MOMENT DUE
TO ENGINE FAILURE,
(C_{LTP})



($\Delta C_{L TRIM}$) POWER 3 ENG.

Figure 14.1.10

LSWT-090 CENTER OF PRESSURE OF LOAD DUE TO ENGINE FAILURE

$\delta_c = 25^\circ/90^\circ$

TRAIL DEF

$C_{M_{AE}} = .5$

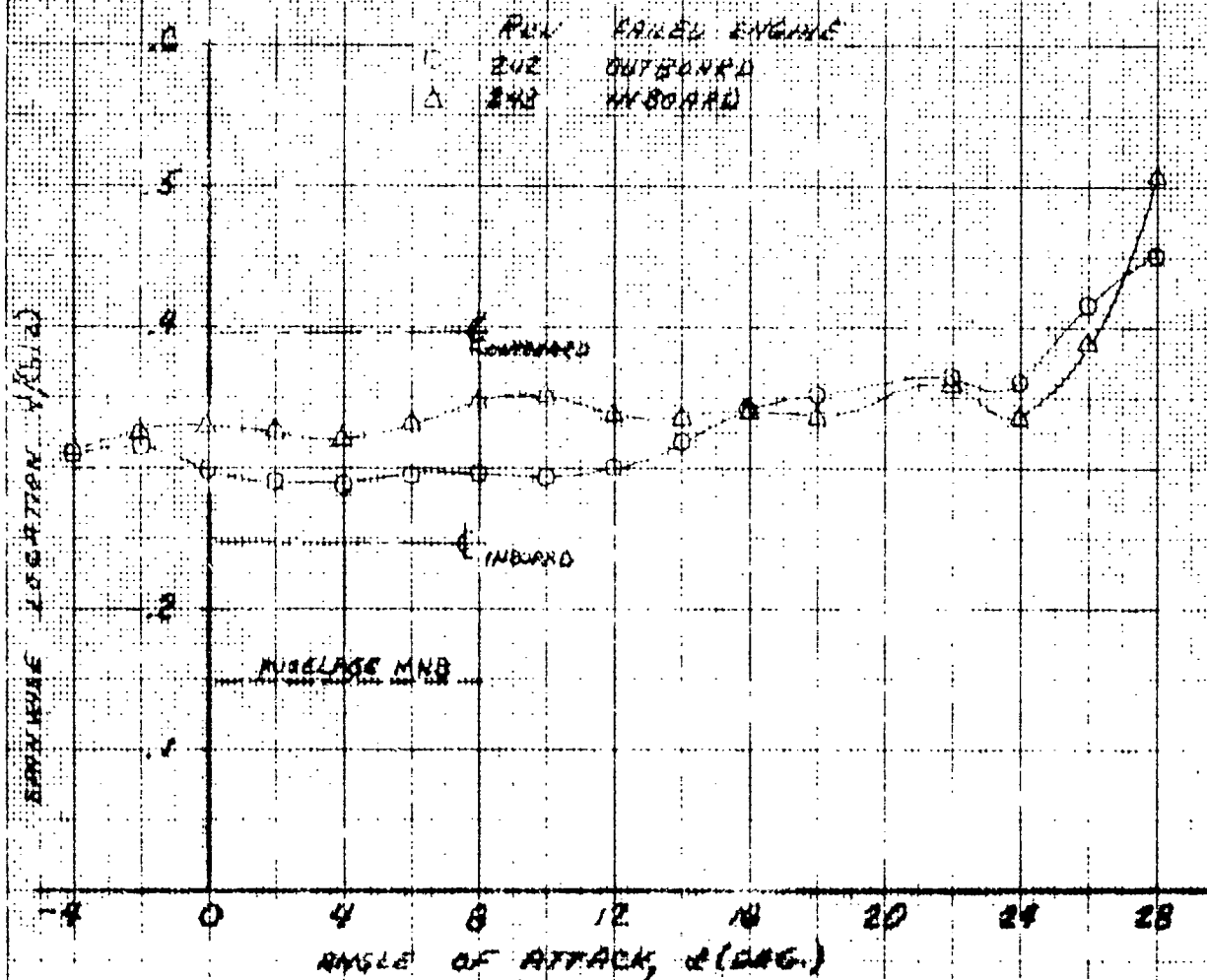


Figure 1d.1.1b

LOWE

CENTER OF PRESSURE OF LOAD DUE TO ENGINE FAILURE

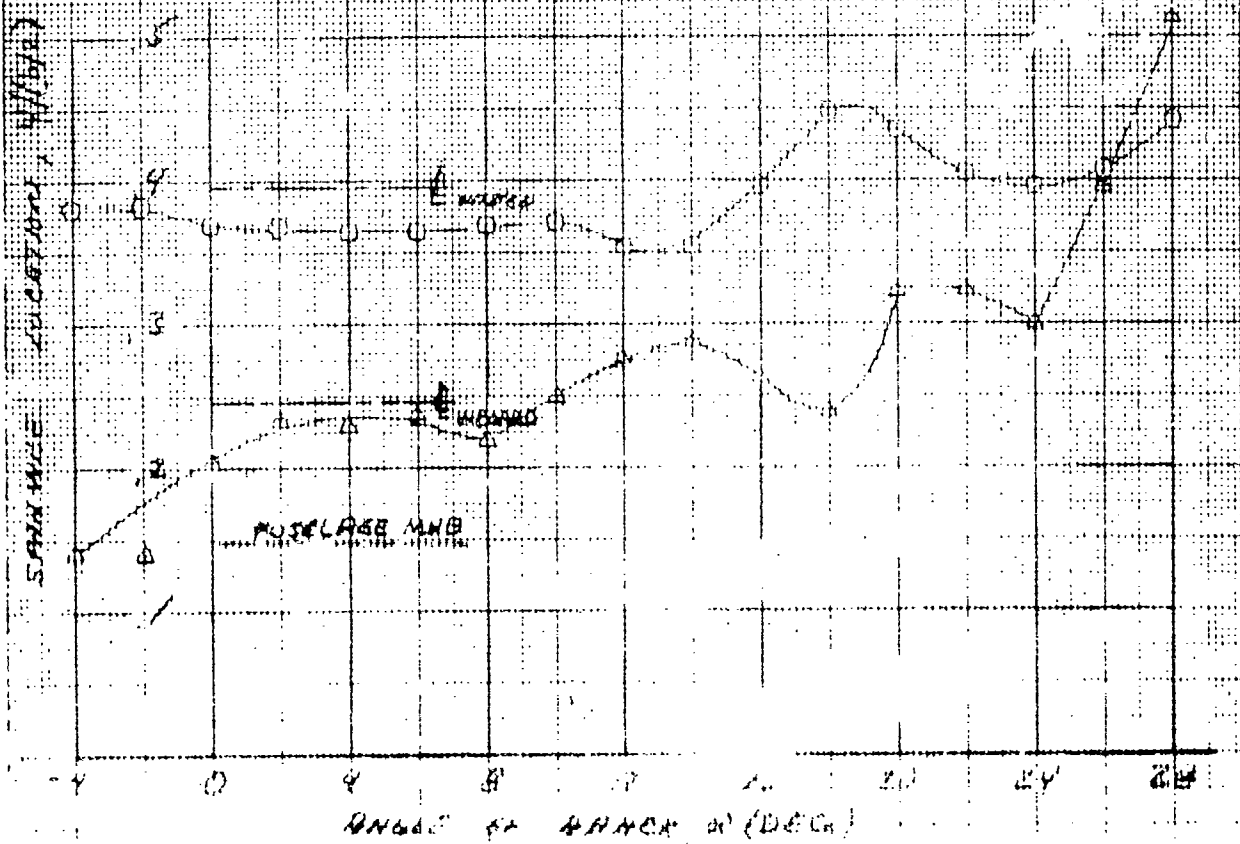
$\beta = 25^\circ 10'$

TAIL DEK

$C_{m,0} = 1.0$

Run	ENGINE
1	242/241
2	242/241

NOTE: CORRECTED FOR ASYMMETRIC GAUGES



LSWT-090
EFFECT OF TAIL ON ROLLING MOMENT
WITH OUTBOARD ENGINE INOPERATIVE

$$\delta_F = 25^\circ/50^\circ$$

$$C_{MN} = .50$$

	RUN	TAIL
O	242	OFF
Δ	259	ON

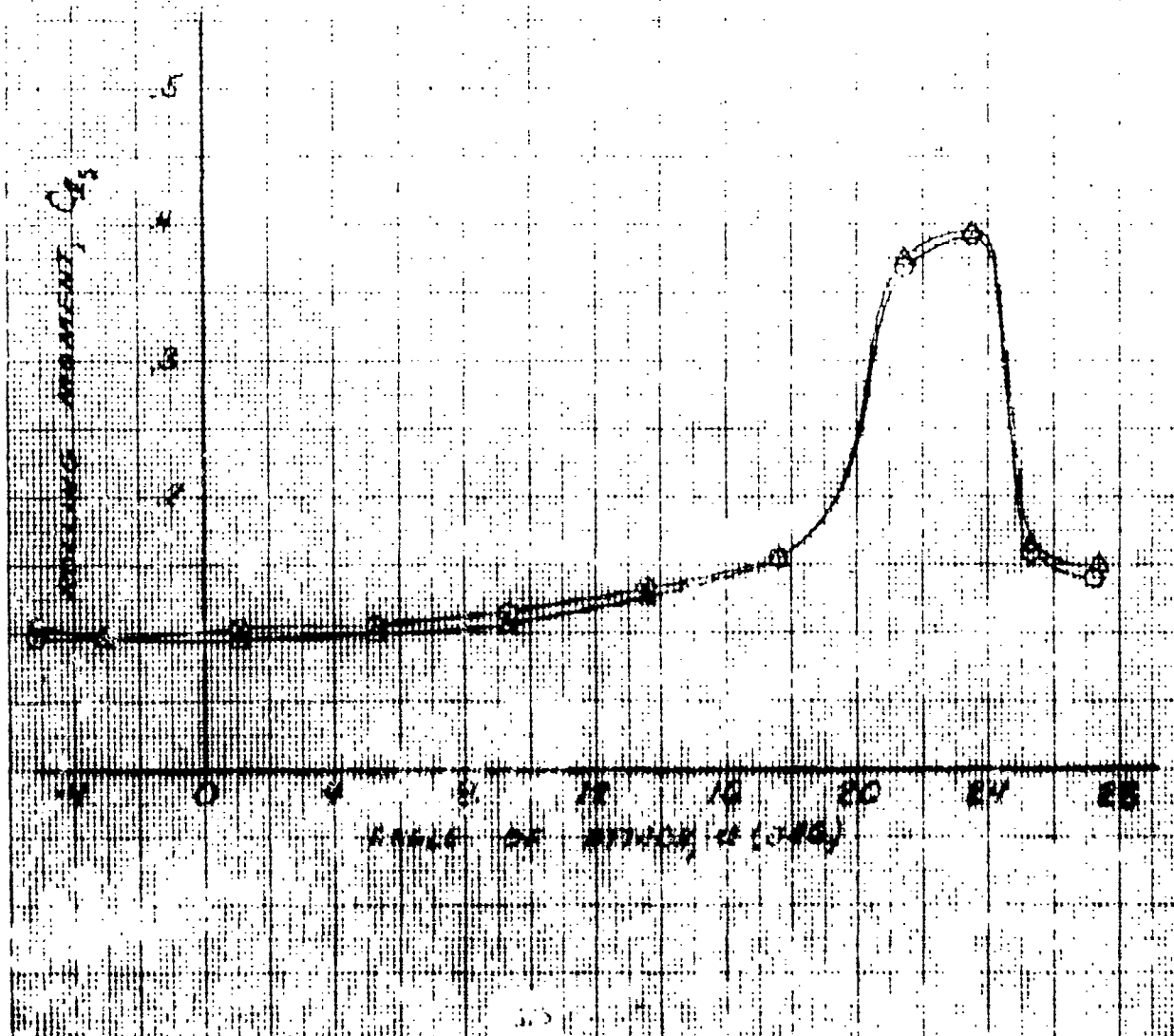


Figure 14.2.1

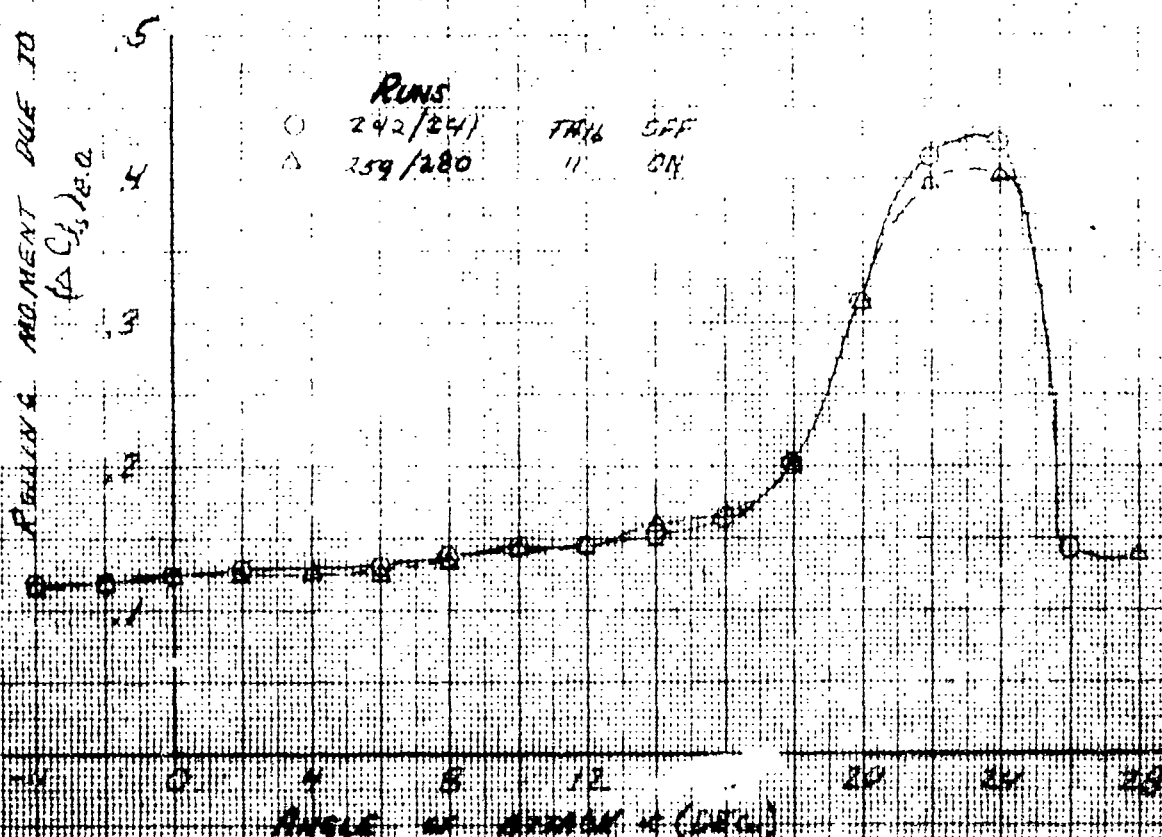
LSWT-090
EFFECT OF TAIL ON ROLLING MOMENT
WITH OUTBOARD ENGINE INOPERATIVE

$$\delta_F = 25^\circ/30^\circ$$

$$C_{M_{tail}} = .50$$

ROLLING MOMENT DUE TO ENGINE FAILURE

(ΔC_L)_{R.O.}

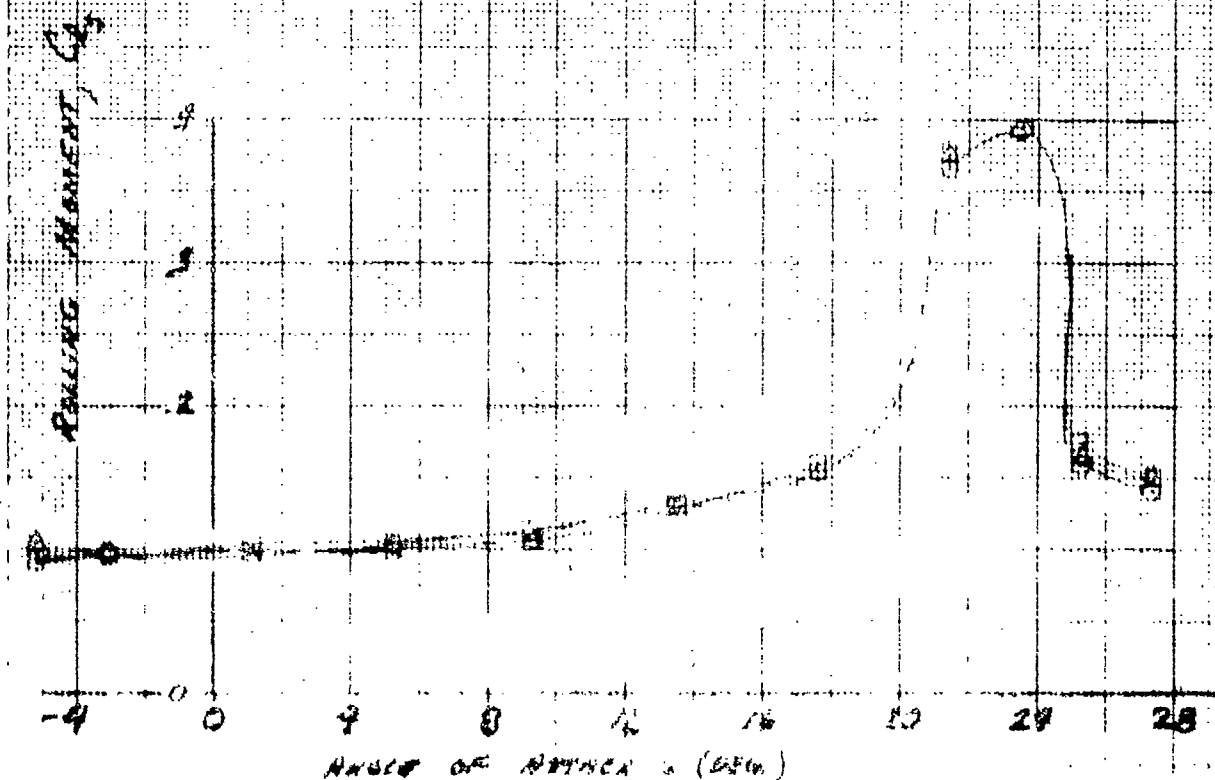


LSWT-280
 EFFECT OF LONG SLOTTED FLENDER ON ROLL
 WITH ALL OUTRIGGER ENGINE FAILURE

$\beta = 25/50$

$C_{LAW} = 5$

	Run	Flare	Flender (OUTBOARD)
○	292	OFF	LONG
△	257	ON	LONG SLOTTED
□	260	"	LONG SLOT/LONG WASSLUT



LSWT-090

EFFECT OF VANE SPOILER ON ROLL DUE TO MAIN SPOILERS

$C_L = 2.0$

$\delta = 25^\circ/50^\circ$

$\delta_{SP} = 10/50$

$\delta_{SP} = 10/40$

TAIL ON

ROLLING MOMENT INCREMENT,
(ΔC_L)_{SP} + δ_{SP}

(ΔC_L)_{SP} + δ_{SP}

2
4
6
8

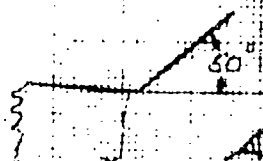
0 4 8 12 16 20 24

ANGLE OF ATTACK, α (DEG.)

ΔC_L
285-280
286-280

δ_{SP}
10/50
10/40

WITH VANE SPOILER



VANE SPOILER

MAIN SPOILER

ROLL INCREMENT DUE TO AIRFLOW

$$S_2 = 207.40'$$

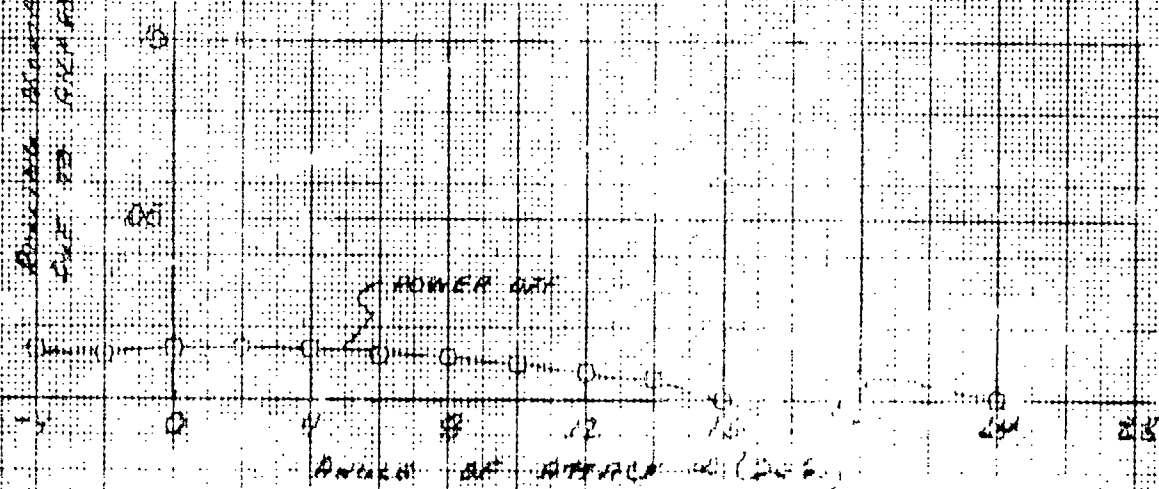
$$S_1 = 25.50'$$

TAKE OFF

$$S_{10} = 10'$$

ROLL INCREMENT DUE TO AIRFLOW
DUE TO AIRFLOW INCREMENT, (S_1, S_2, S_{10})

NAME: GRADE:
DATE: PAGE:



LSWT-090

ROLL INCREMENT DUE TO SPOILER PANELS + AILERON

$$\delta_{\alpha} = 10/50^{\circ}$$

$$\delta_{\beta} = 20/300$$

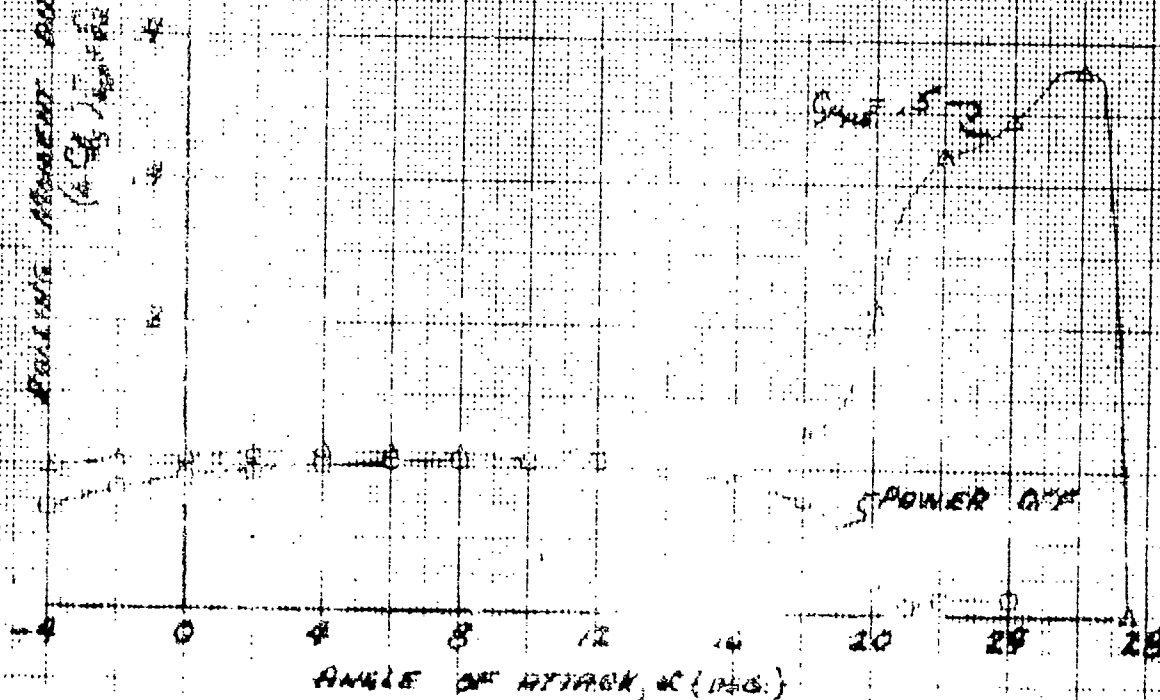
$$\delta_{\gamma} = 25/50^{\circ}$$

TAIL ON

FOUR ENGINE THRUST

	URNS	GRADE
○	12/142	0
△	123/180	1.5"

ROLL INCREMENT DUE TO SPOILER PANELS + AILERON,
($\delta_{\alpha}, \delta_{\beta}, \delta_{\gamma}$)



ROLLING MOMENT DUE TO OUTBOARD SPOILER DEFLECTION

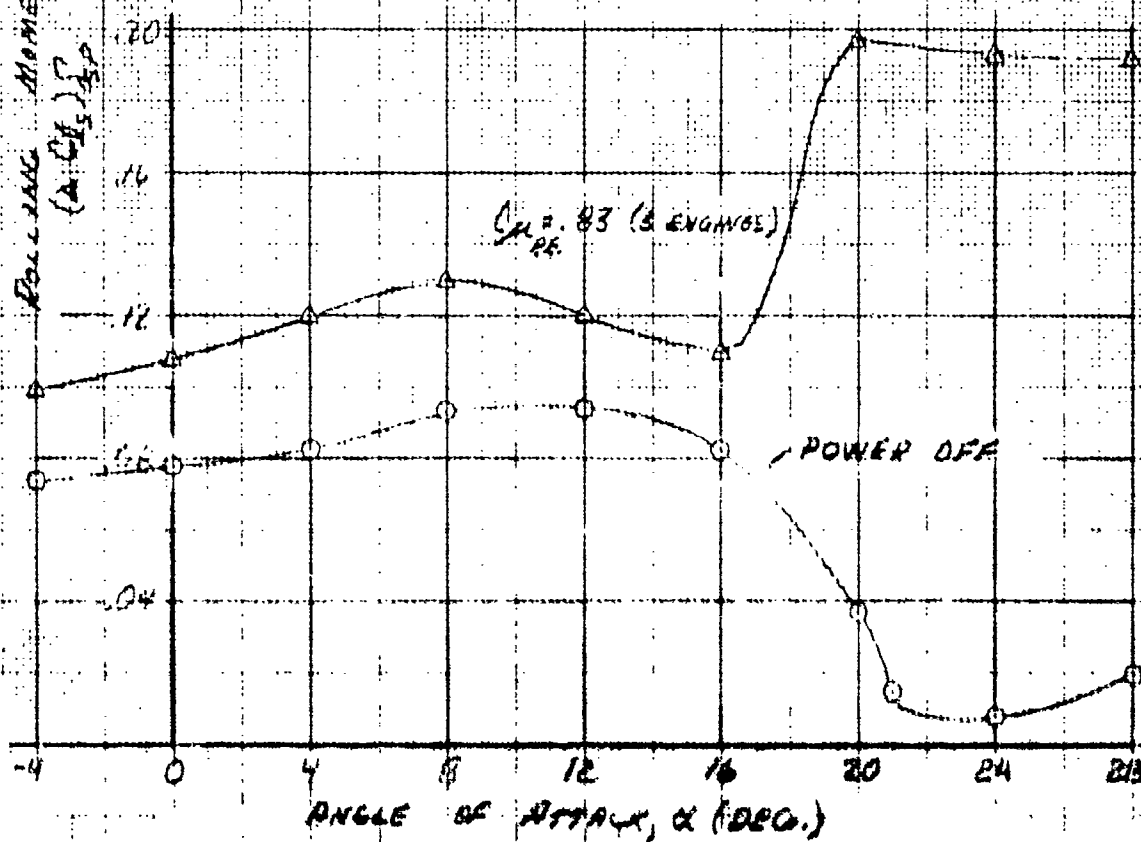
LSWT ~090

$\delta_{SP} = -10^\circ/50^\circ$

TAIL ON $\delta_F = 25^\circ/50^\circ$

RUNS
 O 184-182
 Δ 170-159

$C_{L_{REF}}$
 O
 82 3 ENGINE DATA



ROLL INCREMENT DUE TO OUTBOARD SPOILER (+5)

ROLL INCREMENT DUE TO PROPER AIRWHEELS WITH
WITH/WITHOUT BALANCE

$$\frac{d\theta}{dt} = \frac{2\pi}{T}$$

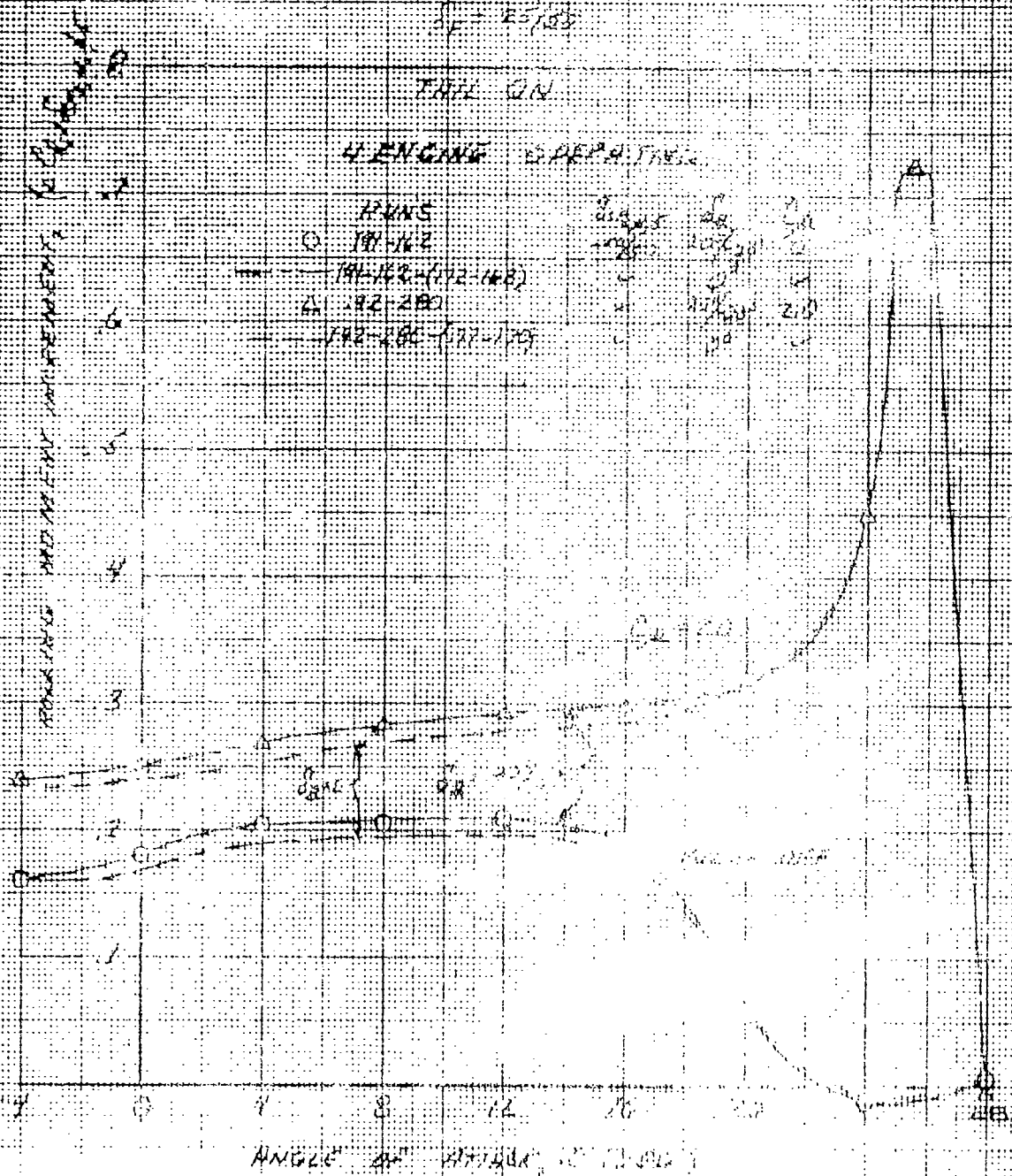
$$T = 25.133$$

TAIL ON

4 ENGINE OPERATIONS

RUNS
 1. 100-162
 2. 141-163-172-168
 3. 192-280
 4. 142-280-177-175

1. 100-162
 2. 141-163-172-168
 3. 192-280
 4. 142-280-177-175

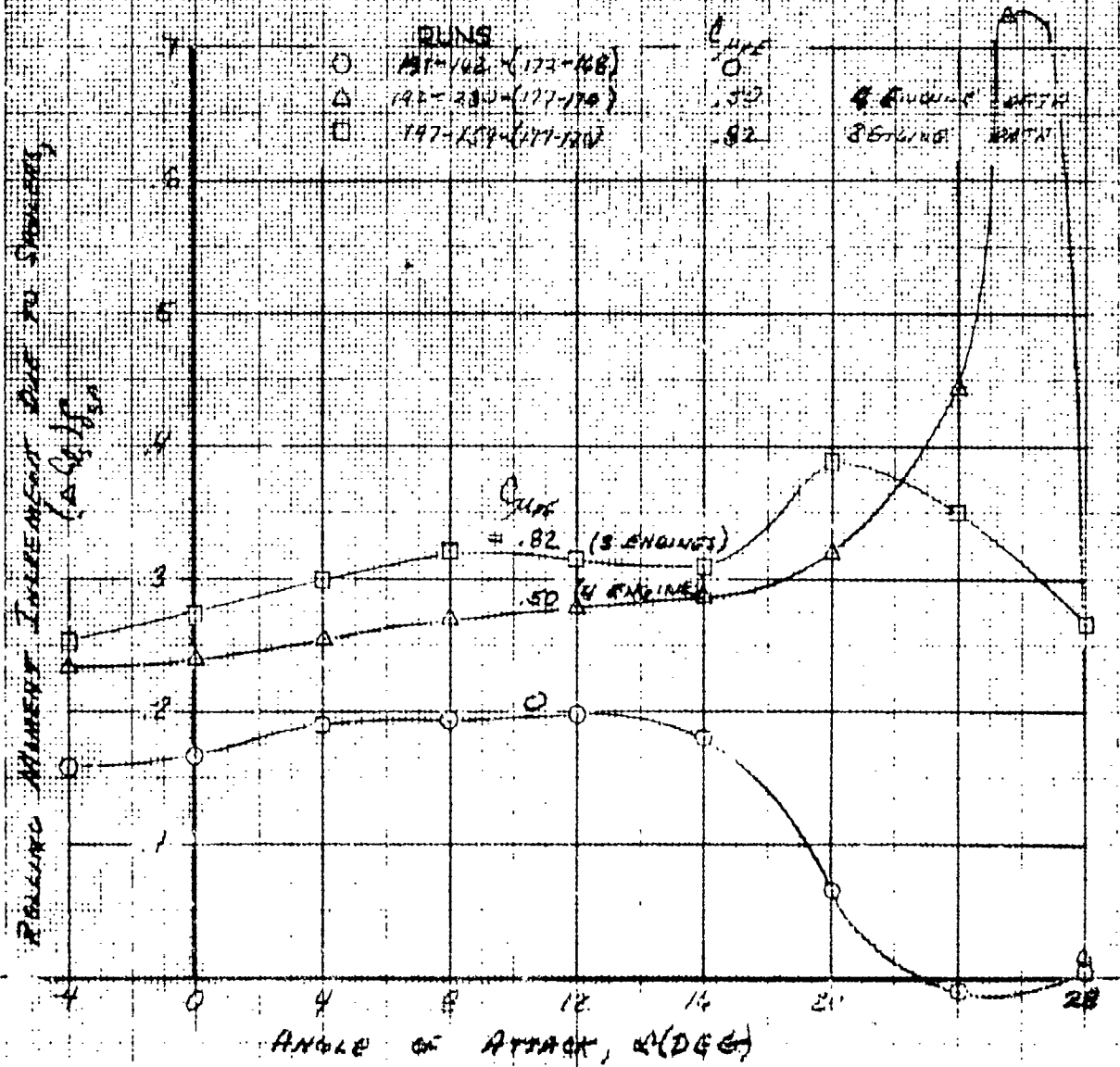


LSWT-090

$$\delta_{\text{roll}} = -\frac{1}{2} \frac{V}{V_0}$$

$$\delta_{\text{roll}} = \frac{25}{50}$$

TAIL ON



ROLL INCREMENT DUE TO SPOILER PANELS 3, 4, & 5

LSWT-090

EFFECT OF SPOILER ON THREE ENGINE LIFT

$\delta = 25^\circ/50^\circ$

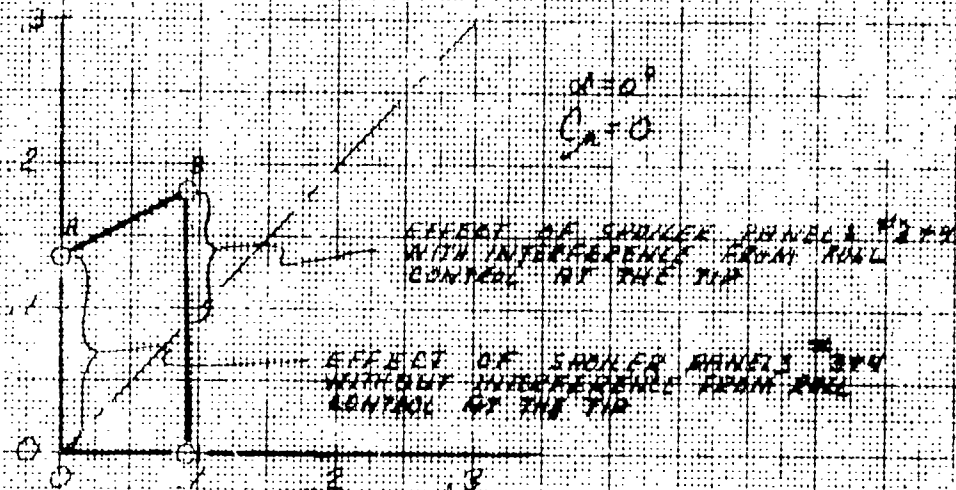
TAKE ON



ROLL CAPABILITY OF THE TIP SPOILER + ALERON WHEN USED WITH #3 AND #4 SPOILER PANELS

TAIL ON

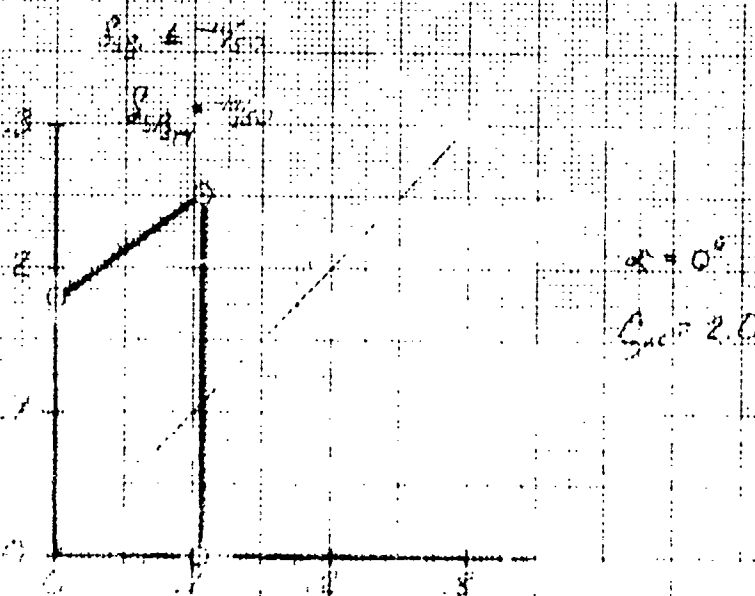
ROLLING MOMENT INCREMENT
DUE TO SPOILER,
(ΔC_L)_{SPOILER}



ROLLING MOMENT INCREMENT
DUE TO SPOILER PLUS ALERON

$$(\Delta C_L)_{SPOILER + ALERON}$$

ROLLING MOMENT INCREMENT
DUE TO SPOILER,
(ΔC_L)_{SPOILER}



ROLLING MOMENT INCREMENT
DUE TO SPOILER PLUS ALERON

$$(\Delta C_L)_{SPOILER + ALERON}$$

LSWT-090 ROLL INCREMENT DUE TO SPOTTER PANELS 1/2

$P_{1/2} = 10^\circ/100^\circ$

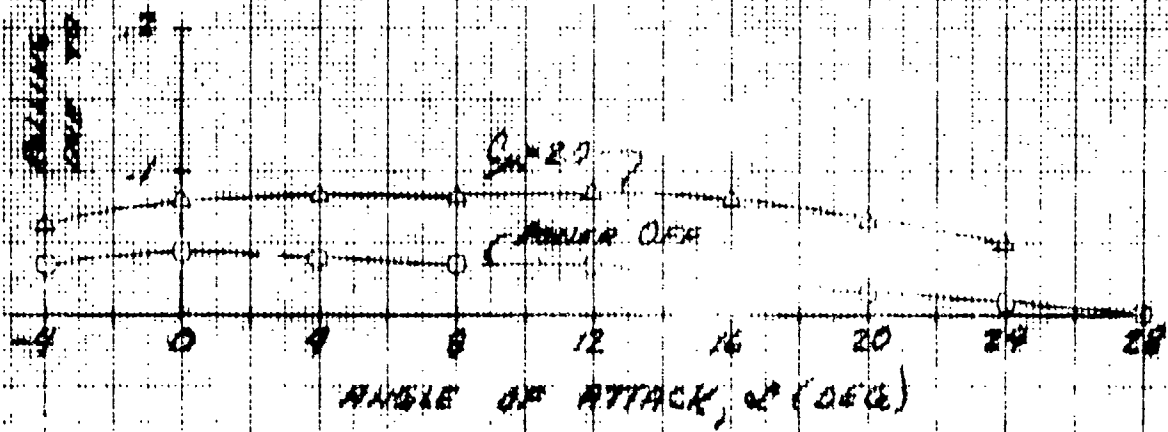
$P_{1/2} = 25^\circ/100^\circ$

TAIL ON

4 ENGINES OPERATING

	Rolls	$P_{1/2}$	$C_{R1/2}$	NOTE
○	495-191 - (178-164)	10/100	0	INCREASING TRENCH WITH PANELS 1/2
△	495-192 - (177-170)	25/100	2.0	

Rolling Moment Increment Due to Spotter Panels 1/2 (2.0) $C_{R1/2}$



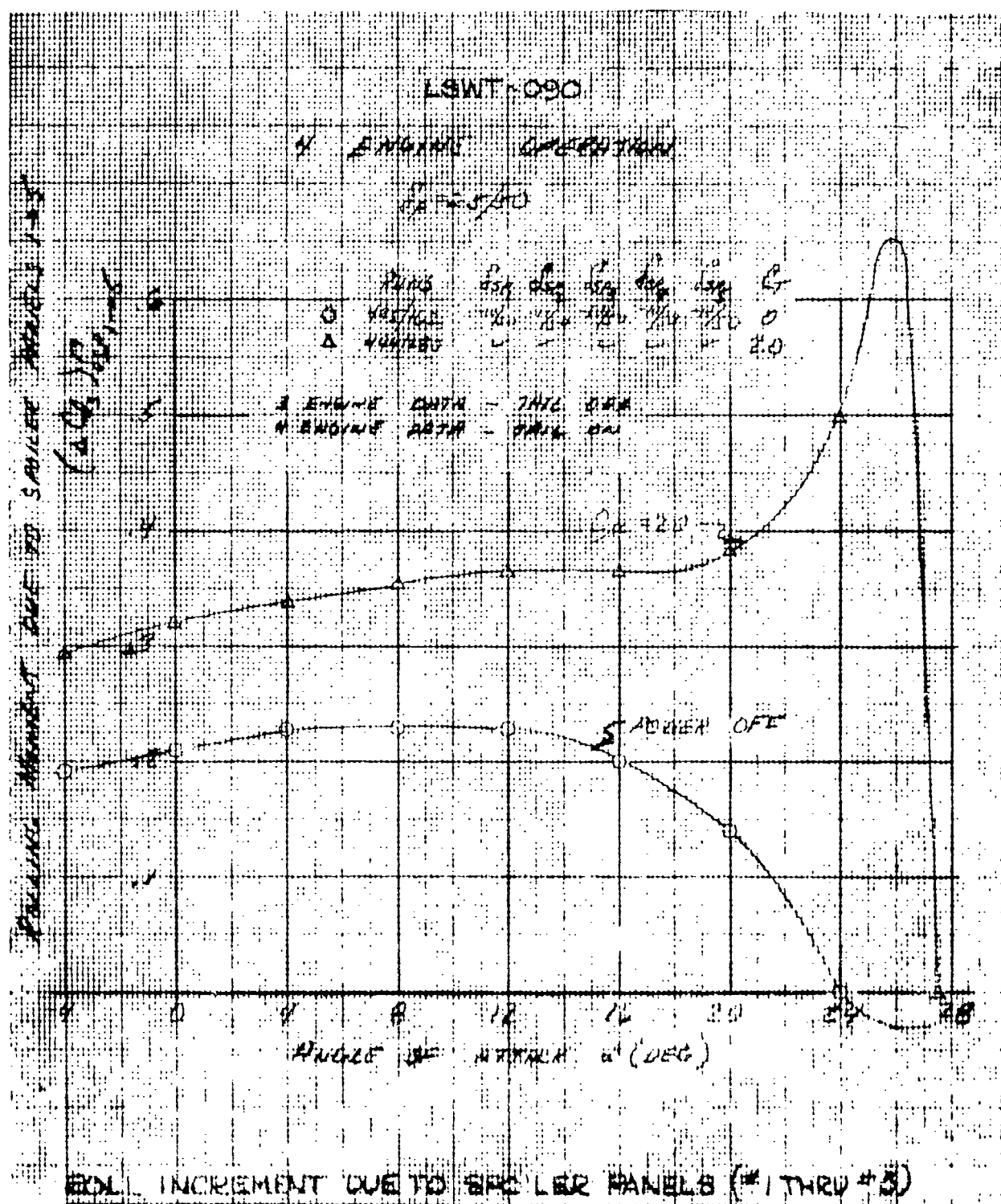


Figure 14.4.10

LSWT-0803

ROLL INCREMENT DUE TO VARIOUS SAILER POWERS

$\Delta = 10$

$\alpha = 0^\circ$

$\delta_1 = 25/50$

TAIL ON

ROLL INCREMENT DUE TO SAILER, $(\Delta \phi)_{\text{roll}}$

24
12
0
-12
-24

24
12
0
-12
-24

24
12
0
-12
-24

SAILER POWERS

7-5

8-4

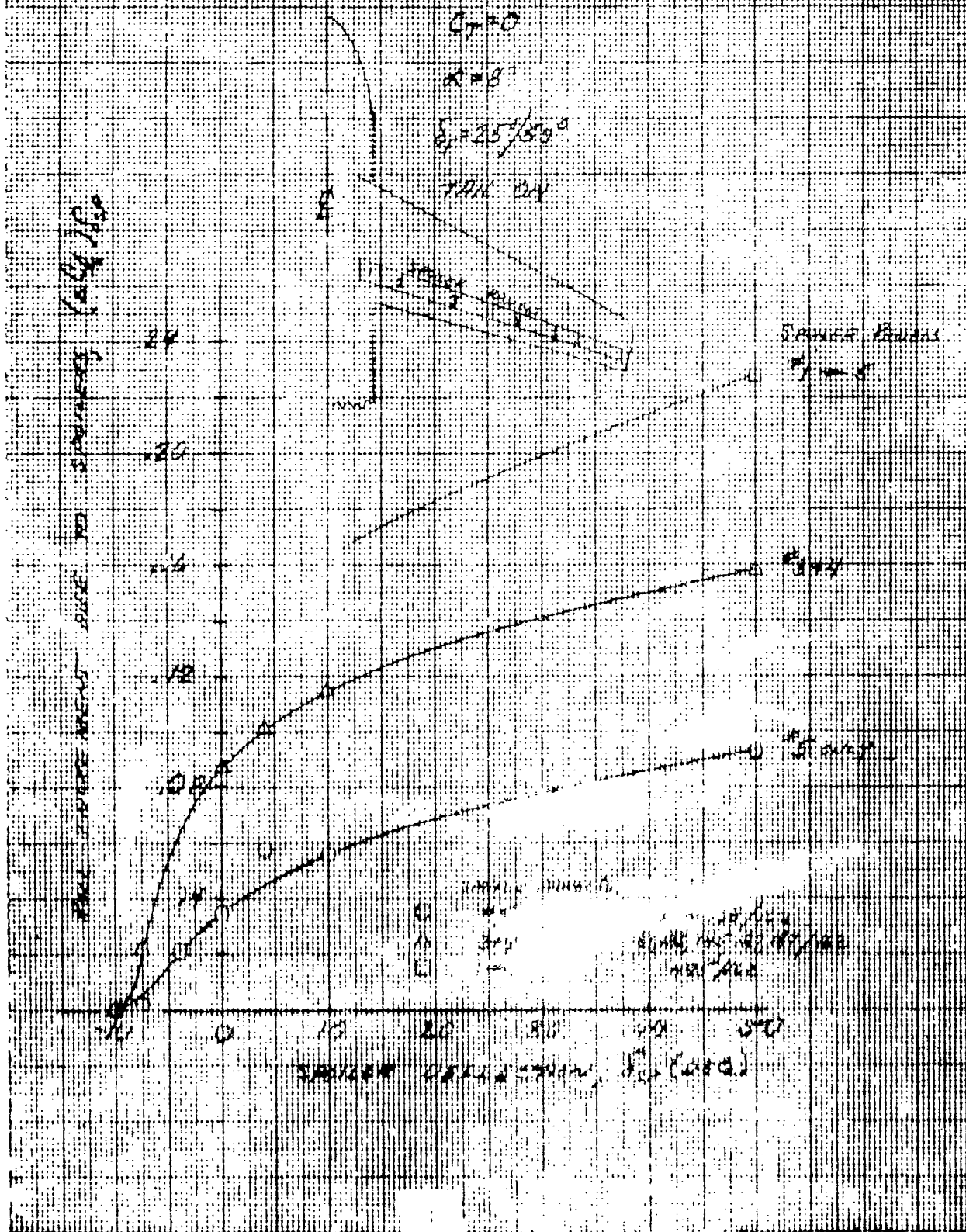
9-3

10
11
12

100, 100, 100
100, 100, 100
100, 100, 100

SAILED IN POSITION (0000)

ROLL INCREMENT DUE TO VARIOUS SPOONER PANELS



ASNT-080

ROLL INCREMENT DUE TO VARIOUS SAKER PANELS

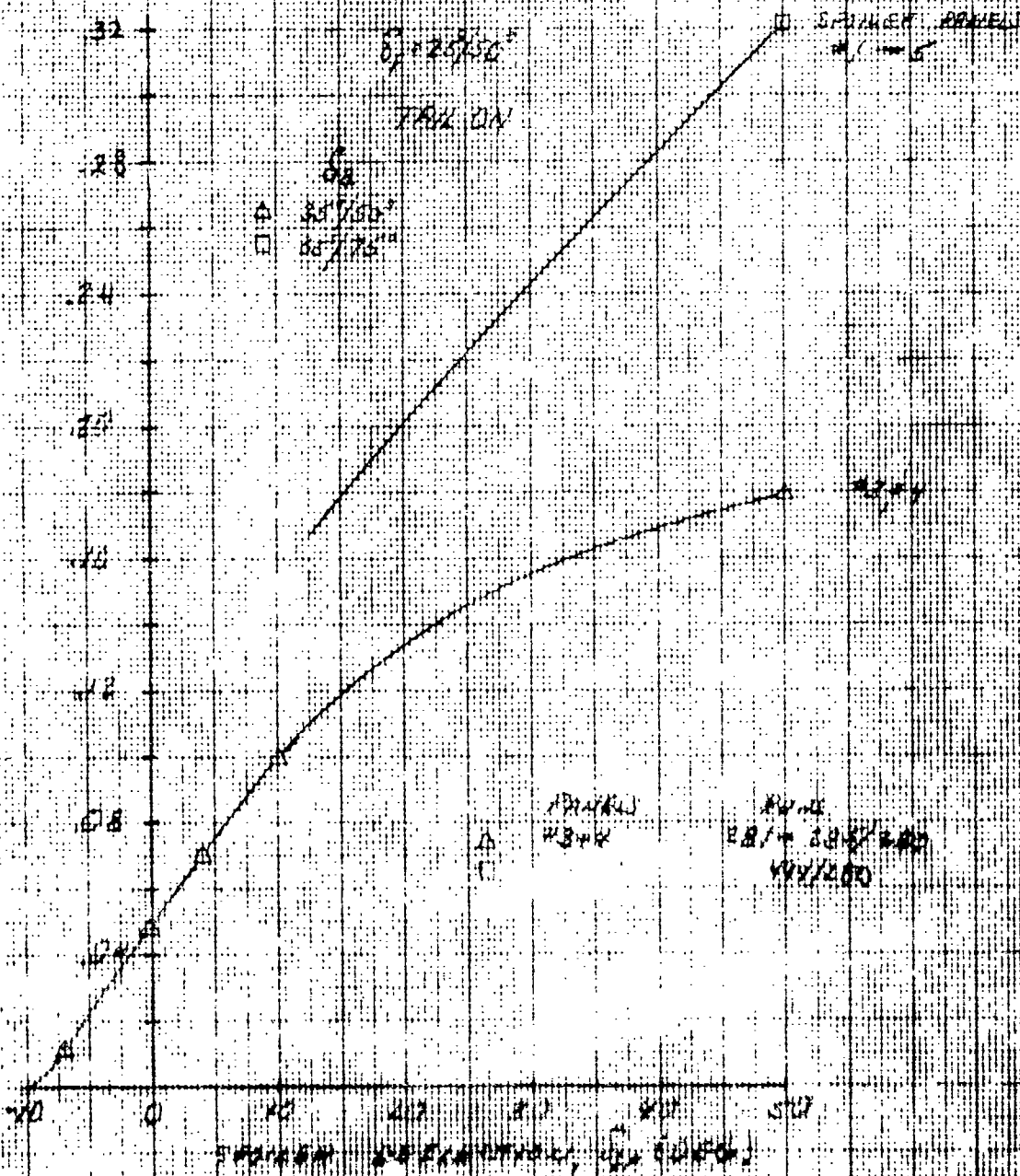
$L = 10$

$\alpha = 0^\circ$

$\delta_p = 25/100^\circ$

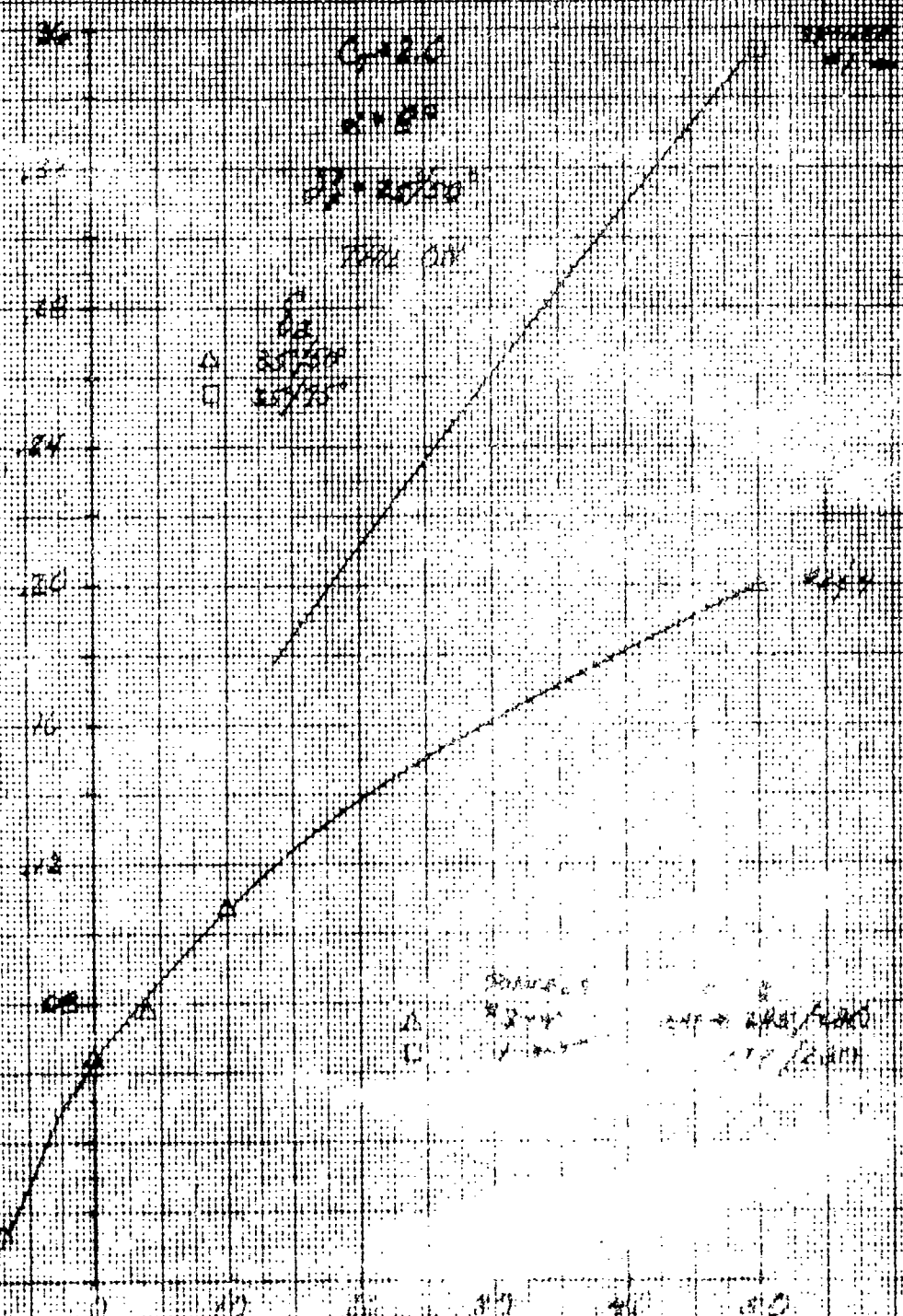
TAIL ON

ROLL INCREMENT DUE TO SAKER PANEL



ROLL INCREMENT DUE TO VARIOUS SOURCES

Roll Increment Due to Various Sources (all in degrees)



Source: $\frac{C}{V^2}$ (all in degrees)

LSWT-090
ROLL DUE TO VARIOUS SPOILERS VERSUS SYMMETRIC LIFT

4 ENGINE OPERATION

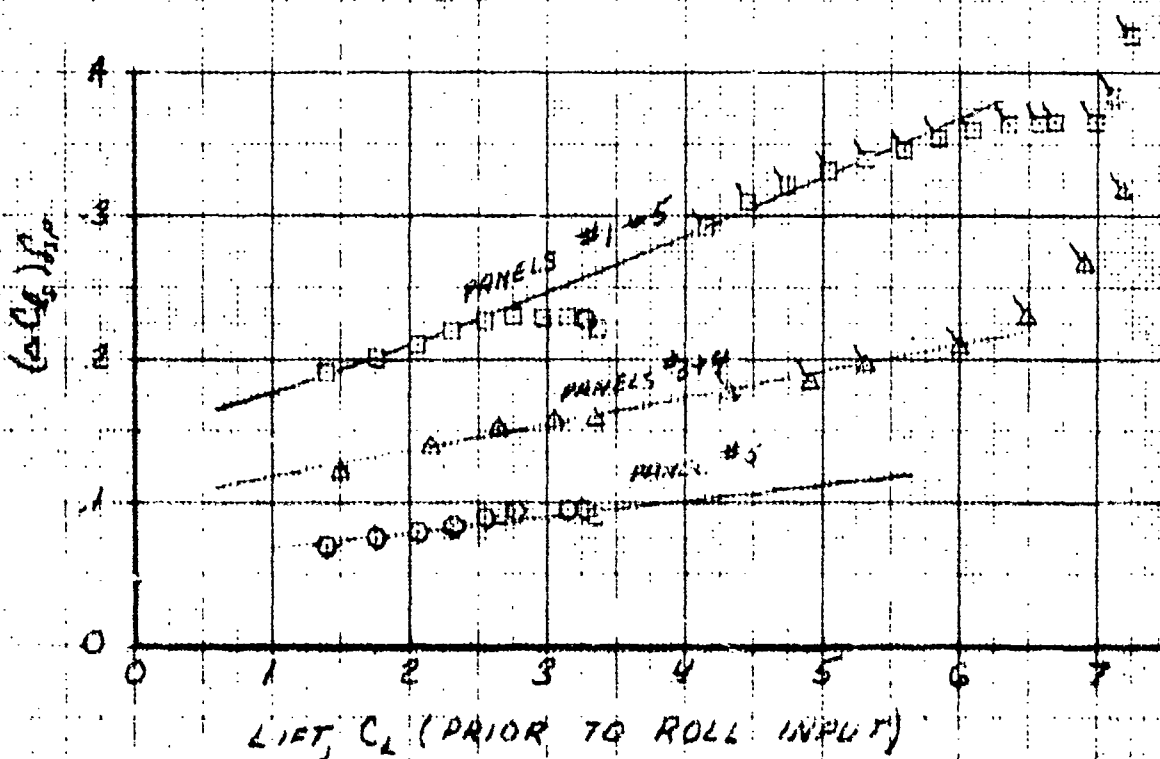
$\delta_F = 25^\circ/50^\circ$

$\delta_{SP} = -14/50$

TAIL ON

	RUNS	PANELS	C_{M0}
○	168/162	*5	0
△	189/162	3+4	✓
△	285/280	-	2.0
□	405/162	*1+5	0
□	499/280	-	2.0

ROLL INCREMENT DUE TO SPOILERS,
 $(\Delta C_L)_{SP}$



LSW 1-03.

ROLL DUE TO SPOILER PLUS DILATION EFFECTS SYMMETRICAL LIFT

$$\delta_1 = 25/50^\circ$$

$$\delta_2 = 10/50^\circ$$

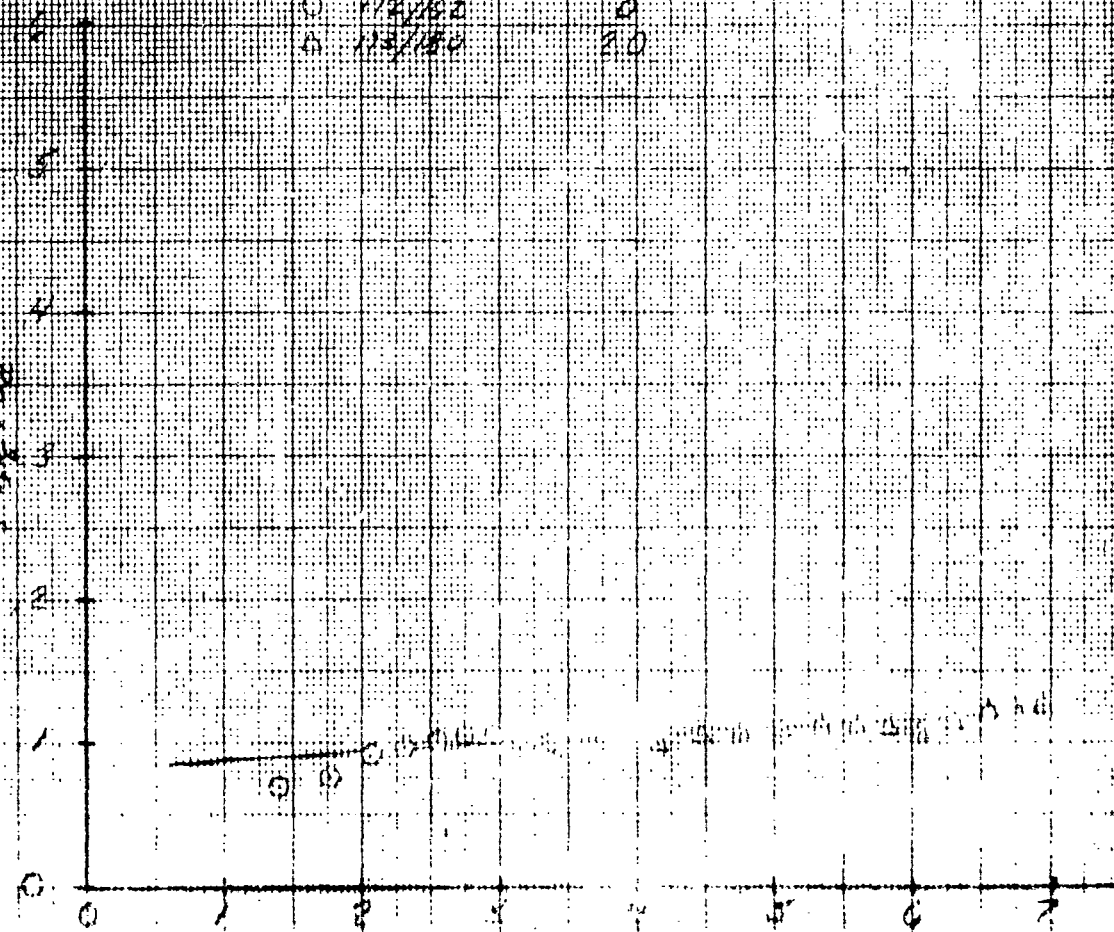
$$\delta_2 = 10/50^\circ$$

4 ENGINES OPERATING
TAIL ON

Roll	CL
172/50	0
113/50	2.0

Roll moment due to spoiler + dilation

$$(a_1 \delta_1) \delta_2 + \delta_2$$



LIFT, CL (deg) and Roll moment

Figure 14.4.16

LSW 1000

ROLL DUE TO VARIOUS SPOILERS VERSUS THREE ENGINE LIFT

$$\dot{\phi} = 2.5^\circ/\text{sec}$$

$$\dot{\phi} = +10^\circ/\text{sec}$$

TAIL ON

#1 ENGINE OUT

RUNS
168/162
170/159

PANELS
#5
#3+4+5

CAL
0
2.5

NOTE

193-194 (177-170)
191-192 (172-148)

0
2.5

EXPERIMENT FOR
AILEMENT

ROLL INCREMENT
DUE TO SPOILERS,
(ΔC_{L2})
%

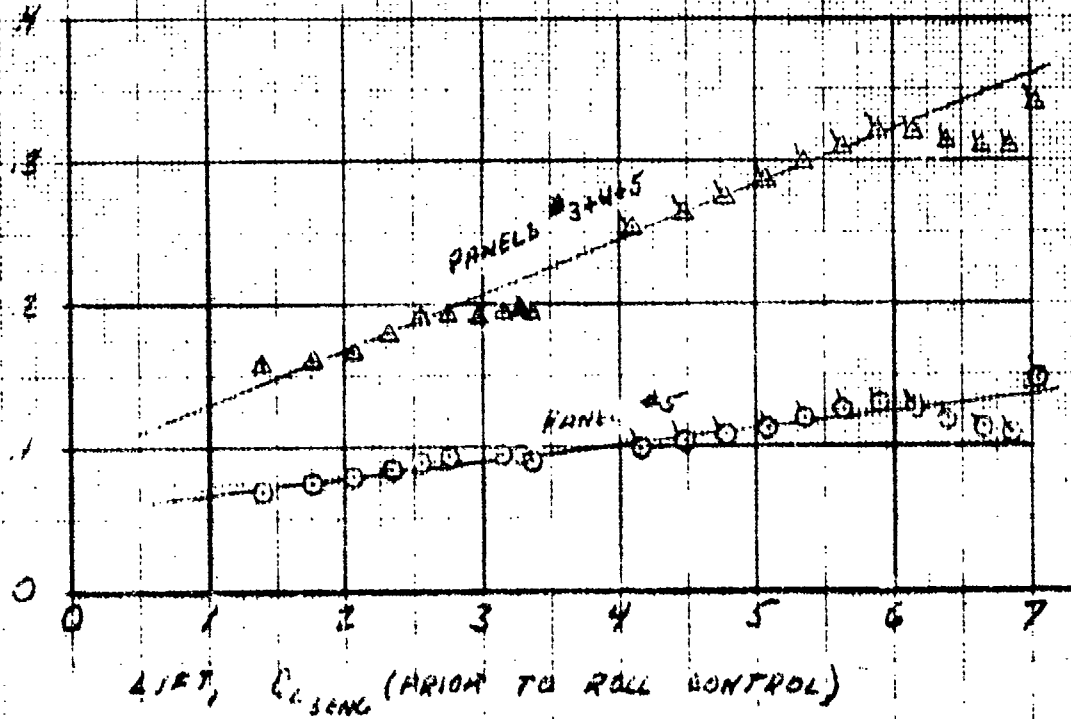
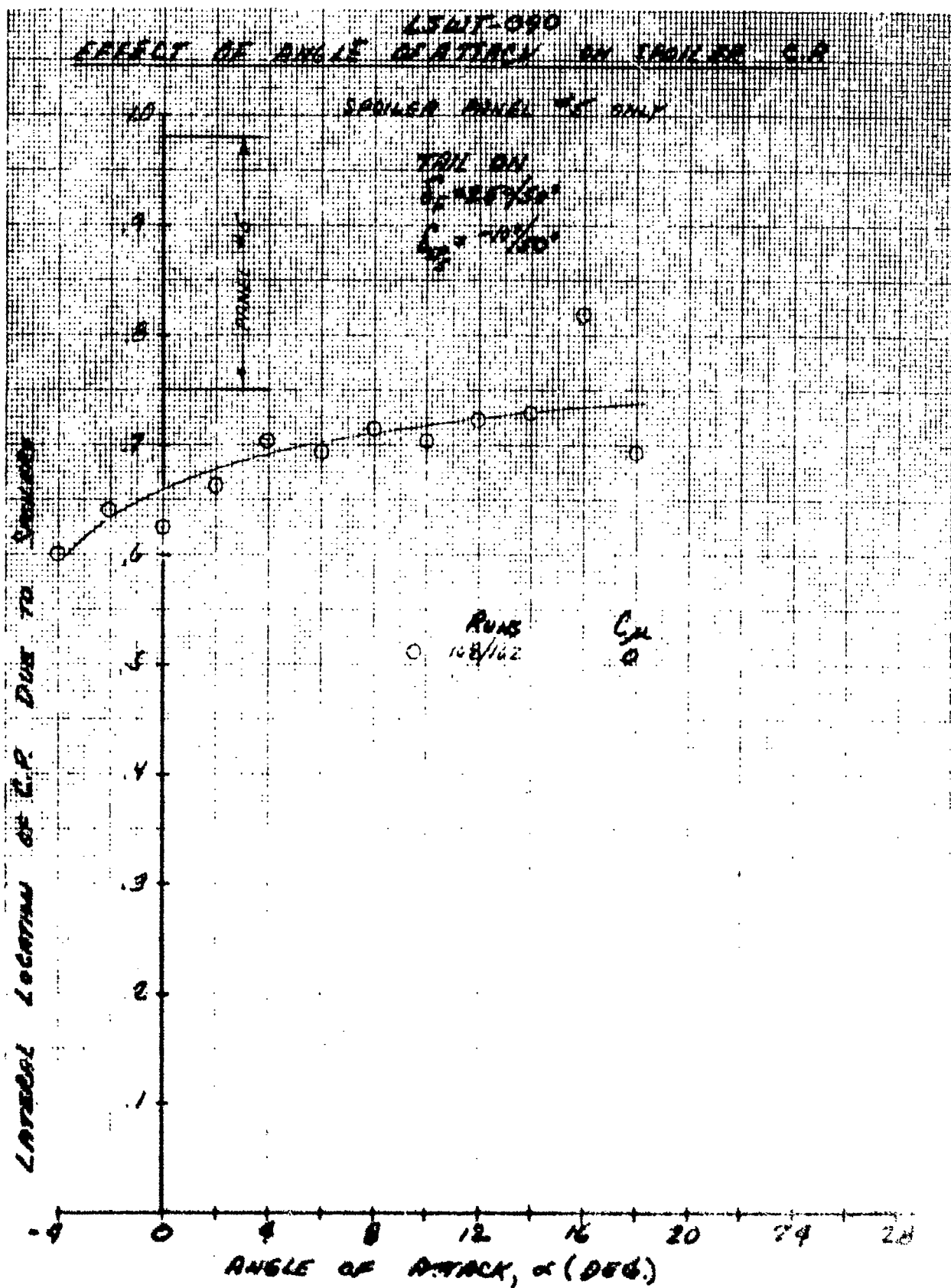
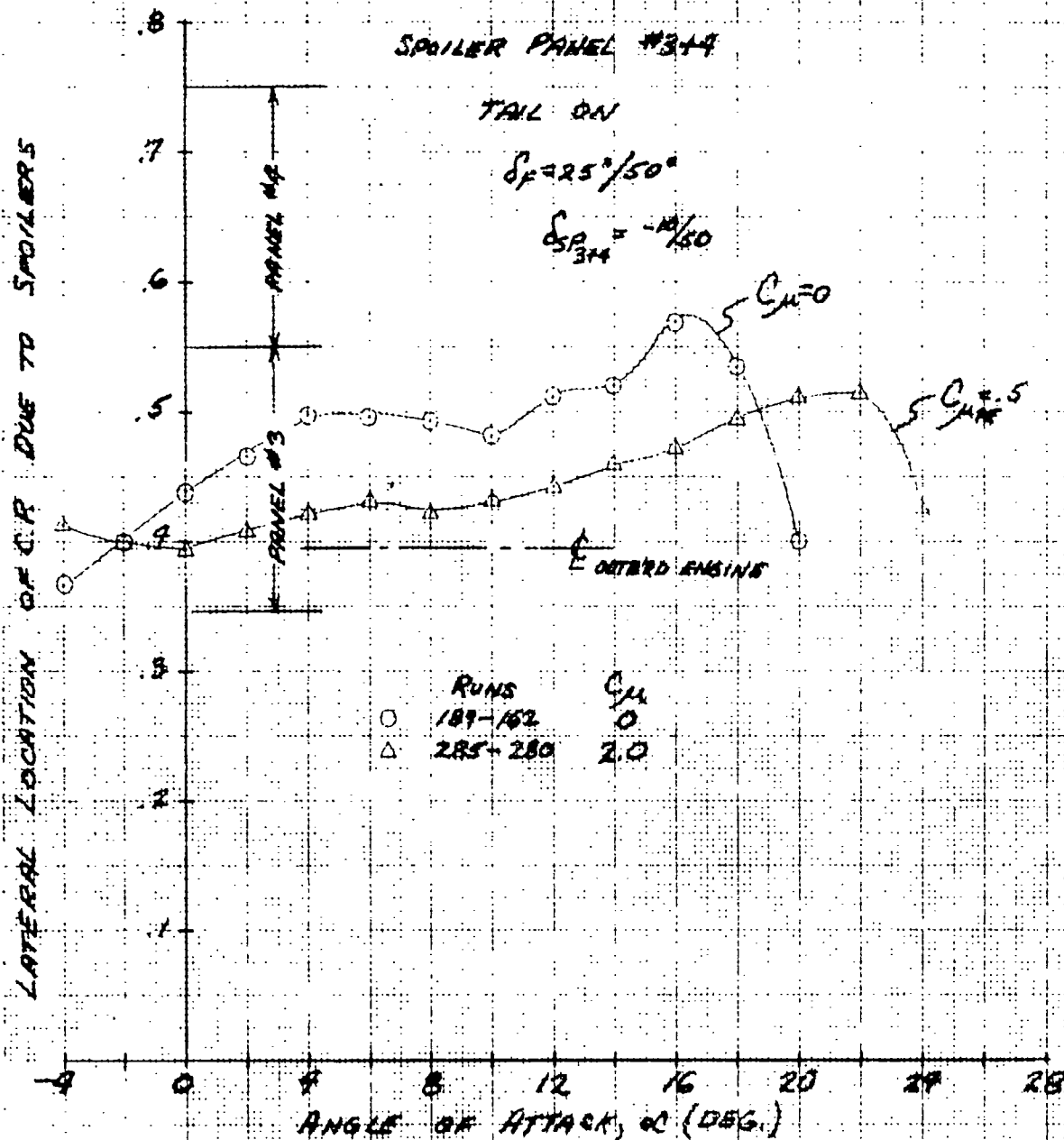


Figure 14.4.17



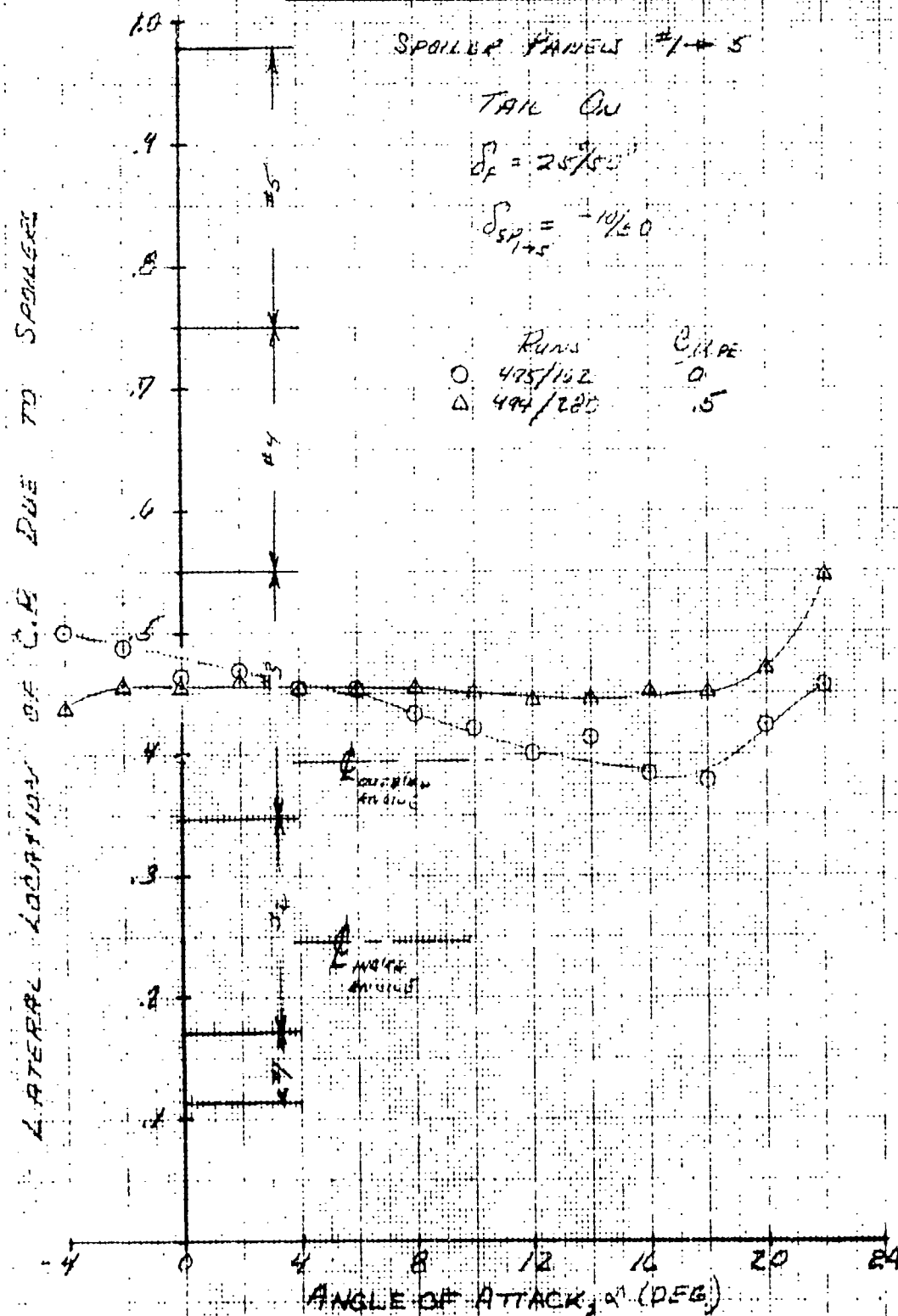
LSWT-090

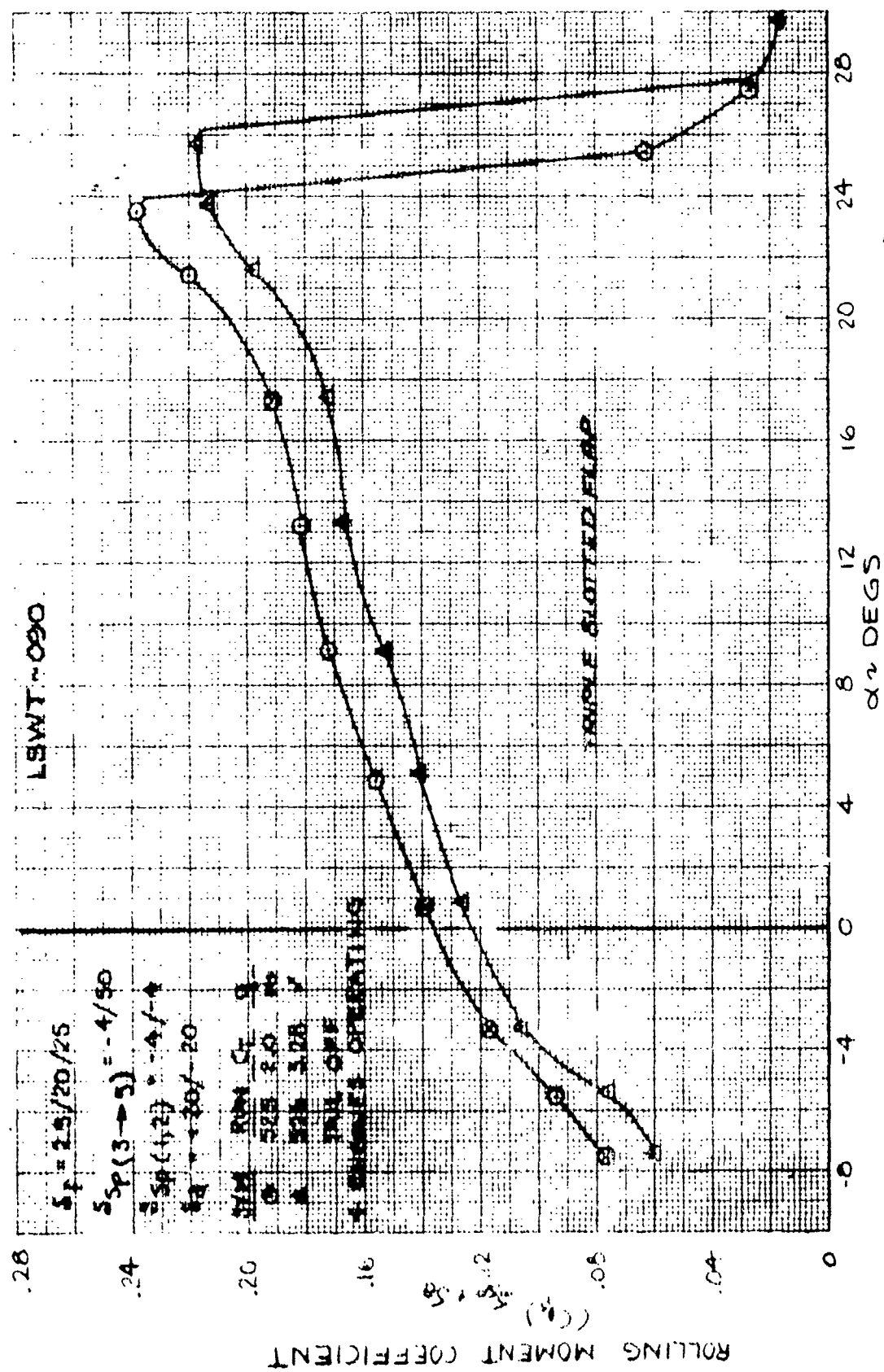
EFFECT OF BLOWING ON SPOILER C.P.



LSWT-090

EFFECT OF BLOWING ON SPOILER C.P.





ROLLING MOMENT DUE TO SPOILER PANEL #3 \rightarrow 5
 WITHAILERONS DEFLECTED

Figure 14.4.21

ROLLING MOMENT COEFFICIENT DUE TO SPOILER AND AILERON DEFLECTION

LSWT-090

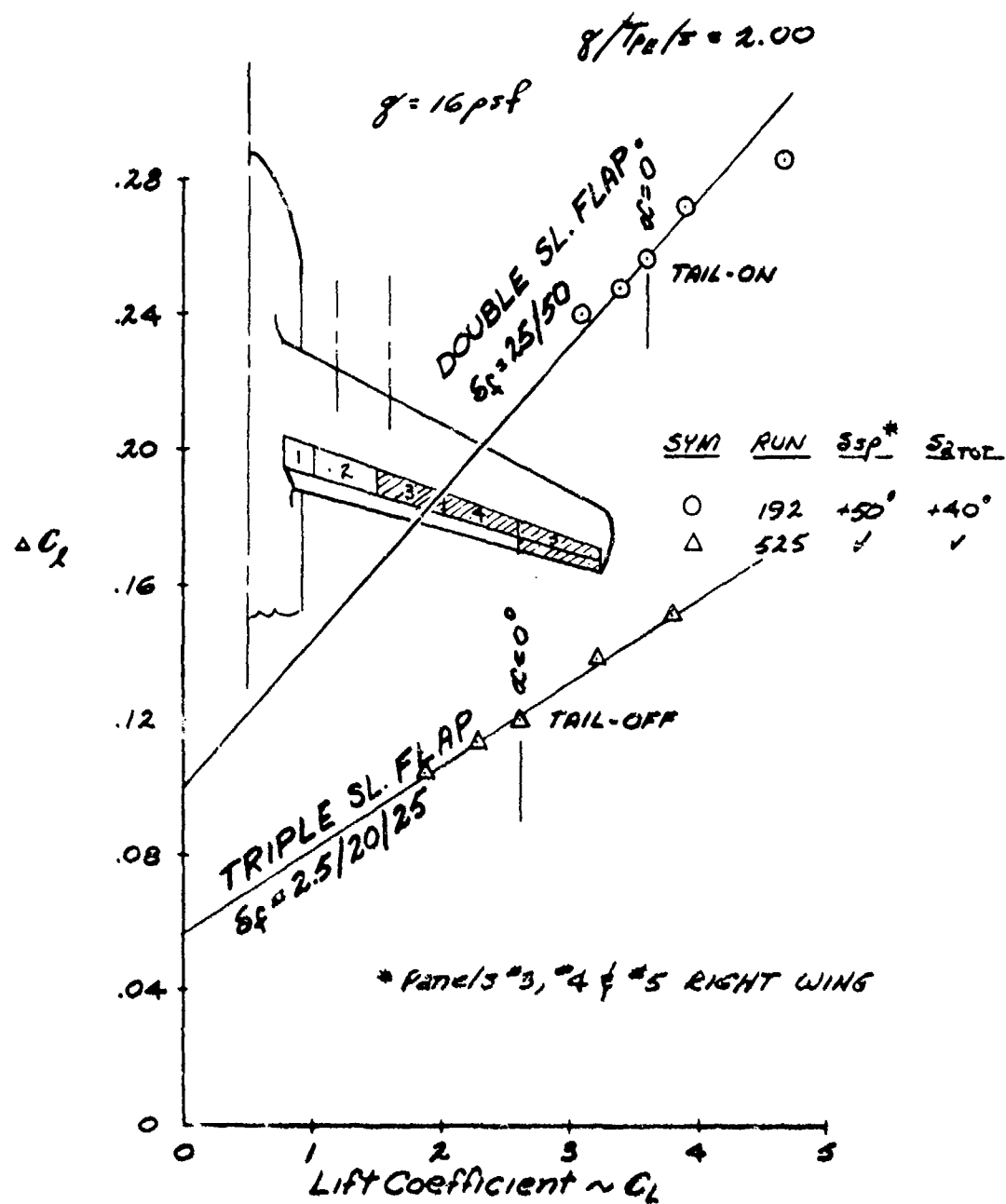
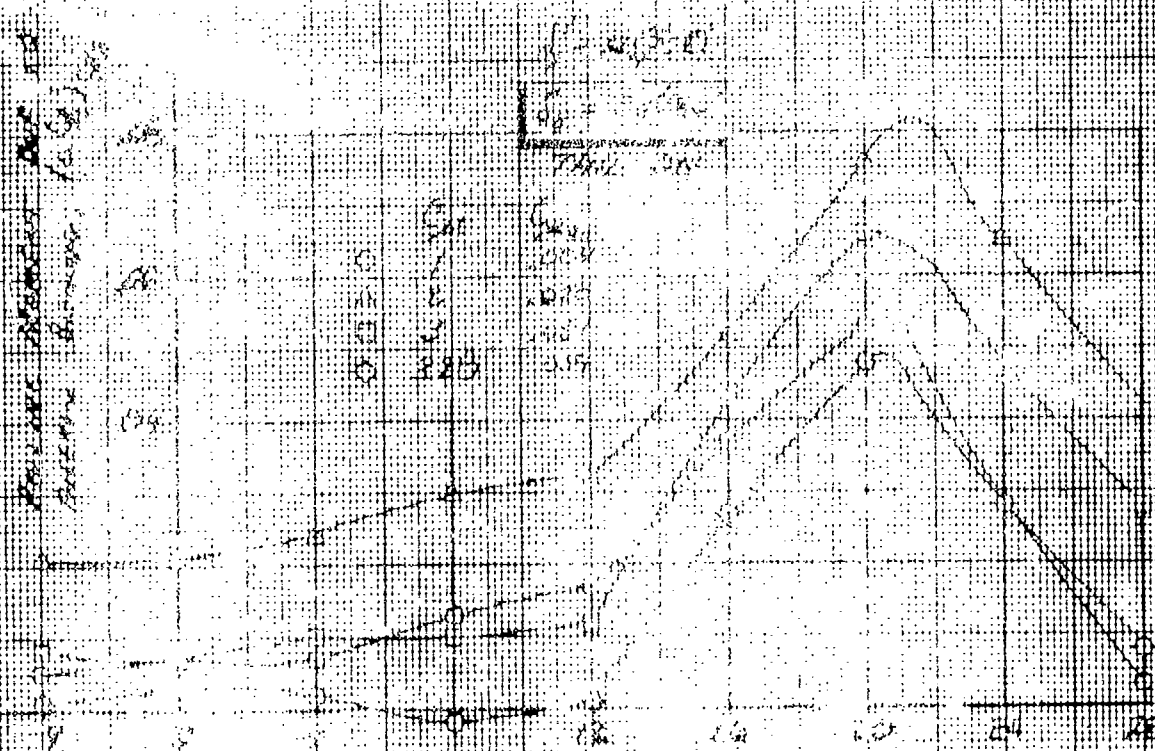
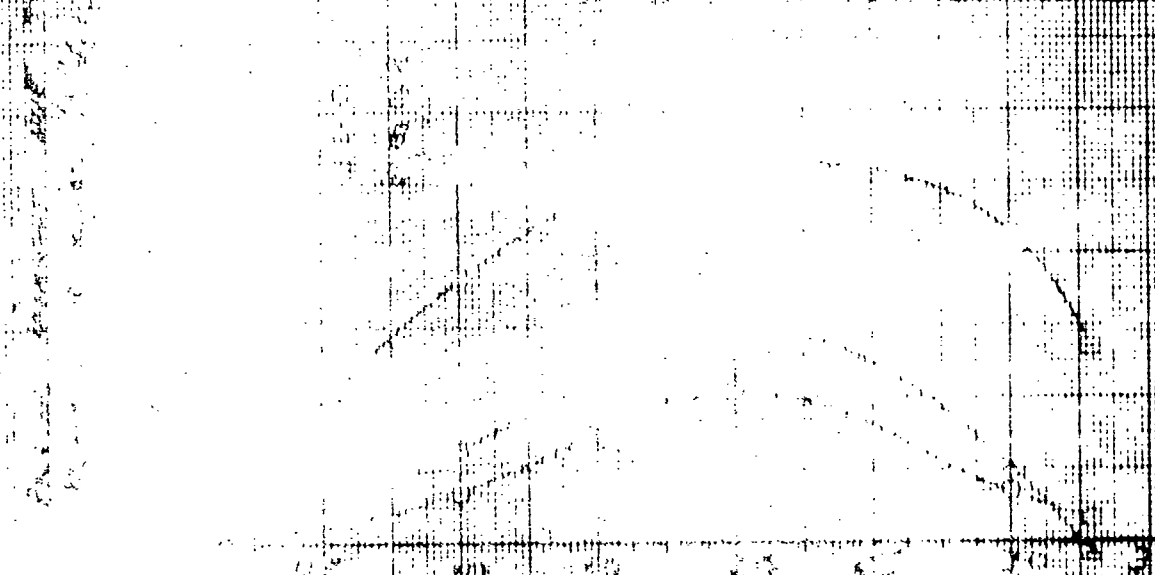


Figure 14.4.22

WELL TO RAILROAD AND RAILROAD (GAS SALES)
 FROM ELEVATION 1000



WELL TO RAILROAD AND RAILROAD (GAS SALES)
 FROM ELEVATION 1000



WELL TO RAILROAD AND RAILROAD (GAS SALES)
 FROM ELEVATION 1000

ROLL DUE TO BLOWING ON AIRCRAFT (ONE SIDE)

ENGINE THRUST

$$C_D = 2.5/20$$

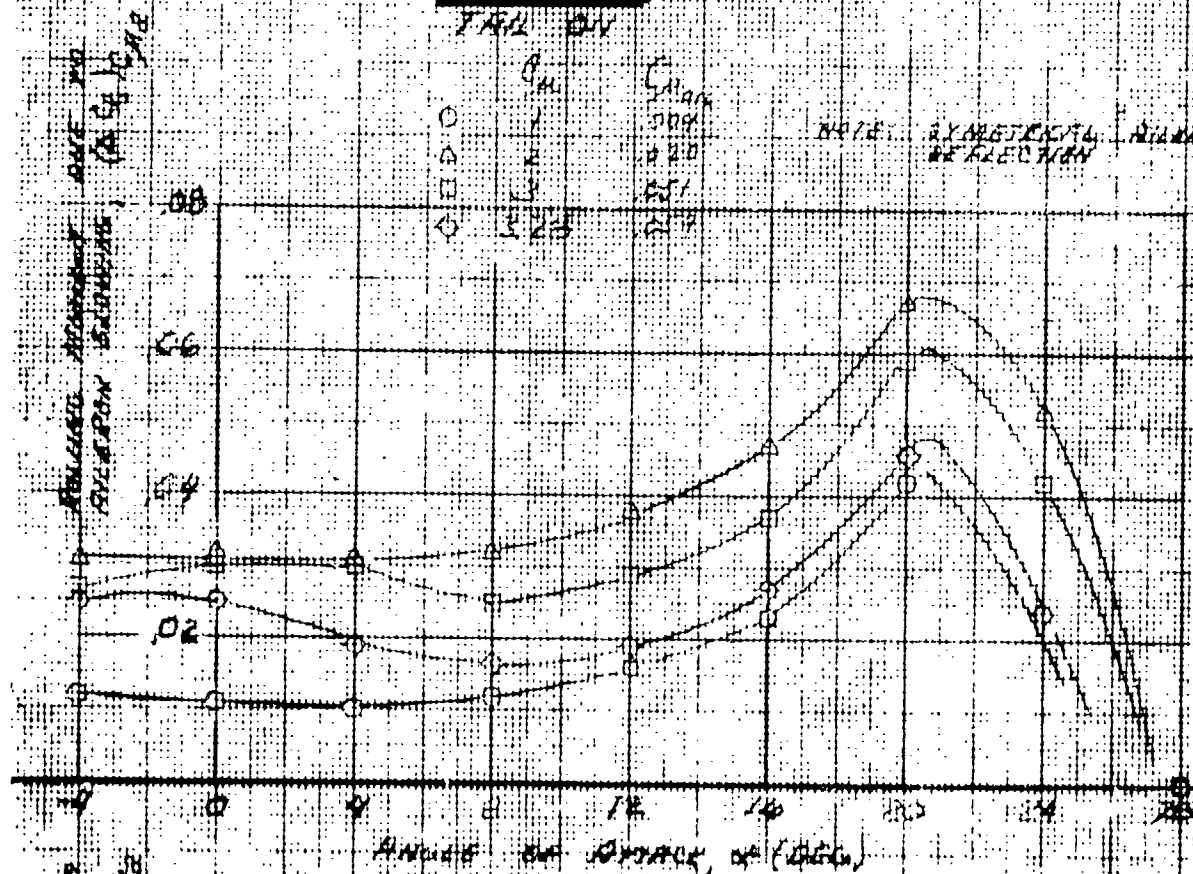
$$C_D = 3.2/20$$

TAIL ON

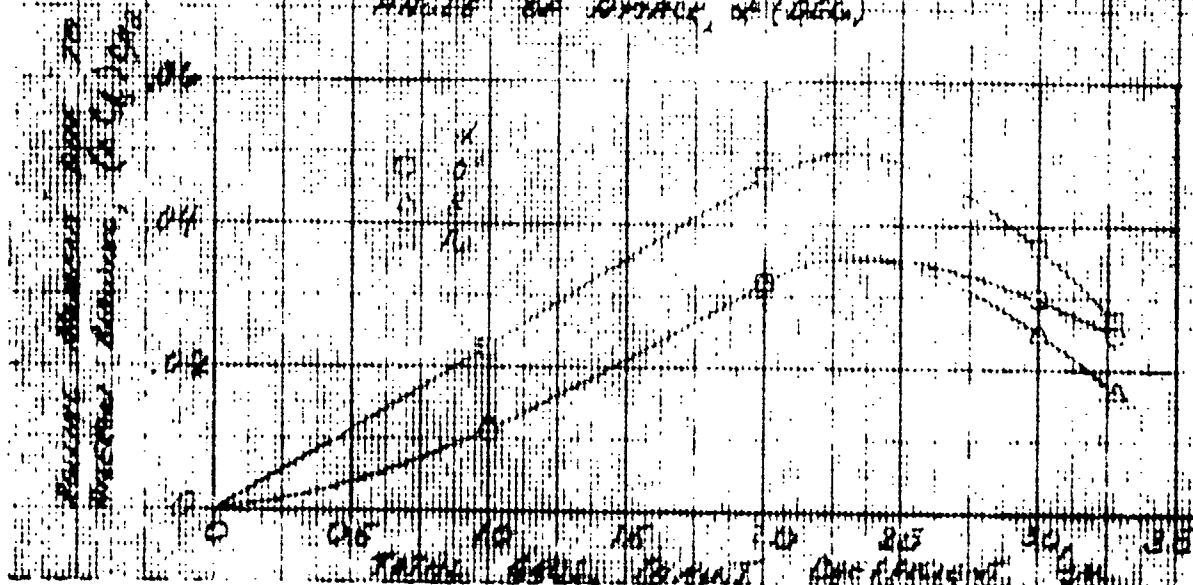
	C_{LH}	C_{LH}/C_D
○	1	0.04
△	2	0.20
□	3	0.51
◇	5.23	2.17

NOTE: SYMMETRICAL AIRFOIL REFLECTION

ROLLING MOMENT DUE TO
ASYMMETRIC BLOWING, (IN $C_L C_D$)



ROLLING MOMENT DUE TO
SYMMETRICAL BLOWING, (IN $C_L C_D$)



ROLL DUE TO BLOWING ON WING (CASE 3)

FOUR ENGINE THRUST

SYMMETRICAL AIRFOIL

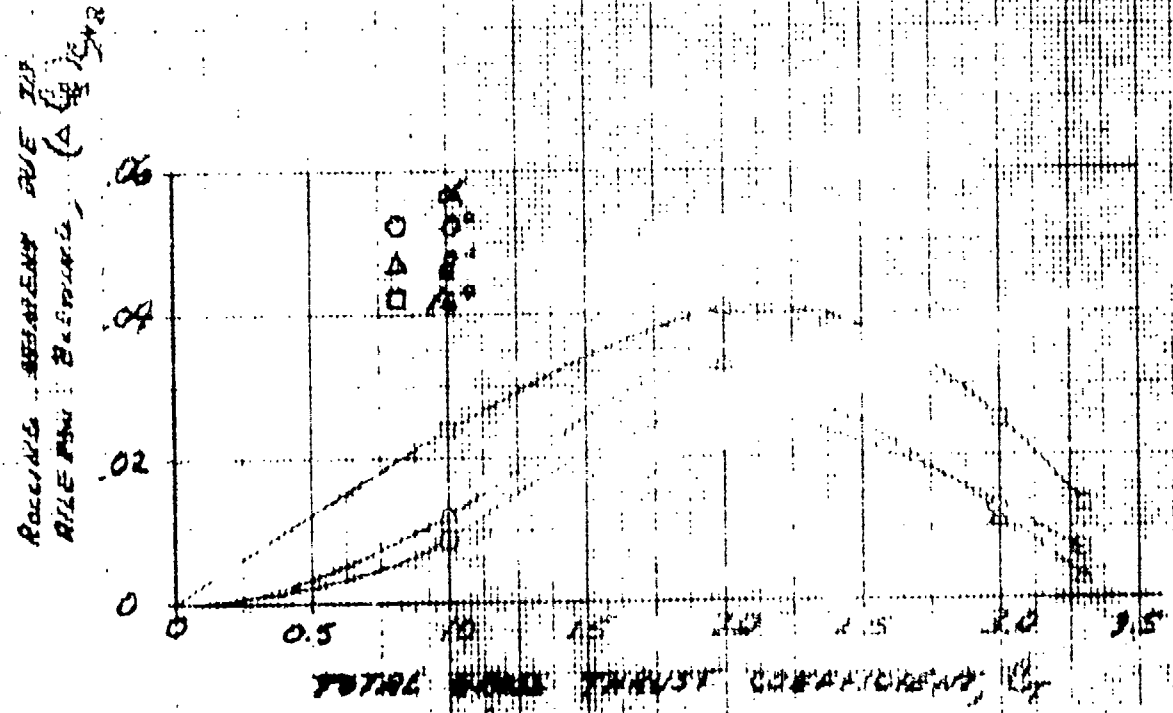
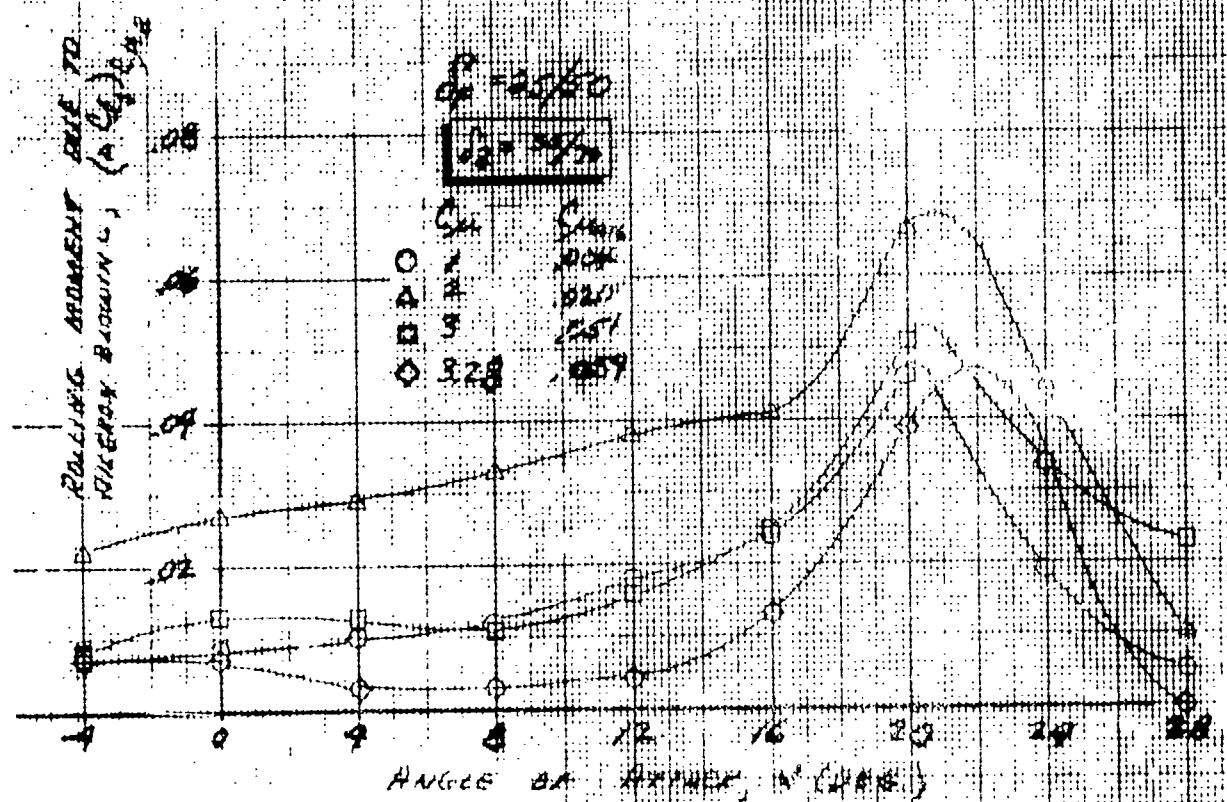


FIGURE 14. N. S. 1

ROLL DUE TO BLOWING ON ALLERON

LSWT-090

(FPGA ENGINE THREAT)

FAIR DIV

ROLLING MOMENT
DUE TO ALLERON BLOWING

$(\frac{1}{2} \rho V^2 S C_L)$

ROLLING MOMENT
DUE TO ALLERON BLOWING

$(\frac{1}{2} \rho V^2 S C_L)$

ROLLING MOMENT
DUE TO ALLERON BLOWING

$(\frac{1}{2} \rho V^2 S C_L)$

$\alpha = 0^\circ$

$\alpha = 6^\circ$

$\alpha = 12^\circ$

$\frac{S}{b} = 25\%$
 $\frac{S}{b} = 30\%$
 $\frac{S}{b} = 35\%$

Engine Thrust, S_u

Engine Thrust, S_u

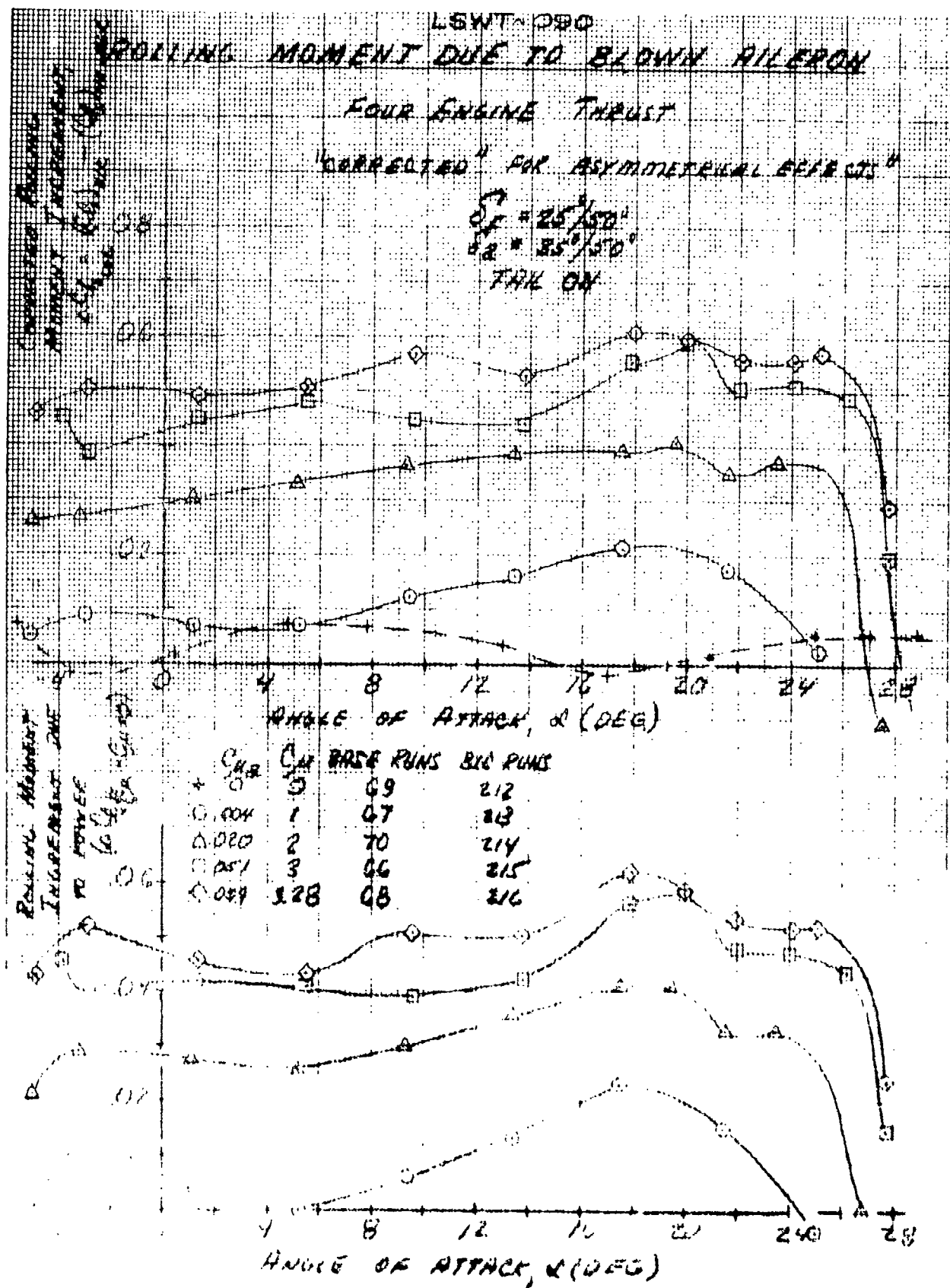


Figure 11.5.7

(SWT-3.1)

AILERON THRUST VERSUS GROSS THRUST

4 ENGINE OPERATION

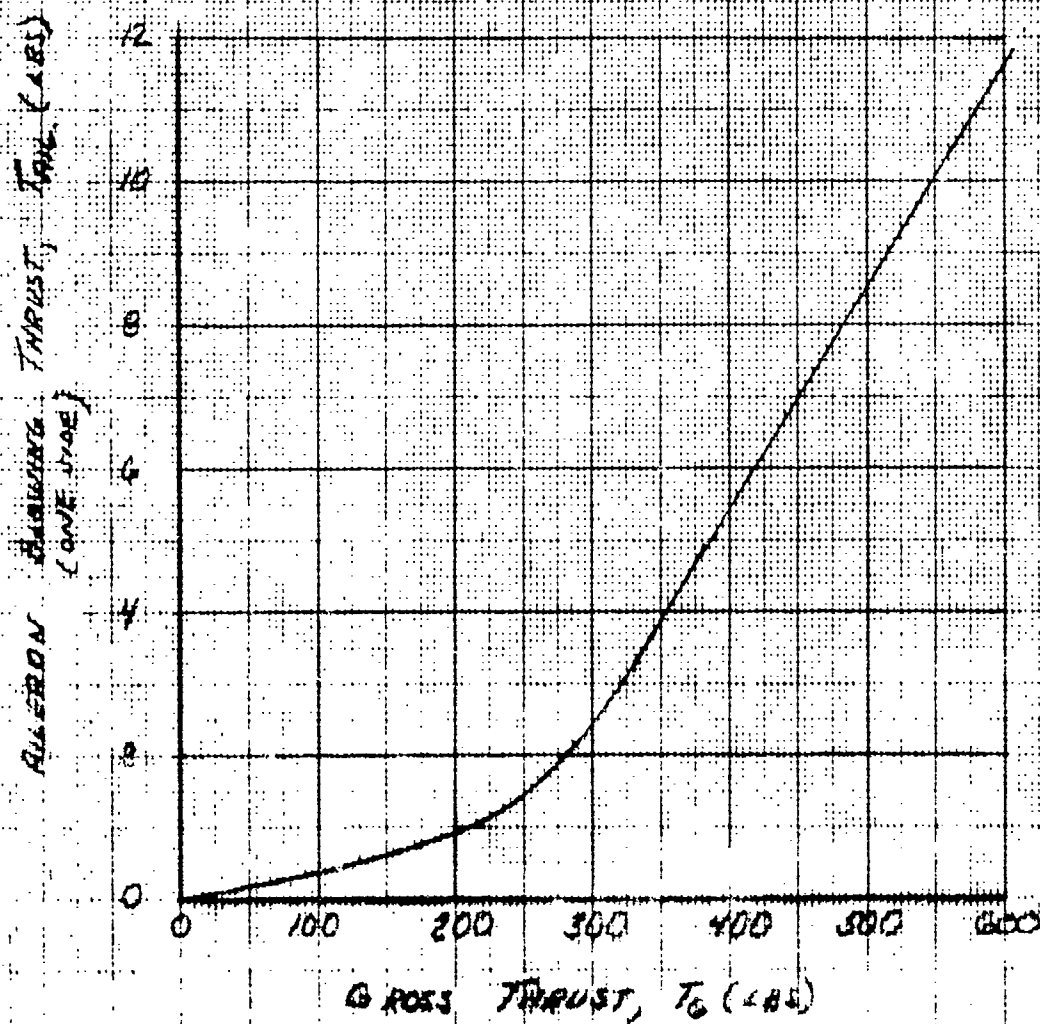
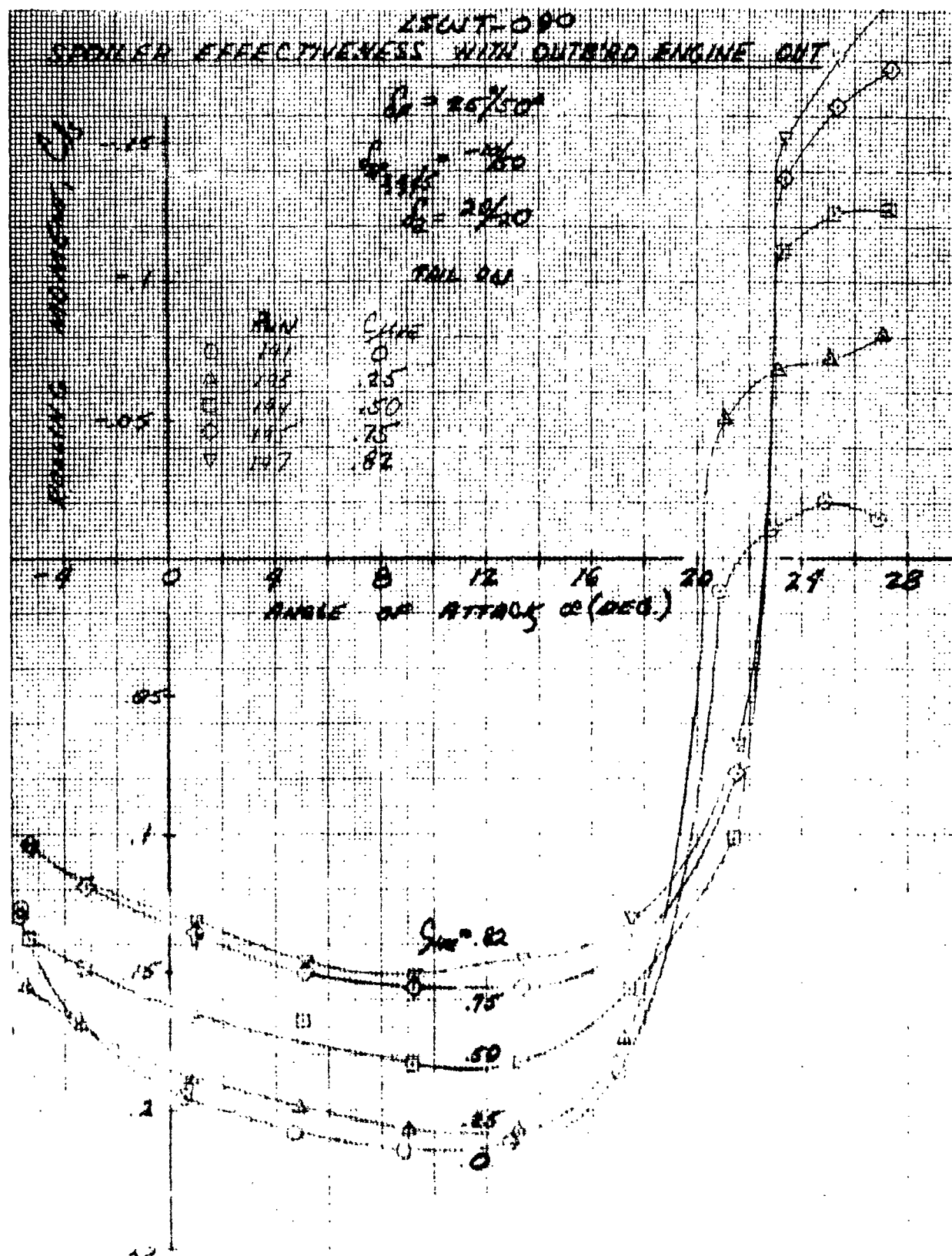


Figure 14.5.6



(the reverse side of this page is blank)

Figure 14.6.1

Section XV

DIRECTIONAL CONTROL

The yaw run data obtained in test LSWT-090 was taken at only two angles of attack, $\alpha_{FRL} = 0^\circ$ and 12° . Data was obtained flaps up and down, tail on and off, with and without engine failures and with and without rudder deflected.

15.1 DIRECTIONAL STABILITY - FLAPS UP AND FLAPS DOWN

Figures 15.1.1 shows the stabilizing effect an application of power has on flaps down total directional stability. Figure 15.1.2 presents the increment.

Similarly, Figure 15.1.3 shows the effects that increasing power has on the flaps deflected total dihedral effect, $C_{l\psi}$ while Figure 15.1.4 presents the increment, showing a decrease in stability.

Figure 15.1.5 shows the effects of power application to the flaps down side force derivative and corresponding increments in side force derivative due to power are presented in Figure 15.1.6.

Some basic yawing moment coefficient wind tunnel data are presented in Figures 15.1.7 and 15.1.8.

15.2 DORSAL OPTIMIZATION

Dorsal fins of three projected side areas were tested. The basic configuration dorsal or the D dorsal was the smallest with a projected side area of 0.0608 ft.². The next in size was the D₃ dorsal with a projected side area of 0.6831 ft.² and the largest dorsal was the D₂ dorsal with a projected side area of 0.8418 ft.².

Figures 15.2.1, 15.2.2 and 15.2.3 represent the stability axis yawing moment coefficient, rolling moment coefficient and side force coefficient versus the angle of yaw, ψ . All three dorsals are shown on these plots for at least two C_{mu} 's each. These figures are basic wind tunnel data plots.

15.3 YAW CHARACTERISTICS WITH ENGINE FAILURE

The model was capable of simulating engine failures by remotely closing either of two valves in the engine air supply line. The engines failed were the left side outboard (Engine #1) and the right side inboard (Engine #3).

Figure 15.3.1 shows the yawing moment for normal engine operation and engine failure at zero flap deflection on model yawing moment coefficient at $\alpha_{FRL} = 0^\circ$. Stability levels are unaffected by engine failure in this flaps up condition.

The normal engine operating directional stability ($C_{n\dot{\psi}}$) is doubled by deflecting the flaps from 0° to $25^\circ/50^\circ$, which is also shown in this figure. Additional engine failure effects on yawing moment coefficient at $\alpha_{FRL} = 0^\circ$ with flaps deflected are presented in Figure 15.3.2. Note that the inboard engine out develops larger yawing moment coefficients than the outboard engine out. This unique behavior is also seen in Figure 15.3.4 the only difference here being $\alpha_{FRL} = 12^\circ$. The causes for the unorthodox engine out yawing moment coefficient tendencies are at this time unresolved. It is possible that highly asymmetric wing spanwise load distributions are being generated with inboard engine out which may induced sizeable sidewash components; the effects of which are reflected in the yawing moment. The need for additional detailed investigations in this case is obvious.

Figure 15.3.3 presents the corresponding side force data for Figure 15.3.2.

Figures 15.3.5 and 15.3.6 show the effects of flap deflection on outboard and inboard engine failed yawing moment coefficients respectively at $\alpha_{FRL} = 0^\circ$. These data show less engine failed yawing moment coefficient results with the flaps at $35^\circ/60^\circ$ than at $25^\circ/50^\circ$.

The total yawing moment coefficient produced by spoiler deflection with the outboard engine failed are shown in Figure 15.3.7 for two double slotted flap deflections at $\alpha_{FRL} = 0^\circ$. Corresponding side force coefficient data is plotted in Figure 15.3.8.

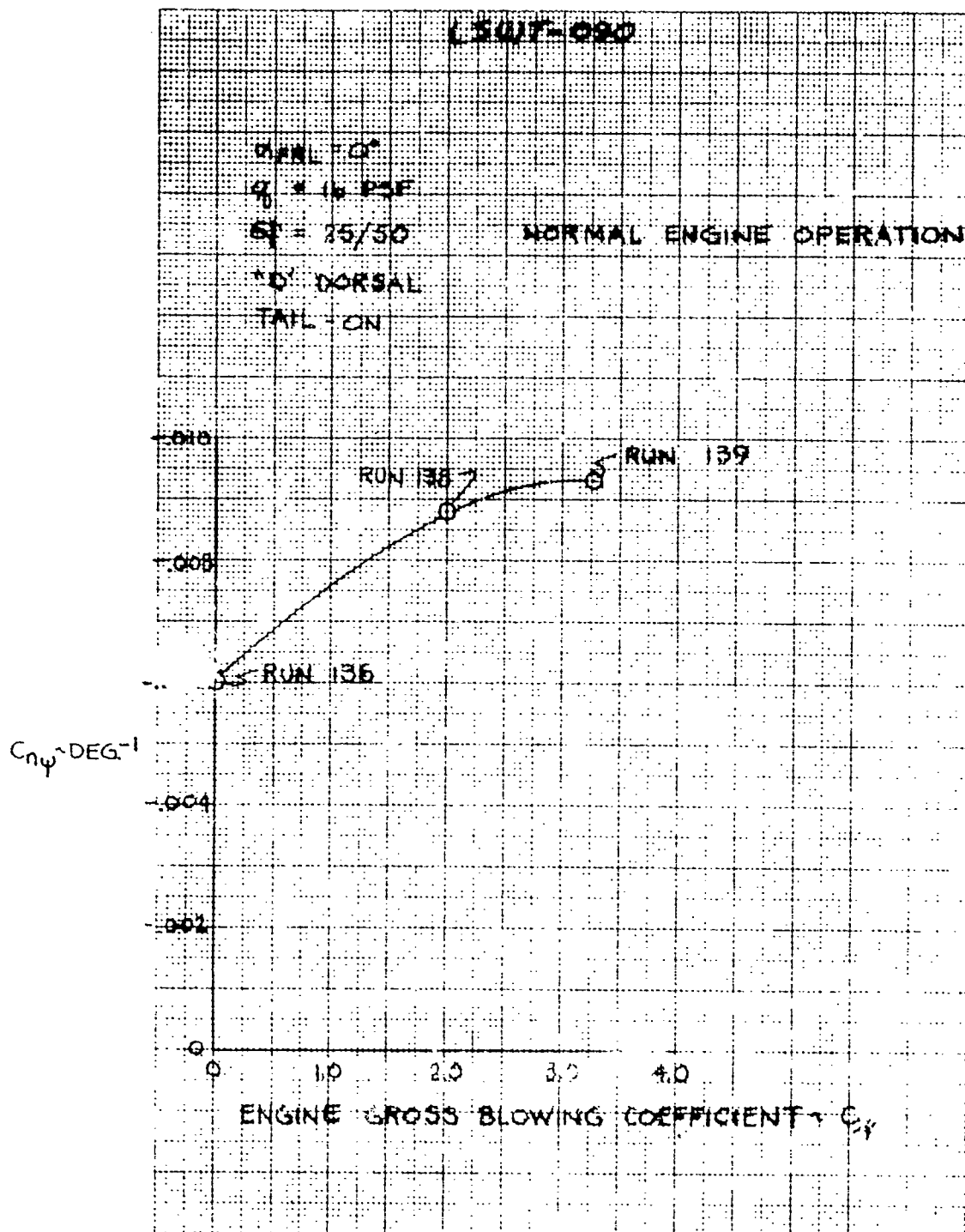
15.4 RUDDER EFFECTIVENESS AND EFFICIENCY

The rudder tested in test LSWT-090 was a double cambered device similar to the elevator. The forward rudder segment (δ_{r1}) was hinged at the vertical fin 55 percent chord element and the rear rudder segment (δ_{r2}) was hinged at the vertical fin 75 percent chord element. The forward rudder segment was tested only at the 0° and 25° deflections with respect to the vertical fin centerline and the rear rudder segment was tested at 0° , 15° , 20° , and 25° deflections with respect to the forward rudder segment centerline.

Figures 15.4.1 and 15.4.2 show the rudder effectiveness for $\delta_f = 25^\circ/50^\circ$ and $35^\circ/60^\circ$ respectively with normal operating engines and one engine failed. The data was taken at $\alpha_{FRL} = 0^\circ$ and with maximum rudder deflection of $\delta_{r1}/\delta_{r2} = 25^\circ/25^\circ$ and at varying sideslip angles.

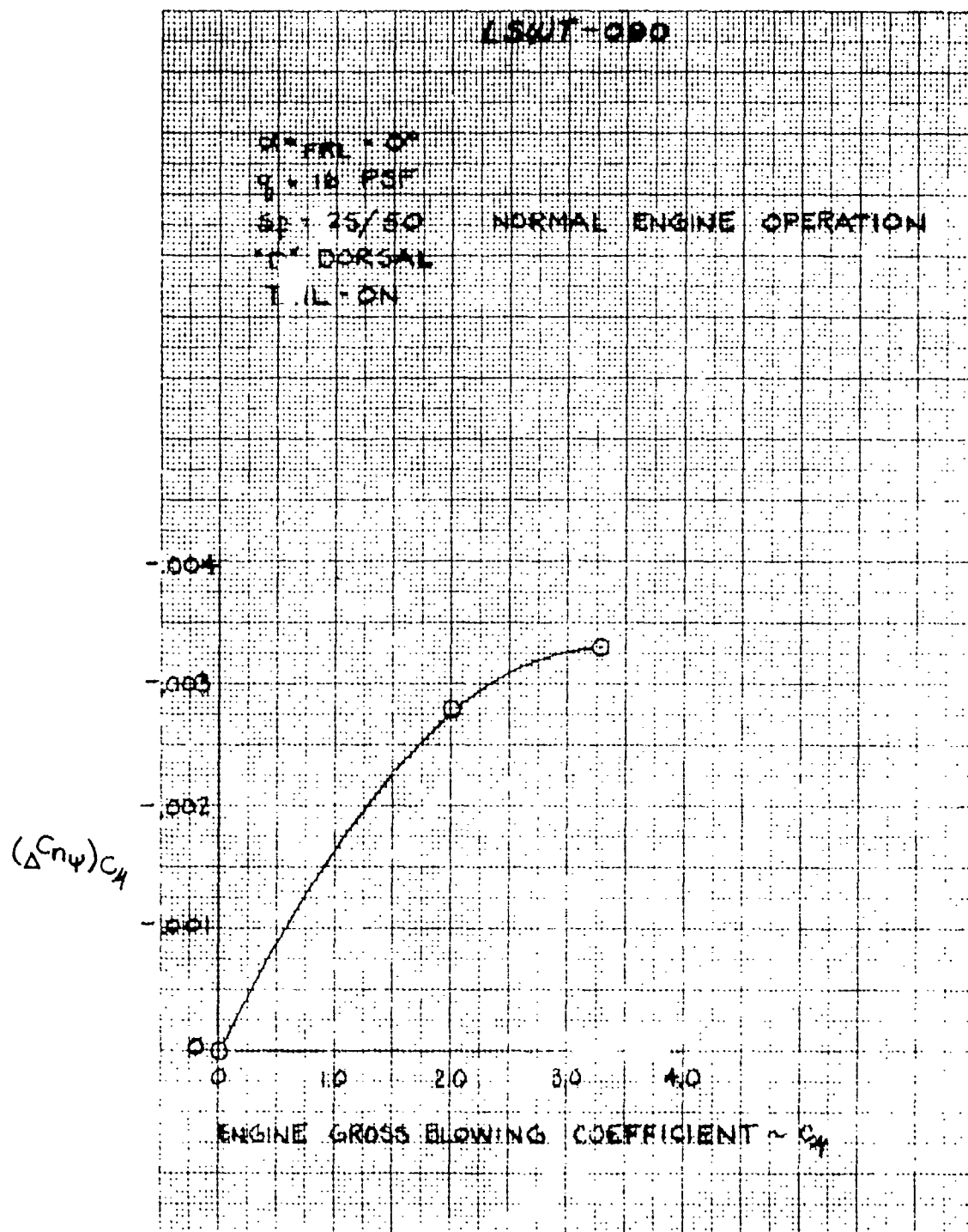
The control capability of the vertical tail with deflected rudder is shown in Figure 15.4.3. The yawing moment coefficient of the vertical tail with corresponding vertical tail lift coefficients is given for varying rudder deflections.

The control surface efficiency of the vertical tail with deflected rudder is shown in Figure 15.4.4 as well as the maximum lift (or side force) coefficient for maximum rudder deflection. Also presented in this figure is a single surface deflection control efficiency versus rudder to vertical tail chord ratio.



POWER EFFECTS ON FLAPS DOWN DIRECTIONAL STABILITY

Figure 15.1.1



CHANGE IN FLAPS DOWN DIRECTIONAL STABILITY
DUE TO POWER EFFECTS

Figure 15.1.2

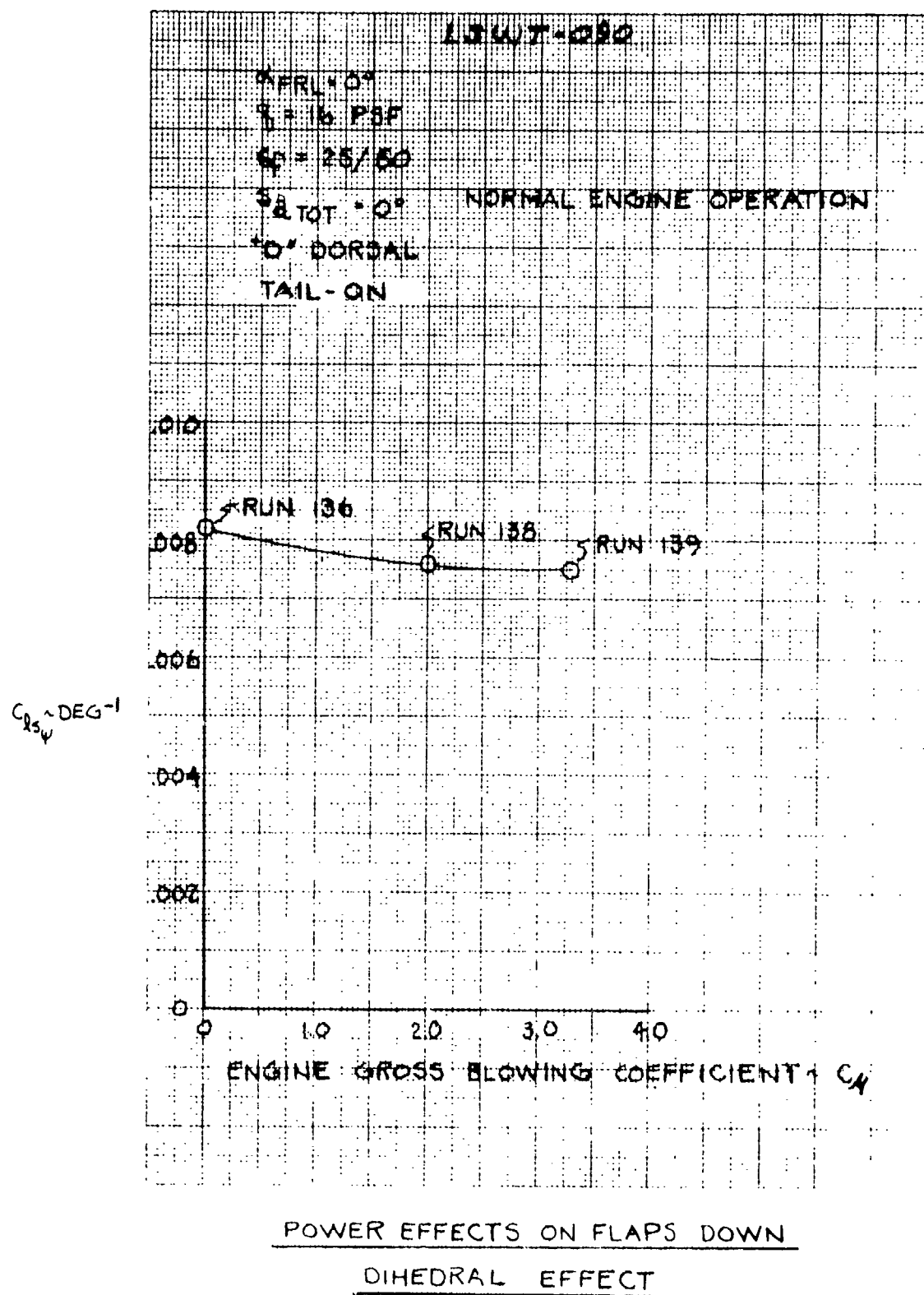


Figure 15.1.3

LSWT - 090

$\alpha_{FRL} = 0^\circ$

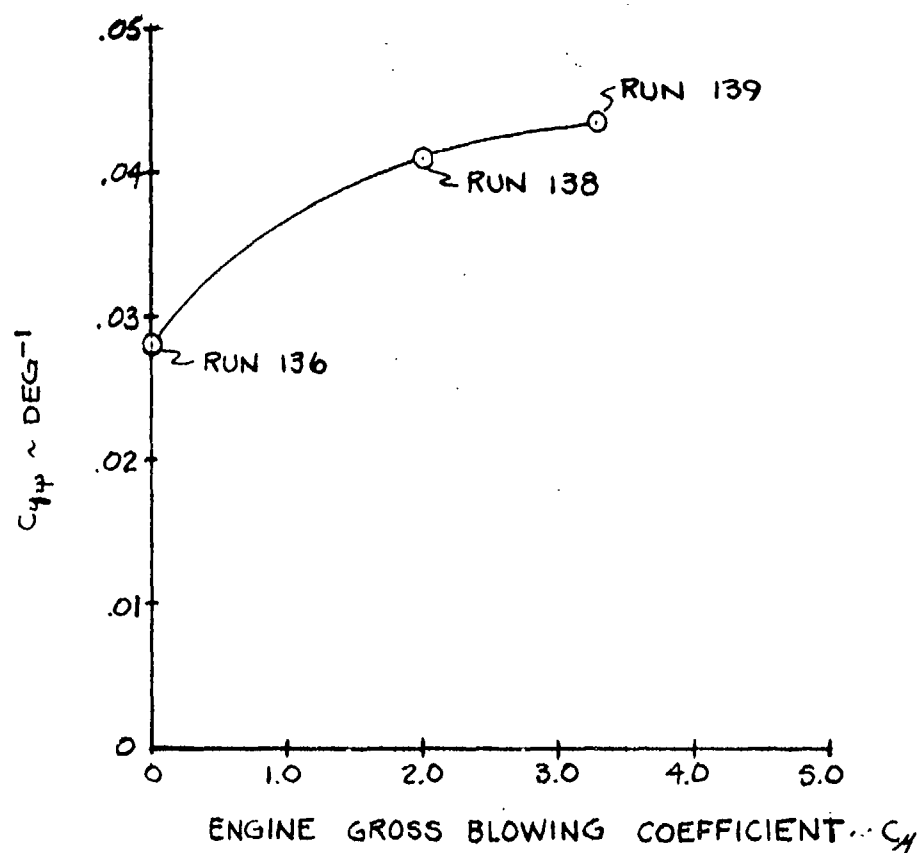
$q = 16 \text{ PSF}$

$S_F = 25/50$

"D" DORSAL

TAIL - ON

NORMAL ENGINE OPERATION



POWER EFFECTS ON FLAPS DOWN SIDE FORCE
DERIVATIVE

Figure 15.1.5

LSWT-090

$\alpha_{FRL} = 0^\circ$

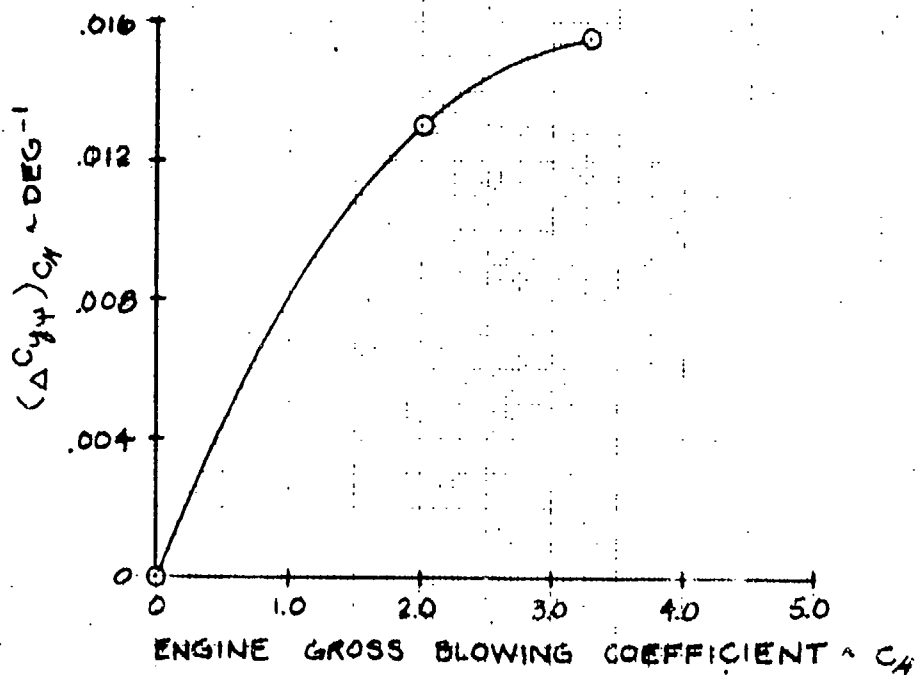
$q = 16 \text{ PSF}$

$Sp = 25/50$

'D' DORSAL

TAIL-ON

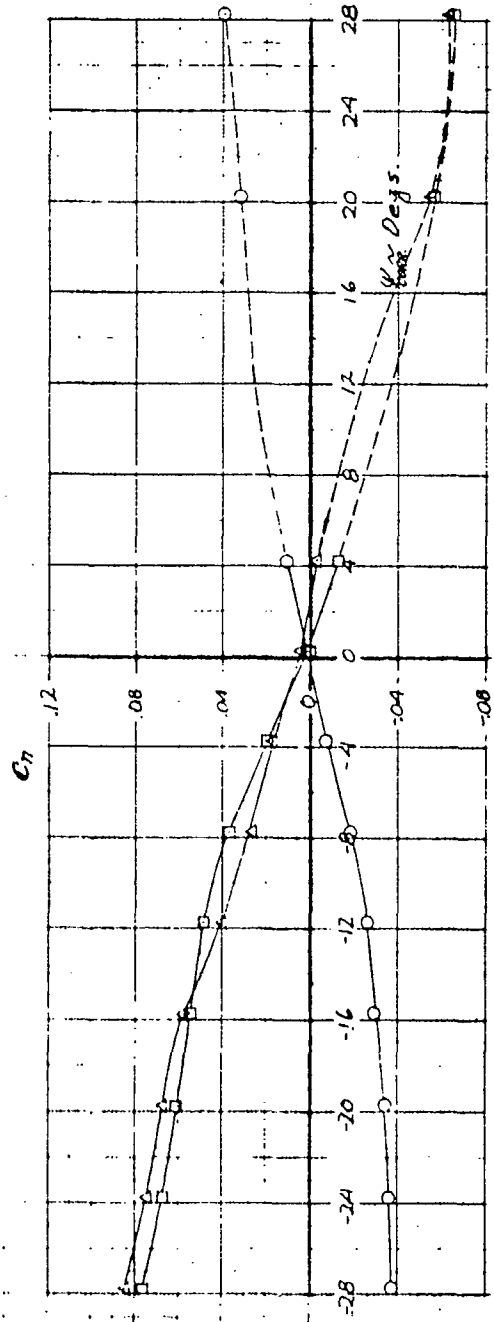
NORMAL ENGINE OPERATION



CHANGE IN FLAPS DOWN SIDE FORCE
DERIVATIVE DUE TO POWER EFFECTS

Figure I5.1.6

DIRECTIONAL STABILITY - FLAPS UP



SYM	RUN	CI	St	VERT	APPLIC
O	129	8.00	0	OFF	OFF
Δ	130	✓	✓	ON	OFF
□	131	✓	✓	ON	ON (4.2°)

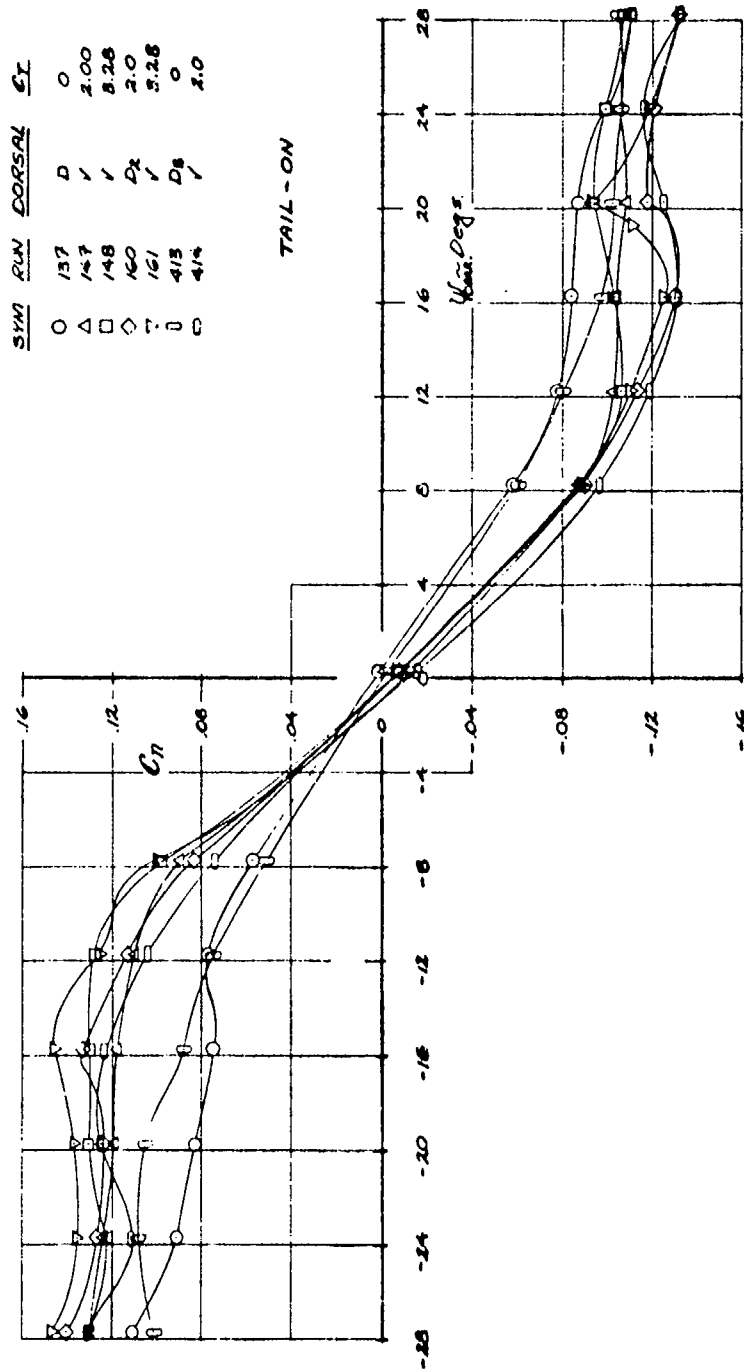
BASIC YAW RUNS $\delta_{FL} = 0^\circ$

LSWT-080

Figure 15.1.7
(The reverse side of this page is blank)

DIRECTIONAL STABILITY - FLAPS DOWN

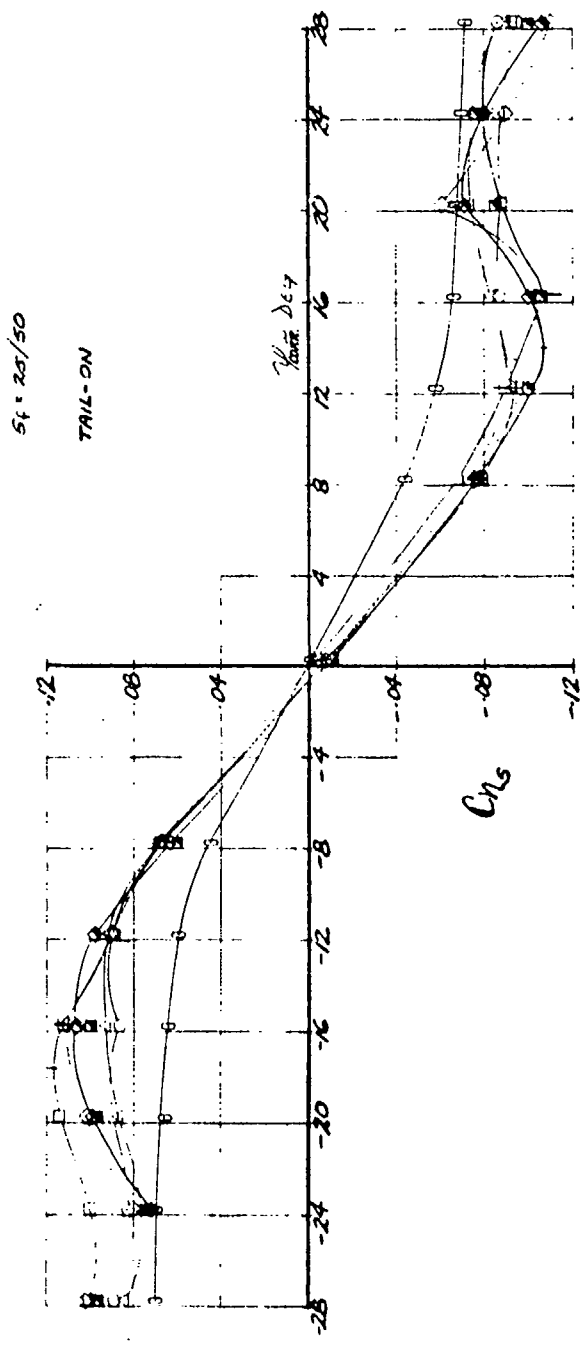
$\alpha_{max} = 12^\circ$ $g = 16 \text{ g}$ $q = 25/50$



LSWT-090

Figure 15.1.8
(The reverse side of this page is blank)

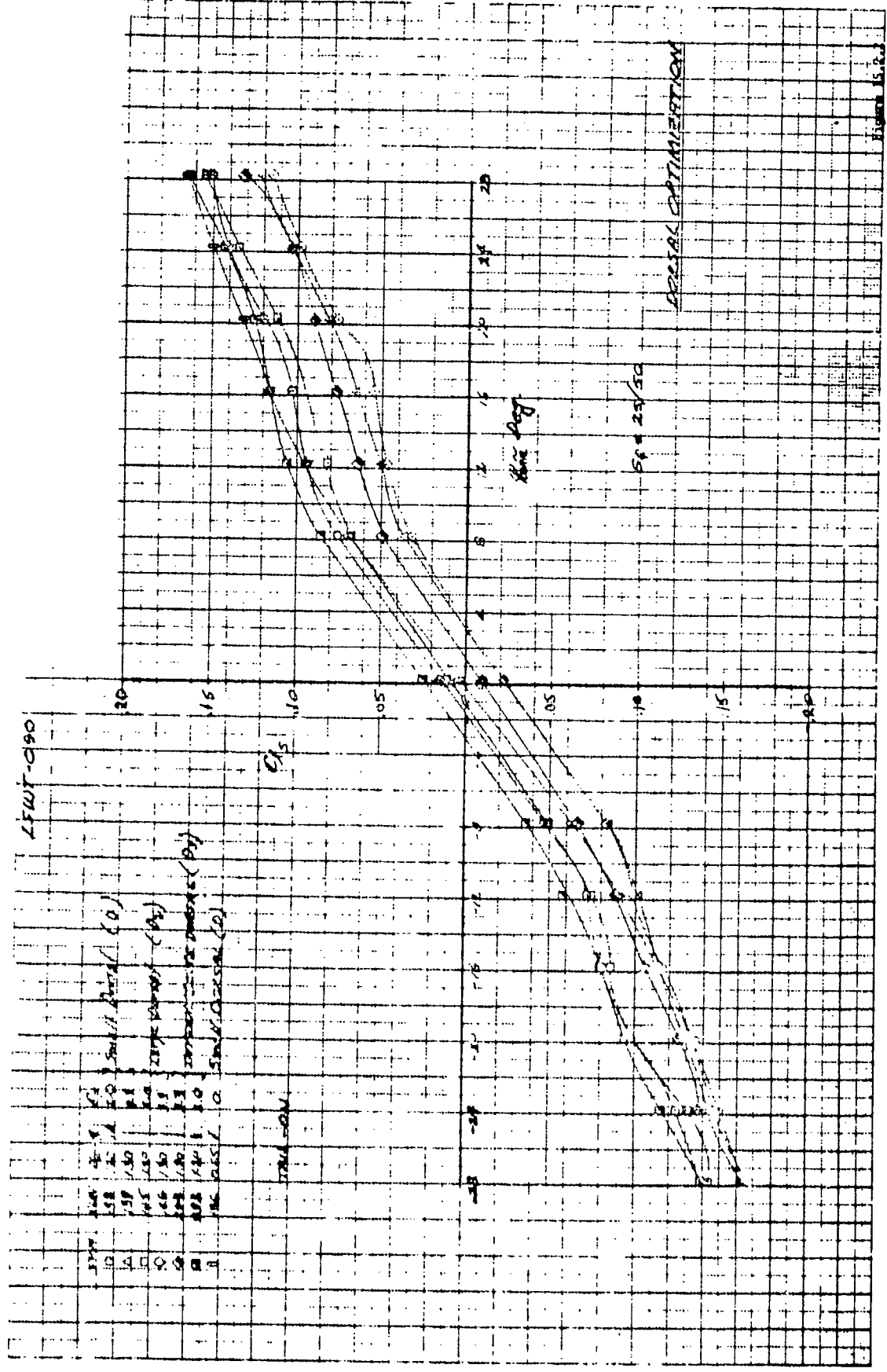
• Sum	Run	Config.	CT	Change	
138	Small beam	2.0	120	1.0	D
139		3.3	130	1.0	D
145	large beam	2.0	120	1.0	D ₂
146		3.3	130	1.0	D ₂
274	Extending	1.3	110	1.0	D ₃
277		2.0	120	1.0	D
136	Small Dorsal	0	0.65	1.0	D



DORSAL OPTIMIZATION & DIRECTIONAL
STABILITY - FLAPS DOWN

LSWT-090 Figure 15.2.1

373 (The reverse side of this page is blank)

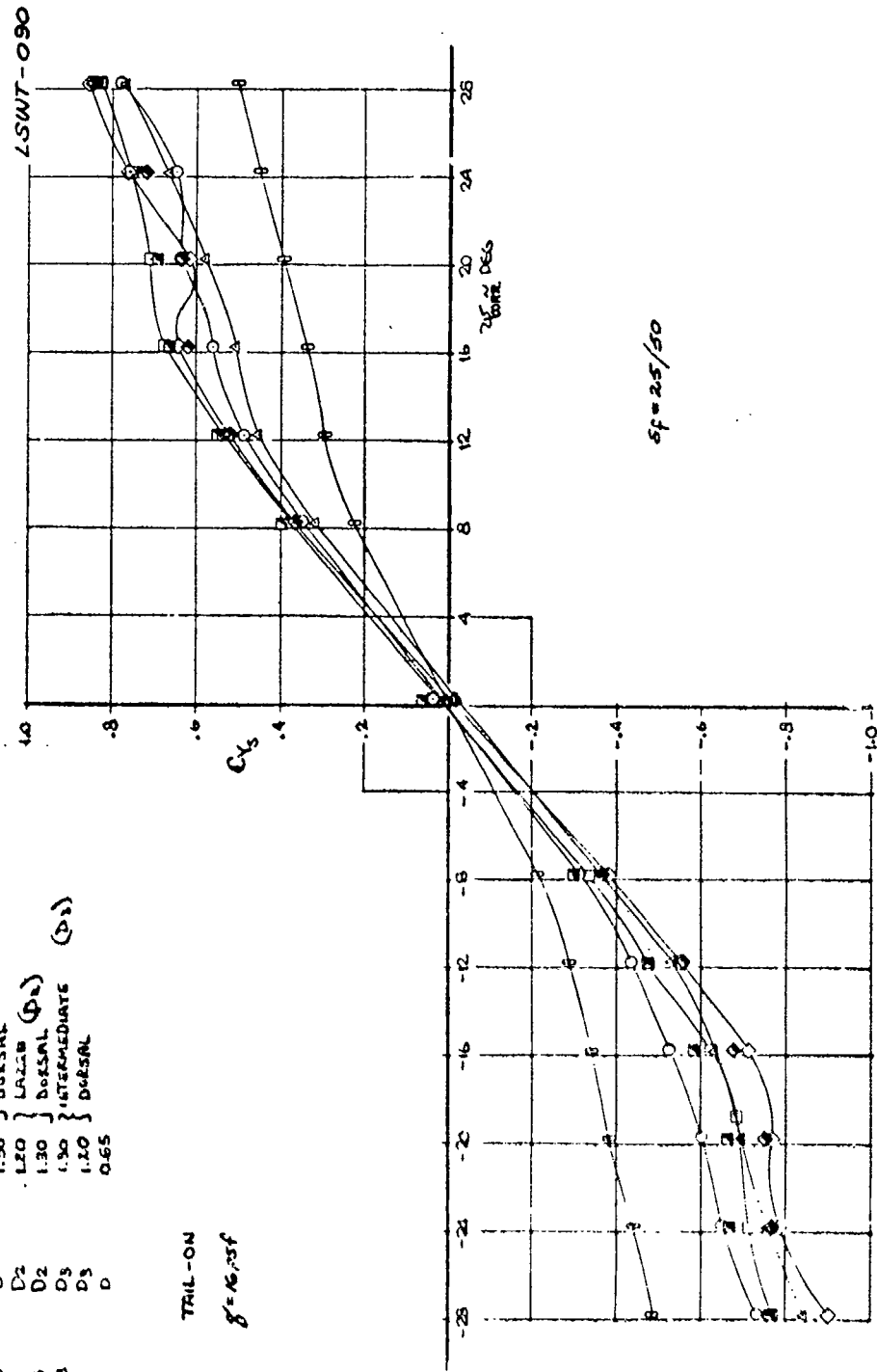


DORSAL OPTIMIZATION

SWT	QJA	Cf	CONFIGURATION	C_{max}	SWT (D)
135	2		D	1.20	SMALL (D)
135	5.3		D	1.50	DORSAL
145	2		D2	1.20	LARGE (D)
145	5.3		D2	1.30	DORSAL
294	5.3		D3	1.30	INTERMEDIATE (D)
292	2		D3	1.20	DORSAL
156	0		D	0.65	

TAIL-ON

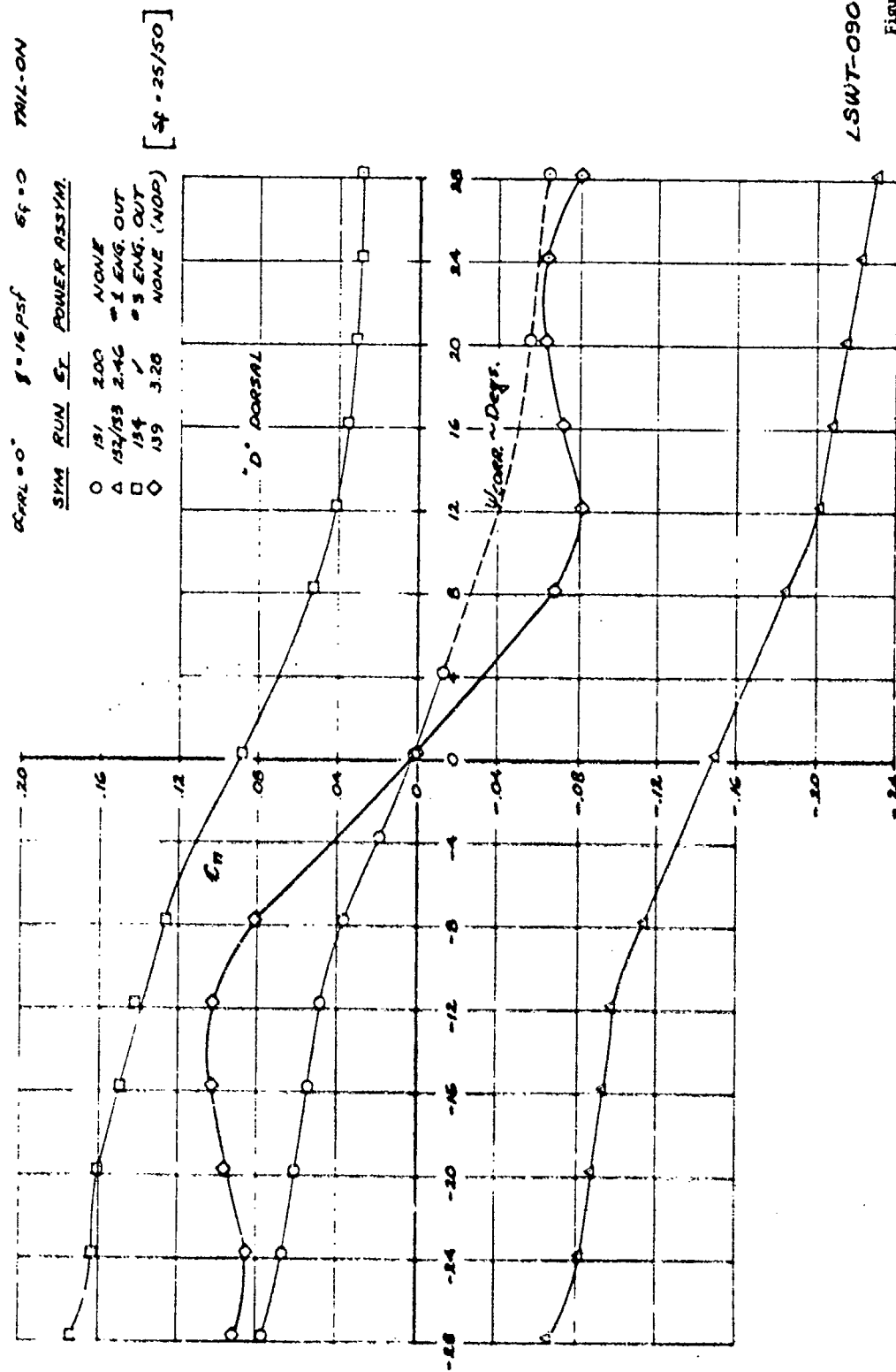
$$g = 16.73f$$



$$S_f = 25/50$$

Figure 15.2.3
377 (The reverse side of this page is blank)

YAW CHARACTERISTICS WITH ENGINE FAILURE



LSWT-090

Figure 15.3.1

379 (The reverse side of this page is blank)

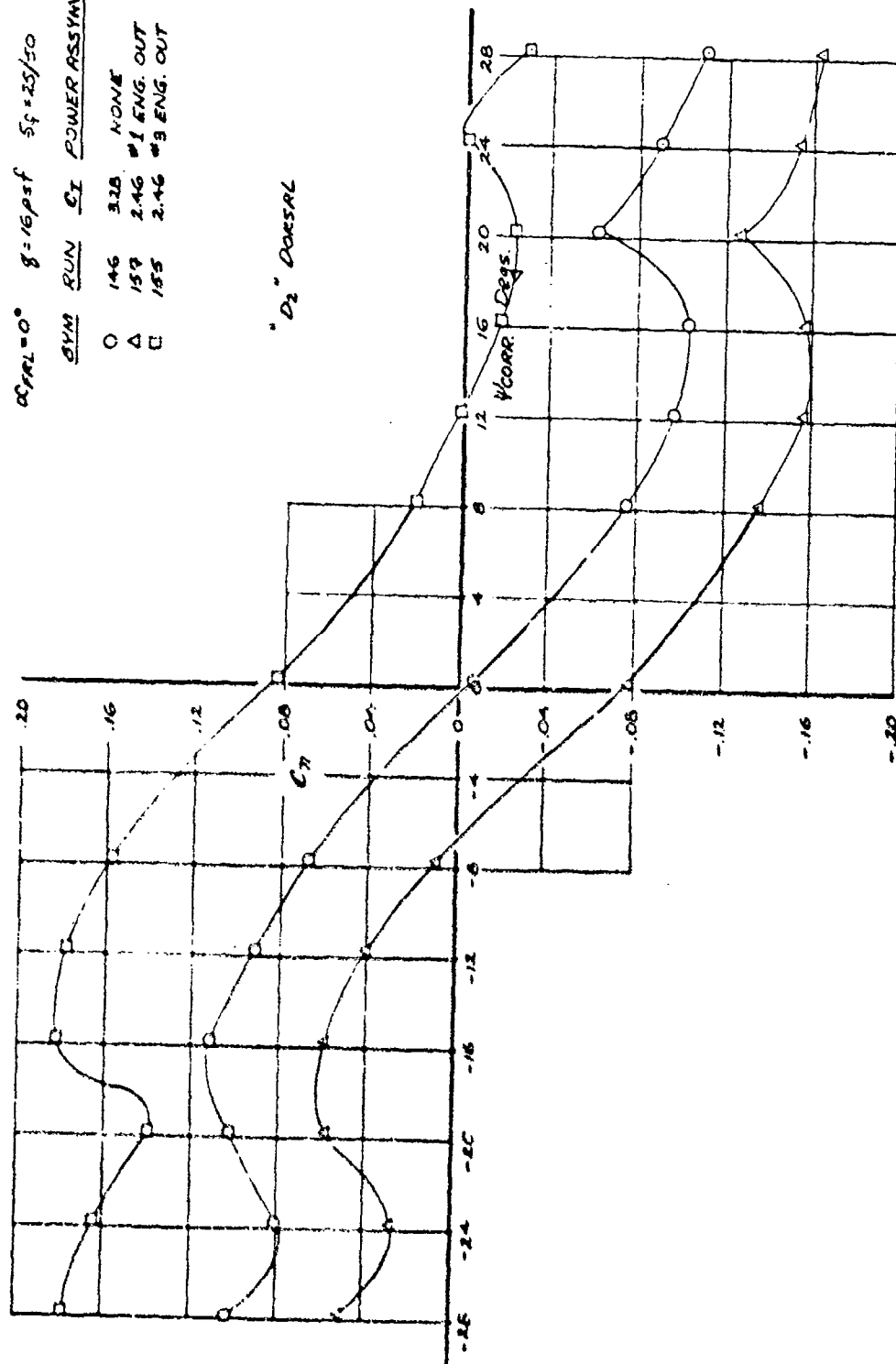
YAW CHARACTERISTICS WITH ENGINE FAILURE

$\alpha_{YAW} = 0^\circ$ $g = 16 \text{ psf}$ $S_f = 25/50$ TAIL-ON

SYM RUN CI POWER ASSYM.

- 146 3.28 NONE
- △ 157 2.46 #1 ENG. OUT
- 155 2.46 #3 ENG. OUT

"D₂" DORSAL

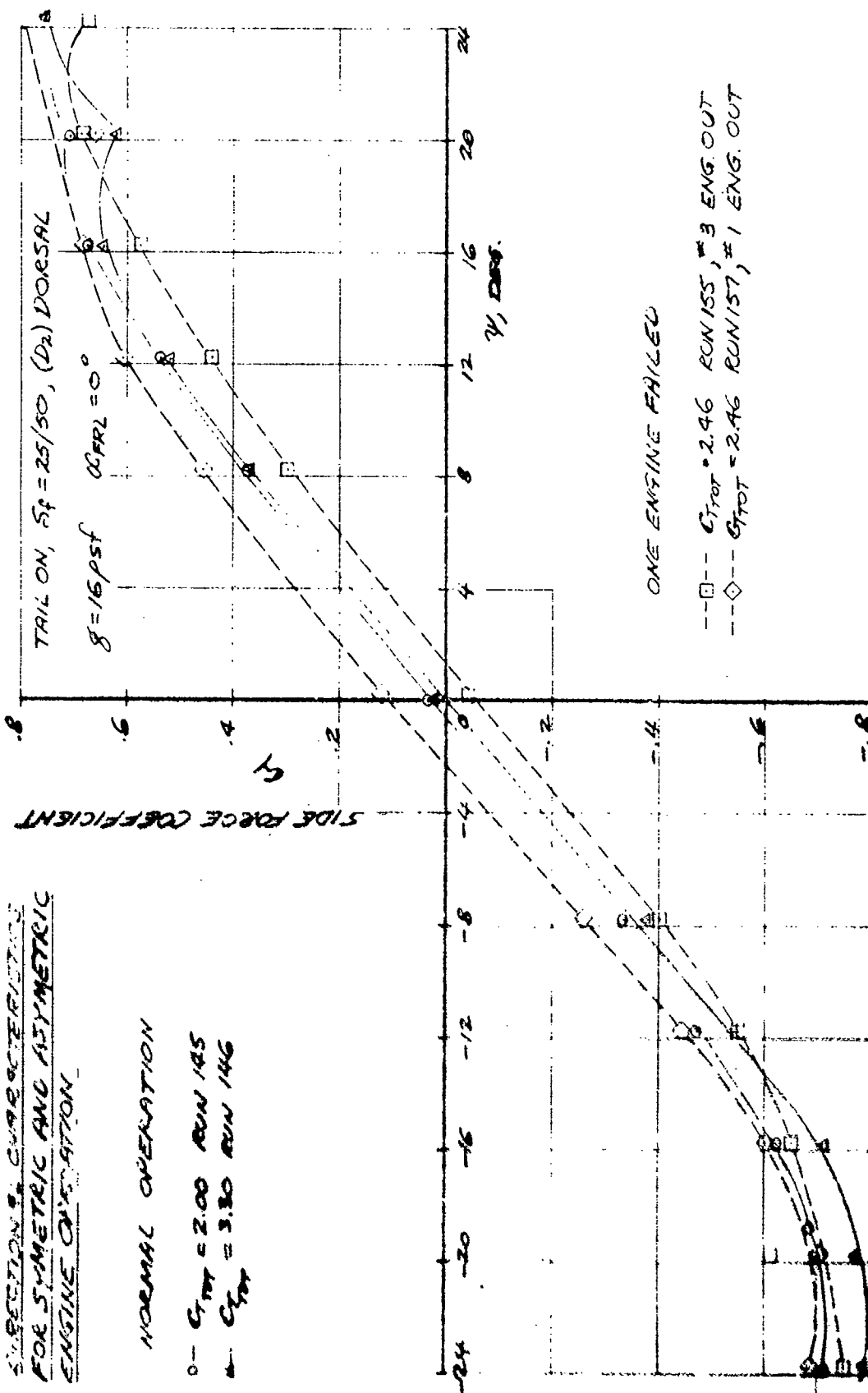


LSWT-090

EXPRESSIONS, CHARACTERISTICS
FOR SYMMETRIC AND ASYMMETRIC
ENGINE OPERATION

NORMAL OPERATION

- $C_{T/TOT} = 2.00$ RUN 145
▲ $C_{T/TOT} = 3.30$ RUN 146



(The reverse side of this page is blank)

Figure 15.3 3

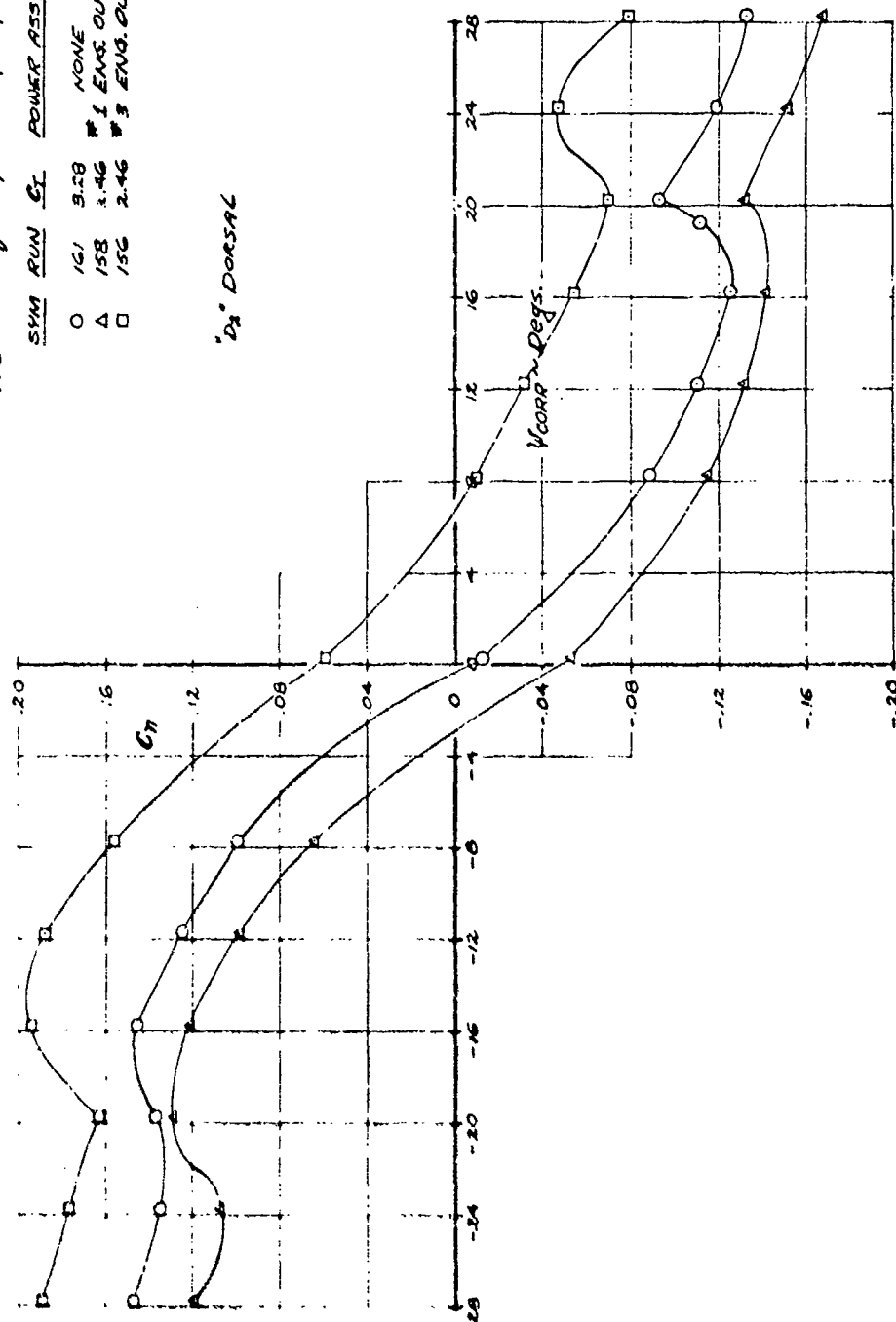
WING CHARACTERISTICS WITH ENGINE FAILURE

$\alpha_{FRL} = 12^\circ$ $g = 16 \text{ gsf}$ $S_f = 25/50$ TAIL-ON

SYM RUN C_L POWER ASSYM.

- 161 3.28 NONE
- △ 158 3.46 #1 ENG. OUT
- 156 2.46 #3 ENG. OUT

"0.1" DORSAL



LSUIT-090
(The reverse side of this page is blank)
Figure 15.3.4

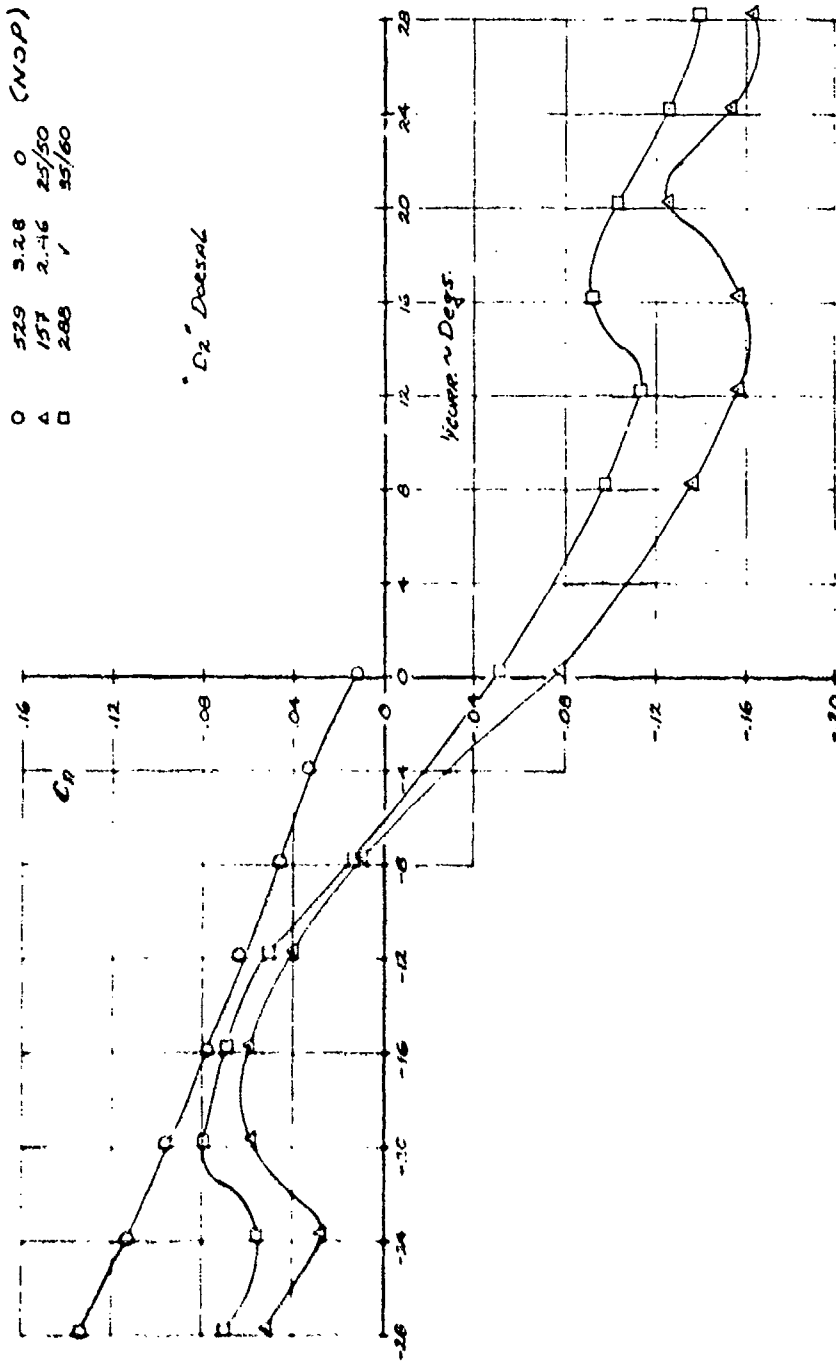
SAW CHARACTERISTICS WITH ENGINE FAILURE

EFFECT OF FLAPS

$\alpha_{FRL} = 0^\circ$ $\delta = 16/50$ TAIL-ON #1 ENG. OUT

SYM	RUN	C_L	C_D
○	529	3.28	0 (N.O.P.)
△	157	2.46	25/50
□	288	1	25/60

"D₂" Does not



LSWT-090

Figure 15.3.5

387 (The reverse side of this page is blank)

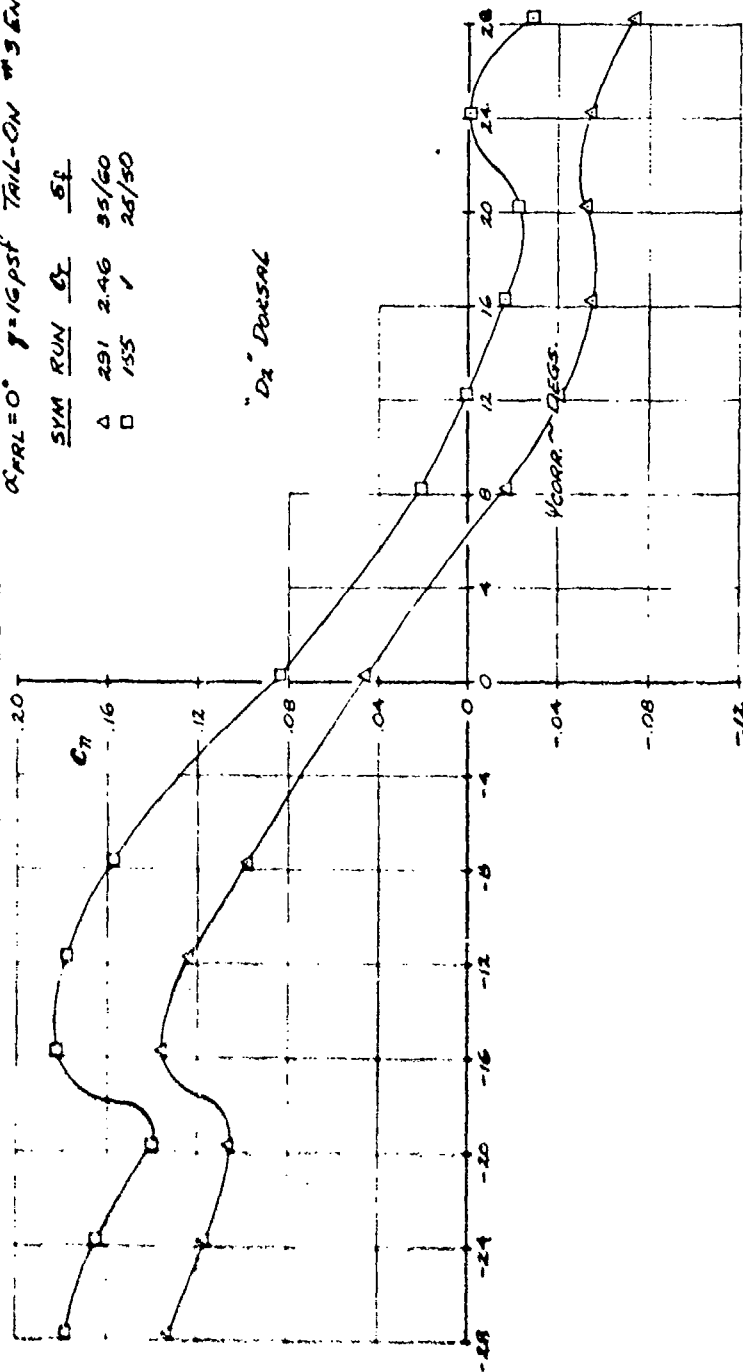
YAW CHARACTERISTICS WITH ENGINE FAILURE

EFFECT OF FLAPS

$\alpha_{FRL} = 0^\circ$ $\gamma = 16 \text{ psf}$ TAIL-ON $\theta = 3 \text{ DEG}$ OUT

SYM	RUN	C_L	C_D
Δ	291	2.46	95/60
\square	155	1	25/50

"D₂" DORSAL



LSWT-090

Figure 15.3.6

389 (The reverse side of this page is blank)

318

LSWT-090

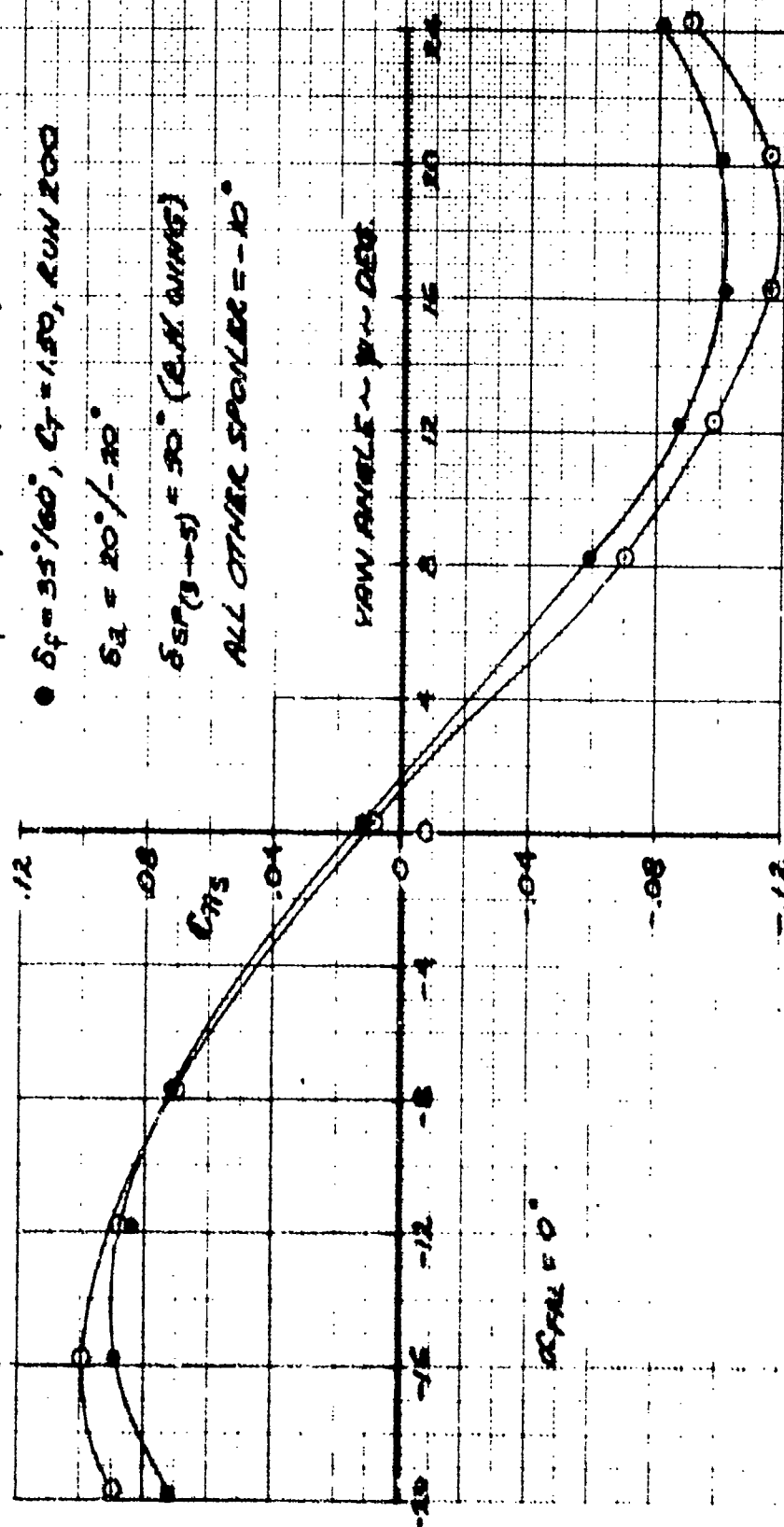
○ $\delta_f = 25^\circ/50^\circ$; $C_f = 150$, RUN 188

● $\delta_f = 35^\circ/60^\circ$; $C_f = 150$, RUN 200

$\delta_a = 20^\circ/-20^\circ$

$\delta_{SP}(3 \rightarrow 5) = 30^\circ$ (E.A. QUINCY)

ALL OTHER SPONDER = -10°



DIRECTIONAL CHARACTERISTICS
CRITICAL (#1) ENGINE OUT

LSWT-090

DIRECTIONAL CHARACTERISTICS

CRITICAL #1) ENGINE OUT, TAIL ON

$\alpha_{FRL} = 0^\circ$

$\delta_a = 20^\circ/-20^\circ$ $\delta_{SF} = 50^\circ$ RH WING ONLY
(ALL OTHERS = -10°)

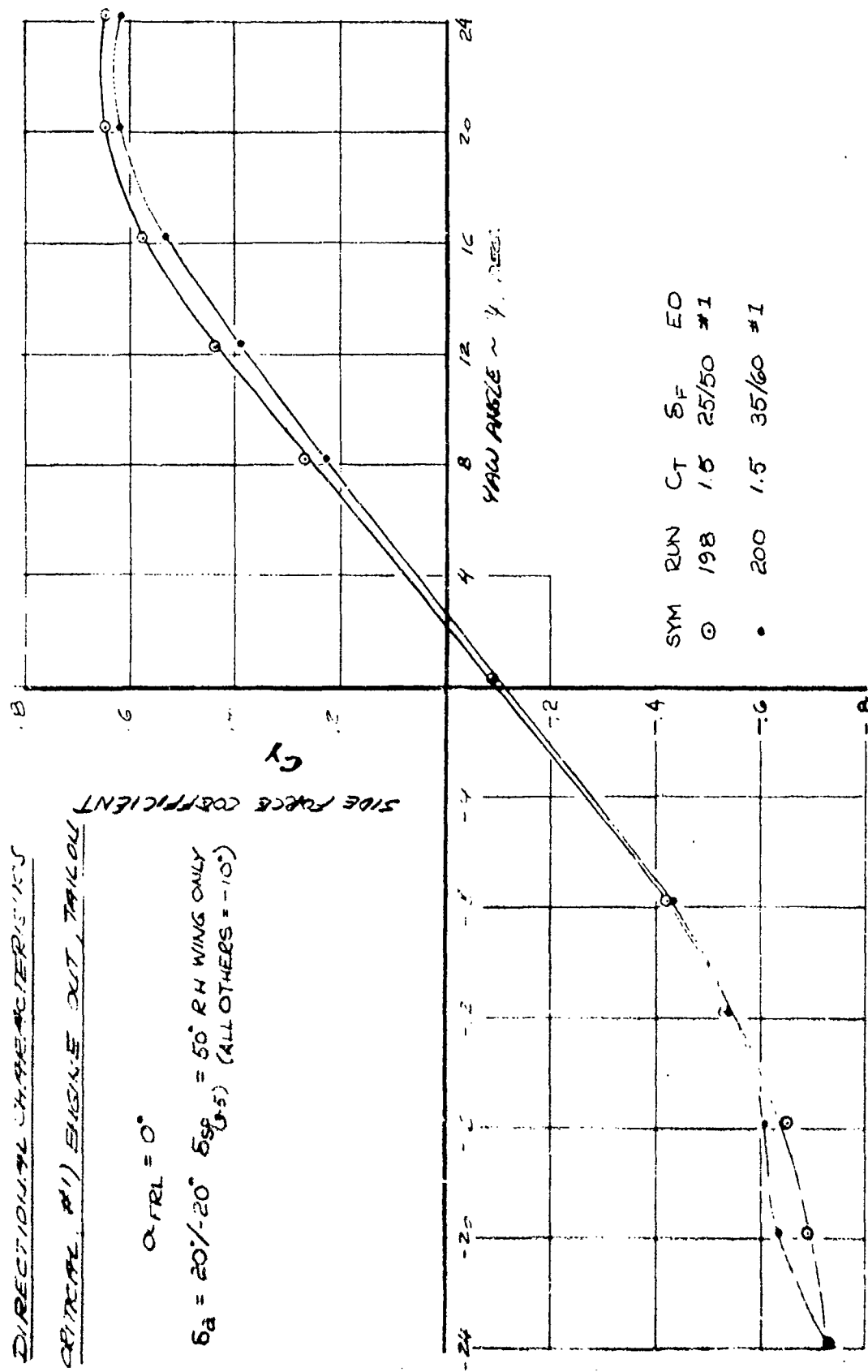
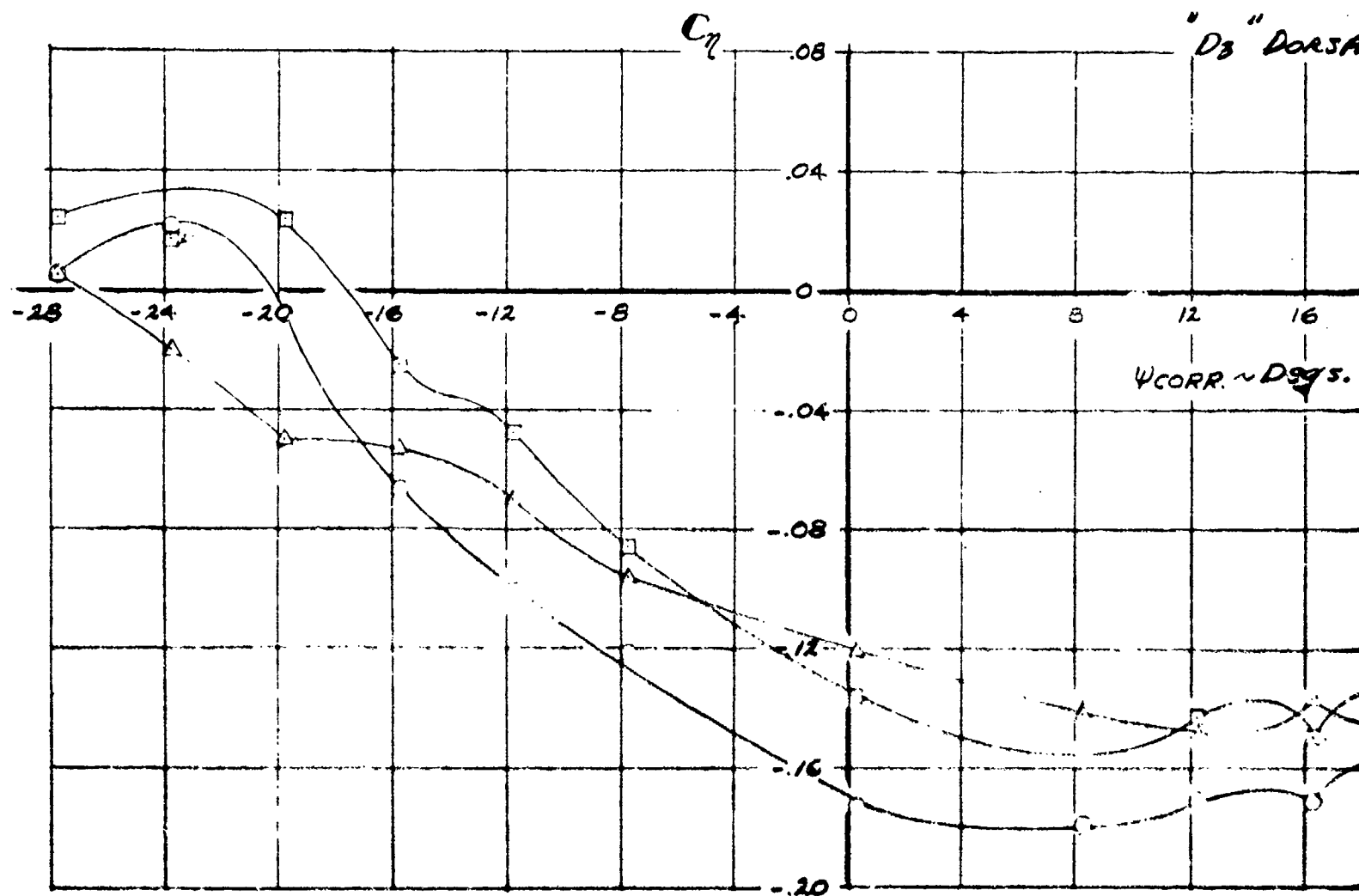


Figure 15.3.8

LSWT-090

YAW CHARACTERISTICS WITH DEFLECTED RUDDER

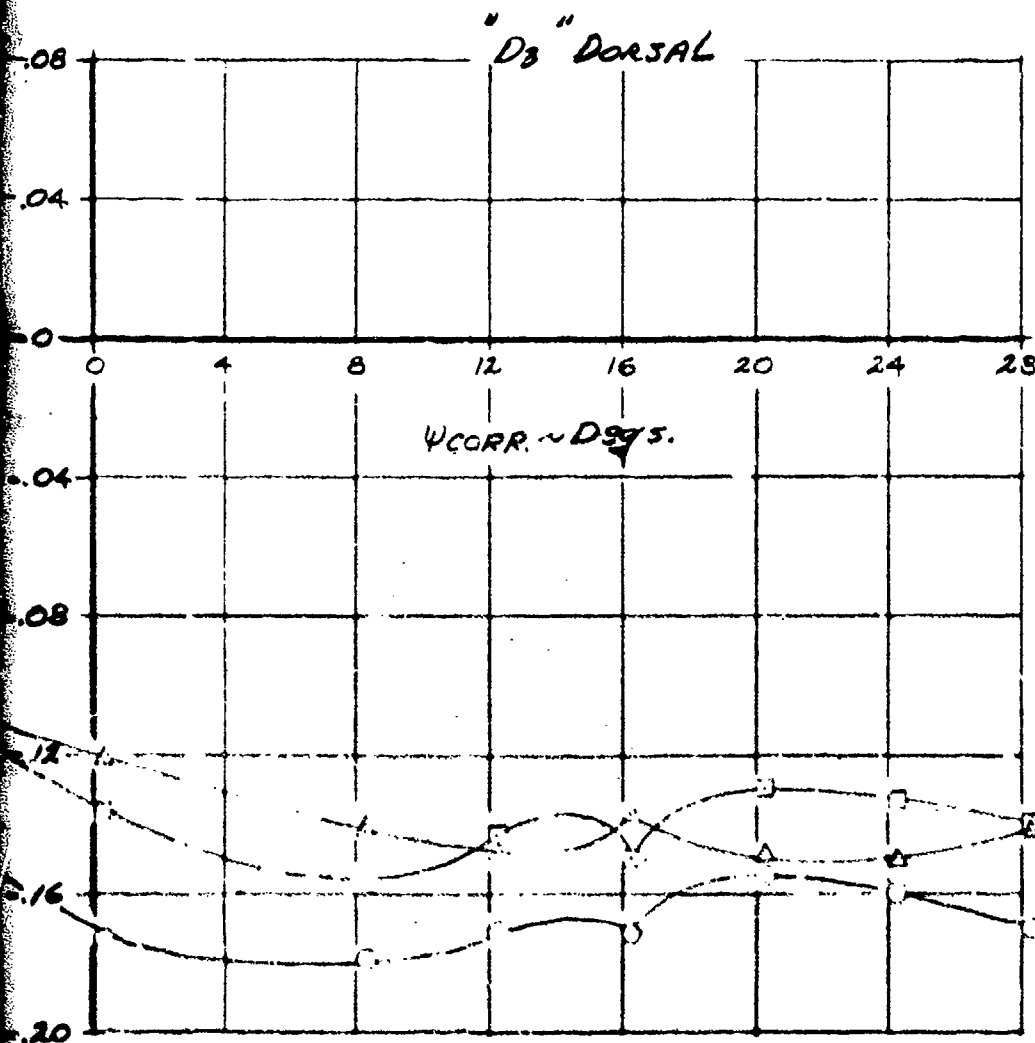


LSWT-090

WITH DEFLECTED RUDDER

$\alpha_{TFL} = 0^\circ$ $g = 16 \text{ psf}$ TAIL-2N ($i_N = 0^\circ$)

<u>SYM</u>	<u>RUN</u>	<u>δ_T</u>	<u>δ_E</u>	<u>S_T/S_E</u>	
○	437	1.5	25/50	25/25	EJ
△	435	0	✓	✓	
□	436	2.0	✓	✓	NOP



(The reverse side of this page is blank)

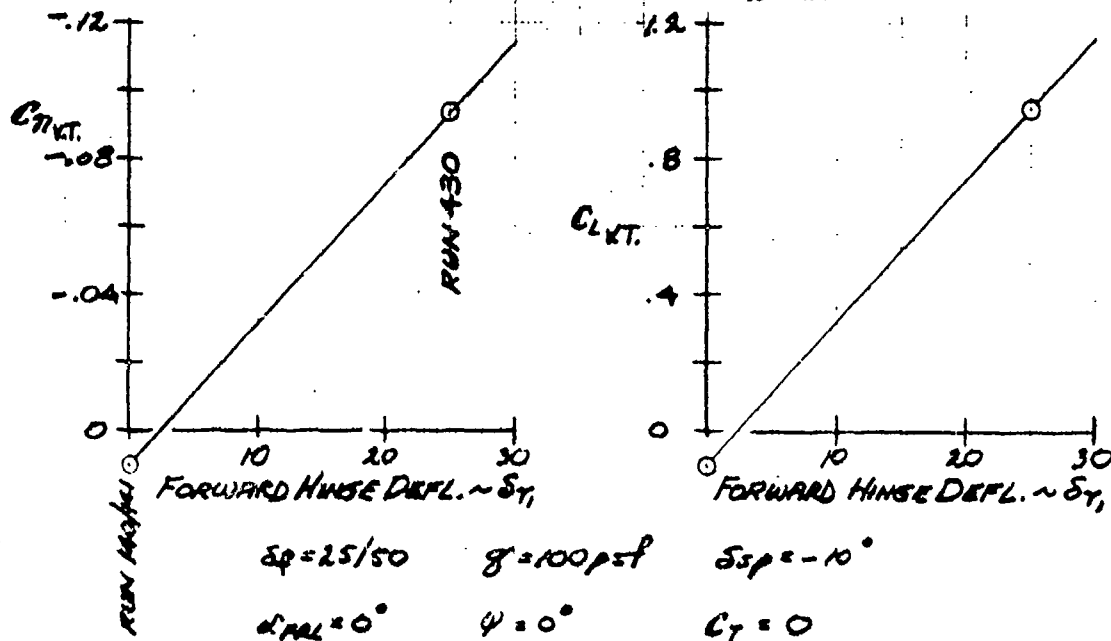
Figure 15.4.1

LSWT-090

CONTROL CAPABILITY OF VERTICAL TAIL
WITH DEFLECTED RUDDER

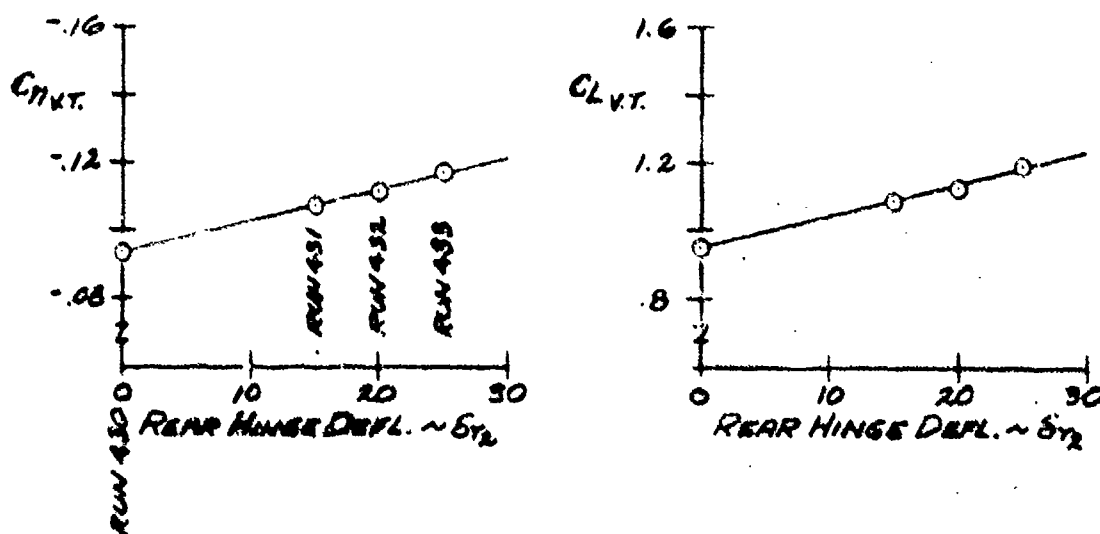
$V_v = 0.0885$

REAR HINGE DEFL. $\sim \delta_{T_2} = 0^\circ$



TAIL-ON ($i_H = 0^\circ$)

FORWARD HINGE DEFL. $\sim \delta_{T_1} = 25^\circ$



A POSITIVE RUDDER DEFLECTION IS TRAILING EDGE LEFT
IN THE PLAN VIEW.

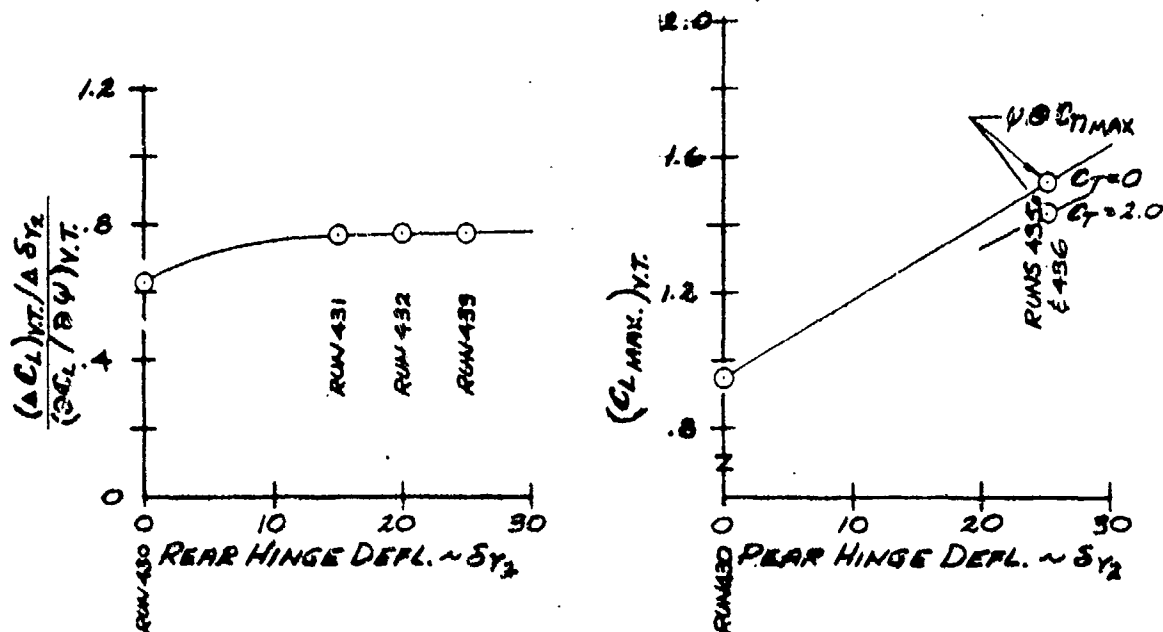
Figure 15.4.3

LSWT-080

CONTROL EFFICIENCY OF VERTICAL TAIL
WITH DEFLECTED RUDDER

$V_V = 0.0985$

FORWARD HINGE DEFL. $\sim \delta_{Y1} = 25^\circ$



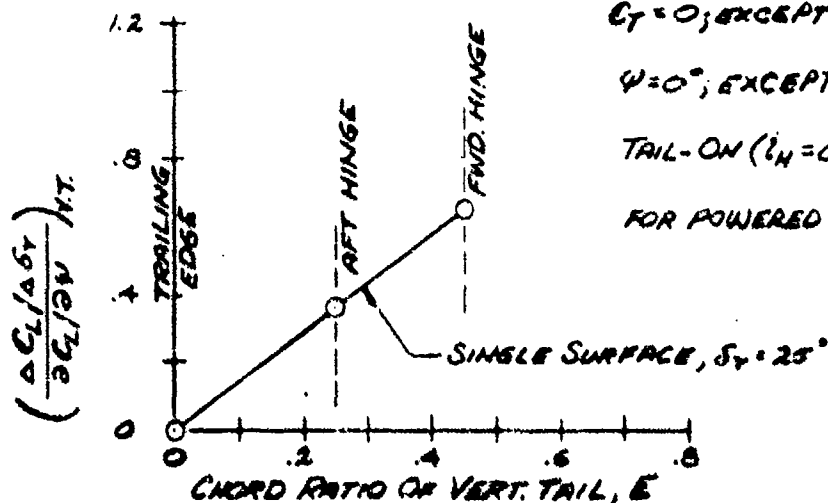
$\delta_T = 25/50$ $\alpha_{TAL} = 0^\circ$

$C_T = 0$; EXCEPT AS NOTED

$\psi = 0^\circ$; EXCEPT AS NOTED

TAIL-ON ($i_H = 0^\circ$)

FOR POWERED RUNS $\rho/\rho_0 = 1.068$



A POSITIVE RUDDER DEFLECTION IN TRAILING EDGE
LEFT IN THE PLAN VIEW.

Figure 15.4.4

Section XVI

CONCLUSIONS

In general all of the objectives enumerated in the Rockwell report NA-71-1121, "STOL Tactical Aircraft Investigation: Wind Tunnel Test Plan for a Research Model of an Externally Blown Flap STOL Transport," dated 7 December 1971 have been met with the exception of the ground plane testing and flow visualization testing. All testing was accomplished at the Lockheed Georgia Company's low speed wind tunnel in a 16 by 23-foot test section between 3 April 1972 and 19 May 1972. The test was designated by Lockheed as LSWT-090.

A great deal of force and pressure data was obtained during this test and a large amount of the force data has been analyzed and is in a form suitable for application to design. Much of the analyzed data has been used in the design of the baseline configuration and in the design compendium update. Some of the data was used in performance tradeoff studies and for the sizing of the horizontal and vertical tails of the baseline configuration.

A comparison analysis of the double and triple slotted flaps has been completed as well as an analysis showing the benefits of the various leading edge extensions and leading edge boundary layer control systems.

An analysis of the data for various roll control devices led to the elimination of the asymmetric leading edge BLC system as a candidate for an adequate roll control system.

Data has been acquired, analyzed and presented in this report showing the capabilities and efficiencies of double cambered rudder and elevator surfaces.

The only pressure data analyzed to date is that acquired with the downwash study rake. The wing pressure data has not been looked at yet. With a test of this magnitude and complexity it is obvious that time would not permit extensive detail testing in any singular area. Yet the analysis reveals that such additional detail testing is required, to better understand the effects of flaps on the downwash flow field or to more accurately define the causes leading to the inboard engine failed being critical in yaw rather than the outboard engine failed. Other areas that need further detailed investigation are, for example, DMC effects on full flaps downwash, static turning angles for all flap deflections and engine nozzle deflections, roll control effectiveness at low engine C_T 's, and basic flaps up yaw data at varying C_T 's. These are only a few of the areas that require additional testing in order for the using aerodynamicists to get an in depth feel for these data.

REFERENCES

1. Papp, P.P., and Hughes, M.T., NA-71-1121, "STOL Tactical Aircraft Investigation: Wind Tunnel Test Plan for a Research Model of an Externally Blown Flap STOL Transport," Rockwell International, Los Angeles Aircraft Division, International Airport, Los Angeles, California, 7 December 1971, revised 18 March 1972
2. Hughes, M.T., NA-72-670, "STOL Tactical Aircraft Investigation Wind Tunnel Test Data of an Externally Blown Flap Model, Contract F33615-71-C-1760", Rockwell International, Los Angeles Aircraft Division, International Airport, Los Angeles, California, 24 August 1972